New Cyclometalating Ligands for Emissive Iridium(III) Complexes for OLED Applications

HELEN BENJAMIN

New Cyclometalating Ligands for Emissive Iridium(III) Complexes for OLED Applications

Helen Benjamin

St. Aidan's College

Department of Chemistry

Durham University

A thesis submitted for the degree of Doctor of Philosophy at Durham University

March 2016

Abstract

Organic light-emitting diodes (OLEDs) are an emerging area in lighting technology, with the potential to be cheaper, lighter and more efficient than traditional filament and fluorescent lighting sources. Emission in OLED devices is produced by relaxation of excitons, excited states of the emissive material formed by the applied electrical current, to the ground state, releasing the energy as light. Excitons exist as either singlets or triplets, which can emit light via fluorescence and phosphorescence, respectively. While phosphorescence is formally forbidden for simple organic molecules, it is allowed for 2^{nd} and 3^{rd} row transition metal complexes due to their strong spin-orbit coupling. This maximises the conversion of electrical energy to light when the complexes are employed as dopants in OLED devices. Iridium(III) complexes are the most widely used, as the emission colour can be tuned easily through relatively simple structural modification, although other d^6 metal centres have been investigated.

In this thesis a new family of sulfone containing ligands was synthesised, with the aim of blue-shifting the emission of the resultant iridium complexes compared to the parent complex, FIrpic. Introducing a sulfone group to the 5-position of dfppy (**19**, **20**, **28**) resulted in a blue-shift of 10 nm compared to FIrpic, due to the lowering of the HOMO with respect to the LUMO. This series of complexes was then extended to include complexes **68**, **69**, **70** and **80**, which contain fewer aromatic fluorines, as these are known to make the complexes unstable in devices. While a red-shift is observed when exchanging one fluorine for a methoxy group, complexes **68**, **69** and **70** still displayed bluer emission than FIrpic. Complex **80** provides a viable fluorine-free alternative to FIrpic, with similar emission wavelength, HOMO/LUMO energies and similar orbital distributions, as indicated by the computational data. To blue-shift the emission further a new ancillary ligand (**133**) was synthesised and combined with some of the sulfone ligands to produce complexes **140** and **141** (analogous to complexes **70** and **80**). Devices fabricated in the Department of Physics retained the blue emission observed in solution and performed comparably with FIrpic. New complexes with oxazoline- and oxazole- based ancillary ligands were also synthesised.

Donor-acceptor chromophoric ligands were also synthesised to investigate the solvent dependent dual emission properties of the resultant complexes. The donor and acceptor components were varied, producing complexes with differing degrees of dual emission character in solution (**90**, **105**, **116** and **117**), which is tentatively assigned to the prescence of a ligand based CT state. While the complexes did not display dual emission properties in the solid state, devices fabricated in the Department of Physics showed favourable performances as blue emitters compared to a FIrpic device.

Statement of Copyright

Declaration

The work in this thesis was carried out in the Department of Chemistry at Durham University between October 2012 and March 2016. All of the work was carried out by the author unless otherwise stated and has not previously been submitted for a degree at this or any other university.

Acknowledgements

I would like thank my supervisor, Martin Bryce, for his support and guidance over the years. I would also like to thank the past and present members of the Bryce group for sharing their expertise and providing such a friendly and instructive environment to work in.

Additional thanks go to Professor Andrew Beeby, and his post-docs, Dr Helen Hsu and Dr Ross Davidson for their help with conducting the photophysical measurements.

Many thanks go to the staff of the analytical services, in particular the NMR service, for their help and patience

Additional thanks go to Dr Mark Fox, for the computational work in chapters 2 and 3, and to Dr Andrei Batsanov and Dr Dmitry Yufit for their expertise in solving X-ray crystal structures from my tiny crystals.

I would also like to thank Durham University for awarding me a scholarship and giving me the opportunity to pursue my studies.

I would also like to thank our collaborators in Professor Monkman's group in the Department of Physics, and Prof. Dongxia Zhu and her collaborators in Northeast Normal University and Jilin University for the device measurements presented in this thesis.

I would like to thank parents and my sister for their love and support during my studies. Thanks also go to my friends, in particular Aidan and the Wynyard crew, for making my time in Durham so wonderful.

Table of contents

List of abbreviations

acac	Acetylacetonate
AMOLEDs	Active matrix organic light-emitting diodes
ASAP	Atmospheric Solids Analysis Probe
$B(O^iPr)_3$	Triisopropyl borate
B_2pin_2	Bis(pinacolato)diboron
CBZ	Chlorobenzene
COSY	Correlation spectroscopy
CT	Charge transfer
CzSi	9-(4-Tert-butylphenyl)-3,6-bis(triphenylsilyl)-9H-carbazole
Dbm	Dibenzoylmethanate
DCM	Dichloromethane
DDQ	2,3-Dichloro-5,6-dicyano-1,4-benzoquinone
dfppy	2-(2,4-Difluorophenyl)pyridine
DFT	Density functional theory
DIPA	Diisopropyl amine
DME	1,2-Dimethoxyethane
DMF	Dimethylformamide
DMSO	Dimethylsulfoxide
dppf	1,1'-Bis(diphenylphosphino)ferrocene
EBL	Electron blocking layer
EDG	Electron-donating group
EPESS	Enhanced phosphorescence emission in the solid state
EQE	External quantum efficiencies
ESI	Electrospray ionisation
E_T	Triplet energy
ETL	Electron transport layer
EtOAc	Ethyl acetate
EWG	Electron-withdrawing group
fac	Facial
fac-$Ir(ppy)_3$	*fac*-Tris[2-phenylpyridinato-C2,N]iridium(III)
Fc	Ferrocene
FIrpic	Bis[2-(4,6-difluorophenyl)pyridinato-C2,N](picolinato)iridium(III)
GCMS	Gas chromatography–mass spectrometry
HBL	Hole blocking layer
HOMO	Highest occupied molecular orbital
HPLC	High-performance liquid chromatography
HRMS	High resolution mass spectrometry
HTL	Hole transport layer
IC	Internal conversion
ICT	Intramolecular charge transfer
ILET	Inter-ligand energy transfer
^iPr	Isopropyl

IQE	Internal quantum efficiency
ISC	Intersystem crossing
ITO	Indium tin oxide
k_{nr}	Non-radiative decay rate
k_r	Radiative decay rate
LC	Ligand-centred
LCD	Liquid crystal display
LDA	Lithium diisopropylamide
LEEC	Light emitting electrochemical cell
LLCT	Ligand-to-ligand charge transfer
LMCT	Ligand-to-metal charge-transfer
LUMO	Lowest unoccupied molecular orbitals
MALDI	Matrix-assisted laser desorption/ionization
MC	Metal-centred
MCH	Methylcyclohexane
mCPBA	*meta*-chloroperoxybenzoic acid
Me	Methyl
mer	Meridonal
mes	Mesityl/2,4,6-Trimethylphenyl
MIDA	methyliminodiacetic acid
MLCT	Metal-to-ligand charge-transfer
MsCl	Methanesulfonyl chloride
^{n}BuLi	n-Butyllithium
NOESY	Nuclear Overhauser effect spectroscopy
OLED	Organic light-emitting diode
OXD-7	2,2'-(1,3-Phenylene)bis[5-(4-tert-butylphenyl)-1,3,4-oxadiazole]
PCy_3	Tricyclohexylphosphine
$Pd(OAc)_2$	Palladium(II) acetate
$Pd(PPh_3)_4$	Tetrakis(triphenylphosphine)palladium(0)
$Pd_2(dba)_3$	Tris(dibenzylideneacetone)dipalladium(0)
PEDOT:PSS	Poly(3,4-ethylenedioxythiophene) polystyrene sulfonate
PET	Photoinduced electron transfer
pic	Picolinate
PLQY/ Φ	Photoluminescence quantum yield
PMMA	Poly(methyl methacrylate)
PPh_3	Triphenylphosphine
ppy	2-Phenylpyridine
p-Tol	*Para*-tolyl
PVK	Poly-(vinylcarbazole)
RT	Room temperature
$Ru(bpy)_3^{2+}$	Ruthenium(II) tris(bipyridine)
S_NAr	Nucleophilic aromatic substitution
SOC	Spin orbit coupling
SPhos	2-Dicyclohexylphosphino-2',6'-dimethoxybiphenyl
T_{50}	Device lifetime (time for the luminance to fall to 50% of the initial value)

TADF	Thermally activated delayed fluorescence
T_d	Decomposition temperature
TF	Triplet fusion
TFA	Trifluroroacetic acid
THF	Tetrahydrofuran
THP-	Tetrahydropyranyl
TLC	Thin-layer chromatography
TMEDA	Tetramethylethylenediamine
TMS	Tetramethylsilane
Tol	Toluene
TPBi	2,2',2"-(1,3,5-Benzinetriyl)-tris(1-phenyl-1-H-benzimidazole)
TsOMe	Methyl 4-methylbenzenesulfonate
TTA	Triplet-triplet annihilation
UGH2	*p*-Bis(triphenylsilyl)benzene
UPS	Ultraviolet photoelectron spectroscopy
VR	Vibrational relaxation
WOLED	White organic light-emitting diode
Xantphos	4,5-Bis(diphenylphosphino)-9,9-dimethylxanthene
ΔE_{ST}	Singlet-triplet splitting
ε	Molar extinction coefficient
λ_{max}	Maximum absorption/emission wavelength
σ_m	*Meta* Hammett parameter
σ_p	*Para* Hammett parameter
τ_{obs}	Observed emission lifetime

Chapter 1: Introduction

Since the first report of electroluminescence from organic molecules in the 1950s,[1] there has been a considerable amount of research into emissive organic materials. The first Organic Light-Emitting Diodes (OLEDs), fabricated by Tang and VanSlyke at Eastman Kodak in 1987,[2] prompted intense study into conducting and emissive materials for display and lighting applications, including conductive and emissive polymers, small molecules and transition metal phosphors. OLEDs have the potential to be more light-weight, cheaper and more efficient than traditional filament and fluorescent lighting sources. OLED devices do not require backlighting, instead consisting of layers of thin films, allowing them to be more light weight than current liquid crystal display (LCD) technology.[3,4] They can also have a wider viewing angle, faster response time and consume less energy when displaying dark images.[3,4] The absence of backlighting allows OLEDs to be deposited onto flexible substrates to form bendable devices.[5] In addition, soluble organic electroactive materials can be deposited by solution processing, which allows the manufacture of devices by inkjet printing techniques, reducing device cost.[5,6] Today Active Matrix OLEDs (AMOLEDs) are used in the displays of many smart phones, and OLED TVs have been produced by Samsung, Sony and LG, although at a high price. In addition, in 2010, Sony debuted a small flexible OLED screen prototype, able to roll around a pencil while still displaying images, highlighting the unique potential of OLED technology.[7]

OLEDs

OLEDs are devices which emit light in response to an applied electric current. They consist of layers of organic semiconducting materials, each of which performs a specific function within the device, sandwiched between two electrodes (one of which is optically transparent) and deposited onto a substrate such as glass or flexible plastic (Figure 1.1). The cathode and anode serve to introduce charges (electrons and holes, respectively) into the device and these pass through the layers and combine in the emissive layer to form excitons, excited states of the emissive molecules.[8] These excited states then collapse back to the ground state, resulting in emission of light from the device with a wavelength corresponding to the energy difference between the excited and ground states. As electrons and holes have spin ½ the excitons can either be singlets (S = 0) or triplets (S = 1) and these are formed in a ratio of 1:3 in devices according to spin statistics and experimental observations.[8,9] Devices utilising purely fluorescent emitters are therefore limited to an internal quantum efficiency (IQE, defined as the ratio of the number of internally generated photons to the number of injected electrons) of only 25% as transitions

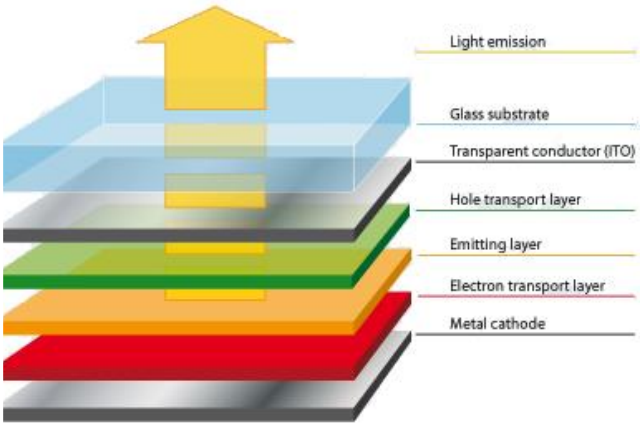

Figure 1.1: Diagram of a typical OLED device.

between states of differing spin quantum number are formally forbidden by the spin selection rules. Materials that can harness the remaining 75% triplet states can theoretically achieve 100% IQE. There are a few methods to do this: 1) using heavy metal complexes in which spin-orbit coupling (SOC) allows formally forbidden emission from the triplet states,[7,10] 2) using a form of delayed fluorescence, either triplet fusion (TF or P-type delayed fluorescence), which can achieve a maximum IQE of 62.5%, or 3) thermally- activated delayed fluorescence (TADF, or E-type delayed fluorescence) which can achieve a theoretical 100% IQE.[11]

Figure 1.2 shows an example energy level diagram for a typical OLED device. The HOMO and LUMO levels of the materials are depicted, and it is evident that it is important for the HOMO/LUMO levels of layers to match up to prevent high injection barriers. In addition, charge mobilities in adjacent layers must also be matched to neighbouring layers. In order to ensure colour purity from a device the excitons must be confined on the emissive molecule; to do this charges within the device must be appropriately balanced.

For this to be achieved electron and hole transport layers (ETLs and HTLs) are inserted next to the cathode and anode, respectively, to facilitate the injection of charges by reducing the injection barrier.[10] Efficient electron transport materials are particularly important, as hole mobility in OLED devices is typically 1000 times greater than electron mobility.[10] To assist in the balancing of charges electron and hole blocking layers (EBLs and HBLs) can be used. These are materials with a high LUMO/low HOMO to prevent charge leakage.

It is necessary to dope most emitters into a host matrix, in order to prevent concentration induced quenching.[10] This is particularly important for phosphorescent emitters, as triplet-triplet annihilation can occur at high concentrations due to the long-lived nature of the excited state.[10] This is a Dexter process wherein two excited triplet states with overlapping wavefunctions collide

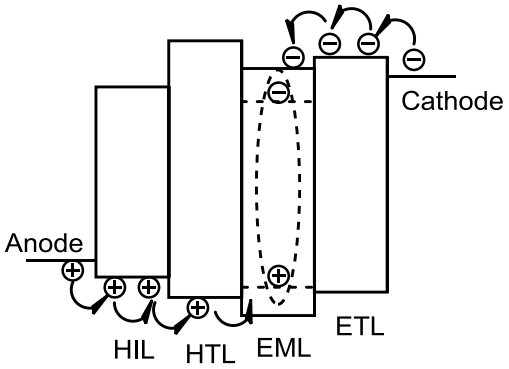

Figure 1.2: Energy level diagram for a typical OLED device.

to produce one molecule in the singlet ground state and one in an excited singlet state. This energy transfer is strongly distance dependent and hence can be reduced by doping a phosphorescent material into a matrix. However, the use of a host brings its own difficulties; host materials must have a triplet energy (E_T) approximately 0.4 eV higher than that of the dopant in order for the energy transfer to be efficient.[10,12,13] Otherwise, triplet states can remain trapped on the host and may undergo quenching. In addition colour purity can also be reduced as the host molecules may emit themselves.[10,14-17]

While red and green emitters for OLEDs are well known, their blue counterparts continue to underperform in devices by comparison. Operational lifetimes (defined here as the time taken for the luminance of a device to fall to 50% of its original value) published in 2007 by DuPont for red and green phosphors were 46,000 h and 230,000 h, respectively,[18] and they recently published a solution-processable green material with a lifetime of 1,000,000 h.[19] In comparison, the blue emitting materials still have a maximum current lifetime of about 40,000 h. [18] The design of efficient blue emitting materials is challenging as blue light requires high energy transitions which can be difficult to obtain.[4,10] In addition the increased energy of the transition can result in an increase in radiationless deactivation pathways, such as M-L bond stretching, solvent deactivation, vibronic coupling to the ground state and, if the potential energy surface of the T_1 state is shallow enough, direct surface crossing between T_1 and S_0.[15,20,21] Another challenge is in designing hosts and other materials that can be used with these high energy emitters; host materials for blue and deep blue materials require large E_Ts and as a result a wide HOMO-LUMO gap E_g,.[10] This can be difficult to obtain as it is normally achieved by decreasing π-conjugation, however this reduces the conductance and is detrimental to device efficiency.[10,16] It is also necessary for the orbital energy levels of the host and emitter to overlap, otherwise efficient energy transfer will not occur.[12]

TRANSITION METALS FOR OLEDs

Luminescent transition metal complexes have attracted great interest in recent years due to their wide variety of applications, including sensitisers for f-block emissive complexes,[22] bioimaging agents,[22-25] singlet oxygen sensitisers,[26] oxygen and fluoride sensors,[27-30] metal ion sensors,[31,32] solar cells,[33,34] luminescent sensors of chiral molecules,[35] photosensitisers for hydrogen generation catalysts,[30,36] photodynamic therapy agents,[37] and photoredox catalysts.[38] Their interesting photophysical properties have also found widespread use in the field of optoelectronics, particularly in OLEDs or light-emitting electrochemical cells (LEECs).

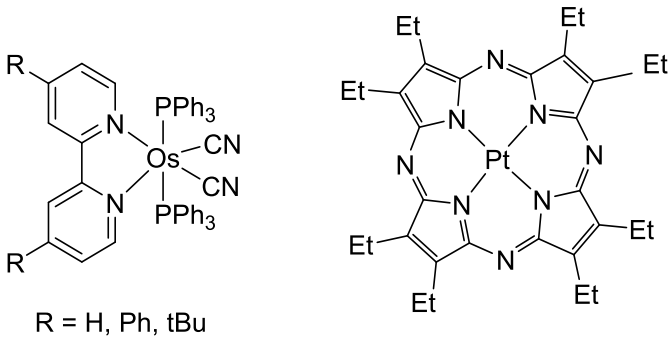

Figure 1.3: LEFT: Electroluminescent osmium complexes. RIGHT: PtOEP, an electroluminescent platinum complex.

Electroluminescence from a transition metal complex in an OLED device was first reported in 1998 by Yuguang Ma *et. al.* from osmium (II) complexes with a chromophoric bipyridine ligand (Figure 1.3).[39] Along with other d_6 metal centres (such as Ru^{II} and Ir^{III}), Os^{II} was identified as a promising centre for emissive phosphorescence materials due to its large ligand field splitting and strong metal-ligand interactions which allow for highly efficient luminescence.[7] In the same year, Thompson and Forrest also reported an OLED device with a platinum porphyrazine (PtOEP, Figure 1.3) complex as the emitter,[40] however, both papers reported a quenching of efficiency in devices due to triplet-triplet annihilation (TTA) as a result of the materials' long phosphorescence lifetimes. In 1999 Thompson and Forrest utilised *fac*-$Ir(ppy)_3$ to produce a green OLED device with an external quantum efficiency (EQE) of 7.5% at 100 cd/m^2 at an operating voltage of 4.3 V.[41] $Ir(ppy)_3$ was identified as promising due to its short phosphorescence lifetime, 2 μs, indicating strong spin-orbit coupling and a reduced effect from TTA.[41] Since then Ir^{III} complexes have been widely studied due to their favourable short phosphorescent lifetimes, strong spin-orbit coupling and large ligand-field splitting due to Ir being a 3rd row transition metal.[42-44] Although iridium is a rare and therefore expensive metal, the quantity required to produce devices is relatively low, as they are doped into a host material. In addition, many of the complexes are robust and efficient, as a result iridium phosphors remain the industry standard for red and green emitters.

To understand how these complexes perform these functions the nature of the excited state must

be considered. In order to do this it is important to understand the different types of excited states and electronic transitions that occur, and how they affect the emissive properties of the complex, such as colour, photoluminescence quantum yield and lifetime. Armed with this understanding, these properties can be tuned through molecular design to produce the features desired for specific applications.

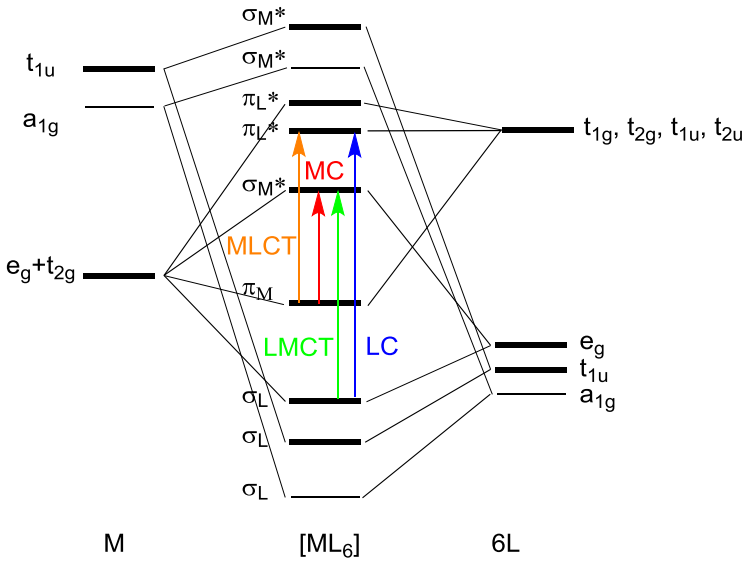

Figure 1.4: Generalised molecular orbital diagram for an octahedral complex ML_6.

A general molecular orbital diagram for an octahedral metal complex ML_6 is shown in Figure 1.4. The energy levels vary depending on the identity of the metal centre M, the oxidation state of the metal, and the choice of ligand. Although the orbitals span the entire molecule it is possible to identify the orbitals with significant ligand character (L) or metal character (M); once the orbitals are labelled as such it is possible to identify four main types of transitions, listed below:

1) Metal-centred (MC) states
2) Ligand-centred (LC) states
3) Metal-to-ligand charge-transfer (MLCT)
4) Ligand-to-metal charge-transfer (LMCT).

The lowest energy excited state can be any one of these, or an admixture of two, depending on the relative energy levels of the orbitals.

Metal-centred (MC) states

These states arise from transitions from metal d orbitals to metal d* orbitals; a transition formally forbidden by the Laporte selection rule, however this can be relaxed by spin-orbit coupling (SOC) for heavier transition metals.[7] As a result d-d* transitions in absorption spectra have lower

oscillator strengths and ε values. As population of these states involves population of antibonding orbitals, they are often significantly distorted compared to the ground state, as a result they can be effective pathways for radiationless deactivation or ligand dissociation.[13] For first row transition metals these states are often low in energy; however for second/third row transition metals they are often higher in energy, as the crystal field splitting parameter increases going down a group.[7,13] The energy level of these states is still important in the design of high energy emissive materials however, as it is important to ensure they are sufficiently high in energy otherwise they can provide an efficient quenching mechanism. An energy difference of 0.37 to 0.50 eV between the emitting and the quenching state is necessary to ensure a sufficiently small Boltzmann factor, and thus a small population of the quenching state, at ambient temperature.[13]

Ligand-centred (LC) states

Ligand-centred transitions arise from electron transfer between the π and π* orbitals localised on the ligands, and resemble the transitions of the free ligand if the change in its structure upon coordination to the metal is minimal.[7] As these transitions do not involve the metal centre directly, spin-orbit coupling (SOC) does not have much of an effect.[7,45] This can be detrimental for the emissive properties in OLEDs, as without a relaxation to the selection rules the $^3LC \rightarrow S_0$ is formally forbidden.[45]

Metal-to-ligand charge transfer (MLCT) states

Metal-to-ligand charge transfer states occur on promotion of an electron from the metal d orbitals to the ligand π*orbitals, resulting in metal oxidation and ligand reduction.[7] Hence the energy of the MLCT state can be related to the difference between first oxidation and reduction potentials. Due to the change in symmetry between the initial and final states these transitions are strongly allowed by the Laporte selection band, resulting in greater extinction coefficients in the absorption spectra than seen for d-d* transitions. As these states involve the metal orbitals directly, spin-orbit coupling can make the transition between the ^{1}MLCT and ^{3}MLCT, and the transition from the ^{3}MLCT to the ground state strongly allowed, resulting in efficient emission.

Ligand-to-metal charge transfer (LMCT) states

Ligand-to-metal states occur on promotion of an electron from a ligand π orbital to metal d orbitals. These states generally arise from early transition metals in high oxidation states or d^{10} metal centres and rarely occur for Ir^{III} complexes.[7]

JABLONSKI DIAGRAM

Another factor to consider is the spin of the excited states; most organic molecules exist as a

ground state singlet (S = 0, all electrons are paired); upon excitation of one electron four possible states are produced, shown in Figure 1.4. The transition that proceeds with no spin flip results in an excited singlet state S_n, and the three transitions where spin flip occurs are described as the triplet state T_n. The triplet states are lower in energy than their corresponding singlet states, due to the exchange interaction. As a result of quantum mechanics, electrons with the same spin are less likely to be found near each other than those with opposite spins, therefore triplet states experience less electron-electron repulsion, hence the lower energy. The splitting between the excited S and T states (ΔE_{ST}) depends on the exchange integral:

$$K = const. \left\langle \pi(r_1)\pi^*(r_2) \left| \frac{1}{r_{12}} \right| \pi(r_2)\pi^*(r_1) \right\rangle \qquad \text{(Equation 1.1)}$$

where π/π* = HOMO/LUMO wavefunctions, r_1, r_2 = electron coordinates and r_{12}= the separation of the two electrons.

Increasing π-conjugation results in a decrease in ΔE_{ST}, as does having distinctly localised HOMO and LUMOs. This can be prominent in transition metal complexes as the inclusion of the metal centre results in increased spatial extension of the wavefunctions and therefore a small gap between singlet and triplet states, which increases the inter-system crossing rate and probability.

The relative energy levels of these possible transitions can be shown on a Jablonski diagram (Figure 1.5). On absorption of light an electron is promoted to a higher energy orbital, creating an excited electronic and vibrational state, typically a singlet state due to the selection rules. From here the molecule can relax to a lower vibrational level through vibrational relaxation, or to a lower energy electronic state through internal conversion. This occurs due to vibrational overlap between the two states and can act as a mechanism to quench emission; however it is not normally a favoured transition to the ground state. Both of these processes are non-radiative. From here a molecule can emit light from its singlet state in a radiative transition to the singlet

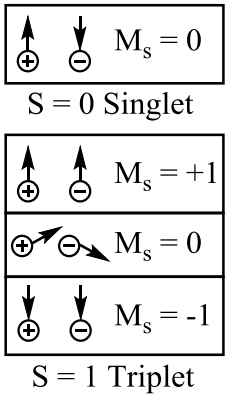

Figure 1.4: Possible excited states generated on excitation of a molecule.

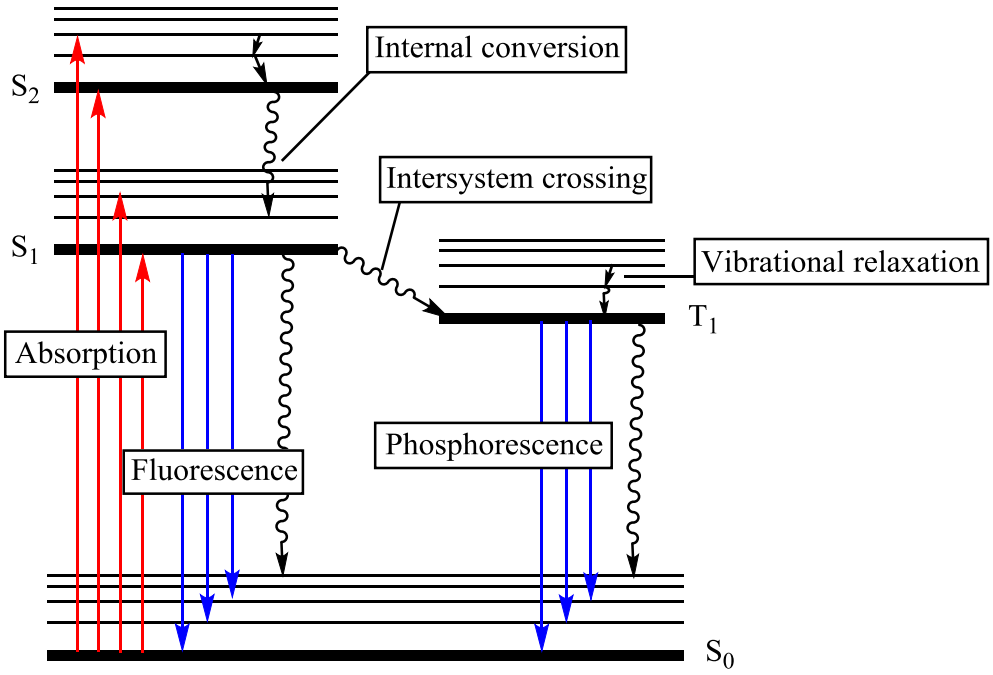

Figure 1.5: Jablonski diagram showing the types of transitions available to a molecule on photoexcitation.

ground state, i.e. fluorescence, which is allowed by the spin selection rules. Another pathway a molecule can take is intersystem crossing, the term given to a non-radiative transition between two states of differing spin multiplicity. This transition is normally slow for organic molecules, as it is forbidden by spin selection rules; however due to spin-orbit coupling it can become more favourable for transition metal complexes. For $Ru(bpy)_3^{2+}$ and $Ir(ppy)_3$, two examples shown later, the efficiency of intersystem crossing can be assumed to be unity.[46] The molecule can also emit from the triplet state to the ground state, a radiative transition referred to as phosphorescence. As with other transitions that involve a change in spin multiplicity it is formally forbidden by selection rules, meaning for organic molecules ISC to the triplet state can provide a quenching route at room temperature, as it is difficult to return to S_1 unless the gap is small. The resulting triplet states have long lifetimes and so are prone to radiationless deactivation such as collisions or quenching with molecular oxygen. Efficient spin-orbit coupling, as can be seen in transition metal complexes, can make phosphorescence a strongly allowed transition resulting in efficient emission and decreasing the lifetime.[13,44]

SPIN-ORBIT COUPLING

Spin-orbit coupling is the coupling of an electron's spin to its orbital motion, and its magnitude (E_{SO}) is given by a matrix element, shown below for zero-order:

$$E_{SO} = \langle \psi_1 | H_{SO} | \psi_2 \rangle \approx \langle \psi_1 | \zeta_{SO} \mu_S \mu_L | \psi_2 \rangle \qquad \text{(Equation 1.2)}$$

where H_{SO} is the spin-orbit coupling operator, ψ_1, ψ_2 initial and final orbitals involved, ζ_{SO} is the spin-orbit coupling

constant, μ_S, μ_L are the magnetic moments due to the spin and orbital angular momentum, respectively.[47]

The spin-orbit coupling constant ζ_{SO} is related to the nuclear charge (Z) an electron experiences during its orbit; for atoms it is proportional to Z^4, for molecules this is a local effect, hence spin-orbit coupling is most effective when the electron is located near the heavy atom.[48] These dependencies explain why transition metal complexes can display efficient spin-orbit coupling, and why complexes with localised ^{3}LC states as the lowest energy states have long lifetimes and lower quantum yields than complexes with a lowest energy ^{3}MLCT state, or complexes with mixing between the LC and MLCT states. Spin-orbit coupling transitions are only possible between states of the same symmetry representation, and there are other restrictions on the SOC routes related to the orbitals involved in the transitions, as well as whether the integral is one- or two-centre. Detailed descriptions of the requirements are available.[13,49]

PHOTOPHYSICAL PARAMETERS

The efficiency of emission from a molecule can be quantified as the photoluminescence quantum yield (PLQY), Φ, defined as the number of photons emitted over the number of photons absorbed. It can also be described in terms of radiative and non-radiative decay rates (k_r and k_{nr})

$$\Phi = \frac{k_r}{k_r + k_{nr}} \qquad \text{(Equation 1.3)}$$

For molecules that emit via phosphorescence, the triplet state T_1 is not normally populated by absorption of light, so we have to consider the rate of intersystem crossing from S_1 to T_1 relative to other processes that deactivate the singlet excited state, which gives the equation shown below:

$$\Phi = \frac{k_{ISC}}{k_f + k_{IC} + k_{ISC}} \times \frac{k_p}{k_p + k_{nr}} \qquad \text{(Equation 1.4)}$$

where k_{ISC} is the rate of intersystem crossing, k_{IC} is the rate of internal conversion, k_f is the rate of fluorescence, and k_p is the rate of phosphorescence, respectively.

However for most complexes considered here the first term can be ignored, as the rate of intersystem crossing is far greater than that of any other pathway.

It is possible to deduce the value of k_r and k_{nr} from experimentally measureable parameters, as Φ can be measured, along with the lifetime τ_{obs}, which can be determined from the rate of decay of luminescence intensity. Typically the decay is first order:

$$I(t) = I(0)e^{-k_{obs}t} \qquad \text{(Equation 1.5)}$$

and τ_{obs} is defined as:

$$\tau_{obs} = \frac{1}{k_{obs}} = \frac{1}{k_r + k_{nr}} \quad \text{(Equation 1.6)}$$

From here, we can see that:

$$\Phi = k_r \times \tau_{obs} \quad \text{(Equation 1.7)}$$

It is clear from these equations that in order to have efficient luminescence from a molecule it is important not only to maximise k_r, but to minimise k_{nr}. k_r is proportional to the transition dipole moment squared, meaning that factors that influence this such as symmetry, the spin selection rule, spin-orbit coupling, nuclear overlap and ΔE_{ST} also influence k_r.[48] Non-radiative decay is often a result of transfer of electronic energy into vibrational energy; hence k_{nr} can be increased by factors such as a large distortion between the ground and excited states or the presence of higher lying states that can be thermally activated and result in bond rupture.

EMISSIVE METAL COMPLEXES

$Ru(bpy)_3^{2+}$

One of the most widely studied luminescent metal complexes is ruthenium(II) tris(bipyridine), $Ru(bpy)_3^{2+}$, shown in Figure 1.6. First synthesised in 1936 by F.H. Burstall as a comparison with the well-known iron analogues,[50] its emissive properties were not reported until 1959, by Paris and Brandt.[51] The emission of $Ru(bpy)_3^{2+}$ was initially assigned to an excited singlet MLCT state; it was later concluded to be from a triplet MLCT state due to its long luminescence lifetime.[52] The absorption and emission spectra shown in Figure 1.6 show a strong absorption band (ε ~ 10,000 M) at ~450 nm, which is responsible for the red colour of the complex. The high extinction coefficient indicates that this is not a Laporte forbidden d-d* transition, but the singlet MLCT

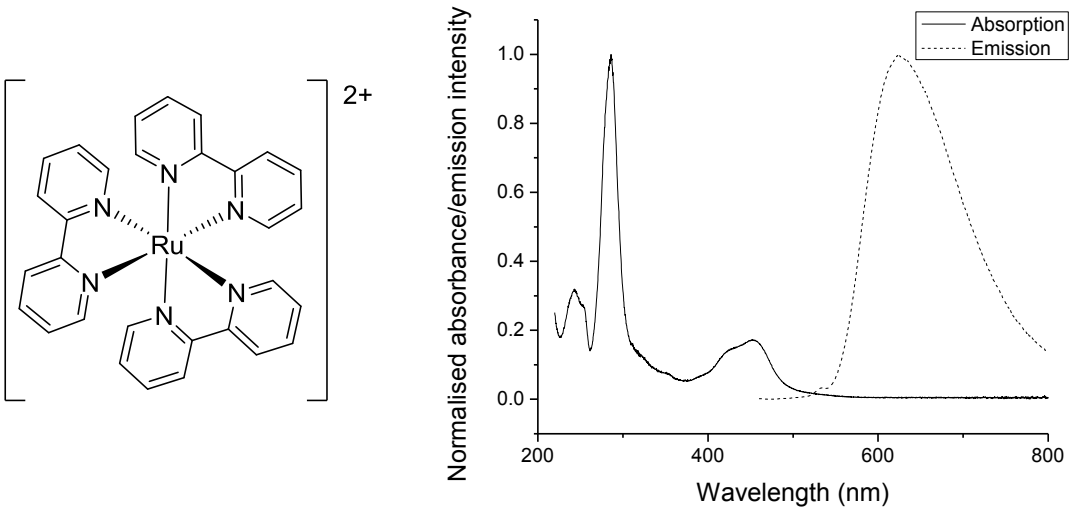

Figure 1.6: LEFT: Structure of $Ru(bpy)_3^{2+}$. RIGHT: Absorption and emission of $Ru(bpy)_3Cl_2$ in water. λ_{ex} = 450 nm.[53]

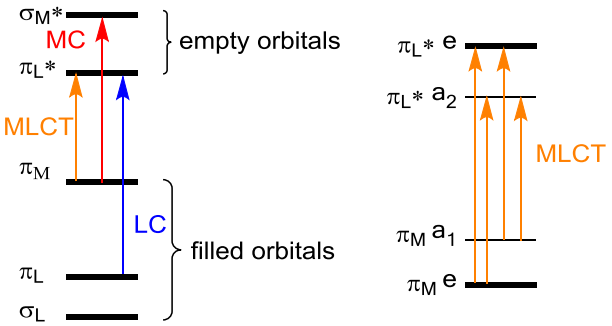

Figure 1.7: LEFT: Simplified molecular orbital diagram for Ru(L^L)$_3^{2+}$ complexes with octahedral geometry. RIGHT: Detailed depiction of the MLCT transition in D_3 symmetry.

(^{1}MLCT) band. The triplet MLCT (^{3}MLCT) band can be seen at longer wavelengths, although is far less intense due to the forbidden nature of the transition. LC bands are also seen at shorter wavelengths, and the molecular orbital diagram showing these transitions is shown in Figure 1.7. The emission spectrum is shown in Figure 1.6; the emission at RT in aqueous solution is relatively broad and featureless, with a λ_{max} of 625 nm. Juris and Balzani published a detailed review of Ru(bpy)$_3^{2+}$ and its properties in 1988.[46] Ru(bpy)$_3^{2+}$ has been widely studied not only due to its photoluminescence properties but also its photostability, and the reversibility and stability of its oxidation states. These properties have led to it and its related complexes being investigated for solar cells, luminescent photosensitisers, photocatalysts and prompted the investigation into transition metal complexes for various photoluminescence applications.

fac-Ir(ppy)$_3$

fac-Ir(ppy)$_3$ (hereafter referred to as Ir(ppy)$_3$) is an efficient green emitting complex, shown in

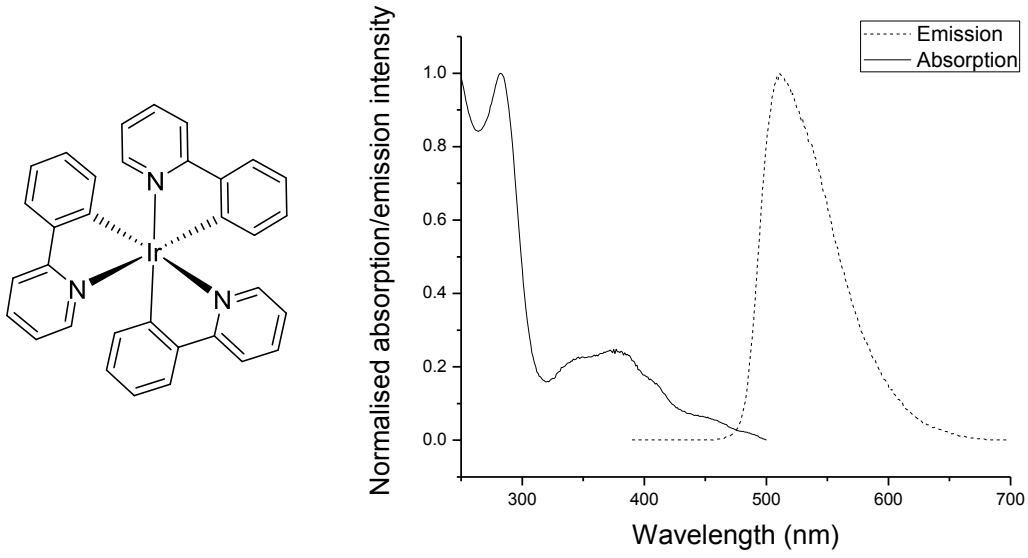

Figure 1.8: LEFT: Structure of *fac*-Ir(ppy)$_3$. RIGHT: Absorption and emission of Ir(ppy)$_3$ in DCM. λ_{ex} = 380 nm.

Figure 1.8. Initially synthesised in 1985 it was identified as an effective photoreducing agent,[54] prompting investigation into the photophysical properties of it and other triply *ortho*-metallatedIr complexes.[55] Its absorption and emission spectra are shown in Figure 1.8. Similar to the absorption spectra of $Ru(bpy)_3$ distinct regions can be seen in the absorption spectra for $Ir(ppy)_3$. Below 300 nm the intense absorption bands can be assigned to the ligand centred π-π* transitions, which are strongly allowed by selection rules. At lower energies (300-400 nm) the ^{1}MLCT transitions can been seen, followed by the formally forbidden ^{3}MLCT transitions between 430-450 nm. The emission at room temperature is broad and unstructured, as expected from an MLCT state, with λ_{max} of 510 nm. The emission is quenched efficiently by oxygen, indicating the triplet character of the emission. $Ir(ppy)_3$ has a short radiative lifetime time of 1.5 – 2 μs in deaerated solution, due to the highly efficient spin-orbit coupling between the ^{3}MLCT and higher lying singlet states. This efficient SOC results in intersystem crossing times on the order of 100 fs, resulting in highly efficient emission.[56] A similar molecular orbital diagram to that shown for $Ru(bpy)_3^{2+}$ can be drawn, showing the possible states and transitions (Figure 1.9). As $Ir(ppy)_3$ has C_3 symmetry in the ground state the t_{2g} orbitals split into two sets, a non-degenerate orbital with *a* representation and a degenerate pair with *e* representation.

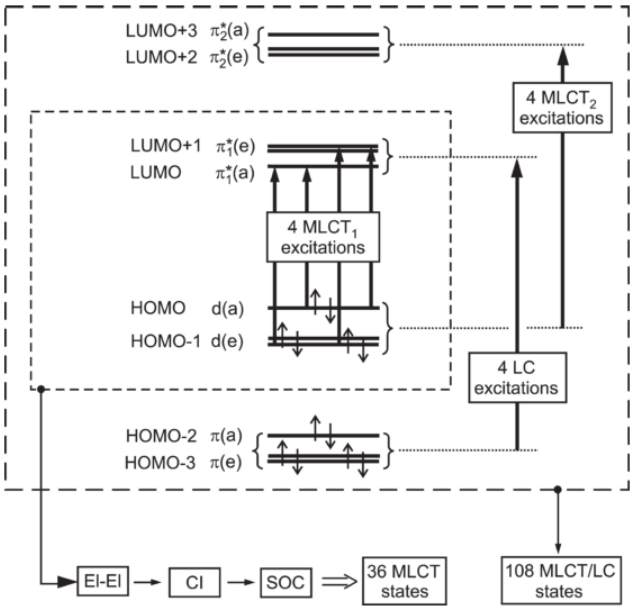

Figure 1.9: Frontier orbitals, MLCT and LC excitations for $Ir(ppy)_3$ with C_3 symmetry. The inner frame shows a simple model with four MLCT transitions. The outer frame includes additional frontier orbitals and transitions. Taken from reference [13].

Combined with symmetry-adapted unoccupied π* orbitals from the ppy ligands the simple model in the centre of Figure 1.9 is produced.[57] Once the electron-electron interactions are taken into account the total number of states resulting from these transitions is 36, 12 of which are doubly

degenerate under C_3 symmetry, although if the complex is doped into a host matrix the symmetry can be reduced and these degeneracies split.[13] This simple model does not fully describe the experimentally observed properties; to obtain a more accurate model higher energy orbitals must also be considered (Figure 1.9). This results in a large number of states of comparable energy, highlighting the complexity of the system. The triplet excited state of *fac*-Ir(ppy)$_3$ has been well studied by Yersin,[58] and details on the relative levels of the triplet substates can be found therein. Use by Forrest and Thompson in an OLED device prompted large scale investigation into Ir(ppy)$_3$ and other iridium complexes. Devices containing Ir(ppy)$_3$ have been fabricated that approach the upper limit for EQE with current device architecture.[59-61]

ANATOMY OF AN IRIDIUM COMPLEX

Phosphorescent iridium(III) complexes for OLEDs are charge neutral species and can be divided into two basic categories: homoleptic complexes contain three identical, bidentate monoanionic ligands, whereas heteroleptic complexes have non-identical ligands. Both classes contain a chromophoric ligand that is responsible for controlling the emission from the complex; these are normally cyclometalating ligands that bind to the metal through a carbanion C and a neutral N (C^N ligands) to form a 5- or 6-membered metallocycle, although C^C and N^N monoanionic ligands are also known.

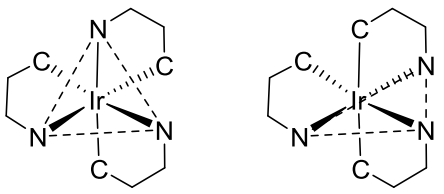

fac-Ir(C^N)$_3$ *mer*-Ir(C^N)$_3$

Figure 1.10: Structural isomers of a homoleptic Ir complex with C^N ligands. Dotted lines illustrate the different geometries.

Homoleptic complexes can exist as two isomers, meridional (*mer*) and facial (*fac*), shown in Figure 1.10. The *mer* isomer is the kinetic product; however it can normally be converted to the thermodynamic *fac* isomer either by photochemical or thermal means.[44,62] As a result of the different symmetry of the *mer* isomer compared to the *fac* the location of the frontier orbitals differs, and consequently so do their electrochemical and photophysical properties.[62] Studies on a selection of *mer* isomers showed they exhibited broader, red-shifted emission and lower luminescence efficiencies compared to their *fac* counterparts along with lower luminescence efficiencies.[44,62] In a study on a selection of homoleptic complexes radiative (k_r) and non-radiative

(k_{nr}) decay rate constants were calculated for each isomer and although k_r showed little variation between isomers, k_{nr} was over an order of magnitude larger for the *mer* isomers, indicating effective quenching mechanisms.[62] It has been suggested that one pathway for non-radiative decay in *mer* isomers is a bond-dissociation in the excited state, resulting in conversion to the *fac* isomers.[62] $Ir(ppy)_3$, described in the previous section, is a classic example of a *fac* homoleptic complex.

As mentioned previously, heteroleptic complexes contain non-identical ligands; typically either one or two chromophoric ligands and then the rest of the coordination sphere filled with ancillary ligands. Ancillary ligands are generally not involved in the excited state that produces the emission,[23,63,64] but can influence its properties and modify emission colour indirectly by varying the electron density around the metal centre.[23] Strong σ-donor or π-acceptor ancillary ligands can raise the energy of the deactivating d-d* states that quench emission, thereby increasing the luminescence efficiency of the complex. Additional functionality, such as charge carrier transport properties and enhanced solubility can also be introduced onto ancillary ligands.[10,63,65] Care must be taken when choosing ancillary ligands, however, as if the triplet energy of the ancillary ligand is lower than that of the chromophoric ligand efficient inter-ligand energy transfer (ILET) can lead to significant red-shifts in emission colour.[66,67] An example of a typical heteroleptic iridium complex is FIrpic (Figure 1.11), the archetypal blue emitter, which will be discussed in more detail in Chapter 2.

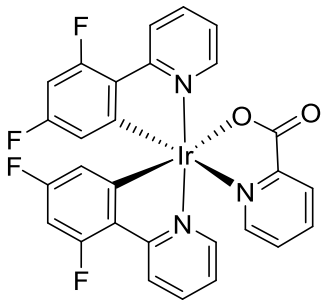

FIrpic

Figure 1.11: Heteroleptic complex FIrpic.

In this thesis a variety of iridium complexes for OLED applications will be discussed; in Chapter 2 sulfone-containing derivatives of FIrpic are synthesised as blue OLED materials and their properties are discussed along with their device performance. Chapter 3 is concerned with an extension to this family; moving towards fluorine-free blue emitters in an attempt to increase complex stability. Their properties and device performance is discussed in comparison to the difluoro complexes presented in Chapter 2. In Chapter 4 the synthesis and photophysical

properties of a selection of dual-emitting complexes is discussed. Investigation into alternative ancillary ligands is conducted in Chapter 5, both for blue emission and efficient emission. In Chapter 6 hexadentate ligands are synthesised with the aim of creating ligands to stabilise carbene complexes, a class of complexes that exhibit deep blue emission but with limited stability.

References

1) A. Bernanose, *Br. J. Appl. Phys.,* 1955, S54-S56
2) C. W. Tang and S. A. Vanslyke, *Appl. Phys. Lett.,* 1987, **51**, 913-915
3) S. J. Yeh, M. F. Wu, C. T. Chen, Y. H. Song, Y. Chi, M. H. Ho, S. F. Hsu and C. H. Chen, *Adv. Mater.,* 2005, **17**, 285-289
4) H. Fu, Y.-M. Cheng, P.-T. Chou and Y. Chi, *Mater. Today,* 2011, **14**, 472-479
5) C. Fan, Y. Li, C. Yang, H. Wu, J. Qin and Y. Cao, *Chem. Mater.,* 2012, **24**, 4581-4587
6) V. N. Kozhevnikov, K. Dahms and M. R. Bryce, *J. Org. Chem.,* 2011, **76**, 5143-8
7) P. T. Chou and Y. Chi, *Chem. Eur. J.,* 2007, **13**, 380-95
8) E. Holder, B. M. W. Langeveld and U. S. Schubert, *Adv. Mater.,* 2005, **17**, 1109-1121
9) S. Y. Takizawa, J. Nishida, T. Tsuzuki, S. Tokito and Y. Yamashita, *Inorg. Chem.,* 2007, **46**, 4308-19
10) L. Xiao, Z. Chen, B. Qu, J. Luo, S. Kong, Q. Gong and J. Kido, *Adv. Mater.,* 2011, **23**, 926-52
11) W.-C. Chen, C.-S. Lee and Q.-X. Tong, *J. Mater. Chem. C,* 2015, **3**, 10957-10963
12) R. J. Holmes, S. R. Forrest, Y. J. Tung, R. C. Kwong, J. J. Brown, S. Garon and M. E. Thompson, *Appl. Phys. Lett.,* 2003, **82**, 2422
13) H. Yersin, *Highly Efficient OLEDs with Phosphorescent Materials,* Wiley-VCH, Darmstadt, 2008
14) H. Sasabe, J. Takamatsu, T. Motoyama, S. Watanabe, G. Wagenblast, N. Langer, O. Molt, E. Fuchs, C. Lennartz and J. Kido, *Adv. Mater.,* 2010, **22**, 5003-7
15) S. Tokito, T. Iijima, Y. Suzuri, H. Kita, T. Tsuzuki and F. Sato, *Appl. Phys. Lett.,* 2003, **83**, 569
16) S. Ye, Y. Liu, C.-a. Di, H. Xi, W. Wu, Y. Wen, K. Lu, C. Du, Y. Liu and G. Yu, *Chem. Mater.,* 2009, **21**, 1333-1342
17) R. J. Holmes, B. W. D'Andrade, S. R. Forrest, X. Ren, J. Li and M. E. Thompson, *Appl. Phys. Lett.,* 2003, **83**, 3818
18) DuPont, http://www2.dupont.com/OLED/en_US/assets/downloads/pdf/DuPont_OLED_Technology.pdf
19) *Nat. Photonics,* 2009, **3**, 441-441
20) C. H. Yang, S. W. Li, Y. Chi, Y. M. Cheng, Y. S. Yeh, P. T. Chou, G. H. Lee, C. H. Wang and C. F. Shu, *Inorg. Chem.,* 2005, **44**, 7770-80
21) T. Sajoto, P. I. Djurovich, A. B. Tamayo, J. Oxgaard, W. A. Goddard, 3rd and M. E. Thompson, *J. Am. Chem. Soc.,* 2009, **131**, 9813-22
22) Z. Q. Chen, Z. Q. Bian and C. H. Huang, *Adv. Mater.,* 2010, **22**, 1534-9
23) H. Wu, T. Yang, Q. Zhao, J. Zhou, C. Li and F. Li, *Dalton Trans.,* 2011, **40**, 1969-76
24) K. K.-W. Lo, C.-K. Chung, T. K.-M. Lee, L.-H. Lui, K. H.-K. Tsang and N. Zhu, *Inorg. Chem.,* 2003, **42**, 6886-6897
25) K. K.-W. Lo, C.-K. Chung and N. Zhu, *Chem. Eur. J.,* 2003, **9**, 475-483
26) R. Gao, D. G. Ho, B. Hernandez, M. Selke, D. Murphy, P. I. Djurovich and M. E. Thompson, *J. Am. Chem. Soc.,* 2002, **124**, 14828-14829
27) M. E. Köse, R. J. Crutchley, M. C. DeRosa, N. Ananthakrishnan, J. R. Reynolds and K. S. Schanze, *Langmuir,* 2005, **21**, 8255-8262
28) Y. You and S. Y. Park, *Adv. Mater.,* 2008, **20**, 3820-3826
29) M. Marín-Suárez, B. F. E. Curchod, I. Tavernelli, U. Rothlisberger, R. Scopelliti, I. Jung, D. Di Censo, M. Grätzel, J. F. Fernández-Sánchez, A. Fernández-Gutiérrez, M. K. Nazeeruddin and E. Baranoff, *Chem. Mater.,* 2012, **24**, 2330-2338
30) C. Ulbricht, B. Beyer, C. Friebe, A. Winter and U. S. Schubert, *Adv. Mater.,* 2009, **21**, 4418-4441
31) J. Brandel, M. Sairenji, K. Ichikawa and T. Nabeshima, *Chem. Commun.,* 2010, **46**, 3958-60
32) P.-H. Lanoë, J.-L. Fillaut, V. Guerchais, H. Le Bozec and J. A. G. Williams, *Eur. J. Inorg. Chem.,* 2011, **2011**, 1255-1259
33) F. Gao, Y. Wang, J. Zhang, D. Shi, M. Wang, R. Humphry-Baker, P. Wang, S. M. Zakeeruddin and M. Gratzel, *Chem. Commun.,* 2008, 2635-7

34) K. S. Chen, W. H. Liu, Y. H. Wang, C. H. Lai, P. T. Chou, G. H. Lee, K. Chen, H. Y. Chen, Y. Chi and F. C. Tung, *Adv. Funct. Mater.,* 2007, **17**, 2964-2974
35) E. Marchi, R. Sinisi, G. Bergamini, M. Tragni, M. Monari, M. Bandini and P. Ceroni, *Chem. Eur. J.,* 2012, **18**, 8765-73
36) F. Gartner, S. Denurra, S. Losse, A. Neubauer, A. Boddien, A. Gopinathan, A. Spannenberg, H. Junge, S. Lochbrunner, M. Blug, S. Hoch, J. Busse, S. Gladiali and M. Beller, *Chem. Eur. J.,* 2012, **18**, 3220-5
37) L. B. Josefsen and R. W. Boyle, *Metal-Based Drugs,* 2008, **2008**,
38) D. A. Nagib, M. E. Scott and D. W. MacMillan, *J. Am. Chem. Soc.,* 2009, **131**, 10875-7
39) Y. Ma, H. Zhang, J. Shen and C. Che, *Synth. Met.,* 1998, **94**, 245-248
40) M. A. Baldo, D. F. O'Brien, Y. You, A. Shoustikov, S. Sibley, M. E. Thompson and S. R. Forrest, *Nature,* 1998, **395**, 151-154
41) M. A. Baldo, S. Lamansky, P. E. Burrows, M. E. Thompson and S. R. Forrest, *Appl. Phys. Lett.,* 1999, **75**, 4-6
42) G. Zhang, F.-I. Wu, X. Jiang, P. Sun and C.-H. Cheng, *Synth. Met.,* 2010, **160**, 1906-1911
43) G. Zhang, H.-H. Chou, X. Jiang, P. Sun, C.-H. Cheng, Y. Ooyama and Y. Harima, *Org. Electron.,* 2010, **11**, 632-640
44) Y. You and S. Y. Park, *Dalton Trans.,* 2009, 1267-1282
45) J. Li, P. I. Djurovich, B. D. Alleyne, M. Yousufuddin, N. N. Ho, J. C. Thomas, J. C. Peters, R. Bau and M. E. Thompson, *Inorg. Chem.,* 2005, **44**, 1713-27
46) A. Juris, V. Balzani, F. Barigelletti, S. Campagna, P. Belser and A. von Zelewsky, *Coord. Chem. Rev.,* 1988, **84**, 85-277
47) N. J. Turro, V. Ramamurthy and J. C. Scaiano, *Principles of Molecular Photochemistry: An Introduction,* University Science Books, 2009
48) S. Haneder, E. Da Como, J. Feldmann, J. M. Lupton, C. Lennartz, P. Erk, E. Fuchs, O. Molt, I. Münster, C. Schildknecht and G. Wagenblast, *Adv. Mater.,* 2008, **20**, 3325-3330
49) S. Obara, M. Itabashi, F. Okuda, S. Tamaki, Y. Tanabe, Y. Ishii, K. Nozaki and M.-a. Haga, *Inorg. Chem.,* 2006, **45**, 8907-8921
50) F. H. Burstall, *J. Chem. Soc.,* 1936, 173-175
51) J. P. Paris and W. W. Brandt, *J. Am. Chem. Soc.,* 1959, **81**, 5001-5002
52) G. A. Crosby, W. G. Perkins and D. M. Klassen, *J. Chem. Phys.,* 1965, **43**, 1498-1503
53) http://omlc.org/spectra/PhotochemCAD/html/085.html
54) K. A. King, P. J. Spellane and R. J. Watts, *J. Am. Chem. Soc.,* 1985, **107**, 1431-1432
55) K. Dedeian, P. I. Djurovich, F. O. Garces, G. Carlson and R. J. Watts, *Inorg. Chem.,* 1991, **30**, 1685-1687
56) G. J. Hedley, A. Ruseckas and I. D. W. Samuel, *Chem. Phys. Lett.,* 2008, **450**, 292-296
57) P. J. Hay, *J. Phys. Chem. A,* 2002, **106**, 1634-1641
58) T. Hofbeck and H. Yersin, *Inorg. Chem.,* 2010, **49**, 9290-9
59) Y. Kawamura, K. Goushi, J. Brooks, J. J. Brown, H. Sasabe and C. Adachi, *Appl. Phys. Lett.,* 2005, **86**, 071104
60) M. S. Park and J. Y. Lee, *Chem. Mater.,* 2011, **23**, 4338-4343
61) H. Sasabe, T. Chiba, S.-J. Su, Y.-J. Pu, K.-i. Nakayama and J. Kido, *Chem. Comm.,* 2008, 5821-5823
62) A. B. Tamayo, B. D. Alleyne, P. I. Djurovich, S. Lamansky, I. Tsyba, N. N. Ho, R. Bau and M. E. Thompson, *J. Am. Chem. Soc.,* 2003, **125**, 7377-87
63) S. Lamansky, P. Djurovich, D. Murphy, F. Abdel-Razzaq, R. Kwong, I. Tsyba, M. Bortz, B. Mui, R. Bau and M. E. Thompson, *Inorg. Chem.,* 2001, **40**, 1704-1711
64) N. Tian, A. Thiessen, R. Schiewek, O. J. Schmitz, D. Hertel, K. Meerholz and E. Holder, *J. Org. Chem.,* 2009, **74**, 2718-25
65) H. Tang, Y. Li, B. Chen, H. Wu, W. Yang and Y. Cao, *Opt. Mater.,* 2011, **33**, 1291-1296
66) Y. You and S. Y. Park, *J. Am. Chem. Soc.,* 2005, **127**, 12438-9

67) X. Gu, T. Fei, H. Zhang, H. Xu, B. Yang, Y. Ma and X. Liu, *Eur. J. Inorg. Chem.,* 2009, **2009**, 2407-2414

Chapter 2: Complexes of ligands containing difluoro and sulfone substituents as blue OLED materials

FIrpic (**1**), shown in Figure 2.1, is the archetypal sky blue emitter. With pale-blue emission exhibiting CIE coordinates of (0.16, 0.29) it is among the most widely investigated bis-cyclometalated iridium complexes; this can be attributed to its facile synthesis and desirable photophysical and electrochemical properties. First reported in 2001, its emission is considerably bluer than that of $Ir(ppy)_3$ due to the presence of the electron withdrawing fluorine substituents on the phenyl ring and the picolinate ancillary.[1,2] Initial devices were reported with EQEs of 5% but recently FIrpic-containing devices have reached 30% EQE, the maximum with current device architectures.[3] As one of the first blue phosphorescent emissive materials for OLEDs, FIrpic is often used as the benchmark for blue phosphors and many derivatives have been synthesised. An extensive review of FIrpic and its properties has been published.[4] Although FIrpic has excelled in many ways there are still some problems, including poor emission colour for RGB display, poor solubility in organic solvents and degradation of the material under thermal evaporation and during device operation.[2,5] The stability of FIrpic and its derivatives will be discussed in Chapter 3; in this chapter strategies for blue-shifting the emission of iridium complexes will be discussed along with examples, followed by the synthesis, results and discussion of a new series of FIrpic analogues.

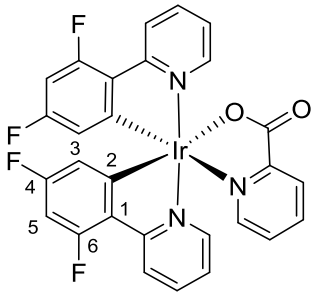

1

Figure 2.1: FIrpic. The positions of the phenyl ring are numbered as they are referred to in this work.

The HOMO/LUMO orbital diagrams for $Ir(ppy)_3$ are shown in Figure 2.2. The HOMO is mostly localised on the iridium d-orbitals and the phenyl ring of the ppy ligand, with negligible contribution on the pyridyl ring, while the LUMO is mostly localised on the pyridine ring, with a small contribution on the 4,6-positions on the phenyl ring.[6,7] This is typical for cyclometalated iridium complexes based on ppy ligands, and as a result of the distinct HOMO/LUMO distributions

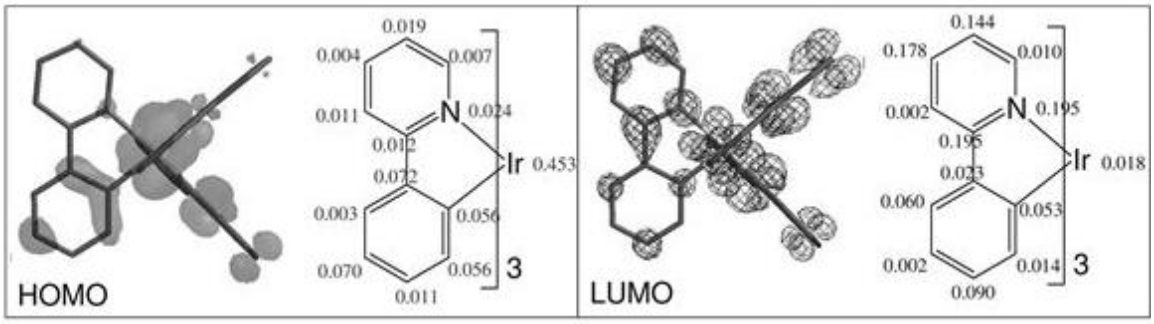

Figure 2.2: MO diagrams of HOMO/LUMO distribution of $Ir(ppy)_3$. Reproduced from reference [8].

their energies can be tuned relatively independently, allowing for colour tuning by varying the structure of the ligands. Some strategies to tune the emission colour of an iridium complex towards the blue region include:[9]

1) Lowering the HOMO with respect to the LUMO by introducing electron-withdrawing groups to positions on the phenyl ring with HOMO localisation
2) Raising the LUMO by either adding electron donating groups to the pyridine ring or replacing the pyridine ring with another heterocycle with higher LUMO energy
3) Using electron withdrawing ancillary ligands to modulate the electron density about the metal centre, thereby affecting the HOMO energy
4) Using strong σ-donor ligands to increase the crystal field splitting, therefore widening the HOMO-LUMO gap and shifting non-emissive d-d* MC states to higher energies.

These strategies can be used in conjunction with each other, and the effects are additive. The work in this chapter primarily considers the first strategy.

Due to the success of FIrpic a large number of complexes have been synthesised based on the dfppy ligand framework. As can be seen from the HOMO/LUMO localisation of FIrpic (Figure 2.3) there is a large density of the HOMO at the 5- position of the difluorophenyl ring, but little

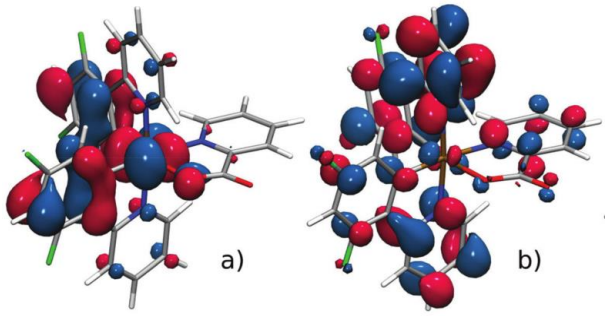

Figure 2.3: FIrpic Kohn–Sham highest occupied (a) and lowest unoccupied (b) orbitals (DFT/M06). Reproduced from reference [4].

contribution from the LUMO. As a result a common strategy to blue-shift the emission relative to FIrpic is to introduce electron withdrawing groups at the 5-position. One example is the homoleptic complex FCNIr (Figure 2.4) which displays deep blue emission, with a λ_{max} of 448 nm and a vibrational side peak at 476 nm.[10] The introduction of the CN substituent results in a blue-shift of 20 nm compared to *fac*-Ir(4,6-dfppy)$_3$ due to the lowering of the HOMO with respect to the LUMO, giving the complex a band gap of 2.8 eV. Devices incorporating FCNIr as the emitter achieved CIE coordinates of (0.15, 0.19) at 5% dopant concentration with an EQE of 4.9% at 300 cd/m^2, significantly bluer than FIrpic devices.[10] This dfppy ligand has also been modified to impart additional solubility to FIrpic-based complexes; replacing one of the fluorines with an alkoxy group results in a slightly bluer emission than FIrpic, as well as an increase in solubility.[2]

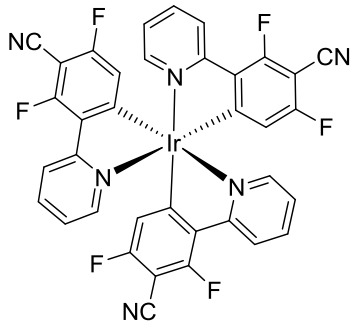

FCNIr λ_{max} = 448, 476 nm

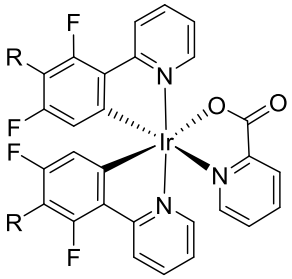

SOFIrpic R = SO_2Tol
λ_{max} = 460, 489 nm
POFIrpic R = $PO(Ph)_2$
λ_{max} = 459, 486 nm

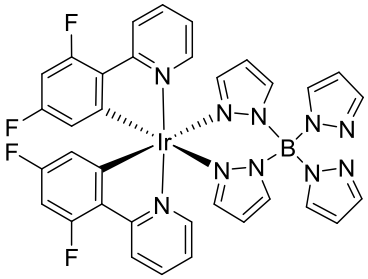

FIr6 λ_{max} = 461, 489 nm

Figure 2.4: Structures of a selection of substituted iridium complexes.

Cao *et al.* synthesised two FIrpic analogues with the SO_2Tol and $PO(Ph)_2$ groups at the 5-position to blue-shift emission (Figure 2.4).[11] Cyclic voltammetry estimations of the HOMO/LUMO levels showed a decrease in the HOMO relative to FIrpic, while the LUMO levels remained fairly similar, resulting in emission peaks of 460 nm and 489 nm for POFIrpic, and 459 and 486 nm for SOFIrpic in DCM solution.[11] This represented a blue-shift relative to FIrpic and the devices fabricated showed comparable performance to the established material FIr6 (Figure 2.4).[11]

The highly electron withdrawing CF_3 group has also been introduced between the two F atoms and some complexes are shown in Figure 2.5.[12] The FIrpic analogue showed a blue-shift in emission of 11 nm as a result of the addition of the CF_3 group, and the HOMO is significantly lowered, based on a 0.24 eV increase in the oxidation potential.[12] Exchange of the picolinate ancillary ligand for a 3-trifluoromethyl-5-(2-pyridyl)-1,2,4-triazolate system (from **2**/**3** to **4**/**5**) prompted further blue-shift; however the EQEs of devices based on these complexes are low.[12]

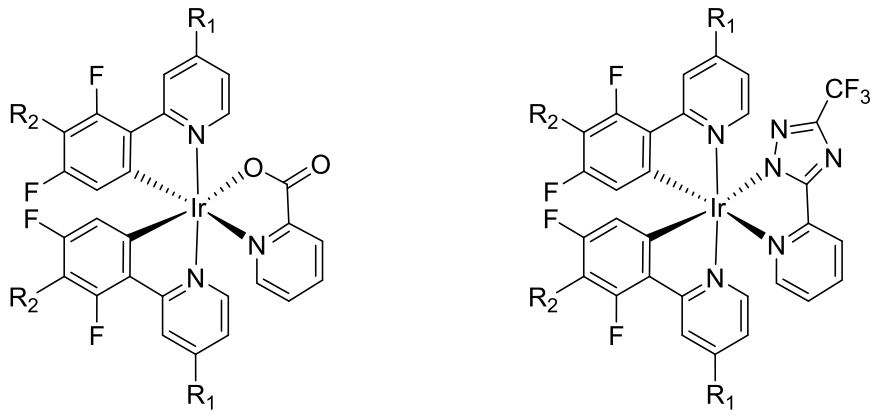

2 R_1 = H, R_2 = CF_3 λ_{max} = 457, 485 nm
3 R_1 = CH_3, R_2 = CF_3 λ_{max} = 454, 481 nm
4 R_1 = H, R_2 = CF_3 λ_{max} = 451, 480 nm
5 R_1 = CH_3, R_2 = CF_3 λ_{max} = 447, 476 nm

Figure 2.5: FIrpic analogues containing CF_3 groups.

Materials involving ester substituents at the 5-position of dfppy have also been synthesised and used as sensors for molecular oxygen (**6a**/**b**, Figure 2.6: left).[13] Blue emitting sensors are highly desirable as they would increase sensor performance in media where there are natural red emitters. The ester group was selected as it could allow grafting of the dye to substrates and the trifluoromethyl ester was predicted to increase solubility and shift further into the blue region, as it has stronger acceptor character.[13] However, while use of the CO_2CF_3 group does result in a blue-shift in emission relative to FIrpic, it should be noted that presence of the CO_2CF_3 group results in the LUMO being mostly localised there.[13] This highlights the need to be aware that introducing different groups within the structure can significantly affect locations of the HOMO/LUMO, which could result in different emission from what may be expected.[13] Related complexes with a perfluorinated alkyl ketone (-$COCF_3$ and –COC_3F_7) were also synthesised by another group (Figure

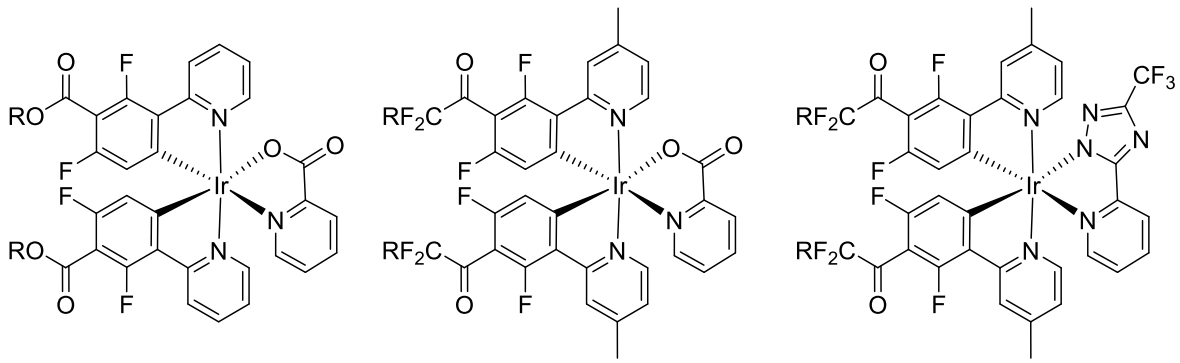

6a R = CH_3 λ_{max} = 463 nm
6b R = CF_3 λ_{max} = 459 nm

7a R = F
λ_{max} = 453, 476 nm
7b R = CF_2CF_3
λ_{max} = 454, 479 nm

8a R = F
λ_{max} = 447, 474 nm
8b R = CF_2CF_3
λ_{max} = 447, 476 nm

Figure 2.6: Structures from a selection of substituted iridium complexes.

2.6: centre, right).[14] These complexes displayed bluer emission than FIrpic, with DFT calculations and optical measurements indicating band gaps of 2.9 eV and triplet energies of 2.77 eV for the pic complexes (**7a**/**b**).[14] The emission was pushed further to the blue by exchange of the picolinate ancillary ligand (**7a**/**b**) for a more electron withdrawing trifluoromethylated triazole ligand (**8a**/**b**).[14] Devices fabricated with **7a** and **8a** showed EQEs of 17.1 and 8.4% and CIE coordinates of (0.141, 0.158) and (0.147, 0.116), respectively, which are among some of the highest reported for deep blue phosphorescent OLEDs.[14] Again, it must be noted that the introduction of these highly electron withdrawing perfluorinated carbonyl substituents shifts the LUMO density onto the phenyl ring of the cyclometalating ligand, an atypical arrangement for iridium complexes based on ppy ligands.

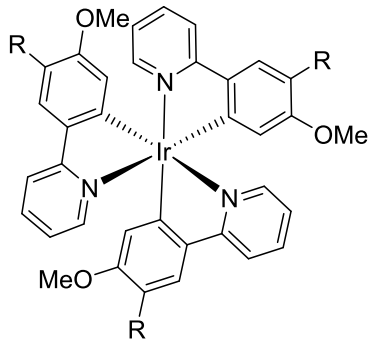

R = H, λ_{max} = 495 nm
R = CHO, λ_{max} = 463, 488 nm
R = CN, λ_{max} = 464, 492 nm
R = SCN, λ_{max} = 486 nm
R = SO_2Me, λ_{max} = 465, 492 nm
R = SO_2Tol, λ_{max} = 465, 492 nm
R = SO_2PhCl, λ_{max} = 463, 491 nm
R = SH, λ_{max} = 511 nm
R = SMe, λ_{max} = 520 nm
R = I, λ_{max} = 491 nm

Figure 2.7: A series of homoleptic complexes with substituents at the 5-position.

For another series of homoleptic complexes a variety of substituents were introduced at the 5-position (Figure 2.7) and the trends in emission colour are as expected, with the EWGs (CHO, CN, SCN, SO_2Ar) resulting in a blue-shift and the thiol/thioether acting as EDGs and red-shifting emission.[15] The SCN group blue-shifts the emission only slightly, whereas the other EWGs do so by approximately 30 nm, resulting in blue emission without using fluorine substituents.[15] These complexes were particularly interesting as the synthesis was conducted 'on complex', allowing the use of groups that could be sensitive to the high reaction temperatures required to synthesise homoleptic complexes.[15]

A different approach to deeper blue emission is to replace the phenyl ring with a more electron deficient group, such as pyridine, as it has been reported that pyridine has a lower HOMO/LUMO than other nitrogen containing heterocycles.[16] For example, the homoleptic bipyridyl complex **9** (Figure 2.8) exhibits bright blue emission when irradiated with UV light. Comparison with the absorption spectra of FIrpic shows a blue-shift in the LC and ^{1}MLCT/^{3}MLCT transitions.[16] The intensities of the MLCT transtions also increase, indicating an increase in spin orbit coupling on

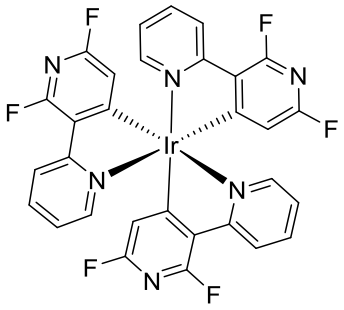

9 λ_{max} = 438, 463 nm

Figure 2.8

switching to a bipyridyl system.[16] Molecular orbital calculations show a lowering of both the HOMO and LUMO relative to $Ir(ppy)_3$, however the HOMO is lowered to a greater extent, resulting in pure blue, more efficient (PLQY = 0.71) emission with CIE coordinates of (0.14, 0.12).[16]

It must be noted, however, that there are some disadvantages to lowering the HOMO; for example, if the level drops too low hole injection from the anode is inhibited.[16] Consequently, simply lowering the HOMO is not the best strategy for producing efficient blue emitting devices, other strategies must be employed in conjunction.

While fluorine is considered a withdrawing group, it is a special case, being both strongly electronegative, and therefore a good inductive withdrawer, and also a weak mesomeric π-donor. The position of the fluorine(s) on the phenyl ring of the iridium complex has a large impact on the emission colour; a study on heteroleptic pic complexes revealed that having the fluorines at the 4- and 6-positions results in the bluest emission, even bluer than having three fluorines distributed at the 3-,4- and 5- positions.[17] Another study conducted on homoleptic complexes with ligands containing 3 and 4 fluorines at the 3,4,6- and 3,4,5,6- positions noted that the F_3ppy complexes demonstrated bluer emission than the F_4ppy complexes, by approximately 10 nm.[18] This was in line with the cyclic voltammetric data, which suggested that the LUMO was lowered on addition

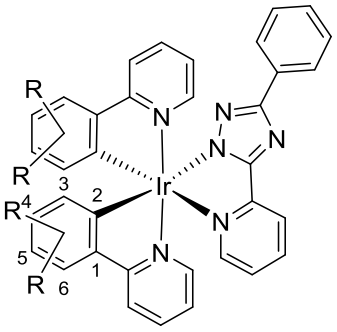

10a R = 4,6 F, λ_{max} = 461, 491 nm
10b R = 3,5 F, λ_{max} = 484, 518 nm
10c R = 4,6 CF_3, λ_{max} = 511, 544 nm
10d R = 3,5 CF_3, λ_{max} = 466, 499 nm
10e R = H, λ_{max} = 489, 517 nm

Figure 2.9

of the fourth fluorine.[18] A theoretical study on the frontier orbitals of some methoxy-substituted heteroleptic complexes noted that a large HOMO density is located at the 5-position of the ppy-based ligand, and suggested that the weak π-donor ability of fluorine was raising the HOMO.[19] Another paper from the DeCola group compared the purely inductive withdrawing CF_3 group to the mesomeric donor but inductively withdrawing F group in a series of heteroleptic complexes (Figure 2.9).[20] Introduction of the fluorine substituents at the 4,6-positions (**10a**) of the phenyl ring results in a blue-shift in the emission compared to the unsubstitued complex **10e**, whereas placing them at the 3,5-positions results in little change in colour (**10b**).[20] On the other hand, introducing the CF_3 group at the 4,6-positions (**10c**) results in a red-shift in emission relative to the parent complex and a blue-shift when they are introduced at the 3,5-positions (**10d**). This behaviour is rationalised by the donor/acceptor character of F versus the purely inductive withdrawing character of CF_3.[20]

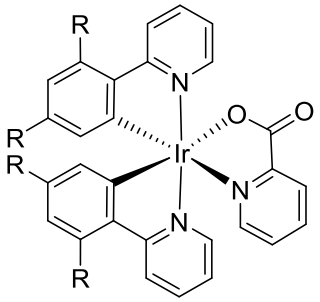

HIrpic R = H, λ_{max} = 505 nm
FIrpic R = F, λ_{max} = 468, 495 nm
ClIrpic R = Cl, λ_{max} = 491, 517 nm
BrIrpic R = Br, λ_{max} = 494, 519 nm

Figure 2.10

The effect of fluorine is even unique among the halogens. In 2012 Baranoff *et. al.* published a comparison of FIrpic to its analogues HIrpic, ClIrpic and BrIrpic (Figure 2.10); here FIrpic resulted in a blue-shift in emission relative to HIrpic, whereas the blue-shift for ClIrpic and BrIrpic was relatively small.[21] The oxidation potentials for all the halogenated complexes were similar, ~0.35 V greater than that of HIrpic, indicating the stabilisation of the HOMO due to the halogens being electron acceptors. However, LUMO energies of ClIrpic and BrIrpic, estimated from the electrochemical HOMO level and optical gap, were much lower than that of FIrpic, resulting in the red-shift.[21] This was correlated with the different values for the Hammett parameters (σ_m and σ_p) for F versus Cl and Br; Cl and Br exert a stronger electron accepting effect than F in the para position, resulting in a lowering of the LUMO as it is localised on the pyridyl ring which is *ortho*/*para* to the halogens.[21]

As noted by De Cola *et. al.* changing the position of substituents can have a large effect on emission colour and properties; a substituent may provide a blue-shift at one position and a red-shift at others.[20] In particular, the introduction of strongly withdrawing groups at the 4-position

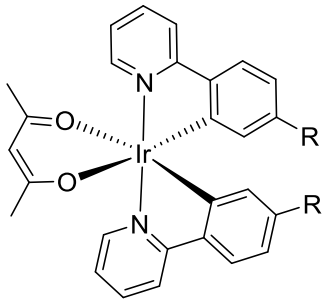

R = SO_2Ph, λ_{max} = 550 nm
R = SPh, λ_{max} = 527 nm
R = OPh, λ_{max} = 505 nm
R = NPh_2, λ_{max} = 533 nm
R = $POPh_2$, λ_{max} = 541 nm
R = $GePh_3$, λ_{max} = 530 nm
R = $SiPh_3$, λ_{max} = 535 nm
R = $B(mes)_2$, λ_{max} = 605 nm

Figure 2.11

seems to result in a red-shift in emission. In one study introducing electron withdrawing groups such as -SO_2Ar, -$PO(Ph)_2$ and -$B(Mes)_2$ at the 4-position of $Ir(ppy)_2acac$ derivatives results in a red-shift in the emission relative to $Ir(ppy)_2(acac)$ (Figure 2.11).[22] For Ir-PO this is due to the strong EW effect of P=O lowering the LUMO; however, for Ir-$B(mes)_2$ and Ir-SO_2Ar there is a significant change in the LUMO location, with less than 50% localised on the pyridyl ring.[22] Both complexes experience an increase in contribution from the phenyl ring with the mesityl group and boron atom also participating in Ir-B and some contribution from the pendant phenyl rings for Ir-SO_2Ar.[22] This highlights the crudeness of the design rule 'introducing electon withdrawing substituents onto the phenyl ring will blue-shift the emission', as it is important to take into account the position of the new substituent and how it impacts the positions *ortho*-, *meta*- and *para*- to it. A paper relating the Hammett parameters (σ_m and σ_p) to the emission colour accounts for these parameters and allows for more effective prediction of molecular properties and design.[23]

RESULTS AND DISCUSSION

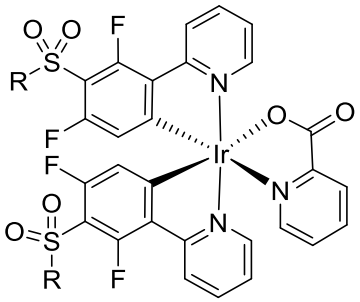

Figure 2.12: General target for a bluer FIrpic analogue.

With the aim of obtaining bluer emission than FIrpic the following general target was designed (Figure 2.12); the sulfone moiety was introduced at the 5-position due to its electron withdrawing power, both inductively and through resonance. It can be seen from the molecular orbital diagram of FIrpic (Figure 2.3) that there is a localisation of the HOMO at this position, but no LUMO localisation, which is a strong indication that introducing an EWG at this position should

result in a selective lowering of the HOMO relative to the LUMO, and therefore a blue-shift in the emission colour. Additionally, the sulfone group was chosen as the R group could be exploited to enhance solubility and potentially add steric shielding to the aromatic fluorines, which have been identified as a source of instability in FIrpic.[24] Enhanced solubility would allow fabrication of devices via solution processing, a much milder technique than the alternative, vacuum deposition, which is routinely used for FIrpic.[4] Vacuum deposition requires high temperatures, and a large proportion of the doping material is lost; it has been shown to result in the defluorination of FIrpic.[24] Some examples of sulfone functionalised C^N ligands in the literature include neutral complexes,[11,15,22,25,26] charged complexes for LEECs,[27-29] an example of a sulfone containing N^N ligand,[30] and even an example of an anionic iridium complex with a disulfinate ligand.[31]

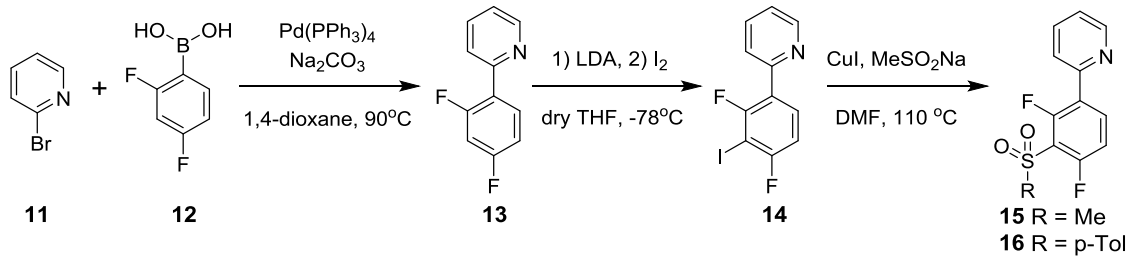

Figure 2.13: Synthesis of target ligands.

Initial choices of R group were R = p-Tol (synthesised in my MSci project[32] and subsequently published by Cao),[11] and R = Me, due to the commercial availability of the required sodium sulfinate salts. The synthetic route to target ligands **15** and **16** is shown in Figure 2.13. The first step involves a Suzuki cross coupling of commercially available 2-bromopyridine (**11**) and 2,4-difluorophenylboronic acid (**12**) using $Pd(PPh_3)_4$ and Na_2CO_3 as the catalyst and base, respectively, to give dfppy (**13**) in 84-96% yield. The next step involves an *ortho*-lithiation using LDA at -78 °C, followed by iodination at low temperature to give dfppy-I (**14**) in 56% yield, a step that is known.[12] The final step in the ligand synthesis is the copper-assisted nucleophilic displacement reaction to form **15** and **16**, based on reaction conditions to produce diarylsulfones investigated by Suzuki and Abe.[33] This step was reproducibly low yielding in both cases, 15% and 26% for **15** and **16** respectively, prompting investigation into improving the synthesis.

Unreacted and deiodinated starting materials (**14** and **13**, respectively) account for ca. 50% of the missing product, suggesting the sulfinate is not acting as a good nucleophile. In the original paper,[33] it is noted that aryl halides with electron donating groups, and a hindered example (C_6Me_5I) react in moderate to good yields, suggesting it is not the steric influence of the *ortho*-fluorine substituents impeding the reaction.[33] Suzuki and Abe noticed improvement in yields of

the diarylsulfones when the CuI/R-sulfinate sodium salt system was replaced with copper(II) bis(arenesulfinate), resulting in yield increases of up to 40% for previously difficult to obtain sulfones. The required material was synthesised from copper(II) sulfate and sodium methanesulfinic acid in water, and the reaction was repeated. The reaction was left for 24 h, then 72 h, but showed no improvement, with isolated yields of 17% and 13%, respectively. Alternative protocols were attempted; the first, a CuI catalysed coupling reaction using ionic liquids as additives,[34] however, the product was not obtained. A mixture of sulfone containing products was isolated, although none of them could be matched to the pure ligand **15** by NMR characterisation and the yield of the mixture was <4%. The second route, a CuI/L- proline catalysed system, was conducted in a sealed tube.[35] Again, this yielded none of the desired product. Other possible conditions were considered, such as a palladium catalysed reaction using $Pd_2(dba)_3$, Xantphos, Cs_2CO_3 as the base and $^nBu_4NCl$ as a salt additive. However, these could not be used as they do not tolerate *ortho*- substituents.[36] As sufficient quantities of the required products **15** and **16** could be obtained via the route in Figure 2.13 further variations were not explored.

Heteroleptic pic complexes **19** and **20**, analogues of FIrpic, were synthesised under modified Lamansky conditions from the intermediate μ-dichloro-bridged dimers (Figure 2.14).[9] Water was omitted from the reaction conditions in order to protect the sensitive aromatic fluorines from nucleophilic aromatic substitution (S_NAr) reactions. Dimer **18** was isolated and characterised previously.[32] However, attempts to rigorously dry dimer **17** for NMR characterisation failed, as it decomposed under ambient conditions over the period of a week. The decomposition products were tentatively identified as mononuclear iridium complexes by NMR, although they were not fully characterised. Henceforth, all syntheses of the heteroleptic pic- complexes proceeded via a one-pot method, unless specified otherwise, to avoid possible decomposition of the intermediate dimer.

Complexes **19** and **20** were synthesised from their respective dimers via the standard method,

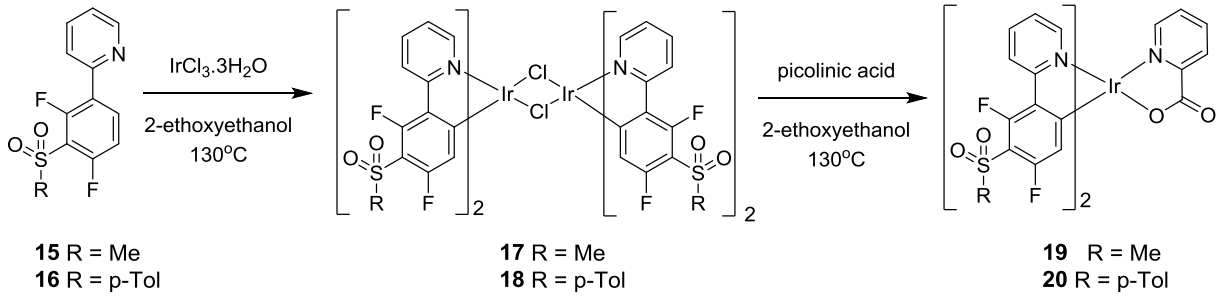

Figure 2.14: Synthesis of initial complexes.

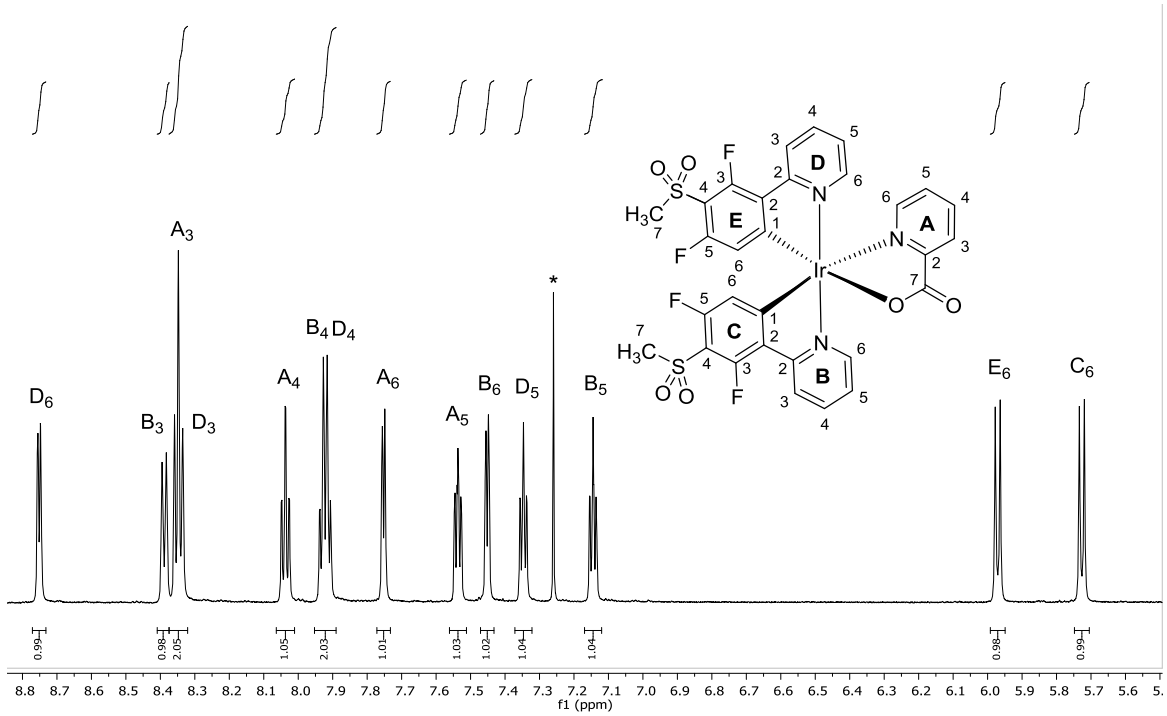

Figure 2.15: ^{1}H NMR spectrum of complex 19.

suspended in 2-ethoxyethanol with a large excess of picolinic acid and heated to reflux overnight. The complexes were obtained in good yield, 85% and 74%, respectively. It was noted that the p-Tol complex **20** was more soluble than **19** in common organic solvents.

The NMR spectra were typical for complexes of this type, and the ^{1}H and ^{13}C spectra of **9** have been fully assigned with the aid of 2D experiments (Figure 2.15, ^{13}C assignments presented in Chapter 7). Using information from the NOESY experiment the stereochemistry about the metal centre could be determined, revealing the *trans*- nitrogen containing structure shown (Figure 2.14). This is the expected product from reactions from the μ-dichloro bridged dimer, and was

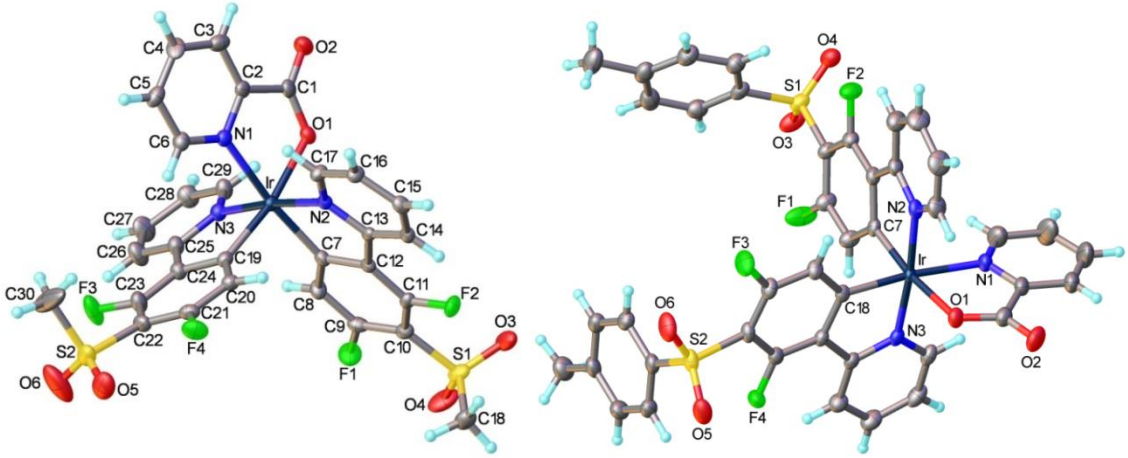

Figure 2.16: LEFT: X-ray molecular structure of 19. RIGHT: X-ray molecular structure of 20.3CH_2Cl_2. Thermal ellipsoids are drawn at the 50% probability level. Solvent omitted for clarity.

confirmed by the X-ray crystal structure.

The X-ray molecular structures of **19** and **20** are shown in Figure 2.16. In both complexes the expected *trans* arrangement of the nitrogens of the C^N ligands is observed, with a distorted octahedral coordination about the iridium centre. In both complexes the ppy ligand framework is almost planar, with small twists of 1.3, 4.0° and 3.0° for complexes **19** and **20,** respectively. Selected bond distances are shown in Table 2.1. The bond lengths are similar to those reported for FIrpic,[21] with the exception of the Ir-C bonds, which are shorter. The electrochemical and photophysical properties of these complexes will be discussed later.

	19	**20**	**FIrpic** [a]
Ir-N(pic)	2.137(3)	2.134(3)	2.135(3)
Ir-N(ppy-1)	2.046(3)	2.029(3)	2.056(3)
Ir-N(ppy-2)	2.028(3)	2.048(3)	2.049(3)
Ir-O(pic)	2.146(2)	2.158(2)	2.158(2)
Ir-C(ppy-1)	1.991(4)	1.989(3)	2.010(3)
Ir-C(ppy-2)	1.974(3)	1.985(3)	2.002(3)

[a]Bond lengths taken from [21]. Ppy-1 and 2 are defined as the ligands with carbon atoms opposite the pic N/O, respectively.

Table 2.1: Selected bond distances.

Previous work conducted in our group suggested introduction of a mesityl group at the 4-position of the pyridyl ring of dfppy can result in a large increase in the EQE of devices compared to that of the parent complex FIrpic, due to the steric shielding it provides.[37] This helps to reduce the concentration quenching effect in devices, allowing for higher complex loadings and therefore brighter devices.

With this in mind it was desirable to combine mesityl and sulfone substituents to create a bluer emitter that is highly efficient under device operation. The initial target was **16**, derived from **9**, as **9** was determined to have slightly bluer emission than **10**. In addition, the mesityl group was predicted to enhance solubility, making the complexes more suitable for solution processing.

The synthetic route is shown in Figure 2.17, and is analogous to that described for **15** and **16**. The mesityl-dfppy was constructed as previously described;[37] an initial Suzuki coupling between 2-chloro-4-iodopyridine (**21**) and 2,4,6-trimethylphenylboronic acid (**22**) to produce **23**. The reaction occurs selectively at the 4-position, as the C-I bond is significantly more reactive than the C-Cl bond. The base and catalyst used here were K_3PO_4 and $Pd_2(dba)_3/PCy_3$ in 1,4-dioxane. The long

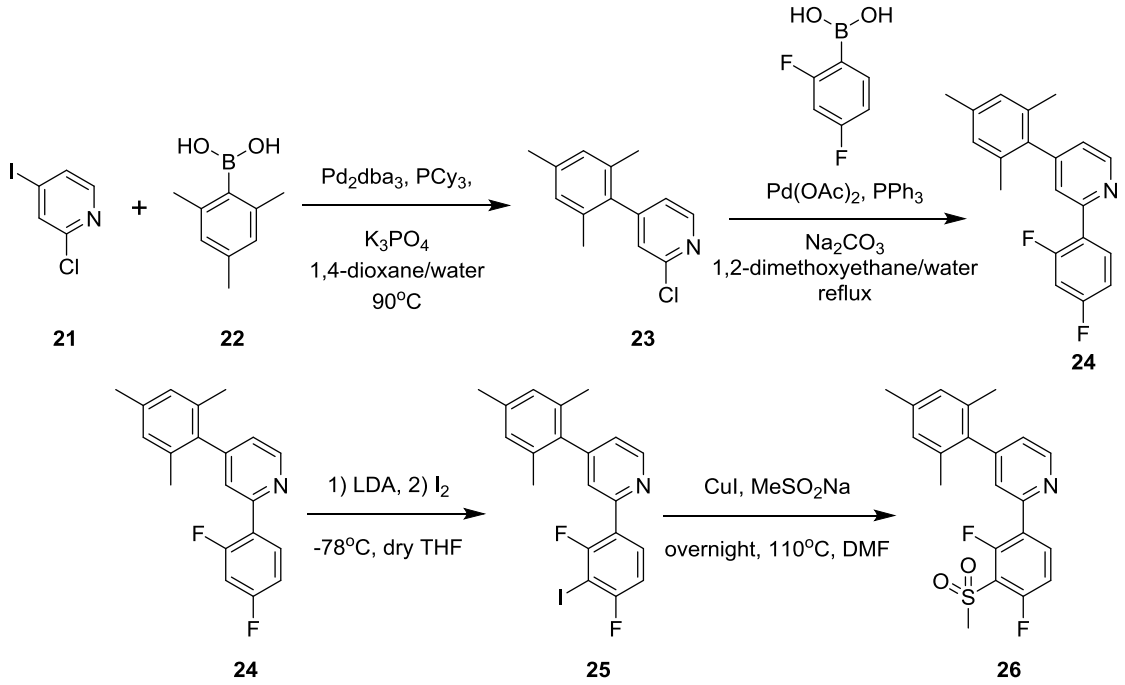

Figure 2.17: Synthesis of mesityl-containing target ligand 26.

reaction time (3 days) is required due to the steric bulk of the boronic acid. The second step involved another Suzuki reaction, with 2,4-difluorophenylboronic acid (**12**) at the C-Cl bond of **23**. The reaction was conducted in 1,2-dimethoxyethane, Na_2CO_3 was used as the base and the catalyst was formed *in situ* from $Pd(OAc)_2$ and PPh_3. The reaction was heated to reflux overnight to give the product **24** in 85-96% yield.

The next step involved the *ortho*-lithiation of **24** between the two fluorines at low temperature (-78 °C) using LDA, followed by iodination with I_2. The reaction proceeds as previously described for the synthesis of **14** from **13**, however, introduction of the mesityl group into the molecule results in a dramatic change in the differences in solubility and properties of **24** and **25** compared to their parent compounds. This required them to be separated by reverse phase column chromatography on the Biotage® Isolera One ™, and the product **25** was obtained in 43% yield. The final step in the ligand synthesis was the copper-assisted nucleophilic displacement reaction to introduce the

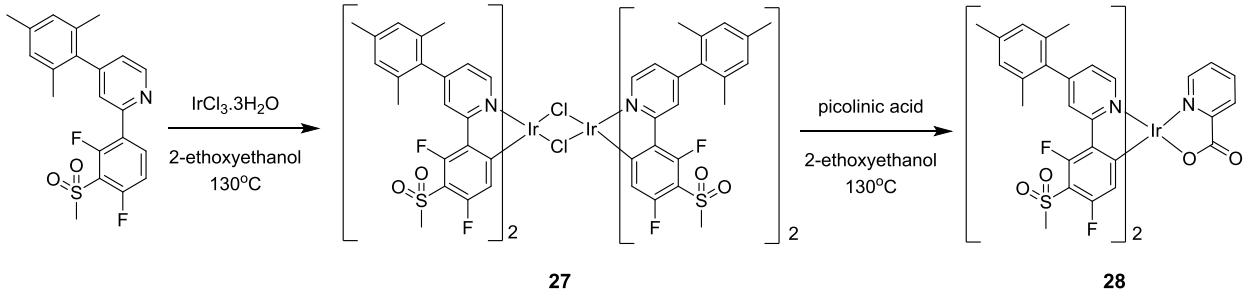

Figure 2.18: Synthesis of heteroleptic complex 28.

sulfone group under the same conditions described for **15** and **16**. After purification, **26** was isolated in 19% yield and, as in the synthesis of **15**, unreacted and deiodinated starting materials **25** and **24** were also isolated.

The heteroleptic pic complex **28** was then synthesised via the dichloro-bridged dimer **27** (Figure 2.18), as with previous iridium complexes, and was obtained in 85% yield. It was noted that the solubility of **28** in common organic solvents such as DCM and ethyl acetate was superior to that of **19**, as had been expected. In addition, **28** appeared to retain the blue emission of the parent compound by visual inspection, as was the case for the FIrpic analogue.[37] The photophysics will be discussed later in this chapter.

The X-ray molecular structure of **28** is shown in Figure 2.19. As can be seen, the C^N ligands adopt the expected *trans* nitrogen arrangement and the coordination around the Ir atom is a distorted octahedron. The structure shows disorder in the mesityl and methylsulfone groups of one ligand, it is disordered between two orientations in a 0.55:0.45 ratio, with the preferred conformer shown here. It can be seen that the methyl groups of the mesityl moiety are sufficient to break conjugation between it and the pyridyl ring, with dihedral angles of 86° for the ordered mesityl and 82° and 73° for the disordered mesityl. This suggests there should not be a large red-shift in emission colour, as the effective conjugation length has not increased.

During the synthesis of ligand **15** an interesting side product was isolated, the disulfone

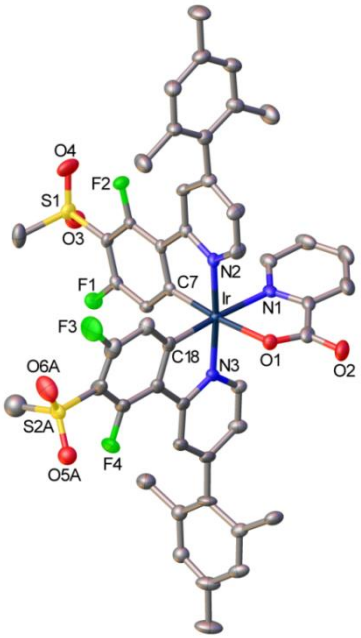

	19	20	28	FIrpic [a]
Ir-N(pic)	2.137(3)	2.134(3)	2.140(5)	2.135(3)
Ir-N(ppy-1)	2.046(3)	2.029(3)	2.033(5)	2.056(3)
Ir-N(ppy-2)	2.028(3)	2.048(3)	2.033(5)	2.049(3)
Ir-O(pic)	2.146(2)	2.158(2)	2.133(4)	2.158(2)
Ir-C(ppy-1)	1.991(4)	1.989(3)	2.000(6)	2.010(3)
Ir-C(ppy-2)	1.974(3)	1.985(3)	1.986(6)	2.002(3)

[a] Bond lengths taken from [21]. Ppy-1 and 2 are defined as the ligands with carbon atoms opposite the pic N/O, respectively.

Figure 2.19: LEFT: X-ray molecular structure of 28. Thermal ellipsoids are drawn at the 50% probability level. Solvent omitted for clarity. RIGHT: Table 2.2: Selected bond distances.

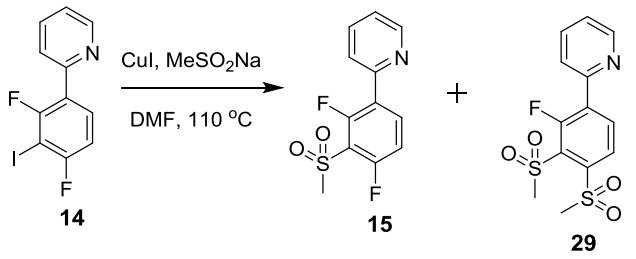

Figure 2.20: Synthesis of disulfone ligand 29.

derivative **29** (Figure 2.20), formed by a nucleophilic aromatic substitution on one of the fluorines. Upon synthesis of **15** from a specific batch of **14** it initially seemed that an increased yield of **15**, approximately 25%, had been isolated. NMR analysis revealed it to be a mixture of two compounds, which were then separated by column chromatography, and identified as **15** (15%) and **29** (5%). The same batch of **14** was also used to synthesise **16** and in this case an increase in yield to 40% from 26% was seen; however, no doubly sulfonated product was identified. This is most likely due to the steric demands of a second substitution on the phenyl ring in the p-tolyl case.

Although the ^{1}H NMR spectrum was clean, it was thought that the batch of **14** was contaminated with iodine from the reaction mixture, as it had a pink-brown tinge. This theory was tested by repeating the reaction with a batch of **14** known to be of the highest purity (as previous reactions using this batch had not produced any disulfone **29**) and adding a small amount of iodine (3 mol%). The reaction was worked up as previously to give ligand **15** in 15% yield and **29** in 2% yield, suggesting iodine may be involved in the formation of **29**. The iodine could coordinate to the nitrogen of the pyridine ring, thereby activating the phenyl ring toward nucleophilic aromatic substitution by increasing the electron withdrawing power of the pyridyl ring. It is thought that the required compound **15** forms first and then, due to its highly electron withdrawing nature, undergoes a further nucleophilic aromatic substitution to replace a F atom. It is likely that steric hindrance prevents replacement of the final fluorine.

NMR experiments were conducted to establish which of the fluorines had been replaced. Pure-shift ^{1}H NMR, a technique that suppresses the homonuclear proton coupling in order to improve the resolution and reduce the complexity of the NMR spectra,[38] was used to reveal the heteronuclear couplings between H and F, which can be obscured in normal ^{1}H spectra by more complicated splitting patterns (Figure 2.21). Inspection of the pure shift spectrum of **15** revealed that the signal at 8.29 ppm shows two splittings of 8 and 6 Hz, while the signal at 7.19 ppm shows only one major splitting of ca. 10 Hz, suggesting that the former is the proton *ortho* to the pyridyl group while the latter is *ortho* to the fluorine. Comparison with the pure-shift spectrum of **29**

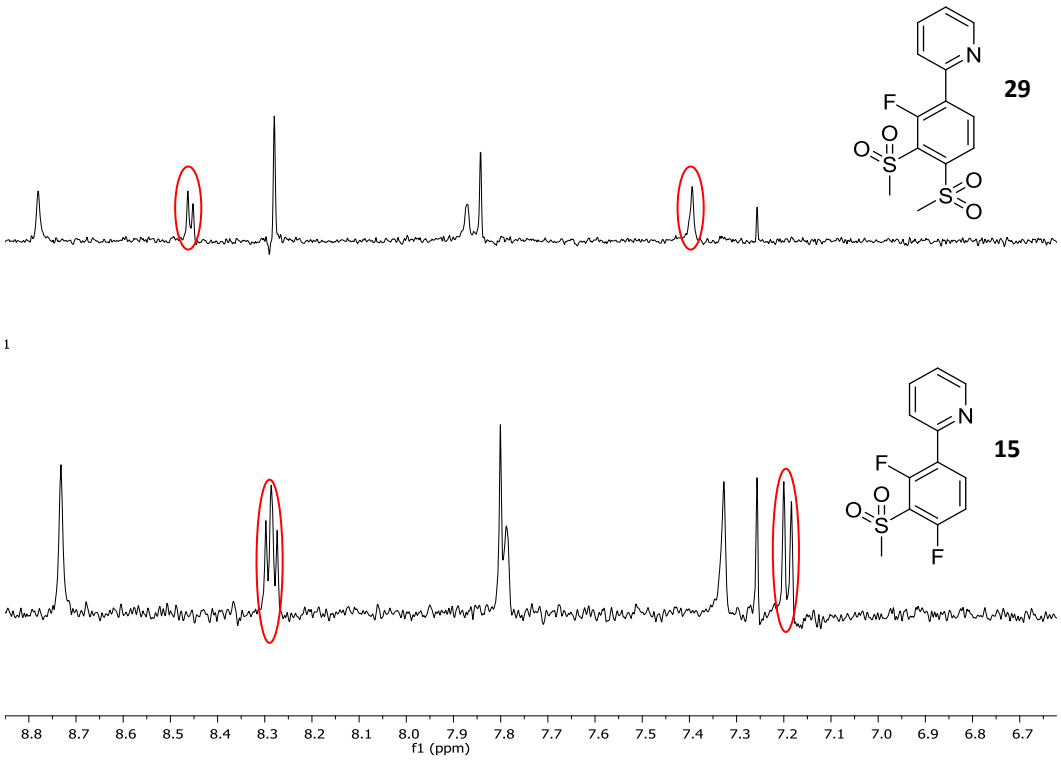

Figure 2.21: Pure shift spectra of 15 and 29. Highlighted in red are the protons on the phenyl ring.

showed only one coupling remained, with a coupling constant of 6.5 Hz at 8.46 ppm. This value suggests it is the fluorine *ortho* to the pyridyl group that is retained; this is supported by $^{1}H/^{19}F$ heteronuclear NOESY (HOESY) and COSY assignments.

In order to compare the effect of a different electron withdrawing group to fluorine at the 4-position, the heteroleptic pic- complex **30** was synthesised from ligand **29** (Figure 2.22). The synthesis was analogous to the complexes previously discussed, and **30** was isolated after column chromatography as a bright yellow solid in 84% yield. The NMR spectra of **30** confirmed the replacement of the *para*- fluorine, as the protons at the 3-position appeared as singlets, indicating they were not adjacent to a fluorine.

The X-ray molecular structure of **30** is shown in Figure 2.23. As with other iridium complexes formed from the μ-dichloro-bridged dimer, the nitrogens of the pyridyl rings are *trans* to each

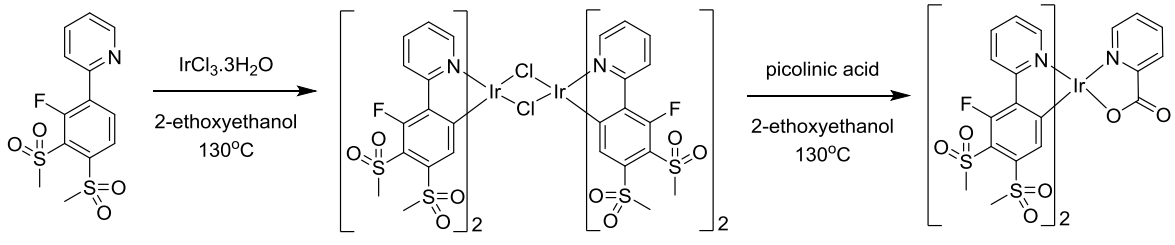

29 **30**

Figure 2.22: Synthesis of complex 30.

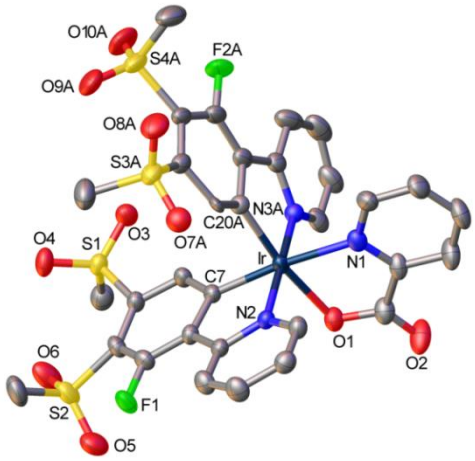

	30
Ir-N(pic)	2.128(3)
Ir-N(ppy-1)	2.040(4). 2.042(5) [a]
Ir-N(ppy-2)	2.064(8)
Ir-O(pic)	2.148(3)
Ir-C(ppy-1)	1.995(4)
Ir-C(ppy-2)	1.951(8), 1.991(5) [a]

[a] Alternative positions of the disordered C^N ligand. Ppy-1 and 2 are defined as the ligands with carbon atoms opposite the pic N/O, respectively.

Figure 2.23: LEFT: X-ray molecular structure of 30.CH_3CN. Thermal ellipsoids are drawn at the 50% probability level. RIGHT: Table 2.3: Selected bond distances.

other. The ppy ligand framework is essentially planar, with a twist angle of only 3.1° between the pyridyl and phenyl rings. Notably, one of the C^N ligands is disordered between two orientations differing by a ca. 10° libration around the Ir atom, with occupancies refined to 0.684(5) and 0.316(5), respectively. The major conformer is shown in Figure 2.23.

The synthesis of the homoleptic complexes of ligands **15** and **16** was attemped,[32] via a method previously used successfully in our group.[39] The route involves synthesis and isolation of the μ-dichloro bridged dimers **17** and **18**, which are then suspended in ethylene glycol with further ligand and heated to reflux overnight (Figure 2.24). Purification of the resulting mixture revealed complexes **31** and **32** as the major products in 29% and 23% yield, respectively. There was no sign of the homoleptic products, and the majority of the material remained at the top of the column as intractable brown solid, suggesting decomposition. The formation of **31** and **32** can be explained by reaction of the sulfone ligand via nucleophilic aromatic substitution from residual water in the solvent, followed by N^O coordination to the iridium. To confirm the instability of the ligands, **16** was exposed to similar reaction conditions, this time without the presence of the iridium dimer

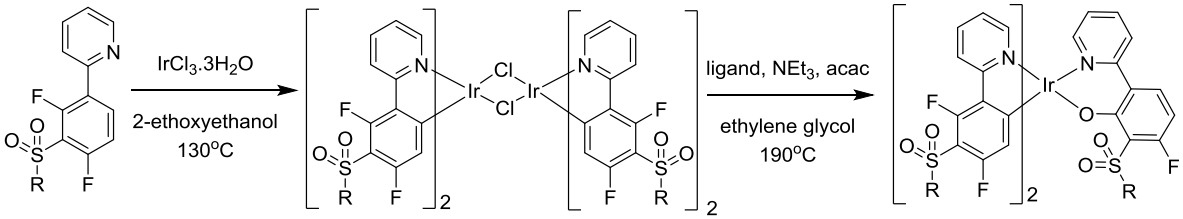

15 R = Me
16 R = p-Tol

17 R = Me
18 R = p-Tol

31 R = Me
32 R = p-Tol

Figure 2.24

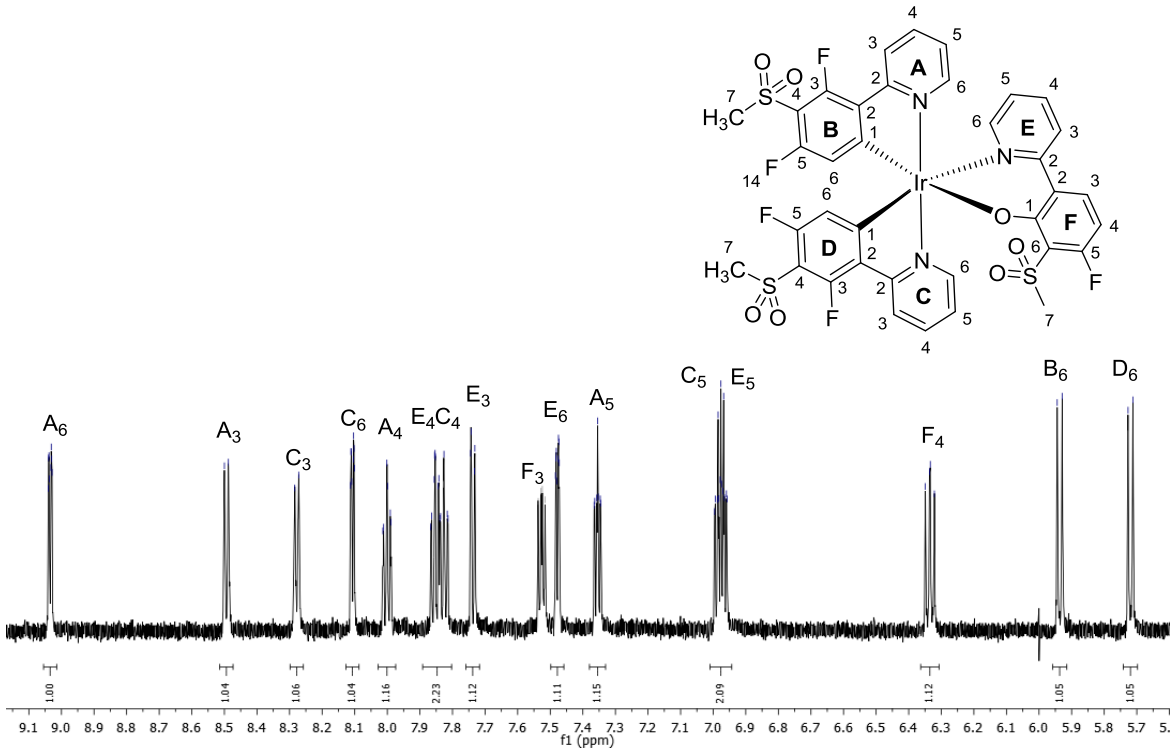

Figure 2.25: ^{1}H NMR assignment of 31.

and at a lower temperature of 160 ^{o}C. The NMR spectra of the reaction mixture was complicated, and the products were not isolated. However from the mass spectrometry data it can be suggested that the ligand undergoes nucleophilic attack by both residual water and the ethylene glycol solvent, resulting in the displacement of fluorines.

Complex **31** was characterised by its ^{1}H NMR spectrum (Figure 2.25), although its poor solubility limited the full assignment of the ^{13}C spectrum. The 2D experiments confirmed the orientation about the Ir centre. In the ^{19}F NMR spectrum five peaks can be seen indicating one fluorine has been replaced. From the COSY spectrum it is clear that the third ligand is not C^N coordinated, as two protons are visible on the phenyl ring, suggesting that the fluorine *ortho* to the pyridyl has been replaced by a group that can coordinate to the iridium centre.

The structure of **32** was unambiguously confirmed by X-ray crystallography, and the X-ray molecular structure is shown in Figure 2.26. The nitrogen atoms of the two C^N ligands are *trans* to each other, indicating direct substitution of the chlorides without isomerisation. The N^O bonded ligand experiences a significant twist between the pyridyl and phenyl rings of 37.1^{o} in order to bind and form a 6-membered chelate, as opposed to the 5-membered chelate ring formed from C^N coordination.

Bidentate ligands that form a 6-membered ring on chelation to Ir are scarce in the literature;[40] a

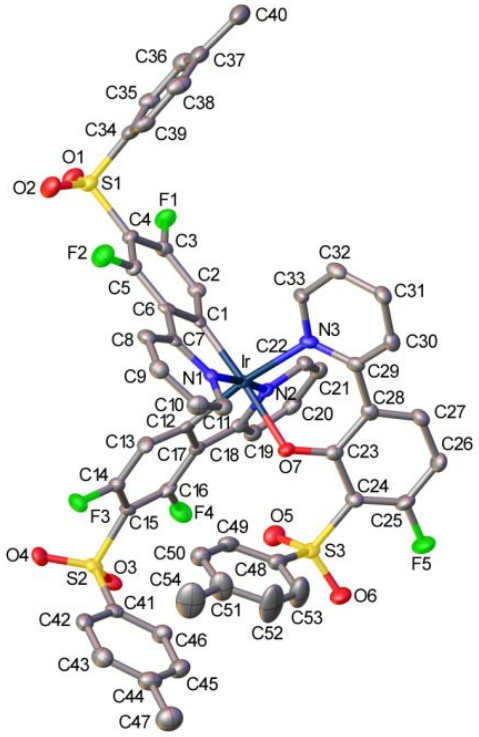

	32
Ir-N(1)	2.161(4)
Ir-N(2)	2.032(4)
Ir-N(3)	2.037(4)
Ir-O(7)	2.151(3)
Ir-C(7)	1.982(5)
Ir-C(19)	1.987(5)

Figure 2.26: LEFT: X-ray molecular structure of 32.2CH_2Cl_2. Thermal ellipsoids are drawn at the 50% probability level. Solvent omitted for clarity. RIGHT: Table 2.4: Selected bond distances.

few examples include [Ir(C^N)$_2$(N^O)] structures with two ppy C^N ligands and 2-(2'-hydroxyphenyl)oxazole,[41] or 2-(2'-hydroxyphenyl)oxazoline,[42] as the ancillary N^O ligand. To our knowledge there are no previous examples of iridium complexes with a 2-(2'-hydroxyphenyl)pyridine-based ligand in the literature.

The instability of these ligands (**15**, **16**) under high temperatures and in the presence of nucleophiles prompted investigation into alternative ligands that contain fewer fluorines to increase stability. This investigation is discussed in Chapter 3.

PHOTOPHYSICAL AND ELECTROCHEMICAL PROPERTIES

Absorption and emission

The absorption spectra for complexes **19**, **20**, **28**, **30**, **31** and **32** in DCM are shown in Figure 2.27. All complexes show strong absorption bands in the 250-300 nm region, assigned to π-π* transitions on the ligand based on the calculations of Hay,[43] and literature precedent.[1] At lower energies the complexes display sets of absorption bands with lower oscillator strengths at 350-420 nm, which are assigned to the ^{1}MLCT transitions, and at even longer wavelengths and smaller oscillator strengths the ^{3}MLCT bands can be identified. As the ^{3}MLCT state is a major component

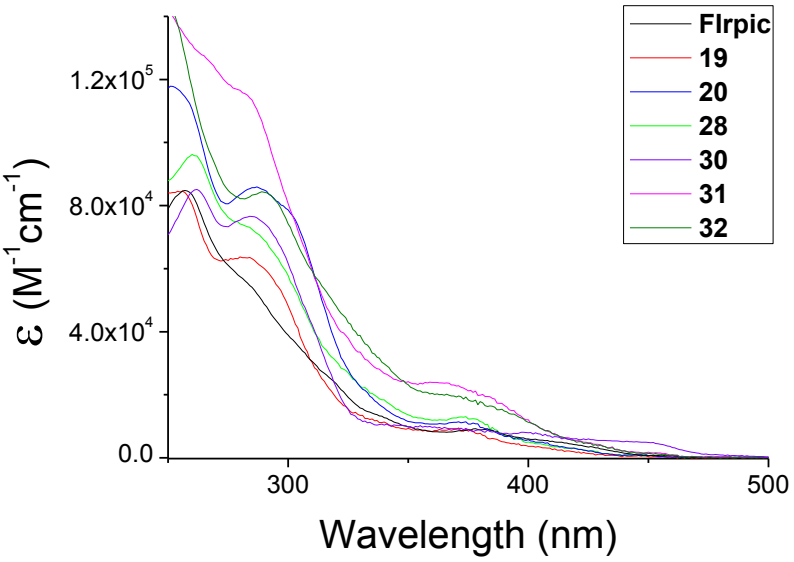

Figure 2.27: Absorption spectra of complexes 19, 20, 28, 30, 31, 32 in DCM [<10^{-5} M].

of the state responsible for the emission of these complexes the wavelength of this absorption band can correlated with the λ_{max} of the emission. For complexes **19**, **20** and **28** the bands are all at similar wavelengths, 443-445 nm, whereas for FIrpic the band is at 454 nm; this difference is reflected in the bluer emission of **19**, **20** and **28** compared to FIrpic. For complex **30** the absorption extends out to 470 nm and smaller bands are present to ~490 nm, suggesting a much lower energy ^{3}MLCT, which is reflected in the greener emission. For the N^O bonded complexes **31** and **32** the absorption spectra were similar to their pic analogues in the low energy region.

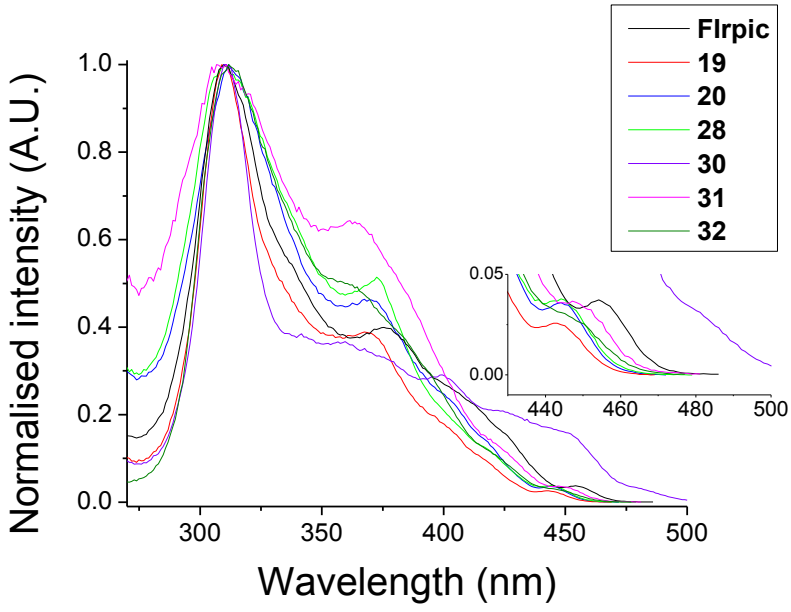

Figure 2.28: Excitation spectra of the selected complexes in DCM [<10^{-5} M]. The emission band observed was the second emission maximum.

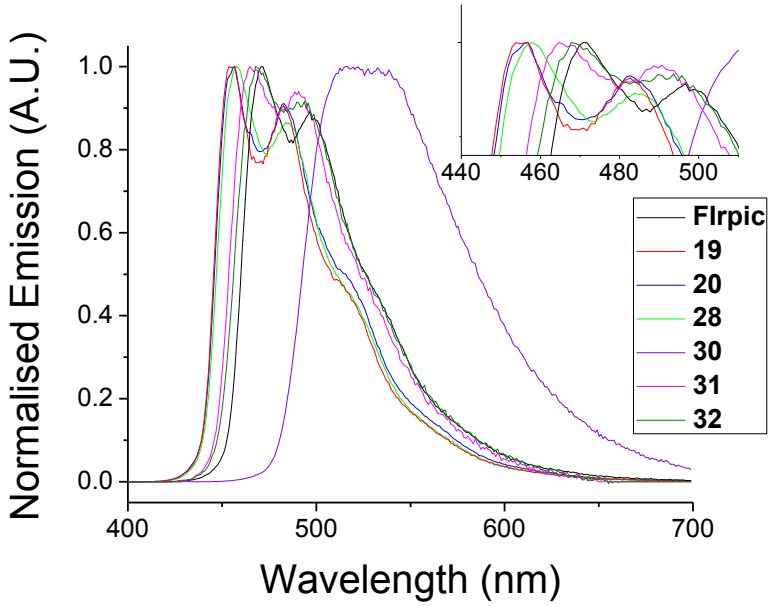

Figure 2.29: Emission spectra of selected complexes in deaerated DCM [<10^{-5} M], λ_{ex} = 380 nm.

Excitation spectra were recorded (Figure 2.28), revealing as expected that the bands from the ^{1}MLCT and ^{3}MLCT states are responsible for the emission from the complexes, while the majority of the lower energy π-π* transitions are dark.

The emission spectra of the complexes are shown in Figure 2.29. The emission of **19**, **20**, **28**, **31** and **32** display a similar profile to that of FIrpic, with an emission maximum, vibronic progression and a shoulder at longer wavelengths, indicating the emission originates from a similar excited state. The presence of defined features in the emission spectra suggests a mixed LC/MLCT nature for the excited state, as broad, featureless emission is associated with CT states, and it has been noted that the emission spectrum of FIrpic is similar to that of the protonated ligand dfppyH^{+}.[21] The emission from **19**, **20**, **28** is blue-shifted by ~10 nm relative to that of FIrpic, indicating the sulfone group is efficient at widening the HOMO-LUMO gap. The emission of **30** is significantly greener, with λ_{max} of 516 nm with a second band at 536 nm of approximately equal intensity. In the case of the N^O bonded complexes **31** and **32** their emission is red-shifted compared to their corresponding pic complexes, but with a similar spectral profile, suggesting a similar source for the emission.

The PLQYs, lifetimes (τ_{obs}) and calculated radiative and non-radiative decay rates (k_r and k_{nr}) are shown in Table 2.5. The PLQYs for the FIrpic analogues are 0.64–0.68, similar to that of FIrpic, and the lifetimes are on the order of 1-2 μs. These are typical values for mono-iridium complexes with efficient spin-orbit coupling between the triplet and singlet states.

Complex	λ_{max}^{abs} (ε) / nm (x10^3 $M^{-1}cm^{-1}$)[a]	λ_{max}^{em} / nm[b]	PLQY / Φ_{PL}[d]	τ_P / μs[b,e]	k_r / 10^5 s^{-1}[f]	k_{nr} / 10^5 s^{-1}[f]
1 FIrpic	277 (50.1), 301 (34.2), 304 (32.6), 337 (13.8, sh), 357 (8.9, sh), 400 (6.2), 454 (0.8)[c]	468, 496, 531 (sh)	0.67	1.72	3.90	1.92
19	255 (88.6), 282 (67.2), 292 (61.7), 371 (9.4), 401 (sh, 3.8), 443 (0.6)[c]	455, 482, 511 (sh)	0.64	2.19	2.92	1.64
20	252 (123.7), 286 (90.4), 300 (83.0), 331 (sh, 23.4), 373 (11.3), 407 (sh, 4.7), 444 (0.8)[c]	457, 483, 515 (sh)	0.68	2.09	3.25	1.53
28	260 (100.4), 283 (76.4), 321 (sh, 30.9), 374 (13.1), 401 (sh, 5.0), 444 (0.9)[c]	457, 485, 517 (sh)	0.68	1.49	4.56	2.15
30	261 (89.1), 284 (80.2), 306 (b, 52.8), 399 (8.2), 452 (4.9), 490 (0.6)[c]	516, 536	0.48	3.53	1.36	1.47
31	264 (95.5), 278 (85.1), 302 (sh, 58.1), 364 (19.4), 382 (sh, 15.9), 421 (sh, 4.3), 447 (1.3)[c]	466, 491, 530 (sh)	0.44	2.90	1.52	1.93
32	250 (sh, 143.2), 266 (sh, 98.7), 290 (83.4), 312 (56.5), 368 (19.6), 414 (sh, 6.7), 449 (1.4)[c]	469, 494, 534 (sh)	0.38	2.85	1.33	2.18

[a] Data obtained in dichloromethane solution at 20 °C. [b] Data obtained in degassed dichloromethane solution with λ_{ex} = 380 nm. [c] Observed lowest energy band from excitation spectra. [d] Measured relative to $Ir(ppy)_3$ Φ_{PL} = 0.46 in degassed dichloromethane at 20 °C; estimated error ±10%. [e] Estimated error ±5%. [f] k_r, k_{nr} values calculated using Equations 1.5/1.6.

Table 2.5: Photophysical data for selected iridium complexes.

Electrochemistry

Cyclic voltammetry can be used to provide an estimate of HOMO and LUMO levels of cyclometalated iridium complexes which, in turn, can provide a reasonable estimate for the energy of the lowest level triplet (T) state. This can help rationalise changes in emission colour and can assess the impact of changing substituents on the basic ligand framework. The HOMO/LUMO levels can be estimated using the formula below:[44]

$$E_{HOMO/LUMO} = -4.8 - E_{ox/red}^{ons} \quad \text{(Equation 2.1)}$$

where E^{ons} = the potential of first onset of the oxidation/reduction peak in question (referenced to Fc/Fc^+).

Alternative equations are:

$$E_{LUMO} = -4.78 - 1.19E_{red}$$ [45] (Equation 2.2)

$$E_{HOMO} = -4.6 - 1.4E_{ox}$$ [46] (Equation 2.3)

These equations resulted from plotting the relationship between the oxidation/reduction potential and the HOMO/LUMO energy as determined by ultraviolet photoelectron spectroscopy (UPS) of thin films. They differ from Equation 2.1 as UPS is conducted on thin films (solid state), whereas the electrochemical measurements are conducted in solution in the presence of supporting electrolyte, as a result solvent effects and image charge effects must be accounted for. These effects are incorporated in the gradient factor.

Using these estimates it is possible to determine the effect of changing substituents on the emission colour and also to evaluate how well the HOMO/LUMO levels will match up with those of the host material in devices. For efficient electroluminescence it is important that the triplet energy (E_T) of the host material is at least as large as that of the emitter, and that they overlap to ensure efficient energy transfer from host to dopant.

Complexes **19**, **20**, **28**, **30**, **31** and **32** were investigated by cyclic voltammetry in solution and compared to the parent compound FIrpic. The voltammograms are shown in Figure 2.30 and the key parameters in Table 2.6. Equation 2.1 is used to calculate the energy of the HOMO.

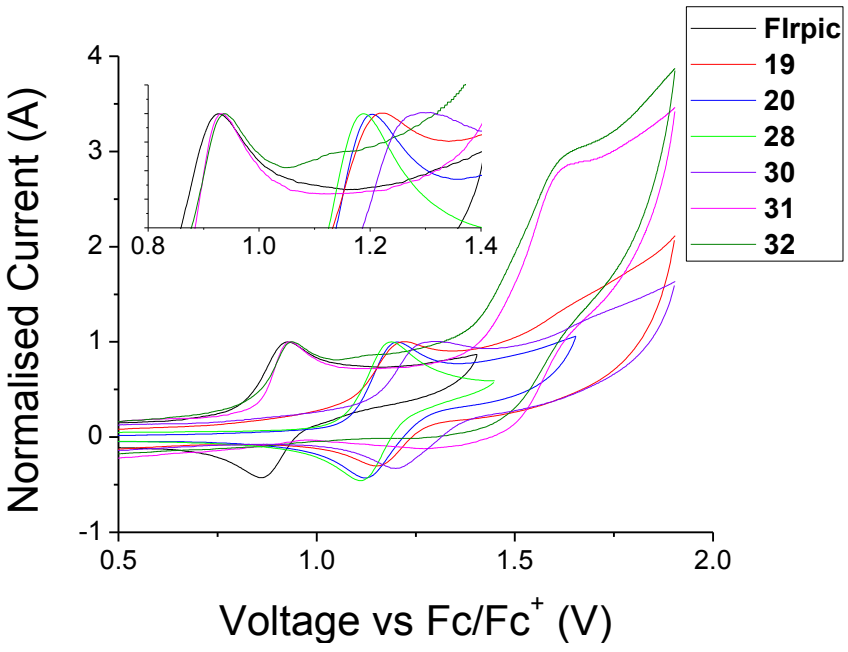

Figure 2.30: Cyclic voltammograms of the iridium complexes.

Complex	$1^{st} E^{ox}_{1/2}$ / V	$2^{nd} E^{ox}_{1/2}$ / V
FIrpic	0.89	-
19	1.19	-
20	1.16	-
28	1.15	-
30	1.25	-
31[a]	0.93 (irr)	1.62 (irr)
32[a]	0.94 (irr)	1.63 (irr)

[a] (irr) denotes an irreversible oxidation. The values reported are the cathodic peak potentials observed on the first scan. All values reported vs Fc/Fc^+ = 0.00 V.

Table 2.6: Electrochemistry data of iridium complexes. Measured in MeCN (0.1 M $^nBu_4NPF_6$) at 298 K.

All the pic complexes show a quasireversible oxidation wave, which is assigned to the Ir^{III}/Ir^{IV} couple. The parent compound FIrpic shows the least positive oxidation potential; this is as expected, as it is known that the introduction of electron withdrawing substituents results in a lowering of the HOMO, thereby increasing the oxidation potential. There is minimal difference in the potentials for **19**, **20** and **28**, suggesting in the cases studied here the identity of R in $–SO_2R$ has little impact,as does the introduction of the mesityl group, confirming there is minimal conjugation between the mesityl and the pyridyl ring. The E_{HOMO} estimates and $E^{ox}_{1/2}$ values for FIrpic and **20** agree with those obtained by Cao *et. al*.[11] Exchange of the *para* fluorine for a second $–SO_2Me$ group (**19** to **30**) results in a further increase in the oxidation potential (by 0.06 V), which can be rationalised by $–SO_2R$ being a stronger withdrawing group than F. As the emission from **30** is green rather than blue, it can be concluded that the LUMO of **30** is lowered more than the HOMO by the introduction of the sulfone group at this position. This can be rationalised, as the HOMO/LUMO molecular orbital plots for FIrpic show a large density of the LUMO at the 4-position however a relatively small HOMO density, suggesting that introducing an electron withdrawing group at this position would lower the LUMO a greater amount than the HOMO and thereby resulting in a smaller HOMO-LUMO gap.[4] This is supported by a report that introducing electron withdrawing groups at the 5-position results in a red-shift in emission relative to the parent compound.[22] No reduction waves were observed within the solvent window for any of the complexes in Table 2.6.

N^O bonded complexes **31** and **32** show significantly different electrochemical behaviour from the pic complexes; an irreversible oxidation occurs at +0.93 V for **31** and +0.94 V for **32**, followed by a second irrreversible oxidation at +1.62 V and +1.63 V. If the scan is reversed before the

second oxidation is reached the first oxidation wave is still irreversible. This suggests a chemical reaction takes place upon oxidation, and could be attributed to the unusual connectivity around the Ir centre. DFT calculations indicate that the HOMO in the N^O complexes is localised over the oxygen atom of the N^O ligand, which could explain the irreversibility of the first oxidation wave and the similarity of the oxidation values for **31** and **32**.

COMPUTATIONAL DATA

Electronic structure calculations were carried out on iridium complexes **19**, **20**, **28**, **30**, **31**, **32** by Dr Mark Fox (Department of Chemistry) to elucidate the nature of the frontier orbitals and the transitions involved in the absorption and emission spectra. The full geometries were optimised at the B3LYP/LANL2DZ:3-21G* level and are denoted **19'**, **20'**, **28'**, **30'**, **31'**, **32'** to distinguish them from experimental data. Comparison with optimised and experimental geometries determined from the X-ray data for **19**, **20**, **28**, **30**, **31**, **32** revealed good agreement for the Ir-X bond distances (Table 2.7).

	Ir-N(ppy)	Ir-N(ppy)	Ir-C *trans* N	Ir-C *trans* O	Ir-O	Ir-N(pic)
10	2.046(3)	2.028(3)	1.991(4)	1.974(3)	2.146(2)	2.136(3)
10'	2.062	2.047	2.013	2.011	2.133	2.162
11	2.048(3)	2.029(3)	1.989(3)	1.985(3)	2.158(2)	2.134(3)
11'	2.061	2.048	2.014	2.011	2.136	2.163
12	2.033(5)	2.033(5)	2.000(6)	1.986(6)	2.133(4)	2.140(5)
12'	2.061	2.048	2.012	2.011	2.135	2.162
13	2.040(4)	2.042(5)	1.995(4)	1.991(5)	2.148(3)	2.128(4)
13'	2.063	2.049	2.01	2.009	2.134	2.165
15	2.037(4)	2.032(4)	1.989(5)	1.982(5)	2.151(3)	2.161(4)
15'	2.065	2.043	2.009	2.008	2.114	2.198
23	2.042(4)	2.035(4)	1.988(5)	1.985(5)	2.143(4)	2.129(4)
23'	2.061	2.048	2.015	2.013	2.14	2.164

Table 2.7: Comparison of experimental (10-13, 15, 23) and optimised (10'-13', 15', 23') bond lengths involving the iridium atom.

The frontier orbital energies were computed for all complexes, and the HOMO energies show good agreement with the observed oxidation potentials. The HOMO/LUMO distributions of selected complexes **19'**, **30'**, and **31'** are shown in Figure 2.31. The HOMO energies of the sulfone

	MO	Orbital	eV	Ir	Py(Pic)	CO_2(Pic)	Py(ppy)	Ph(ppy)
Firpic 1	138	LUMO	-1.87	2	81	10	5	2
	137	HOMO	-5.49	44	2	7	7	41
19'	178	LUMO	-2.23	1	52	7	27	12
	177	HOMO	-6.09	44	2	9	7	39
20'	218	LUMO	-2.15	1	61	8	21	9
	217	HOMO	-5.97	42	2	8	6	41
28'	242	LUMO	-2.15	1	70	9	13	6
	241	HOMO	-6.01	44	2	9	7	39
30'	210	LUMO	-2.46	3	4	1	47	46
	209	HOMO	-6.15	44	2	10	6	37
31'	215	LUMO	-2.2	5	2	2	65	27
	214	HOMO	-5.8	20	8	64	3	5
32'	275	LUMO	-2.04	4	16	6	50	23
	274	HOMO	-5.61	21	6	63	3	7

Table 2.8: HOMO/LUMO energies and % MO contributions for the complexes.

complexes are all lower than that of **FIrpic** (**1**), reflecting the electron withdrawing properties of the sulfone moiety. For complexes **19'**, **20'**, **28'** and **30'** the HOMO is localised on the phenyl rings of the cyclometalating ligands and on the iridium d-orbitals, as is the case with FIrpic (Table 2.8). The LUMOs for **19'**, **20'** and **28'** are distributed across the pyridyl of the picolinate ancillary and across the pyridyl ring of the ppy ligands, with a small contribution from the phenyl rings. This is slightly different to FIrpic, wherein the LUMO is mostly localised on the pic ancillary ligand (91% total). This results in the sulfone complexes having lower LUMO energies than FIrpic **1'**, however, in the case of **19'**, **20'** and **28'** this shift is small compared to the decrease in the HOMO levels. As a result complexes **19'**, **20'** and **28'** exhibit larger HOMO-LUMO gaps than FIrpic, and their emission is predicted to be blue-shifted, which agrees with experimental observation. In the case of **30'** the LUMO is almost totally (93%) located on a ppy ligand, with a notable density at the 4-position of the phenyl ring, where the additional sulfone is located. The influence of the *para* sulfone results in a lower LUMO energy for **30** than for the other pic complexes, as a result the HOMO-LUMO gap is lower, resulting in the green emission.

Complexes **31'** and **32'** exhibit significantly different HOMO distributions to the pic- complexes; the HOMOs are localised on the phenyloxy group of the N^O bonded ligand (Figure 2.31) rather

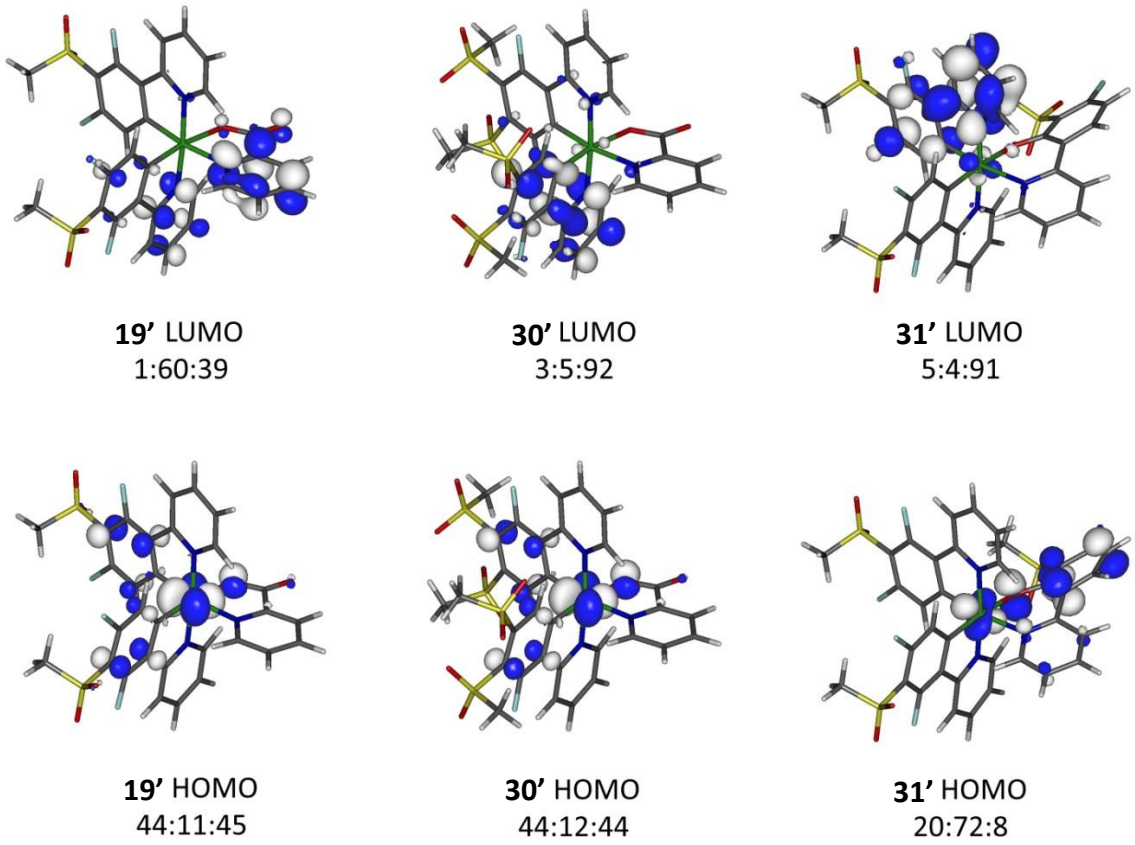

Figure 2.31: Frontier molecular orbitals for 19', 30' and 31'. All contours are plotted at ±0.05 (e/bohr^3)$^{1/2}$. Ir : pic or oppy : ppy % orbital contribution ratio listed for each orbital.

than on the iridium d-orbitals or the phenyl ring of the C^N ppy ligands. As a result, the HOMO levels for **31'** and **32'** are higher than those of the pic complexes (**19'**, **20'**, **28'**). The unusual HOMO distribution is reflected in the oxidation potentials for **31** and **32**, which are irreversible and at lower oxidation potentials. The LUMOs are also lowered relative to the pic complexes, and distributed over C^N ppy ligands, resulting in the smallest HOMO-LUMO gaps for all the complexes, including FIrpic.

TD-DFT computations were carried out on the S_0 optimized geometries of **19'**, **20'**, **28'**, **30'**, **31'** and **32'** to predict the emission wavelengths. The initial excitation is assumed to give the lowest energy singlet excited state S_1 which then undergoes intersystem crossing (ISC) due to the SOC induced by the iridium centre to form the triplet excited state T_1. Phosphorescence is then observed from the $S_0 \leftarrow T_1$ process. Most of the complexes display small Stokes shifts (**30** is the exception), suggesting that the T_1 geometry is similar to the corresponding S_0 geometry. The reverse process $S_0 \leftarrow T_1$ is therefore considered to have the same nature as the computed $S_0 \rightarrow T_1$

process, with the predicted emission wavelength adjusted to take into account the Stokes shift. The predicted and observed emission wavelengths are shown in Table 2.8, and it can be seen that there is good agreement for most of the complexes, with the exception of **30'-32'**.

Complexes **30**-**32** exhibit lower PLQYs and longer lifetimes than the rest of the pic complexes, suggesting the emission is likely to be from a different excited state. In the case of **30** the large Stokes shift suggests substantial rearrangement in the excited state, a suggestion supported by the T_1 larger vertical energy for **30'** (0.30 eV) compared to **19'** (0.27 eV) and **31'** (0.28 eV). In the case of **31'** and **32'** it is notable that there is a relatively small contribution to the HOMO from the metal d-orbitals (20% and 21%, respectively) compared to the rest of the complexes, whereas for the HOMO-1 the Ir d orbitals contribute 45% and 38% for **31'** and **32'**, respectively. This suggests that the $S_0 \leftarrow T_1$ transition may not be the transition responsible for the emission due to its low metal character, which may reduce the rate of intersystem crossing between S_1 and T_1. This is supported by the spin density calculations conducted on the optimised T_1 geometries; spin densities for **19'**, **30'** and **31'** were 0.36, 0.46 and 0.13, respectively. The low spin density value for **31'** implies that a higher energy triplet state (T_n, $n > 1$) is responsible for the emission in **31'** and, by extension, **32'**. Calculations for the emission from the $S_0 \leftarrow T_2$ transition reveal a better agreement with experimental data (474 nm and 472 nm for **31'** and **32'**, respectively).

DEVICE DATA

OLEDs containing complexes **19**, **20** and **28** were fabricated by Dr Hameed Al Atter in the Department of Physics at Durham University and compared to a reference device containing FIrpic. The hole transporting layer and emissive layer were deposited by solution processing techniques, and the electron transporting, electron injection layers and the cathode were then fabricated by vacuum deposition. The device structure is as follows: ITO/PEDOT:PSS (45

Complex	λ_{ELmax} / nm	Brightness / cd/m^2	turn-on voltage / V [a]	EQE / %	current efficiency / cd/A	power efficiency / lm/W	CIE coordinates / (x,y) [b]
FIrpic 1	475	7340	6.2	5.4	12.2	5.1	(0.19, 0.38)
19	463	776	6.8	3.0	2.0	0.8	(0.19, 0.29)
20	463	2464	8.0	3.9	8.2	2.9	(0.20, 0.36)
28	465	2368	8.0	4.0	7.8	2.0	(0.18, 0.30)

[a] Measured at a brightness of 10 cd/m^2. [b] Measured at 12 V.

Table 2.8: Summary of device data.

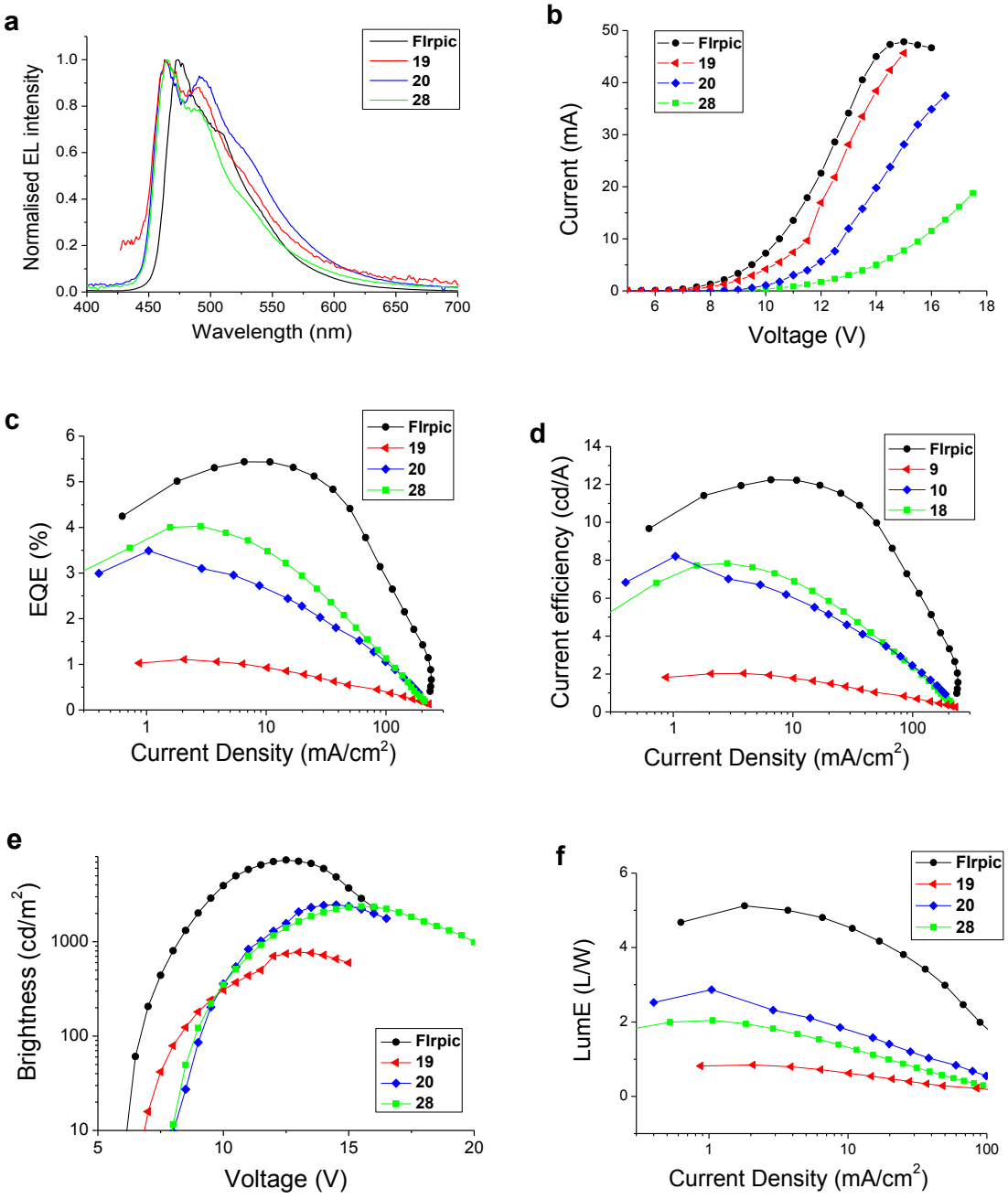

Figure 2.32: Device data for complexes 19, 20, 28.

nm)/PVK:OXD-7(30%):**Ir complex**(15%)(60 nm)/TPBi (30 nm)/LiF/Al. The electroluminescence (EL) spectra from the devices are shown in Figure 2.31; for all complexes the EL spectra are similar to the photoluminescence (PL) spectra, indicating good exciton confinement to the emissive molecule. The EQE and brightness of the devices are shown in Figure 2.31 (panels c and e). As can be seen, the devices containing **28** and **20** performed better than the devices of **19**, with EQEs of 4.0% and 3.9%. This can be rationalised by the increased steric shielding due to the mesityl substituent in the case of **28**, and the p-Tol substituent in the case of **20**. These complexes also displayed greater solubility than **19**, which is beneficial for solution processing. All the complexes

display lower maximum brightnesses (panel e) than the FIrpic device; however it is notable that their electroluminescence is bluer.

CONCLUSION

New sulfone containing ligands were synthesised with the aim of blue-shifting the emission of the resultant iridium complexes compared to the parent complex, FIrpic. Heteroleptic pic complexes **19**, **20**, **28** were synthesised, and exhibited bluer emission than FIrpic (~10 nm) while maintaining comparable PLQYs and emission lifetimes. Electrochemical study indicated the introduction of the sulfone group at the 5- position (**19**, **20**, **28**) resulted in a lowering of the HOMO energy, suggesting the LUMO energy was not significantly affected. Complex **30**, containing disulfone ligand **29**, highlights the importance of the position of substitution, as it displays green emission due to a lowering of the LUMO level. Complexes **31** and **32**, heteroleptic complexes with a novel ancillary ligand, were also synthesised, bringing to light the instability of these sulfone ligands to nucleophilic attack, a feature which will be discussed more extensively in Chapter 3. The computed bond lengths and oxidation potentials showed good agreement with the experimental data, and the HOMO/LUMO distributions of the pic complexes (**19**, **20**, **28**, **30**) were comparable to parent complex FIrpic. Devices of complexes **19**, **20** and **28** were fabricated by solution processing in the Department of Physics retain the blue emission obseved in the PL spectra. Complexes **20** and **28** were the best performing, with the device of **28** displaying CIE coordinates of (0.18, 0.30) at 12 V and a maximum EQE of 4.0%, however all complexes performed less favourably than the FIrpic device.

References

1) C. Adachi, R. C. Kwong, P. Djurovich, V. Adamovich, M. A. Baldo, M. E. Thompson and S. R. Forrest, *Appl. Phys. Lett.,* 2001, **79**, 2082
2) V. N. Kozhevnikov, K. Dahms and M. R. Bryce, *J. Org. Chem.,* 2011, **76**, 5143-8
3) H. Shin, S. Lee, K.-H. Kim, C.-K. Moon, S.-J. Yoo, J.-H. Lee and J.-J. Kim, *Adv. Mater.,* 2014, **26**, 4730-4734
4) E. Baranoff and B. F. Curchod, *Dalton Trans.,* 2015, **44**, 8318-29
5) C. Zhong, C. Duan, F. Huang, H. Wu and Y. Cao, *Chem. Mater.,* 2011, **23**, 326-340
6) P. T. Chou and Y. Chi, *Chem. Eur. J.,* 2007, **13**, 380-95
7) H. Wu, T. Yang, Q. Zhao, J. Zhou, C. Li and F. Li, *Dalton Trans.,* 2011, **40**, 1969-76
8) H. Yersin, *Highly Efficient OLEDs with Phosphorescent Materials,* Wiley-VCH, Darmstadt, 2008
9) S. Lamansky, P. Djurovich, D. Murphy, F. Abdel-Razzaq, R. Kwong, I. Tsyba, M. Bortz, B. Mui, R. Bau and M. E. Thompson, *Inorg. Chem.,* 2001, **40**, 1704-1711
10) S. H. Kim, J. Jang, S. J. Lee and J. Y. Lee, *Thin Solid Films,* 2008, **517**, 722-726
11) C. Fan, Y. Li, C. Yang, H. Wu, J. Qin and Y. Cao, *Chem. Mater.,* 2012, **24**, 4581-4587
12) S.-y. Takizawa, H. Echizen, J.-i. Nishida, T. Tsuzuki, S. Tokito and Y. Yamashita, *Chem. Lett.,* 2006, **35**, 748-749
13) M. Marín-Suárez, B. F. E. Curchod, I. Tavernelli, U. Rothlisberger, R. Scopelliti, I. Jung, D. Di Censo, M. Grätzel, J. F. Fernández-Sánchez, A. Fernández-Gutiérrez, M. K. Nazeeruddin and E. Baranoff, *Chem. Mater.,* 2012, **24**, 2330-2338
14) S. Lee, S. O. Kim, H. Shin, H. J. Yun, K. Yang, S. K. Kwon, J. J. Kim and Y. H. Kim, *J. Am. Chem. Soc.,* 2013, **135**, 14321-8
15) Y. Hisamatsu and S. Aoki, *Eur. J. Inorg. Chem.,* 2011, **2011**, 5360-5369
16) S. J. Lee, K. M. Park, K. Yang and Y. Kang, *Inorg. Chem.,* 2009, **48**, 1030-7
17) M. Xu, R. Zhou, G. Wang and J. Yu, *Inorg. Chim. Acta.,* 2009, **362**, 2183-2188
18) R. Ragni, E. A. Plummer, K. Brunner, J. W. Hofstraat, F. Babudri, G. M. Farinola, F. Naso and L. De Cola, *J. Mater. Chem.,* 2006, **16**, 1161
19) M. Zhang, Z.-S. Li and J.-Z. Sun, *J. Mol. Struct.,* 2009, **919**, 204-209
20) P. Coppo, E. A. Plummer and L. De Cola, *Chem. Commun.,* 2004, 1774-5
21) E. Baranoff, B. F. Curchod, F. Monti, F. Steimer, G. Accorsi, I. Tavernelli, U. Rothlisberger, R. Scopelliti, M. Gratzel and M. K. Nazeeruddin, *Inorg. Chem.,* 2012, **51**, 799-811
22) G. Zhou, C.-L. Ho, W.-Y. Wong, Q. Wang, D. Ma, L. Wang, Z. Lin, T. B. Marder and A. Beeby, *Adv. Funct. Mater.,* 2008, **18**, 499-511
23) J. Frey, B. F. Curchod, R. Scopelliti, I. Tavernelli, U. Rothlisberger, M. K. Nazeeruddin and E. Baranoff, *Dalton Trans.,* 2014, **43**, 5667-79
24) V. Sivasubramaniam, F. Brodkorb, S. Hanning, H. P. Loebl, V. van Elsbergen, H. Boerner, U. Scherf and M. Kreyenschmidt, *J. Fluorine Chem.,* 2009, **130**, 640-649
25) M. Tavasli, S. Bettington, I. F. Perepichka, A. S. Batsanov, M. R. Bryce, C. Rothe and A. P. Monkman, *Eur. J. Inorg. Chem.,* 2007, **2007**, 4808-4814
26) R. Ragni, E. Orselli, G. S. Kottas, O. H. Omar, F. Babudri, A. Pedone, F. Naso, G. M. Farinola and L. De Cola, *Chem. Eur. J.,* 2009, **15**, 136-48
27) D. Tordera, A. M. Bünzli, A. Pertegás, J. M. Junquera-Hernández, E. C. Constable, J. A. Zampese, C. E. Housecroft, E. Ortí and H. J. Bolink, *Chem. Eur. J.,* 2013, **19**, 8597-8609
28) E. C. Constable, C. D. Ertl, C. E. Housecroft and J. A. Zampese, *Dalton Trans.,* 2014, **43**, 5343-56
29) C. D. Ertl, J. Cerda, J. M. Junquera-Hernandez, A. Pertegas, H. J. Bolink, E. C. Constable, M. Neuburger, E. Orti and C. E. Housecroft, *RSC Advances,* 2015, **5**, 42815-42827
30) S. Ladouceur, L. Donato, M. Romain, B. P. Mudraboyina, M. B. Johansen, J. A. Wisner and E. Zysman-Colman, *Dalton Trans.,* 2013, **42**, 8838-47
31) V. H. Nguyen, H. Q. Chew, B. Su and J. H. Yip, *Inorg. Chem.,* 2014, **53**, 9739-50
32) H. Benjamin, MSci, University of Durham, 2012

33) H. Suzuki and H. Abe, *Tetrahedron Lett.,* 1995, **36**, 6239-6242
34) M. Bian, F. Xu and C. Ma, *Synthesis,* 2007, **2007**, 2951-2956
35) W. Zhu and D. Ma, *J. Org. Chem.,* 2005, **70**, 2696-700
36) S. Cacchi, G. Fabrizi, A. Goggiamani, L. M. Parisi and R. Bernini, *J. Org. Chem.,* 2004, **69**, 5608-14
37) V. N. Kozhevnikov, Y. Zheng, M. Clough, H. A. Al-Attar, G. C. Griffiths, K. Abdullah, S. Raisys, V. Jankus, M. R. Bryce and A. P. Monkman, *Chem. Mater.,* 2013, **25**, 2352-2358
38) J. A. Aguilar, S. Faulkner, M. Nilsson and G. A. Morris, *Angew. Chem. Int. Ed.,* 2010, **49**, 3901-3903
39) Y. Zheng, A. S. Batsanov, R. M. Edkins, A. Beeby and M. R. Bryce, *Inorg. Chem.,* 2012, **51**, 290-7
40) S. Ladouceur and E. Zysman-Colman, *Eur. J. Inorg. Chem.,* 2013, **2013**, 2985-3007
41) Y. You, J. Seo, S. H. Kim, K. S. Kim, T. K. Ahn, D. Kim and S. Y. Park, *Inorg. Chem.,* 2008, **47**, 1476-87
42) K. Chao, K. Shao, T. Peng, D. Zhu, Y. Wang, Y. Liu, Z. Su and M. R. Bryce, *J. Mater. Chem. C,* 2013, **1**, 6800
43) P. J. Hay, *J. Phys. Chem. A,* 2002, **106**, 1634-1641
44) I. A. Wright, P. J. Skabara, J. C. Forgie, A. L. Kanibolotsky, B. Gonzalez, S. J. Coles, S. Gambino and I. D. W. Samuel, *J. Mater. Chem.,* 2011, **21**, 1462-1469
45) P. I. Djurovich, E. I. Mayo, S. R. Forrest and M. E. Thompson, *Org. Electron.,* 2009, **10**, 515-520
46) B. Dandrade, S. Datta, S. Forrest, P. Djurovich, E. Polikarpov and M. Thompson, *Org. Electron.,* 2005, **6**, 11-20

Chapter 3: Towards 'fluorine-free' emission

While fluorinated ligands are widely used in emissive Ir^{III} complexes there are problems associated with their stability. A study of FIrpic devices by HPLC/MS showed that isomerisation occurred during device fabrication and it was also noted that degradation of FIrpic with loss of one F occurred during the deposition process.[1] This is detrimental for the colour purity as the fluorine moieties are introduced to blue-shift the emission. In this study the devices were stressed (i.e. under operation) for 24 h and the proportion of defluorinated species increased during operation.[1] Other studies have also shown degradation of FIrpic via loss of the picolinate ancillary ligand, or loss of CO_2 from the ancillary ligand, followed by reaction with other species.[2,3] The instability of fluorinated complexes in LEECs has also been observed, and a correlation drawn between increasing the number of fluorines present on the ligands and a decrease in device stability.[4]

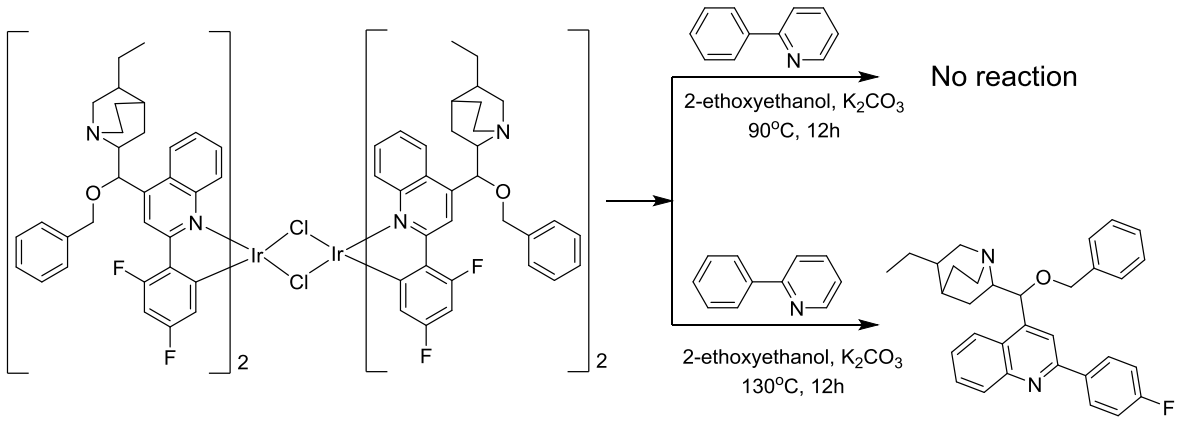

Figure 3.1: Defluorination and decyclometalation of ligands upon attempts to split a dichlorobridged dimer.

Defluorination does not occur solely during device operation; several complexes undergo defluorination during synthesis. Attempts to split the Ir-dimer shown in Figure 3.1 with ancillary ligands such as acac and dbm (dibenzoylmethane) resulted in the formation of the required complex, however defluorinated free ligand was also isolated in increasing yield as the reaction temperature was raised.[5] In addition, when attempts were made to split the Ir dimer with ppy the dimer decomposed to give defluorinated ligand.[5]

In another example, an attempt to synthesise the homoleptic complex of 2,4-difluoro-phenylisoquinoline (Figure 3.2) resulted in mono-defluorination of all three ligands around the Ir

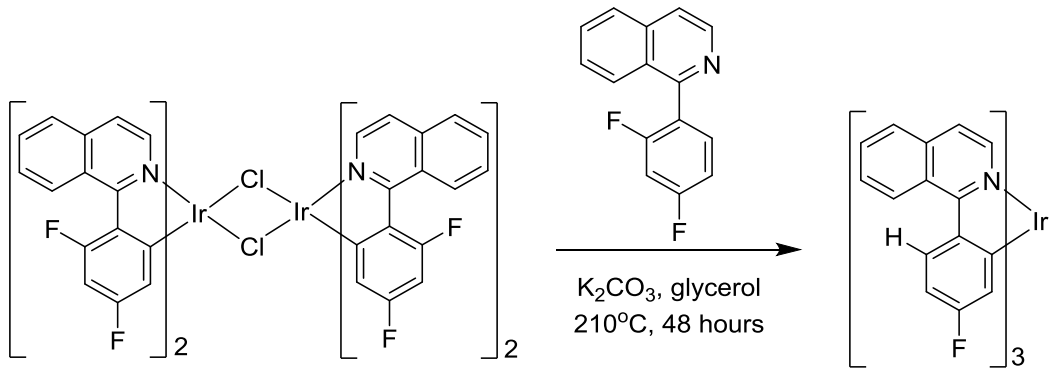

Figure 3.2: Defluorination of 2,4-difluoro-phenylisoquinoline ligands.

centre.[6] Interestingly, when attempts were made to crack the equivalent non-fluorinated dimer with both 2,4-difluoro-phenylisoquinoline and 2,4-difluorophenylpyridine none of the expected products were observed.[6] Instead, the major products were the homoleptic complexes of the mono-defluorinated ligand that had been introduced to crack the dimer.[6]

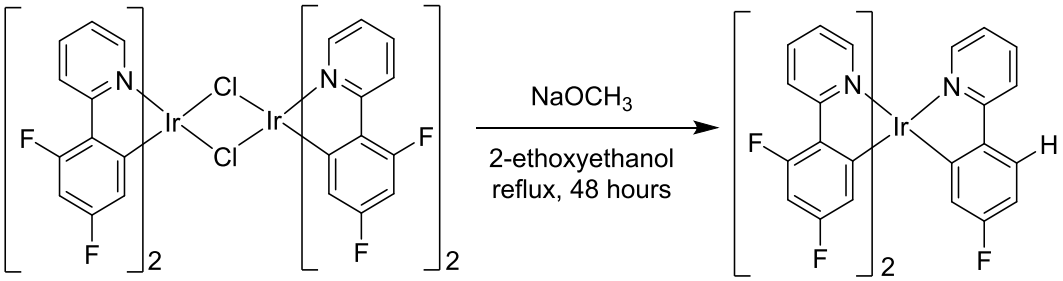

Figure 3.3: Partial defluorination and decomposition of an iridium dimer.

Partial defluorination is also observed when reacting the dfppy dimer with $NaOCH_3$, resulting in the formation of a heteroleptic complex, shown in Figure 3.3.[7] A mechanism is proposed to explain this behaviour involving Ir-H and Ir-F intermediates. In another example from our laboratory attempts to thermally convert a *mer* complex of 2-phenyl-γ-carboline ligands (Figure 3.4) to the *fac* isomer resulted in regioselective defluorinaton.[8] When the *mer*-isomer was heated to 290 ^{o}C in glycerol the fluorine *ortho* to the pyridyl group was replaced on all three ligands and the *fac*-defluorinated product formed. The *mer*-isomer was successfully converted to the *fac*-isomer via UV irradiation.[8] The stability of the fluorinated *fac*-isomer was tested but no defluorination was observed when refluxing in glycerol for 48 h, indicating that defluorination occurred from the *mer*-isomer in 58% yield.[8] This also confirms that the γ-carboline system imparts additional thermal stability to the *fac*-complex, as comparable treatment of *fac*-Ir(dfppy)$_3$ results in decomposition within 2 h.[8] It is interesting to note that in all these cases the fluorine atom that is replaced is the one that is *ortho* to the pyridyl substituent; this position is presumably

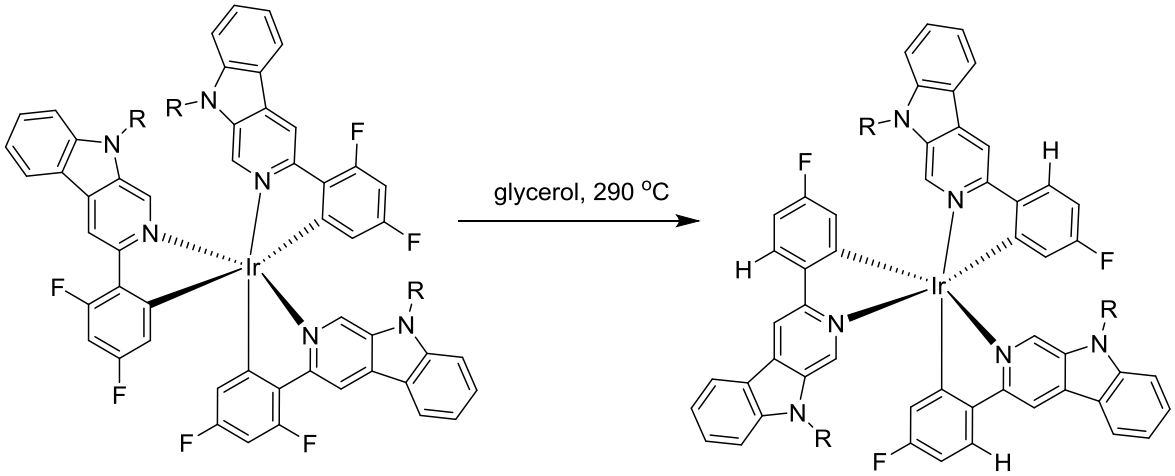

Figure 3.4: Defluorination upon attempted thermal conversion from a *mer* to *fac* isomer.

more activated by the inductive withdrawing effect of the pyridyl ring.[8] Attempts to make homoleptic complexes of 1-(2-fluorophenyl)isoquinoline and 1-(4-fluorophenyl)isoquinoline (Figure 3.5) from their dimers resulted in the isolation of the required product for the latter, while the former experienced defluorination on all three ligands, indicating the regioselective nature of the defluorination.[6] The poor stability of fluorinated Ir complexes has been noted elsewhere, in a series of cationic complexes (Figure 3.6). It was observed that the stability of the LEECs they were used in decreased as the number of fluorinated ligands increased.[9]

These examples highlight the need for care when using fluorinated ligands to synthesise iridium complexes for OLED devices, as cleavage of C-F bonds will not only distort the colour of emission

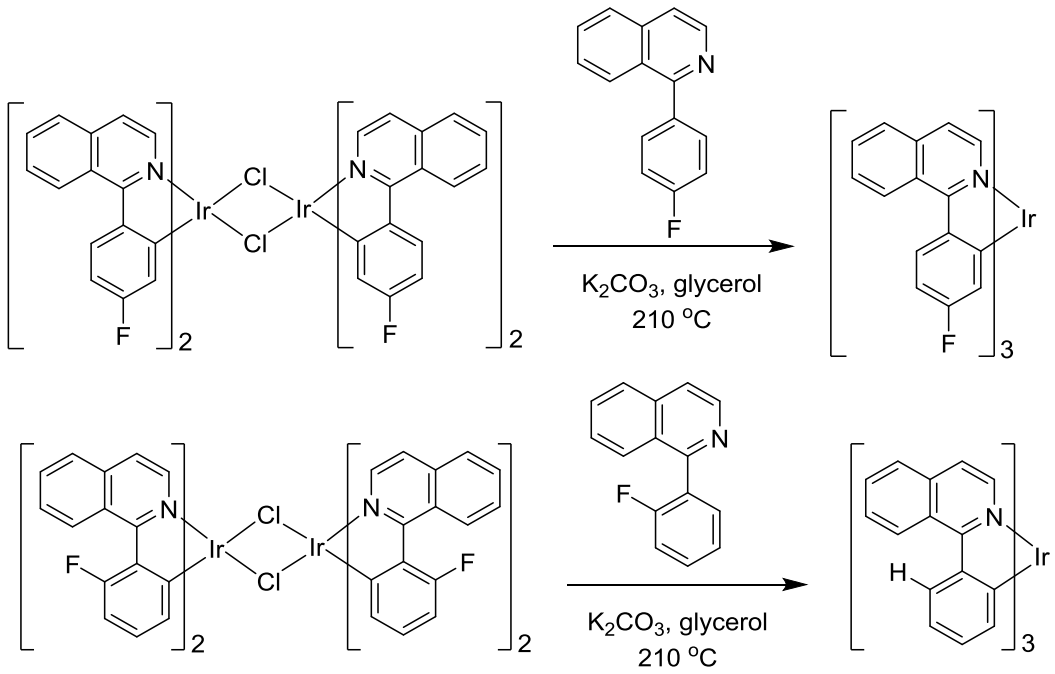

Figure 3.5: Regioselective defluorination of fluorinated isoquinoline ligands.

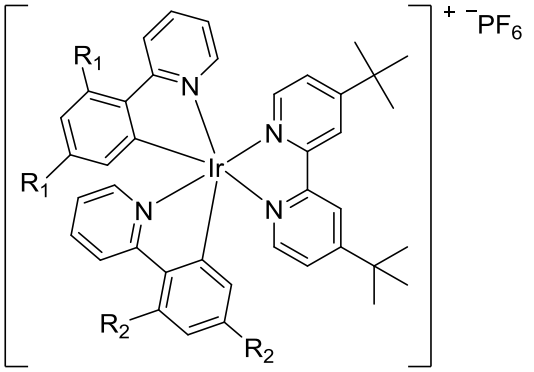

$R_1 = H \quad R_2 = H$
$R_1 = H \quad R_2 = F$
$R_1 = F \quad R_2 = F$

Figure 3.6: A selection of cationic complexes for LEECs.

but also potentially produce reactive species that could interact with other nearby organic materials, thereby affecting the device performance. As a result there is an interest both in moving away from fluorinated ligands and in finding ways of stabilising them.

There are a few ways of achieving 'fluorine-free' blue emission including:

1) Modifying existing fluorinated ligands by replacing fluorines with electron donating groups
2) Exchanging the pyridine or phenyl rings in ppy for another heterocycle in order to increase the π- π* gap (such as a carbene, imidazole, pyrazole or triazole)
3) Utilising ancillary ligands that widen the HOMO-LUMO gap and shift quenching d-d* states to higher energies, such as carbenes or phosphines.

This chapter is concerned with the first two methods, although carbene ligands will be discussed in more detail in Chapter 6, and there is discussion of ancillary ligands in Chapter 5.

As was noted in Chapter 2 introducing electron withdrawing groups onto the phenyl ring of ppy based ligands is not guaranteed to blue-shift the emission colour; the position and identity of the substituent also matters, with fluorine appearing to be a special case among electron withdrawing groups. Our paper reported that fluorines can be exchanged for alkoxy groups with a minimal red-shift in the emission, despite the fact the alkoxy groups are electron donating.[10] This observation was explained and generalised in a paper by Baranoff which details the correlation between the Hammett σ_m and σ_p parameters of substituents on ppy ligands and the oxidation and reduction potentials of the resultant homoleptic complexes.[11] These data allow reasonable predictions of emission λ_{max}, provided the localisations of the HOMO and LUMO remain on the phenyl ring/iridium d orbitals and pyridyl ring, respectively.[11] A series of complexes (**35**, **36**, **38**, **39**, **42**)

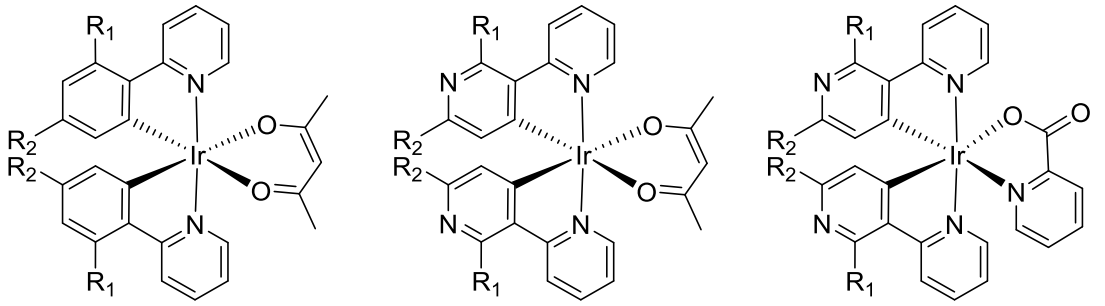

33 $R_1 = R_2 = H$
34 $R_1 = R_2 = F$
35 $R_1 = R_2 = OMe$
36 $R_1 = Me$, $R_2 = OMe$

37 $R_1 = R_2 = F$
38 $R_1 = R_2 = OMe$
39 $R_1 = Me$, $R_2 = OMe$

40 $R_1 = R_2 = F$
41 $R_1 = R_2 = OMe$
42 $R_1 = Me$, $R_2 = OMe$

Figure 3.7

were then synthesised that replaced the electron withdrawing fluorines with donating methoxy and methyl moieties (Figure 3.7). These displayed significant blue-shifts in emission compared to the unsubstituted reference compound **33**, although they were not as blue as the fluorinated analogues (**34**, **37**). The blue-shift induced by fluorine substituents is attributed to it being a strong acceptor towards the *meta* position ($\sigma_m = 0.34$), thereby stabilising the HOMO more than the LUMO ($\sigma_p = 0.06$). However, for methoxy/methyl substituents it is their ability to act as strong donors towards the *para* position ($\sigma_p = -0.17$ for Me, $\sigma_p = -0.27$ for OMe), thus destabilising the LUMO relative to the HOMO, that is responsible for the blue-shift.[11]

A series of complexes with this motif have been synthesised via a route that exploits the instability of complexes with fluorinated ligands; attempts were made to synthesise a series of

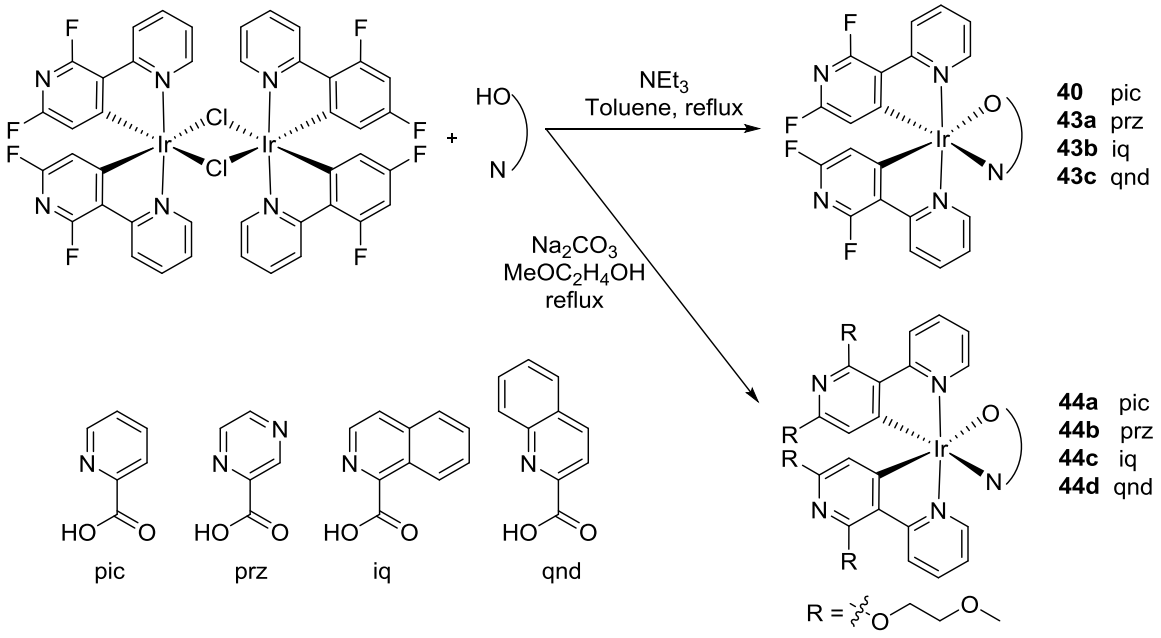

Figure 3.8

heteroleptic complexes containing the 2',6'-difluoro-2,3'-bipyridine (dfpypy) ligand as the chromophore (**40**, **43a**-**c**) under standard conditions, shown in Figure 3.8.[12] However, instead the complexes underwent nucleophilic aromatic substitution due to attack at the aromatic fluorines by the solvent, methoxyethanol, which produced complexes **44a**-**d** in 33-63% from the μ-dichloro bridged dimer.[12] Interestingly, when the ligand was subjected to the reaction conditions without the presence of iridium the substitution was not observed, indicating that the chelation to the Ir(III) centre enhances the susceptibility of the fluorines to nucleophilic attack.[12] Complex **41** was also synthesised in this study. The two pic complexes **41** and **44a** in particular exhibit sky-blue emission comparable to FIrpic, with λ_{max} = 454 nm for **44a** and λ_{max} = 467 nm for **41**, and good quantum yields (0.75 and 0.70 in solution, respectively).

An alternative to exchanging fluorines for donor groups is to exchange the phenyl group in the ppy framework for a more electron deficient alternative. Complexes using a pyrimidine instead of the phenyl ring were synthesised (Figure 3.9) as an attempt to achieve blue emission without fluorinated aromatic ligands (the ancillary ligand contains a CF_3 group).[13] Pyrimidine was chosen as the ligands were easy to synthesise and the electron deficient nature of the ring would help increase the ligand π-π* gap, thereby achieving blue emission.[13] For both the 4- and 5-substituted pyridyl pyrimidine derivatives the emission colour was shown to be highly dependent on the substitution position.[13] The complex with 4-substitution **46** displayed green emission (λ_{max} = 535 nm) while the corresponding 5-substituted complex **45b** exhibited sky-blue emission (λ_{max} = 457 nm) similar to FIrpic.[13] The difference was attributed to the ability of the nitrogen atoms in the 4-substituted ligand to extend the conjugation via a resonance effect, which is not possible in the 5-substituted isomer, thereby reducing the HOMO-LUMO gap.[13]

This approach can be used in conjunction with the use of donors, as in the series of complexes shown in Figure 3.10.[14,15] Here, donating methoxy groups have been introduced onto 2,3'-

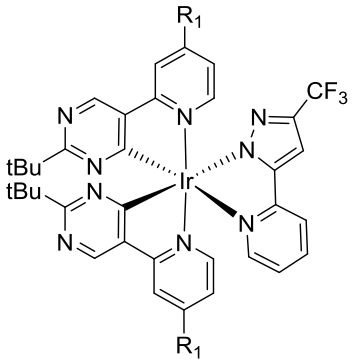

45a R_1 = H λ_{max} = 456, 488, 521 nm
45b R_1 = tBu λ_{max} = 457, 489, 521 nm

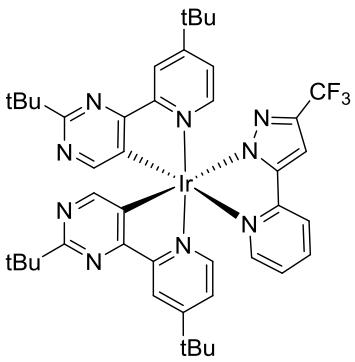

46 λ_{max} = 535 nm

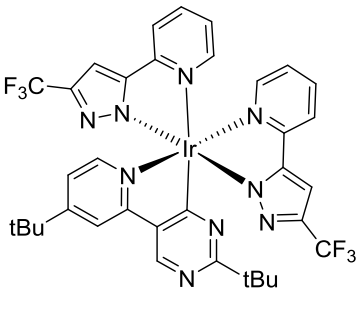

47 λ_{max} = 452, 483, 516 nm

Figure 3.9

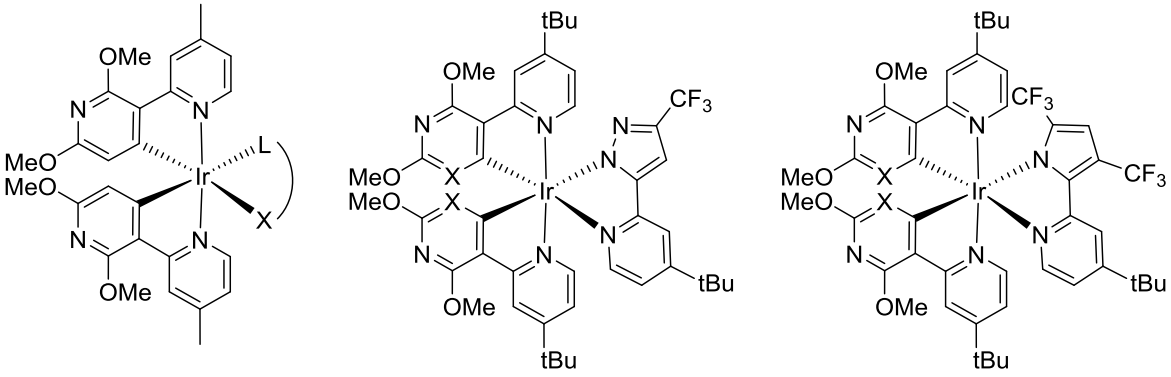

48a L^X = acac
λ_{max} = 468 nm
48b L^X = pic
λ_{max} = 462 nm

49a R = CH
λ_{max} = 458, 488, 510 nm
50a R = N
λ_{max} = 444, 472, 493 nm

49b R = C
λ_{max} = 458, 488, 510 nm
50b R = N
λ_{max} = 458, 476, 507 nm

Figure 3.10

bipyridine (pypy) and 2-(pyrimidin-5-yl)-pyridine (pmpy) ligands to create aromatic fluorine-free complexes (**48-50a/b**).[14] DFT/TD-DFT calculations indicate the electron withdrawing nitrogen atoms in the cyclometalating ligand effectively stabilise the ligand π-orbitals, while the donating methoxy groups both increase the ligand π* orbitals and lower the electron density of the iridium dπ orbitals.[14] Emission from all four complexes is in the sky-blue region, with the bluest complex being **50a**, and they are highly emissive (ϕ = 0.79-0.93).[14] The bluer emission of **50a** relative to **49a** can be rationalised by the greater ligand π-π* gap in the former, however in the case of the complexes with the pyrrole-containing ancillary ligand (**49b** and **50b**) the authors note a different emission profile for **50b** compared to **49b**, and do not observe a blue-shift.[14] The reasons for this are not clear, although it is noted that **50b** has significant HOMO distribution on the ancillary ligand (31%), whereas the others do not.[14]

A water soluble, fluorine-free blue iridium complex has also been synthesised for biological applications (Figure 3.11). In this case 1-methyl-3-(2'-pyridyl)pyridinium was used as the C^N ligand and substituents on the N^N bipyridine ancillary ligand were varied.[16] The resulting complexes were blue/blue-green emitters, highlighting the effect of a strongly electron

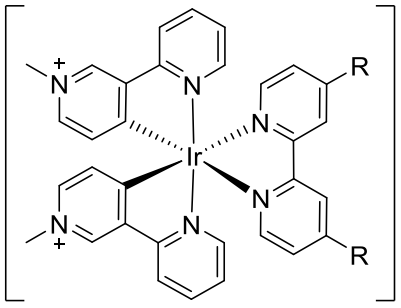

51a R = H λ_{max} = 444, 474, 504, 548 nm
51b R = CF_3 λ_{max} = 466, 494, 525, 574 nm
51c R = tBu λ_{max} = 440, 470, 502, 546 nm

Figure 3.11

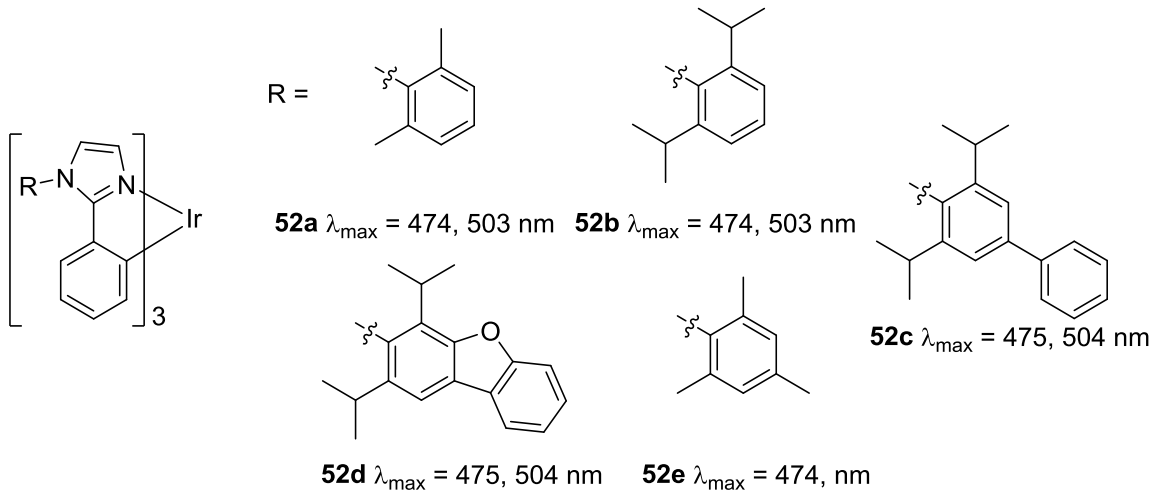

Figure 3.12

withdrawing pyridinium fragment *para* to the cyclometalating carbon.

The pyridine fragment can also be replaced with other moieties that increase the ligand π-π* gap; one example is carbenes, which will be discussed in Chapter 6. These are strong σ-donors that increase the energy of d-d* states as well as the emissive states. Another example is N-aryl/alkyl imidazoles, whose increased donor ability compared to pyridine results in a larger shift of the LUMO than the HOMO, leading in turn to an increased HOMO-LUMO gap compared to ppy ligands.[17] A collection of blue emitting N-aryl imidazole complexes is shown in Figure 3.12.[18,19] Here, aryl groups with *ortho* substituents have been chosen to avoid extending the conjugation, and thereby red-shifting the emission.[19] These complexes displayed sky blue emission and two exhibited increased thermal stability compared to FIrpic (T_d = 429 °C for **52b**, T_d = 416 °C for **52b** , and T_d = 412 °C for **52e** compared to T_d = 344 °C for FIrpic [20]). All the complexes also showed increased device stability compared to FIrpic, with test devices of **52a-d** achieving T_{50} values (defined as the time when luminance of a device has dropped to half its initial value) of 4.6-5.8 h, whereas T_{50} = 0.1 h for the comparable FIrpic device.[18,19]

Another fragment that can be used to replace the pyridine group in ppy-based ligands is the triazole group; examples of sky-blue triazole complexes are shown in Figure 3.13.[21] Due to the unsymmetrical substitution on the phenyl rings the ligands display atropisomerism, and upon complexation diastereomers are formed which can be separated by column chromatography.[21] The isomers show slight differences in photophysical properties, with small changes in spectral width and λ_{max}. The *ortho* methyl group ensures a break in conjugation between the phenyl and triazole ring, which prevents a red-shift in emission.[21]

A pyrazole group has also been used, with some complexes shown in Figure 3.14. Although the

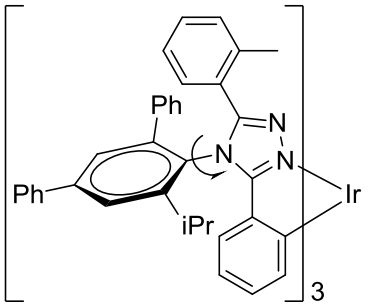

Δ/Λ chirality at Ir:
53a Λ- MMM/Δ-PPP
53b Δ-MPP/Λ-PMM
53c Λ-MPP/Δ-PMM
53d Δ-MMM/Λ-PPP

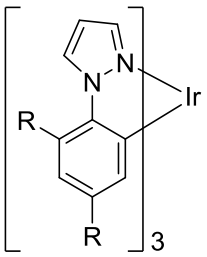

54a R = H
λ_{max} (77 K) = 412 nm
ϕ(298 K) < 0.01
54b R = F
λ_{max} (77 K) = 388 nm
ϕ(298 K) < 0.01

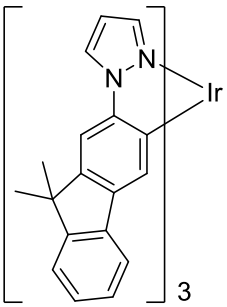

54c Ir(flz)$_3$
λ_{max} (298 K) = 478 nm
ϕ(298 K) = 0.81

Figure 3.13: LEFT: Triazole complexes for fluorine-free sky blue emission. RIGHT: Pyrazole complexes for fluorine-free sky/deep blue emission.

pyrazole group is effective at blue-shifting the emission colour it pushes the energy of the emissive state close enough to non-radiative states that emission is not observable at room temperature for most homoleptic complexes.[22] However, complex Ir(flz)$_3$ (**54c**) is emissive at room temperature, due to the extended conjugation of the fluorene unit red-shifting the emission away from the non-radiative state.[22]

RESULTS AND DISCUSSION

Prompted by the formation of novel complexes **31** and **32** and the interesting product of nucleophilic aromatic substitution **29**, nucleophilic aromatic substitution (S_NAr) on the sulfone ligand system was investigated. Due to the withdrawing pyridyl-, fluorine- and sulfone-substituents the phenyl ring should be highly activated towards S_NAr via an addition-elimination reaction at the C-F bonds. Additionally, as identified in the introduction to this chapter, aromatic fluorines in particular have been identified as unstable during device operation and fabrication resulting in a desire to achieve bluer emission without utilising them.

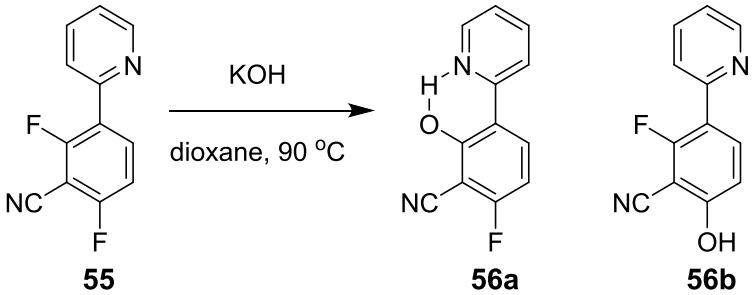

55 **56a** **56b**

Figure 3.14: Nucleophilic aromatic substitution on ligand 55.

The first attempt was to replicate results from earlier work in our group, wherein hydroxide was used to displace one of the fluorines on cyano substituted dfppy **55**.[10] In that work an aqueous solution of KOH (4 M) was added to a solution of ligand **55** in 1,4-dioxane and the mixture heated to reflux for 2 h. There was no selectivity as to which fluorine was replaced, resulting in the two isomers **56a** and **56b** (Figure 3.14) which could not be separated by column chromatography. Their differing solubility in DCM, which allowed them to be separated by a series of filtrations, was ascribed to the ability of **56a** to form intramolecular hydrogen bonds, while **56b** can only form intermolecular hydrogen bonds, which greatly reduced its solubility.[10] As CN and SO_2R are both strongly electron withdrawing it was thought that the new system could also undergo substitution.

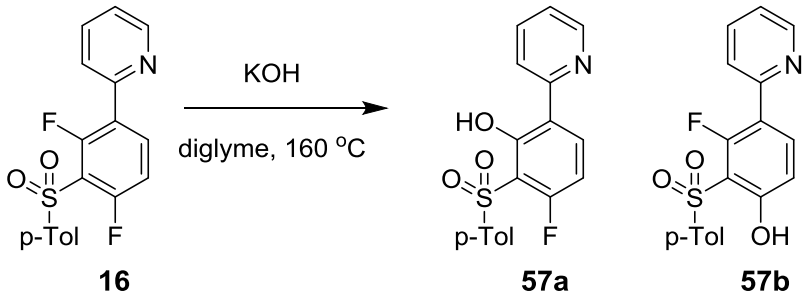

Figure 3.15.

Compound **16** was chosen as the test ligand and the conditions detailed above for **55** were replicated; however TLC analysis of the product mixture revealed only a very small conversion of the starting material. Increasing the reaction time to 72 h produced no detectable change, indicating an increased stability of ligand **16** towards S_NAr compared to **55**. This is consistent with the observation made in Chapter 2, as ligand **16** only underwent a nucleophilic substitution reaction when the temperature was significantly greater than 130 °C (160 °C), as no substitution is seen during synthesis of the heteroleptic complexes. A higher reaction temperature was needed and diglyme (2-methoxyethyl ether) was chosen as the solvent, as it has a high boiling point (162 °C), is water miscible and non-nucleophilic. The last property is particularly important as ethylene glycol was shown to react with **16** at 160 °C. TLC analysis of the reaction in diglyme indicated a much greater conversion than was observed for the reaction in dioxane. NMR analysis confirmed that the reaction was unselective, with both isomers **57a** and **57b** being formed (Figure 3.15).

Attempts to separate **57a** and **57b** by the method described for the **56a**/**b** failed as there seemed to be no difference in their solubility. This was attributed to the presence of the oxygens on the sulfone; these are adjacent to the OHs and could therefore hydrogen bond with them, thus

removing the solubility difference as no isomer is more prone to intramolecular H-bonding than the other. The product mixture was initially obtained in 50% yield (increased to 84% on a second attempt, as the work-up was changed) with an approximately 50:50 ratio of the two isomers (30:70 for **57a**:**57b** on the second attempt) by ^{1}H NMR analysis.

The aim was to emulate previous work by alkylating **57a** and **57b** to produce soluble alkoxy derivatives. It was anticipated that the two alkylated derivatives would suffer similar separation issues to **57a** and **57b**, and so we sought a selective alkylation route. The aim was to use a sterically hindered base to selectively deprotonate the *para* hydroxyl group of **57b**, and then to alkylate the resulting anion. This should result in the formation of the *para* alkoxy compound **58**, with the *ortho* hydroxyl **57a** left unreacted; the mixture could then be purified by column chromatography or using a basic work-up to deprotonate **57a** and potentially solubilise it in the water layer.

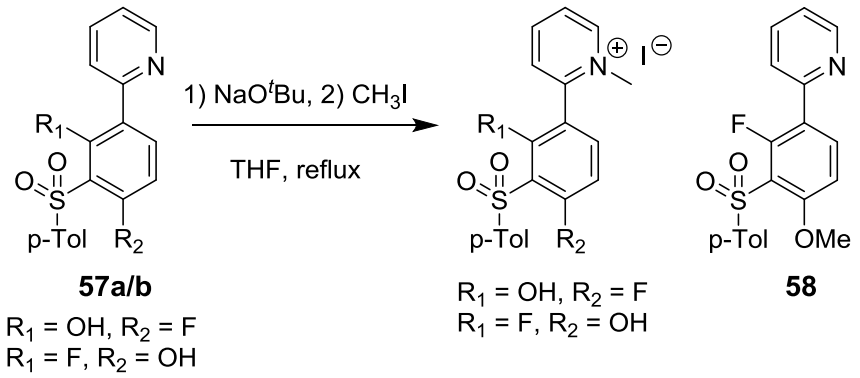

Figure 3.16.

The base chosen was NaO^{t}Bu, and the first alkylating agent investigated was MeI (Figure 3.16); this was selected as there is no possibility of an elimination side reaction occurring, which can happen with hindered bases and alkyl halides. The mixture of **57a** and **57b** was dissolved in dry THF and NaO^{t}Bu and one equivalent of MeI (based on the ratio of the mixture) was added. After work up, the ^{1}H NMR characterisation and TLC analysis revealed that, although the methylation of the hydroxyl was selective for the isomer desired, the majority of the product and starting material were converted into N-methyl pyridinium salts. An attempt was made to convert the salts to free pyridines using PPh_3,[23] however even with long reaction times and at high temperatures (150 ^{O}C) the yield was low (29%) and there was concern that longer reaction times would result in decomposition. Methyl tosylate was chosen as an alternative alkylating agent, however it produced similar results; after work-up and purification by column chromatography **58** was obtained in 18% yield, with unreacted starting material **57a**/**b** (32%) and (presumed)

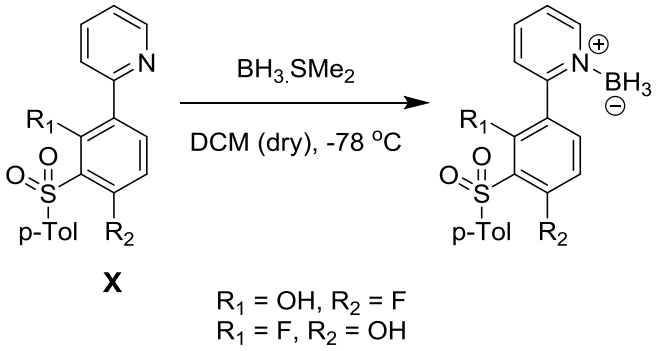

Figure 3.17.

pyridinium salts (30%) also isolated. The alkylating agent was then changed to a less reactive alkyl bromide, 1-bromooctane, and the reaction was conducted as before. Unreacted starting material **57a**/**b** (60%) and pyridinium ions were isolated but there was no evidence of any desired product formation.

As the pyridine lone pair was proving problematic an attempt was made to introduce a protecting group. An N-oxide was considered; however alkyl halides are known to react with N-oxides to give O-alkylated products and it was thought that N-oxides could be difficult to remove without reaction at the sulfone. Another option was the use of a borane as a protecting group, as detailed by Zajac.[24] In this case $BH_3.SMe_2$ was used to protect the pyridyl nitrogen in a molecule containing an aminopyridine and an alkyl halide, as on treatment with base, if the pyridyl nitrogen is unprotected, intramolecular cyclisation occurs.[24] This approach could potentially be applied to the pyridyl in **57a**/**57b** (Figure 3.17), however, boron is known to coordinate well with oxygen and therefore could easily coordinate to the sulfone or the hydroxyl instead, which would inhibit reaction with the alkylating agent or prompt unwanted side reactions. A small sample was tested; the starting material mixture was dissolved in dry DCM and cooled to -78 °C. Then $BH_3.SMe_2$ was slowly added, and the solution was stirred at -78 °C for 30 min. After the reaction was worked up the product was characterised by ^1H and ^{11}B NMR, which indicated the formation of multiple products. In particular the ^{11}B NMR showed three distinct peaks, none of which corresponded to

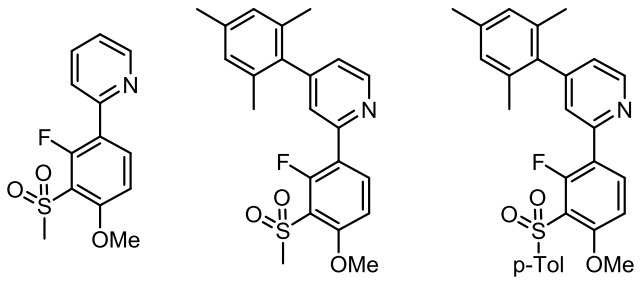

Figure 3.18.

the starting material, which is reported to give a peak at -20.2 ppm in $CDCl_3$.[25] This suggests that coordination to other sites in the molecule is occurring, which prevents the use of BH_3 as a protecting group for this system.

Due to the small amount of ligand obtained from this route the synthesis was changed. The previous work conducted on the ligands derived from **56a**/**b** noted no difference in emission colour between the complexes with the methoxy *para*- or *ortho*- to the pyridyl group, although the *para* complex displayed a slightly higher PLQY;[10] hence we chose the target ligand with a *para* methoxy substituent. The required boronic acid **59** became commercially available, allowing for a route analogous to that described for the difluoro-complexes in chapter 2 to be followed. The targets **64** and **65**, shown in Figure 3.18, were identified as they were analogous to **15** and **16**, and **66** was later synthesised due to solubility concerns with the heteroleptic complexes of **64** and **65**.

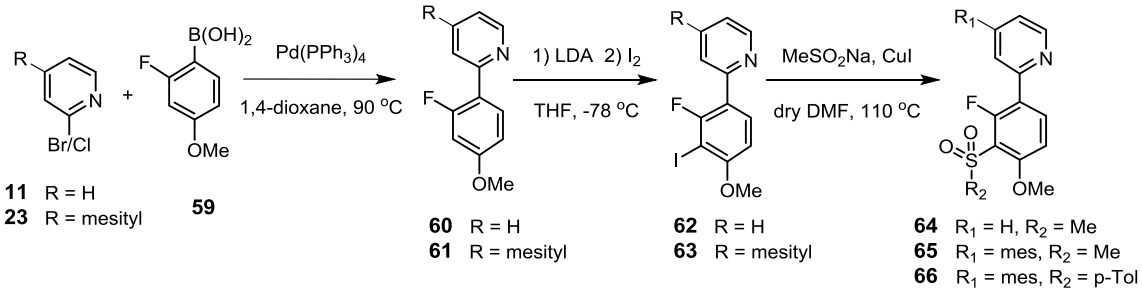

Figure 3.19: Synthesis of target ligands.

The first step (Figure 3.19) for all ligands involved a Suzuki coupling between boronic acid **59** and the required 2-halopyridine derivative **11**, **23**, which was high yielding in both cases (91% and 78%, respectively). The second step introduced iodine by *ortho*-lithiation; this proceeded in comparable yields to the difluoro analogues (58% for **60**, 55% for **61**) and the products were both easily separated from their corresponding starting materials by column chromatography.

The final step in the synthesis was the copper-assisted nucleophilic displacement to introduce the sulfone unit, as used for the difluoro complexes.[26] For the previous difluoro-substituted ligands **15**, **16** and **26** the yields were low (26%, 17% and 19%, respectively), and attempts to improve them proved unsuccessful. However, in the case of **64** and **65** the yields were significantly higher (45% and 53%, respectively). For **64** the unreacted starting material **62** and the de-iodination product **60** accounted for 27% and 25% of the missing product, respectively. The improved yields could be due to the ability of the methoxy- substituent to better coordinate the copper during the C-I insertion step. For **66** the yield was still low, 21%, the reason for which is unclear.

Prompted by the synthetic route for the dimethoxy- ligand **79**, which will be discussed later in this

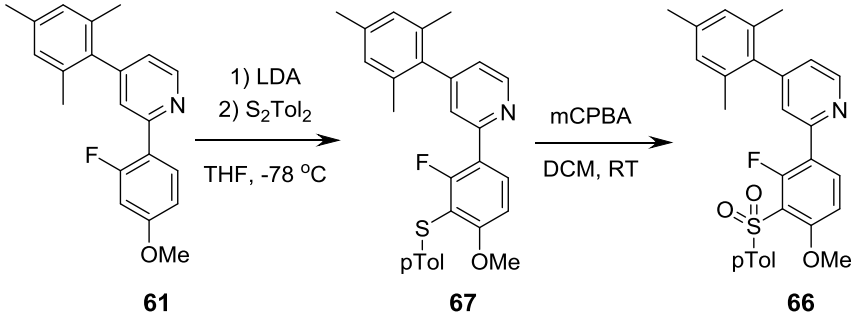

Figure 3.20

chapter, an alternative route was tested for ligand **66** (Figure 3.20). Instead of a lithiation/iodination protocol to create **63**, p-tolyl disulfide was used as the electrophile to yield thioether **67** in 21% yield.

The low yield for this reaction is possibly due to the steric demands of the electrophile. Compound **67** was then oxidised using mCPBA to give the product **66** in 63% yield. Care must be taken at this step to avoid competing oxidation of the pyridine to the N-oxide, as removal of this without reducing the sulfone can prove difficult.

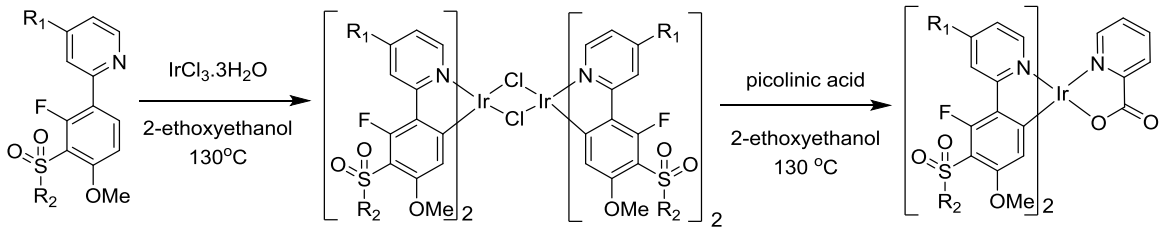

64 R_1 = H, R_2 = Me
65 R_1 = mes, R_2 = Me
66 R_1 = mes, R_2 = p-Tol

68 R_1 = H, R_2 = Me
69 R_1 = mes, R_2 = Me
70 R_1 = mes, R_2 = p-Tol

Figure 3.21: Synthesis of heteroleptic pic complexes.

Once the ligands **64**-**66** were obtained the heteroleptic pic complexes **68**, **69** and **70** were synthesised under modified Lamansky conditions, as described in chapter 2 (Figure 3.21). Water was excluded from the reaction mixture due to the noted sensitivity of fluoroaromatics bearing a strong electron-withdrawing group to nucleophilic attack,[10,12,27] although this risk should be lessened with the exchange of one fluorine for an alkoxy group. The complexes **68**, **69** and **70** were obtained as yellow powders after purification by column chromatography followed by trituration with hot ethanol in the case of **68** (54%) and **69** (70%), and recrystallisation from ethanol in the case of **70** (83%). The fact that a recrystallisation rather than trituration can be carried out for **70** indicates its increased solubility, a property favourable for device applications.

The NMR spectra of the complexes were as expected for heteroleptic pic complexes, and the ^{1}H

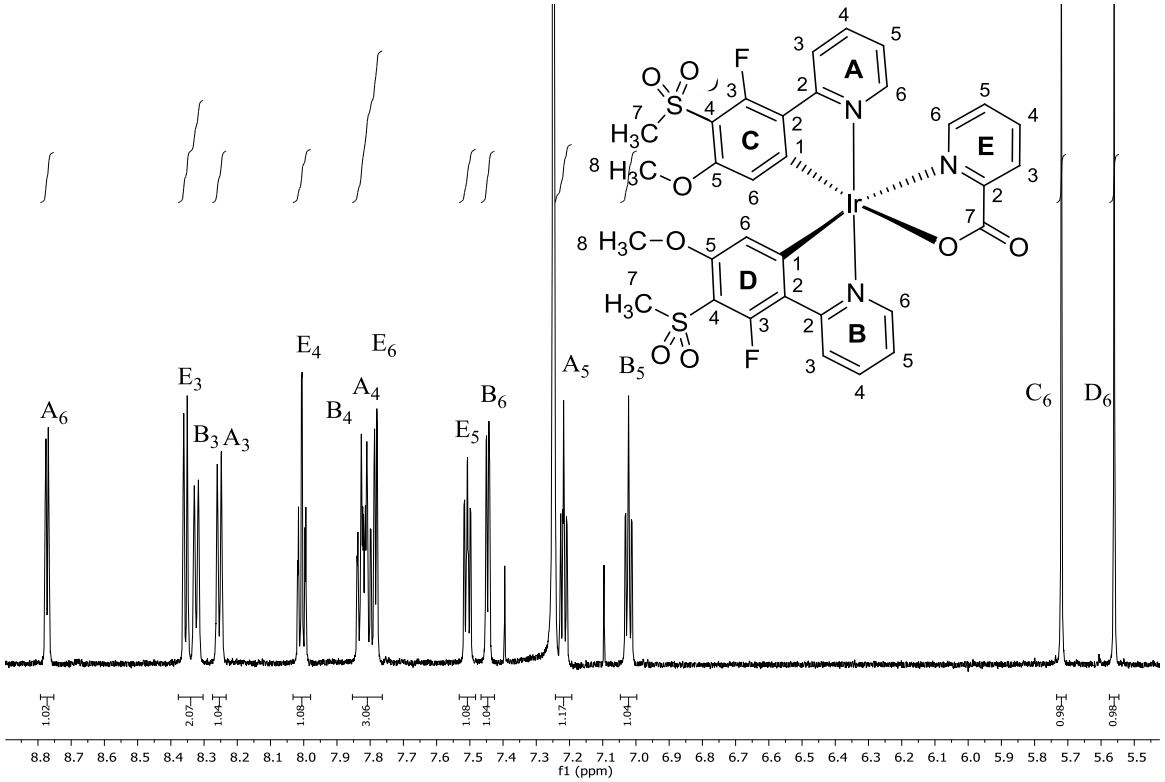

Figure 3.22: ^{1}H NMR spectrum of complex 68.

and ^{13}C spectra of **68** have been fully assigned with the aid of 2D experiments (Figure 3.22, ^{13}C assignment present in the experimental section). As with **19** and **31** the stereochemistry about the metal centre was determined using the NOESY, revealing the expected *trans* orientation of the C^N ligand's nitrogens about the iridium centre, which was confirmed by the crystal structure.

The X-ray crystal structures of **68** and **69** are shown in Figure 3.23, although it should be noted that the crystals of **69** diffracted poorly, giving only a low resolution structure. Both complexes show the expected orientation of ligands around the metal centre for complexes synthesised from the dichloro-bridged dimer; the nitrogens of the chromophoric ligands are *trans* to each other. In

	19	**28**	**68**	**69**
Ir-N(pic)	2.137(3)	2.140(5)	2.129(4)	2.147(7)
Ir-N(ppy-1)	2.046(3)	2.033(5)	2.041(4)	2.008(7)
Ir-N(ppy-2)	2.028(3)	2.033(5)	2.035(4)	2.014(9)
Ir-O(pic)	2.146(2)	2.133(4)	2.142(3)	2.134(12)
Ir-C(ppy-1)	1.991(4)	2.000(6)	1.990(4)	2.006(8)
Ir-C(ppy-2) [b]	1.974(3)	1.986(6)	1.987(4)	1.973(7)

Ppy-1 and 2 are defined as the ligands with carbon atoms opposite the pic N/O, respectively.

Table 3.1: Selected bond distances.

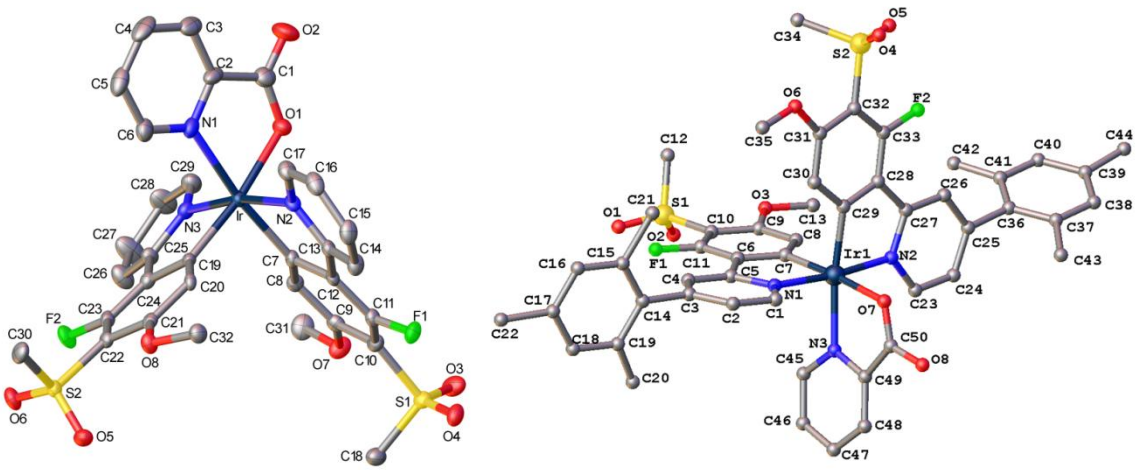

Figure 3.23: LEFT: Molecular structure of 68.CH_2Cl_2, thermal ellipsoids set at 50%, solvent omitted for clarity. RIGHT: Molecular structure of 69.

the case of **69** the twist between the phenyl and pyridyl rings is 0.6-3.4°, whereas for **68** it is much larger (12.7° and 14.7°). The structure for **69** shows significant disorder of the mesityl ring, possibly due to difficulties in cooling the crystal and the presence of disordered solvent in the structure. The dihedral angles between the mesityl and pyridyl rings for **69** were 73.4 and 91.0°, highlighting again the effectiveness of the *ortho* methyl substituents at restricting the conjugation with the pyridyl ring. Selected bond lengths are shown in Table 3.1 and compared to those of FIrpic and the relevant difluoro analogues. The photophysics and electrochemistry of these complexes will be discussed later.

To further extend the 'fluorine-free' idea an analogue of **28** and **69** was designed, namely the dimethoxy-ligand complex **80**, which contains no fluorines. An attempt was made to synthesise ligand **79** via a route analogous to that of the difluoro- (**15**, **16**, **28**) and 2-fluoro-4-methoxy- (**64**-**66**) ligands (Figure 3.24). The first step was a Suzuki coupling between **23** and **71** to give **72** in 68% yield. However, attempted iodination to give **73** failed. It was anticipated that it would not be possible to deprotonate **72** with LDA, as the electron-donating ability of the methoxy substituents reduces the acidity of the proton between them, and, as all the starting material **72** was

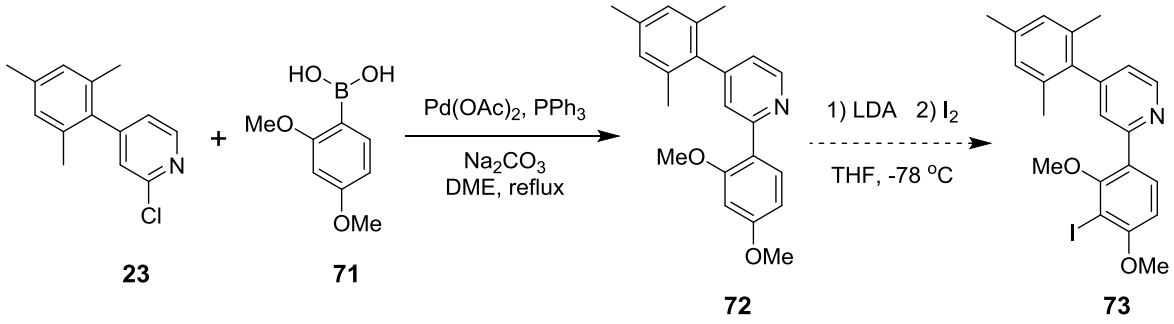

23 **71** **72** **73**

Figure 3.24

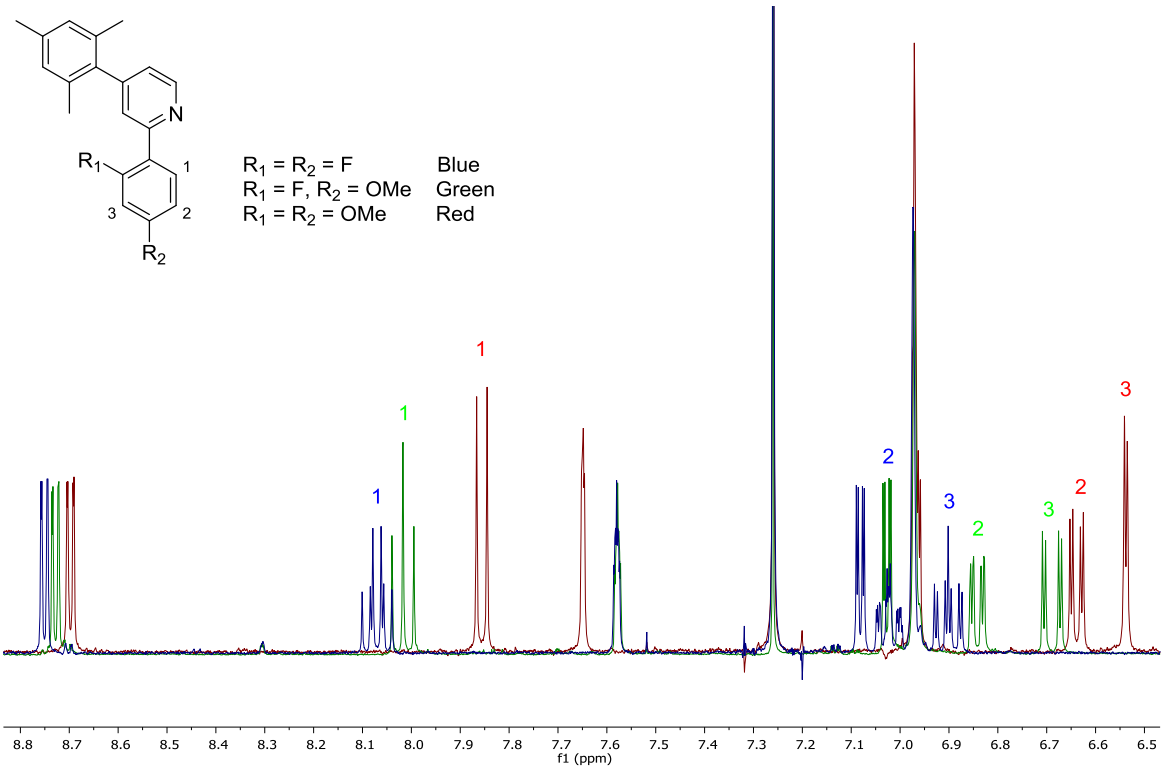

Figure 3.25: ^{1}H NMR spectra of ligand precursors 24, 61 and 72 with protons on the phenyl ring highlighted.

recovered, this was assumed to be the case. Stronger bases such as n-butyllithium were considered; however, pyridyl groups are known to undergo nucleophilic substitution with alkyllithium reagents.[28-30] The change in acidity of the phenyl ring protons upon exchange of each fluorine for a methoxy group can be seen from the ^{1}H NMR spectra (Figure 3.25). Protons 1, 2 and 3 are increasingly shielded with each replacement of fluorine, with the proton nearest to the introduced methoxy group showing the largest shift.

A new route (Figure 3.26) was therefore devised where a methylsulfide substituent was introduced. The first step involves introduction of the methyl sulfide group via *ortho*-lithiation of 1,3-dimethyoxybenzene **74** to give literature compound **75** in 81% yield.[31] Compound **75** is highly activated towards electrophilic aromatic substitution due to the three electron donating substituents, hence monobromination of **75** to give **76** was achieved, using one equivalent of bromine to avoid oversubstitution, in quantitative yield, as described in the literature.[31] The novel boronic acid **77** was then synthesised by lithium-halogen exchange, followed by reaction with $B(OMe)_3$/$B(O^iPr)_3$ and aqueous workup (51% yield). It was noted that **77** is relatively unstable; it deborylates upon storage under ambient conditions over a period of weeks.

Boronic acid **77** was then coupled to **23** via a Suzuki reaction using $Pd(OAc)_2$/PPh_3 as the catalytic system to give **78** in 60% yield, followed by oxidation of the sulfide **78** using *m*-

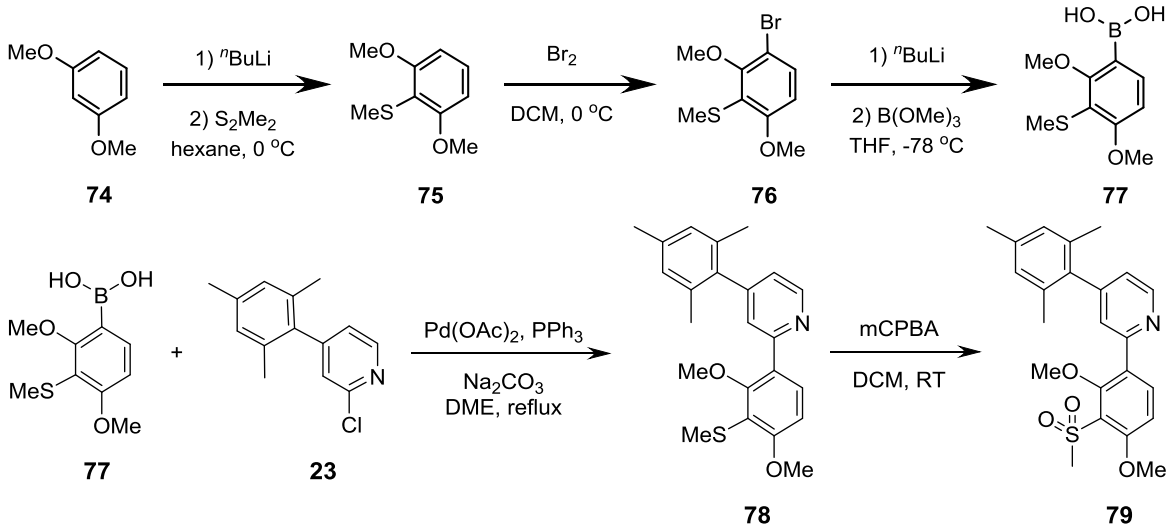

Figure 3.26: Synthesis of target ligand 79.

chloroperoxybenzoic acid to give the sulfone **79** in 83% yield);. During the oxidation a significant amount of material appeared to stick at the top of the column; this was removed with highly polar solvents (water/MeOH) and identified as the pyridine N-oxide by NMR and mass spectroscopy analysis. This was observed even when only two equivalents of mCPBA were used, and it proved difficult to selectively reduce this N-oxide without also reducing the sulfone.

During the course of this work it was discovered that the pyridine nitrogen could be 'protected' as the pyridinium HCl salt **78a**, which minimised N-oxide formation. After oxidation the reaction mixture was treated with a basic workup to deprotonate the HCl salts, and **79** was isolated after column chromatography in 83% yield. The sulfide group was not oxidised prior to the Suzuki coupling due to concerns that a sulfone group may interfere with the lithiation steps.

Initial attempts to synthesise complex **80** from $IrCl_3.H_2O$ and **79** proved unsuccessful; the dimer did not appear to form, as a result when picolinic acid was added to the mixture the major product was $Ir(pic)_3$. Difficulties inducing cyclometalation of ligands containing methoxy

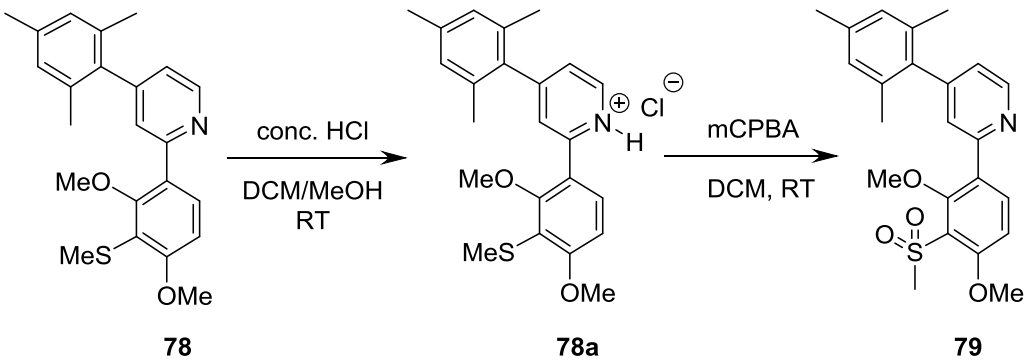

Figure 3.27: Protection of the pyridine nitrogen.

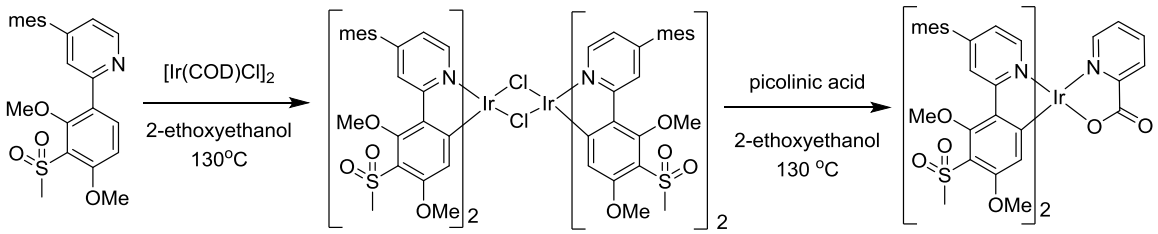

Figure 3.28

substituents have been reported previously, and in that case the alternative iridium source $[Ir(COD)Cl]_2$ was used to synthesise the dimers with great success.[11] $[Ir(COD)Cl]_2$ typically reacts with cyclometalating ligands via oxidative addition, due to the low oxidation state of the metal, whereas $IrCl_3$ cyclometalates via electrophlic aromatic substitution.[32] The $[Ir(COD)Cl]_2$ was prepared by refluxing $IrCl_3.3H_2O$ with 1,5-cyclooctadiene in isopropanol/water overnight, and upon repeating the reaction the intermediate dimer now appeared to form. This was reacted *in situ* with a minimum amount of picolinic acid in an attempt to suppress ligand exchange. The product **80** was isolated after column chromatography as an off-yellow solid in 40% yield (Figure 3.28).

PHOTOPHYSICAL AND ELECTROCHEMICAL PROPERTIES

Absorption and emission

The absorption spectra for complexes **68**-**70** and **80** in DCM are shown in Figure 3.29. As with the difluoro complexes, they show strong absorption bands in the 250-300 nm region; these were

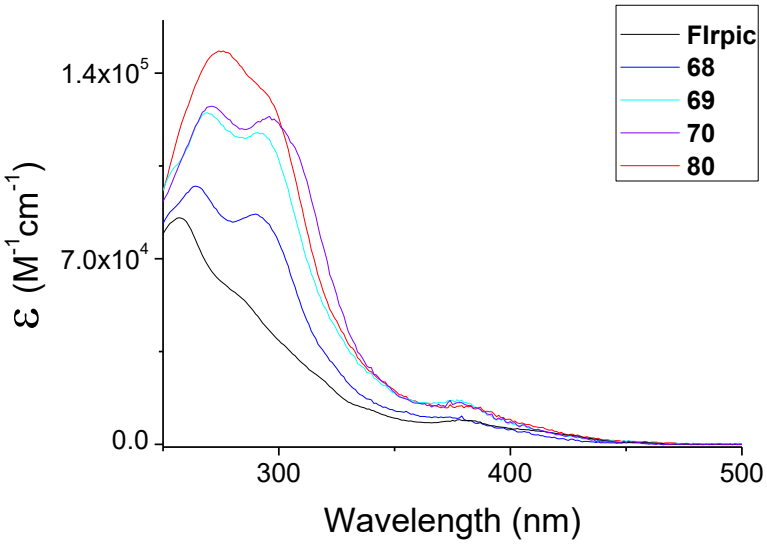

Figure 3.29: Absorption spectra of listed complexes in DCM [<10^{-5} M].

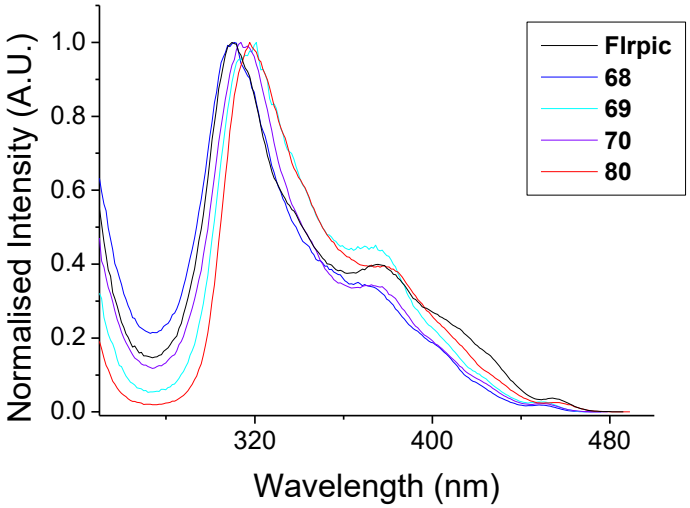

Figure 3.30: Excitation spectra of the complexes in DCM [<10^{-5} M]. The emission band observed was the second emission maximum.

assigned to π-π* transitions on the ligand based on the calculations of Hay,[33] and literature precedent.[34] At lower energies the complexes display sets of absorption bands with lower oscillator strengths at 350-420 nm, assigned to the ^{1}MLCT transitions, and at even longer wavelengths and smaller oscillator strengths the ^{3}MLCT bands can be identified. As with the difluoro complexes the ^{3}MLCT state is a major component of emissive state of these complexes, and the wavelength of this absorption band correlates with the λ_{max} of the emission. For complexes **68**, **69** and **70** the bands are all at similar wavelengths, 449-450 nm, indicating that the R group in the -SO_2R substituent and the addition of the mesityl group both have little effect.

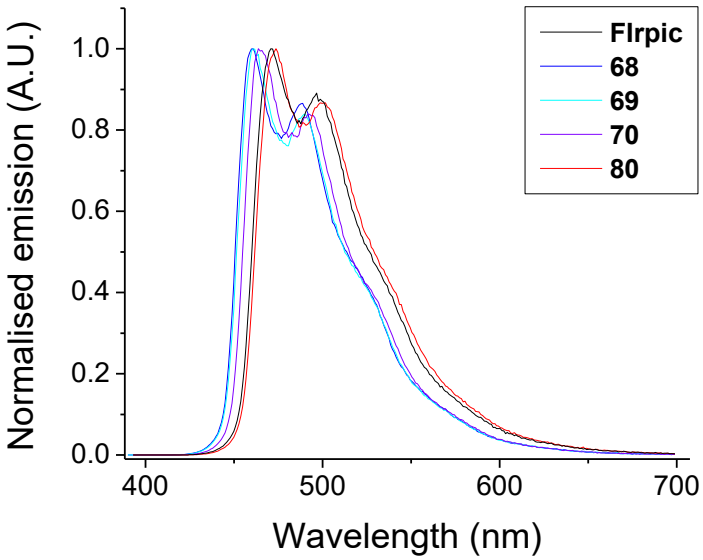

Figure 3.31: Emission spectra of the complexes in deaerated DCM [<10^{-5} M], λ_{ex} = 380 nm.

There is approximately 5 nm of red-shift compared to their difluoro analogues (**19**, **20** and **28**), indicating that the donating methoxy substituent results in a small decrease in the $\Delta E_{HOMO\text{-}LUMO}$.

Importantly, this is still a blue-shift compared to FIrpic, which has a λ_{max} at 454 nm. The ^{3}MLCT band for the dimethoxy- complex **80** has a λ_{max} at 456 nm, suggesting that the emission colour of the two complexes should be similar, provided the bandwidth of the spectra are comparable.

Excitation spectra for all complexes were recorded (Figure 3.30), revealing that the bands from the ^{1}MLCT and ^{3}MLCT states are responsible for the emission from the complexes, as expected, while the majority of the lower energy π-π* transitions are dark.

The emission spectra of the complexes are shown in Figure 3.31. The spectra of **68**, **69**, **70** and **80** also exhibit a similar profile to that of FIrpic, with an emission maximum, vibronic progression and a shoulder at longer wavelengths, indicating that the emission originates from a similar excited state. As with the of difluoro complexes the emission is consistent with a mixed LC/MLCT state, due to the vibronic nature of the emission. The emission from **68**, **69** and **70** is blue-shifted by 6-8

Complex	λ_{max}^{abs} (ε) / nm (x10^3 M^{-1}cm^{-1})[a]	λ_{max}^{em} / nm[b]	PLQY / Φ_{PL}[a,d]	τ_P / μs[a,e]	k_r / 10^5 s^{-1} [f]	k_{nr} / 10^5 s^{-1} [f]
1 FIrpic	277 (50.1), 301 (34.2), 304 (32.6), 337 (13.8, sh), 357 (8.9, sh), 400 (6.2), 454 (0.8)[c]	468, 496, 531 (sh)	0.67	1.72	3.90	1.92
68	253 (89.0), 264 (97.7), 290 (87.0), 319 (sh, 35.6), 372 (10.2), 406 (s sh, 4.5), 449 (0.6)	460, 489, 522 (sh)	0.63	2.67	2.36	1.39
69	255 (99.0), 269 (118.1), 291 (110.6), 336 (s sh, 27.6), 376 (15.9), 402 (sh, 6.8), 450 (0.9)	461, 489, 523 (sh)	0.67	1.79	3.74	1.84
70	258 (s sh, 108.5), 271 (128.6), 297 (123.4), 307 (sh, 112.5), 339 (s sh, 29.2), 379 (15.7), 450 (1.0)	462, 490, 524 (sh)	0.67	1.78	3.76	1.85
80	275 (104.4), 291 (101.9), 324 (sh, 47.8), 381 (14.5), 405 (sh, 7.9), 456 (0.9)	469, 497, 536 (sh)	0.58	2.13	2.72	1.97

[a] Data obtained in dichloromethane solution at 20 °C. [b] Data obtained in degassed dichloromethane solution with λ_{ex} = 380 nm. [c] Energy difference between lowest energy excitation maxima and highest energy excitation maxima. [d] Measured relative to Ir(ppy)$_3$ Φ_{PL} = 0.46 in degassed dichloromethane at 20 °C; estimated error ±5%. [e] Estimated error ±5%. [f] k_r, k_{nr} values calculated using Equations 1.5/1.6.

Table 3.2: Photophysical data for selected iridium complexes

nm relative to that of FIrpic, a red-shift of only ~2 nm compared to the analogous difluoro-complexes **19** and **20**. This indicates that the methoxy group is less effective than fluorine at blue-shifting the emission, although the change is small when only one fluorine is exchanged.

The PLQYs, lifetimes (τ_{obs}) and calculated radiative and non-radiative decay rates (k_r and k_{nr}) are shown in Table 3.2. The PLQYs for complexes **68**, **69**, **70** and **80** are all comparable with their analogous difluoro complexes (**19**, **20**, **28**). The lifetimes are on the order of 1-3 μs. These are typical values for mono-iridium complexes with efficient spin-orbit coupling between the triplet and singlet states.[35]

Electrochemistry

The electrochemical behaviour of complexes **68**-**70** and **80** was investigated using cyclic voltammetry and compared to the parent compound FIrpic and their difluoro analogues (**19**, **20**, **28**). The voltammograms are shown in Figure 3.32 and the key parameters in Table 3.3. Formula 2.1 is used to calculate the energy of the HOMO.

Complex	$E^{ox}_{1/2}$ / V	HOMO / eV
FIrpic	0.89	-5.69
68	1.02	-5.82
69	1.02	-5.82
70	1.01	-5.81
80	0.89	-5.69

All values reported vs Fc/Fc^+ = 0.00 V.

Table 3.3: Electrochemistry data of iridium complexes. Measured in MeCN (0.1 M $^nBu_4NPF_6$) at 298 K.

The complexes all show a quasireversible oxidation wave which was assigned to the Ir^{III}/Ir^{IV} couple. Compared to the difluoro complexes (**19**, **20**, **28**), all the mono-fluoro complexes (**68**-**70**) display less positive oxidation potentials, with a difference of 0.13-0.17 V. This is expected, as the HOMO is localised on the phenyl rings of the C^N ligand, and an electron withdrawing fluorine has been exchanged for an electron donating methoxy group which will raise the orbital energies. The oxidation potentials are still more positive than that of FIrpic, suggesting that if the LUMO remains at a similar energy the HOMO-LUMO gap for the mono fluoro complexes (**68'**, **69'**, **70'**) will be larger, and the emission bluer, than that of FIrpic. This is supported by experimental observation. As with the difluoro complexes there is little variation upon changing the identity of R in $–SO_2R$, or upon addition of the mesityl group. The dimethoxy complex **80** has a similar oxidation potential to FIrpic, and as the emission colour is similar it suggests that the HOMO-

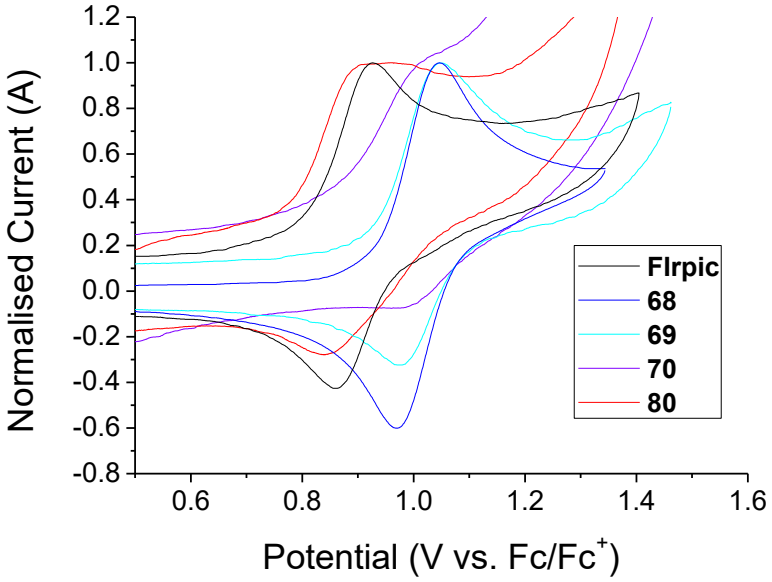

Figure 3.32: Cyclic voltammograms of 68, 69, 70 and 80.

LUMO gap is similar, creating a 'fluorine-free' alternative. No reduction waves were observed within the solvent window.

COMPUTATIONAL DATA

Electronic structure calculations were carried out on iridium complexes **68**-**70** and **80** by Dr Mark Fox (Department of Chemistry) to elucidate the nature of the frontier orbitals and the transitions involved in the absorption and emission spectra. The full geometries were optimised at the B3LYP/LANL2DZ:3-21G* level of theory and are denoted **68'**, **69'**, **70'**, **80'** to distinguish them from experimental data. Comparison with optimised and experimental geometries determined from the X-ray data for **68** revealed good agreement for the Ir-X bond distances (Table 3.4). The orbital energies were computed for **68'**, **69'**, **70'**, **80'** and show good agreements with the observed

	68	**68'**
Ir-N(ppy)	2.042(4)	2.061
Ir-N(ppy)	2.035(4)	2.048
Ir-C *trans* N	1.988(5)	2.015
Ir-C *trans* O	1.985(5)	2.013
Ir-O	2.143(4)	2.140
Ir-N(pic)	2.129(4)	2.164

Table 3.4: Comparison of the experimental (68) and optimised (68') bond lengths involving the iridium atom.

Complex	HOMO / eV	Calc HOMO / eV	Calc LUMO / eV	Calc ΔE_{HL} gap
FIrpic 1	-5.69	-5.49	-1.87	3.62
68	-5.82	-5.82	-2.06	3.76
69	-5.82	-5.74	-2.00	3.74
70	-5.81	-5.64	-1.94	3.70
80	-5.69	-5.53	-1.89	3.64

Table 3.5: Comparison between experimental HOMO energies (estimated from observed oxidation potentials) and the calculated HOMO/LUMO energies.

oxidation potentials (Table 3.5). As expected, the exchange of a fluorine for a methoxy (**19'** to **68'**, **28'** to **69'** then **80'**) results in an increase of the HOMO level relative to the LUMO, resulting in a decrease in the HOMO-LUMO gap, which correlated well with the observed emission λ_{max}. This reflects the greater donor ability of the methoxy group compared to fluorine. The frontier orbital distributions for **68'**, **69'**, **70'**, **80'** are similar to FIrpic, with the HOMO largely localised on the metal d orbitals (39-41%) and the phenyl ring (42-45%) and the LUMO localised mostly on thepyridine of the pic ligand (78-82%). Notably the orbital distribution and energies of **80'** and FIrpic are very similar, suggesting **80** should be a good replacement for FIrpic in devices.

TD-DFT computations were carried out on the S_0 optimised geometries of **68'**, **69'**, **70'** and **80'** to predict emission wavelengths of these iridium complexes. The initial excitation is assumed to give the lowest energy singlet excited state S_1 which then undergoes intersystem crossing (ISC) due to the SOC induced by the iridium centre to form the triplet excited state T_1. Phosphorescence is then observed from the $S_0 \leftarrow T_1$ process. Complexes **68'**, **69'**, **70'** and **80'** display small Stokes shifts, suggesting that the T_1 geometry is similar to the corresponding S_0 geometry. The reverse

Complex	$S_0 \leftarrow T_1$ nm[a]	Complex	Observed λ_{max}^{em} / nm[b]
1'	471	**1**	471
68'	463	**68**	460
69'	467	**69**	461
70'	467	**70**	464
80'	473	**80**	474

[a] Values from TD-DFT data on S_0 optimized geometries with scaling energy factor of 0.945 based on dichloromethane at 298 K. [b] Observed highest energy band from emission spectra.

Table 3.6: Comparison between calculated and observed emission wavlengths.

process $S_0 \leftarrow T_1$ is therefore considered to have the same nature as the computed $S_0 \rightarrow T_1$process, with the predicted emission wavelength adjusted to take into account the Stokes shift. The predicted and observed emission wavelengths are shown in Table 3.6, it can be seen that there is good agreement for all complexes.

DEVICE DATA

OLEDs containing complexes **68**, **69**, **70** and **80** were fabricated by Dr Hameed Al Attar in the Department of Physics at Durham University and compared to a reference device containing

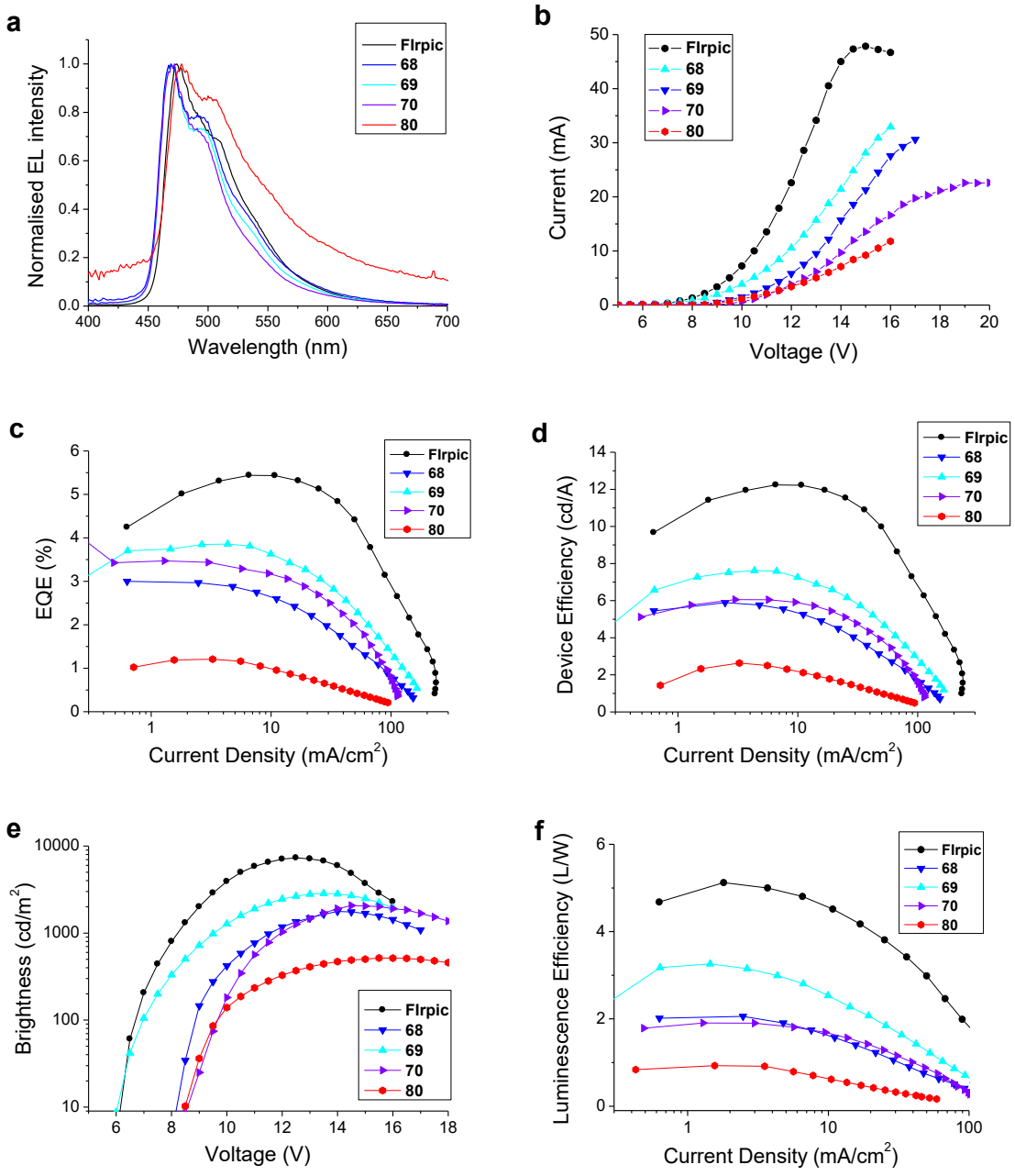

Figure 3.34: Device data for complexes 68, 69, 70, 80

FIrpic. The hole transporting layer and emissive layer were deposited by spin-coating and the electron transporting, electron injection layers and the cathode were then fabricated by vacuum deposition. The device structure is as follows: ITO/PEDOT:PSS (45 nm)/PVK:OXD(30%):**Ir complex**(15%)(60 nm)/TPBi (30 nm)/LiF/Al. The electroluminescence (EL) spectra from the devices are shown in Figure 3.35, panel a; for all complexes the EL spectra are similar to the photoluminescence (PL) spectra, indicating good exciton confinement on the emissive molecule. Complexes **69** and **70** containing the mesityl substituent were the best performing of the complexes synthesised in this chapter, with maximum EQEs of 3.9% and 3.4%, respectively (panel c). Complexes **68** and **80** gave less efficient devices; in the case of **68** this can be rationalised by the lack of the mesityl substituent, however, the reason for the poor performance of **80** is unclear. Compared to FIrpic, all complexes gave lower EQEs (panel c), lower efficiencies (panel d) and lower maximum brightnesses (panel e), although the mono-fluorinated complexes (**68**, **69**, **70**) display bluer electroluminescene than FIrpic (panel a), which could be partially responsible for their lower performance. The device of **69**, however, exhibits a lower turn on voltage than the FIrpic device, and comparable brightness when operated at less than 7 V (panel e).

Complex	λ_{ELmax} / nm	Brightness / cd/m^2	turn-on voltage / V [a]	EQE / %	current efficiency / cd/A	power efficiency / lm/W	CIE coordinates / (x,y)[b]
FIrpic 1	475	7340	6.2	5.4	12.2	5.1	(0.19, 0.38)
68	469	1772	8.1	3.0	5.9	2.1	(0.17, 0.33)
69	469	2851	6.0	3.9	7.6	3.3	(0.17, 0.32)
70	470	2072	8.5	3.5	6.1	1.9	(0.16, 0.30)
80	478	516	8.5	1.2	2.6	0.9	(0.22, 0.40)

[a] Measured at a brightness of 10 cd/m^2. [b] Measured at 12 V.

Table 3.7: Summary of device data.

CONCLUSION

The family of sulfone-containing complexes introduced in Chapter 2 has been extended by the synthesis of complexes **68**, **69**, **70** and **80**, which contained fewer aromatic fluorines. The photophysical and electrochemical properties were compared to the parent complex FIrpic, and the difluorinated sulfone containing complexes **19**, **20**, **28**. While a small red-shift is observed on exchanging one fluorine for a methoxy group, complexes **68**, **69**, **70** still displayed bluer emission than FIrpic, as well as comparable quantum yields and lifetimes. Complex **80** provides a viable fluorine-free alternative to FIrpic, with similar emission wavelength, HOMO/LUMO energies and

similar orbital distributions, as indicated by the computational data. Devices of all complexes fabricated in the Department of Physics retain the blue emission obseved in the PL spectra, and the best two complexes, **69** and **70**, performed comparably to the best of the difluoro complexes of Chapter 2, **28**. Devices were fabricated by solution processing, and the solubility has been enhanced compared to FIrpic by the sulfone and mesityl groups.

References

1) V. Sivasubramaniam, F. Brodkorb, S. Hanning, H. P. Loebl, V. van Elsbergen, H. Boerner, U. Scherf and M. Kreyenschmidt, *J. Fluorine Chem.,* 2009, **130**, 640-649
2) S. Scholz, D. Kondakov, B. Lüssem and K. Leo, *Chem. Rev.,* 2015, **115**, 8449-8503
3) K. F. Jeltsch, G. Lupa and R. T. Weitz, *Org. Electron.,* 2015, **26**, 365-370
4) D. Tordera, J. J. Serrano-Pérez, A. Pertegás, E. Ortí, H. J. Bolink, E. Baranoff, M. K. Nazeeruddin and J. Frey, *Chem. Mater.,* 2013, **25**, 3391-3397
5) W.-H. Zhang, X.-H. Zhang, A. L. Tan, M. A. Yong, D. J. Young and T. S. A. Hor, *Organometallics,* 2012, **31**, 553-559
6) M. Lepeltier, F. Dumur, J. Marrot, E. Contal, D. Bertin, D. Gigmes and C. R. Mayer, *Dalton Trans.,* 2013, **42**, 4479-86
7) L. Li, F. Wu, S. Zhang, D. Wang, Y. Ding and Z. Zhu, *Dalton Trans.,* 2013, **42**, 4539-43
8) Y. Zheng, A. S. Batsanov, R. M. Edkins, A. Beeby and M. R. Bryce, *Inorg. Chem.,* 2012, **51**, 290-7
9) D. Tordera, M. Delgado, E. Ortí, H. J. Bolink, J. Frey, M. K. Nazeeruddin and E. Baranoff, *Chem. Mater.,* 2012, **24**, 1896-1903
10) V. N. Kozhevnikov, K. Dahms and M. R. Bryce, *J. Org. Chem.,* 2011, **76**, 5143-8
11) J. Frey, B. F. Curchod, R. Scopelliti, I. Tavernelli, U. Rothlisberger, M. K. Nazeeruddin and E. Baranoff, *Dalton Trans.,* 2014, **43**, 5667-79
12) H. Oh, K.-M. Park, H. Hwang, S. Oh, J. H. Lee, J.-S. Lu, S. Wang and Y. Kang, *Organometallics,* 2013, **32**, 6427-6436
13) C. H. Chang, Z. J. Wu, C. H. Chiu, Y. H. Liang, Y. S. Tsai, J. L. Liao, Y. Chi, H. Y. Hsieh, T. Y. Kuo, G. H. Lee, H. A. Pan, P. T. Chou, J. S. Lin and M. R. Tseng, *ACS Appl. Mater. Interfaces,* 2013, **5**, 7341-51
14) T. Duan, T.-K. Chang, Y. Chi, J.-Y. Wang, Z.-N. Chen, W.-Y. Hung, C.-H. Chen and G.-H. Lee, *Dalton Trans.,* 2015, **44**, 14613-14624
15) J. Lee, H. Oh, J. Kim, K.-M. Park, K. S. Yook, J. Y. Lee and Y. Kang, *J. Mater. Chem. C,* 2014, **2**, 6040-6047
16) B. J. Coe, M. Helliwell, S. Sanchez, M. K. Peers and N. S. Scrutton, *Dalton Trans.,* 2015, **44**, 15420-15423
17) H. J. Bolink, F. De Angelis, E. Baranoff, C. Klein, S. Fantacci, E. Coronado, M. Sessolo, K. Kalyanasundaram, M. Gratzel and M. K. Nazeeruddin, *Chem. Comm.,* 2009, 4672-4674
18) J. Zhuang, W. Li, W. Su, Y. Liu, Q. Shen, L. Liao and M. Zhou, *Org. Electron.,* 2013, **14**, 2596-2601
19) J. Zhuang, W. Li, W. Wu, M. Song, W. Su, M. Zhou and Z. Cui, *New J. Chem.,* 2015, **39**, 246-253
20) I. R. Laskar, S.-F. Hsu and T.-M. Chen, *Polyhedron,* 2006, **25**, 1167-1176
21) J. Feldman, G. D. Vo, C. D. McLaren, T. C. Gehret, K.-H. Park, J. S. Meth, W. J. Marshall, J. Buriak, L. M. Bryman, K. D. Dobbs, T. H. Scholz and S. G. Zane, *Organometallics,* 2015, **34**, 3665-3669
22) T. Sajoto, P. I. Djurovich, A. B. Tamayo, J. Oxgaard, W. A. Goddard, 3rd and M. E. Thompson, *J. Am. Chem. Soc.,* 2009, **131**, 9813-22
23) U. Berg, R. Gallo and J. Metzger, *J. Org. Chem.,* 1976, **41**, 2621-2624
24) M. A. Zajac, *J. Org. Chem.,* 2008, **73**, 6899-6901
25) C. S. Shiner, C. M. Garner and R. C. Haltiwanger, *J. Am. Chem. Soc.,* 1985, **107**, 7167-7172
26) H. Suzuki and H. Abe, *Tetrahedron Lett.,* 1995, **36**, 6239-6242
27) H. Benjamin, MSci, University of Durham, 2012
28) G. Fraenkel and J. C. Cooper, *Tetrahedron Lett.,* 1968, **9**, 1825-1830
29) R. K. Bansal, *Heterocyclic Chemistry,* New Age International Limited, 1999
30) C. S. Giam and J. L. Stout, *J. Chem. Soc. D,* 1969, 142-142
31) P. Jacob and A. T. Shulgin, *J. Med. Chem.,* 1981, **24**, 1348-1353
32) S. M. W. Rahaman, S. Dinda, T. Ghatak and J. K. Bera, *Organometallics,* 2012, **31**, 5533-5540
33) P. J. Hay, *J. Phys. Chem. A,* 2002, **106**, 1634-1641

34) C. Adachi, R. C. Kwong, P. Djurovich, V. Adamovich, M. A. Baldo, M. E. Thompson and S. R. Forrest, *Appl. Phys. Lett.,* 2001, **79**, 2082
35) H. Meng and N. Herron, *Organic Small Molecule Materials for Organic Light Emitting Diodes* in *Organic Light-Emitting Materials and Devices*, Ed. Z. M. Li, H., CRC Press, 2006, 369

Chapter 4: Dual emissive phosphorescent materials

Compounds that display broad emission spectra are of great interest for lighting applications, including white OLEDs (WOLEDs).[1,2] One origin of broad spectral emission is dual emission, wherein emission occurs approximately simultaneously from two distinct excited states of the same compound. For iridium complexes one method of accomplishing this is to incorporate them into polymer chains containing other emissive materials of different colours, details of which can be found in the following reviews: Farinola *et*. *al*.,[2] Xiao *et*. *al*.,[3] and Ulbricht *et*. *al*.[4] The other alternative involves emission from two distinct excited states of a single iridium complex; reports of this in the literature are rare, and among the reported examples there are a variety of mechanisms responsible for the dual emission character.

In the case of complex **81b** (Figure 4.1), a neutral *mer*- homoleptic complex, the two main emission features are vibronic bands in the blue region (P_1 400-500 nm) and a broad, featureless band in the red region (P_2 550 nm).[5] On lowering the temperature the intensity of the P_1 increases dramatically, along with an increase in the lifetime (4.9 ns at 298 K to 236 ns at 218 K).[5] Experimental observations and TD-DFT calculations ascribed the dual phosphorescence character to the existence of two triplet states: an intra-ligand charge transfer (ILCT) state of pyrazolate → pyridine character, with a small MLCT contribution (10%), and a second localised ligand to ligand charge transfer (LLCT) state of pyrazolate → pyridine character, with a greater MLCT contribution (20%).[5] Although the LLCT state is predicted to have higher energy than the ILCT state by TD-DFT, due to the increased MLCT character of the LLCT state the Ir-L bond lengths are predicted to be lengthened, resulting in a lowering of the LLCT state. The P_1 band is therefore assigned to the

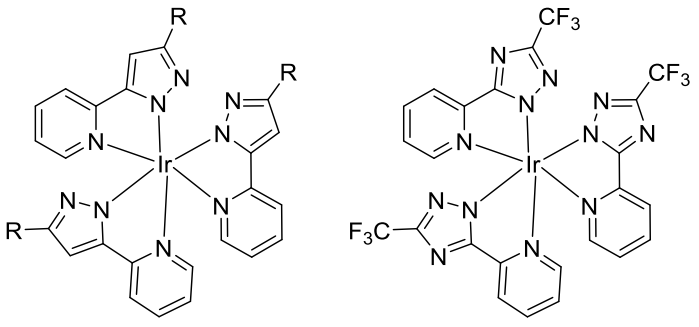

81a R = ^{t}Bu
81b R = CF_3

81c

Figure 4.1: Structures of dual emitting complexes.

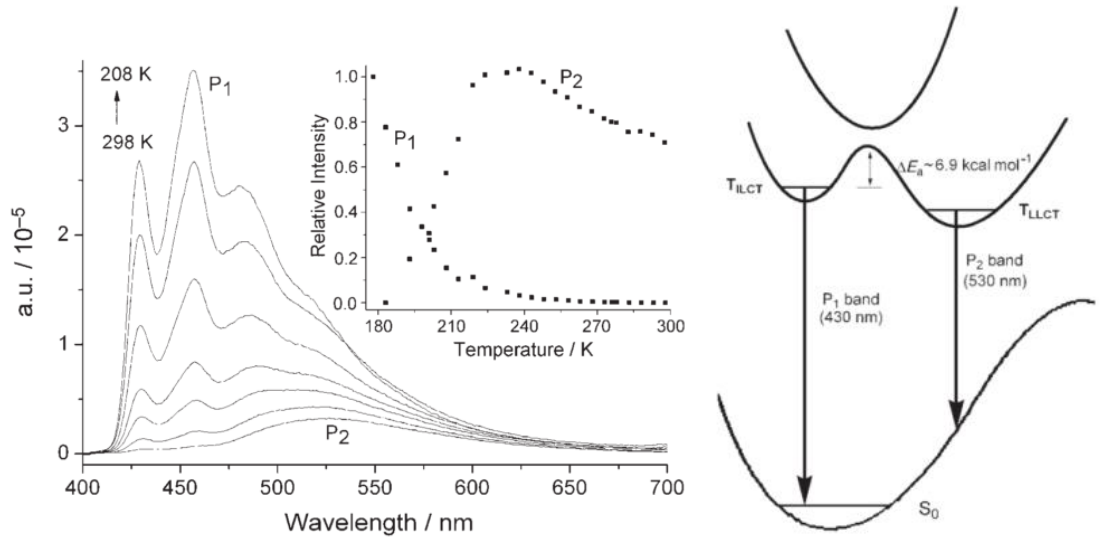

Figure 4.2: LEFT: Selected temperature dependent luminescent spectra of 81b in Ar saturated DCM. Inset: the intensity changes of the P_1 and P_2 emission bands with temperature. RIGHT: The proposed mechanism of dual emission in 94b. Adapted from reference [5].

ILCT state, and the P_2 band to the LLCT state. The proposed mechanism of the dual emission of **81b** is shown in Figure 4.2.

An example of a neutral heteroleptic complex that exhibits dual emission is shown in Figure 4.3.[6] Complex **82a** shows broad green emission in aerated and non-aerated DCM, but blue-shifted emission that displays fine structure in acetonitrile. The emission profile in 2-methyl THF and 1:1 MeOH:EtOH is somewhat intermediate (Figure 4.4).[6] By comparison, the emission profile for the related complex **82b** shows only unstructured emission with a λ_{max} of 602 nm with only minor solvatochromic effects.[6] The absorption spectrum of **82a** was invariant to changes in the solvent, and the excitation spectra obtained in MeCN for various emission wavelengths showed little variation and matched well with the absorption spectra, indicating that the complicated features in the emission spectra were indeed from one species.[6] Additionally, ^{1}H NMR titration

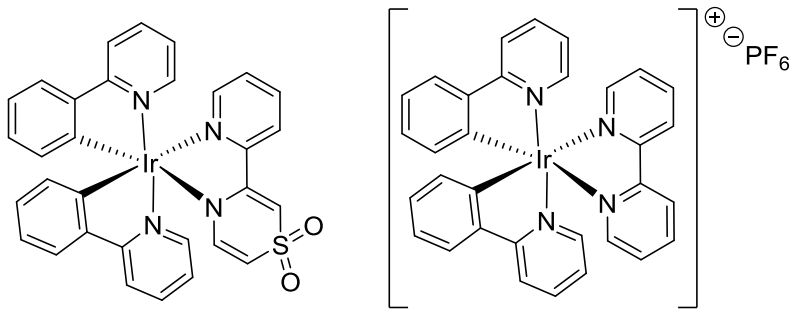

82a **82b**

Figure 4.3

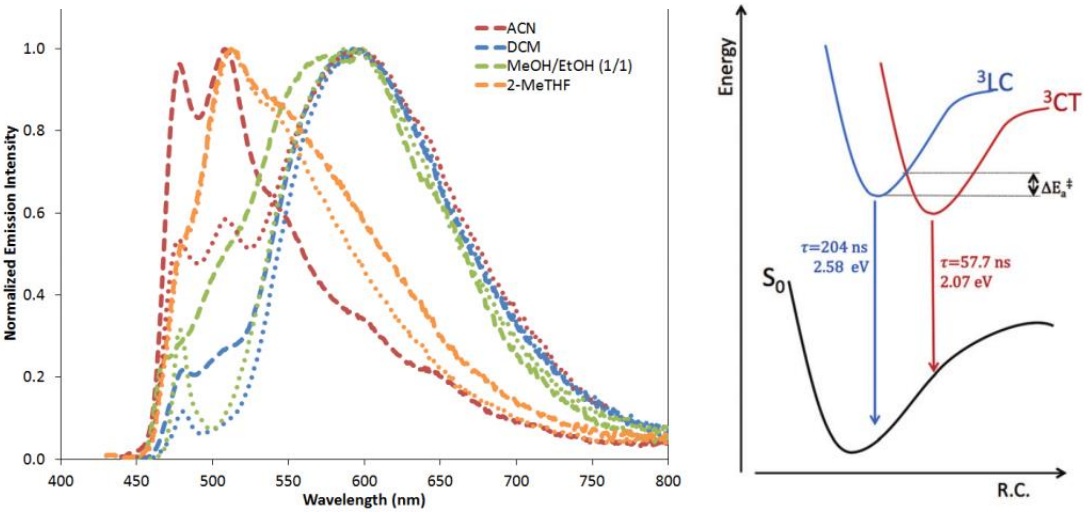

Figure 4.4: LEFT: Emission spectra of 82a in various solvents, at 298K. The dotted lines represent aerated and the dashed lines represent deareated spectra. RIGHT: The proposed mechanism for dual emission from 82a. Adapted from reference [6].

experiments showed no evidence of direct solvent interactions, although solvent interactions in the excited state cannot be completely excluded.[6] The influence of oxygen ($^3O_2$) on the emission was also investigated, with higher energy bands (480 nm and 505 nm) showing a much greater oxygen sensitivity than the lower energy band (600 nm).[6] As was the case with complex **81b**, the higher energy emission was assigned to a ^{3}LC state with low metal character while the lower energy emission was assigned to a ^{3}CT state with significant metal character (Figure 4.4).[6] The relative energy of the ^{3}CT state is thought to be solvent dependent based on the emission spectra, although it was noted that the exact nature of the CT state was difficult to determine computationally based on the electronic distribution of the frontier molecular orbitals.[6]

Examples of dual emitting iridium complexes have been employed as biological sensors; a family of such complexes are shown in Figure 4.5.[7] Here, the amide group has been modified to include

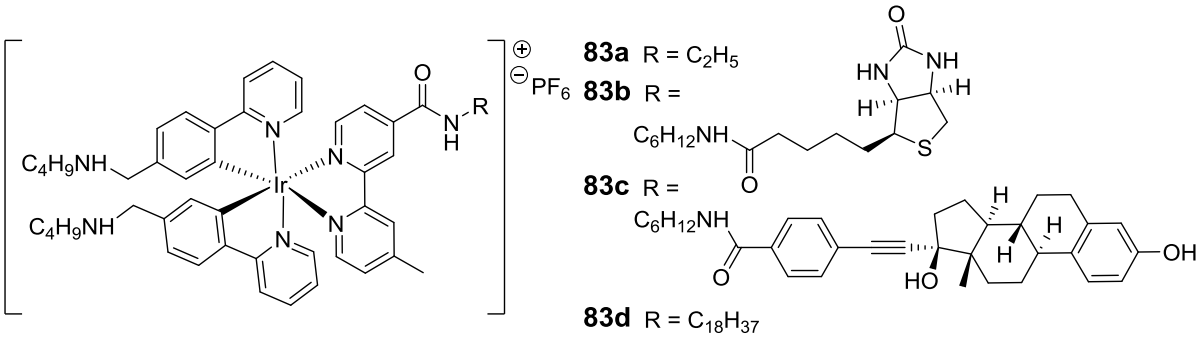

Figure 4.5: Dual emissive complexes with biologically active groups.

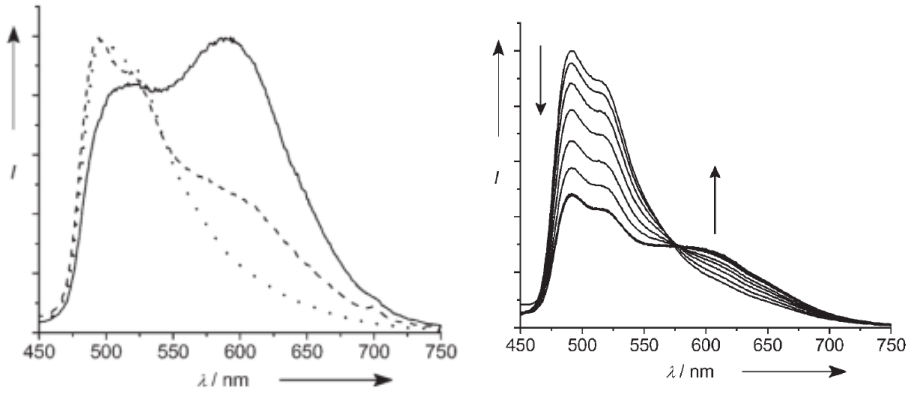

Figure 4.6: LEFT: Normalised emission spectra of 83a in deaerated DCM (line), CH_3CN (dash) and phosphate buffer (dot) at 298 K. RIGHT: Emission of 83b in aerated phosphate buffer at 298 K on addition of avidin. Reproduced from reference [7].

biologically active groups (biotin **83b** and estradiol **83c**), as well as a long, hydrophobic $C_{18}H_{37}$ chain (**83d**).[7] Parent compound **83a** exhibits dual emission in organic solvents at room temperature, with a structured high energy band at ~500 nm (τ_o = 1.1 – 2.5 μs) and a broad, lower energy band at ~593 – 619 nm (τ_o = 0.1 – 0.3 μs).[7] As solvent polarity is increased (from DCM to MeCN/MeOH) the intensity of the lower energy band decreases until, in the case of the aqueous deareated phosphate buffer, the emission becomes completely dominated by the higher energy band (Figure 4.6).[7] The intensity of both bands decreases in aerated solutions, with the higher energy band being more strongly affected.[7] The emission bands of **83a** were assigned to an intra-ligand (^{3}IL/LC) excited state for the higher energy band, and a mixed ^{3}MLCT/^{3}LLCT excited state.[7] Complexes **83b** and **83c** display similar dual-emissive properties to **83a** in organic solvents and aqueous buffer, with the high energy band being dominant in aqueous aerated buffer solutions. On addition of the appropriate proteins (avidin and estrogen receptor α (ERα), respectively) the

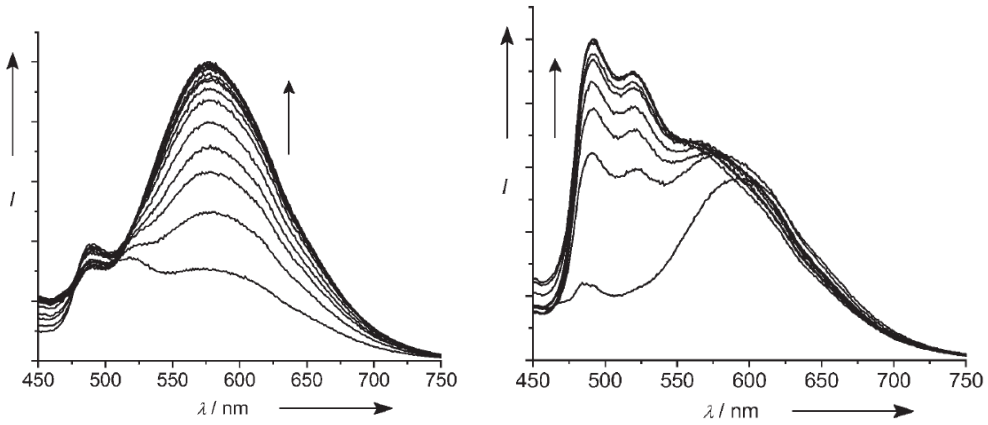

Figure 4.7: LEFT: Emission of 83c in aerated phosphate buffer at 298 K on addition of ERα. RIGHT: Emission of 83d in aerated phosphate buffer at 298 K on addition of HSA. Reproduced from reference [7].

biologically active groups bind with the protein, causing an increase in the intensity of the lower energy band, and a decrease in the intensity of the higher energy band (Figures 4.6 and 4.7). This was attributed to the increased hydrophobic character of the local environment of the complexes upon binding with the protein. In the case of complex **83d**, the long hydrophobic $C_{18}H_{37}$ chain is thought to 'wrap around' the complex in aqueous buffer solutions, resulting in emission dominated by the lower energy band. Upon interaction with either human serum albumin (HSA, a protein known to bind lipids) or β-cyclodextrin (known to bind aliphatic chains) to aerated buffer solutions the intensity of the higher energy band increases relative to the lower energy band, resulting in a blue-shift of the emission colour (Figure 4.7). It is proposed that the binding of the aliphatic chains results in the iridium core being exposed to the hydrophilic buffer solution, enhancing the higher energy band. A mechanism for the dual emission of these complexes is not proposed, although it is noted that the parent complex, which lacks the amine groups on the ppy ligands, does not show dual emission.

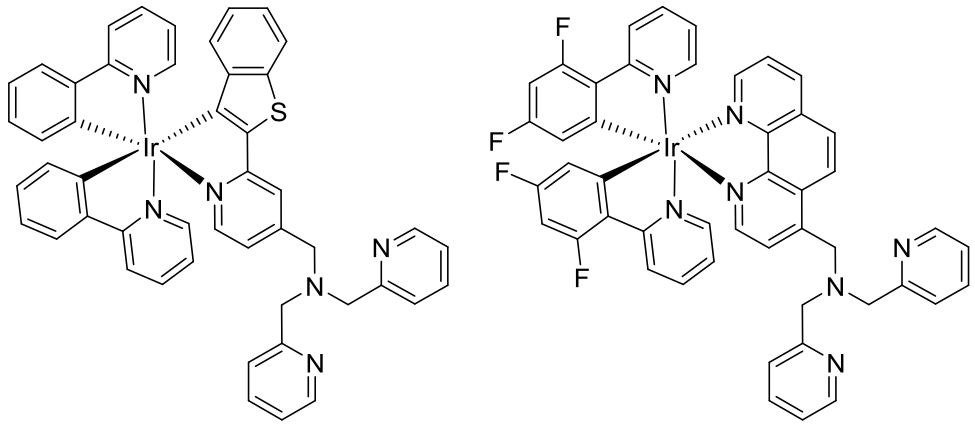

84a **84b**

Figure 4.8: Dual emitting complexes for metal sensing.

Other examples of dual emitting iridium complexes used for biological sensors are shown in Figure 4.8; complex **84a** is a selective sensor for Cu(II) ions,[8] while complex **84b** is a sensor for Zn(II),[9] although it is less selective. In both cases dual emission is observed from the complexes in solution when no metal ions are present; for **84a** this is attributed to emissive states originating from both the ppy (475-550 nm) and the 2-(2'-benzo[*b*]thienyl)pyridine (btp) ligands (575-700 nm),[8] for **84b** the higher energy band (461, 491 nm) is associated with the dfppy ligand and the lower energy band is associated with emission from the phenanthroline (phen) ligand (528 nm), although it is noted that this emission exhibits a large degree of charge transfer character.[9] When **84a** is exposed to Cu^{2+} ions the emission from the btp ligand is quenched while the ppy emission

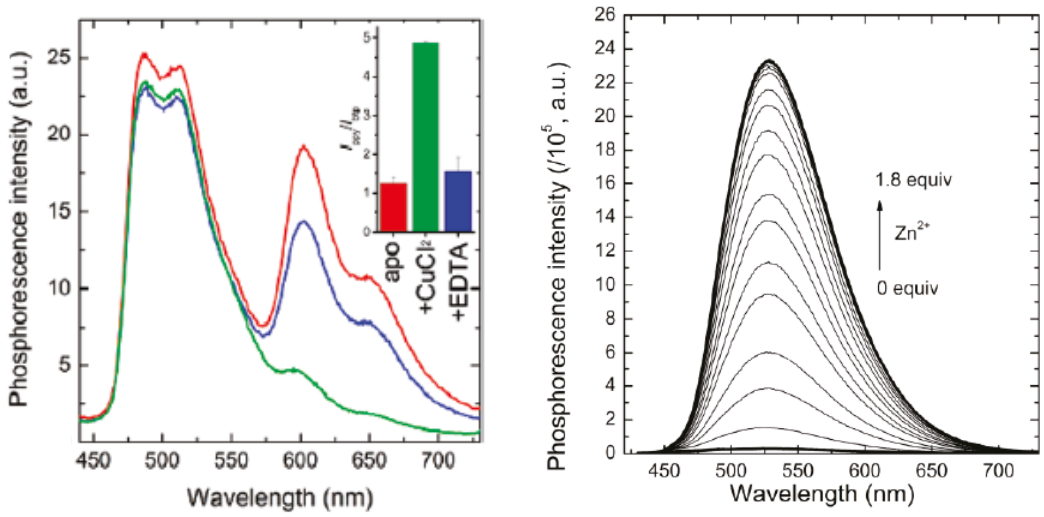

Figure 4.9: LEFT: Reversible change in the phosphorescence spectrum of 84a in response to $CuCl_2$ (red line, Cu(II)-free state; green line, in the presence of $CuCl_2$ (1 equiv); blue line, after subsequent addition of Na_2EDTA (100 equiv) to the mixture). The inset depicts the corresponding change in phosphorescence intensity ratio of green vs red bands. Adapted from reference [8]. RIGHT: Change in phosphorescence spectrum of 84b with increasing total zinc concentration. Adapted from reference [9].

remains intense (Figure 4.9). This results in a colour change on binding of copper, and is selective even in the presence of other metal ions, such as Na^+, K^+, Mg^{2+}, Ca^{2+}, Zn^{2+}, Fe^{2+}, Ni^{2+}, Cr^{2+} and Co^{2+}.[8] In the case of **84b**, the emission intensity of the free complex is poor at RT, with a PLQY of 0.02; on binding of Zn^{2+} an enhancement in the intensity of the lower energy band is observed, increasing the PLQY to 0.58.[9] Compound **84b** selectively binds Zn^{2+} in the presence of Na^+, Mg^{2+}, K^+, Ca^{2+}, and Mn^{2+}, although paramagnetic ions Fe^{2+}, Co^{2+}, Ni^{2+} and Cu^{2+} bind more strongly with the complex, however their binding also quenches the emission.[9]

An example of a white-light emitting iridium complex with a very simple structure is shown in Figure 4.10.[10] When excited within the ligand π-π* and MLCT absorption bands **85** displays broad, relatively featureless emission covering almost the whole visible region, from 440 nm to 800 nm, that is independent of the excitation wavelength.[10] The emission spectra were independent of concentration (over a range of 10^{-3} to 10^{-7} M) showing that the emission was not due to excimer formation.[10] TD-DFT calculations indicated that the LUMO, LUMO+1 (which are based over the cyclometalating ligands) and LUMO+2 (which possesses mainly acac character) are close in energy, resulting in several excited states that are close in energy (<0.1 eV).[10] The authors note that they have no evidence for dual emission from **85**, rather that the emission results from an excited state of mixed character, as suggested by the calculations.[10] The authors propose that vibronic coupling between bright (such as the imidazole-based transition) and dark states (such as the acac-based transition) may be the cause of the spectral broadening observed in **85**. The PLQY

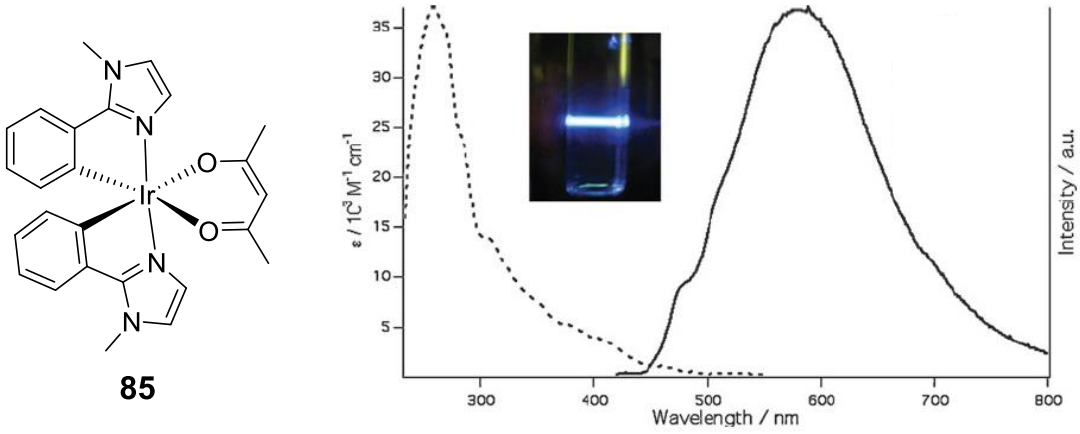

Figure 4.10: LEFT: Complex 85. RIGHT: Absorption and emission spectra (λ_{ex} = 355 nm) of 95 in DCM.

of **85** has been measured in solution, in a PMMA matrix, and a thin film emulating the emissive layer of an OLED, and it is low in all cases (0.015, 0.07 and 0.05, respectively).

RESULTS AND DISCUSSION

A series of complexes synthesised by previous members of the group is shown in Figure 4.11. The emission spectra of complexes **86**, **87**, **88**, **89**, **90** are shown in Figure 4.12; with the exception of complex **90** the emission spectra is typical of mono iridium complexes, the vibronic structure is

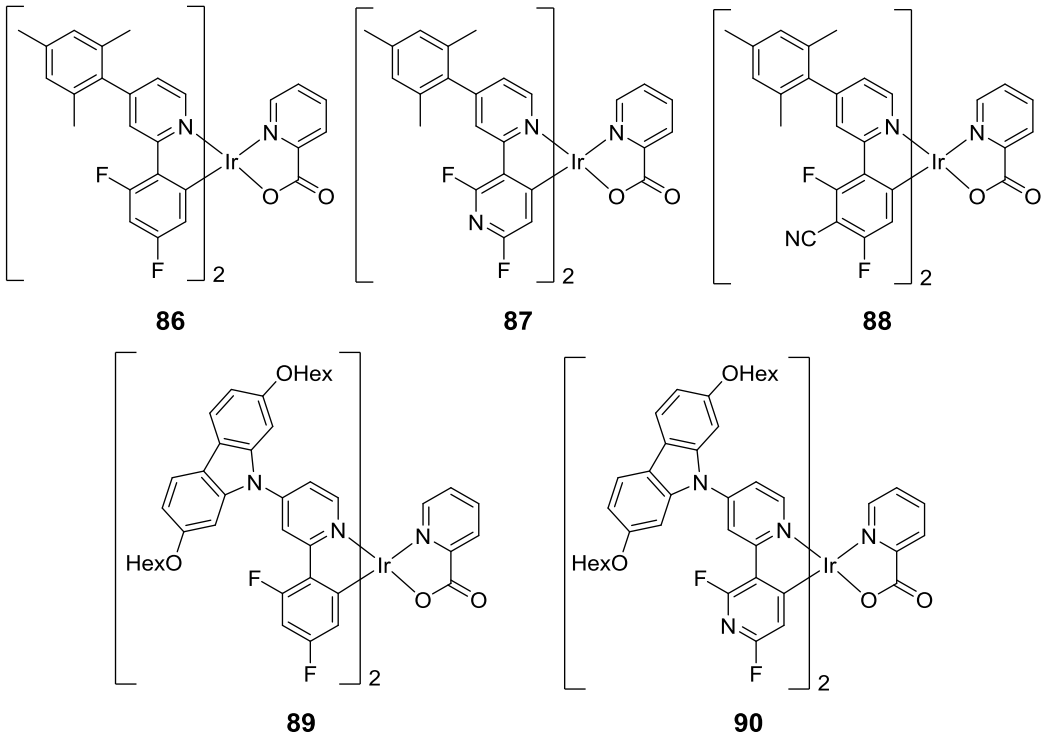

Figure 4.11: Iridium complexes synthesised by previous members in our group.

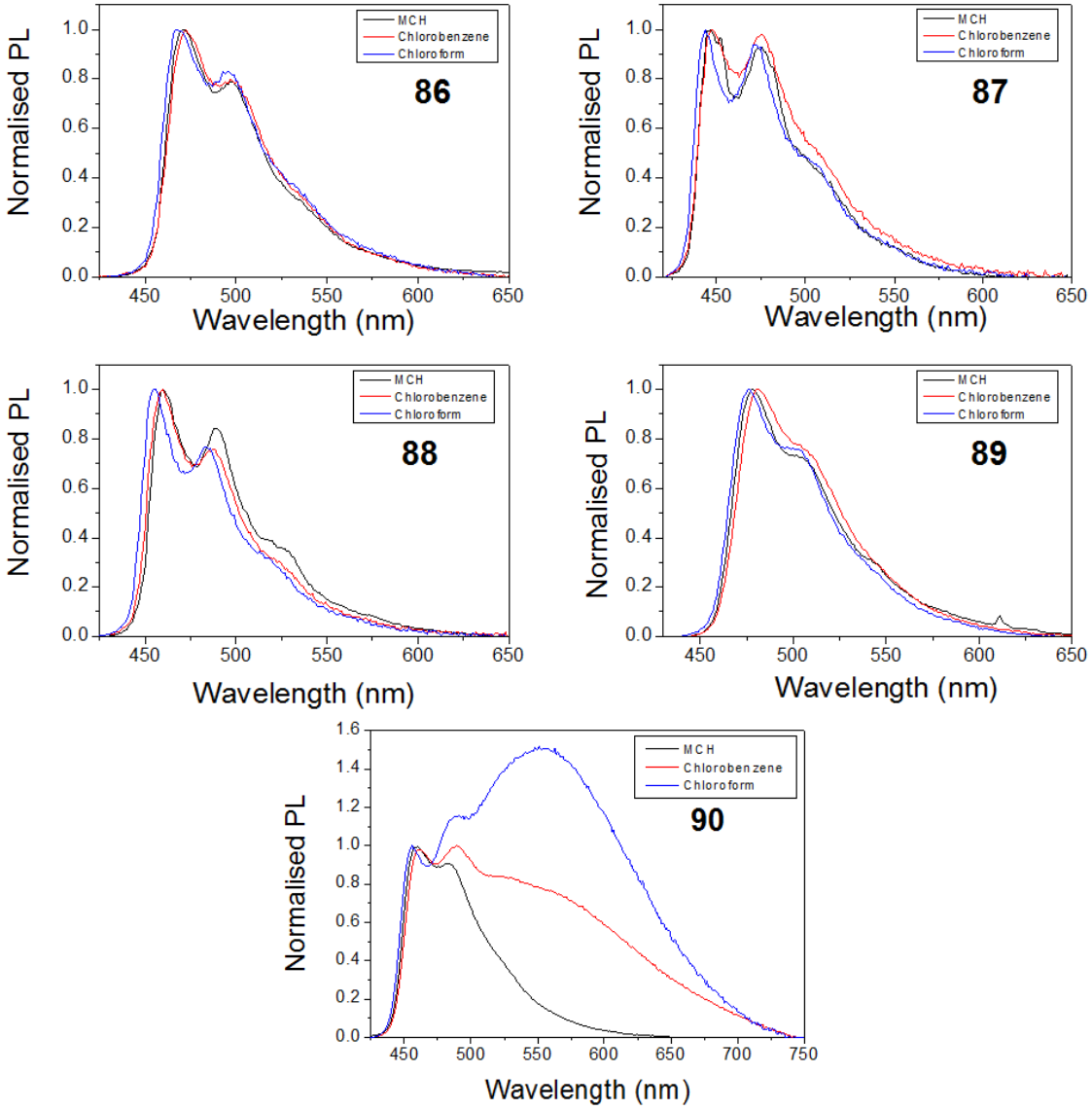

Figure 4.12: Emission spectra of the complexes in degassed solvent at 298 K.

indicative of a mixed LC/MLCT state and little variation in emission profile is seen upon changing solvents, indicating that the charge transfer character is low. In the case of **90**, however, a lower energy band (λ_{max} = 570 nm) develops on increasing the solvent polarity, which results in broadened emission. We were interested in investigating **90** for white OLEDs, and in developing design rules for the synthesis of further dual emitting iridium complexes.

The analogous complex **89** does not exhibit dual emission, despite containing the same dialkoxy substituted carbazole moiety (a strong electron donor), and neither did complex **87**, which contains the 2,4-difluoro-3-pyridyl group (a strong electron acceptor). This observation, and the fact that the second band grows in at lower energy, is consistent with the emission originating from a charge-transfer interaction between the donor and acceptor moieties in **90**. Hence we

have now varied the identity of the donor/acceptor units to determine whether other strong donors/acceptors would produce the same effect. Initially the 2,4-difluoro-3-cyanophenyl group was chosen to allow comparison with existing complex **88**. Additional quantities of complex **90** were synthesised for further study.

The route to target ligands **101** and **102** is shown in Figure 4.13. The first section of the synthesis involves construction of 2,7-dimethoxycarbazole (**95**). The first step involved synthesis of the boronic acid **92**, via a Grignard reaction in 90% yield. This was followed by a Suzuki coupling reaction with 1-bromo-2-nitro-4-methyoxybenzene **93** to form the required biphenyl derivative **94** in 92% yield.

The ring closure reaction was then achieved using $P(OEt)_3$, which was freshly distilled prior to use. The carbazole **95** (formed in 85% yield) was then coupled with 2-chloro-4-iodopyridine **21** in an Ullman-type reaction to give **96** (96% yield). The methoxy ethers were then deprotected with BBr_3 to give the phenol **97** (72%) and hexyl chains were added to improve the solubility of the resulting

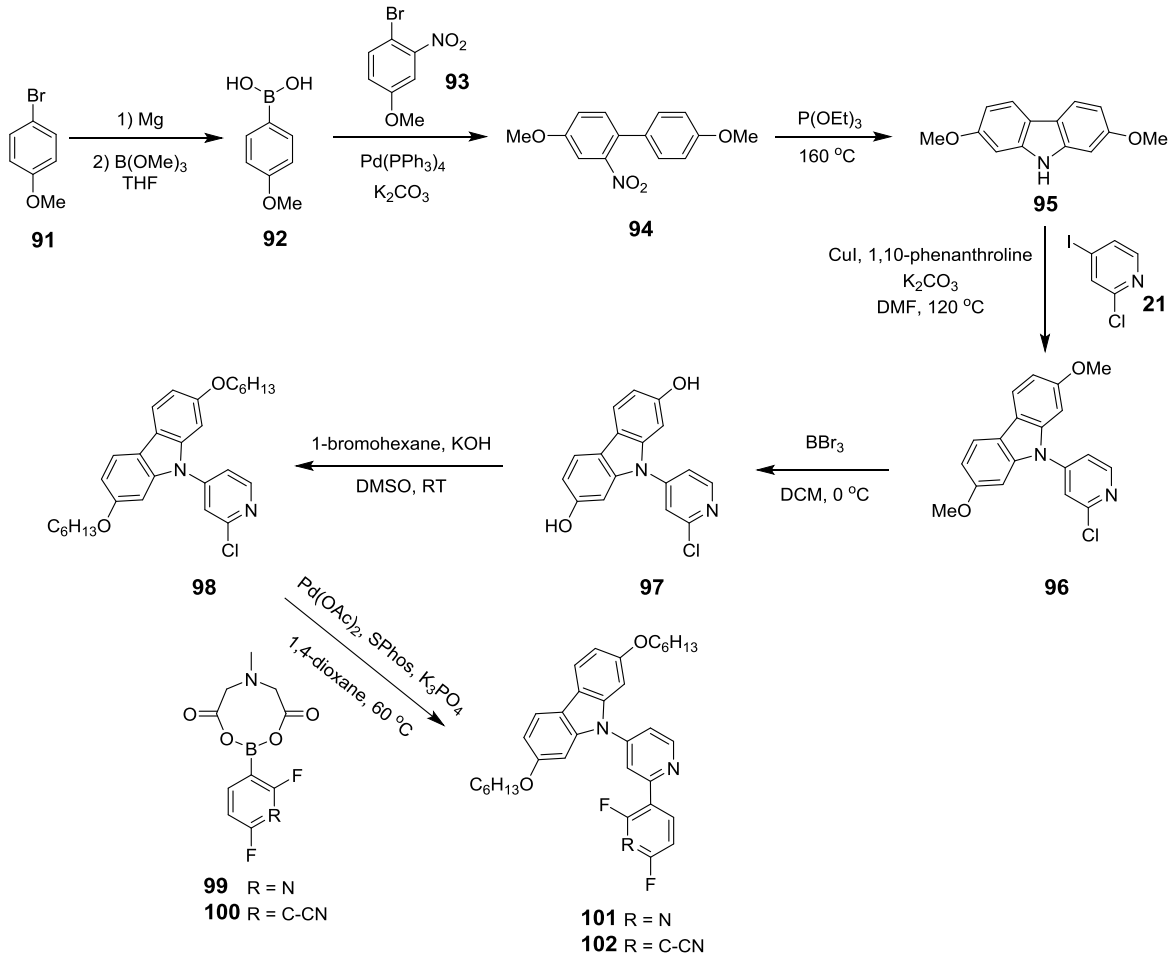

Figure 4.13: Synthesis of target ligands.

complexes, via a Williamson ether synthesis to give **98** (79%).

The next step was to perform Suzuki coupling reactions with the desired MIDA boronates; **99** was available in our laboratory, and **100** was synthesised via the route shown in Figure 4.14.

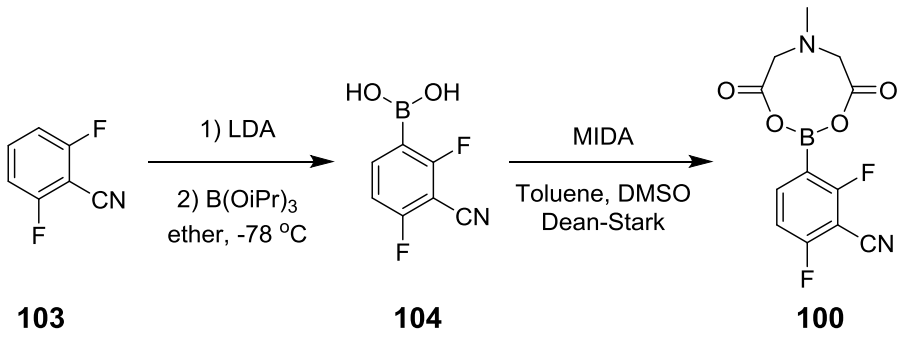

Figure 4.14: Synthesis of the required MIDA-boronic ester.

First *ortho* lithiation of **103** with LDA was used to introduce the boronic acid group into the required position (72%), then the MIDA ester **100** was synthesised via a condensation reaction between **104** and MIDA. The reaction was conducted in a Dean-Stark apparatus to remove the water produced and the product was obtained in good yield (72%). The MIDA esters were used due to the instability of the parent boronic acids under the reaction conditions. Longer reaction times, as required for coupling reactions with the less active 2-chloropyridine derivatives, suffer from competing deborylation, particularly for highly electron-deficient boronic acids.[11,12]

The Suzuki couplings between boronic esters **99**/**100** and **98** followed the protocol described by Burke *et al*.[11] The initial synthesis of **101**, conducted in refluxing dioxane, resulted in a poor yield (<10%), and no unreacted MIDA boronic ester was isolated, suggesting decomposition. The MIDA esters are thought to operate by releasing the active boronic acid species in the presence of base, and the rate of thisrelease can be controlled via choice of base and reaction temperature. Hence the reaction temperature was lowered to 60 ^{o}C, which resulted in an improved yield (87%) of **101**. The reaction conditions were repeated with **100** and the ligand (**102**) was isolated in 83% yield.

The target heteroleptic pic complexes **90** and **105** were then synthesised (Figure 4.15). Reaction of the ligands (**101**, **102**) with $IrCl_3.3H_2O$ gave yellow precipitates presumed to be the intermediate μ-dichloro-bridged dimers, which were not isolated. Picolinic acid was then added and the solution heated to reflux. TLC analysis revealed a large number of yellow spots, suggesting the formation of many iridium complexes. The desired complexes **90** and **105** were isolated in low yields (9% and 13%); and in the case of complex **90** each additional spot was isolated by column chromatography. From the mass spectra it could be seen that each spot corresponded to the

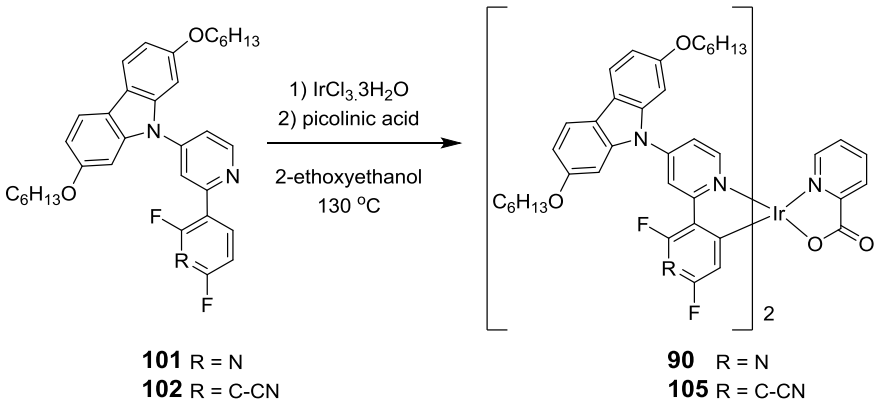

Figure: 4.27: Synthesis of heteroleptic complexes.

replacement of one fluorine with an ethoxyethanol group (Figure 4.16). The ^{1}H NMR spectra of the spots are complex, which can be attributed to a lack of selectivity in the fluorine replacement, resulting in a mixture of isomers all with a similar polarity. This instability of aromatic fluorines towards nucleophilic attack has been discussed in Chapters 2 and 3, although for the complexes synthesised in this thesis so far this instability has not been observed at temperatures below 160 ^{o}C, indicating the increased electron withdrawing nature of the pyridine nitrogen in **90** compared to the sulfone moiety described in Chapters 2 and 3. As detailed in Chapter 2, the instability of the 2,4-difluoro-2',3-bipyridine ligand under the standard reaction conditions has been observed before, wherein the methoxyethanol solvent attacks the ligands and the tetra alkoxylated heteroleptic complex is isolated as the major product in good yield (Figure 3.8).[13] As a result, the temperature of the reaction was dropped to 120 ^{o}C, and the yields improved to 33% and 54% for **90** and **105**, respectively. The photophysics of the complexes, along with the device performance

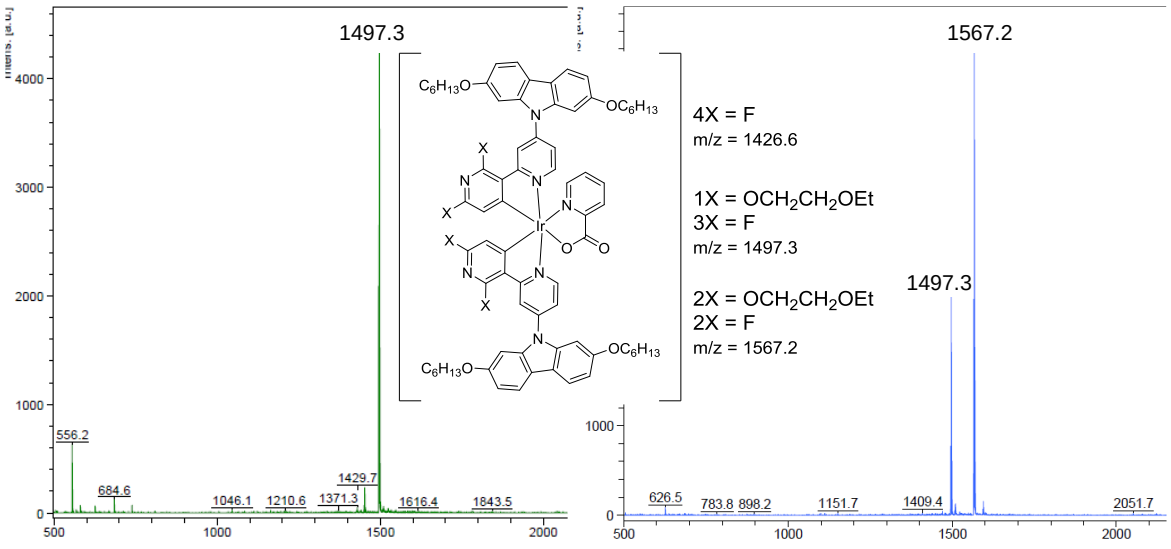

Figure 4.16: Mass spectra of two products isolated from the reaction of 101 with IrCl.3H$_2$O and picolinic acid in ethoxyethanol at 130 ^{o}C.

will be discussed later.

Due to the noted instability of complexes **90** and **105**, there was interest in removing some of the fluorines from the acceptor portion of the molecules. As a result complex **116** was designed, which exchanges the carbazole moiety for a more strongly donating dialkoxy-phenothiazine unit to compensate for the weakening in acceptor strength from removing the fluorine. The synthesis of target ligand **113** is shown in Figure 4.17, and is analogous to that of **101** and **102**. First, amine **107** was constructed via a Buchwald-Hartwig type reaction between **91** and **106**, which proceeded in 62% yield, and then the ring was closed using elemental sulfur and iodine to give the phenothiazine **108** in 30% yield.[14] An Ullmann type reaction was then used to couple **108** with 2-chloro-4-iodopyridine to give **109** (52%), followed by deprotection of the ethers with BBr_3 to give **110** (95%) and then a Williamson ether reaction with hexyl bromide to give **111** (76%).

The final step in the ligand synthesis was a Suzuki coupling with the MIDA ester, **112**. This was conducted under the conditions previously described for **101** and **102**; however no product was

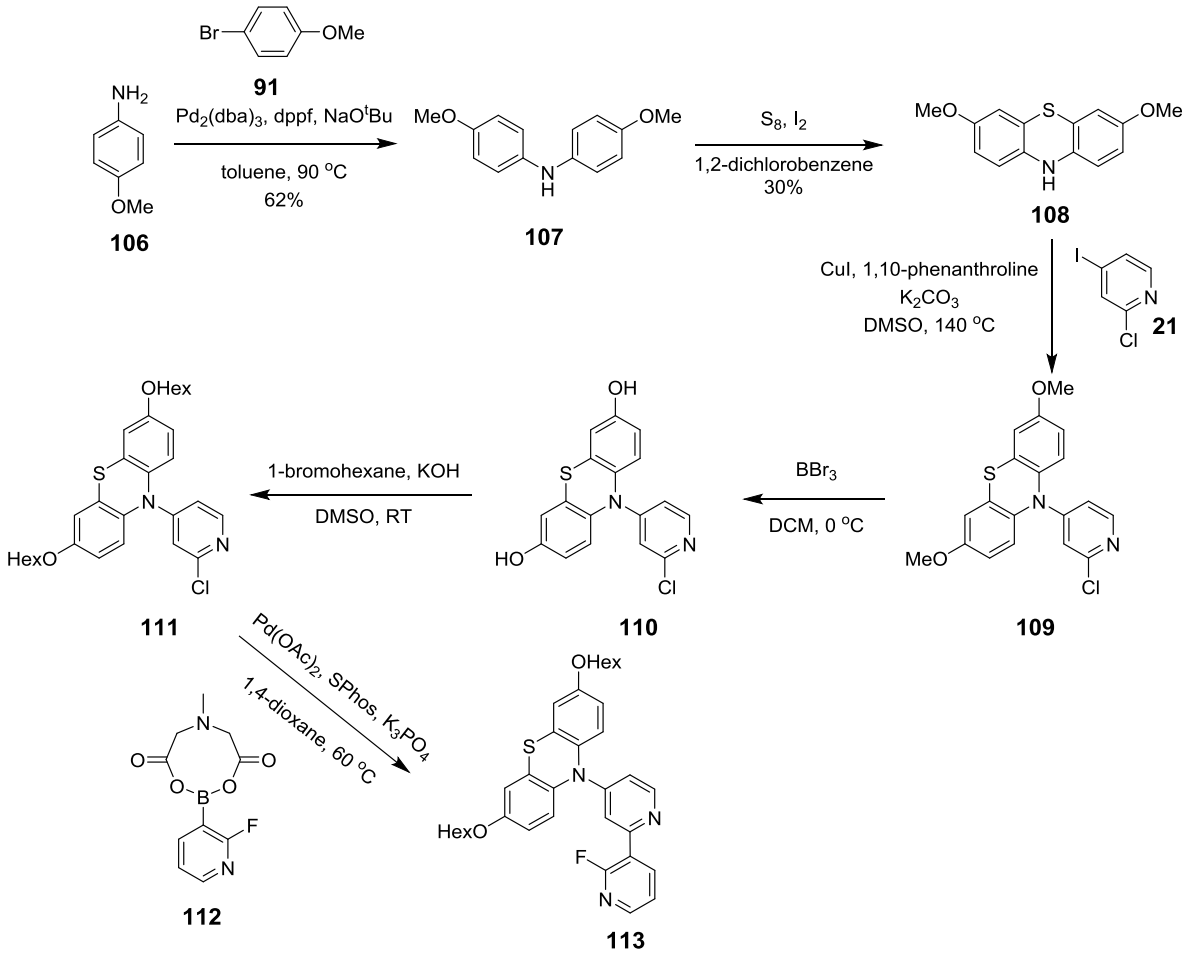

Figure 4.17: Synthesis of target ligand 113.

obtained. The catalytic system was therefore changed to $Pd(OAc)_2/PPh_3$ in dimethoxyethane (DME) with Na_2CO_3 to give the product **113** in 81% yield.

The required MIDA boronic ester was synthesised in the manner previously described for **100** (Figure 4.18). The intermediate boronic acid **115** was synthesised via lithiation *ortho* to the fluorine of **114** (crude yield 92%), followed by a condensation reaction with MIDA to form MIDA boronate **112** in 55% yield (51% over the two steps).

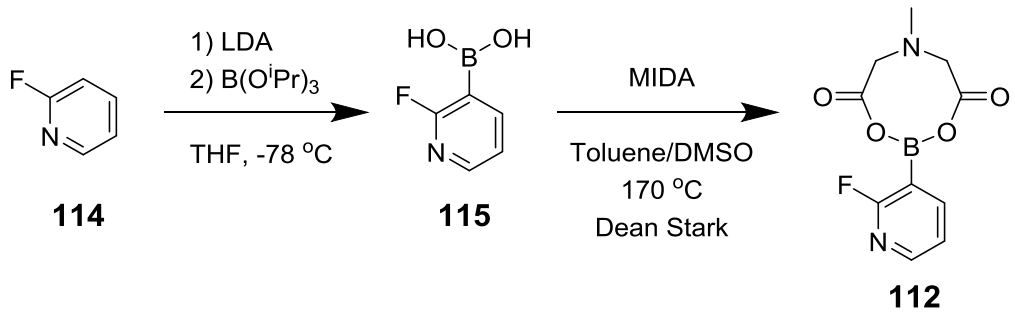

Figure 4.18: Synthesis of required MIDA-boronic ester.

The synthesis of complex **116** is shown in Figure 4.19. The reaction was conducted in toluene at 115 °C in an attempt to prevent the degradation of the material, as observed with **90** and **105**, however, no product was observed. TLC showed a small amount of free ligand **113** remained, and analysis of the ^{1}H NMR spectrum indicated that the dimer had formed, however it had not spilt to form the complex **116**. The crude reaction mixture was redissolved in 2-ethoxyethanol, further picolinic acid was added and the reaction was repeated. Upon purification the desired product **116** was isolated in low yield (9%). Repeating the reaction in the non-nucleophilic solvent diglyme gave **116** in a higher yield (26%).

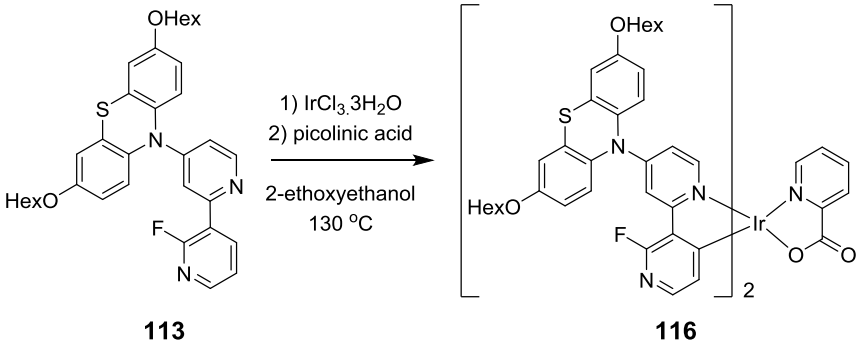

Figure 4.19: Synthesis of complex 116.

The photophysics, device performance and electrochemistry of complexes **90**, **105** and **116** will be discussed later, however it is noted that while the complexes exhibited dual emission properties in solution state with increasing solvent polarity this emission could not be replicated in solid

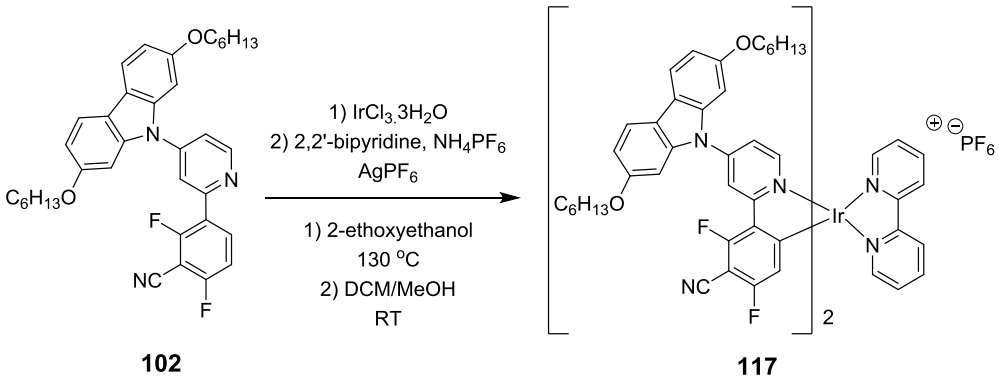

102 **117**

Figure 4.20: Synthesis of complex 117.

state films or devices. As a polar medium stabilised the lower energy emission band it was considered that a charged analogue may exhibit a broad spectrum emission in a light-emitting electrochemical cell (LEEC). With this in mind complex **117** was synthesised (Figure 4.20); the first step was to form the intermediate μ-dichloro bridged dimer from ligand **102** (dry diglyme, 130 °C), followed by reaction with bipyridine, NH_4PF_6 and $AgPF_6$ according to the procedure described by Bünzli *et. al.*[15] The final complex **117** was isolated as an off yellow solid in 22% yield.

PHOTOPHYSICAL AND ELECTROCHEMICAL PROPERTIES

Absorption and emission

The absorption spectra of complexes **86-90**, **105**, **116** and **117** in toluene are shown in Figure 4.21. The complexes possessing extended aromatic systems, namely carbazole and phenothiazine show larger extinction coefficients than the other complexes (**86**-**89**). The strong bands between 290-

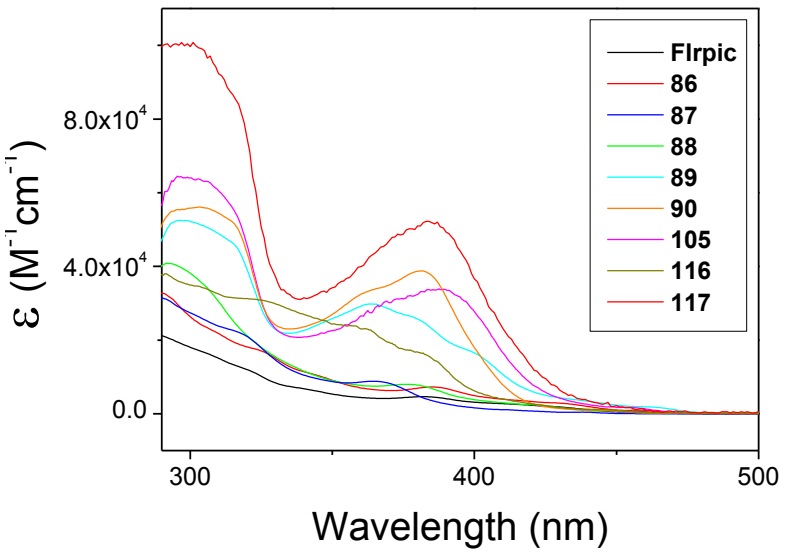

Figure 4.21: UV-Vis absorption spectra of the complexes in toluene [10^{-5} M].

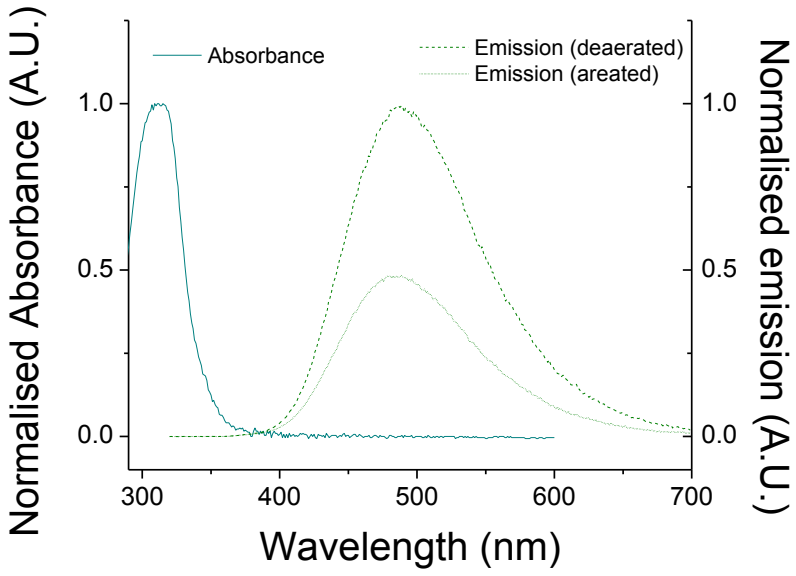

Figure 4.22: Absorption and emission (λ_{ex} = 310 nm) of ligand 102 in toluene [<10^{-5} M].

325 nm are assigned to π-π* transitions on the ligand based on the calculations of Hay[16] and the absorption spectra of ligand **102** (Figure 4.22). The intense bands at 350-425 nm are assigned to the ^{1}MLCT bands, as they are not present in the ligand spectrum, and at much lower oscillator strengths (0.8-1.8 x 10^{3} dm^{3}/mol cm) the ^{3}MLCT bands can be seen.

Excitation spectra for all complexes (Figure 4.23), reveal, as expected, that the bands from the ^{1}MLCT states are responsible for the emission from the complexes, while the majority of the higher energy π-π* transitions are dark.

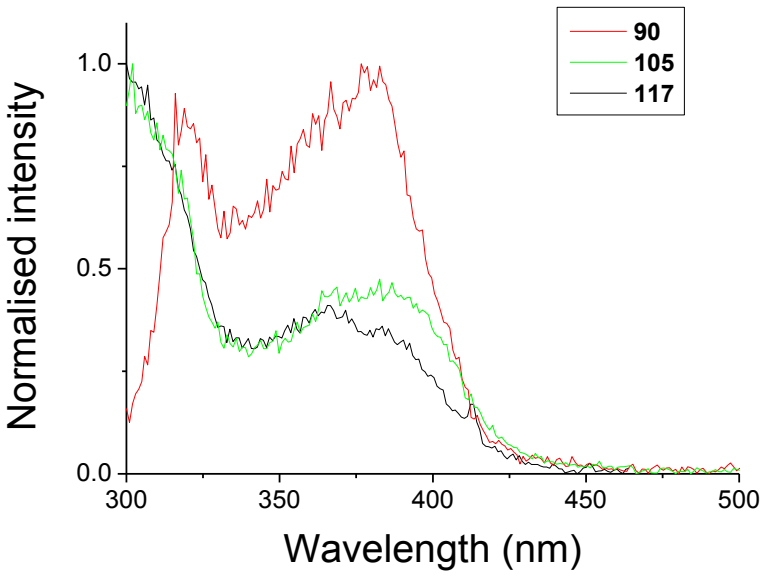

Figure 4.23: Excitation spectra for complexes 90, 105 and 117 in chlorobenzene [<10^{-5} M]. The emission band observed was the second emission maximum. An excitation spectra for 116 could not be measured.

The emission spectra of complexes **90**, **105**, **116** and **117** in various solvents are shown in Figure 4.24. It can be seen that that complexes **90**, **105** and **116** exhibit dual emission on increasing the solvent polarity (from methyl cyclohexane, to chlorobenzene, to chloroform). Emission from complex **117** shows some variation on moving to different solvents, however, there is no sign of a broad feature, suggesting a lack of charge transfer. Compared to **90**, the effect of solvent polarity on the emission of **105** is weaker, as the ratio between the phosphorescence band assigned to the LC/MLCT state and the charge transfer band is greater. In the case of **116**, the additional peak is present even in non-polar methyl cyclohexane (MCH), and it shifts to a longer wavelength in more polar solvents, such as chlorobenzene and chloroform. Complex **117** could not be dissolved in MCH, and the emission spectra were recorded in chlorobenzene, chloroform and ethanol.

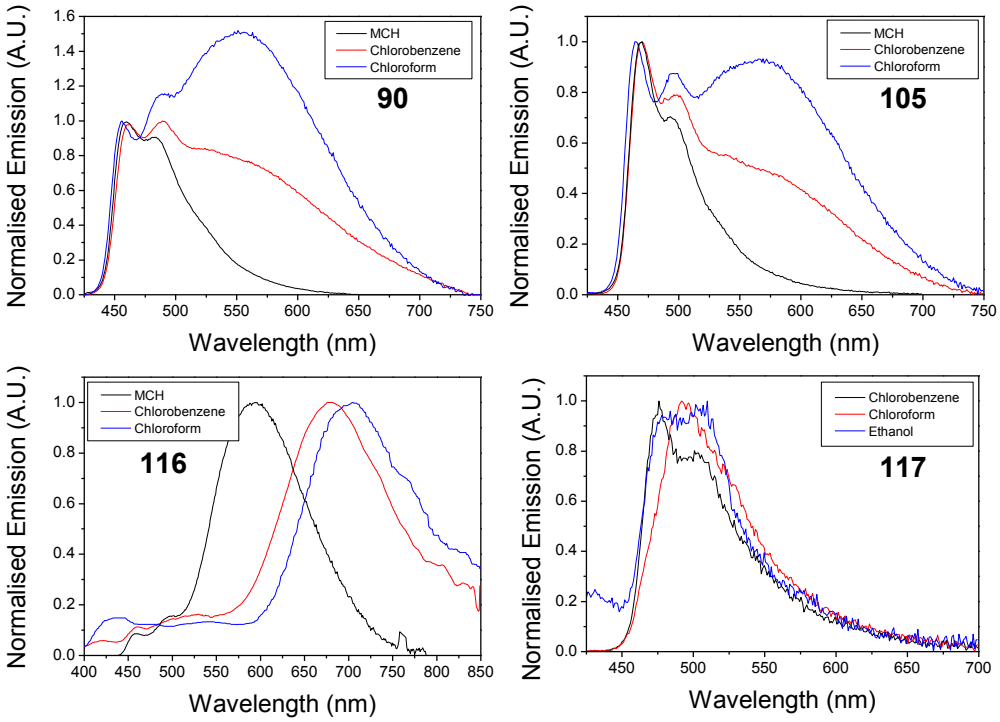

Figure 4.24: Emission spectra of complexes 90, 105, 116 and 117. The emission spectra for complex 116 were smoothed.

The emission spectrum of ligand **102** is shown in Figure 4.22; it is broad and featureless with a λ_{max} = 488 nm, and shows a large Stokes shift, indicating distortion in the excited state. Based on the structure of the ligand, with a strong donor and strong acceptor component, the emission could be due to intramolecular charge transfer. The emission is quenched slightly by oxygen (Figure 4.22), and the emission band has a lifetime of 0.98 µs in deaerated toluene solution, and 0.64 µs in aerated toluene solution. The lifetime data also indicated the presence of a short decay component (<60 ns), although this could not be measured on the experimental set up, suggesting,

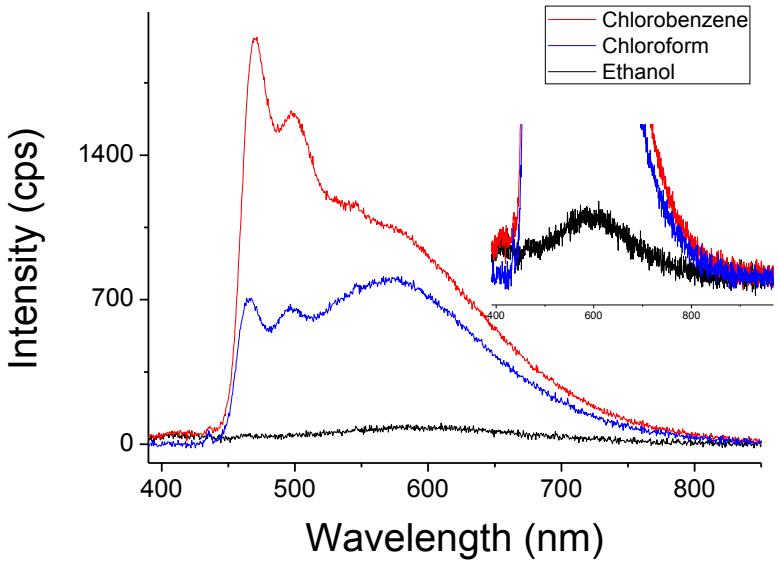

Figure 4.25: Emission spectra of complex 105 in a chlorobenzene, chloroform and ethanol [<10^{-5}] showing the relative intensity of the emission bands.

along with the lifetime measurements, the possibility of a delayed emission mechanism.

The PLQYs and lifetimes of complexes **90**, **105**, **116** and **117** are shown in Table 4.1. For complex **105** the PLQY was measured in chlorobenzene, chloroform and ethanol, to determine the effect of the solvent polarity on the efficiency of the emission. Unfortunately the PLQY could not be measured in methyl cyclohexane, as the solubility of **105** was so low that the absorbance could not be detected. Upon increasing the solvent polarity a decrease in the PLQY is observed, in conjunction with an increase in the intensity of the lower energy band (Figure 4.25). A plot of the relative solvent polarity against the PLQY is shown in Figure 4.26. As the solvent polarity increases

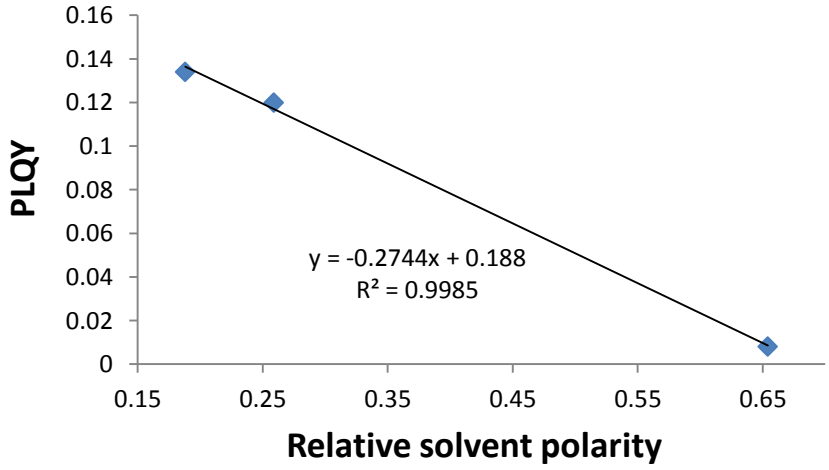

Figure 4.26: Plot of relative solvent polarity against PLQY measured in degassed solvent. The values for relative polarity are normalized from measurements of solvent shifts of absorption spectra and were taken from reference [17].

the intensity of the CT band relative to the LC/MLCT band increases dramatically, although the PLQY falls sharply. This effect has been documented previously, both for charge transfer complexes,[18,19] and for compounds, such as porphyrins, that possess intramolecular charge transfer (ICT) states or undergo photoinduced electron transfer (PET).[20-22] In these cases the use of more polar solvents increases the efficiency of the ICT/CT/PET processes, however the quantum yields of the compounds decrease. This is attributed to non-radiative solvent dissociation or, in the case of the CT complexes, solvent stabilised ionic separation. This observation therefore supports the assignment of the lower energy band to a state with strong CT character. For complexes **94**, **116** and **117** the PLQYs were measured in chlorobenzene, as the complexes could not be dissolved in methyl cyclohexane. The PLQYs of **116** and **117** are significantly lower than those of **90** and **105**. In the case of **116** this can be partially explained by the significant red-shift in emission colour compared to **90** and **105**; lower energy excited states are more susceptible to direct radiationless deactivation to the ground state. Another possible

Compound	λ_{max}^{abs} (ε) / nm (x10^3 M^{-1} cm^{-1})[a]	λ_{max}^{em} / nm[b]		PLQY / Φ_{PL}[c]	τ_P / μs[d]
90	306 (55.9), 313 (53.0), 365 (33.8), 382 (38.7), 445 (0.9)	MCH	456, 482	-	-
		CBZ	460, 487, 521 (sh)	0.30	0.83 (460) 0.79 (550)
		$CHCl_3$	456, 486, 526	-	-
105	296 (64.5), 308 (62.3), 372 (31.0), 389 (33.8), 454 (1.7)	MCH	462, 490	-	-
		CBZ	469, 499, 550 (sh)	0.13	0.52 (470) 0.49 (550)
		$CHCl_3$	464, 496, 550	0.12	-
		EtOH	600	0.008	-
116	304 (34.5), 325 (30.8), 360 (23.0), 382 (16.5), 445 (1.2)	MCH	459, 501, 570	-	-
		CBZ	459, 493, 654	0.01	
		$CHCl_3$	456, 486, 655	-	
117	301 (100.8), 316 (85.3), 368 (45.4), 385 (51.9)	CBZ	475, 504	0.005	0.45 (475)
		$CHCl_3$	494, 523 (sh)	-	0.57 (495)
		EtOH	481, 507	-	0.2 (495) 0.23 (505)
Ligand 102	312	Tol	487	-	0.98
					[0.64]

[a] Data obtained in toluene solution at 20 °C. [b] Data obtained in degassed solvent, with λ_{ex} = 365 nm. MCH = methylcyclohexane, CBZ = chlorobenzene, Tol = toluene. [c] Measured in degassed solvent, relative to quinine sulfate Φ_{PL} = 0.546 in 0.5 M H_2SO_4 at 20 °C; estimated error ±5%. [d] Estimated error ±5%, measured in deaerated solvent. The number within ( ) refers to the wavelength corresponding to the lifetime. [ ] refers to a lifetime in aerated solvent.

Table 4.1: Photophysical data for selected compounds.

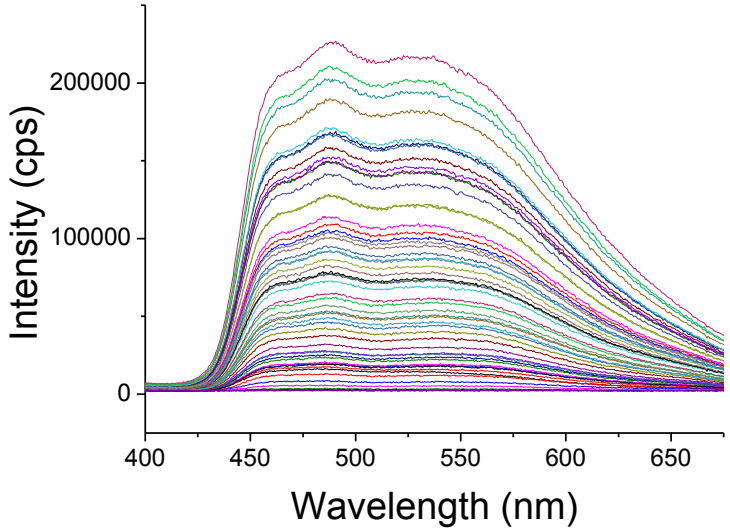

Figure 4.27: The decay profile of complex 90 in chlorobenzene (λ_{ex} = 355 nm).

cause is the apparent increase in charge transfer character (suggested by the fact that the broad emission feature is present even in non-polar solvents), resulting in more efficient quenching via radiationless deactivation in solution.

For complexes **90**, **105** and **117** the lifetimes of the two bands were measured, and are shown in Table 4.1. The values for the two features are the same within experimental error. This is highlighted by the decay profile of complex **90** (Figure 4.27), which shows no significant change in spectral features during the decay, suggesting that the decays come from states similar in origin.

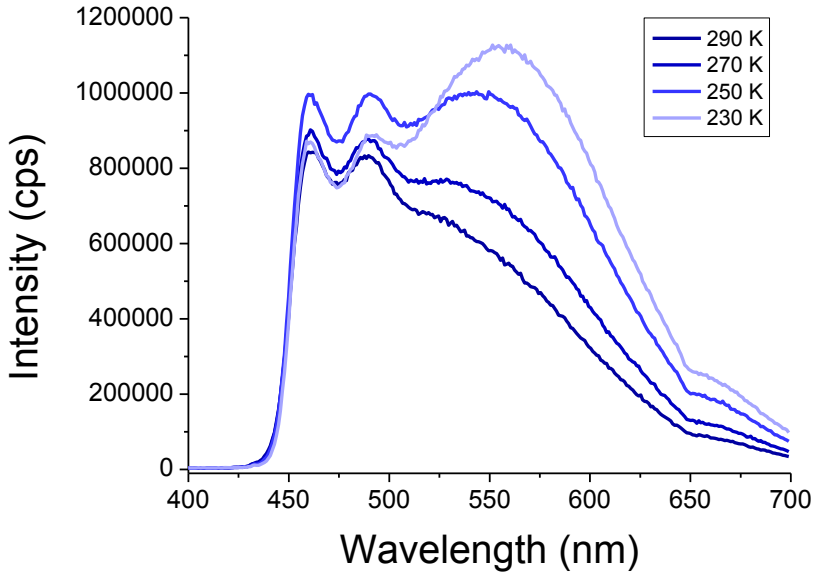

Figure 4.28: The emission profile of 90 in chlorobenzene at varying temperatures.

The effect of temperature on the emission spectra of complex **90** was also investigated (Figure 4.28). On decreasing the temperature from room temperature to 230 K the ratio between emission bands changes, with an increase in the intensity of the lower energy feature relative to the higher energy feature. This can be rationalised by the difference in the degree of CT character between the two bands; the PLQY of the complexes and the intensity of the lower energy band show a strong dependence on solvent polarity, suggesting the stabilisation of a state with increased dipole moment (CT state) on moving to more polar solvents. Upon cooling the chlorobenzene solution (m.pt. = 228 K) the viscosity of the solution increases, decreasing the rate with which solvent molecules that support the CT state can dissociate, resulting in an enhancement of the 550 nm emission. The higher energy feature, assigned to a mixed LC/MLCT state, is not as substantially affected, as it has less CT character that requires solvent stabilisation.

Electrochemistry

Complexes **90**, **105**, **116** and **117** were investigated by cyclic voltammetry, and the cyclic voltammograms are shown in Figure 4.29. Complexes **90**, **105** and **117**, which contain the 2,7-dialkoxycarbazole moiety, show a change in the voltammogram profile on increasing the number

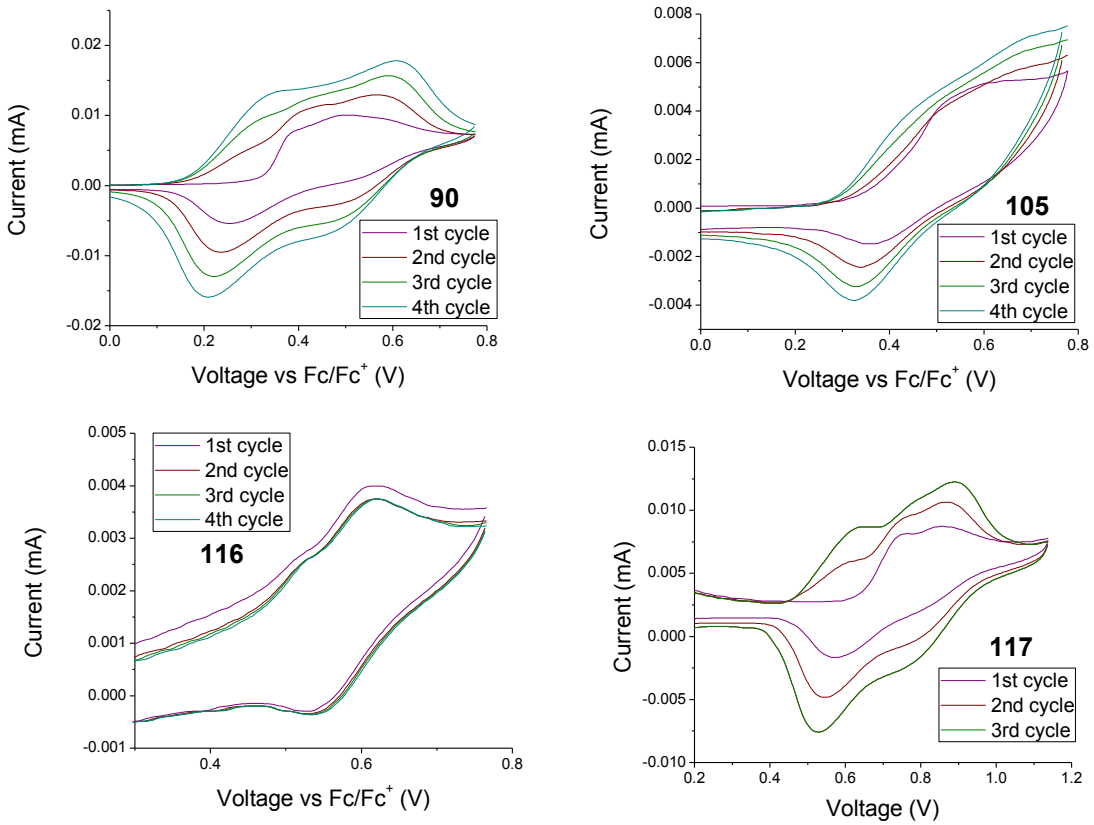

Figure 4.29: Cyclic voltammograms of complexes 90, 105, 116 and 117.

of cycles. On the first scan all the complexes initially show two oxidation waves, which can be assigned to the Ir^{3+}/Ir^{4+} couple, and the oxidation of the carbazole moiety. On the reverse scan, the oxidations of the carbazoles are quasireversible; however, another reduction wave emerges. On additional forward scans a new oxidation is seen to grow in before the oxidation assigned to the iridium oxidation. It is known that upon oxidation of carbazole units a radical cation is formed, and is localised at the 3- and 6-positions of the carbazole subunit. From here, due to the close proximity of the molecules on the surface of the electrode, two radical cations can dimerise. This gives rise to the additional reduction on the first back-scan. The additional oxidation peak observed in the subsequent scans is assigned to the oxidation of dimer species formed.[23] It is noted that if the 3- and 6- position are blocked this behaviour is not observed. Complex **116** does not contain the carbazole subunit and instead shows two quasireversible oxidations, assigned to the Ir^{3+}/Ir^{4+} couple and the oxidation of the phenothiazine moiety.

Complex	E^{ox} Ir^{3+}/Ir^{4+} / V[a]	$E^{ox}_{1/2}$ [Het] / V	$E^{ox}_{1/2}$ dimer / V	HOMO / eV
FIrpic	0.89	-	-	-5.69
90	0.40	0.52	0.27	-5.20
105	0.55	0.64	0.40	-5.35
116	0.52	0.58	-	-5.32
117	0.75	0.82	0.57	-5.55

[a] Values for this oxidation are the aniodic peak potential. [Het] refers to the heterocycle, either carbazole of phenothiazine. All values reported vs Fc/Fc^+ = 0.00 V.

Table 4.1: Electrochemical data for selected complexes. Measured in DCM (0.1 M $^nBu_4NPF_6$) at 298 K.

DEVICE DATA

To our knowledge, no devices have been reported that use complexes that display dual emissive properties in solution as the emissive material. Complexes containing ligands with donor and acceptor groups, both on the same ligand,[24] and on different ligands,[25] that do not show dual emission properties in solution have been used in OLED devices, and display favourable performances due to their charge transport properties. OLEDs using complexes **86**-**90**, **105**, **116** and **117** as the emitters were fabricated by Dr Gareth Griffiths in the Department of Physics at Durham University and compared to a reference device containing FIrpic. The hole transporting layer and emissive layer were deposited by solution processing techniques, and the electron transporting, electron injection layers and the cathode were then fabricated by vacuum deposition. The device structure is as follows: ITO/PEDOT:PSS (50 nm)/PVK:OXD:**Ir complex** [100:50:8] (75 nm)/TPBi (25 nm)/LiF (1 nm)/Al. The electroluminescence (EL) spectra from the

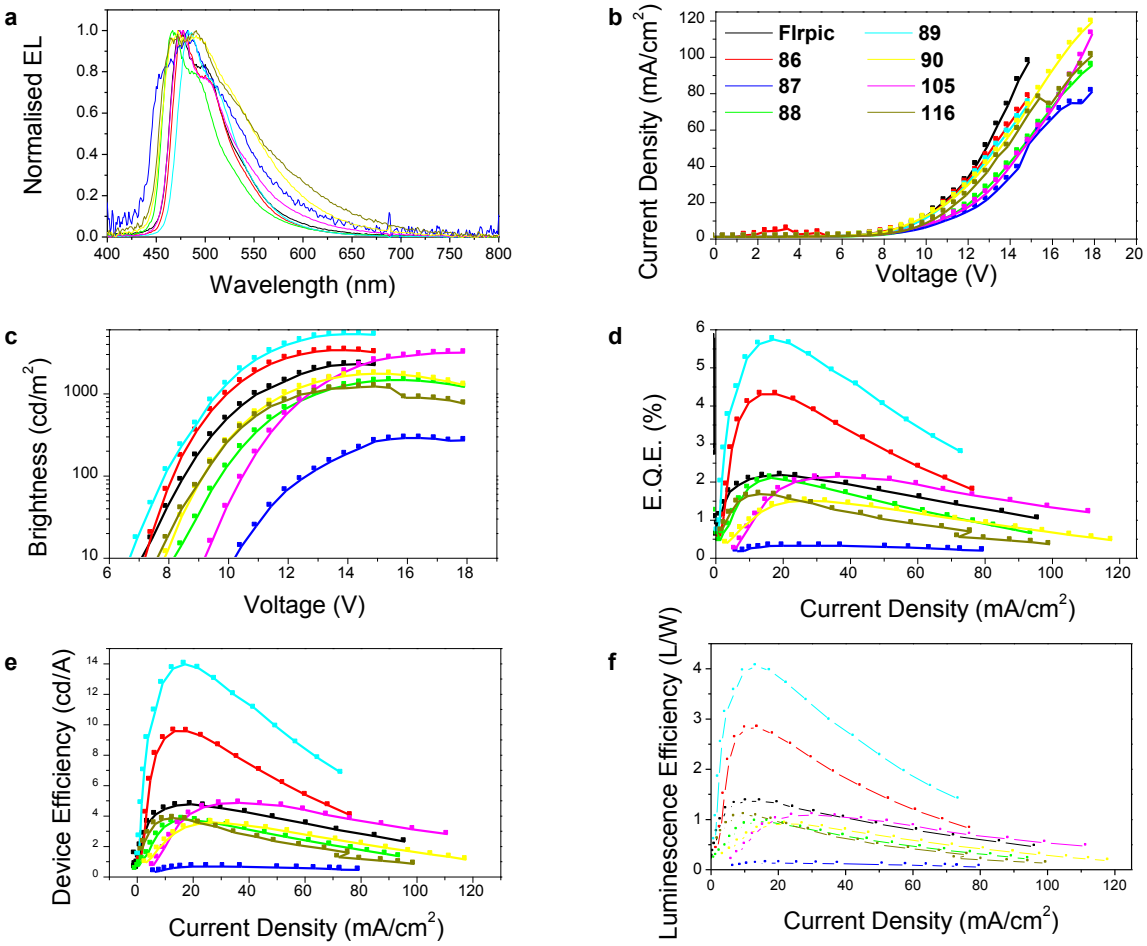

Figure 4.30: Device data for complexes 86-90, 105 and 116.

devices are shown in Figure 4.30, panel a; for complexes **90**, **105** and **116** the EL spectra show no sign of the dual emissive properties present in the PL spectra. Thin films of complexes also only display emission from the LC/MLCT band; this is not unexpected as in a solid, non-polar environment the conformations required for population of, and emission from, the CT state may not be accessible. Complexes **90** and **116** are less efficient than FIrpic, with lower EQEs (panel d), brightnesses (panel c) and device efficiencies (panel e). Complex **105**, however, performs

Complex	λ_{ELmax} / nm	Brightness / cd/m^2	turn-on voltage / V [a]	EQE / %	current efficiency / cd/A	power efficiency / lm/W	CIE coordinates / (x,y) [b]
FIrpic 1	473	2179	7.2	2.14	4.63	1.36	(0.17, 0.37)
90	472-491	1657	9.3	1.46	3.44	0.91	(0.22, 0.38)
105	476	2988	8.0	2.09	4.73	1.09	(0.19, 0.38)
116	467-490	1158	7.7	1.63	3.72	1.09	(0.24, 0.37)

[a] Measured at a brightness of 10 cd/m^2. [b] Measured at 12 V.

Table 4.2: Summary of device data.

comparably with the FIrpic device, with a maximium EQE of 2.09% and higher maximum brightness (2988 cd/m^2), although **105** requires higher driving voltages to achieve comparable brightnesses to the FIrpic device. Due to the loss of the dual emission feature the EL spectra of the complexes (particularly complex **105**) are comparable. Key device parameters are shown in Table 4.2.

CONCLUSION

Complexes **105**, **116** and **117** were synthesised to probe the origin of the dual emission properties seen in **90**, and to establish design rules for synthesising new dual-emitting complexes. The photophysical and electrochemical properties were investigated, and compared to FIrpic, as well as other related complexes (**86**-**89**) synthesised by previous members of our group. Taking into account the structural motifs that are present in the complexes that display dual emission (namely, the presence of strong donor and acceptor components), the response of the new spectral features to solvent polarity, and consideration of the free ligand spectra, the origin of the dual emissive character is tentatively assigned to the presence of a ligand based CT state. Unfortunately, the complexes did not display dual emission properties in the solid state, although it is noted that no solid state or OLED device data has been reported for the dual emissive complexes detailed in the introduction. Nevertheless, devices fabricated in the Department of Physics showed favourable performances as blue emitters compared to the FIrpic device. It remains a challenge to exploit the properties of dual emissive compounds for WOELDs.

References

1) K. T. Kamtekar, A. P. Monkman and M. R. Bryce, *Adv. Mater.,* 2010, **22**, 572-82
2) G. M. Farinola and R. Ragni, *Chem. Soc. Rev.,* 2011, **40**, 3467-3482
3) L. Xiao, Z. Chen, B. Qu, J. Luo, S. Kong, Q. Gong and J. Kido, *Adv. Mater.,* 2011, **23**, 926-52
4) C. Ulbricht, B. Beyer, C. Friebe, A. Winter and U. S. Schubert, *Adv. Mater.,* 2009, **21**, 4418-4441
5) Y. S. Yeh, Y. M. Cheng, P. T. Chou, G. H. Lee, C. H. Yang, Y. Chi, C. F. Shu and C. H. Wang, *ChemPhysChem,* 2006, **7**, 2294-7
6) S. Ladouceur, L. Donato, M. Romain, B. P. Mudraboyina, M. B. Johansen, J. A. Wisner and E. Zysman-Colman, *Dalton Trans.,* 2013, **42**, 8838-47
7) K. K. Lo, K. Y. Zhang, S. K. Leung and M. C. Tang, *Angew. Chem. Int. Ed.,* 2008, **47**, 2213-6
8) Y. You, Y. Han, Y. M. Lee, S. Y. Park, W. Nam and S. J. Lippard, *J. Am. Chem. Soc.,* 2011, **133**, 11488-91
9) Y. You, S. Lee, T. Kim, K. Ohkubo, W.-S. Chae, S. Fukuzumi, G.-J. Jhon, W. Nam and S. J. Lippard, *J. Am. Chem. Soc.,* 2011, **133**, 18328-18342
10) H. J. Bolink, F. De Angelis, E. Baranoff, C. Klein, S. Fantacci, E. Coronado, M. Sessolo, K. Kalyanasundaram, M. Gratzel and M. K. Nazeeruddin, *Chem. Comm.,* 2009, 4672-4674
11) D. M. Knapp, E. P. Gillis and M. D. Burke, *J. Am. Chem. Soc.,* 2009, **131**, 6961-3
12) G. R. Dick, E. M. Woerly and M. D. Burke, *Angew. Chem. Int. Ed.,* 2012, **51**, 2667-72
13) H. Oh, K.-M. Park, H. Hwang, S. Oh, J. H. Lee, J.-S. Lu, S. Wang and Y. Kang, *Organometallics,* 2013, **32**, 6427-6436
14) X.-Q. Zhu, Z. Dai, A. Yu, S. Wu and J.-P. Cheng, *J. Phys. Chem. B,* 2008, **112**, 11694-11707
15) A. M. Bünzli, E. C. Constable, C. E. Housecroft, A. Prescimone, J. A. Zampese, G. Longo, L. Gil-Escrig, A. Pertegás, E. Ortí and H. J. Bolink, *Chem. Sci. ,* 2015, **6**, 2843-2852
16) P. J. Hay, *J. Phys. Chem. A,* 2002, **106**, 1634-1641
17) C. Reichardt, *Solvent Effects on the Absorption Spectra of Organic Compounds* in *Solvents and Solvent Effects in Organic Chemistry*, Ed. Wiley-VCH Verlag GmbH & Co. KGaA, 2004, 329-388
18) J. Prochorow, *Chem. Phys. Lett.,* 1973, **19**, 596-600
19) J. Prochorow and E. Bernard, *J. Lumin.,* 1974, **8**, 471-487
20) V. Novakova, P. Zimcik, M. Miletin, L. Vachova, K. Kopecky, K. Lang, P. Chabera and T. Polivka, *Phys. Chem. Chem. Phys.,* 2010, **12**, 2555-2563
21) M. Isosomppi, N. V. Tkachenko, A. Efimov and H. Lemmetyinen, *J. Phys. Chem. A,* 2005, **109**, 4881-4890
22) L. Fajari, P. Fors, K. Lang, S. Nonell and F. R. Trull, *J. Photochem. Photobiol., A,* 1996, **93**, 119-128
23) M. Gantenbein, M. Hellstern, L. Le Pleux, M. Neuburger and M. Mayor, *Chem. Mater.,* 2015, **27**, 1772-1779
24) H. Tang, Y. Li, B. Chen, H. Wu, W. Yang and Y. Cao, *Opt. Mater.,* 2011, **33**, 1291-1296
25) X. Xu, X. Yang, J. Dang, G. Zhou, Y. Wu, H. Li and W.-Y. Wong, *Chem. Comm.,* 2014, **50**, 2473-2476

Chapter 5: New ancillary ligands

As discussed in Chapter 1, emissive heteroleptic complexes consist of one or two chromophoric ligands, with the rest of the coordination sphere occupied by so called 'ancillary' ligands. These ligands are typically not directly involved in the excited state that produces the emission,[1-3] but can influence its properties and modify emission colour indirectly. They can also be used to introduce additional functionality to the complex, such as electron or hole transporting groups,[2,4] or increased steric shielding to reduce triplet-triplet annihilation.[5] Functionalised ancillary ligands have been used in iridium complexes for sensitisation of lanthanide ions, which are important for biological imaging applications.[5] Complexes with β-diketonate ancillary ligands have been synthesised that display enhanced phosphorescence emission in the solid state (EPESS), a phenomenon that could be exploited in bioimaging.[3] Addition of promesogenic groups onto the ancillary ligand of charged iridium complexes, results in complexes that undergo reversible colour tuning in response to surface stress or heating, promising properties for device applications.[6] Ancillary ligands can also be used to incorporate iridium complexes into polymers without interfering with their photophysical properties; polymers containing iridium complexes have a variety of uses, for example as single molecule white light emitters, as described in Chapter 4.[7]

Ancillary ligands with singlet and triplet energies significantly higher than those of the other ligands are referred to as non-chromophoric, and emission from the excited state predominantly arises from the$(C^N)_2$Ir fragment.[8-10] Here, while the ancillary ligand is not directly involved in the excited state, it can still influence the emission of the complex by modifying the electron density at the iridium centre.[3,8,9,11,12] Electron withdrawing ancillary ligands stabilise metal d-orbitals, and as the HOMO for emissive iridium complexes is partially localised on the Ir centre this results in a lowering of the HOMO relative to the LUMO, thereby blue-shifting the emission.[8] For complexes

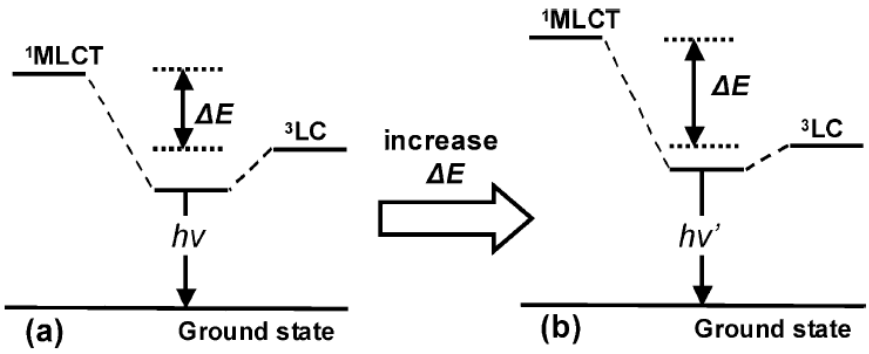

Figure 5.1: Illustrative energy level diagrams showing the effect of raising the ^{1}MLCT energy on the emission energy. Adapted from reference [8].

with ppy based ligands the excited state is typically of mixed ^{3}LC/^{3}MLCT character, as the HOMO is of Ir d-orbital and cyclometalating ligand character, while the LUMO is mainly on the cyclometalating ligand. Lowering the HOMO level by using ancillary ligands therefore increases the separation between the $^{1/3}$MLCT and ^{3}LC states by raising the energy of the MLCT states, thus resulting in an increase in emission energy, as shown in Figure 5.1.[8] Care must be taken with this approach, however, as the contribution from states involving the iridium atom (i.e. the MLCT states) is required to allow the spin orbit coupling; increased ^{3}LC emission character is associated with smaller radiative rates (k_r) and lower PLQYs.[8,9]

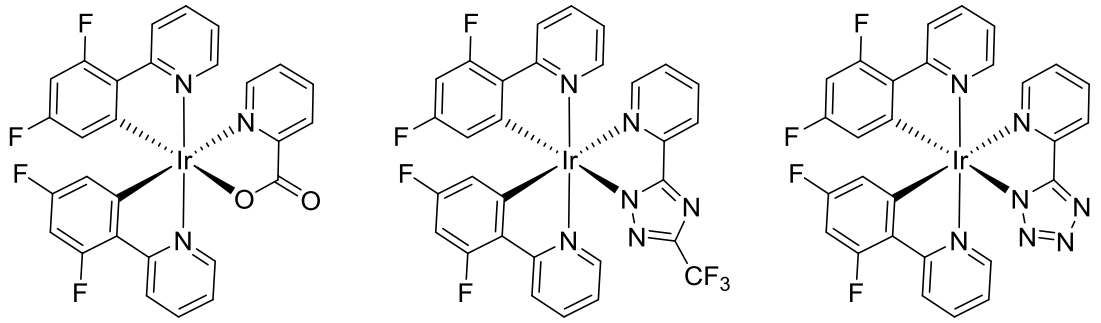

Figure 5.2: A selection of iridium complexes with blue-shifting ancillary ligands.

A selection of complexes that illustrate this approach is shown in Figure 5.2. Here, replacing the pic ligand of FIrpic with a triazole (**118a**, FIrtaz) or tetrazole (**118b**, FIrN4) results in a blue-shift in emission λ_{max} of ~ 10 nm.[13] Typically, azole ligands act as strong σ-donors and weak π-acceptors due to the electron-rich nature of the triazole ring.[14] Devices using **118b** as the dopant emitter were compared to a reference device containing FIrpic; the **118b** devices retained the blue emission present in the PL spectrum, and the CIE coordinates of (0.15, 0.24) were bluer compared to those reported for the FIrpic device- (0.15, 0.28), although the electroluminescence efficiencies and EQEs were lower.[14]

A series of complexes containing pyrazolyl based ancillary ligands (Figure 5.3, **119a**-**e** and **119h**) also demonstrate this effect, as the electron withdrawing nature of the ancillary ligand is increased (from **119a**<**119b**<**119e**) a blue-shift in the emission colour is observed.[12] Cyclic voltammetry data confirmed that the reduction potentials were largely unaffected by the change of ancillary ligand, with the potentials for all complexes remaining in a narrow range (-2.62 – -2.68 V), while the oxidation potentials increase with increasing withdrawing capability of the ancillary ligand.[12] These complexes are of additional interest, as the pyrazole ancillary ligands of **119e** could

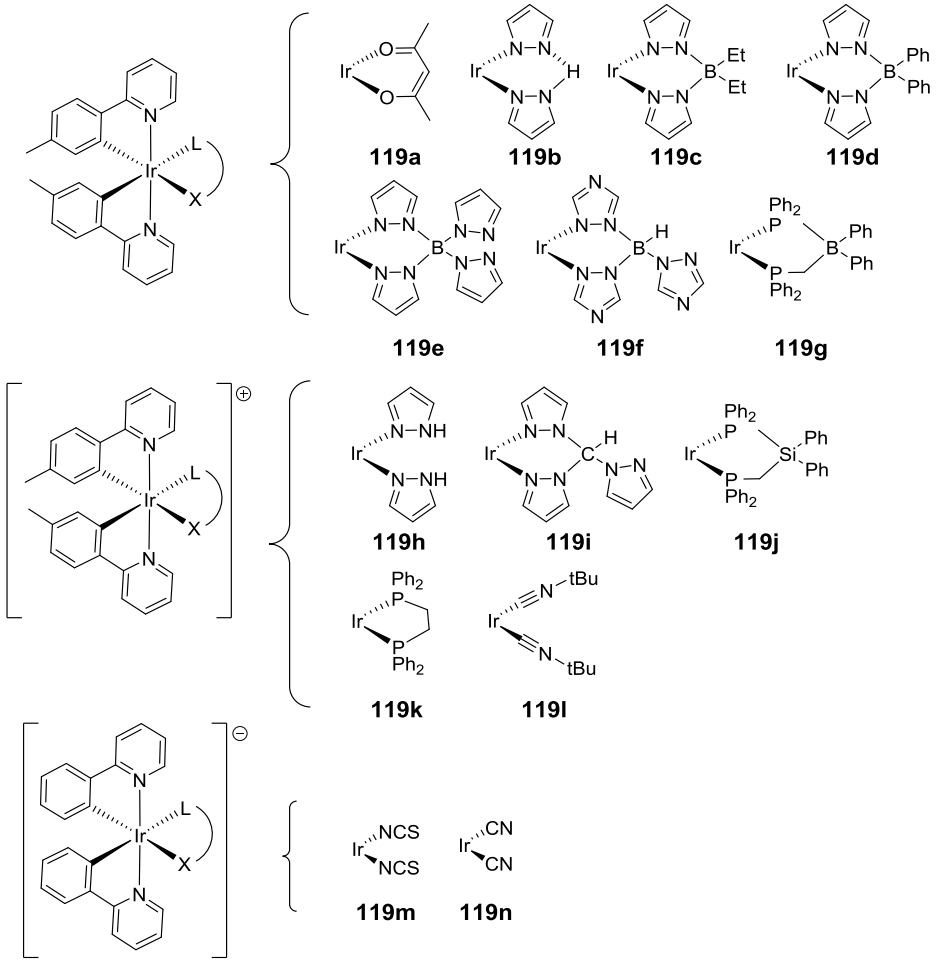

Figure 5.3

be used to coordinate other metal centres.[12] A further study extended the series to include the ancillary ligands (**119f**, **g** to **119i**-**n**) and a larger series of cationic complexes; in both series increasing the electron withdrawing potential of the ancillary ligand resulted in a blue-shift in emission. However, this was coupled with the expected decrease in radiative decay rates associated with a decrease in MLCT character in the excited state.[8] The PLQYs of the complexes vary with the choice of ancillary ligand, however the non-radiative decay values (k_{nr}) appear to follow the energy gap law, implying that any decrease in PLQY with increasing emission energy is due to the decrease of MLCT character in the excited state rather than an increase in non-radiative decay pathways.[8]

The substituent on the triazole ancillary ligand can effect the emission properties of the complexes; those shown in Figure 5.4 possess phenyl rings substituted with either electron donating or electron withdrawing substituents at the 3-position of the triazole ring display emission colours ranging from blue-green to near UV.[14] The complexes with electron donating

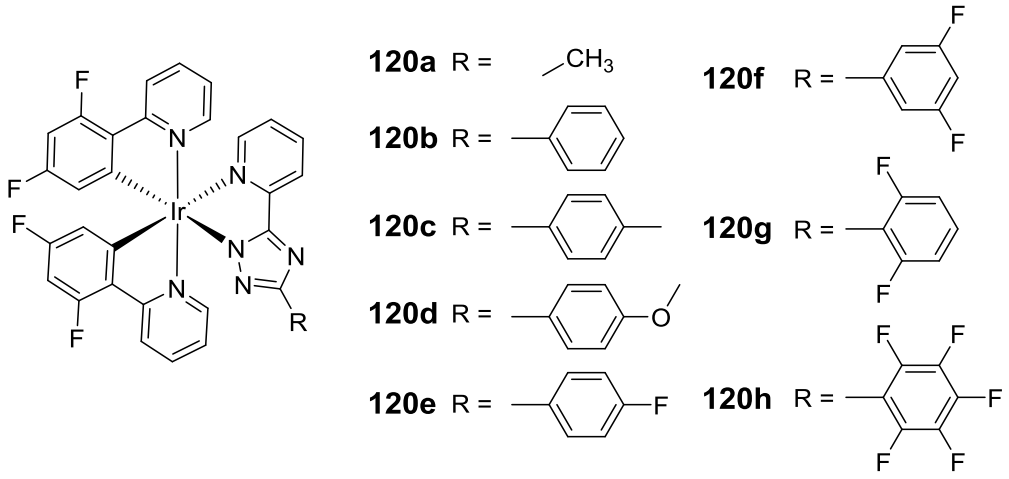

Figure 5.4

groups (**120c**, **d**) exhibit greener emission, due to a tail into the green region of the spectra, attributed to either the presence of a ligand-to-ligand charge transfer (LLCT) or an aggregation-induced effect.[14] The bluest emission is from complex **120h**, and it is observed that an increase in the twist angle between the triazole and the substitued phenyl ring (**120g**, **120h** vs **120e**, **120f**) results in a blue-shift in emission, and a switch from a pyridyl-triazole based MLCT state to an MLCT state based on the cyclometalating dfppy ligands.[14]

A variation on this strategy is to use strong field ancillary ligands, either strong σ-donors or π-acceptors, to increase the ligand field splitting, thereby lowering the energy of the metal d-orbitals and resulting in an increase in the emission energy. Strong field ligands also increase the energy of the d* antibonding orbitals, thereby increasing the energy of deactivating d-d* states and improving the efficiency of the complex.[15-17] Additionally, the lack of extended conjugation in the bidentate phosphine ligands reduces the participation of the ancillary ligand in the frontier orbitals of the complex, ensuring colour purity.[15-17] A variety of complexes containing non-

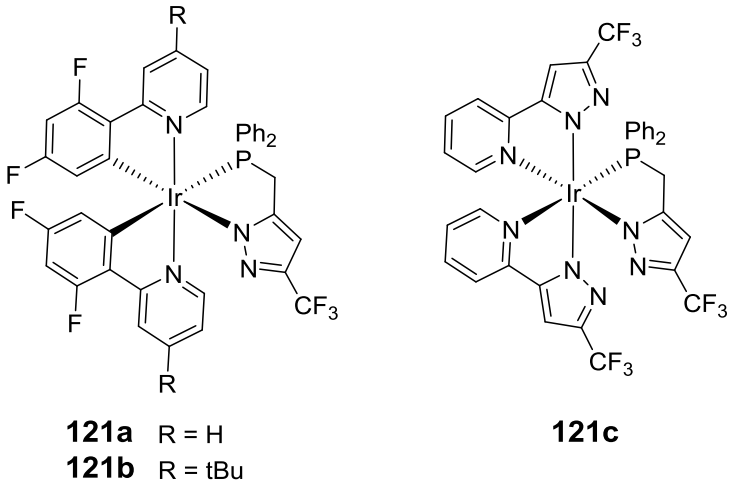

Figure 5.5

conjugated bidentate phosphine ligands are shown in Figure 5.5. Complexes **121a** and **121b**, containing a non-conjugated (P^N)H ligand, display blue emission, with λ_{max} of 455 nm, representing a significant blue-shift compared to FIrpic, and PLQYs of > 0.70.[16] On exchanging the dfppy based ligand for a phenylpyrazole cyclometalating ligand in **121c** the emission profile changes, three emission maxima are now observed at 431, 458, and 482 nm, resulting in true-blue emission insolution. The PLQY of complex **121c** was low in solution (0.02), but improved in the solid state when measured into a host material (0.25-0.35).[16] Devices of **121b** and **121c** displayed blue and deep blue emission, respectively, with CIE coordinates of (0.154, 0.215) and (0.163, 0.145), respectively.[16] The device of complex **121b** showed a peak EQE and luminance efficiency of 12.6% and 20.3 cd A^{-1}, while the device of complex **121c** gave a peak EQE and luminance efficiency of 6.9% and 8.1 cd A^{-1}, representing reasonable to high efficiencies for devices with these coordinates.[16]

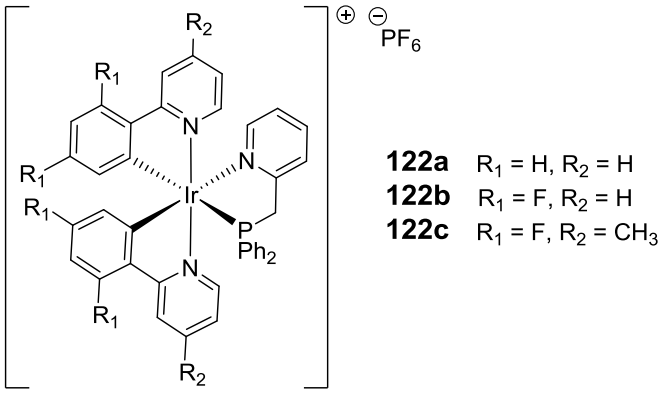

Figure 5.6

A comparable phosphine ancillary ligand was used in a series of cationic complexes **122a**-**c** (Figure 5.6).[18] Complex **122b**, an analogue of FIrpic, displayed blue emission with λ_{max} of 452 and 481 nm and, although the solution PLQY was very low (0.013 in DCM, 0.002 in ethanol), it improved to 0.18 when doped into a PMMA film.

Complexes containing charged ancillary ligands possessing a neutral phosphine and a cyclometalating phenyl ring have also been synthesised; complexes **123a**-**c** show first λ_{max} of 456-469 nm, with **123a** and **123b**, containing the fluorinated phosphine ligand, showing a significant blue-shift compared to FIrpic (λ_{max} = 470 nm).[19] The complexes show moderate (0.19 and 0.06 for **123a** and **123c**, respectively) to high (0.67 for **123b**) PLQYs, and a device containing **123b** displayed CIE coordinates of (0.156, 0.199) at 100 cd/m^2, a blue-shift compared to complexes such as FIrpic and FIrtaz (**118a**).[19] This work was later extended to include complexes **124a** and **124b**, analogues of **123c** and **123a**, respectively, with a pyridyl-pyrazole chromophoric ligand (Figure 5.7).[15] The complexes displayed deep-blue emission in solution, with λ_{max} of 430, 458 nm and 428,

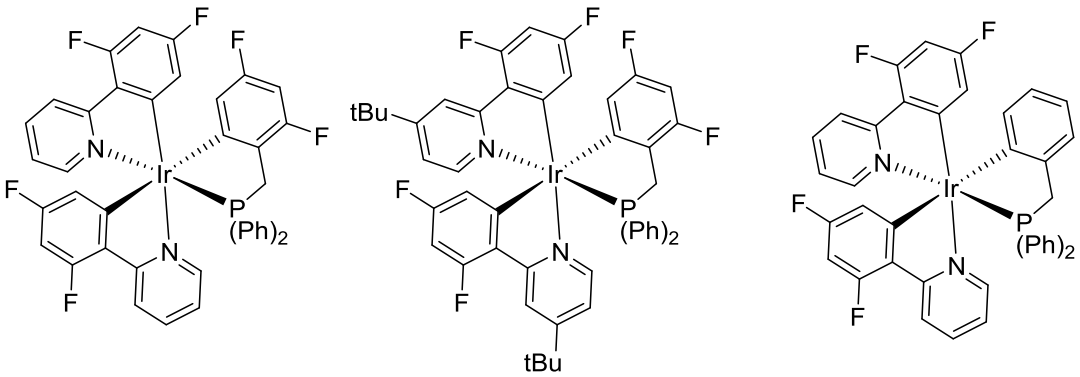

Figure 5.6

455 nm for **124b** and **124c** respectively, although the solution PLQYs were low (<0.01).[15] The PLQYs of the complexes improved dramatically when doped into films of host materials UGH2 and CzSi, presumably due to the restriction of intramolecular twisting and/or torsional motions. Devices using **124b** and **124c** as the dopants with UGH2 and CzSi as host materials, and displayed CIE coordinates of (0.152, 0.110) and (0.155, 0.106), respectively, close to the ideal coordinates of (0.14, 0.08) for true-blue emission.[15,17]

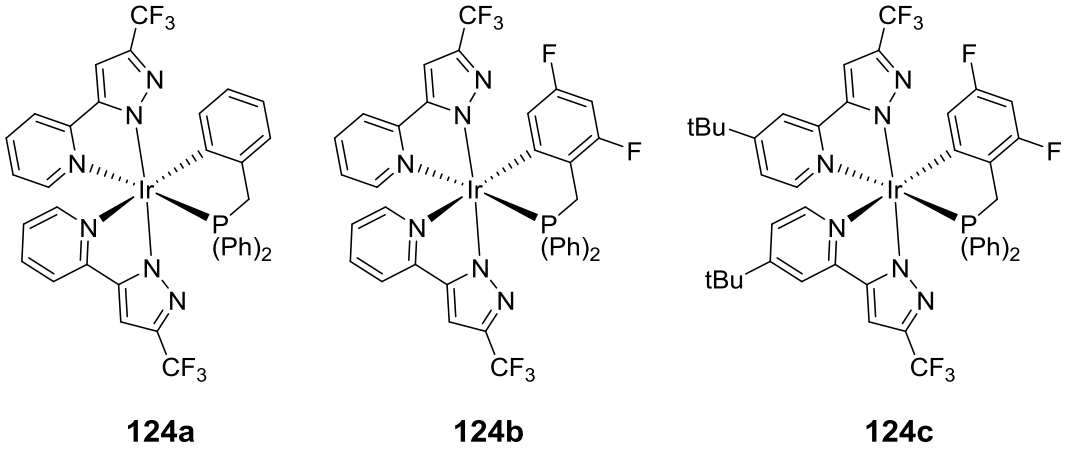

Figure 5.7

More exotic ancillary phosphine ligands can be seen in Figure 5.8; here the tridentate P^C_2 chelate was designed to offer long term stability to the complexes in devices and its saturated nature enables facile fine tuning of the emission by varying the substituent on the triazole ligand.[20] There is little variation in the emission colour on varying the monodenate phosphine ligands, although it does have a profound effect on the efficiency of emission; on increasing the donating ability of the phosphine the radiative rates increase due to the increase in energy of the deactivating MC state relative to the emissive state and an increase in MLCT participation in the emissive state.[20] The complexes performed well in devices, with a device of complex **125g** exhibiting CIE coordinates of (0.169, 0.247) and an EQE of 8.5% at a brightness of 100 cd/m^2.[20]

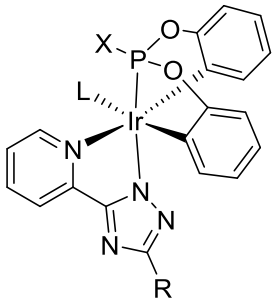

125a L = PPh_3, R = tBu, X = OPh
125b L = PPh_2Me, R = tBu, X = OPh
125c L = $PPhMe_2$, R = tBu, X = OPh
125d L = $P(OPh)_3$, R = tBu, X = OPh
125e L = $P(OPh)_3$, R = CF_3, X = OPh
125f L = PPh_2Me, R = tBu, X = Ph
125g L = PPh_2Me, R = 2-pyridyl, X = Ph

Figure 5.8

The phosphine moiety has also been combined with a o-carborane to create a strong field ancillary ligand; the phosphine acts as a strong σ-donor/π-acceptor and o-carborane can act as a good σ-donor, resulting in a ligand that forms stable metal-ligand bonds.[21] Additionally, due to the electron deficiency and lack of π-orbitals, the o-carborane fragment was predicted to have little involvement in the HOMO and therefore also in the electronic transitions.[21] Complexes **126a** and **126b** (Figure 5.9) displayed blue/blue-green emission in solution, with **126b** being significantly bluer than FIrpic.[21] The quantum yields of the complexes in solution were low, however they were enhanced in doped films; this effect was attributed to potential twisting and/or torsional motions of the carborane in solution.[21] The electrochemical properties of the complexes showed an increase in oxidation potential relative to FIrpic and *mer*-$(dfppy)_3$, highlighting the strong field character of the ancillary ligand.[21]

In addition to chelating ancillary ligands strong field monodentate ligands can also be used to blue-shift emission, including phosphines,[22,23] cyanide,[22,24] iso-cyanide and thiocyanate.[23] Complexes of the form $Ir(F_2Meppy)(PPhMe_2)_2(H)(X)$, where X = Cl (**127a**), NCMe (**127b**) and CN (**127c**) (Figure 5.10) all exhibit blue emission with λ_{max} of 439-446 nm in solution, although the PLQYs are low (<0.07).[22] As the field strength of the ancillary ligand increases (Cl < NCMe < CN) the emission is blue-shifted, and the (calculated) HOMO level drops significantly (0.29 eV), as expected.[22] In another series of complexes of the form $Ir(dfppy)_2(RNC)CN$ (**128a**-**f**,Figure 5.10) the

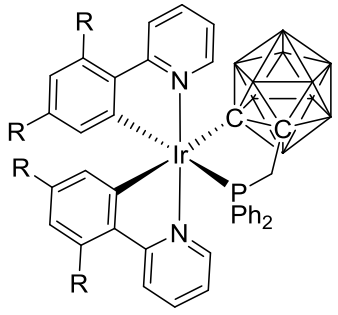

126a R = H
126b R = F

Figure 5.9

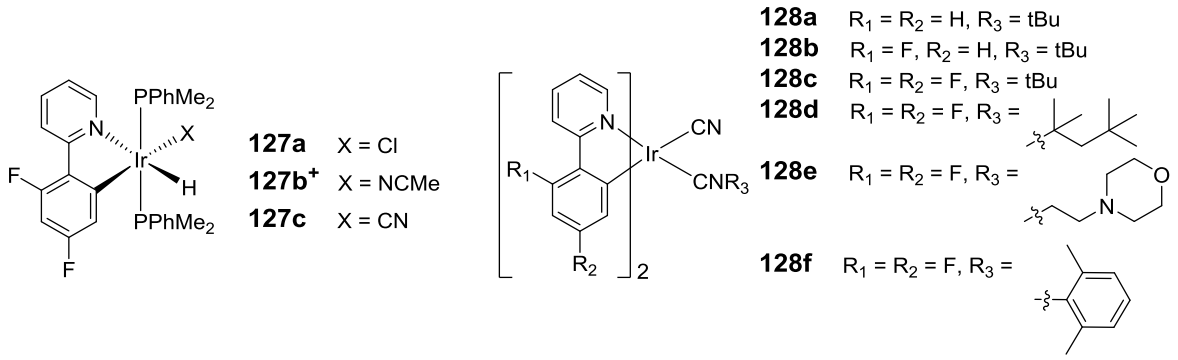

Figure 5.10

cyanide and isocyanate ancillary ligands serve to blue-shift the emission due to their strong electron-withdrawing ability, resulting in complexes that all exhibit bluer emission than FIrpic (λ_{max} = 469 nm), although the choice of R group in RNC had little effect on the emissive properties.[24] Additionally, the strong field nature of the ligands can also shift the deactivating MC d-d* states to higher energies, resulting in efficient emission at room temperature (PLQYs > 0.60).[24]

'Chromophoric' ancillary ligands, i.e. those that participate in the excited state provide another mechanism for tuning the emission colour.[25] When the triplet state of the ancillary ligand is lower than that of the ^{3}MLCT transition centred on the chromophoric ligand an interligand energy transfer (ILET) process can occur, resulting in subsequent emission from the lower energy ^{3}LC state, red-shifting the emission.[25,26] Ancillary ligands can also participate in the excited state via LLCT mechanisms, wherein either the HOMO or, more commonly, the LUMO is localised on the ancillary ligand, while the other frontier orbital is located on the cyclometalating ligand. The ILET effect can be seen in the family of complexes shown in Figure 5.11; the complexes all contain dfppy as the cyclometalating ligand while the ancillary ligands are all related to picolinic acid.[9,25]

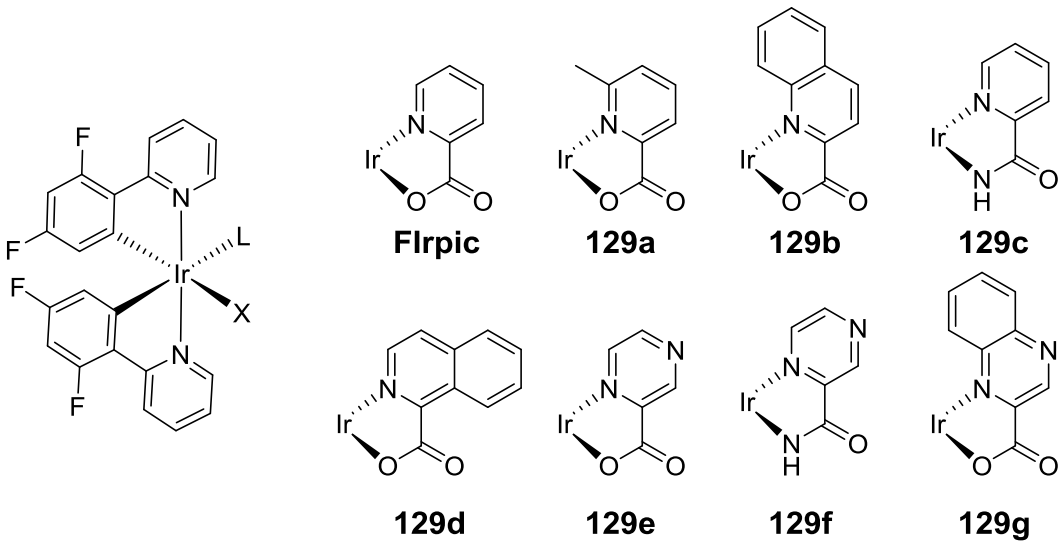

Figure 5.11

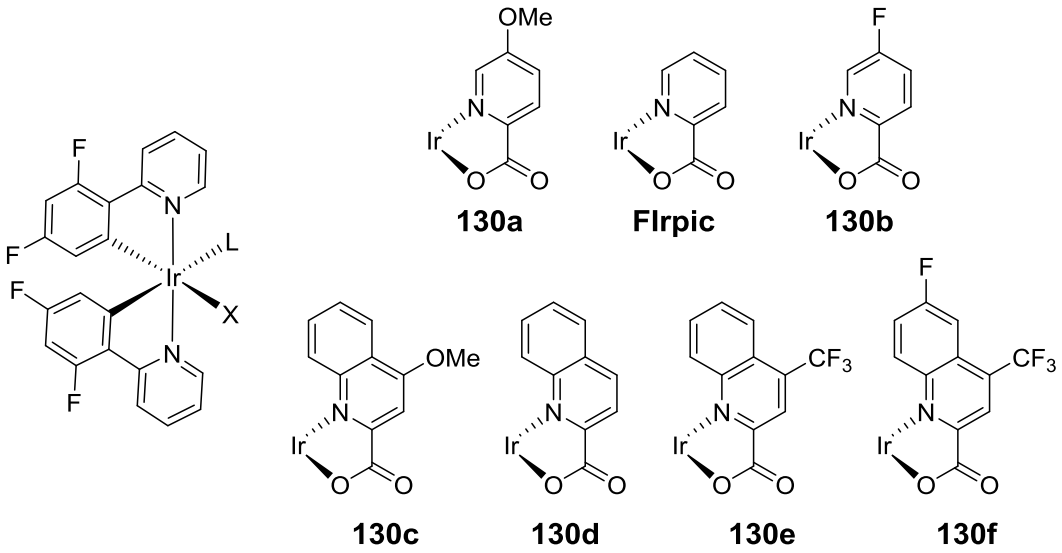

Figure 5.12

FIrpic and **129a** displayed blue/green emission, with vibronic features characteristic of emission from a mixed ^{3}LC/^{3}MLCT state localised on the dfppy ligand, while the remaining complexes (**129b**-**g**) display featureless, red-shifted emission.[9,25] Electrochemical analysis indicated that the HOMO levels of the complexes were all similar in energy, while the LUMO levels decrease across the series.[9,25] Based on the DFT calculations and the experimental data it was concluded that the cyclometalating ligands are preferentially excited, the energy is then rapidly transferred to the ancillary ligand, followed by ancillary ligand centred phosphorescence.[9,25] Similar complexes were described by Zhou (Figure 5.12); here the complexes are divided into two series, a FIrpic based series (**130a**,**b**, **FIrpic**) and a FIrqui based series(**130c**-**f**), which displayed ILET emission.[27] The substitution of the pyridine ring in the FIrpic series had no impact on the colour of the emission, as was to be expected, as the ancillary ligand is not directly involved in the excited state, however the intensity of the emission does vary.[27] In the case of the ILET series the introduction of substituents onto the quinoline ring affects both the emission colour and the intensity, as the ancillary ligand is directly involved in the excited state.[27]

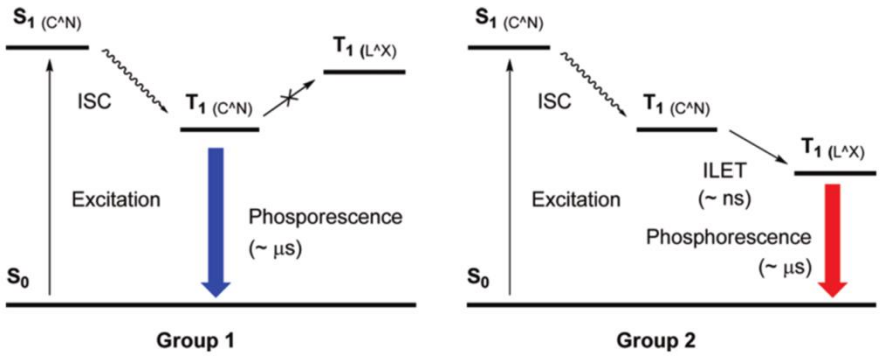

Figure 5.13: Initial mechanism proposed for the ILET process. Adapted from reference [28].

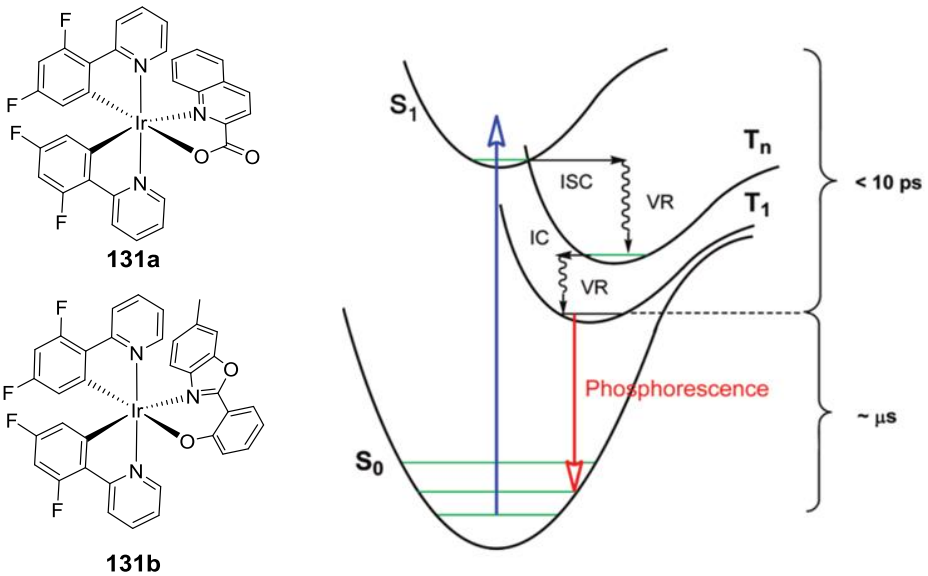

Figure 5.14: LEFT: complexes 131a,b. RIGHT: Proposed energy level diagrams of complexes 131a,b and mechanism of emission. IC = internal conversion, ISC = intersystem crossing, VR = vibrational relaxation. Adapted from reference [28].

There is a debate in the literature around the exact mechanism of the 'ILET' process. The initial suggestion involved a nanosecond ILET process between the triplet state of the C^N chromophoric ligand (^{3}C^N) and the triplet state of the ancillary ligand (^{3}L^X), followed by phosphorescence from this state on a microsecond timescale (Figure 5.13), when the ^{3}L^X state is lower in energy than the ^{3}C^N state.[29] However, a later study on complexes **131a** and **131b** (Figure 5.14) revealed no sign of a nanosecond timescale process; the complexes were studied by time-correlated single photon counting (TCSPC), revealing a single exponential decay to a resolution of 300 ps.[28] Femto-picosecond transient absorption spectroscopy revealed an ultrafast (<1 ps) intersystem crossing process ($S_1 \rightarrow T_n$), followed by a rapid (<10 ps) internal conversion/vibrational relaxation process ($T_n \rightarrow T_1$) to populate the lowest energy triplet state, which then decays by phosphorescence (µs), with no evidence of a nanosecond process.[28]

As can be seen from the complexes that have been discussed in Figures 5.11 and 5.12, extending

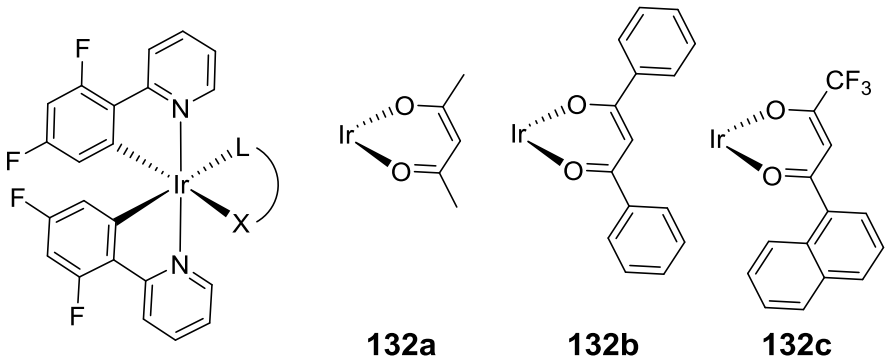

Figure 5.15

the conjugation in the ancillary ligand commonly results in activation of an ILET/ILCT-type process.[26] Some further examples of this are shown in Figure 5.15; on increasing the conjugation in the ancillary ligand across the series (**132a** to **132b**) the emission is red-shifted, and electrochemical and computational data support a shift in the LUMO from the cyclometalating ligand to the ancillary ligand, resulting in a decrease in the HOMO-LUMO gap.[26]

NEW ANCILLARY LIGANDS FOR BLUE IRIDIUM COMPLEXES – RESULTS AND DISCUSSION

Due to the success of the sulfone ligands discussed in Chapters 2 and 3 there was interest in devising new ancillary ligands to further blue-shift the emission, in particular to be paired with the mono-fluoro and 'fluorine-free' ligands **66** and **79** synthesised in Chapter 3. Pyrazolepyridine ligands (and the related triazolepyridines) have been used as blue-shifting ancillary ligands due to their high acidity, reducing the electron density around the metal centre and thereby reducing the HOMO level relative to the LUMO.[8,12,11] They are also used as the chromophoric ligands in N-heterocyclic carbene complexes,[30] and in conjunction with a variety of other ligands, such as difluorophenylpyridine ligands and chelating phosphine ligands.[17,31,32] Ligand **133** was chosen as the initial target, as the CF_3 group is strongly electron withdrawing,[33,34] and our group has shown that a mesityl substituent can increase the PLQY and efficiency of complexes in devices.[35] The route to ligand **133** is shown in Figure 5.16, and can be generalised to other ligands of the same type.

2-Acetyl-4-chloropyridine (**137**) was identified as a key synthetic intermediate, as from here a

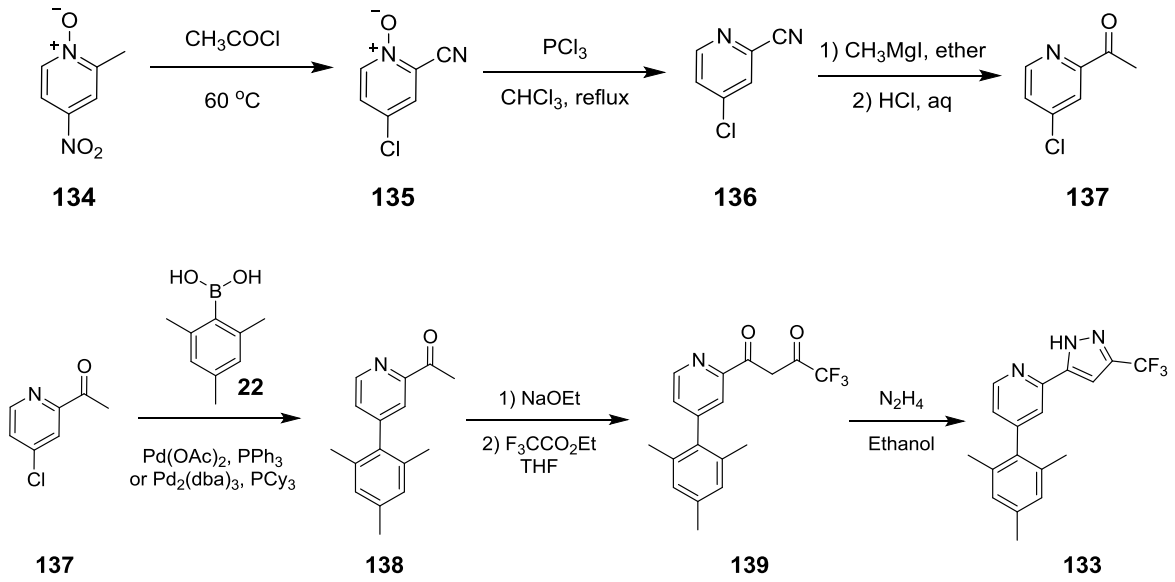

Figure 5.16: Synthesis of target ligand 133.

choice of R_1 and R_2 groups can be introduced to create a variety of ancillary ligands. The synthesis of **137** started with a reaction between 4-nitro-α-picoline N-oxide **134** and acetyl chloride.[36] The nitro group is replaced by a chloride and the reagent generated (thought to be acetyl nitrite) attacks the ortho-methyl group to produce an oxime intermediate, which results in the desired nitrile **135**.[36,37] This reaction has been documented in 2-methylpyridine, 2-methylquinoline and 2-methyl pyridazine N-oxides.[37,38] Although the yield is low (23%), 2-cyano-4-chloropyridine **135** was produced in sufficient quantity to continue, and the starting material **134** was inexpensive, compared to the high cost of **136** and **137**. The next step was to remove the N-oxide using PCl_3, which produced **136** in good yield (73%). Then a reaction with methyl magnesium chloride resulted in the formation of the ketone **137** upon acidic workup.

From **137** it would be possible to synthesis a wide variety of ligands; however for the target molecule **133** the next step was a Suzuki coupling with mesitylboronic acid (**22**) to give **138**, followed by a crossed Claisen condensation type reaction with ethyl trifluoroacetate to give a diketone intermediate **139**. The crude material was used in the next step directly, and reacted with hydrazine hydrate to give **133** via a ring closing condensation reaction.[39]

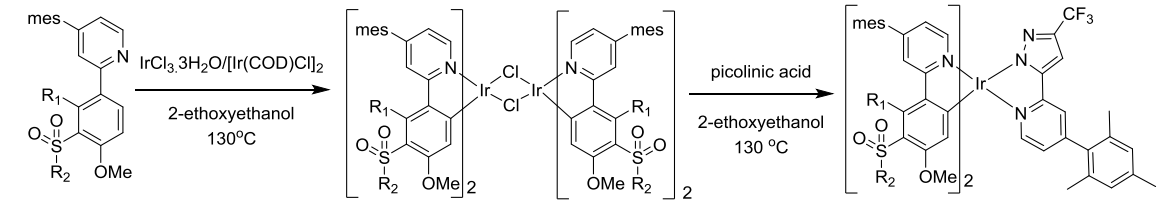

Figure 5.17

Once ligand **133** was obtained, it remained to synthesise the desired complexes. Ligands **66** and **79**, the synthesises of which are described in Chapter 3, were chosen as the chromophoric ligands due to the promising performance of complex **70** derived from **66**, and the desire to create a bluer fluorine-free complex than **80** (derived from **79**). The complexes **140** and **141** were synthesised as shown in Figure 5.17. The routes were analogous to those used for the corresponding pic complexes **70** and **80**, with complex **140** being obtained in 70% yield from ligands **66** and **133** using $IrCl_3.3H_2O$, and complex **141** being obtained in 27% yield from ligands **79** and **133** using $[Ir(COD)Cl]_2$.

PHOTOPHYSICAL AND ELECTROCHEMICAL PROPERTIES

Absorption and emission

The absorption spectra of complexes **140** and **141**, analogous pic complexes **70** and **80** and FIrpic

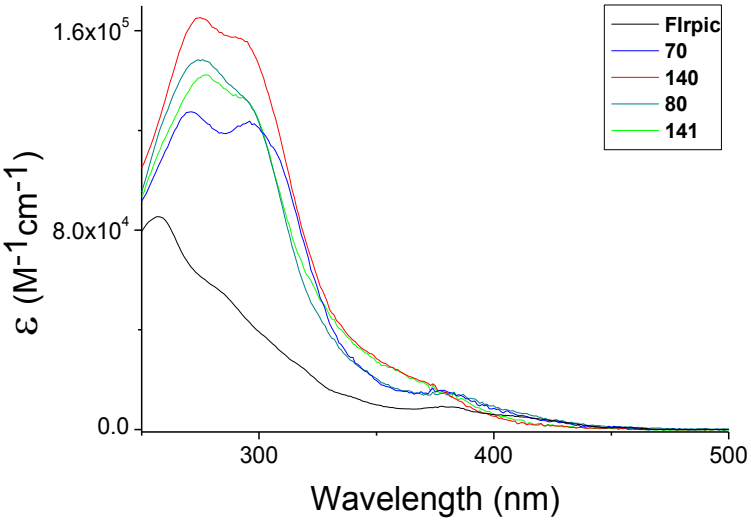

Figure 5.18: UV absorption spectra of the complexes in DCM [<10^{-5} M].

are shown in Figure 5.18. As with complexes **70** and **80**, **140** and **141** show strong absorption bands (with oscillator strengths of >100 x 10^3 dm^3/mol cm) in the 250-325 nm region, assigned to the π-π* transitions on the ligands, based on the calculations of Hay,[40] and literature precedent.[41] At lower energies and oscillator strengths the complexes display another set of absorption bands, assigned to the ^{1}MLCT transitions. Here, we see differences between the pic complexes **70** and **80** and **140** and **141**; the ^{1}MLCT bands appear to have moved to higher energies on replacing the pic ligands with ligand **133**, suggesting **133** has indeed decreased the energy of the metal d-orbitals. At very low oscillator strengths (>1x10^3 dm^3/mol cm) the ^{3}MLCT bands can be seen between 450-456 nm.

The excitation spectra of complexes FIrpic, **70**, **80**, **140** and **141** are shown in Figure 5.19, revealing as expected that the bands from the ^{1}MLCT and ^{3}MLCT states are responsible for the emission

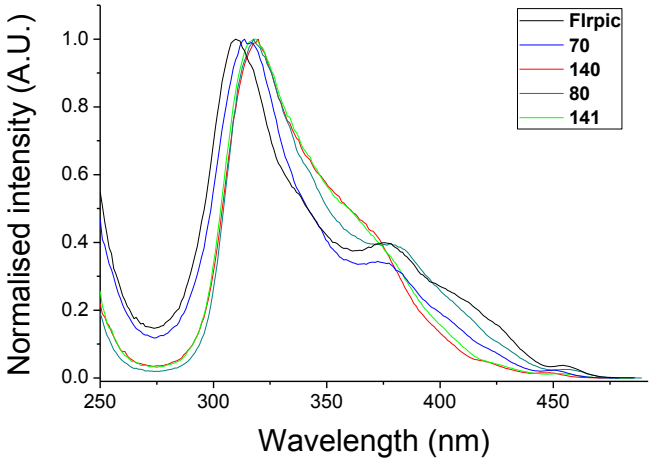

Figure 5.19: Excitation spectra of the complexes in DCM [<10^{-5} M]. The emission band observed was the second emission maximum.

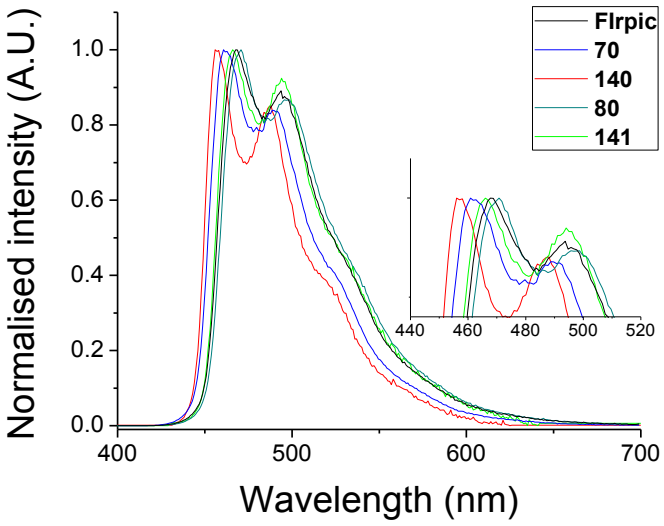

Figure 5.20: Emission spectra of selected complexes in deaerated DCM, λ_{ex} = 380 nm.

from the complexes, while the majority of the lower energy π-π* transitions are dark.

The emission spectra of the complexes are shown in Figure 5.20. The spectra of **140** and **141** display a similar profile to that of FIrpic and the analogous pic complexes **70** and **80**, with an emission maximum, vibronic progression and a shoulder at longer wavelength, indicating the

Complex	λ_{max}^{abs} (ε)/ nm (x10^3 $M^{-1}cm^{-1}$)[a]	λ_{max}^{em} / nm[b]	PLQY / Φ_{PL}[a,d]	τ_P / μs[a,e]	k_r / $10^5 s^{-1}$ [f]	k_{nr} / $10^5 s^{-1}$ [f]
1 FIrpic	277 (50.1), 301 (34.2), 304 (32.6), 337 (13.8, sh), 357 (8.9, sh), 400 (6.2), 454 (0.8)	468, 496, 531 (sh)	0.67	1.72	3.90	1.92
70	258 (s sh, 108.5), 271 (128.6), 297 (123.4), 307 (sh, 112.5), 339 (s sh, 29.2), 379 (15.7), 450 (1.0)	462, 490, 524 (sh)	0.67	1.78	3.76	1.85
140	274 (144.4), 293 (136.7), 370 (19.4), 419 (sh,2.7), 447 (0.7)	457, 486, 521 (sh)	0.62	2.30	2.70	1.65
80	275 (104.4), 291 (101.9), 324 (sh, 47.8), 381 (14.5), 405 (sh, 7.9), 456 (0.9)	469, 497, 536 (sh)	0.58	2.13	2.72	1.97
141	255 (sh, 100.4), 277 (125.8), 292 (133.5), 321 (59.6) (sh), 375 (16.3), 406 (sh, 5.1), 454 (0.8)	466, 494, 531 (sh)	0.52	3.13	1.66	1.53

[a] Data obtained in dichloromethane solution at 20 °C. [b] Data obtained in degassed dichloromethane solution with λ_{ex} = 380 nm. [c] Energy difference between lowest energy excitation maxima and highest energy excitation maxima. [d] Measured relative to $Ir(ppy)_3$ Φ_{PL} = 0.46 in degassed dichloromethane at 20 °C; estimated error ±5%. [e] Estimated error ±5%.%. [f] k_r, k_{nr} values calculated using Equations 1.5/1.6.

Table 5.1: Photophysical data for selected iridium complexes.

emission originates from a similar excited state. This is consistent with a mixed LC/MLCT state, due to the vibronic nature of the emission. The emission λ_{max} for **140** and **141** is blue-shifted by 5 nm and 4 nm relative to their analogous pic complexes, respectively. This represents blue-shift of 11 nm and 3 nm relative to that of FIrpic, indicating the new ancillary ligand is effective at blue-shifting the emission.

The PLQYs, lifetimes (τ_{obs}) and calculated radiative and non-radiative decay rates (k_r and k_{nr}) are shown in Table 5.1. The PLQYs for complexes **140** and **141** are comparable to their pic analogues, **70** and **80**, although the lifetimes of **140** and **141** are slightly longer.

Electrochemistry

The electrochemical behaviour of complexes **140** and **141** was investigated using cyclic voltammetry and compared FIrpic and their pic analogues **70** and **80**. The voltammograms are shown in Figure 5.21, panel a, and the key parameters in Table 5.2. Formula 2.1 is used to calculate the energy of the HOMO.

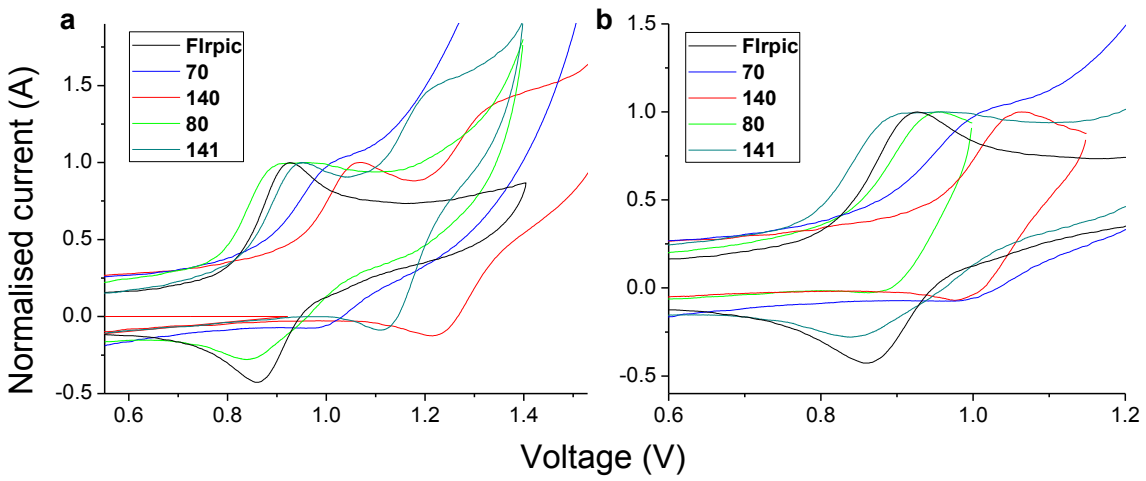

Figure 5.21: Cyclic voltammograms of the iridium complexes. Panel a: full oxidation scan. Panel b: scan reversed after first oxidation.

Whereas the pic complexes **70** and **80** show a single quasireversible oxidation wave, complexes **140** and **141** show an initial oxidation that appears irreversible, followed by a second reversible oxidation at higher potentials. If the scan is reversed before the second oxidation is reached the oxidation wave is quasireversible (Figure 5.21, panel b). As both complexes (**140** and **141**) contain the same ancillary ligand it is assumed the second oxidation occurs either on this ligand or is due to an interaction this ligand has with the metal. Notably, in both cases exchanging the pic ancillary ligand for ligand **133** (**70** to **140**, **80** to **141**) results in an increase in the oxidation potential of the Ir^{3+}/Ir^{4+}couple, suggesting that ligand **133** is effective at lowering the energy of the HOMO. No

Complex	$1^{st} E^{ox}_{1/2}$ / V	$2^{nd} E^{ox}_{1/2}$ / V	HOMO / eV
FIrpic	0.89	-	-5.69
70	1.01	-	-5.81
80	0.89	-	-5.69
140	1.02 (1.07)	1.28	-5.82
141	0.91 (0.95)	1.17	-5.71

Values in ( ) denote the cathodic peak potential observed on the first scan. All values reported vs Fc/Fc^+ = 0.00 V.

Table 5.2: Electrochemistry data of iridium complexes.

reduction waves were observed within the solvent window [to 2.0 – -2.5 V].

DEVICE DATA

OLEDs containing complexes **140** and **141** were fabricated by Dr Hameed Al Attar in the Department of Physics at Durham University and compared to a reference device containing FIrpic, and devices containing related complexes **70** and **80**.The hole transporting layer and emissive layer were deposited by solution processing techniques, and the electron transporting, electron injection layers and the cathode were then fabricated by vacuum deposition. The device structure is as follows: ITO/PEDOT:PSS (45 nm)/PVK:OXD(30%):**Ir complex**(15%)(60 nm)/TPBi (30 nm)/LiF/Al.

The electroluminescence (EL) spectra from the devices are shown in Figure 5.22, panel a; for all complexes the EL spectra are similar to the photoluminescence (PL) spectra, indicating good exciton confinement on the emissive molecule. Complex **140** was less efficient than the corresponding pic complex **70**, with lower brightness (panel e), lower EQEs (panel c), and lower

Complex	λ_{ELmax} / nm	Brightness / cd/m^2	turn-on voltage / V [a]	EQE / %	current efficiency / cd/A	power efficiency / lm/W	CIE coordinates / (x,y) [b]
FIrpic 1	475	7340	6.2	5.4	12.2	5.1	(0.19, 0.38)
70	470	2072	8.5	3.5	6.1	1.9	(0.16, 0.30)
80	478	516	8.5	1.2	2.6	0.9	(0.22, 0.40)
140	464	1066	9.5	2.3	4.1	1.2	(0.17, 0.28)
141	473	456	7.9	1.7	3.9	1.4	(0.23, 0.40)

[a] Measured at a brightness of 10 cd/m^2. [b] Measured at 12 V.

Table 5.3: Summary of device data.

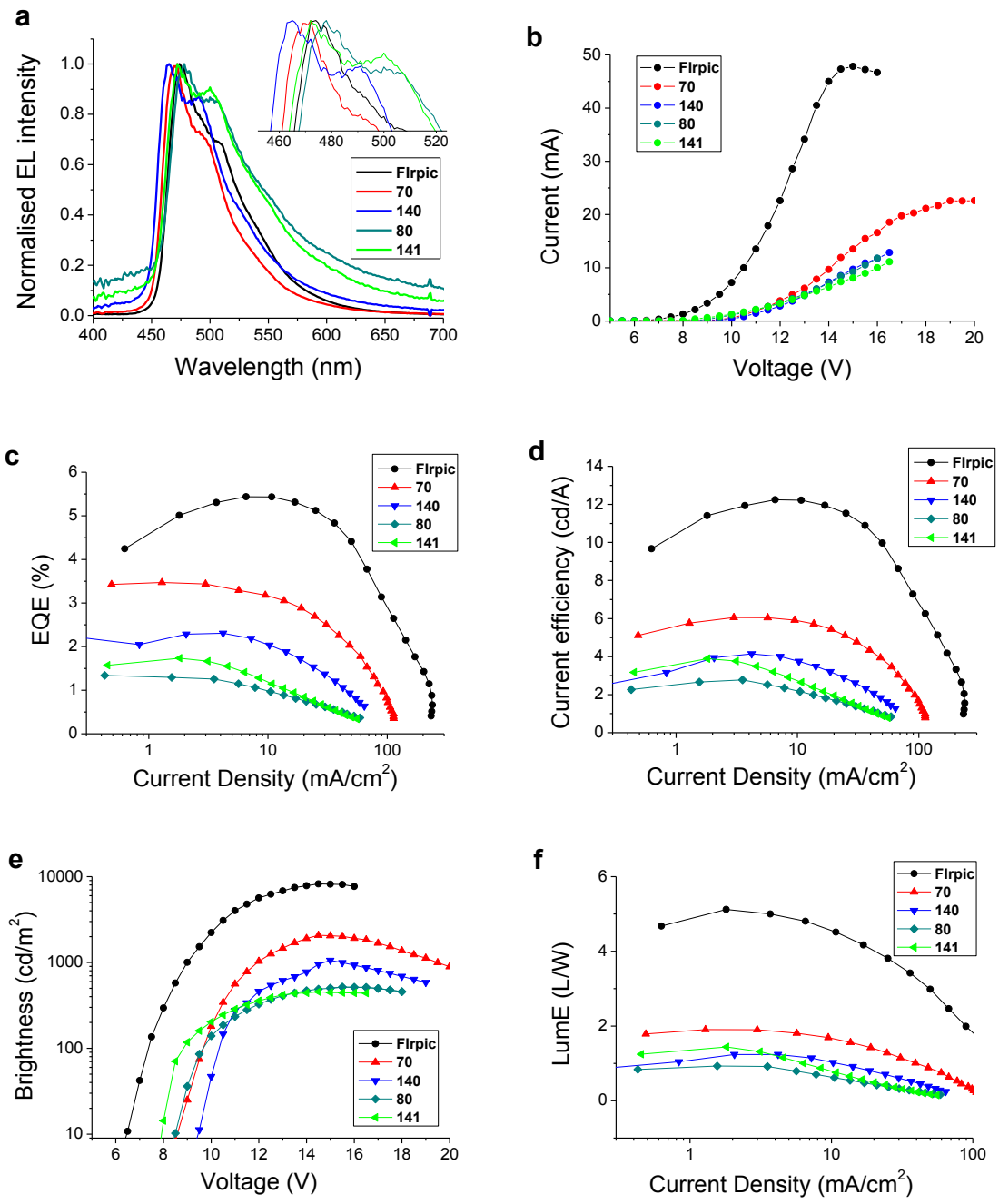

Figure 5.22: Device data for complexes 70, 80, 140, 141.

current and power efficiencies (panels d and f), although it is noted that the emission is significantly bluer (6 nm) and, based on the electrochemical data, the HOMO is lower in energy, which could be partially responsible for the reduced performance. Complex **141**, however, performed slightly better than **80**, with comparable brightness and turn on voltage (panel e), but superior EQEs, current and power efficiencies. The electroluminescent λ_{max} of **141** is also blue-shifted relative to **80**, making **141** a very promising aromatic fluorine-free blue emitter. Key device parameters are summarised in Table 5.3.

CONCLUSION

A new ancillary ligand **133** was devised with the aim of blue-shifting emission, and was paired with ligands **66** and **79**, the syntheses of which are described in Chapter 3, to create complexes **140** and **141**, analogous to **70** and **80**. The photophysical and electrochemical properties were compared to FIrpic and their parent complexes; ligand **133** successfully blue-shifted the emission of **140** and **141** relative to the pic complexes, and quantum yields were comparable. Devices of complexes **140** and **141** were fabricated in the Department of Physics, and retain the blue emission observed in the PL spectra. Future work would involve expanding this ancillary ligand family, with the aim of optimising device performance.

INVESTIGATING A NEW FAMILY OF ANCILLARY LIGANDS – RESULTS AND DISCUSSION

In 2013 complexes **142a** and **142b** (Figure 5.23) were published by Zhu, Bryce *et*.*al*. featuring novel oxazoline/thiazoline containing ancillary ligands.[42] Complexes **142a** and **142b** showed promising device performance, with low turn on voltages (3.5-3.7 V), high maximum brightnesses of 61,560 cd/m^2 (at 16 V) and 21,350 cd/m^2 (at 14.5 V), and maximum EQEs of 17.1% and 8.5%, respectively.[42] The exchange of the oxazoline (**142a**) for the thiazoline (**142b**) results in a broadening of the emission spectra, giving rise to a change in the emission colour from green to yellow/orange.[42] Also of interest is the unusual localisation of the frontier orbitals in these complexes; the LUMO is located on the pyridyl ring of the cyclometalating ligand, as expected, while the HOMO is localised on the Ir d-orbitals and the phenoxylate of the 'ancillary' ligand.[42]

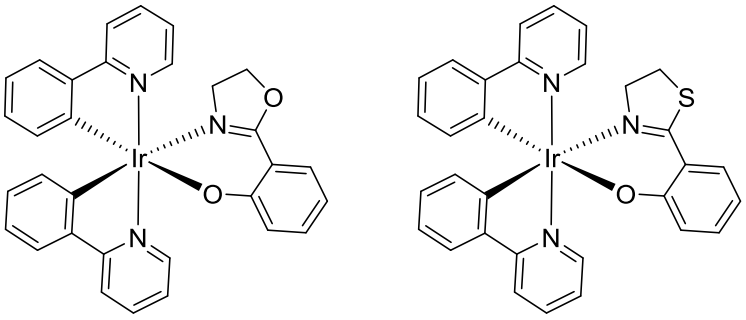

142a **142b**

Figure 5.23: Iridium complexes containing oxazoline/thiazoline ancillary ligands.

Other similar complexes have been synthesised, such as those shown in Figure 5.24; here enantiomerically pure chiral oxazoline ancillary ligands are used to separate the Δ/Λ isomers of the complexes **143a-d**.[43] The diastereomers each have similar photophysical properties, and were considered in future applications as luminescent sensors of chiral molecules.[43] A similar series

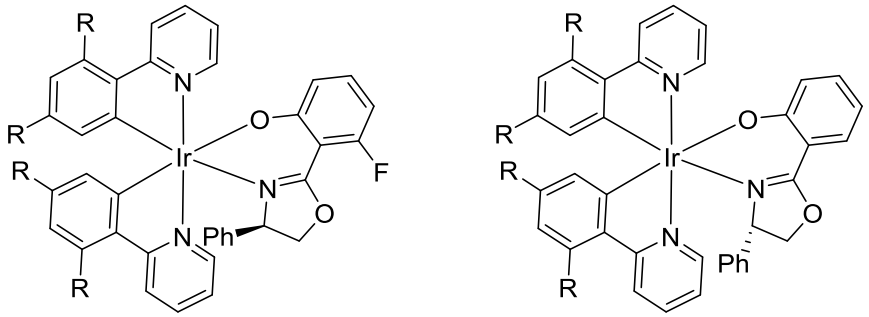

143a R = F
143b R = H

143c R = F
143d R = H

Figure 5.24

shown in Figure 5.25 has an oxazole (rather than oxazoline) based ancillary ligand, and the conjugation length of this ligand was increased (**144a** to **144c**).[44] In this case the HOMO is localised on the Ir d-orbitals and the phenolate ring of the ancillary ligand, while the LUMO is located mostly on the cyclometalating ligands, although as the conjugation length of the ancillary ligand increases a greater portion is localised on the oxazole ring.[44] DFT calculations reveal participation from higher lying unoccupied orbitals (LUMO+1, LUMO+2) in the lowest energy triplet state of the complexes, resulting in emission dominated by the 'ancillary' ligand.[44] Oxazoline, oxazole and benzoxazole ligands have also been used as the chromophoric ligand for iridium complexes for use as photosensitisers for water splitting.[45]

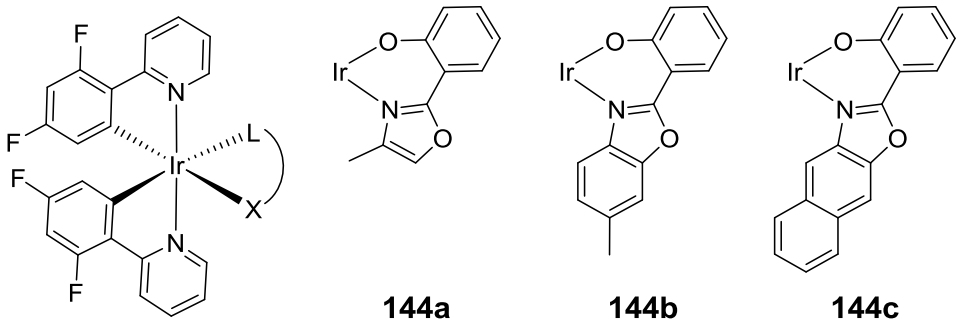

144a **144b** **144c**

Figure 5.25

As the oxazoline/oxazole ligands described above have produced complexes with interesting properties it was of interest to expand the family of complexes to further probe the effect of substituents, both on the chromophoric and ancillary ligands. This work was conducted in collaboration with Prof. Dongxia Zhu of Northeast Normal University, Changchun, China. The initial aim was to retain the good device performance, and the narrow emission bandwidth of **142a**, while blue-shifting the emission by choice of chromophoric cyclometalating ligand. Complex **142a** displays an unusual HOMO-LUMO distribution, with the LUMO based on the pyridine ring of the ppy ligand, while the HOMO is localised on the iridium atom, and the

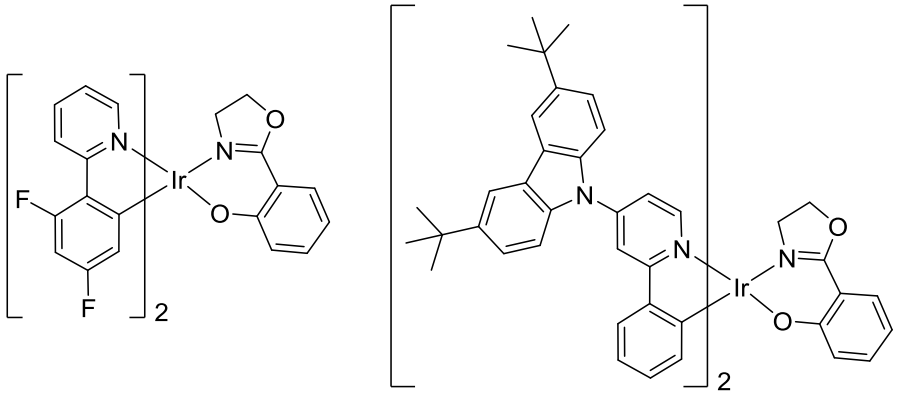

145 **146**

Figure 5.26: Initial target complexes.

phenolate ring of the 'ancillary' ligand. As a result the two initial target complexes are shown in Figure 5.26, **145** and **146**. Compound **145** was chosen as the fluorines are known to result in a blue-shift in emission compared to typical ppy-based complexes. However in this system it was thought they may not be as effective, as the HOMO is not localised on the phenyl ring. Utilising a dfppy (**13**) cyclometalating ligand could still affect the emission colour by withdrawing electron density from the metal d-orbitals, where the HOMO is partially located. Complex **146** was chosen in an attempt to raise the energy of the LUMO relative to the HOMO by virtue of the strongly electron-donating carbazole unit.

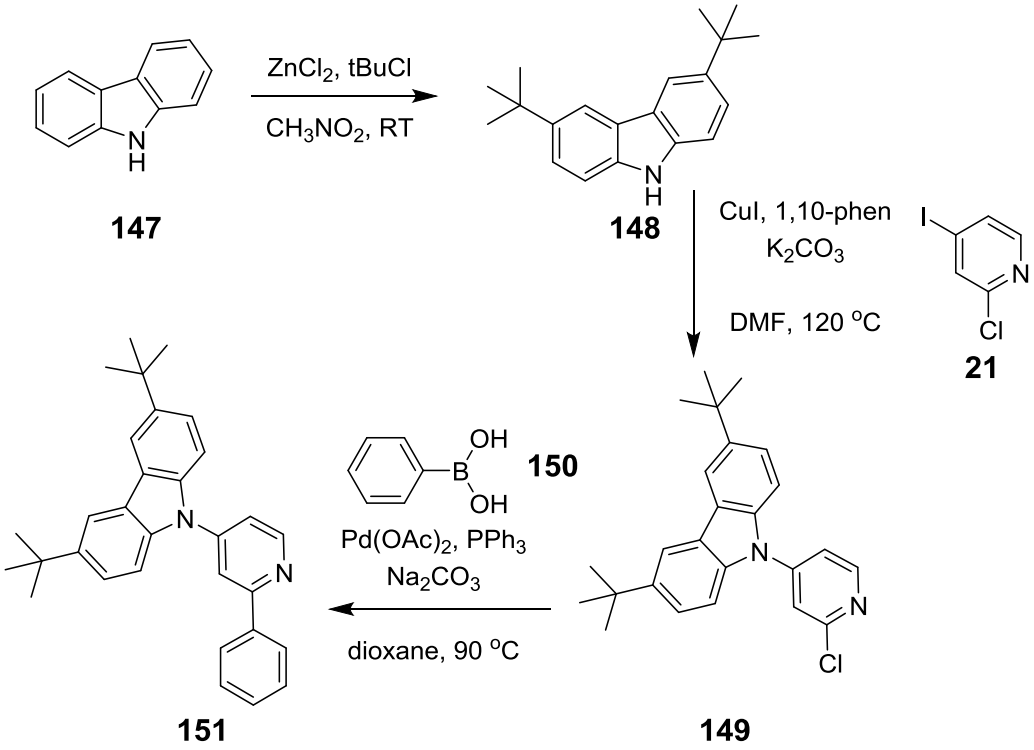

Figure 5.27: Synthesis of ligand 151

The synthesis of dfppy **13** is shown in Figure 2.13, and the synthesis of ligand **151** is shown in Figure 5.27. Ligand **13** was synthesised from a Suzuki reaction between commercially available boronic acid **12** and 2-bromopyridine **11**, as described in Chapter 2. For ligand **151**, the first step involved synthesis of the 3,6-(bistertbutyl)carbazole **148** from carbazole **147** via a Friedel-Crafts type alkylation (19% yield). The next step was an Ulmann-type reaction between **148** and **21** to give **149** (79%), followed by the final Suzuki coupling between **149** and phenylboronic acid **150** using $Pd(PPh_3)_4$ as the catalyst and Na_2CO_3 as the base. Compound **151** was obtained in quantitative yield.

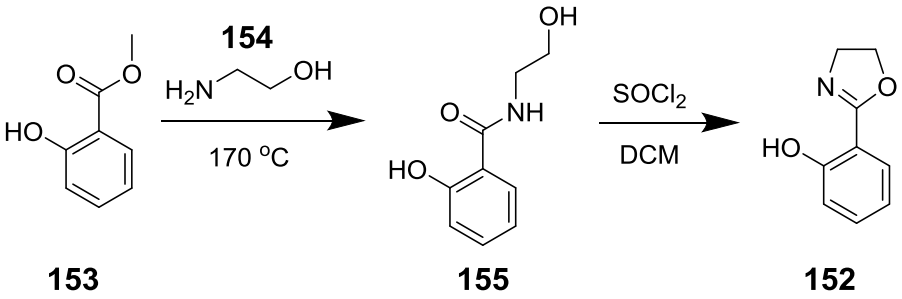

Figure 5.28: Synthesis of ancillary ligand 152.

The synthesis of ancillary ligand **152** is shown in Figure 5.28, and proceeded as described.[42] First, commercially available ester **153** was refluxed with amine **154** to produce **155** in 82% yield. Then, the reaction of **155** with thionyl chloride gave the product **152** in 94% yield.

Complexes **145** and **146** were synthesised via the standard one-pot method (Figure 5.32); the ligands **13** and **151** were each reacted with $IrCl_3.3H_2O$ in 2-ethoxyethanol to produce precipitates presumed to be the intermediate dichloro-bridged dimers. Ancillary ligand **152** and Na_2CO_3 were then added, and after purification complexes **145** and **146** were isolated as yellow and orange powders, in 79% and 19% yield, respectively.

The low yield of complex **146** was attributed to difficulties in the purification; the complex appeared unstable on silica. It is possible the stability is due to reaction with the chlorinated

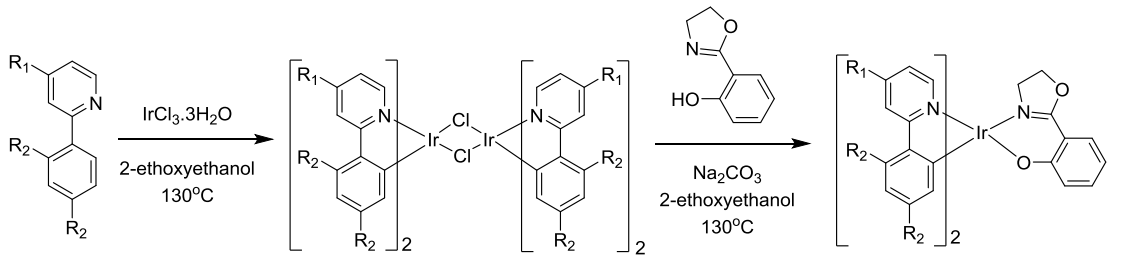

13 R_1 = H, R_2 = F
151 R_1 = 3,6-tBu carbazole, R_2 = H

145 R_1 = H, R_2 = F
146 R_1 = 3,6-tBu carbazole, R_2 = H

Figure 5.29

solvent when exposed to acidic media, such as silica, however the expected dichloro dimer did not contaminate the samples of **146**.[46] This mechanism of instability will be discussed in further detail later, with complexes **163** and **164**, as they were more strongly affected. The photophysics, electrochemistry and device performance of these complexes is discussed later.

Crystals of **145** suitable for X-ray crystallographic analysis were grown by Guangfu Li (Northeast Normal University) and the structure (solved by Dr Baiqiao Song at Northeast Normal University) is shown in Figure 5.30. As expected for a complex synthesised via the dichloro-bridged dimer the nitrogen atoms of the cyclometalating ligands are *trans* oriented about the iridium centre. Both the cyclometalating ppy ligands show relatively small twist angles between the pyridyl and phenyl rings, with values of 0.2° and 5.7°, respectively. The ancillary ligand, on the other hand, experiences a larger twist angle of 8.3° to accommodate the 6-membered chelate. Notably, this deformation is far smaller than that experienced by **31**, highlighting the difference in angles required by a coordinating 5-membered heterocycle (oxazoline) and 6-membered heterocycle (pyridine). Selected bond lengths are shown in Table 5.4 and compared to those of parent complex **142a**.

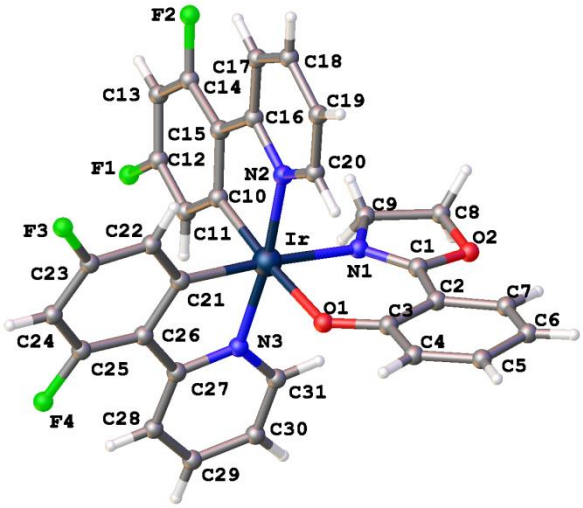

	142a[a]	145
Ir-N(1)	2.124(3)	2.119 (3)
Ir-N(2)	2.035(3)	2.031(4)
Ir-N(3)	2.046(3)	2.043(4)
Ir-O(1)	2.146(3)	2.133(3)
Ir-C(10)	1.988(5)	1.982(4)
Ir-C(21)	2.006(5)	2.000(5)

[a] Values for complex **114a** taken from reference [42]

Figure 5.30: Crystal structure of complex 145.MeOH, solvent omitted for clarity. Table 5.4: Selected bond lengths.

It was also of interest to synthesise the oxazole analogue **156** of ancillary ligand **152** to determine the effect of additional heteroaromaticity on the properties of the resultant complex. The initial route to ligand **156** was to oxidise ligand **152** using MnO_2, however the yield was low (28%) despite a large excess (>18 molar equivalents) of oxidising agent. As a result, a new route was devised, shown in Figure 5.31. The first step is analogous to the first step in the synthesis of **152**, namely a condensation reaction between ester **157** and an amine **158**, containing an aldehyde

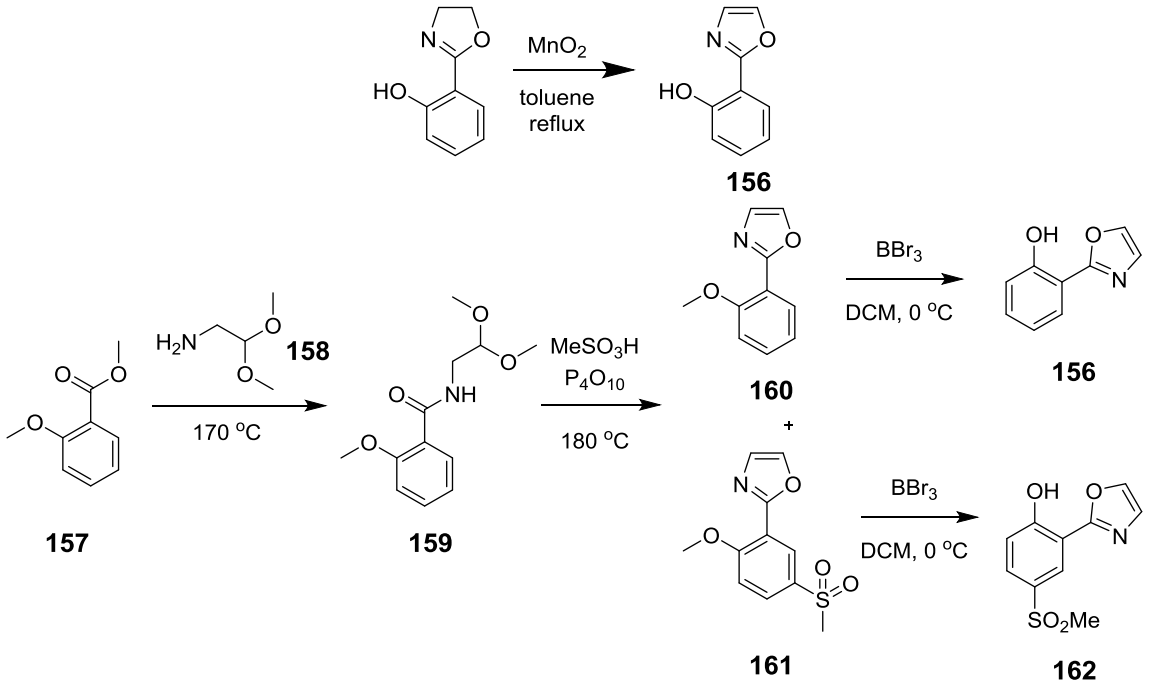

Figure 5.31: Synthesis of ancillary ligand precursors 160 and 161.

masked as a dimethylacetal moiety, to give the amide **159** in 40% yield.

Oxazole **160** is then synthesised by a ring closure reaction; amide **159** was treated with Eaton's reagent (made in house by mixing methanesulfonic acid and P_4O_{10}) as described for a similar compound.[47] Upon work up of the reaction mixture TLC analysis revealed the presence of two spots, neither of which corresponded to starting material **159**. The products were identified as **160** and **161**, and isolated in 19% and 18% yield, respectively. Compound **161** is the result of the reaction between product **160** and the methanesulfonic acid used to form Eaton's reagent; on reviewing the literature alkyl sulfonic acids have been observed to react with aryl rings in the presence of phosphorus reagents.[48] The sulfone moiety in **161** is introduced *para* to the o/p-directing methoxy group.

Once **160** and **161** were obtained the final step was to deprotect the ethers to leave the final phenol products, **156** and **162**. The initial conditions used were those described previously, using conc. HBr (48% aq.).[47] However, the unreacted starting materials were recovered in 100% yield. As a result, the deprotection was performed with BBr_3 to give the two phenols, **156** and **162**, in 68% and 39% yield, respectively (Figure 5.32). As the HOMO for parent complex **142a** and complex **145** (DFT calculations discussed later) is located on the phenoxylate section of the ancillary ligand it was thought that the complex of side-product **162** could be of interest, as it may provide colour tuning by shifting the HOMO.

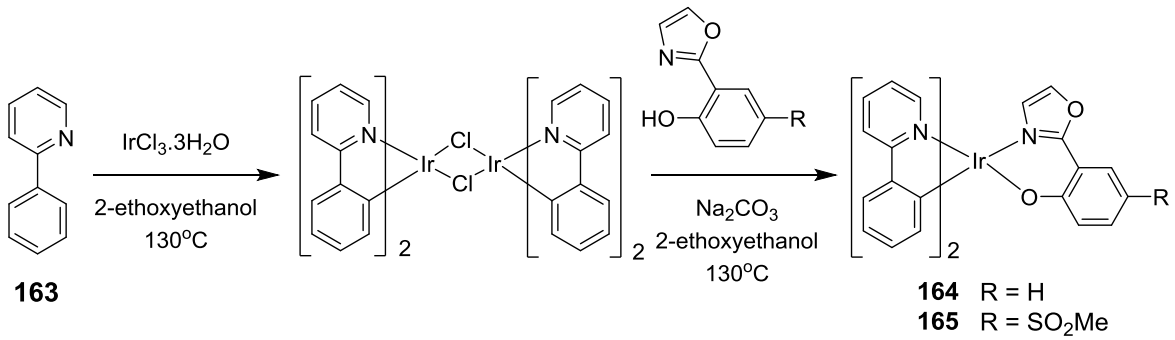

Figure 5.33

Complexes **164** and **165** were synthesised using standard conditions, shown in Figure 5.33, analogous to the synthesis of complexes **145** and **146**. The complexes were synthesised via a one-pot method; ppy **163** was reacted with $IrCl_3.3H_2O$ in 2-ethoxyethanol to produce precipitates presumed to be the intermediate dichloro-bridged dimers. Addition of the required ancillary ligand **156** or **162** and Na_2CO_3 followed, and after work up attempts were made to purify the complexes by column chromatography. Here, problems were encountered; complexes **164** and **165** were highly insoluble in solvents other than DCM, however, with a mixture containing DCM as the column solvent the isolated product was contaminated with traces of the intermediate dichloro-bridged dimer, which could be easily identified by ^{1}H NMR. This trace impurity persisted through multiple columns, despite a clear separation between complex **164** and **165** and the dichloro-bridged dimer on TLC. It is known in the literature that in the presence of an acid and a

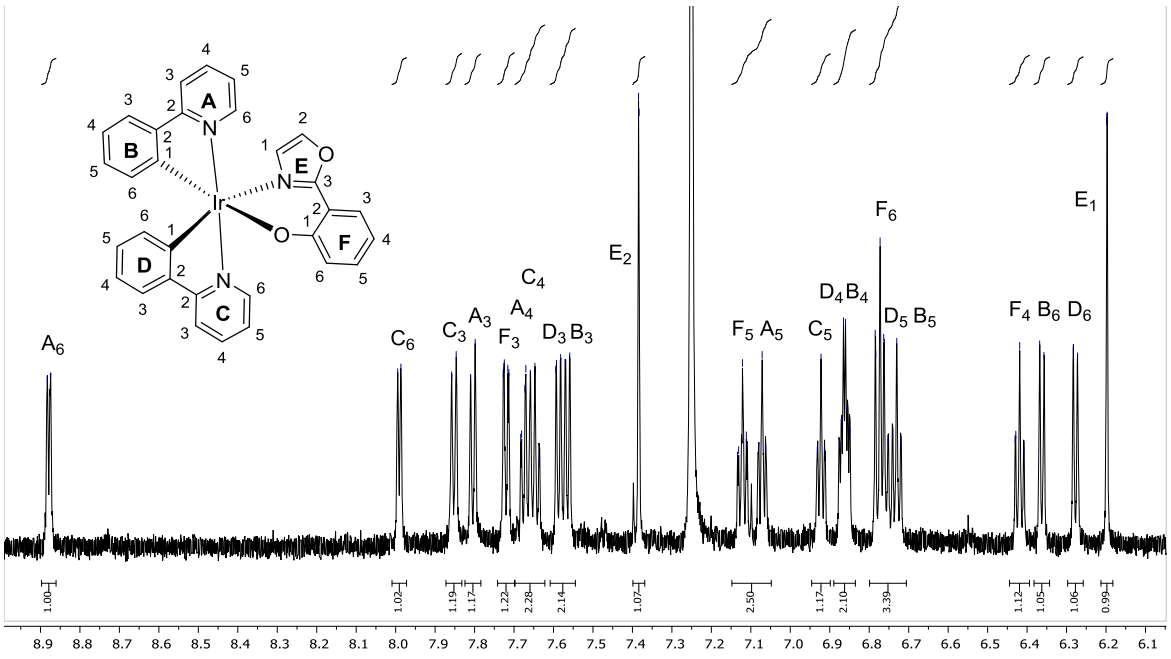

Figure 5.34: ^{1}H NMR spectrum of complex 164.

chloride source the N^O and O^O ligands, such as pic and acac, of heteroleptic complexes can be cleaved, and the intermediate dichloro-bridged dimer is reformed.[46] With this knowledge it was assumed that the use of DCM as a column solvent and the acidic silica provided a source of chloride ions and acid, respectively, resulting in the generation of dichloro dimer impurities during the column chromatography. As a result the purification of **164** and **165** was repeated, this time utilising neutral alumina as the stationary phase and treating the eluent DCM with K_2CO_3 to remove any acid impurities before it was used. Complexes **164** and **165** were thereby obtained in high purity as bright yellow powders in 35% and 57% yield.

The ^{1}H and ^{13}C NMR spectra of complex **164** have been fully assigned with the aid of 2D experiments (Figure 5.34, ^{13}C assignment is in the experimental section). As with complexes **19**, **31** and **68**, described in previous chapters, the stereochemistry about the metal centre was determined using the NOESY experiment, revealing the expected *trans* orientation of the C^N ligands nitrogens about the iridium centre.

Crystals of complex **165** were grown that were suitable X-ray crystallography analysis, and the molecular structure is shown in Figure 5.35. As expected for a complex synthesised via the dichloro- bridged dimer the nitrogen atoms of the cyclometalating ligands are *trans* oriented about the iridium centre, and the ligands are arranged in a distorted octahedral geometry. The twist angles between the phenyl and pyridyl rings of the cyclometalating ligands are small, 0.7° and4.8°, and a similar twist angle is observed for the ancillary ligand, 4.5°. Selected bond lengths are shown in Table 5.5 and compared to those of parent complex **142a**. Notably, the Ir-N1 bond length (the bond to the N of the oxazole/oxazoline) is longer for **165** than for complexes **142a** and **145**, potentially due to the decreased basicity of the oxazole nitrogen compared to that of oxazoline.

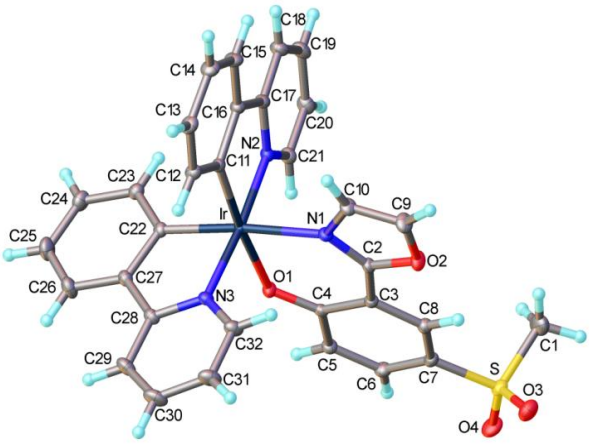

	142a[a]	145	165
Ir-N(1)	2.124(3)	2.119 (3)	2.1373(10)
Ir-N(2)	2.035(3)	2.031(4)	2.0349(10)
Ir-N(3)	2.046(3)	2.043(4)	2.0418(10)
Ir-O(1)	2.146(3)	2.133(3)	2.1452(8)
Ir-C(10/1)	1.988(5)	1.982(4)	1.9894(11)
Ir-C(21/2)	2.006(5)	2.000(5)	2.0003(12)

Figure 5.35: Crystal structure of complex 165.2THF, solvent omitted for clarity. Table 5.5: Selected bond lengths.

PHOTOPHYSICAL AND ELECTROCHEMICAL PROPERTIES

Absorption and emission

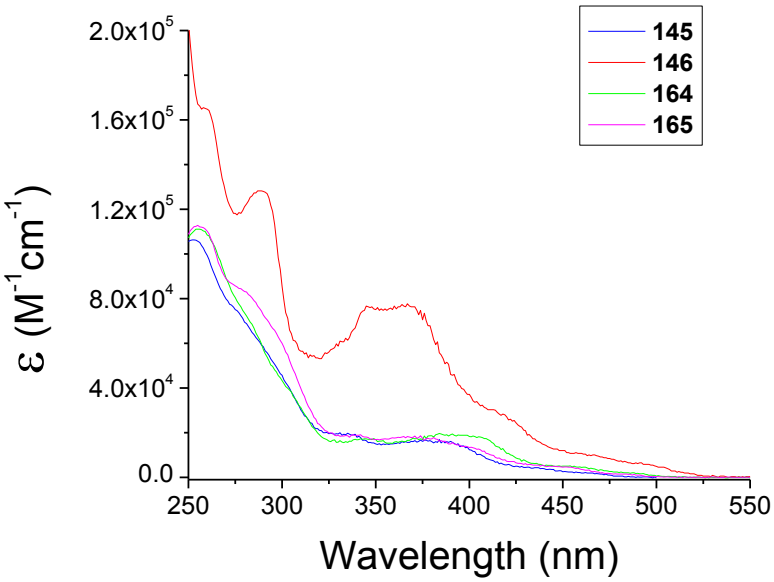

Figure 5.36: Absorption spectra of complexes 145, 146, 164 and 165 in DCM [<10^5].

The absorption spectra of complexes **145**, **146**, **164** and **165** are shown in Figure 5.36. The strong bands between 250-320 nm are assigned to π-π* transitions on the ligand based on the calculations of Hay,[40] and literature precedent. The intense bands at 350-400 nm are assigned to the ^{1}MLCT bands, and at much lower oscillator strengths (1.1-5.2 x 10^3 dm^3/mol cm) the ^{3}MLCT bands can be seen. The extinction coefficients and absorption profiles of complexes **145, 164** and **165** are similar, as they all possess similar cyclometalating and ancillary ligands. The extinction coefficients for complex **146** are significantly higher; this is consistent with the introduction of large, conjugated groups such as carbazoles into the molecular structure.

Excitation spectra for all complexes were recorded (Figure 5.37), revealing as expected that the bands from the ^{1}MLCT states are responsible for the emission from the complexes, while the majority of the higher energy π-π* transitions are dark.

The emission spectra of the complexes are shown in Figure 5.38. All four complexes display a similar emission profile to that of parent complex **142a**, the emission is broad and largely featureless, indicating a strong MLCT contribution to the emission. Introducing the fluorine atoms onto the phenyl ring of the ppy ligands (from **142a** to **145**) results in a blue-shift of 21 nm, this is expected due to the electron-withdrawing ability of the fluorine groups. Even though the computational work (discussed in a later section) indicates phenyl ring contribution to the HOMO is small, the introduction of fluorines here can still lower the HOMO energy by decreasing the

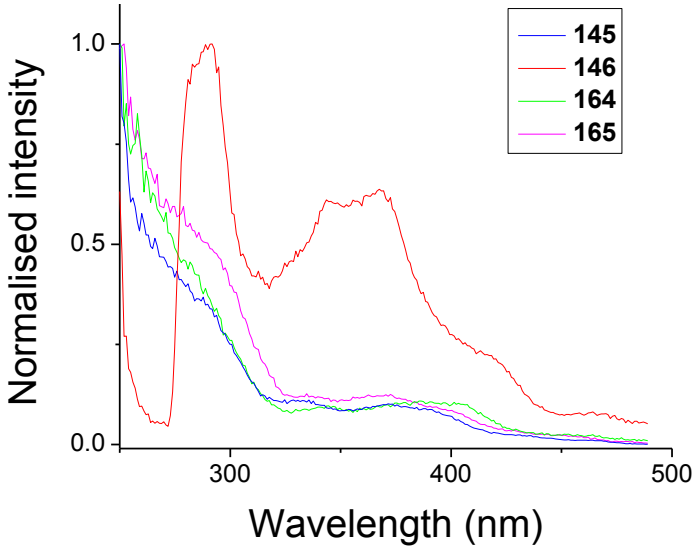

Figure 5.37: Excitation spectra of complexes 145, 146, 164 and 165 in DCM [<10^5 M].

energy of the metal d orbitals by coordination. Introducing the carbazole moiety onto the pyridyl ring of the ppy ligand (from **142a** to **146**) results in a red-shift of 12 nm; it was thought that introducing an electron donating group to the pyridyl ring would shift the LUMO to higher energies, resulting in a blue-shift in emission. In this case, while the HOMO level does not seem to have been affected according to the electrochemical data, the complex displays a red-shift in emission. This suggests the LUMO has been lowered, rather than raised, by the introduction of the carbazole unit. A reason for this may be an increase in conjugation, or a change in LUMO distribution.

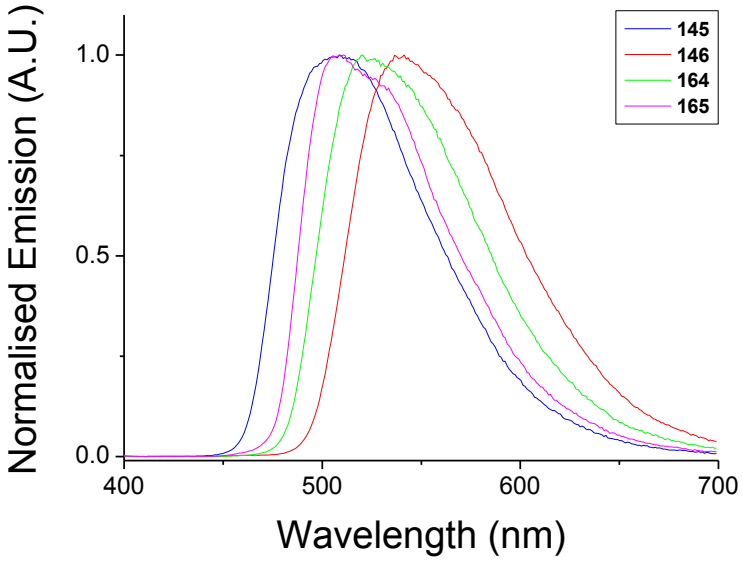

Figure 5.38: Emission spectra of complexes 145, 146, 164 and 165 in degassed DCM [<10^5 M], λ_{ex} = 355 nm.

Exchanging the oxazoline fragment for the more conjugated oxazole moiety (from **142a** to **163**) results in a small blue-shift of 6 nm, this could be due to the increased electron-withdrawing capability of the oxazole fragment, compared to the oxazoline, as a result of the extended conjugation. The introduction of the sulfone moiety onto the phenoxylate ring of the 'ancillary' ligand results in a further blue-shift of 13 nm. As the HOMO in the oxazoline complexes (**142a**, **145**) is localised on the phenoxylate ring, and literature precedent suggests that this is likely to be true for the oxazole complexes (**164** and **165**) [44] it is expected that introduction of an electron withdrawing SO_2Me group would result in a blue-shift in emission.

The PLQYs, lifetimes (τ_{obs}) and calculated radiative and non-radiative decay rates (k_r and k_{nr}) are shown in Table 5.6. The PLQYs for complexes all complexes are comparable to the literature (0.42-0.65 vs 0.55 for **142a**), with complex **145** having the highest PLQY, 0.65. The lifetimes for all four complexes are between 0.85-1.8 μs, typical values for an iridium complex.

Complex	λ_{max}^{abs} (ε) / nm (x10^3 $M^{-1}cm^{-1}$)[a]	λ_{max}^{em} / nm[b]	PLQY / Φ_{PL}[a,c]	τ_P / μs[a,d]	k_r / 10^5 s^{-1} [e]	k_{nr} / 10^5 s^{-1} [e]
142a[f]	249, 340 (sh), 377 (sh), 443 (sh)	527	0.55	0.34	1.61	1.32
145	252 (104.8), 275 (sh, 74.2), 334 (18.7), 374 (16.0), 390 (14.7), 438 (3.9), 464 (1.8)	506	0.65	1.52	4.28	2.30
146	260 (166.5), 288 (129.8), 330 (sh, 60.1), 346 (77.3), 368 (78.3), 418 (28.4), 464 (10.4), 499 (5.2)	539	0.52	0.87	5.98	5.52
164	255 (119.3), 280 (sh, 79.3), 303 (sh, 43.3), 386 (20.8), 402 (18.5), 456 (5.2), 488 (2.0)	521	0.45	1.71	2.63	3.22
165	253 (111.0), 279 (83.2), 297 (64.1), 339 (18.9), 365 (18.3), 380 (17.3), 401 (13.4), 451 (4.5), 483 (1.2)	508	0.42	1.80	2.33	3.22

[a] Data obtained in dichloromethane solution at 20 °C. [b] Data obtained in degassed dichloromethane solution with λ_{ex} = 380 nm. [c] Measured in degassed DCM relative to quinine sulfate Φ_{PL}= 0.546 in 0.5 M H_2SO_4 at 20 °C; estimated error ±5%. [d] Estimated error ±5%. [e] k_r, k_{nr} values calculated using Equations 1.5/1.6. [f] Values for complex **142a** taken from reference [42].

Table 5.6: Photophysical data for selected iridium complexes.

It was observed in the synthesis of complexes **145**, **146**, **164**, **165** that the complexes were unstable in the presence of chlorinated solvents and acid; while attempting to obtain the photophysical measurements decomposition was observed in three of the complexes, **146**, **164** and **165**. A peak was observed to grow in at 460 nm. The intensity of this peak varied in the complexes, and also varied with the batches of DCM used. As the ^{1}H NMR spectra showed no degradation, the emission spectra of complex **146** was recorded in toluene, which showed no sign of decomposition, indicating the decomposition had occurred in the DCM solution. Fresh solutions in DCM were prepared, and exhibited no sign of decomposition. As the complexes have been known to degrade in chlorinated solvents due to acidic impurities, it is possible that this is the cause of the decomposition, with each complex possessing a different rate of decomposition. Complex **146** was observed to be particularly unstable, which could explain the shorter lifetime (0.87 μs) and high non-radiative decay rate. Spectra of the complexes after 72 h of exposure to ambient conditions are shown in Figure 5.39. In all cases, the emission λ_{max} shifts (a blue-shift for **145** and **146**, red-shifts for **164** and **165**) and the intensity of the emission drops. An additional peak is observed for all four complexes, at 445–460 nm. It is proposed that over time the acidic impurities in the DCM solvent attack the complexes, resulting in the formation of their precursor dichloro dimers, resulting in the release of the ancillary ligands **152**, **156**, **162**, which emit in the blue region. With additional time, the rate of decomposition could be probed with NMR spectroscopy.

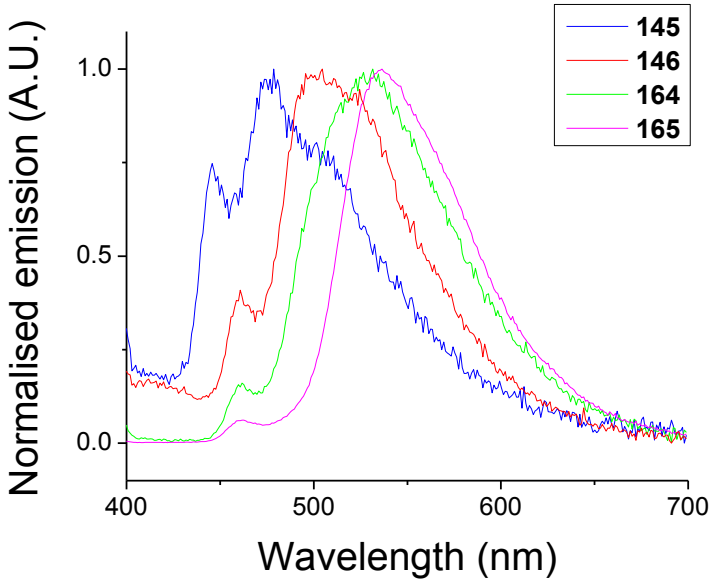

Figure 5.39: Emission spectra of solutions of complexes 145, 146, 164 and 165 in degassed DCM after exposure to ambient conditions for 72 h. [<10^{5} M], λ_{ex} = 355 nm.

Electrochemistry

The electrochemical behaviour of complexes **145**, **146**, **164** and **165** were investigated using cyclic voltammetry and compared to the parent compound **142a**. The voltammograms are shown in Figure 5.39 and the key parameters in Table 5.7. Formula 2.1 is used to calculate the energy of the HOMO.

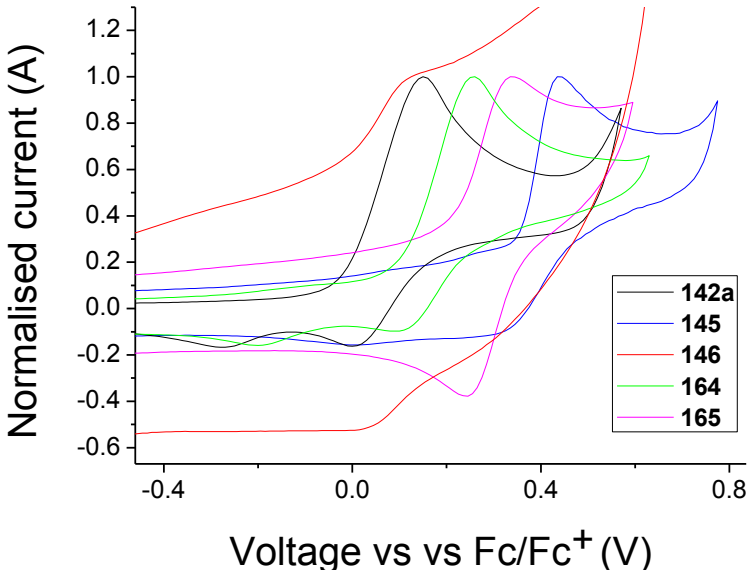

Figure 5.39: Cyclic voltammograms of complexes 145, 146, 164 and 165. Measured in DCM (0.1 M $^{n}Bu_4NPF_6$) at 298 K.

Complexes **145**, **146**, **164** and **165** all show an electrochemically quasi/irreversible oxidation at 0.08-0.37 V vs Fc/Fc^+, similar to that of the parent complex **142a** (Figure 5.39). Complex **142a** shows an oxidation potential of 0.08 V, with no reductions observed in the solvent window. Exchanging the ppy ligand for dfppy (**142a** to **145**) results in an increase of 0.29 V in the oxidation potential, indicating the HOMO level has been shifted to lower energies, as desired. For complex **146** the oxidation potential is 0.08 V, similar to that of parent complex **142a**; this is as expected, as there is no localisation of the HOMO on the pyridyl ring of the cyclometalating ligand, therefore

Complex	$E^{ox}_{1/2}$ / V a	HOMO / eV
142a	0.08	-4.88
145	0.37	-5.17
146	0.08	-4.88
164	0.18	-4.98
165	0.30	-5.10

All values reported vs Fc/Fc^+ = 0.00 V.

Table 5.7: Electrochemistry data of iridium complexes. Measured in DCM (0.1 M $^{n}Bu_4NPF_6$) at 298 K.

the oxidation potential is not expected to vary significantly on introduction of substituents here. Upon replacing the oxazoline fragment with an oxazole (**142a** to **164**) the oxidation potential increases by 0.1 V. As the HOMO for **142a** is localised on the iridium d-orbitals and across the phenoxylate ring it is possible that switching from an oxazoline to an oxazole results in a lowering of the HOMO energy due to the increased electron withdrawing ability of the oxazole compared to the oxazoline. Introducing the sulfone group (**165** vs **164**) results in an increase in the oxidation potential of 0.12 V; if the HOMO of **164** is still localised on the phenoxylate ring of the ancillary ligand introducing an electron withdrawing group such as a sulfone should lower the HOMO level. In the voltammograms of both **142a** and **164** a reduction appears on the reverse sweep. When the cyclic voltammogram of **142a** was obtained at -78 ^{o}C (achieved by cooling the DCM solution with a dry ice/acetone bath), the reduction features disappeared, suggesting they result from decomposition of the complex. Complex **164** began to precipitate out of solution on lowering the temperature, hence a voltammogram at -78 ^{o}C could not be measured. The trends in oxidation potentials are consistent with the observed photophysical properties; introducing electron withdrawing groups onto the cyclometalating or the ancillary ligand results in a lowering of the HOMO energy, and a widening of the HOMO-LUMO gap. Introducing the electron donating carbazole group (**146**) results in no change in the oxidation potential, and a red-shift in the emission relative to **142a**, suggesting the shift is due to a lowering of the LUMO. No reduction features were observed within the solvent window (-1.5 V vs Fc/Fc^{+}).

COMPUTATIONAL DATA

Electronic structure calculations were carried out on iridium complex **145** by Dr Yun Geng (Northeast Normal University) to elucidate the nature of the frontier orbitals and the transitions involved in the excitation spectra. The full geometry was optimised at the B3LYP/LANL2DZ:6-21G* level and is denoted **145'** to distinguish it from experimental data. The computed orbital energies for **145'** show good agreement with the observed oxidation potentials (Table 5.7).The HOMO of

Transition energy[a]	Participating MO	Transition character[b]	Energy gap / eV
452.33 nm	HOMO→LUMO	L_CL_ACT+ ML_ACT	3.35
439.30 nm	HOMO→LUMO+1	L_CL_BCT+ML_BCT+L_CL_ACT	
376 nm	HOMO→LUMO+2	L_CL_ACT+L_CL_BCT+ML_ACT+ML_BCT	

[a] Excitation energies calculated for the excited states. [b] Ligand notation: A, B =2-(2,4-difluorophenyl)pyridine; C =2 -(2'-hydroxyphenyl)-2-oxazoline

Table 5.8: TD-DFT calculation results for complex 145'

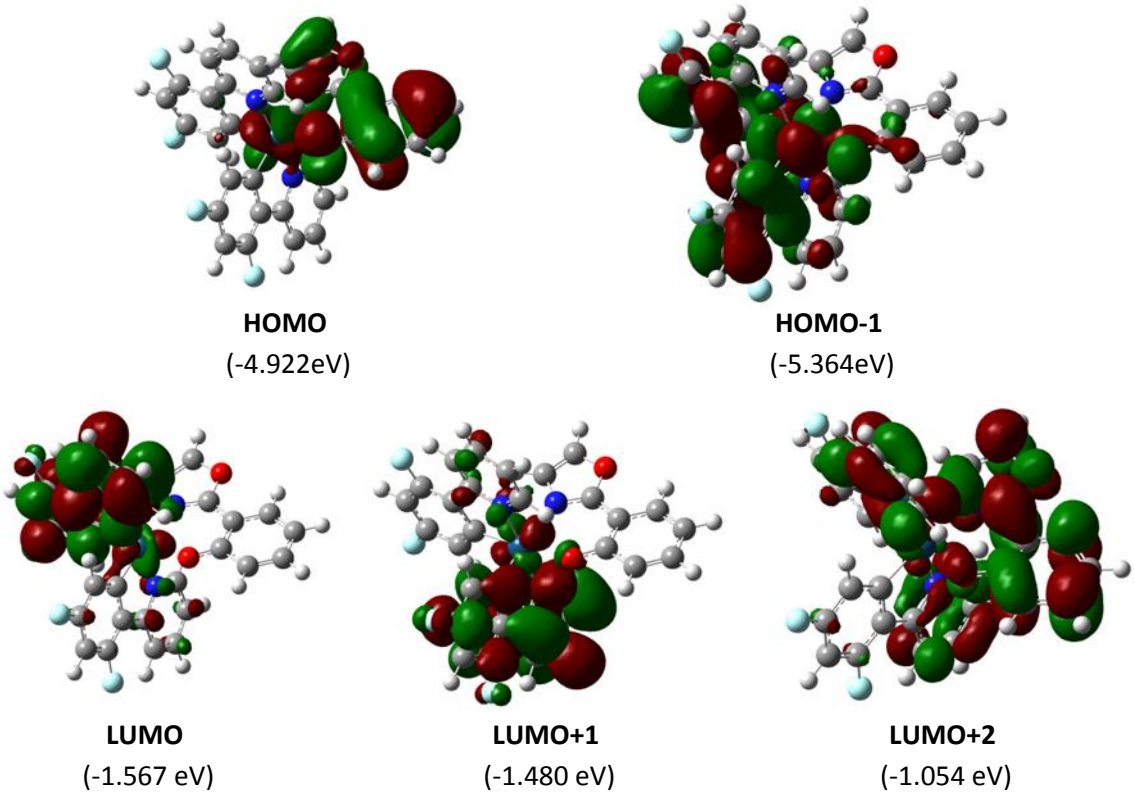

Figure 5.40: The contour plots of the HOMOs and LUMOs of complex 145'.

145' is localised mainly across the central iridium atom and the phenoxylate ring of the ancillary ligand, with a small contribution from the oxazole ring. The LUMO is localised on a ppy ligand, across the pyridine and phenyl rings. The frontier orbitals are shown in Figure 5.40. The first three transition energies are shown in Table 5.8; the lowest energy transition (HOMO → LUMO) is of LLCT/MLCT character, with an energy gap of 3.35 eV. This represents an increase in energy compared to parent complex **142a**, for which an energy gap of 3.22 eV was calculated.

DEVICE DATA

Devices of complexes **145** and **164** were fabricated by Prof. Yu Liu (Jilin University). The device structure is as follows: ITO/NPB (40 nm)/CBP:**Ir complex**(5 or 10%) (30 nm)/TPBI (25 nm)/LiF/Al. The layers were deposited by vacuum disposition. Complexes **146** and **165** would not sublime, and so devices were not fabricated. The electroluminescence (EL) spectra from the devices are shown in Figure 5.41, panel a; for all complexes the EL spectra are similar to the photoluminescence (PL) spectra, indicating good exciton confinement on the emissive molecule. Additionally, there is little variation in the emission spectra on variation of the complex loading

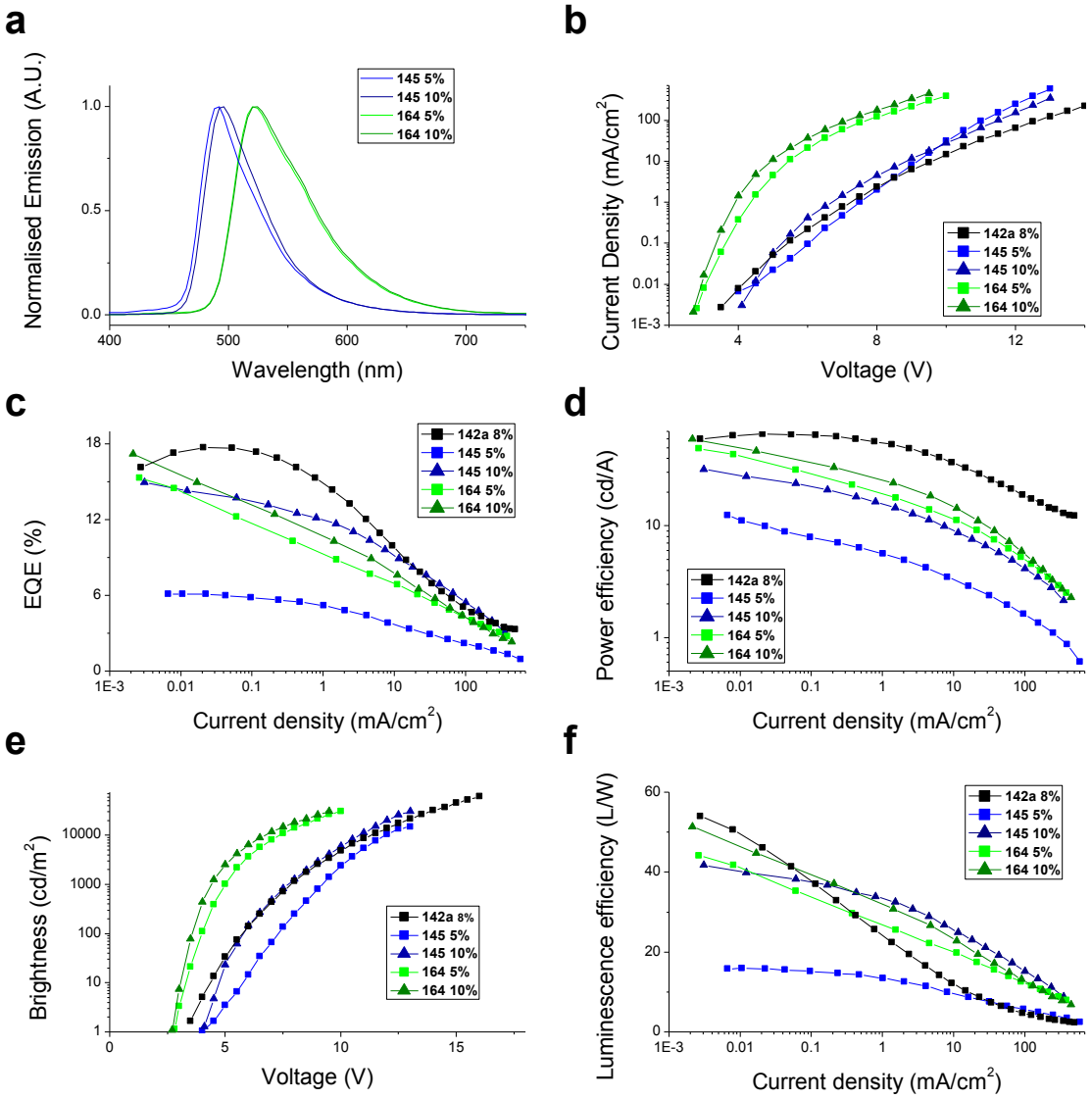

Figure 5.41: Device data for complexes 142a, 145 and 164. Data for complex 142a taken from reference [42]. X% refers to the weight % of complex in the emissive layer.

(5% or 10%) in the CBP host in the devices, suggesting no significant aggregation of the complex. The increase in complex loading results in an increase in performance for both complexes, although the effect is more significant for **145**. Notably, the devices of complex **163** achieved high brightness at lower voltages than those required for the devices of **142a** and **145** (panel e). Complex **145** was less efficient in devices than both complexes **142a** and **164**; this can be rationalised by the fact that **145** exhibits bluer emission (panel a). The two complexes achieved good EQEs (14.0% and 14.2% for **145** and **164**, respectively, panel c), comparable to the literature compound **142a**.[42]

Complex	Wt. %	λ_{ELmax} / nm	Brightness / cd/m^2	turn-on voltage[a] / V	EQE[b] / %	current efficiency[b] / cd/A	power efficiency[b] / lm/W	CIE coordinates / (x,y)
142a	8%	530	61560	4.4	17.7	66.1	47.2 (54.0)	(0.35, 0.61)
145	5%	492	14860	5.8	5.6 (6.1)	8.3 (12.5)	15.3 (15.9)	(0.19, 0.42)
	10%	496	31230	4.7	14.0 (15.0)	26.1 (32.0)	39.3 (41.8)	(0.18, 0.53)
164	5%	522	31050	3.3	12.8 (15.3)	34.6 (49.5)	36.8 (44.2)	(0.33, 0.61)
	10%	523	31140	3.1	14.2 (17.2)	38.2 (59.8)	42.5 (51.4)	(0.33, 0.61)

[a] measured at a brightness of 10 cd/m^2. [b] Values reported are the maximum values above a brightness of 10 cd/m^2, while the values in brackets report the overall maximum values.

Table 5.9: Summary of device data.

CONCLUSION

A family of four complexes, **145**, **146**, **164** and **165**, related to the known complex **142a** were synthesised. Exchanging a ppy ligand for a dfppy ligand (from **142a** to **145**) resulted in a blue-shift of 21 nm, indicating that the introduction of the fluorine atoms was effective at widening the HOMO-LUMO gap. Replacing an oxazoline with an oxazole ring on the ancillary ligand (from **142a** to **164**) resulted in a small blue-shift in the emission colour. Addition of the sulfone moiety onto the phenyl ring of oxazole ancillary ligand **156** resulted in an additional blue-shift of 13 nm, as the HOMO in these complexes is located on the ancillary ligand. As introducing electron withdrawing groups on to both the cyclometalating ligand and the ancillary ligand resulted in a blue-shift in emission, these two approaches could be combined in the future to produce bluer complexes. All complexes displayed good PLQYs (0.42-0.65) in solution. Devices of complexes **145** and **164**, fabricated by vacuum deposition, retained the emission observed in the PL spectra, and performed favourably compared to the literature compound **142a**. Further work to be conducted would be to investigate the properties of complex **146** and **165** in devices, fabricated by solution processing.

References

1) S. Lamansky, P. Djurovich, D. Murphy, F. Abdel-Razzaq, R. Kwong, I. Tsyba, M. Bortz, B. Mui, R. Bau and M. E. Thompson, *Inorg. Chem.,* 2001, **40**, 1704-1711
2) N. Tian, A. Thiessen, R. Schiewek, O. J. Schmitz, D. Hertel, K. Meerholz and E. Holder, *J. Org. Chem.,* 2009, **74**, 2718-25
3) H. Wu, T. Yang, Q. Zhao, J. Zhou, C. Li and F. Li, *Dalton Trans.,* 2011, **40**, 1969-76
4) H. Tang, Y. Li, B. Chen, H. Wu, W. Yang and Y. Cao, *Opt. Mater.,* 2011, **33**, 1291-1296
5) Z. Q. Chen, Z. Q. Bian and C. H. Huang, *Adv. Mater.,* 2010, **22**, 1534-9
6) E. I. Szerb, A. M. Talarico, I. Aiello, A. Crispini, N. Godbert, D. Pucci, T. Pugliese and M. Ghedini, *Eur. J. Inorg. Chem.,* 2010, **2010**, 3270-3277
7) Q. Zhao, S. J. Liu and W. Huang, *Macromol Rapid Commun,* 2010, **31**, 794-807
8) J. Li, P. I. Djurovich, B. D. Alleyne, M. Yousufuddin, N. N. Ho, J. C. Thomas, J. C. Peters, R. Bau and M. E. Thompson, *Inorg. Chem.,* 2005, **44**, 1713-27
9) Y. You and S. Y. Park, *Dalton Trans.,* 2009, 1267-1282
10) Y. Chi and P. T. Chou, *Chem. Soc. Rev.,* 2010, **39**, 638-55
11) H.-J. Seo, K.-M. Yoo, M. Song, J. S. Park, S.-H. Jin, Y. I. Kim and J.-J. Kim, *Org. Electron.,* 2010, **11**, 564-572
12) J. Li, P. I. Djurovich, B. D. Alleyne, I. Tsyba, N. N. Ho, R. Bau and M. E. Thompson, *Polyhedron,* 2004, **23**, 419-428
13) S. J. Yeh, M. F. Wu, C. T. Chen, Y. H. Song, Y. Chi, M. H. Ho, S. F. Hsu and C. H. Chen, *Adv. Mater.,* 2005, **17**, 285-289
14) E. Orselli, G. S. Kottas, A. E. Konradsson, P. Coppo, R. Frohlich, L. de Cola, A. van Dijken, M. Buchel and H. Borner, *Inorg. Chem.,* 2007, **46**, 11082-93
15) Y.-C. Chiu, J.-Y. Hung, Y. Chi, C.-C. Chen, C.-H. Chang, C.-C. Wu, Y.-M. Cheng, Y.-C. Yu, G.-H. Lee and P.-T. Chou, *Adv. Mater.,* 2009, **21**, 2221-2225
16) Y. C. Chiu, Y. Chi, J. Y. Hung, Y. M. Cheng, Y. C. Yu, M. W. Chung, G. H. Lee, P. T. Chou, C. C. Chen, C. C. Wu and H. Y. Hsieh, *ACS Appl. Mater. Interfaces,* 2009, **1**, 433-42
17) H. Fu, Y.-M. Cheng, P.-T. Chou and Y. Chi, *Mater. Today,* 2011, **14**, 472-479
18) A. F. Ma, H. J. Seo, S. H. Jin, U. C. Yoon, M. H. Hyun, S. K. Kang and K. Y. Inn, *Bull. Korean Chem. Soc.,* 2009, **30**, 2754-2758
19) J. Y. Hung, Y. Chi, I. H. Pai, Y. C. Yu, G. H. Lee, P. T. Chou, K. T. Wong, C. C. Chen and C. C. Wu, *Dalton Trans.,* 2009, 6472-5
20) C. H. Lin, Y. Y. Chang, J. Y. Hung, C. Y. Lin, Y. Chi, M. W. Chung, C. L. Lin, P. T. Chou, G. H. Lee, C. H. Chang and W. C. Lin, *Angew. Chem. Int. Ed.,* 2011, **50**, 3182-6
21) T. Kim, J. Lee, S. U. Lee and M. H. Lee, *Organometallics,* 2015, **34**, 3455-3458
22) H. W. Ham, K. Y. Jung and Y. S. Kim, *Thin Solid Films,* 2010, **518**, 6199-6204
23) X. Shen, X.-H. Hu, F.-L. Wang, F. Sun, Y.-Q. Yang, Y. Xu, S. Chen and D.-R. Zhu, *Inorg. Chem. Commun.,* 2010, **13**, 1096-1099
24) K. Dedeian, J. Shi, E. Forsythe, D. C. Morton and P. Y. Zavalij, *Inorg. Chem.,* 2007, **46**, 1603-11
25) Y. You and S. Y. Park, *J. Am. Chem. Soc.,* 2005, **127**, 12438-9
26) X. Gu, T. Fei, H. Zhang, H. Xu, B. Yang, Y. Ma and X. Liu, *Eur. J. Inorg. Chem.,* 2009, **2009**, 2407-2414
27) Y. Zhou, W. Li, Y. Liu, L. Zeng, W. Su and M. Zhou, *Dalton Trans.,* 2012, **41**, 9373-81
28) H.-S. Duan, P.-T. Chou, C.-C. Hsu, J.-Y. Hung and Y. Chi, *Inorg. Chem.,* 2009, **48**, 6501-6508
29) Y. You, K. S. Kim, T. K. Ahn, D. Kim and S. Y. Park, *J. Phys. Chem. C,* 2007, **111**, 4052-4060
30) C. H. Hsieh, F. I. Wu, C. H. Fan, M. J. Huang, K. Y. Lu, P. Y. Chou, Y. H. Yang, S. H. Wu, I. C. Chen, S. H. Chou, K. T. Wong and C. H. Cheng, *Chem. Eur. J.,* 2011, **17**, 9180-7
31) L. Shi, B. Hong, W. Guan, Z. Wu and Z. Su, *J. Phys. Chem. A,* 2010, **114**, 6559-64
32) J. M. Fernandez-Hernandez, J. I. Beltran, V. Lemaur, M. D. Galvez-Lopez, C. H. Chien, F. Polo, E. Orselli, R. Frohlich, J. Cornil and L. De Cola, *Inorg. Chem.,* 2013, **52**, 1812-24

33) C.-H. Yang, M. Mauro, F. Polo, S. Watanabe, I. Muenster, R. Fröhlich and L. De Cola, *Chem. Mater.,* 2012, **24**, 3684-3695
34) C.-H. Chang, C.-C. Chen, C.-C. Wu, C.-H. Yang and Y. Chi, *Org. Electron.,* 2009, **10**, 1364-1371
35) V. N. Kozhevnikov, K. Dahms and M. R. Bryce, *J. Org. Chem.,* 2011, **76**, 5143-8
36) E. Bisagni, M. Rautureau and C. Huel, *Heterocycles,* 1989, **29**, 1815
37) G. Jones and D. J. Baty, *Quinoline N-Oxides* in *Chemistry of Heterocyclic Compounds: Quinolines*, Ed. G. Jones, John Wiley & Sons, Inc., 2008, 377-605
38) T. Itai, *Pyridazine N-Oxides* in *Chemistry of Heterocyclic Compounds: Pyridazine*, Ed. R. N. Castle, John Wiley & Sons, Inc., 2008, 675-753
39) C.-C. Cheng, W.-S. Yu, P.-T. Chou, S.-M. Peng, G.-H. Lee, P.-C. Wu, Y.-H. Song and Y. Chi, *Chem. Comm.,* 2003, 2628-2629
40) P. J. Hay, *J. Phys. Chem. A,* 2002, **106**, 1634-1641
41) C. Adachi, R. C. Kwong, P. Djurovich, V. Adamovich, M. A. Baldo, M. E. Thompson and S. R. Forrest, *Appl. Phys. Lett.,* 2001, **79**, 2082
42) K. Chao, K. Shao, T. Peng, D. Zhu, Y. Wang, Y. Liu, Z. Su and M. R. Bryce, *J. Mater. Chem. C,* 2013, **1**, 6800
43) E. Marchi, R. Sinisi, G. Bergamini, M. Tragni, M. Monari, M. Bandini and P. Ceroni, *Chem. Eur. J.,* 2012, **18**, 8765-73
44) Y. You, J. Seo, S. H. Kim, K. S. Kim, T. K. Ahn, D. Kim and S. Y. Park, *Inorg. Chem.,* 2008, **47**, 1476-87
45) F. Gartner, S. Denurra, S. Losse, A. Neubauer, A. Boddien, A. Gopinathan, A. Spannenberg, H. Junge, S. Lochbrunner, M. Blug, S. Hoch, J. Busse, S. Gladiali and M. Beller, *Chem. Eur. J.,* 2012, **18**, 3220-5
46) E. Baranoff, B. F. Curchod, J. Frey, R. Scopelliti, F. Kessler, I. Tavernelli, U. Rothlisberger, M. Gratzel and M. K. Nazeeruddin, *Inorg. Chem.,* 2012, **51**, 215-24
47) S.-K. Khim, J. Bauman, J. Evans, B. Freeman, B. King, T. Kirkland, M. Kochanny, D. Lentz, A. Liang, L. Mendoza, G. Phillips, J.-L. Tseng, R. G. Wei, H. Ye, L. Yu, J. Parkinson and W. J. Guilford, *Bioorg. Med. Chem. Lett.,* 2008, **18**, 3895-3898
48) US5015775 (A), 1991

Chapter 6: 'Hemicage Ir complexes' for enhanced stability

In the search for deep-blue emitters focus has shifted from phenylpyridine-based ligands to ligands containing alternative heterocycles, such as pyrazoles, or carbenes. Pyrazoles raise the energy of the LUMO, thus widening the HOMO-LUMO gap and blue-shifting the emission.[1] Carbenes, as strong σ-donor ligands, firstly destabilise the LUMO, and secondly, increase the energy of non-radiative MC states as a result of the strong metal-ligand bonds formed.[1,2] This results in deep-blue to near-UV emission from carbene complexes at room temperature, with some complexes even displaying solution PLQYs of up to 0.40.[3,4] Carbene ancillary ligands can also be used to blue-shift the emission and increase PLQYs by shifting deactivating states to higher energies.[5,6] Some examples of carbene-Ir complexes are shown in Figure 6.1.

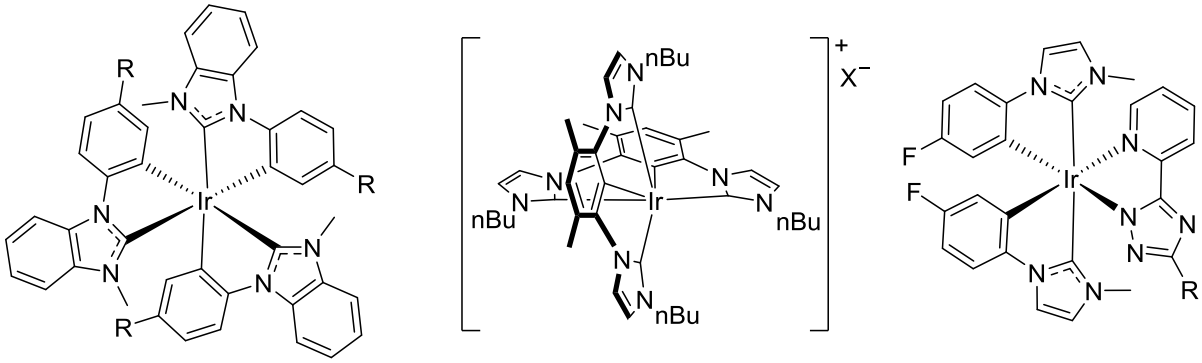

166a R = H
166b R = CF_3
166c R = CN
166d R = OCH_3

167a X = I
167b X = PF_6

168a R = Me
168b R = Ph

Figure 6.1: Carbene complexes 166a-d taken from reference [7]. Complexes 167a, b taken from reference [3]. Complexes 168a, b are taken from reference [8].

However, despite the favourable emission properties of carbene complexes there are still some disadvantages; some carbene complexes have been reported to have long excited state lifetimes (>20 μs), resulting in increased triplet-triplet annihilation at high brightnesses.[9,10] Carbene complexes are known to be unstable in OLEDs for long periods of device operation,[11] and it is thought that one mechanism for radiationless deactivation is cleavage of the iridium-carbene bond to form a five-coordinate intermediate.[12] Once bond rupture occurs, the ligand cannot recoordinate, resulting in decomposition. Methods of preventing this include increasing the rigidity of the ligands to restrict the complex from achieving the required structural conformation for bond dissociation, or utilising tripodal or hexadentate type chelates to form hemicage structures around the iridium centre. Advantages of hemicage complexes include a decrease in

reactivity, as the reactive metal centre is effectively encapsulated within the ligand structure.[13] Quenching of the luminescence by agents such as molecular oxygen, or solvent can therefore be inhibited, which can result in increased quantum yields in solution.[14] Formation of cage or hemicage complexes can also lead to a decrease in the non-radiative decay rate, as non-radiative vibrational processes can be inhibited by the increased rigidity of the system.[12,15,16]

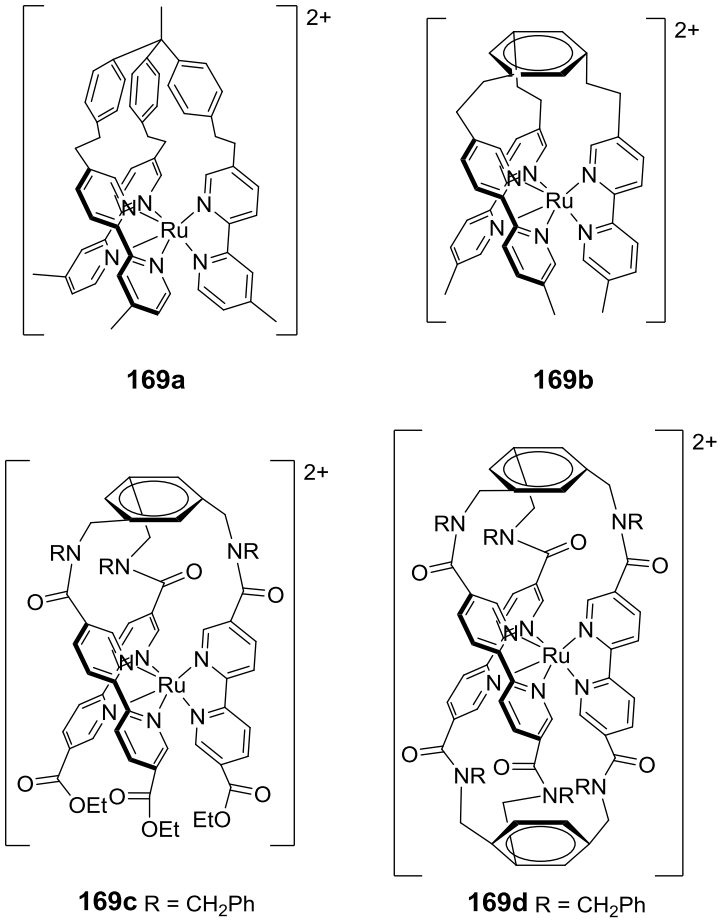

Figure 6.2: Complexes 169a/b taken from reference [15]. Complexes 169c/d taken from reference [17].

Few examples of iridium cage/hemicage complexes have been reported in the literature, however several ruthenium(II) complexes have been reported.[15,17-19] Some examples of caged and hemicaged ruthenium complexes are shown in Figure 6.2; in particular, complexes **169c** and **169d** showed increased photostability, with the photodecomposition rate of **169d** estimated to be at least 10^4 times smaller than that of $[Ru(bpy)_3][PF_6]_2$.[17] Complexes **169a** and **169b** also show significantly enhanced (1-7 times) quantum yields compared to their parent compounds.[15]

The first iridium hemicage complex was reported by Schaffner-Hamann *et. al*. in 2004, complex **170** (Figure 6.3).[20] Building on their previous work with ruthenium(II) and iron(II) complexes,[21] an enantiomerically pure ligand containing pinene units was complexed to produce a single isomer,

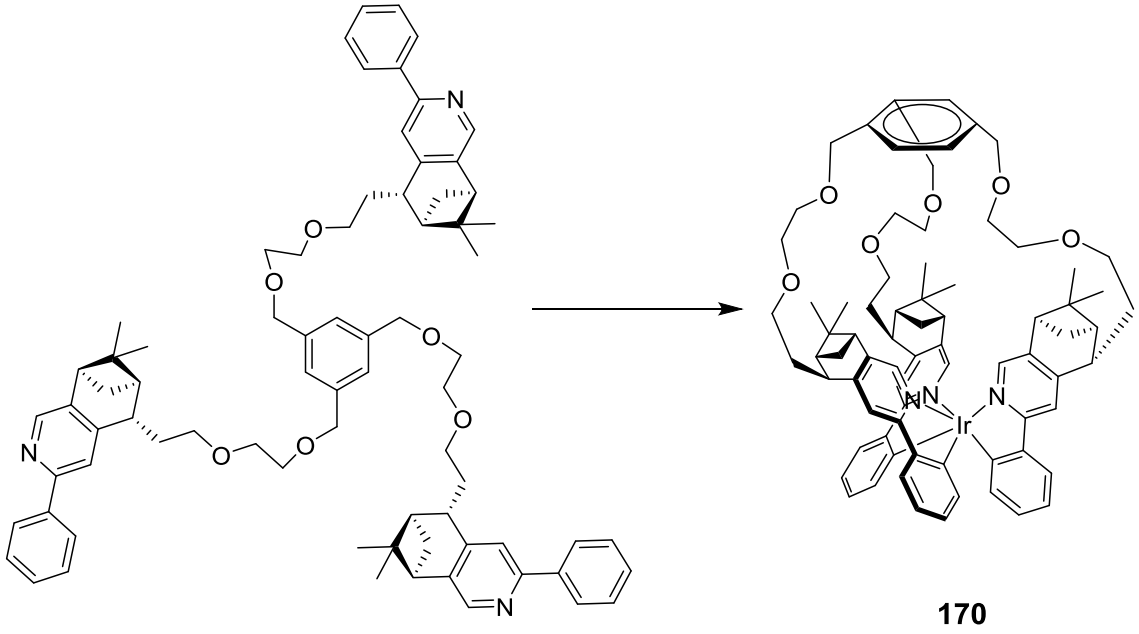

Figure 6.3

chiral complex **170**, which exists as the Λ-fac isomer.[20] In terms of photophysical properties, **170** displays similar absorption and emission spectra to the parent complexes, with a slightly lower PLQY (0.51 vs 0.64). The stability of **170** relative to the parent complexes was not investigated.

The first iridium complex with a caged structure was synthesised in 2010 by Ruggi *et*. *al*. and is shown in Figure 6.4.[14] Hemicage complex **172** was synthesised by reacting tripodal ligand **171** with $IrCl_3/CF_3CO_2Ag$, and the ester moieties were then reacted with another equivalent of the tris(2-aminoethyl)amine cap to give the caged complex **173**.[14] The photophysical properties of complexes **172** and **173**, such as quantum yield, excited state lifetime and emission wavelength are similar.[14] The effect of shielding on the oxygen sensitivity of complexes **172** and **173** was measured by producing a Stern-Volmer plot, and comparing the results to that of related complex

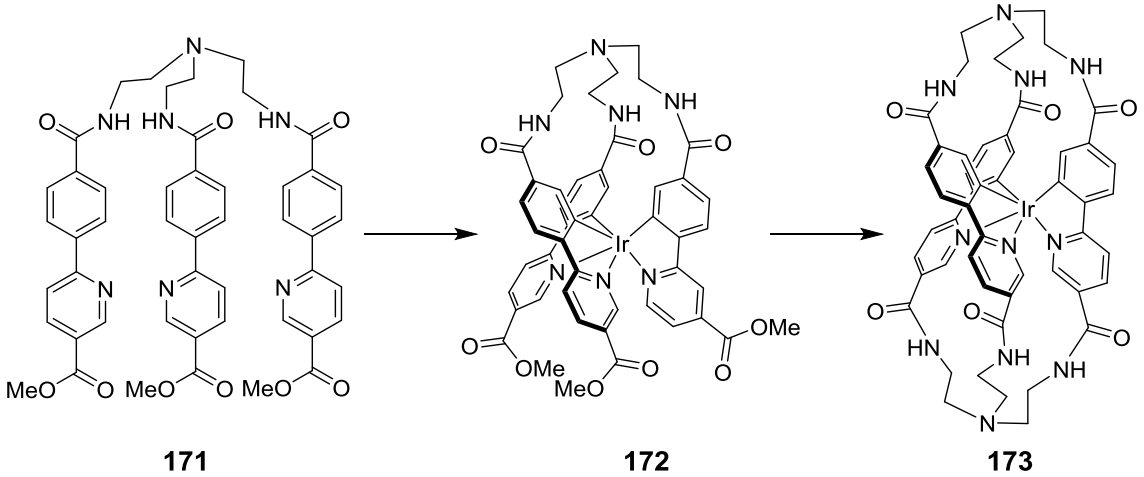

Figure 6.4

$Ir(ppy)_3$; it was found that the hemicage and cage complexes **172** and **173** showed a dramatic decrease in the quenching constant (40% and 80%, respectively) compared to $Ir(ppy)_3$, highlighting the effectiveness of the cage structure at protecting the iridium centre.[14] These complexes therefore have potential for application in biological systems, as these environments are often oxygen rich.[14]

The final examples of iridium hemicage complexes are shown in Figure 6.5, reported by St-Pierre *et. al*.[13] Complexes **174a** and **174b** are related to $Ir(ppy)_3$, with the tethers connected on the pyridine ring for **174a**, and on the phenyl ring for **174b**.[13] The photophysical properties of **174a** and **174b** are similar, with **174b** exhibiting stronger solvatochromism; this is attributed to the difference in the orientation of the dipole moments within the molecule.[13] The two complexes exhibit high quantum yields in polar aprotic solvents, such as acetonitrile or butylnitrile, 76% and 79% for **174a** and **174b**, respectively.[13] This is comparable to the value obtained for $Ir(ppy)_3$ in the same solvent, and the lifetimes are also comparable.[13]

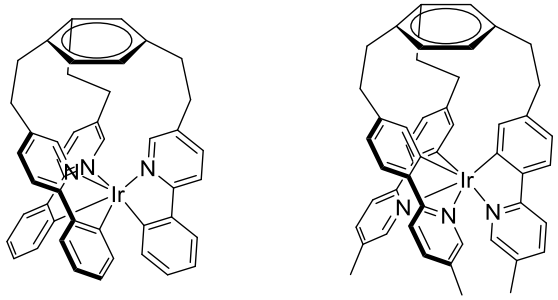

174a **174b**

Figure 6.5

RESULTS AND DISCUSSION

Inspired by these iridium and ruthenium hemicage complexes, the aim was to synthesise a tripodal, hexadentate ligand containing carbenes, with the goal of creating complexes that are more photochemically and thermodynamically stable, in the hope that they would exhibit superior performance under device operation. In addition, the cage effect has been shown on several occasions to enhance the PLQYs of emissive complexes; switching to tridentate carbene ligands produced complexes that displayed near-UV emission with PLQYs of over 0.40.[3] The synthesis of the initial target **180** is shown in Figure 6.6; the choice of tether unit was inspired by a paper by McDaniel *et. al* concerning the synthesis of Cr(III) complexes.[22] The first step involved the reaction of triethanolamine **175** with thionyl chloride to produce the trichloroammonium salt

176 in 95% yield.[23] Next was a triple nucleophilic substitution reaction using the sodium salt of 4-bromophenol as the nucleophile to give **177** in 49% yield after purification.[24] Also isolated was the disubstituted intermediate, in 24% yield. A small excess of NaOH base was used to account for the fact the starting material was an HCl salt. Once **177** was obtained the next step was to introduce the imidazole fragment, via three Ullman coupling reactions, using CuI/1,10-phenanthroline as the catalyst system, and Cs_2CO_3 as the base. Product **178** was isolated after recrystallisation in 46% yield. The final step was to create the carbene precursor, imidazolium salt **179**. This was attempted by treating a solution of **178** with three equivalents of CH_3I. A solid was isolated that was later identified as the methylated ammonium salt of the desired product **179** (50%), indicating the alkylation was not selective.

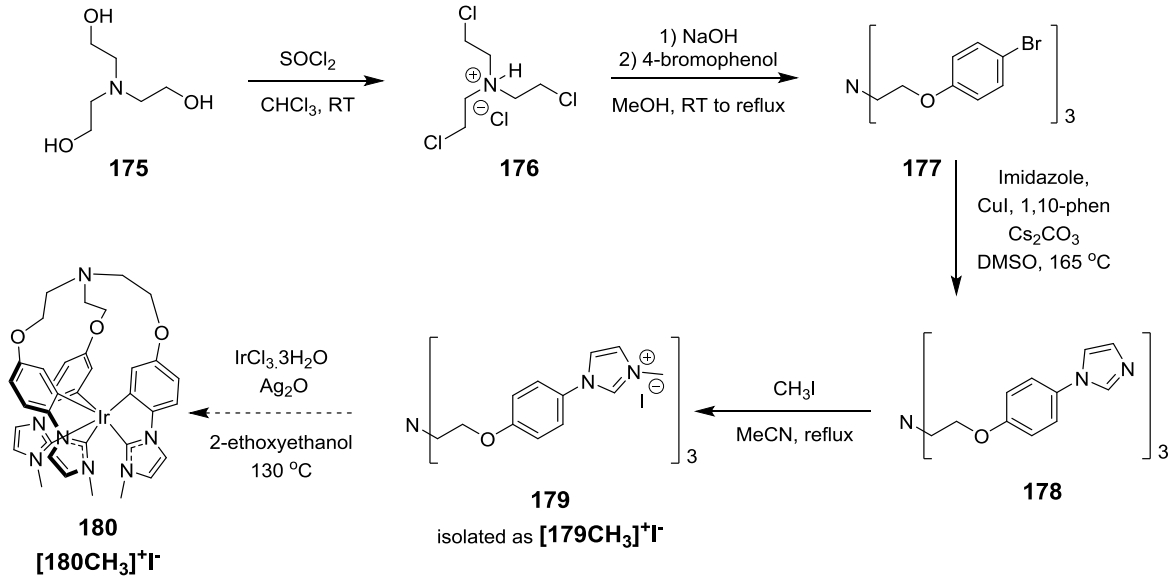

Figure 6.6: Attempted synthesis of target complex 180.

It was decided to attempt to synthesise an iridium complex from the ammonium salt **179CH$_3$I**, as it may be possible to remove the methyl group later. The ligand **179CH$_3$I** was combined with $IrCl_3.3H_2O$ and Ag_2O in 2-ethoxyethanol, shielded from light, and the reaction was heated to reflux overnight, as described in the literature for analogues.[1] After work up the reaction mixture was subjected to column chromatography, and although many fractions were obtained, none appeared to contain the desired complex **[180CH$_3$]$^+$I$^-$**. Analysis of the ^{1}H NMR spectrum suggested extensive decomposition of the ligand had occurred. It was not clear whether this was due to (i) strain within the ligand structure due to the short connection between the ligand fragment and the amine tether; (ii) the choice of iridium starting material or (iii) issues with the carbene formation. As a result, it was decided that the analogous ppy ligand **183** should be synthesised, to identify if the problem was ligand specific or not.

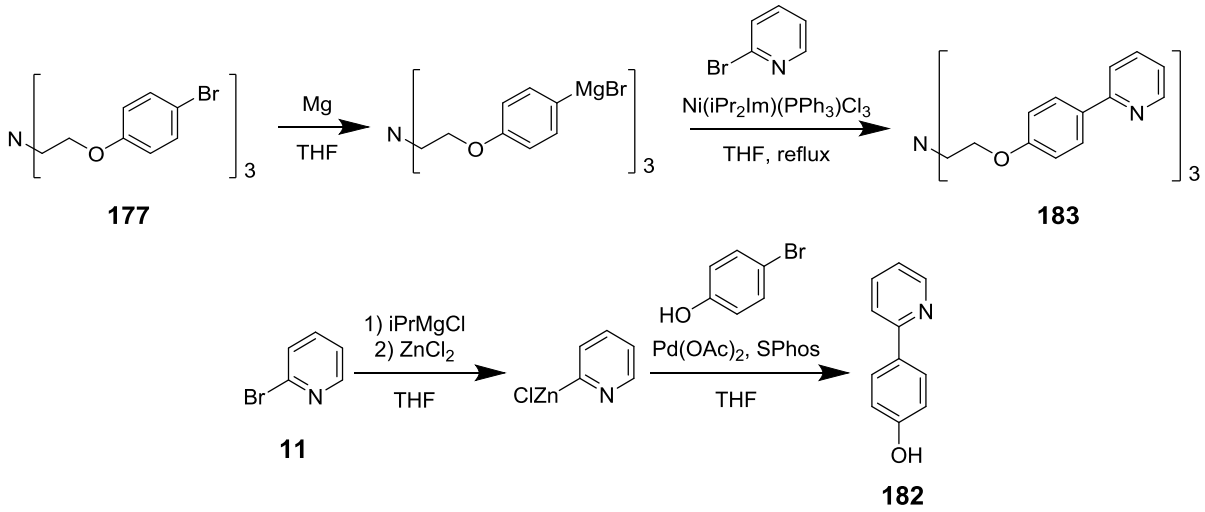

Figure 6.7

Initially the aim was to use intermediate **177** to synthesise the ligand **183**, and a variety of coupling procedures were attempted, as shown in Figure 6.7. A nickel catalysed Kumada coupling was attempted, as was a Negishi coupling on 4-bromophenol, however, NMR spectra revealed no sign of product **182**. Due to the known difficulties preparing 2-pyridyl Grignard reagents and 2-pyridyl boronic acids,[25,26] and the commercial availability of boronic acid **181** the synthesis was revised (Figure 6.8). For the new route the first step involved synthesis of **182** from 2-bromopyridine **11** and commercially available boronic acid **181** to give the product in 84% yield, as described in the literature.[27] There then followed a nucleophilic substitution reaction of **182** with **176** to give the desired product **183** in 40% yield after purification by reverse phase column chromatography. An advantage of this route over the previously outlined route for **179** is that it reduces the number of threefold reactions.

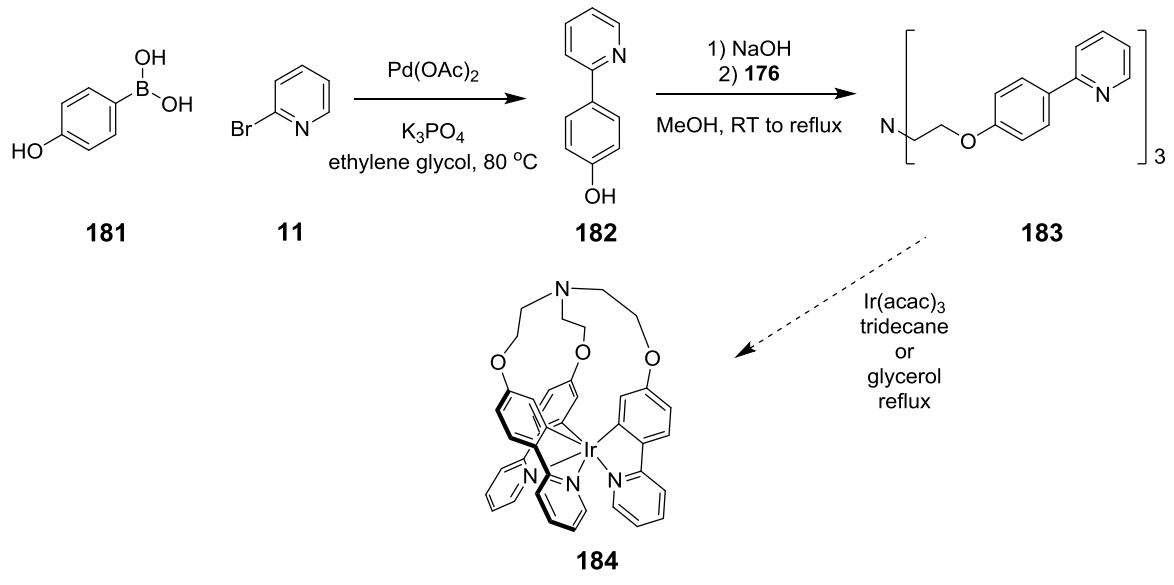

Figure 6.8

To form the desired iridium complex **184** it was thought that the use of $IrCl_3.3H_2O$ may be an issue as this requires the reaction to proceed via the intermediate dichloro dimer, which involves a *trans* arrangement of the nitrogen atoms of the cyclometalating ligands about the iridium centre. This is the incorrect stereochemistry for the *fac*-isomer, and due to the tether it is possible that the third arm of the ligand would not be able to reach the iridium centre. Therefore, $Ir(acac)_3$ was used instead, as the arms of the tripod can sequentially coordinate with the correct stereochemisty. The first set of conditions tried involved heating to reflux a mixture of $Ir(acac)_3$ and ligand **183** in tridecane, a high boiling solvent, overnight. TLC analysis revealed no sign of reaction; both **183** and the $Ir(acac)_3$ were reclaimed after column chromatography. When the solvent was switched to glycerol, another solvent frequently used to synthesise *fac*-iridium complexes, and the reaction was reattempted. This time, the $Ir(acac)_3$ and ligand were consumed and a new, fluorescent spot appeared on TLC. The spot did not move off the baseline unless extremely polar solvent mixtures were used (DCM, 0-100% ethanol), and once obtained the NMR spectrum was complicated, and no product could be identified. It was considered that the ligand might have reacted with the iridium source to form a network structure rather than a mononuclear cage complex, possibly due to the length of the linker. It was therefore decided to extend the linker by two ethylene glycol units, as this is comparable to complex **170** synthesised by Schaffner-Hamann *et.al.*[20]

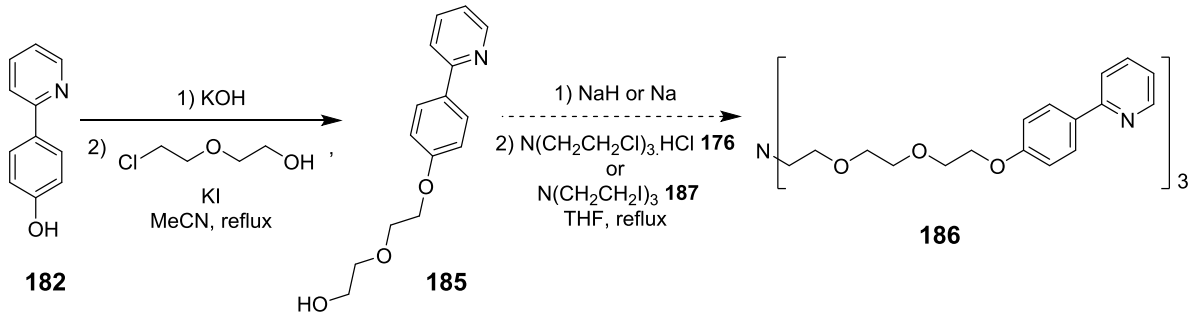

Figure 6.9

The initial route is shown in Figure 6.9, and the first step involved a one pot *in situ* Finkelstein reaction and nucleophilic substitution to attach a diethylene glycol unit to the phenolpyridine **182**. The desired product (**185**) was isolated in 87% yield. The next step involved making the sodium salt of **185** and using it as a nucleophile to attack **176**. This was attempted first using NaH as the base, then by using sodium to generate the sodium salt directly (Figure 6.11). In both cases, while it appeared the sodium salt had formed, only a trace amount (<1%) of product could be isolated despite heating the reaction to reflux overnight. The chloride **176** was transformed to the iodide free base **187** via a Finkelstein reaction, and the reaction was repeated with **185** and **187**.

However, again, only a small amount of product was isolated. In all three cases, **185** was isolated as the major component from the reaction. The poor yields of these reaction may reflect the poor stability of the central amine unit.

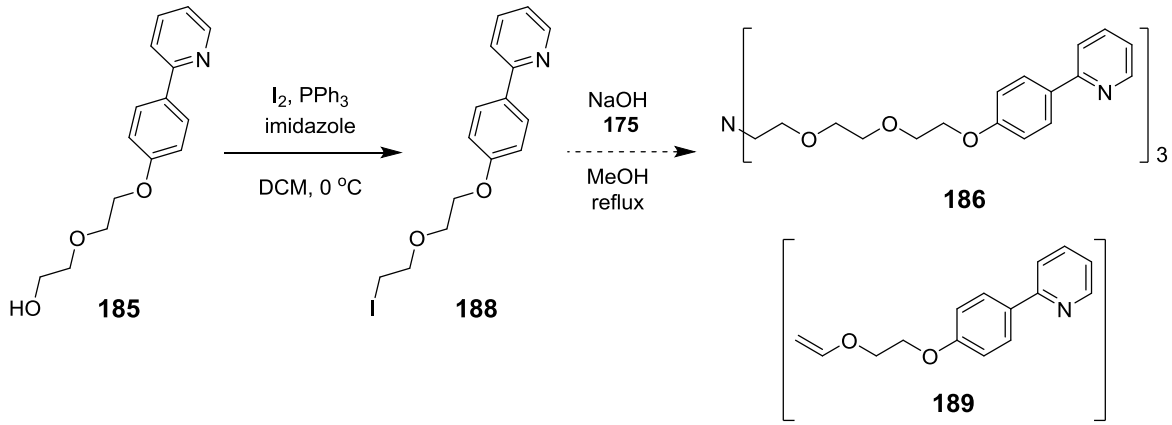

Figure 6.10

The next tactic was to exchange the nature of the reaction sites, as shown in Figure 6.10. Here, triethanol amine **175** was used as the nucleophile and reacted with **188**, which was synthesised via an Appel reaction from **185** (Figure 6.7, 82% yield). Triethanolamine **175** was then treated with NaOH, and **188** was added, and the mixture was heated to reflux overnight. However, no product **186** was isolated, instead, unreacted **188** was identified, along with species displaying doublets of doublets in the 4.5-6.8 ppm region, suggesting formation of the elimination product **189** (Figure 6.10).

Due to the synthetic difficulties described above, a new route shown in Figure 6.11 was devised, analogous to the synthesis of complex **170** by Schaffner-Hamann *et.al*.[20] Following the literature route THP-protected diethylene glycol unit **191**; the reaction was conducted as described in the literature and **191** was obtained in 93% yield.[20] Next, **191** was converted to the sodium salt, which was then reacted with **176** to give **192** in 63% yield. The next step was to remove the THP protecting group, typically achieved using a catalytic amount of acid. In this case the crude NMR revealed no sign of product **193**, instead indicating cleavage of one of the ether linkages to give triethanolamine **175**.

Therefore, the synthesis was redesigned to avoid any protecting groups that require removal with acid. Patent literature reports the synthesis of **193** directly from diethylene glycol **190** and the free base of **176**, $N(CH_2CH_2Cl)_3$, prepared by washing **176** with an aqueous Na_2CO_3 solution and extracting.[28] The mono-sodium salt of **190** was synthesised by adding sodium into stirred diethylene glycol **190**; when the sodium had completely dissolved $N(CH_2CH_2Cl)_3$ was added and the solution heated to reflux overnight. The residual diethylene glycol was removed via distillation

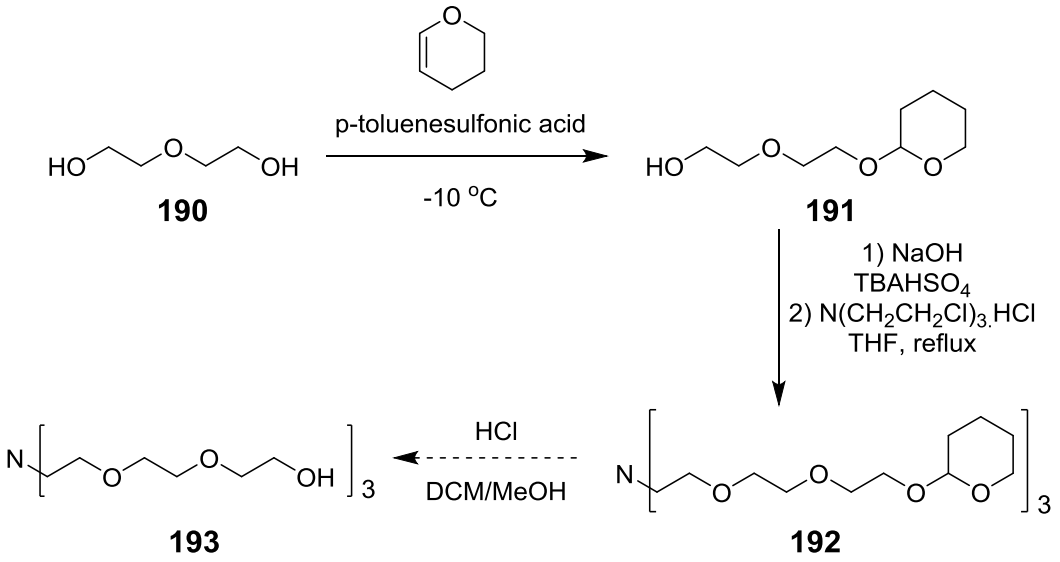

Figure 6.11

to give the desired product **193** in 99% yield.

The next step was to replace the alcohol moieties with halides to allow an analogous synthesis with that of **183.** Initially an Appel reaction with CCl_4/PPh_3 was attempted (Figure 6.12), however analysis of the crude MS data indicated the presence of product **194**, starting material **193**, as well as mono and disubstituted compounds. This route was then abandoned in favour of that proposed in the paper (Figure 6.12);[20] the alcohol moieties of **193** were transformed to mesylates, by a combination of mesyl chloride and base (NEt_3) to give a mixture containing **195** and mesylated diethylene glycol. As there did not appear to be any diethylene glycol present in the

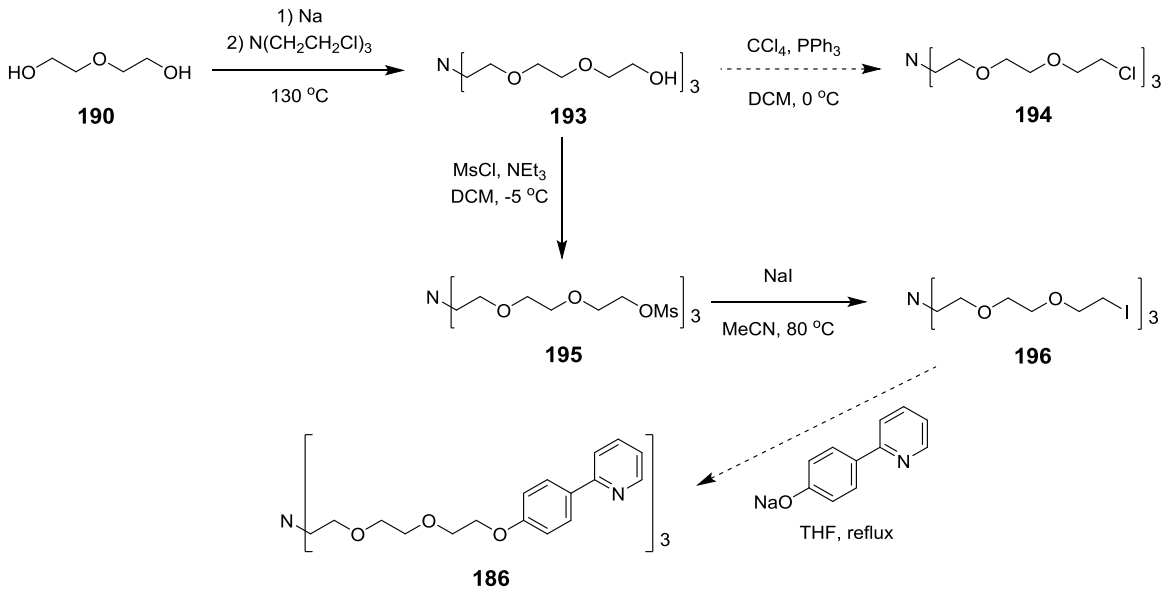

Figure 6.12

material (**193**) obtained in the previous step it is possible that the product **195** decomposed during the reaction or the purification. The crude mixture was then reacted with NaI to give a mixture of **196** and bis(2-iodoethyl) ether. The yield of the reaction appeared to be low, and the impurity was not removed due to concerns about the stability of compound **196**.

To synthesise the ligand **186**, a nucleophilic substitution of the iodides of **196** with the sodium salt of **182** was attempted (Figure 6.12); the initial conditions utilised NaOH as the base, and the reaction was conducted in MeOH. After work up the crude reaction mixture was subjected to reverse phase column chromatography, both phenol **182** and phenolate salt of **182** were isolated, along with the product of the nucleophilic substitution of bis(2-iodoethyl) ether, however none of the desired product **186** was isolated. Due to the synthetic difficulties and the apparent instability of the amine core, this synthetic target was abandoned.

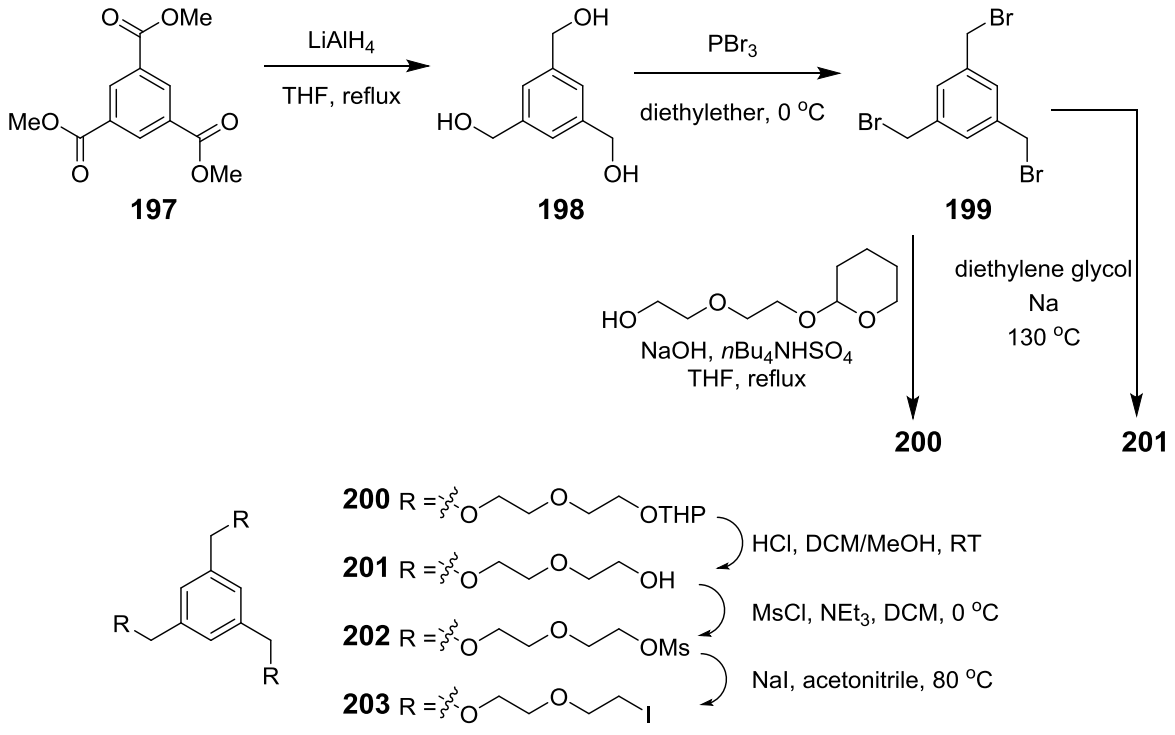

Figure 6.13

Due to the success of complex **170**, the amine core was exchanged for a phenyl ring and a new target (**203**) was designed. The synthesis of key intermediate **203** is shown in Figure 6.13, and the initial steps follow those described by Schaffner-Hamann *et.al.*[20] First, 1,3,5-tricarboxylate **197** was reduced to the trialcohol **198** using $LiAlH_4$ (in quantative yield), then the alcohols were transformed into bromines using PBr_3 to give **199** in 74% yield after purification. The next step was to introduce the glycol chains, achieved by reacting the sodium salt of the THP-protected

glycol **191** with **199** to produce **200** in 30% yield. The THP protecting groups were then removed by catalytic conc. HCl to give **201** in 75% yield.

A small amount of diethylene glycol was observed in the NMR spectrum, despite being carefully removed in the previous step. This was thought to be due, again, to cleavage of one of the ether linkages, as seen for **192** (Figure 6.11). Hence a route analogous to the synthesis of **193** directly from **190** was attempted to avoid the use of the protecting group, and is shown in Figure 6.13. As with the synthesis of **193**, the sodium salt of **190** was formed by adding sodium to diethylene glycol, followed by the addition of **199**. Some residual diethylene glycol sodium salts remained, however, as both the product and impurity were readily soluble in water these could not be extracted. Due to the high polarity of the product it was not suitable for normal phase column chromatography, and little separation between these salts and the product **201** was observed on utilising reverse phase chromatography. As a result the impurity was left for removal at a later stage.

The alcohol groups of **201** were then transformed to mesylates, as described for **193**, to give **202**, along with the mesylate diethylene glycol impurity. **202** was then subjected to Finkelstein conditions to replace the mesylates with iodides. At this stage the bis(2-iodoethyl) ether could be easily removed by distillation (b.pt. 110-120 ^{o}C at 0.66 mbar [29]) to give **203** in 54% yield over the three steps.

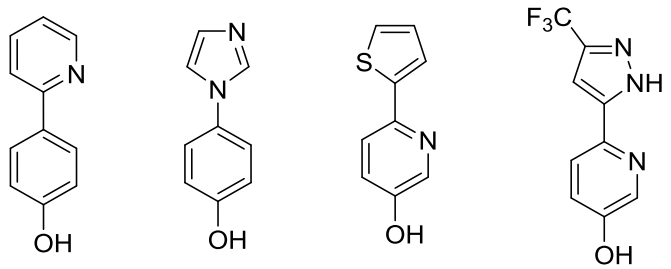

182 **204** **205** **206**

Figure 6.14

From here it remained to attach the appropriate phenols, shown in Figure 6.14, to create the final ligands. Phenols **182** and **204** have already been identified as targets, with the synthesis of **182** described previously. At this point, two other targets were identified, **205** and **206**. Compound **205** was chosen to expand the family to include an orange/red emitter, as *fac*-Ir(thpy)$_3$ [thpy = 2-(2-thienyl)pyridine] is well known.[30] Compound **206** was chosen as it was noted by Yeh *et. al*. that the *fac*- isomer of **81b** had not been synthesised, but computational work suggested that it would

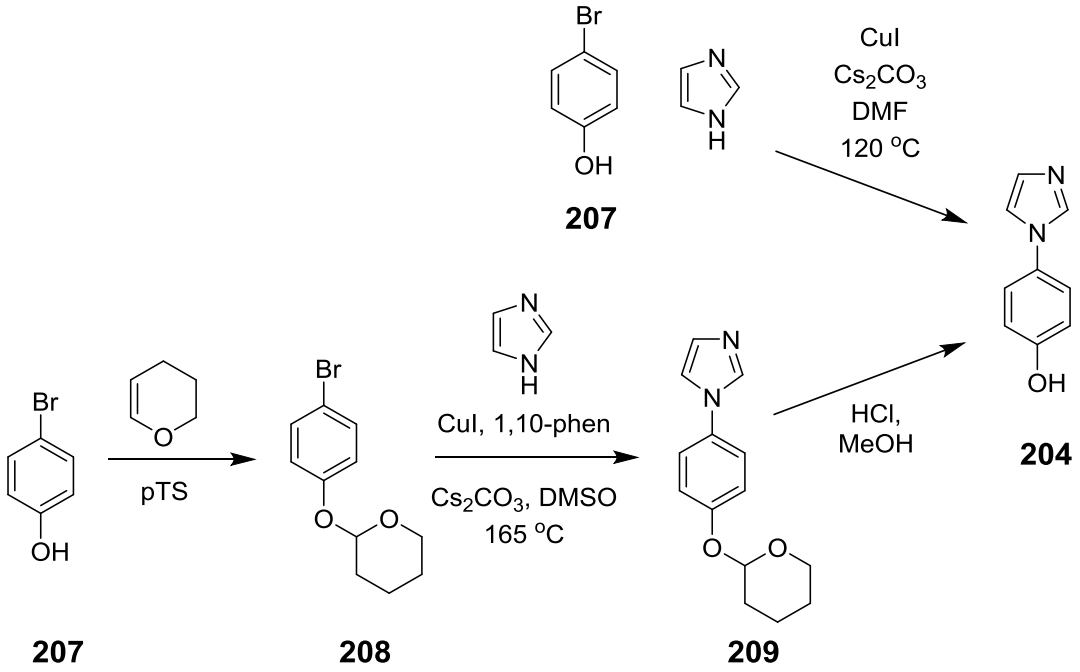

Figure 6.15

be a true-blue emitter, without the dual emissive properties that are observed in the *mer*-isomer **81b**.[31] The hexadentate ligand structure would ensure the formation of the *fac* geometry, as the tethers prevent the approach of the third ligand once the first two have assumed the *trans* nitrogen arrangement required for the *mer* geometry.

The initial attempt at the synthesis of **204** (Figure 6.15) followed the literature procedure described by Zhu *et*. *al*.:[32] an Ullmann reaction using CuI as the catalyst, and Cs_2CO_3 as the base. Unfortunately, the product was obtained in only 14% yield, and additional precautions, such as thoroughly dried reagents and degassed solvent, did not result in any improvement. As the coupling between **177** and imidazole had previously proceeded in good yield (46% for a threefold reaction) it was thought that the issue may be interference from the free -OH group of **207**. As a result, the phenol **207** was protected using the THP group (Figure 6.15), which is base resistant and easily removed with acid. The protected phenol **208** was isolated in 37% yield. The Ullmann coupling was then repeated with **208** and imidazole, this time using conditions that have

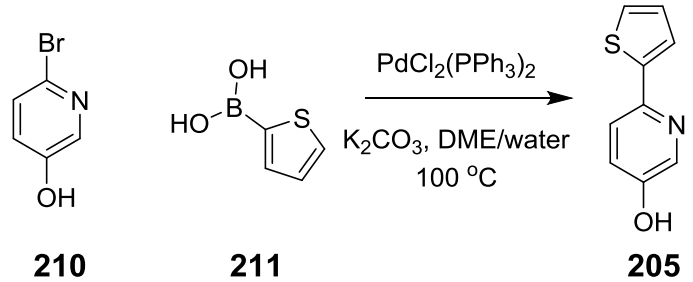

Figure 6.16

previously proved successful, using CuI/1,10-phen as the catalytic system and Cs_2CO_3 as the base. The product **209** was isolated in 69% yield, and the THP group was removed with conc. HCl to give the desired phenol **204** in quantitative yield.

Phenol **205** was synthesised in 69% yield via a Suzuki coupling between **210** and **211** using $PdCl_2(PPh_3)_2$ as the catalyst and K_2CO_3 as the base, as shown in Figure 6.16.

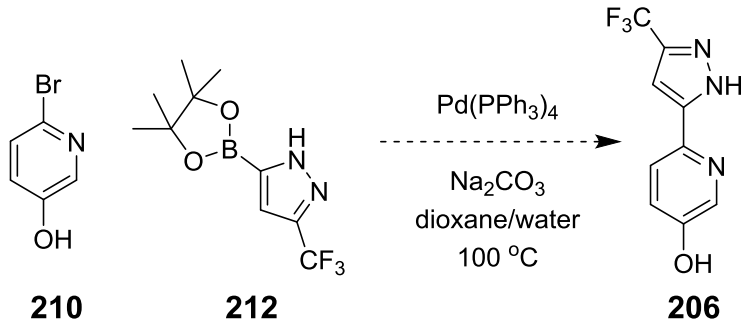

Figure 6.17

The first route attempted to synthesise **206** was a Suzuki coupling between boronic ester **212** and commercially available bromide **210** (Figure 6.17). The boronic ester **212** was synthesised according to the literature procedure, shown in Figure 6.18, and was isolated in 73% yield.[33] Compounds **210** and **212** were subjected to Suzuki conditions, with $Pd(PPh_3)_4$ and Na_2CO_3 as the catalyst and base, respectively. Upon purification starting material **210** and deborylated pyrazole **213** were isolated, with no sign of desired product **206**. As **210** had been shown to perform well under Suzuki conditions with boronic acid **211,** it was decided that the free NH of the pyrazole **212** should be protected. Therefore, THP derivative **214** was synthesised in 24% yield. The order of

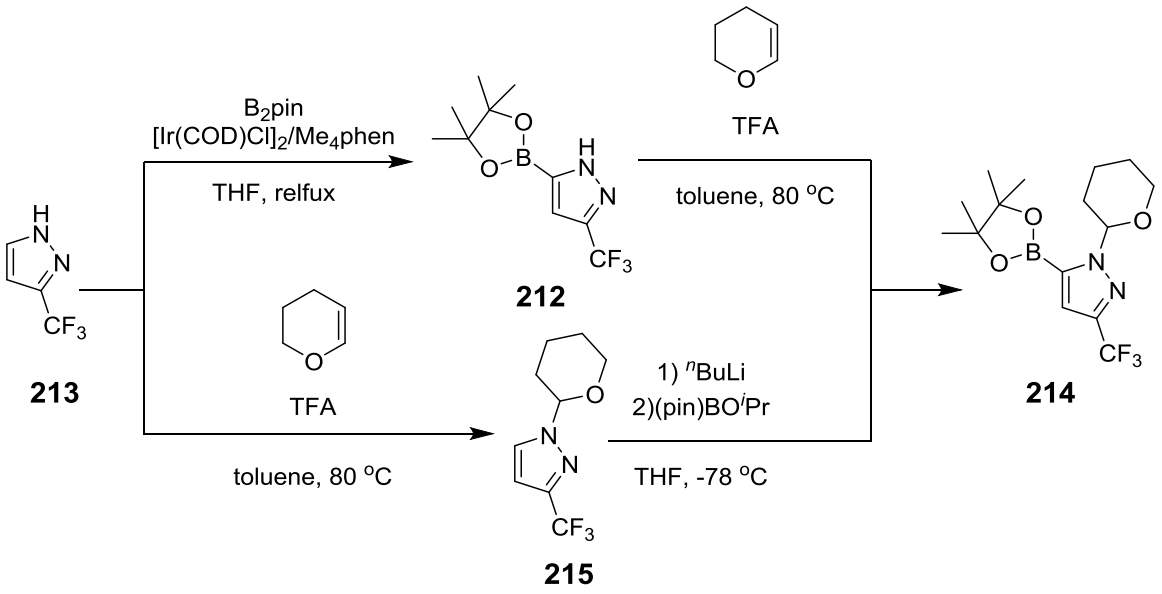

Figure 6.18

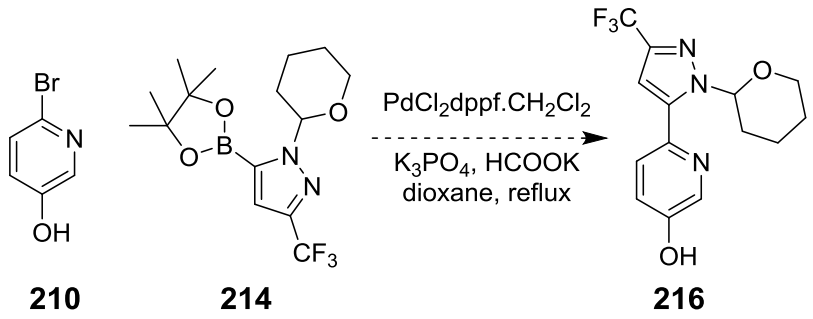

210 **214** **216**

Figure 6.19

reactions was also reversed, with pyrazole **213** protected with THP to give **215** in 95% yield, followed by lithiation and introduction of the Bpin group to give **214** in 41% yield. Boronic ester **214** was then subjected to Suzuki conditions (Figure 6.19) that had been utilised previously in our group for coupling a variety of N-substituted 3-trifluoromethylpyrazole boronic esters to both electron rich and electron poor haloarenes.[34] These conditions had been shown to reduce both the incidence of homo-coupling of the boronic ester and the rate of protodeboronation.[34] In our case, after work up of the crude reaction mixture ^{1}H NMR peaks corresponding to the product could be found, and a large amount of starting material **210** remained.

As a result, this route was abandoned in favour of a route analogous to the synthesis of ligand **144**, which involves constructing the pyrazole ring from a diketone intermediate. The proposed route is shown in Figure 6.20, and starts from the low-cost, commercially available amine **217**. The first step involved introducing the alcohol group via a diazonium salt, synthesised according to the

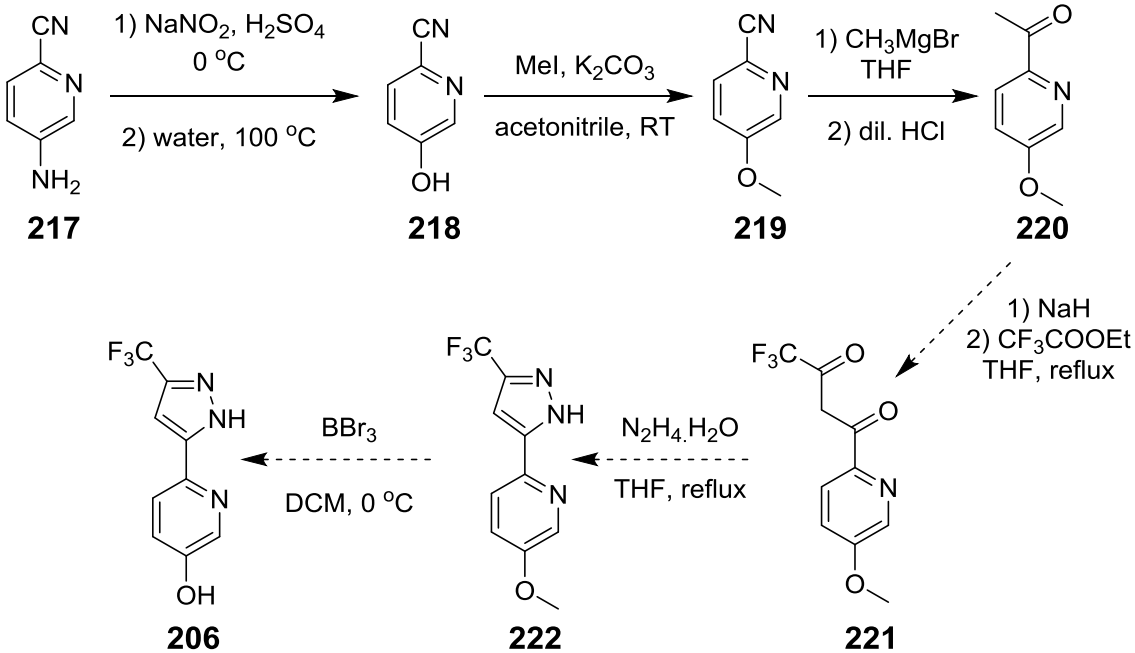

217 **218** **219** **220** **221** **222** **206**

Figure 6.20

literature method.[28] Product **218** was obtained in quantitative yield. The alcohol substituent of **218** was then protected as methoxy derivative **219**, which was then isolated in 23% yield. The cyano group was then transformed into an acetyl via reaction of **219** with MeMgBr followed by acid work up to give **220** in 56% yield. It remained to form the diketone intermediate **221** via a crossed Claisen condensation with ethyl trifluoroacetate, followed by a ring closing condensation with hydrazine hydrate to give pyrazole **222**. The final step would be to deprotect the methyl group with BBr_3 to give the desired phenol **206**. Unfortunately, this synthesis was not completed due to lack of time during the course of this work.

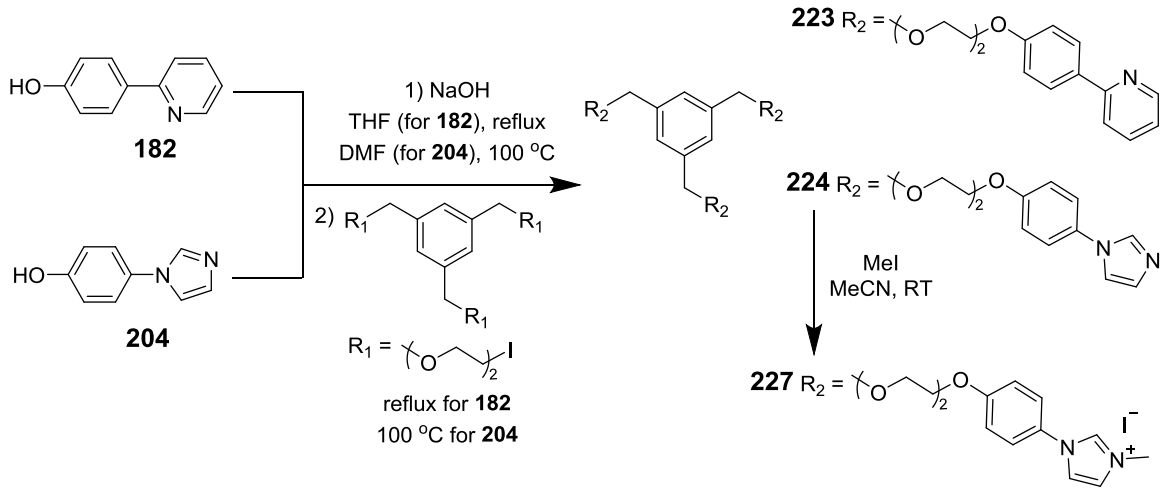

Figure 6.21: Synthesis of tripodal ligands 223 and 224.

With the alcohol derivatives **182**, **204** and **205** in hand the next step was to synthesise the final ligands. NaOH was added to solutions of **182** and **204** in THF, and the mixtures were heated to reflux until all the base had reacted (Figures 6.21 and 6.22). Then the tri-iodo core reagent **203** was added, and the solution heated to reflux overnight. The solvent was removed and the residues were purified by reverse phase column chromatography to give **223** in 66% yield. In the case of **205**, the major product isolated was the doubly substituted product **225**, in 84% yield. The reaction was repeated, and again, **225** was the major product. It is unclear why the reaction appears to stop at this stage. When the reaction was repeated, this time adding **225**, instead of the iodo centre **203**, the desired product **226** was isolated in 50% yield.

In the case of **204**, the reaction was attempted in THF; however, on deprotonation of **204** the sodium salt began to precipitate out. Nonetheless, reagent **203** was added anyway; however no product was isolated. With dioxane as the solvent no increase in solubility was observed. DMF was also tried, and the sodium salt of **204** proved soluble. Reagent **203** was then added, however after attempted purification by column chromatography a residual unidentified impurity was

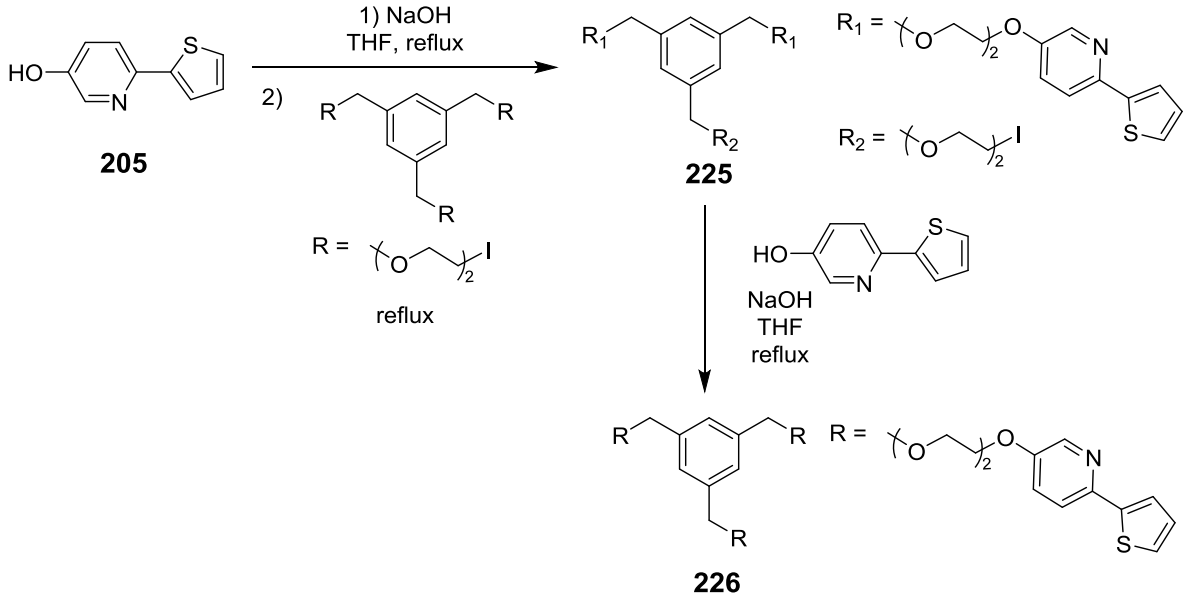

Figure 6.22

observed by NMR. This impurity appears to contain alkyl chains and some aromatic protons. One suspected product is the result of an elimination reaction on the iodo centre to leave an alkene fragment; this is supported by the appearance of two doublets of doublets at 6.50 ppm in the ^{1}H NMR spectrum. The reaction was repeated at a lower temperature of 50^{o}C, in an attempt to suppress the formation of this side-product, however no improvement was observed. An attempt was made to continue through to the final carbene precursor, **227** (Figure 6.23), by reacting the crude **224** with three equivalents of MeI, however the NMR spectrum of the crude material revealed the presence of two species. Attempted resolution of these species both with reverse phase column chromatography and with normal phase chromatography in highly polar solvent mixtures (water/MeCN and KNO_3 solution) was unsuccessful. Analytical HPLC showed some

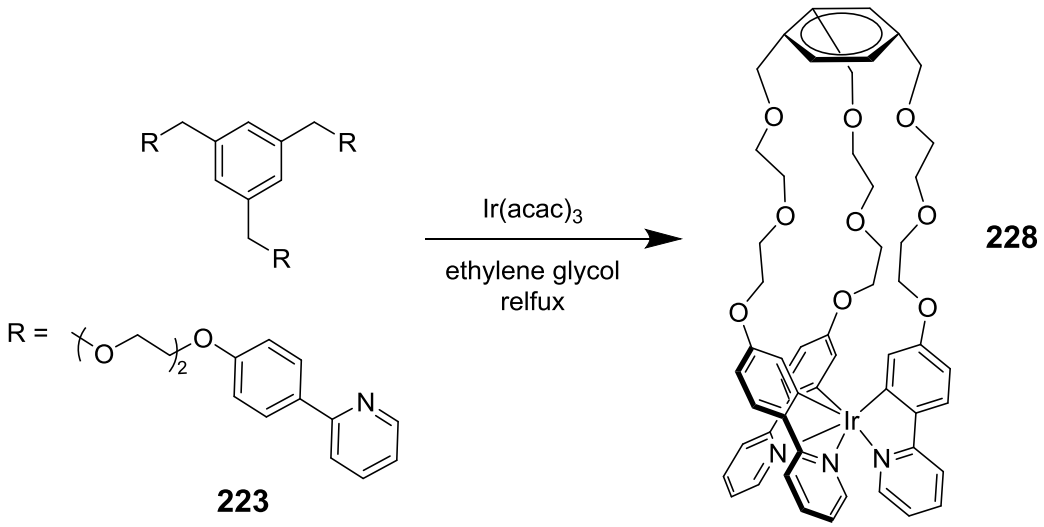

Figure 6.23: Synthesis of target complex.

Reaction	Temperature (°C)	Dilution (ml/mg)	Yield (%)
1	160	4.7	0
2	reflux	2.3	32
3	reflux	0.9	0
4	reflux	3	0
5	reflux	1.9	23

Table 6.1: Reaction conditions for synthesis of complex 228.

promise in separating the precursor **224** and the impurity; however, there was not sufficient time to conduct this on a preparative scale during the course of this work.

Using ligands **223** and **226** the final step was to synthesise the desired complexes **228** and **229**. Based on the procedures outlined by **170** for the synthesis of Schaffner-Hamann *et.al.*,[20] and previous related work conducted by Beeston *et*. *al*. on ruthenium cage complexes,[15] the reactions were conducted under high dilution (approx. 2-3 ml per mg of ligand) in an attempt to ensure formation of the desired cage species, as opposed to polymeric species.

Ligand **223** was suspended in ethylene glycol and $Ir(acac)_3$ was added. The solution was heated to reflux for 24 h, with vigorous stirring. The reaction was attempted five times, at a variety of temperatures and concentrations, as shown in Table 6.1. At the lower temperature of 160 °C no formation of product was observed, and both the unreacted ligand **223** and the $Ir(acac)_3$ were isolated (reaction 1). The temperature was increased to reflux (b.pt. 197 °C), and the volume reduced, and this time product **228** was isolated in 32% and 23% yields (reactions 2 and 5). Due to the difficulties associated with removing the large volume of ethylene glycol in the work up the reaction was attempted at a much higher concentration (reaction 3), in line with those reported

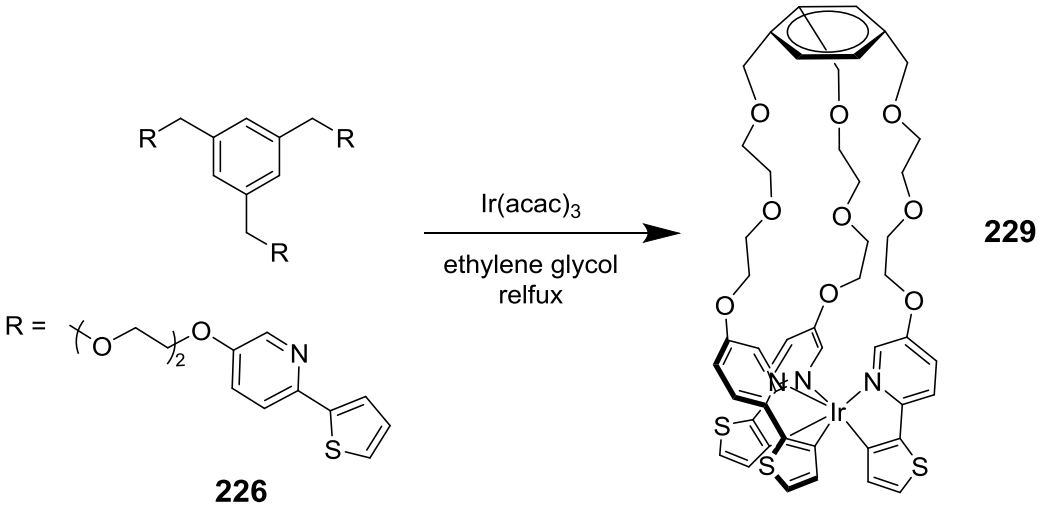

Figure 6.24: Synthesis of complex 229.

by Ruggi *et*. *al*. in the synthesis of **172**,[14] and St-Pierre *et*. *al*. in the synthesis of **174a**/**b**.[13] In the case of **228**, no complex was isolated, instead a large quantity of emissive material that proved difficult to move on TLC except in the most polar solvent mixtures, suggesting formation of polynuclear species. This is contrary to that observed by Ruggi *et*. *al*. and St-Pierre *et*. *al*., who reported yields of 20% for **172** and 33-37% for **174a** and **174b**, respectively. However, this can be explained by the fact the tethers to the core in the case of **228** are much longer, allowing more freedom of movement and possibly reducing the rate of complex formation, allowing the separate arms more opportunities to come into contact with other metal centres than if the chains were shorter.

On one occasion (reaction 4), under similar conditions to the two successful reactions, the reaction failed, with $Ir(acac)_3$ and ligand **223** being identified on TLC. It is not clear the reason for this, but it could be due to the difficulties ensuring adequate heating, stirring and degassing across such a large volume of solvent. Ideally, another iridium source would be used as $Ir(acac)_3$ is known to produce lower yields than reagents such as $IrCl_3.3H_2O$, or the μ-dichloro dimers, and is also more costly.[35,36]

For complex **229** the synthesis was analogous to that of **228**; ligand **226** and $Ir(acac)_3$ were combined in a large volume of ethylene glycol and the solution was heated to reflux for 24 h

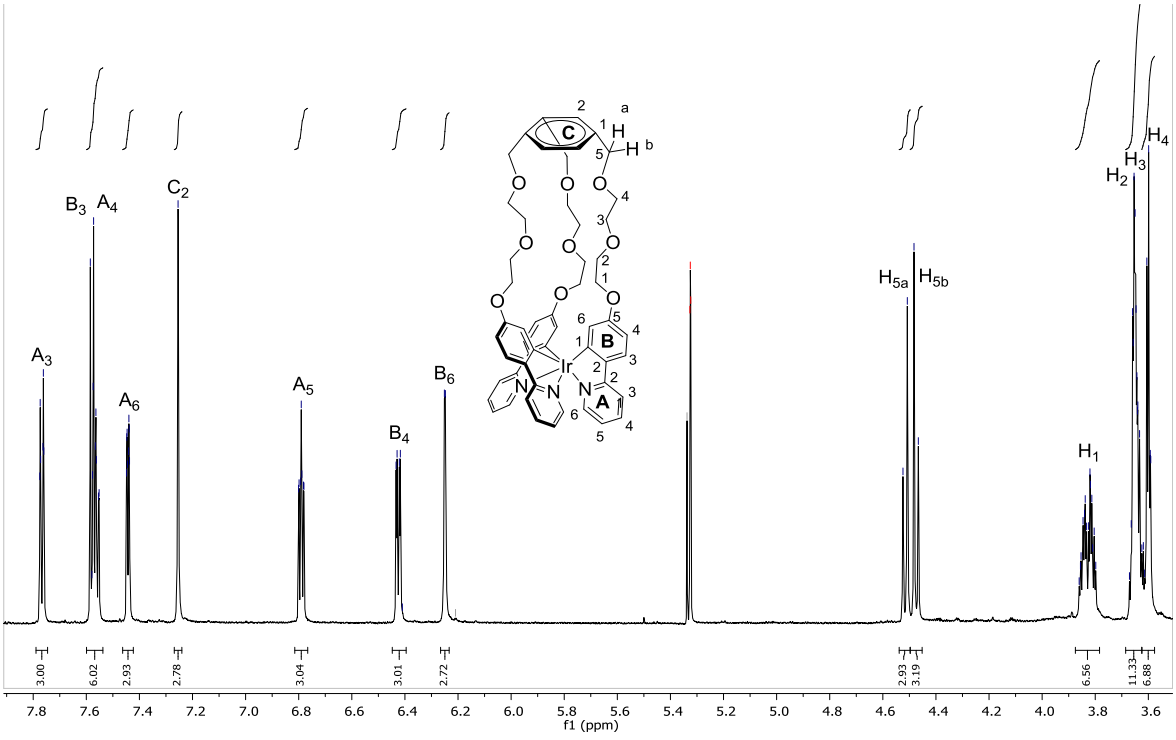

Figure 6.25: ^{1}H NMR spectrum of complex 228 in CD_2Cl_2.

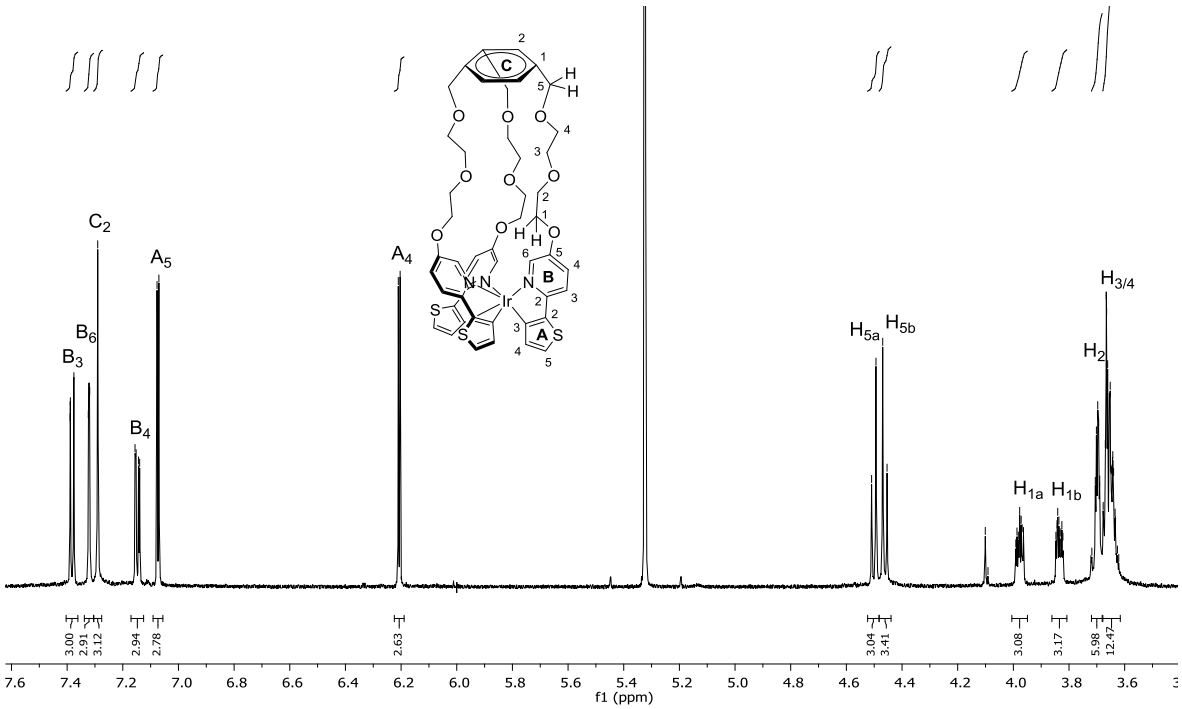

Figure 6.26: ^{1}H NMR spectrum of complex 229 in CD_2Cl_2.

(Figure 6.24). The reaction was worked up as described for **228**, by distillation of the ethylene glycol solvent, followed by purification by column chromatography to give **229** as an orange powder in 8% yield. A significant quantity of black, intractable solid remained at the top of the column, a possible explanation for the low yield of this reaction compared to the synthesis of **229**.

The ^{1}H NMR spectra of complexes **228** and **229** have been fully assigned with the aid of 2D experiments, and are shown in Figure 6.25 and Figure 6.26, respectively. The *fac*- geometry of the complexes is clear from the relative simplicity of the NMR spectra, highlighting the C_3 symmetry of the complexes in solution. It is also notable that the closest methylene protons to the phenyl core (protons H5a and H5b for complex **228** and **229**) appear as two signals with a coupling constant of 12.2 Hz and the signals are roofed. This is due to the reduced flexibility of the chains close to the core, as a result of the geometry required for the cage coordination. This results in the geminal protons becoming diastereotopic due to the inherent chirality of the $Ir(ppy)_3$ unit.[14] There is also a similar splitting for the H1 protons, with the splitting much more significant for complex **229** than for **228**.

Photophysical and electrochemical properties

Absorption and emission

The absorption spectra of complexes **228** and **229** are shown in Figure 6.28. The strong bands

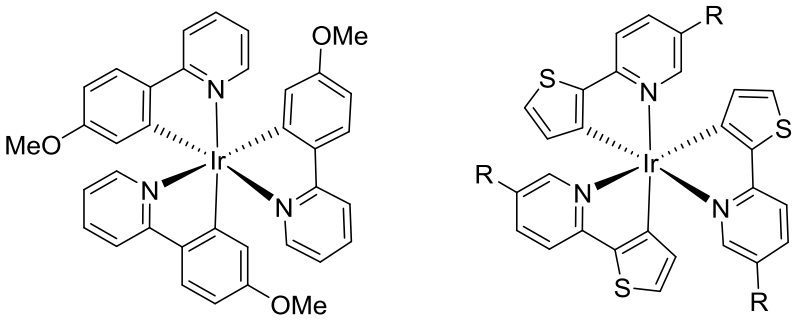

230

231 R = OMe
232 R = H

Figure 6.27: Parent and related complexes.

between 250-320 nm are assigned to π-π* transitions on the ligand based on the calculations of Hay,[37] and literature precedent. The intense bands at 350-400 nm are assigned to the ^{1}MLCT bands.

The lower energy ^{3}MLCT bands could not be easily distinguished. The absorption spectrum of complex **228** bares a strong resemblance to that of parent complex **230**,[38] shown in Figure 6.20, indicating that the addition of the tether unit has had little effect on the absorption of the complex. The parent complex of **229** is not known (**231**); however, the absorption spectrum of **229** does resemble that of related complex **232** (Figure 6.27).[30]

Excitation spectra for all complexes were recorded (Figure 6.29), revealing as expected that the bands from the ^{1}MLCT states are responsible for the emission from the complexes, while the

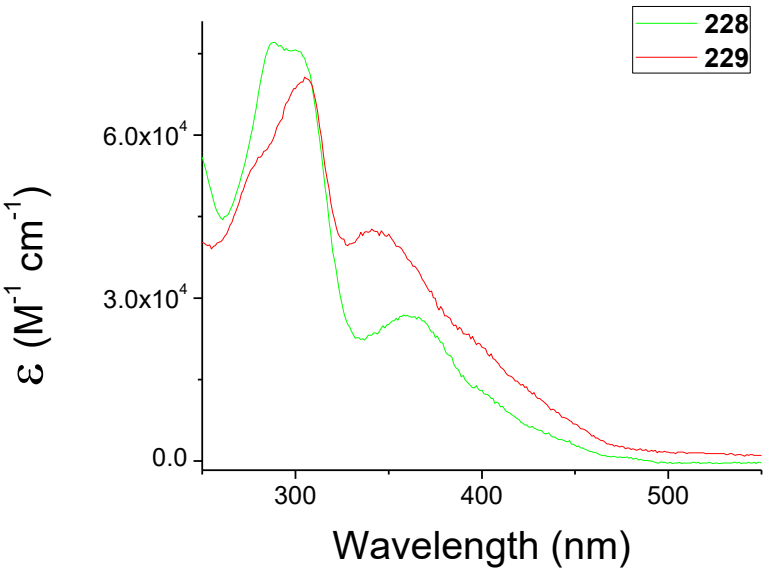

Figure 6.28: Absorption spectra of complexes 228 and 229 in DCM [<10^5 M].

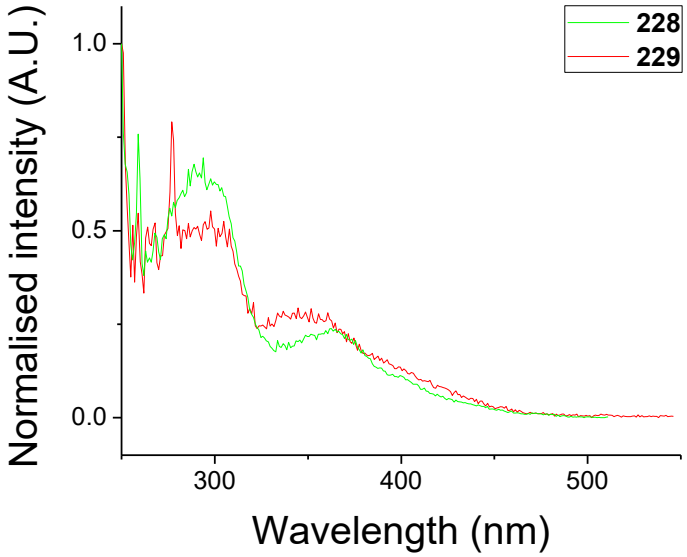

Figure 6.29: Excitation spectra of 228 and 229 in dearated DCM [<10^5 M]. The emission band observed was in the 500-560 nm range.

majority of the higher energy π-π* transitions are dark.

The emission spectra of the complexes are shown in Figure 6.30. The spectrum of **228** is similar to that of parent complex **230**, broad, featureless emission indicative of a large MLCT contribution to the excited state. The emission of complex **229** displays a similar profile to that of complex **232**, with the presence of strong vibronic features. Emission from the *fac* thienylpyridine (thpy)-based iridium complexes is known to display significant LC character.[30,39] In both cases, this suggests

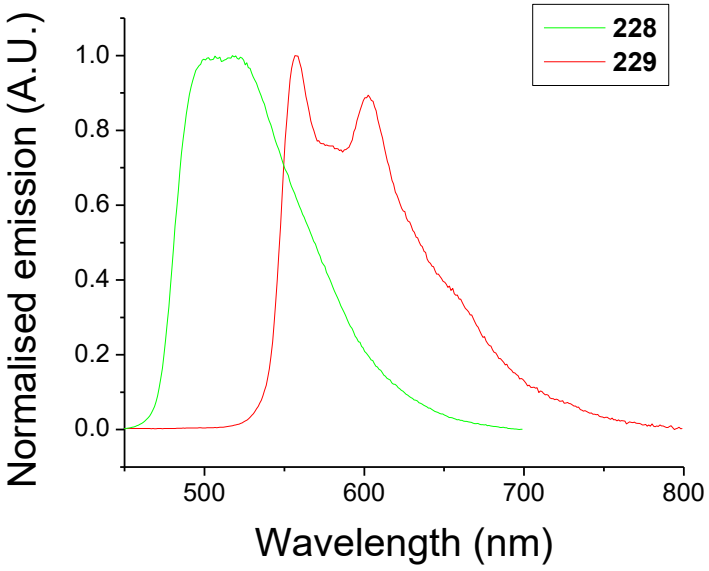

Figure 6.30: Emission spectra of selected complexes in deaerated DCM [<10^5 M], λ_{ex} = 355 nm.

Complex	λ_{max}^{abs} (ε) / nm (x10^3 $M^{-1}cm^{-1}$)[a]	λ_{max}^{em} / nm[b]	PLQY / Φ_{PL}[a,c]	τ_P / μs[a,d]	k_r / $10^5 s^{-1}$ [e]	k_{nr} / $10^5 s^{-1}$ [e]
228	287 (78.3), 303 (76.6), 362 (27.0), 402 (12.3, sh), 446 (3.3), 477 (0.6)	503, 519	0.92	1.87	4.92	0.43
229	279 (54.6), 305 (70.1), 344 (42.1), 385 (24.9, sh), 514 (1.6)	558, 602, 653 (sh)	0.43	7.20	0.60	0.79
230[f]	289, 360	495	0.65	1.80	3.61	1.94
232[g]	300 (35.5), 343 (15.9), 398 (11.9, sh)	548, 592, 643	0.40	7.10	0.56	0.85

[a] Data obtained in dichloromethane solution at 20 °C. [b] Data obtained in degassed dichloromethane solution with λ_{ex} = 380 nm. [c] Measured in degassed DCM relative to quinine sulfate Φ_{PL}= 0.546 in 0.5 M H_2SO_4 at 20 °C; estimated error ±5%. [d] Estimated error ±5%. [e] k_r, k_{nr} values calculated using Equations 1.5/1.6. [f] Values for complex **230** are taken from reference [38]. [g] Values from complex **232** are taken from reference [40].

Table 6.2: Photophysical data for selected iridium complexes

that the introduction of a tethering unit has not significantly impacted the nature of the excited state.

The PLQYs, lifetimes (τ_{obs}) and calculated radiative and non-radiative decay rates (k_r and k_{nr}) for complexes **228** and **229** are shown in Table 6.2, and compared to literature data for complexes **230** and **232**. The phosphorescent lifetime of **228** is comparable to that measured for parent complex **230**, but the PLQY is higher (0.92 vs 0.65). This could indicate an increased stability towards quenching mechanisms, whether via vibrations or solvent quenching, for the hemicage complex **228**. This is in line with previously reported hemicage/cage iridium complexes. In the case of complex **229** the PLQY and the lifetime are both comparable to the related complex **232**. Other complexes containing substituted thpy ligands also display long phosphorescent lifetimes, this is consistent with a reduced MLCT contribution to the excited state, as the spin-orbit coupling is less allowed. For both **228** and **229** the complexes appear to show reduced k_{nr} values relative to the untethered complexes, suggesting that the tethers may indeed rigidify the complexes as desired.

Electrochemistry

The electrochemical behaviour of complexes **228** and **229** was investigated using cyclic

voltammetry and compared to the literature data for parent compound **230**. Literature data could not be found for related complex **232**. The voltammograms are shown in Figure 6.31 and the key parameters in Table 6.3. Formula 2.1 is used to calculate the energy of the HOMO.

Complex	$E^{ox}_{1/2}$ / V	HOMO / eV
228	0.17	-4.97
229	0.13	-4.93
230	0.30	-5.10

All values reported vs Fc/Fc^+ = 0.00 V.

Table 6.3: Electrochemistry data of iridium complexes. Measured in DCM (0.1 M $^nBu_4NPF_6$) at 298 K.

The complexes both show a reversible oxidation wave which was assigned to the Ir^{III}/Ir^{IV} couple. Introduction of the tethering unit results in a small (0.1 V) decrease in the oxidation potential of **228** compared to **230**, which is reflected in the red-shift in emission (8 nm) spectra. Complex **229** exhibited a less positive oxidation potential compared to **228**, consistent with the red-shift in the emission spectra compared to **228**. No reduction peaks were observed within the solvent window.

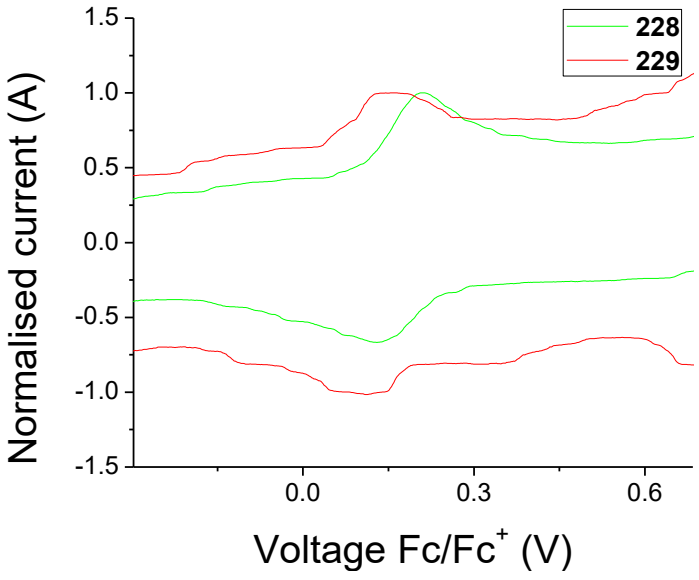

Figure 6.31: Cyclic voltammograms of 228 and 229.

CONCLUSION

Two tripodal ligands, **223** and **226**, and their respective iridium complexes, **228** and **229**, were synthesised. The complexes displayed comparable or superior PLQYs and lifetimes to the parent/related complexes, and the ^1H NMR data suggested some limited motion in solution. It

remains to complete the synthesis of the other target ligands derived from alcohols **204** and **206**, and their iridium complexes. The performance of the complexes in devices remains to be investigated. The complexes could also be tested as sensors for metal cations, as the cavity created between the phenyl-centre and the complex could be large enough to house a metal ion, and the PEG chains provide a coordinating environment. It's anticipated that coordination of a metal ion may induce changes in the photophysical properties, such as the PLQY, lifetime, or even the λ_{max} of the emission.

References

1) T. Sajoto, P. I. Djurovich, A. Tamayo, M. Yousufuddin, R. Bau, M. E. Thompson, R. J. Holmes and S. R. Forrest, *Inorg. Chem.,* 2005, **44**, 7992-8003
2) R. Visbal and M. C. Gimeno, *Chem. Soc. Rev.,* 2014, **43**, 3551-74
3) N. Darmawan, C. H. Yang, M. Mauro, M. Raynal, S. Heun, J. Pan, H. Buchholz, P. Braunstein and L. De Cola, *Inorg. Chem.,* 2013, **52**, 10756-65
4) J. Lee, H. F. Chen, T. Batagoda, C. Coburn, P. I. Djurovich, M. E. Thompson and S. R. Forrest, *Nat. Mater.,* 2016, **15**, 92-8
5) F. Monti, F. Kessler, M. Delgado, J. Frey, F. Bazzanini, G. Accorsi, N. Armaroli, H. J. Bolink, E. Orti, R. Scopelliti, M. K. Nazeeruddin and E. Baranoff, *Inorg. Chem.,* 2013, **52**, 10292-305
6) Y. Zhou, J. Jia, W. Li, H. Fei and M. Zhou, *Chem. Commun.,* 2013, **49**, 3230-2
7) K. Tsuchiya, S. Yagai, A. Kitamura, T. Karatsu, K. Endo, J. Mizukami, S. Akiyama and M. Yabe, *Eur. J. Inorg. Chem.,* 2010, **2010**, 926-933
8) H. Li, Y.-M. Yin, H.-T. Cao, H.-Z. Sun, L. Wang, G.-G. Shan, D.-X. Zhu, Z.-M. Su and W.-F. Xie, *J. Organomet. Chem.,* 2014, **753**, 55-62
9) Y. Wang, N. Sun, B. F. E. Curchod, L. Male, D. Ma, J. Fan, Y. Liu, W. Zhu and E. Baranoff, *J. Mater. Chem. C,* 2016,
10) H. Sasabe, J. Takamatsu, T. Motoyama, S. Watanabe, G. Wagenblast, N. Langer, O. Molt, E. Fuchs, C. Lennartz and J. Kido, *Adv. Mater.,* 2010, **22**, 5003-7
11) J.-A. Seo, S. K. Jeon, M. S. Gong, J. Y. Lee, C. H. Noh and S. H. Kim, *J. Mater. Chem. C,* 2015, **3**, 4640-4645
12) T. Sajoto, P. I. Djurovich, A. B. Tamayo, J. Oxgaard, W. A. Goddard, 3rd and M. E. Thompson, *J. Am. Chem. Soc.,* 2009, **131**, 9813-22
13) G. St-Pierre, S. Ladouceur, D. Fortin and E. Zysman-Colman, *Dalton Trans.,* 2011, **40**, 11726-31
14) A. Ruggi, M. Berenguel Alonso, D. N. Reinhoudt and A. H. Velders, *Chem. Comm.,* 2010, **46**, 6726-6728
15) R. F. Beeston, W. S. Aldridge, J. A. Treadway, M. C. Fitzgerald, B. A. DeGraff and S. E. Stitzel, *Inorg. Chem.,* 1998, **37**, 4368-4379
16) Y. You and S. Y. Park, *Dalton Trans.,* 2009, 1267-1282
17) F. Barigelletti, L. De Cola, V. Balzani, P. Belser, A. Von Zelewsky, F. Voegtle, F. Ebmeyer and S. Grammenudi, *J. Am. Chem. Soc.,* 1989, **111**, 4662-4668
18) H. Duerr, R. Schwarz, C. Andreis and I. Willner, *J. Am. Chem. Soc.,* 1993, **115**, 12362-12365
19) P. Belser, L. De Cola and A. von Zelewsky, *J. Chem. Soc., Chem. Commun.,* 1988, 1057-1058
20) C. Schaffner-Hamann, A. von Zelewsky, A. Barbieri, F. Barigelletti, G. Muller, J. P. Riehl and A. Neels, *J. Am. Chem. Soc.,* 2004, **126**, 9339-48
21) C. Hamann, A. von Zelewsky, A. Neels and H. Stoeckli-Evans, *Dalton Trans.,* 2004, 402-406
22) A. M. McDaniel, H. W. Tseng, E. A. Hill, N. H. Damrauer, A. K. Rappe and M. P. Shores, *Inorg. Chem.,* 2013, **52**, 1368-78
23) A. S. Singh and P. K. Bharadwaj, *Dalton Trans.,* 2008, 738-741
24) A. S. Singh, B.-Y. Chen, Y.-S. Wen, C. Tsai and S.-S. Sun, *Org. Lett.,* 2009, **11**, 1867-1870
25) L. Ackermann, H. K. Potukuchi, A. R. Kapdi and C. Schulzke, *Chem. Eur. J.,* 2010, **16**, 3300-3303
26) G. R. Dick, E. M. Woerly and M. D. Burke, *Angew. Chem. Int. Ed.,* 2012, **51**, 2667-72
27) J. S. Ward, J. M. Lynam, J. W. B. Moir, D. E. Sanin, A. P. Mountford and I. J. S. Fairlamb, *Dalton Trans.,* 2012, **41**, 10514-10517
28) WO2006045096 (A2), 2006
29) D. F. Taber and J. L. Schuchardt, *Tetrahedron,* 1987, **43**, 5677-5684
30) M. G. Colombo, T. C. Brunold, T. Riedener, H. U. Guedel, M. Fortsch and H.-B. Buergi, *Inorg. Chem.,* 1994, **33**, 545-550
31) Y. S. Yeh, Y. M. Cheng, P. T. Chou, G. H. Lee, C. H. Yang, Y. Chi, C. F. Shu and C. H. Wang, *ChemPhysChem,* 2006, **7**, 2294-7
32) L. Zhu, P. Guo, G. Li, J. Lan, R. Xie and J. You, *J. Org. Chem.,* 2007, **72**, 8535-8538

33) M. A. Larsen and J. F. Hartwig, *J. Am. Chem. Soc.,* 2014, **136**, 4287-4299
34) K. M. Clapham, A. S. Batsanov, M. R. Bryce and B. Tarbit, *Org. Biomol. Chem.,* 2009, **7**, 2155-2161
35) A. B. Tamayo, B. D. Alleyne, P. I. Djurovich, S. Lamansky, I. Tsyba, N. N. Ho, R. Bau and M. E. Thompson, *J. Am. Chem. Soc.,* 2003, **125**, 7377-87
36) C.-H. Lin, Y.-C. Chiu, Y. Chi, Y.-T. Tao, L.-S. Liao, M.-R. Tseng and G.-H. Lee, *Organometallics,* 2012, **31**, 4349-4355
37) P. J. Hay, *J. Phys. Chem. A,* 2002, **106**, 1634-1641
38) Y. Hisamatsu and S. Aoki, *Eur. J. Inorg. Chem.,* 2011, **2011**, 5360-5369
39) A. Tsuboyama, H. Iwawaki, M. Furugori, T. Mukaide, J. Kamatani, S. Igawa, T. Moriyama, S. Miura, T. Takiguchi, S. Okada, M. Hoshino and K. Ueno, *J. Am. Chem. Soc.,* 2003, **125**, 12971-12979
40) K. Beydoun, M. Zaarour, J. A. G. Williams, H. Doucet and V. Guerchais, *Chem. Comm.,* 2012, **48**, 1260-1262

Chapter 7: Conclusions

During the course of this work a variety of ligands were synthesised with the aim of tuning the emissive properties of the resultant iridium complexes. The distinct localisations of the HOMO and LUMO in iridium(III) complexes with phenylpyridine-based ligands allows for the facile tuning of the emission colour by introduction of substituents with electron-withdrawing/donating properties onto positions with high HOMO or LUMO density. This manipulation of orbital energies was used in the design of the sulfone-containing ligands of Chapters 2 and 3. Here, electron-withdrawing sulfone moieties were introduced at the 5-position of the phenyl ring, a position with a large HOMO localisation, in order to blue-shift the emission relative to that of the parent complex, FIrpic. Complexes **19**, **20** and **28**, containing a sulfone and two fluorine substituents, were synthesised and exhibited bluer emission than FIrpic (~10 nm) while maintaining comparable PLQYs and emission lifetimes. Investigation of their electrochemical properties indicated that the introduction of the sulfone group resulted in a lowering of the HOMO energy, as predicted. As fluorine substituents are known to be unstable during device operation there was interest in synthesising ligands with fewer fluorines, while still retaining blue emission. Complexes **68**, **69** and **70**, containing one fluorine, one methoxy and one sulfone substituent on the phenyl ring, displayed similar emission to their difluoro analogues, with only a small red-shift of 2-3 nm being observed. Complex **80**, a fluorine-free analogue containing two methoxy groups and one sulfone unit, displayed a similar emission wavelength and oxidation potential to FIrpic, suggesting it could be a viable fluorine-free alternative.

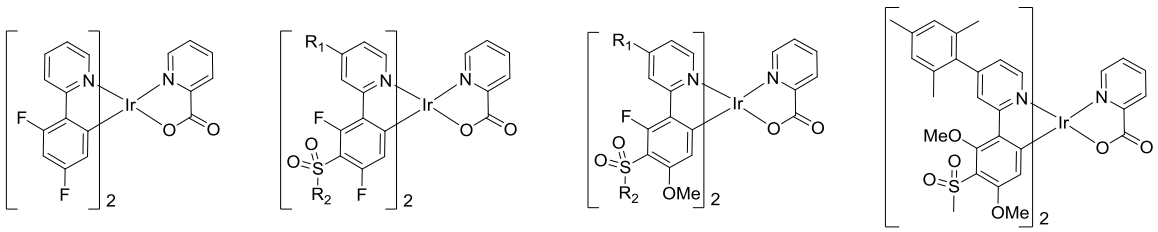

Figure 7.1: FIrpic analogues containing

The emissive properties of iridium(III) complexes can also be tuned by the choice of ancillary ligand; electron-deficient ancillary ligands can indirectly affect the emission of iridium complexes by lowering the energy of the d-orbitals, thereby lowering the energy of the HOMO. In Chapter 5 a new ancillary ligand **133** was devised with the aim of blue-shifting emission while also increasing complex solubility and steric shielding of the Ir core. Exchanging the pic ancillary ligand in **70** and

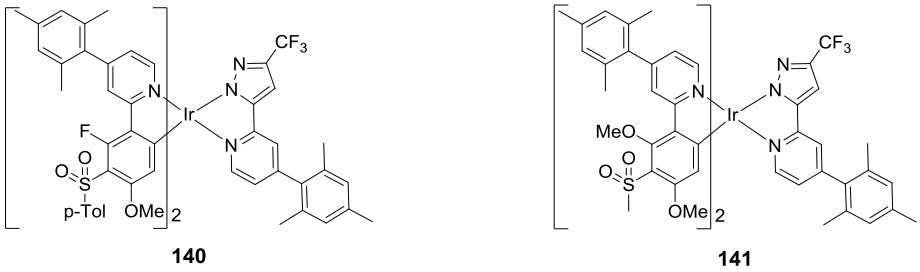

140 **141**

Figure 7.1: Analogues to complexes 70 and 80, containing new ancillary ligand 133.

80 for the new ancillary ligand **133** produced complexes **140** and **141**, which exhibited a 3-5 nm blue-shift in emission relative to their parent complexes.

Attention must be paid to the relative energy levels of the ligands in heteroleptic complexes, for a ligand to be truly ancillary it should play no part in the excited state, requiring a deeper HOMO and a higher LUMO than that of the cyclometalating ligand. In the case of complexes **145**, **146**, **164** and **165** (Chapter 5) and their literature analogue **142a**, the HOMO resides on the phenolate ring of the 'ancillary' ligand, rather than on the cyclometalating ligand, while the LUMO still resides on the pyridyl ring of the phenylpyridine-based ligand. The emission colour of these systems could still be tuned, with the exchange of a ppy ligand for a dfppy ligand (from **142a** to **145**) resulting in a blue-shift of 21 nm, indicating that the introduction of the fluorine atoms was effective at widening the HOMO-LUMO gap, despite the phenyl ring of dfppy not being involved in the HOMO. Addition of the sulfone moiety onto the phenyl ring of oxazole ancillary ligand **156** resulted in an additional blue-shift of 13 nm (from **164** to **165**), as the HOMO in these complexes is located on the ancillary ligand. As introducing electron withdrawing groups on to both the

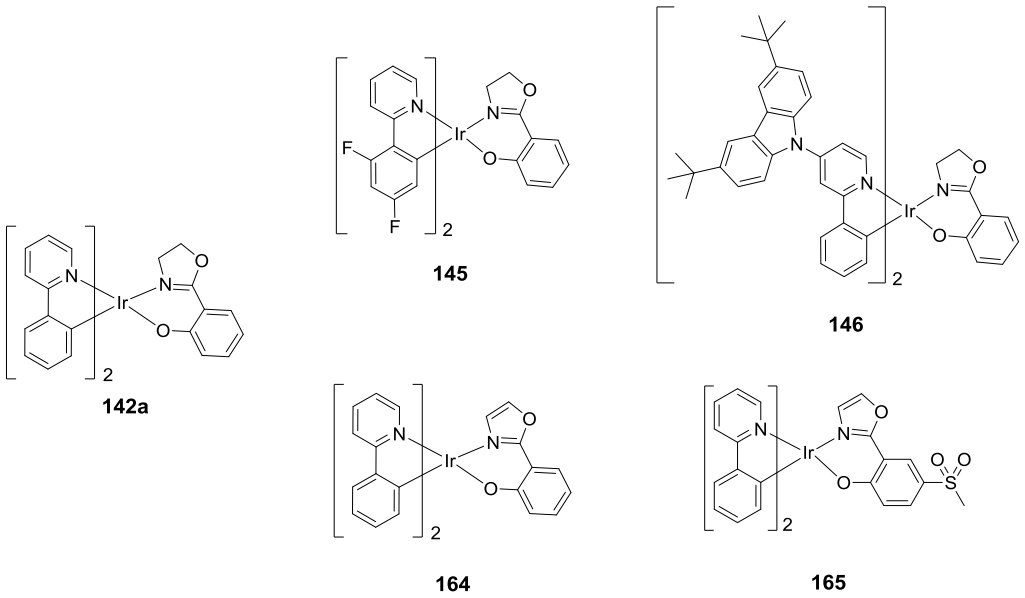

142a **145** **146** **164** **165**

Figure 7.3: Complexes containing oxazoline/oxazole ancillary ligands.

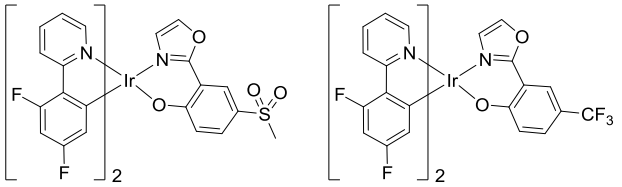

Figure 7.4: Proposed structures for further blue-shifting the emission relative to literature complex 142a.

cyclometalating ligand (**145**) and the ancillary ligand (**165**) resulted in a blue-shift in emission, these two approaches could be combined in future work to produce bluer complexes. Some proposed structures are shown in Figure 7.4.

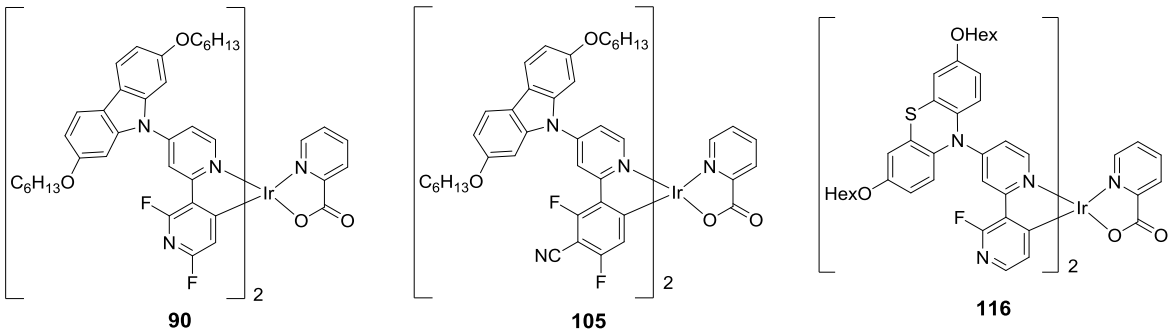

90 **105** **116**

Figure 7.5: Complexes containing ligands with donor-acceptor character.

Combinations of substituents have also been shown to produce some interesting photophysical effects. Complexes **90**, **105** and **116** (Chapter 4), containing ligands with strong donor and acceptor components, displayed solvent dependant dual-emission properties. The origin of this dual emissive character was tentatively assigned to the presence of a ligand based CT state.

It is also possible to affect other emissive properties, such as the PLQY and emission lifetime, of a complex through structural modification. Two hexadenate tripodal ligands **223** and **226** were synthesised derived from known cyclometalating ligands, and the tripodal complexes **228** and **229**

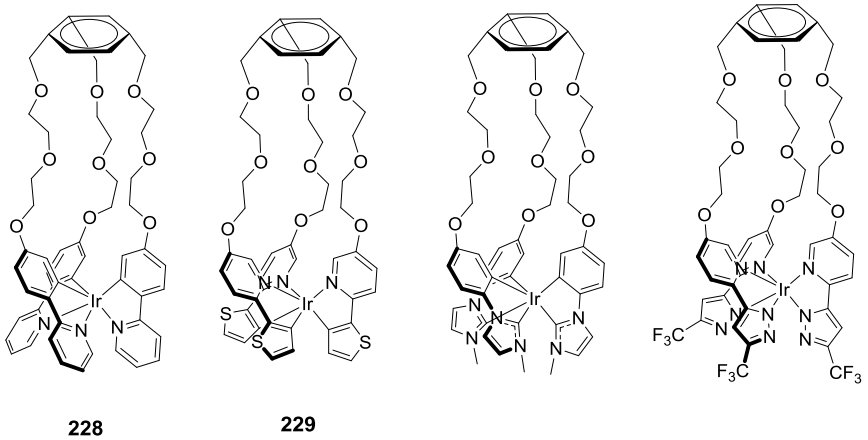

228 **229**

Figure 7.6: Tripodal complexes synthesised in this work, and proposed future complexes.

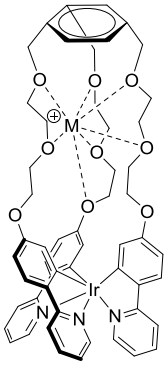

Figure 7.7: Proposed potential coordination of metal ions within the cage structure of complex 128.

were synthesised with the aim that using a single hexadentate, ligand as opposed to three bidentate ligands would increase complex stability and reduce quenching. Complexes **228** and **229** displayed comparable or superior PLQYs and lifetimes to the parent/related complexes, and the ^{1}H NMR data suggested some limited motion in solution. Further derivatives remain to be synthesised, and their properties investigated in devices. Additionally, these complexes have the potential to be used in the sensing of metal ions, as the cavity created between the phenyl-centre and the complex could be large enough to house a metal ion, and the PEG chains provide a coordinating environment, as shown in Figure 7.7.

To conclude, the emissive properties, such as emission colour, efficiency and lifetime, of cyclometalated iridium(III) complexes have been modified by the choice of substituents on the ligands. The emissive properties of heteroleptic complexes have also been modified by the choice of the 'ancillary' ligand. It is important to consider not only the nature of the substituent (electron-withdrawing/donating ability) but also their position on the ligands; for example, introducing a sulfone group at the 5-position results in a blue-shift in emission, while introducing it at the 4-position results in a dramatic red-shift in emission. Care must also be taken when using the molecular orbital distributions to decide which substituents to introduce and where; once a substituent is introduced the orbital distributions can change significantly, meaning the effect of a substituent on the emissive properties is not always predictable.

Chapter 8: Experimental Data

General procedures

All commercially available chemicals were used without further purification unless stated otherwise. Reactions requiring an inert atmosphere were performed under a blanket of argon gas, which was dried over a phosphorus pentoxide column. Anhydrous solvents were dried through an HPLC column on an Innovative Technology Inc. solvent purification system. Column chromatography was performed using 40-60 μm mesh silica gel. Analytical TLC was performed on plates pre-coated with silica gel (Merck, silica gel $60F_{254}$) and visualised using UV light (254, 315, 365 nm). NMR spectra were recorded on Bruker Avance 400 MHz, Varian Mercury 200, and 400 MHz, Varian Inova 500 MHz or Varian VNMRS 600 and 700 MHz spectrometers. Chemical shifts are referenced to tetramethylsilane [TMS, $Si(CH_3)_4$] at 0.00 ppm. Melting points were determined in open ended capillaries using a Stuart Scientific SMP3 melting point apparatus at a ramping rate of 1 ^{o}C/min. They are recorded to the nearest 0.1 ^{o}C. ESI and MALDI mass spectra were recorded on a Thermo-Finnigan LTQ FT (7.0 T magnet) spectrometer. ASAP mass spectra were recorded on a Waters Xevo QTOF spectrometer. GCMS spectra were recorded on a Thermo-Finnigan Trace GCMS (EI and CI ion sources). Elemental analyses were obtained on an Exeter Analytical Inc. CE-440 elemental analyser. Where solvent mixtures are mentioned any percentage/ratio is by volume.

Electrochemistry

Cyclic voltammetry experiments were recorded using a BAS CV50W electrochemical analyser fitted with a three-electrode system consisting of a Pt disk (Ø = 1.8 mm) as the working electrode, a Pt wire as an auxiliary electrode and either an $Ag/AgNO_3$ (0.1 M$[NEt_4][ClO_4]$ in CH_3CN) system or an additional platinum wire as the reference electrode. Solvents and supporting electrolytes will be specified in each chapter. Experiments were conducted at a scan rate of 100 mV/s, unless otherwise specified.

Chapters 2, 3 and 5i: Cyclic voltammetry experiments were conducted in dry acetonitrile solution with $^{n}Bu_4NPF_6$ (0.1 M) as the supporting electrolyte. The reference electrode was an $Ag/AgNO_3$ (0.1 M$[NEt_4][ClO_4]$ in CH_3CN) system; this was assumed to be stable and was referenced externally to ferrocene and decamethylferrocene, which displayed potentials ($E_{1/2}$) of -0.41 V and +0.10 V versus $Ag/AgNO_3$ under these condtions. It was not possible to use ferrocene as an internal reference as upon addition (of both Fc and $Me_{10}Fc$) some form of interaction was observed, resulting in the distortion of the complexes redox waves.

Chapters 4, 5ii and 6: Cyclic voltammetry experiments were conducted in dry DCM solution with $^{n}BuNPF_6$ (0.1 M) as the supporting electrolyte. The reference electrode was a platinum wire, and the complexes were internally referenced to ferrocene (Fc/Fc^{+}) for chapter 4, and decamethylferrocene for chapters 5ii and 6.

Solution photophysics

Solution state photophysical data were obtained using freshly prepared solutions of the complexes in the solvent specified. Emission and lifetime measurements were taken using thoroughly degassed solutions achieved by three freeze−pump−thaw cycles, and obtained using a quartz cuvette with a path length of 1 cm. The solutions had absorbance below 0.10 to minimise inner filter effects. All UV-vis absorption measurements were recorded using a Unicam UV2-100 spectrometer operated with the Unicam Vision(ver. 3.50) software. Baseline correction was achieved by reference to pure solvent in the same cuvette. Absorption measurements were obtained using quartz cuvettes with a path length of 2 cm.

Solution PLQYs were recorded in degassed solvent, and determined using the relative method, with either quinine sulfate (Φ_{PL} = 0.546 in 0.5 M H_2SO_4) or $Ir(ppy)_3$ (Φ_{PL} = 0.46 in degassed dichloromethane) as the reference. The PLQYs are computed according to the following equation:

$$\Phi_x = \Phi_{ref}\frac{Grad_x}{Grad_{ref}}.\left(\frac{\eta_x}{\eta_{ref}}\right)^2$$

where subscripts 'x' and 'ref' denote the material being measured and the reference, respectively. Φ represents the PLQY, Grad is the gradient of the gradient from the plot of integrated fluorescence intensity vs absorbance, and η is the refractive index of the solvent.

There is considerable debate in the literature surrounding the PLQY value of $Ir(ppy)_3$, with the originally reported value of 0.40 suggested to be inaccurate; values reported vary from 0.40 to 1.00 in a variety of solvents.[1-3] The value used in this thesis was determined by measuring the PLQY of $Ir(ppy)_3$ using quinine sulfate as the reference (Φ_{PL} = 0.546 in 0.5 M H_2SO_4). Fifteen solutions of $Ir(ppy)_3$ were measured, and the data was fitted using OLS linear regression, resulting in an R^2 value of 0.99, and a standard error of 2%, a satisfactory level of accuracy for this measurement.

The data for the solutions of $Ir(ppy)_3$ used as a reference were also plotted and fitted using OLS linear regression to give an R^2 value of 0.99 and a standard error of 2%. This indicates that the PLQY for $Ir(ppy)_3$ was consistent across several measurements within the level of accuracy of the

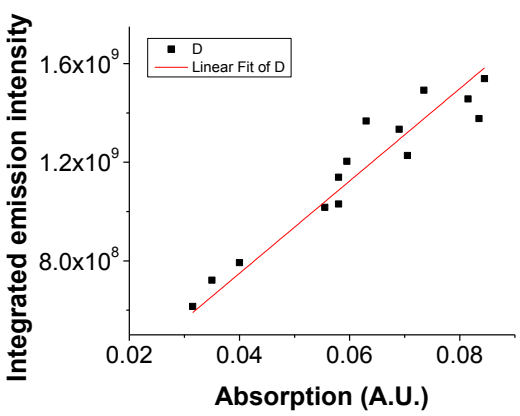

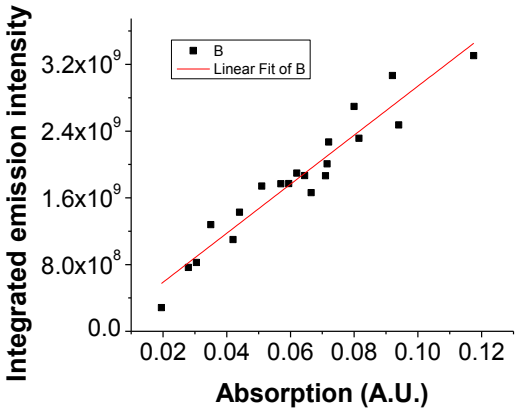

Adj. R^2 0.99349

	Value	Standard Error
Intercept	0	--
Slope	1.87E+10	4.05E+08

Adj. R^2 0.98916

	Value	Standard Error
Intercept	0	--
Slope	2.94E+10	6.88E+08

Figure 7.1: LEFT: Plot of absorbance vs. integrated emission intensity used to determine the PLQY of $Ir(ppy)_3$. RIGHT: Plot of absorbance vs. integrated emission intensity for the reference solutions of $Ir(ppy)_3$ used to determine the PLQYs of the complexes described in chapters 2, 3 and 5i. Below each graph are the tables describing the linear fit and standard error.

experiment.

Chapters 2, 3 and 5i: Excitation and emission spectra were recorded on a Jobin−Yvon−Horiba SpexFluoromax 3 Spectrometer. Quantum yields were determined in degassed DCM in comparison with a standard [$Ir(ppy)_3$ = 0.46]. Solutions of the complexes in degassed DCM [$<10^{-5}$ M] were used for decay measurements. Samples were excited with a pulsed Nitrogen laser emitting at 337.1 nm. Emission was focused onto a spectrograph and detected on a sensitive gated iCCD camera (Stanford Computer Optics) with sub-nano-second resolution.

Chapter 4: Emission spectra for complex **105** were recorded using a custom spectrometer. The sample was excited by the output of a UV-LED (356 nm) and the luminescence collected at 90° and imaged onto the entrance slit of a CCD-spectrograph (Ocean Optics MayaPro spectrometer equipped with a 100µm entrance slit and a HA1 grating) and controlled by the manufacturer's software (SpectraSuite). Spectra were typically acquired using a 1 second integration time and averaged over 1-16 spectra and dark signals were subtracted. Emission spectra for the remaining complexes were recorded on a Jobin−Yvon−Horiba SpexFluoromax 3 Spectrometer or a Horiba Jobin Yvon SPEX Fluorolog 3-22 spectrofluorometer. Quantum yields were determined in degassed solvent in comparison with a standard [quinine sulfate = 0.546 in 0.5 M H_2SO_4]. Solutions of the complexes in degassed solvent [$<10^{-5}$ M] were used for decay measurements. The

sample was excited by the output of a pulse laser diode which produced a 1 kHz train of pulses of 20 ns duration at 405 nm. The luminescence was collected at 90° and focused onto the entrance slit of a monochromator (Bethan TM 300V). The emission was detected by a photon counting PMT and the arrival times of photons at the detector were determined using a multichannel scaler.

Chapters 5ii and 6: Excitation and emission photoluminescence spectra were recorded on a Horiba Jobin Yvon SPEX Fluorolog 3-22 spectrofluorometer. Quantum yields were determined in degassed DCM in comparison with a standard [quinine sulfate = 0.546 in 0.5 M H_2SO_4]. Solutions of the complexes in degassed DCM [$<10^{-5}$ M] were used for decay measurements, using the set up described for Chapter 4.

X-ray crystallography

The X-ray crystal structures for **19**, **20**, **28**, **30**, **32** and **165** were solved by Dr Andrei Batsanov (Durham University). The X-ray crystal structures for **68**, **69** were solved by Dr Dmitry S. Yufit (Durham University). The X-ray crystal structure of **145** was solved by Dr Baiqiao Song (Northeast Normal University, Jilin, China).

General synthetic procedures

General procedure for *ortho* lithiation followed by iodination:

Procedure A: The substrate (1 eq.) was dissolved in THF (dry) under argon, and the solution was cooled to -78 ^{o}C. LDA (1.2 eq.) was added dropwise with stirring over 20 min. The solution was stirred for 1 h at -78 ^{o}C. A solution of I_2 (1.1 eq.) in dry THF (30 ml) was added to the flask dropwise. The solution was stirred for 90 min then allowed to warm to RT overnight. Once warmed, the solution was quenched with an aqueous solution of NaS_2O_3 to remove unreacted LDA and I_2. The solution was then extracted with DCM (3 x 75 ml), and the organic phases combined, dried over $MgSO_4$, filtered and the solvent was reduced *in vacuo*. The residue was passed through a silica plug (eluent: DCM/ethyl acetate) to remove baseline impurities revealed by TLC. The solvent was removed and the crude product was either triturated with cold hexane, or purified by column chromatography, to remove any unreacted starting material. The purified product was then dried on a high vacuum line to leave pure product.

Procedure B: ^{n}BuLi (1.2 eq.) was added to a stirred solution of DIPA (1.3 eq.) in THF (dry) at 0 ^{o}C and the solution was stirred for 30 min. The temperature was then lowered to -78 ^{o}C and a solution of the substrate (1 eq.) in THF (dry) was added in portions via cannula and the mixture was stirred for a further 1 h. A solution of I_2 (1.1-1.3 eq.) in THF (dry) was added to the flask

dropwise. The solution was stirred at -78 ^{o}C and allowed to warm to RT overnight. The reaction was then worked up as described in procedure A to give the pure product.

General procedure for sulfone synthesis:

The iodo compound (1 eq.), the required sodium sulfinate derivative (1.6 eq.) and CuI (1.5 eq.) were dissolved in DMF (dry) and stirred under argon. The mixture was heated at 110 ^{o}C overnight. The mixture was cooled to RT and water (20 ml) and DCM (20 ml) were added. The solid was filtered off and washed with more DCM. The organic layer was separated, dried over $MgSO_4$ and the solvent was removed *in vacuo*. The product was then purified by column chromatography to give pure product, unless otherwise specified. This is in accordance with the method described in the literature.[4]

General procedure for synthesis of Iridium pic complexes:

Method A: $IrCl_3.3H_2O$ (1 eq.) was added to a stirred solution of the cyclometalating ligand (2.1-2.2 eq.) in 2-ethoxyethanol. The mixture was heated to reflux at 130 ^{o}C under an atmosphere of argon overnight. The mixture was then left to cool and the solvent was removed *in vacuo*. The yellow solid, presumed to be the intermediate bis(μ-Cl)dimer complex, was washed with cold hexane to remove any free ligand and dried. Where possible, the intermediate bis (μ-Cl) dimer was characterised. The dimer was then suspended in 2-ethoxyethanol and picolinic acid (<3 eq.) was added. The mixture was stirred and heated to reflux (130 ^{o}C) under an atmosphere of argon overnight. The mixture was allowed to cool to room temperature and the solvent was removed. The product was then purified by column chromatography to give pure product, unless otherwise specified.

Method B: The reaction was conducted via a one-pot method, as a result the intermediate bis(μ-Cl) dimer was not isolated. Otherwise, the reaction was conducted as described in Method A.

Experimental details for chapter 2: complexes of ligands containing difluoro and sulfone substituents as blue OLED materials

2-(2,4-Difluorophenyl)pyridine 13

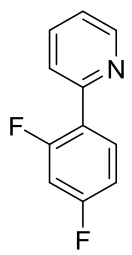

A solution of 2-bromopyridine **11** (15.60 g, 98.7 mmol) and 2,4-difluorophenylboronic acid **12** (16.50 g, 104.5 mmol) in 1,4-dioxane (200 ml) was degassed with argon for 30 min. Separately a 2 M solution of Na_2CO_3 (12.72 g in 60 ml water) was degassed with argon for 20 min. The solutions were combined and $Pd(PPh_3)_4$ (0.51 g, 0.44 mmol) was added. The mixture was refluxed and stirred vigorously at 90 ^{o}C for 20 h. Once cooled the reaction mixture was poured into distilled water (ca.

100 ml) and the aqueous layer was extracted with DCM (3 x 150 ml). The organic phase was dried over $MgSO_4$ and concentrated *in vacuo*. The product **13** was separated from the crude reaction mixture via vacuum distillation (bpt. 125-130 ^oC, 20 mbar), leaving a pale yellow oil (18.35 g, 96%); δ_H (400 MHz; $CDCl_3$; Me_4Si) 8.71 (1H, dt, *J* 4.0 1.4), 8.00 (1H, td, *J* 8.8 6.6), 7.72-7.80 (2H, m), 7.23-7.30 (1H, m), 7.01 (1H, dddd, *J* 8.8 7.8 2.6 1.0), 6.92 (1H, ddd, *J* 11.3 8.8 2.5); δ_F (400 MHz, $CDCl_3$, Me_4Si) -109.30 (1F, p, *J* 7.8), -112.97 (1F, q, *J* 9.5). NMR data are consistent with the literature data.[5]

2-(2,4-Difluoro-3-iodophenyl)pyridine 14

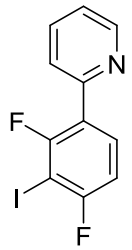

Method 1: The reaction was conducted using the general procedure A for lithiation followed by iodination. The following reagents were used in the stated quantities: 2-(2,4-difluorophenyl)pyridine **13** (5.00 g, 26.15 mmol), LDA (15.7 ml, 2 M in THF), I_2 (7.30 g, 28.77 mmol) and THF (70 ml, dry). The reaction was worked up as described in the general procedure, and the product was purified by trituration with cold hexane to remove any unreacted starting material. The purified product was then dried on the high vacuum line to leave a pale pink tinged solid, 2-(2,4-difluoro-3-iodophenyl)pyridine **14** (5.59 g, 67%); δ_H (400 MHz, $CDCl_3$, Me_4Si) 8.70 (1H, ddd, *J* 4.8 1.8 1.0), 7.98 (1H, td, *J* 8.7 6.5), 7.70-7.80 (2H, m), 7.29 (1H, td, *J* 4.9 2.4), 7.03 (1H, ddd, *J* 8.7 6.9 1.5); δ_F (400 MHz, $CDCl_3$, Me_4Si) -91.08 (1F, q, *J* 5.6), -98.94 (1F, d, *J* 8.0). NMR data are consistent with the literature data.[6]

Method 2: The reaction was conducted using the general procedure B for lithiation followed by iodination. The following reagents were used in the stated quantities: ^{n}BuLi (7.06 ml, 2.5 M), DIPA (2.67 ml, 19.05 mmol) in THF (35 ml, dry), 2-(2,4-difluorophenyl)pyridine **13** (2.81 g, 14.7 mmol) in THF (dry, 20 ml), I_2 (4.66 g, 18.36 mmol) in THF (10 ml, dry). The reaction was worked up as described in the general procedure, and purified as described above to give **14** (2.67 g, 65%).

2-(2,4-Difluoro-3-[methanesulfonyl]phenyl)pyridine 15

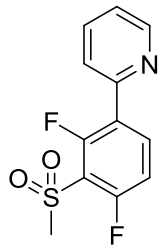

Method 1: The reaction was conducted using the general procedure for sulfone synthesis. The following reagents were used in the stated quantities: 2-(2,4-difluoro-3-iodophenyl)pyridine **14** (1.00 g, 3.15 mmol), sodium methanesulfinate (0.515 g, 5.05 mmol), copper iodide (0.90 g, 4.73 mmol), DMF (3 ml, dry). The reaction was worked up as described in the general procedure, and purified by column chromatography (4% EtOAc in DCM, increased to 20% EtOAc in DCM). The product was then recrystallised from a mixture of hexane and DCM to give **15** as a white solid (0.133, 15%); m.pt. 95.2-97.0 ^oC; δ_H (400 MHz; $CDCl_3$; Me_4Si) 8.72 (1H, dt, *J* 4.8 1.4), 8.27 (1H, td, 8.6 6.0), 7.71-7.87 (2H, m), 7.32 (1H, ddd, *J* 6.7 4.8 2.1), 7.18 (1H, td, 9.2 1.6), 3.34 (3H, s); δ_F (376 MHz, $CDCl_3$,

Me_4Si) -106.14 (1F, dd, *J* 9.3 6.2), -111.50 (1F, d, *J* 8.3); δ_C (101 MHz, $CDCl_3$, Me_4Si) 159.86 (dd, *J* 262.6 4.0), 157.50 (dd, *J* 262.6 3.9), 150.89, 150.18, 137.32 (dd, *J* 10.9 5.8), 136.90, 125.80 (dd, *J* 13.7 4.1), 124.63 (d, *J* 9.5), 123.42, 118.55 (dd, *J* 17.3 15.5), 113.80 (dd, *J* 23.1 4.0), 45.88 (t, *J* 2.4); HRMS (FTMS+ESI): calcd for $[C_{12}H_9F_2NO_2S+H]^+$: 270.03948. Found: 270.03938.

Method 2: i) Copper(II) sulphate (0.38 g, 2.37 mmol) was dissolved in water (10 ml). Sodium methanesulfinate (0.48 g, 4.73 mmol) was added. The solution changed from blue to green and a white precipitate formed. The solution was filtered and the water evaporated to leave an orange-brown solid. The solid was washed with DCM and dried on the high vacuum line for 3 h. It was then dried in the oven overnight at 50 ^oC and dried on the vacuum line for a further 4 h to give an orange-brown solid, presumed to be copper(II) bis(methanesulfinate).

ii) 2-(2,4-difluoro-3-iodophenyl)pyridine **14** (1.00 g, 3.15 mmol) and the orange-brown solid were dissolved in DMF (3 ml, dry) and stirred under argon, and the mixture was heated at 110 ^oC overnight. The mixture was cooled to RT and water (20 ml) and DCM (20 ml) were added. The solid was filtered off and washed with more DCM. The organic layer was separated, dried over $MgSO_4$ and the solvent was removed *in vacuo*. The crude product mixture was separated by column chromatography (1:2 EtOAc in DCM, increased to 1:1). Unreacted starting material was recovered, and **15** was obtained as a white crystalline solid (0.150 g, 17%). The NMR data was consistent with that obtained previously.

The reaction was repeated using copper(II) sulphate pentahydrate (0.59 g, 2.36 mmol), sodium methanesulfinate (0.48 g, 4.73 mmol) and 2-(2,4-difluoro-3-iodophenyl)pyridine **14** (1.00 g, 3.15 mmol). The copper compound which formed was dried for 72 h in the oven and the reaction was heated at 110 ^oC for 72 h. The reaction was worked up as before and the product was obtained, 2-(2,4-difluoro-3-[methanesulfonyl]phenyl)pyridine **15** (109 mg, 13%). The NMR data was consistent with that obtained previously.

2-(2,4-Difluoro-3-[methanesulfonyl]phenyl)pyridine 15 and **2-(2-fluoro-3,4-di[methanesulfonyl]phenyl)pyridine 29**

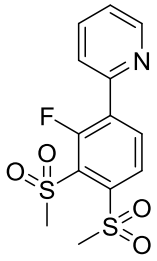

The reaction was conducted using the general procedure for sulfone synthesis. The following reagents were used in the stated quantities: 2-(2,4-difluoro-3-iodophenyl)pyridine **14**[1] (1.00 g, 3.15 mmol), sodium methanesulfinate (0.515 g, 5.05 mmol), CuI (0.90 g, 4.73 mmol), DMF (3 ml, dry). The reaction was worked up as described in the general procedure, and the crude product mixture was subjected to column chromatography (1:2 EtOAc in DCM, increased to 1:1 to elute final fraction).

[1] The 2-(2,4-difluoro-3-iodophenyl)pyridine **14** used for this experiment was from a batch containing trace iodine.

Upon NMR analysis a mixture of products was revealed. The mixture was columned for a second time (10% EtOAc in DCM) to give two white solid products, 2-(2,4-difluoro-3-[methanesulfonyl]phenyl)pyridine **15** (125 mg, 15%) and 2-(2-fluoro-3,4-di[methanesulfonyl]phenyl)pyridine **29** (56 mg, 5%); m.pt. 194.0-198.1 ^{o}C; δ_H (400 MHz; $CDCl_3$; Me_4Si) 8.78 (1H, d, *J* 4.7), 8.46 (1H, dd, *J* 8.4 6.9), 8.28 (1H, dd, *J* 8.3 1.1), 7.83 – 7.91 (2H, m), 7.81 – 7.76 (m, 1H), 7.35 – 7.44 (1H, m), 3.58 (3H, s), 3.49 (3H, s); δ_F (376 MHz, $CDCl_3$, Me_4Si) -106.57 (1F, d, *J* 6.9); δ_c (101 MHz, $CDCl_3$, Me_4Si) 159.10 (d, *J* 265.4), 150.49, 150.13 (d, *J* 1.8), 143.03, 137.01, 136.64 (d, *J* 5.2), 135.16 (d, *J* 15.3), 129.59 (d, *J* 14.7), 128.15 (d, *J* 3.5), 125.20 (d, *J* 9.8), 124.34, 46.27, 45.28; HRMS (FTMS+ESI): calcd for $[C_{13}H_{12}FNO_4S_2+H]^+$: 330.0270. Found: 330.0273. As the starting material **14** appeared to be contaminated with iodine the reaction was repeated using rigorously purified **14** (1.00 g, 3.15 mmol), sodium methanesulfinate (0.515 g, 5.05 mmol), CuI (0.90 g, 4.73 mmol) and additional iodine (27 mg, 0.10 mmol, 3 mole %). The reaction was worked up as before to give 2-(2,4-difluoro-3-[methanesulfonyl]phenyl)pyridine **15** (124 mg, 15%) and 2-(2-fluoro-3,4-di[methanesulfonyl]phenyl)pyridine **29** (24 mg, 2%).

2-(2,4-Difluoro-3-[(4-methylbenzene)sulfonyl]phenyl)pyridine 16

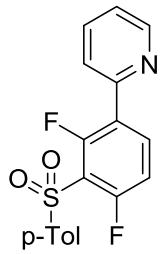

The reaction was conducted using the general procedure for sulfone synthesis. The following reagents were used in the stated quantities: 2-(2,4-difluoro-3-iodophenyl)pyridine **14** (2.67 g, 8.42 mmol), sodium p-toluenesulfinate (2.40 g, 13.47 mmol), CuI (2.40 g, 12.60 mmol), DMF (15 ml, dry). The reaction was worked up as described in the general procedure, and the product was purified by column chromatography (EtOAc (0-5%) in DCM), followed by recrystallisation from a hexane/DCM mixture to give **16** as white crystals (550 mg, 20%); m.pt. 99.5-100.9 ^{o}C; δ_H (400 MHz; $CDCl_3$; Me_4Si) 8.64 (1H, d, *J* 5.2), 8.15 (1H, td, *J* 8.6, 6.0), 7.95 (2H, d, *J* 8.0), 7.70-7.81 (2H, m), 7.30 (2H, d, *J* 8.1) 7.23-7.27 (1H, m), 7.07 (1H, td, *J* 9.2, 1.6), 2.38 (3H, s); δ_F (376 MHz; $CDCl_3$; Me_4Si) -105.24 (1F, t, *J* 7.5), -110.44 (1F, d, *J* 8.1); HRMS (FTMS+ESI): calcd for $[C_{18}H_{13}F_2NO_3S+H]^+$: 346.0713. Found: 346.0692. NMR data is consistent with the literature data.[7]

2-(2,4-Difluoro-3-[(4-methylbenzene)sulfonyl]phenyl)pyridine 16

The reaction was conducted using the general procedure for sulfone synthesis. The following reagents were used in the stated quantities: 2-(2,4-difluoro-3-iodophenyl)pyridine **14**[2] (3.00 g, 9.46 mmol), sodium p-toluenesulfinate (2.70 g, 15.14 mmol) and CuI (2.70 g, 14.19 mmol). The reaction was worked up as described in the general procedure, and the product was purified by

[2] The 2-(2,4-difluoro-3-iodophenyl)pyridine **14** used for this experiment was from a batch containing trace iodine.

column chromatography (EtOAc (0-5%) in DCM) and the product was recrystallised from a hexane/DCM mixture to give **16** as white crystals (1.32 g, 40%). The NMR data was consistent with that obtained previously.

Iridium complex 19

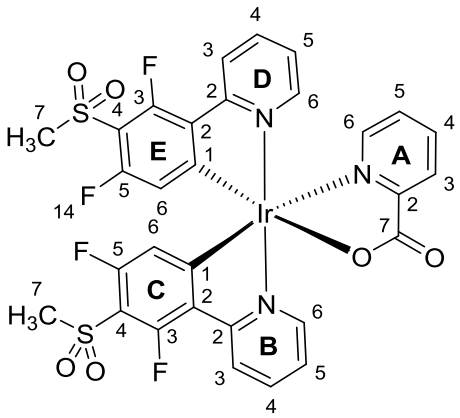

The reaction was conducted as described in the general procedure for synthesis of iridium pic complexes, Method A. The following reagents were used in the stated quantities: $IrCl_3.3H_2O$ (107 mg, 0.30 mmol), 2-(2,4-difluoro-3-[methanesulfonyl]phenyl)pyridine **15** (180 mg, 0.67 mmol), picolinic acid (154 mg, 1.25 mmol) and 2-ethoxyethanol (10 ml). Attempted purification of a small portion of the intermediate μ-dichloro dimer resulted in rapid decomposition under ambient conditions, so no characterization data were obtained. The reaction was worked up according to the general procedure, and purified by column chromatography (DCM:acetone, 1:1) to leave **19** as a yellow solid (190 mg, 85%); Anal. Calc. for $C_{30}H_{20}F_4IrN_3O_6S_2$: C, 42.35; H, 2.37; N, 4.94. Found: C, 42.17; H, 2.23; N, 4.88; δ_H (700 MHz; $CDCl_3$; Me_4Si) 8.75 (1H, dt, *J* 5.8, 1.3, H_{D6}), 8.39 (1H, d, *J* 8.4, H_{B3}), 8.35 (1H, d, *J* 7.8, H_{A3}), 8.34 (1H, d, *J* 8.8, H_{D3}), 8.04 (1H, td, *J* 7.8, 1.6, H_{A4}), 7.93 (1H, td, *J* 6.4, 1.6, H_{B4}), 7.91 (1H, td, *J* 6.4, 1.7, H_{D4}), 7.75 (1H, dt, *J* 5.1, 1.4, H_{A6}), 7.54 (1H, ddd, *J* 7.8, 5.4, 1.5, H_{A5}), 7.45 (1H, dd, *J* 5.7, 1.4, H_{B6}), 7.35 (1H, ddd, *J* 7.3, 5.8, 1.4, H_{D5}), 7.14 (1H, ddd, *J* 7.4, 5.8, 1.4, H_{B5}), 5.97 (1H, d, *J* 10.0, H_{E6}), 5.73 (1H, d, *J* 10.1, H_{C6}), 3.27 (3H, s, H_{E7}), 3.21 (3H, s, H_{C7}); δ_F (376 MHz, $CDCl_3$, Me_4Si) -105.12 (1F, d, 9.8), -106.30 (1F, d, 10.0), -109.57 (1F, s), -110.28 (1F, s); δ_C (176 MHz; $CDCl_3$; Me_4Si) 172.36 (s, C_{A7}), 164.19 (d, *J* 6.8,C_{B2}), 162.97 (d, J 6.4, C_{D2}), 161.34 (d, *J* 8.1, C_{C2}), 160.60 (d, *J* 8.5, C_{E2}), 159.66 (dd, *J* 268.2, 2.82, C_{E5}), 159.19 (dd, *J* 266.4, 3.0, C_{C5}), 157.54 (dd, *J* 271.1, 3.50, C_{E3}), 157.33 (dd, *J* 270.0, 4.5, C_{C3}), 151.11 (s, C_{A2}), 148.89 (s, C_{D6}), 148.41 (s, C_{B6}), 148.32 (s, C_{A6}), 139.58 (s, $C_{B/D4}$), 139.57 (s, $C_{B/D4}$), 139.46 (s, C_{A4}), 130.10 (m, C_{C1}), 129.92 (m, C_{E1}), 129.18 (s, $C_{A3/5}$), 129.11 (s, $C_{A3/5}$), 124.49 (d, J 21.8, C_{B3}), 124.21 (s, C_{D5}), 124.14 (s, C_{B5}), 124.00 (d, *J* 20.6, C_{D3}), 116.64 (d, *J* 19.3, C_{E6}), 116.45 (d, *J* 19.1, C_{C6}),111.83 (t, *J* 16.6, C_{C4}), 111.22 (t, *J* 16.5, C_{E4}), 45.94 (s, $C_{C7/E7}$), 45.90 (s, $C_{C7/E7}$); HRMS (FTMS+ESI): calcd for $[C_{30}H_{20}F_4N_3O_6S_2{}^{191}Ir+H]^+$: 850.0414. Found: 850.0439.

Iridium complex 20

The reaction was conducted as described in the general procedure for synthesis of iridium pic complexes, Method A. The following reagents were used in the stated quantities: $IrCl_3.3H_2O$ (278

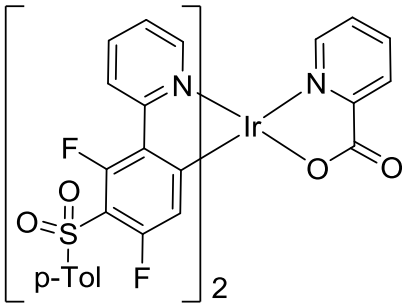

mg, 0.79 mmol), 2-(2,4-difluoro-3-[(4-methylbenzene)sulfonyl]phenyl)pyridine **16** (600 mg, 1.78 mmol), 2-ethoxyethanol (20 ml) to give the intermediate μ-dichloro dimer as a yellow solid (700 mg, 96%); δ_H (400 MHz; $CDCl_3$; Me_4Si) 8.91 (4H, dd, *J* 6.2, 1.4), 8.35 (4H, d, *J* 8.5), 7.88-7.94 (4H, m), 7.83 (8H, d, *J* 8.1), 7.24 (8H, d, *J* 8.5), 6.87 (4H, ddd, *J* 7.4, 5.8, 1.4), 5.24 (4H, d, *J* 10.6), 2.36 (12H, s); δ_F (376 MHz; $CDCl_3$; Me_4Si) -105.27 (4F, d, *J* 10.4), -109.88 (4F, s); HRMS (FTMS+ESI): calcd for $[C_{72}H_{48}Cl_2F_8{}^{191}Ir_2N_4O_8S_4+Na_2]^{2+}$: 939.0320. Found: 939.0303.

The reaction was continued as described in the general Method A. The following reagents were used in the stated quantities: Ir dimer (500 mg, 0.27 mmol), picolinic acid (336 mg, 2.73 mmol), 2-ethoxyethanol (10 ml). The reaction was worked up as previously described, and the product was purified by column chromatography (THF/DCM, 3:7 v/v), followed by recrystallisation from DCM/hexane to leave **20** as a yellow solid (421 mg, 77%). Anal. Calc. for $C_{42}H_{28}F_4IrN_3O_6S_2$: C 50.29; H 2.81; N 4.19. Found: C 50.03; H 2.96; N 4.01; δ_H (400 MHz; acetone-d_6, Me_4Si) 8.65 (1H, dt, *J* 5.7, 1.1), 8.37 (2H, t, *J* 8.3), 8.19–8.07 (4H, m), 7.94 (1H, d, *J* 5.2), 7.87 (4H, t, *J* 7.6), 7.80 (1H, d, *J* 5.8), 7.62 (1H, ddd, *J* 6.6, 5.4, 2.6), 7.55 (1H, ddd, *J* 7.4, 5.8, 1.4), 7.43-7.34 (5H, m), 6.01 (1H, d, *J* 10.7), 5.70 (1H, d, *J* 10.6), 2.41 (3H, s), 2.40 (3H, s); δ_F (376 MHz; acetone-d_6; Me_4Si) -107.87 (1F, dd, *J* 10.7, 4.1), -108.61 (1F, dd, *J* 10.6, 3.6), -110.89 (1F, s), -111.59 (1F, s); HRMS (FTMS+ESI): calcd for $[C_{42}H_{28}O_6N_3F_4{}^{191}IrS_2+Na]^+$: 1026.0883. Found: 1026.0870. Crystals for X-ray analysis were grown by slow evaporation of a DCM/hexane solution of **20**.

2-Chloro-4-(2,4,6-trimethylphenyl)pyridine 23

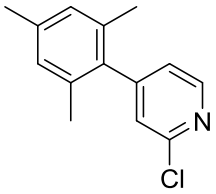

A solution of 2-chloro-4-iodo-pyridine **21** (5.00 g, 20.88 mmol) and 2,4,6-trimethylphenylboronic acid **22** (3.46 g, 21.09 mmol) in 1,4-dioxane (50 ml) was degassed for 20 min. Separately, a solution of K_3PO_4 (5.63 g, 26.52 mmol in 15 ml) was degassed for 15 min. The solutions were combined, PCy_3 (117 mg, 0.42 mmol) and $Pd_2(dba)_3$ (191 mg, 0.21 mmol) was added. The mixture was degassed for a further 5 min and then heated to reflux under an atmosphere of argon for 3 days with stirring. The mixture was allowed to cool and the solution volume was halved *in vacuo*, followed by addition of DCM (50 ml). The layers were separated, and the organic layer was washed with water (2 x 30 ml) then dried over $MgSO_4$. The residue was purified by column chromatography (hexane:EtOAc 1:4). The product containing fractions were combined and the solvent removed. Any residual 2-chloro-4-iodo-pyridine **21** was distilled using a Kugelrohr apparatus to leave 2-

chloro-4-(2,4,6-trimethylphenyl)pyridine **23** as a clear oil (2.68 g, 6.90 mmol, 69%); δ_H (400 MHz; $CDCl_3$; Me_4Si) 8.78 (1H, dd, *J* 5.0 0.9), 8.10 (1H, td, *J* 8.8 6.7), 7.61 (1H, dt, *J* 2.3 1.1), 7.11 (1H, dd, *J* 4.9 1.5), 7.05 (1H, dddd, *J* 8.8 7.8 2.6 1.0), 7.00 (2H, s), 6.93 (1H, ddd, *J* 11.3 8.8 2.5), 2.37 (3H, s), 2.07 (6H, s); δ_F (376 MHz, $CDCl_3$, Me_4Si) -109.16 (1F, m), -112.69 (1F, q, *J* 9.4). NMR data were consistent with the literature.[8]

2-(2,4-Difluorophenyl)-4-(2,4,6-trimethylphenyl)pyridine 24

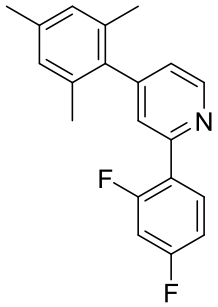

A solution of 2-chloro-4-(2,4,6-trimethylphenyl)pyridine **23** (1.88 g, 8.11 mmol), 2,4-difluorophenylboronic acid **12** (1.92 g, 12.2 mmol), $Pd(OAc)_2$ (111 mg, 0.49 mmol) and triphenylphosphine (551 mg, 2.10 mmol) in 1,2-dimethoxyethane (70 ml) was degassed with argon for 25 min. Separately a 2 M aqueous solution of Na_2CO_3 (3.51 g, 33.11 mmol in 17 ml) was degassed for 15 min. The solutions were combined and the mixture was heated to reflux under argon atmosphere for 24 h. The reaction mixture was then cooled to room temperature and DCM (50 ml) was added, followed by brine (50 ml). The organic layer was separated and dried over $MgSO_4$. The solvent was removed *in vacuo* and the residue was purified by column chromatography (EtOAc:hexane 1:6 v:v) to give **24** as a yellow-tinged liquid (2.38 g, 95%); δ_H (400 MHz; $CDCl_3$; Me_4Si) 8.78 (1H, dd, *J* 5.0 0.9), 8.10 (1H, td, *J* 8.8 6.7), 7.61 (1H, dt, *J* 2.3 1.1), 7.11 (1H, dd, *J* 4.9 1.5), 7.05 (1H, dddd, *J* 8.8 7.8 2.6 1.0), 7.00 (2H, s), 6.93 (1H, ddd, *J* 11.3 8.8 2.5), 2.37 (3H, s), 2.07 (6H, s); δ_F (376 MHz, $CDCl_3$, Me_4Si) -109.16 (1F, m), -112.69 (1F, q, *J* 9.4). NMR data were consistent with the literature.[8]

2-(2,4-Difluoro-3-iodophenyl)-4-(2,4,6-trimethylphenyl)pyridine 25

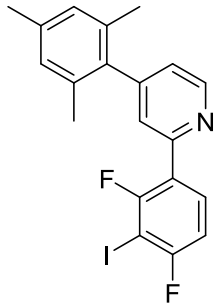

Method 1: The reaction was conducted using the general procedure A for lithiation followed by iodination. The following reagents were used in the stated quantities: 2-(2,4-difluorophenyl)-4-(2,4,6-trimethylphenyl)pyridine **24** (800 mg, 2.59 mmol), LDA (1.55 ml, 2M in THF), I_2 (689 mg, 2.71 mmol in 5 ml THF, dry) and THF (20 ml). The reaction was worked up as described in the general procedure, and the product was purified by column chromatography (EtOAc (0-2%) in DCM) and impure fractions were further purified by using the Biotage® Isolera One ™ purification system to leave **25** as a white semi-solid (360 mg, 32%); δ_H (400 MHz, $CDCl_3$, Me_4Si); 8.77 (1H, dd, *J* 5.0 0.9), 8.07 (1H, td, *J* 8.7 6.4), 7.59 (1H, dt, *J* 2.4 1.3), 7.12 (1H, dd, *J* 4.9 1.5), 7.05 (1H, ddd, *J* 8.6 6.9 1.5), 6.98 (2H, s), 2.35 (3H, s), 2.06 (6H, s); δ_F (376 MHz, $CDCl_3$, Me_4Si) -90.98 (1F, q, *J* 5.7), -93.59 – -93.67 (1F, m); δ_C (101 MHz, $CDCl_3$, Me_4Si) δ_C (101 MHz, $CDCl_3$, Me_4Si)

161.85 (dd, *J* 249.4 5.4), 158.83 (dd, *J* 250.2 5.9), 152.15 (d, *J* 3.4), 150.31, 150.07, 137.75, 136.13, 135.20, 132.31 (dd, *J* 9.2, 4.2), 128.50, 125.50 (d, *J* 9.4), 124.46 (dd, *J* 14.4, 3.7), 123.96, 111.94 (d, *J* 3.7), 111.71 (d, *J* 3.7), 72.01 (dd, *J* 30.9, 29.3), 21.16, 20.71; HRMS (FTMS+ESI): calcd for $[C_{20}H_{16}NF_2I+H]^+$: 436.0374. Found: 436.0378.

Method 2: The reaction was conducted using the general procedure B for lithiation followed by iodination. The following reagents were used in the stated quantities: ^{n}BuLi (3.69 ml, 2.5 M), DIPA (1.40 ml, 9.99 mmol), 2-(2,4-difluorophenyl)-4-(2,4,6-trimethylphenyl)pyridine **24** (2.38 g, 7.68 mmol), I_2 (2.14 g, 8.43 mmol) and THF (45 ml, dry). The reaction was worked up as described in the general procedure, and purified using the Biotage® Isolera One ™ purification system to leave **25** as a white semi-solid (2.50 g, 75%).

2-(2,4-Difluoro-3-[methanesulfonyl]phenyl)-4-(2,4,6-trimethylphenyl)pyridine 26

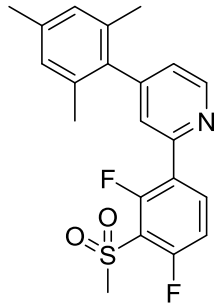

The reaction was conducted using the general procedure for sulfone synthesis. The following reagents were used in the stated quantities: 2-(2,4-difluoro-3-iodophenyl)-4-(2,4,6-trimethylphenyl)pyridine **25** (657 mg, 1.51 mmol), sodium methanesulfinate (247 mg, 2.42 mmol), CuI (431 mg, 2.26 mmol) and DMF (3 ml, dry). The reaction was worked up as described in the general procedure, and the product was purified by column chromatography (2.5% EtOAc in DCM, increased to 10% v/v) to give **26** as an off-white solid (130 mg, 22%); m.pt. 74.6-77.5 ^{o}C; δ_H (400 MHz; $CDCl_3$; Me_4Si) 8.77 (1H, d, *J* 5.0), 8.36 (1H, td, *J* 8.6 6.0), 7.58-7.64 (1H, m), 7.21 (1H, td, *J* 9.0, 1.5), 7.13-7.17 (1H, m), 6.96 (2H, d, *J* 1.1), 3.33 (3H, s), 2.33 (3H, s), 2.03 (6H, s); δ_F (376 MHz, $CDCl_3$, Me_4Si) -106.14 (1F, dd, *J* 10.2, 8.6), -111.40 (1F, d, *J* 11.0); δ_C (101 MHz, $CDCl_3$, Me_4Si) 159.81 (dd, *J* 262.6, 4.0), 157.46 (dd, *J* 262.0, 4.0), 156.18 (d, *J* 3.9), 151.00 (d, *J* 2.1), 150.59, 150.25, 137.83, 137.31 (dd, *J* 10.8, 5.7), 135.79, 135.03, 128.47, 125.96 – 125.56 (m), 124.43, 118.54 (dd, *J* 17.6, 15.5), 113.77 (dd, *J* 23.1, 3.9), 45.79 (t, *J* 2.4), 21.09, 20.64; HRMS (FTMS+ESI): calcd for $[C_{21}H_{19}F_2NO_2S+H]^+$: 388.1183. Found: 388.1170.

Ir complex 28

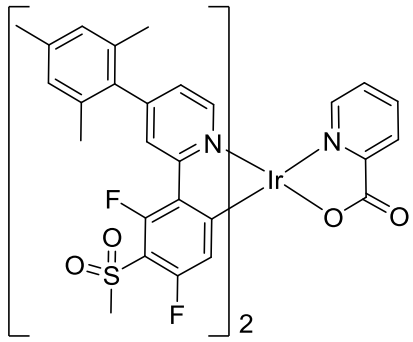

The reaction was conducted as described in the general procedure for synthesis of Iridium pic complexes, Method A. The following reagents were used in the stated quantities: $IrCl_3.3H_2O$ (40 mg, 0.11 mmol), 2-(2,4-difluoro-3-[(4-methylbenzene)sulfonyl]phenyl)pyridine **26** (90 mg, 0.232 mmol), 2-ethoxyethanol (6 ml) to give the intermediate μ-dichloro dimer **27** as a yellow solid. A small sample was set

aside for purification, and the NMR spectra of the product was consistent with the intermediate bis(μ-Cl)dimer complex: δ_H (400 MHz; $CDCl_3$; Me_4Si) 9.52 (4H, d, *J* 5.9), 8.23 (4H, s), 6.97-7.05 (12H, m), 5.34 (4H, d, *J* 10.8), 3.18 (3H, s), 2.40 (3H, s), 2.11 (3H, s), 2.07 (3H, s); δ_F (376 MHz, $CDCl_3$, Me_4Si) -105.73 (4F, d, *J* 12.0), -110.17 (4F, s).

The reaction was continued as described in the general Method A. The following reagents were used in the stated quantities: Ir dimer, picolinic acid (90 mg, 0.731 mmol) and 2-ethoxyethanol (6 ml). The reaction was worked up as previously described, and the product was purified by column chromatography (30% EtOAc in DCM) to leave Ir complex **28** as a yellow solid (105 mg, 85%); Anal. Calc. for $C_{48}H_{40}F_4IrN_3O_6S_2.0.5CH_2Cl_2$: C, 51.57; H, 3.66; N, 3.72. Found: C, 51.32; H, 3.62; N, 3.69; δ_H (400 MHz; $CDCl_3$; Me_4Si) 8.82 (1H, dd, *J* 6.0 0.7), 8.40 – 8.48 (1H, m), 8.21 (1H, t, *J* 1.7), 8.15 (1H, t, *J* 1.7), 8.09 (td, *J* 7.8 1.6), 7.89 (1H, ddd, *J* 5.4 1.6 0.8), 7.60 (1H, ddd, *J* 7.8 5.3 1.5), 7.50 (1H, dd, *J* 6.0 0.7), 7.21 (1H, dd, *J* 5.9 1.7), 6.95 – 7.04 (5H, m), 5.94 (1H, d, *J* 10.3), 5.73 (1H, d, *J* 10.4), 3.25 (3H, s), 3.20 (3H, s), 2.35 (6H, s), 2.12 (3H, s), 2.09 (3H, s), 1.96 (3H, s); δ_F (376 MHz, $CDCl_3$, Me_4Si) -105.58 (1F, dd, *J* 10.9 3.5), -106.77 (1F, dd, *J* 11.4 3.3), -109.82 (1F, d, *J* 4.1), -110.61; HRMS (FTMS+ESI): calcd for $[C_{48}H_{40}F_4N_3O_6S_2{}^{191}Ir + H]^+$: 1086.1979. Found: 1086.1978.

Iridium complex 30

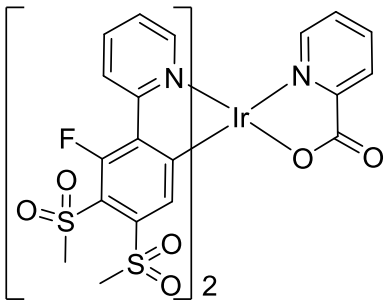

The reaction was conducted as described in the general procedure for synthesis of Iridium pic complexes, Method A. The following reagents were used in the stated quantities: $IrCl_3.3H_2O$ (94 mg, 0.27 mmol), 2-(2-fluoro-3,4-bis(methylsulfonyl)phenyl)pyridine **29** (194 mg, 0.59 mmol), and 2-ethoxyethanol (8 ml) to give an orange-yellow solid presumed to be the bis(μ-Cl)dimer, which was used without further purification. Due to its very poor solubility NMR data could not be obtained.

The reaction was continued as described in the general Method A. The following reagents were used in the stated quantities: Ir dimer, picolinic acid (245 mg, 1.99 mmol), 2-ethoxyethanol (8 ml). The reaction was worked up as described in the general procedure, and the product was purified by column chromatography (DCM:Acetone 1:1 v/v) to give **30** as a yellow solid (208 mg, 80%); Anal. Calc. for $C_{32}H_{26}F_2IrN_3O_{10}S_4$: C, 39.58; H, 2.70; N, 4.33. Found: C, 39.42; H, 2.61; N, 4.42; δ_H (400 MHz; $CDCl_3$; Me_4Si); 8.85 (1H, d, *J* 5.2), 8.52 (1H, d, *J* 8.6), 8.48 (1H, d, *J* 8.6), 8.36 (1H, d, *J* 7.5), 7.97-8.10 (3H, m), 7.70 (1H, d, *J* 5.2), 7.62 (1H, d, *J* 6.0), 7.57 (1H, t, *J* 6.4), 7.49 (1H, t, *J* 6.4), 7.29 (1H, t, *J* 6.6), 7.14 (1H, s), 6.83 (1H, s), 3.43 (3H, s), 3.41 (3H, s), 3.37 (3H, s), 3.36 (3H, s); δ_F (376 MHz, $CDCl_3$, Me_4Si) -105.51 (1F, s), -106.32 (1F, s); HRMS (FTMS+ESI): calcd for $[C_{32}H_{26}F_2N_3O_{10}S_4{}^{191}Ir+H]^+$: 970.0153. Found: 970.0177. Crystals for X-ray analysis were grown by

slow evapouration of a DCM/acetonitrile mixture of **30**.

Iridium complex 31

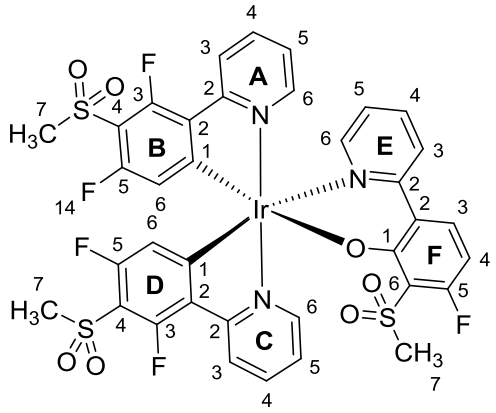

$IrCl_3.3H_2O$ (69 mg, 0.20 mmol) was added to a stirred solution of 2-(2,4-difluoro-3-[methanesulfonyl]phenyl)pyridine **15** (116 mg, 0.67 mmol) in 2-ethoxyethanol (8 ml). The mixture was heated to reflux at 130 ^{o}C under an atmosphere of argon overnight. The mixture was then left to cool and the solvent was removed *in vacuo* to leave a yellow solid, presumed to be the bis(μ-Cl)dimer, which was used without further purification. The dimer was dissolved in ethylene glycol (8 ml) and the 2-(2,4-difluoro-3-[methanesulfonyl]phenyl)pyridine **15** (58 mg, 0.22 mmol), NEt_3 (0.1 ml) and acetylacetone (0.1 ml) were added. The mixture was stirred under argon and heated to reflux at 190 ^{o}C overnight. The mixture was then left to cool. DCM (25 ml) and water (25 ml) were added and the organic layer was separated and washed with water (2 x 60 ml) to remove the majority of the ethylene glycol. The solvent was removed *in vacuo* to leave a brown liquid residue. This was washed with water (5 ml) to remove any residual ethylene glycol. The residue was then purified by column chromatography (DCM/Methanol 29:1 followed by DCM/EtOAc 80:20) to give iridium complex **31** as a yellow solid (56 mg, 29%); δ_H (700 MHz; CD_2Cl_2; Me_4Si) 9.03 (1H, ddd, *J* 5.7, 1.7, 0.8, H_{A6}), 8.49 (1H, d, *J* 8.5, H_{A3}), 8.27 (1H, d, *J* 8.5, H_{C3}), 8.10 (1H, ddd, *J* 5.7, 1.7, 0.8, H_{C6}), 8.00 (1H, td, *J* 8.0, 7.4, 1.6, H_{A4}), 7.85 (1H, ddd, *J* 8.2, 7.4, 1.7, H_{E4}), 7.82 (1H, ddd, *J* 8.4, 7.6, 1.6, H_{C4}), 7.73 (1H, dd, *J* 8.0, 1.1, H_{E3}), 7.52 (1H, dd, *J* 8.8, 6.0, H_{F3}), 7.47 (1H, ddd, *J* 5.7, 1.7, 0.8, H_{E6}), 7.35 (1H, ddd, *J* 7.3, 5.7, 1.4, H_{A5}), 6.98 (1H, ddd, *J* 7.4, 5.8, 1.4, H_{C5}), 6.96 (1H, ddd, *J* 7.4, 5.8, 1.4, H_{E5}), 6.33 (1H, dd, *J* 10.6, 8.8, H_{F4}), 5.93 (1H, d, *J* 10.5, H_{B6}), 5.71 (1H, d, *J* 10.5, H_{D6}), 3.20 (3H, s, $H_{B/D7}$), 3.19 (3H, s, $H_{B/D7}$), 2.74 (3H, s, H_{F7}); δ_F (376 MHz, $CDCl_3$, Me_4Si) -105.39 (1F, dd, *J* 10.1, 6.2), -105.70 (1F, dd, *J* 10.1, 2.8), -106.70 (1F, dd, *J* 9.9, 2.6), -109.10 (1F, s), -109.94 (1F, s); δ_C (176 MHz, $CDCl_3$, Me_4Si) 167.68 (C_{F1}), 163.85 (C_{C2}), 162.72 (C_{A2}), 162.45 (C_{F5}), 159.03 (C_{B5}, *J* 262.5), 158.33 (C_{D5}, *J* 272.9), 155.38 (C_{E2}), 150.91 (C_{C6}), 150.41 (C_{E6}), 149.08 (C_{A6}), 139.94 (C_{A4}), 139.68 (C_{C4}), 139. 53 (C_{E4}), 136.07 (C_{F3}), 131.78 (C_{D1}), 130.56 (C_{B1}), 125.92 (C_{E3}), 125.71 (C_{F2}), 124.98 (C_{A3}), 124.51 (C_{C3}), 124.26 (C_{A5}), 123.82 (C_{E5}), 123.19 (C_{C5}), 120.95 (C_{F6}), 117.23 (C_{B6}, d, *J* 18.1), 116.46 (C_{D6}, d, *J* 17.8), 104.60 (C_{F4}, d, *J* 24.1), 46.33 (C_{B+D7}), 45.49 (C_{F7}); HRMS (FTMS+ESI): calcd for $[C_{36}H_{25}F_5N_3O_7S_3{}^{191}Ir+H]^+$: 994.0459. Found: 994.0478.

Iridium complex 32

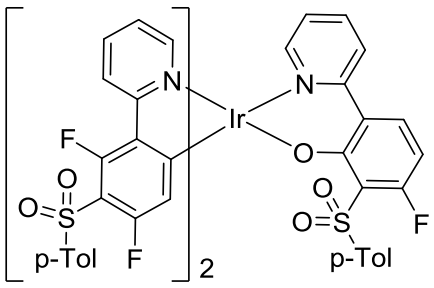

$IrCl_3.3H_2O$ (136 mg, 0.39 mmol) was added to a stirred solution of 2-(2,4-difluoro-3-[(4-methylbenzene)sulfonyl]phenyl)pyridine **16** (293 mg, 0.85 mmol) in 2-ethoxyethanol (10 ml). The mixture was heated to reflux at 130 ^{O}C under an atmosphere of argon overnight. The mixture was then left to cool and the solvent was removed *in vacuo* to leave a yellow solid, presumed to be the bis(μ-Cl)dimer, which was used without further purification. The dimer was dissolved in ethylene glycol (8 ml) and the 2-(2,4-difluoro-3-[(4-methylbenzene)sulfonyl]phenyl)pyridine **16** (130 mg, 0.38 mmol), NEt_3 (0.1 ml) and acetylacetone (0.1 ml) were added. The mixture was stirred under argon and heated to reflux at 190 ^{O}C overnight. The mixture was then left to cool. DCM (25 ml) and water (25 ml) were added and the organic layer was separated and washed with water (2 x 60 ml) to remove the majority of the ethylene glycol. The solvent was removed *in vacuo* to leave a brown liquid residue. The residue was then purified by column chromatography (DCM/Methanol 29:1 followed by DCM/EtOAc 80:20) to give iridium complex **32** as a yellow solid (110 mg, 23%); Anal. Calc. for $C_{54}H_{35}F_5IrN_3O_7S_3$: C, 53.11; H, 2.89; N, 3.44. Found: C, 52.64; H, 2.89; N, 3.37; δ_H (400 MHz; $CDCl_3$; Me_4Si) 8.36 (1H, d, *J* 8.5), 8.25 (1H, d, *J* 8.5), 7.93 (3H, dd, *J* 6.3, 1.8), 7.89 – 7.78 (4H, m), 7.71 (2H, tdd, *J* 8.1, 6.2, 1.7), 7.62 – 7.55 (1H, m), 7.42 (1H, dd, *J* 8.9, 6.0), 7.36 – 7.26 (3H, m), 7.15 – 7.05 (2H, m), 6.99 – 6.91 (2H, m), 6.91 – 6.76 (5H, m), 6.28 (1H, dd, *J* 10.4, 8.8), 5.92 (1H, d, *J* 10.3), 5.40 (1H, d, *J* 10.6), 2.41 (3H, s), 2.37 (3H, s), 2.19 (3H, s); δ_F (376 MHz; $CDCl_3$; Me_4Si) -105.11 – -105.21 (2F, m), -108.21 (1F, dd, *J* 10.7, 3.1), -108.35 (1F, d, *J* 4.3), -108.90 – -108.97 (1F, m); HRMS (FTMS+ESI): calcd for $[C_{54}H_{35}F_5N_3O_7S_3{}^{191}Ir+H]^+$: 1222.13925. Found: 1222.13928. Crystals for X-ray analysis were grown from slow evaporation of a solution of **32** in DCM/hexane/MeOH (1:2:1) at RT.

Experimental details for chapter 3: Toward 'fluorine-free' emission

3-Fluoro-6-(pyridin-2-yl)-2-tosylphenol 57a and 3-fluoro-4-(pyridin-2-yl)-2-tosylphenol 57b

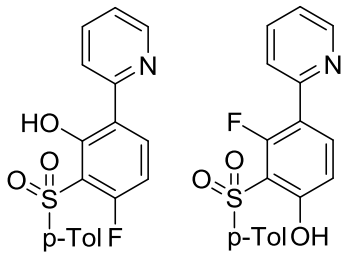

Attempt 1: An aqueous solution of potassium hydroxide [4M KOH (214 mg, 3.85 mmol) in water (1 ml)] was added to a solution of 2-(2,4-difluoro-3-[(4-methylbenzene)sulfonyl]phenyl)pyridine **16** (400 mg, 1.15 mmol) in 1,4-dioxane (7 ml). The mixture was heated to reflux (90 ^{o}C) for 2 h and then evaporated to a volume of ca. 1 ml. Water (20 ml) was added, upon which a yellow-white precipitate formed. Aqueous

acetic acid (conc. AcOH (2 ml) in H_2O (8 ml)) was added, which led to precipitate formation. The precipitate was collected, washed with water, and dried under vacuum. TLC analysis indicated a majority of the starting material remained unconverted. The reaction was set up again and left for 72 h, however this produced little change.

Attempt 2: The reaction mixture was dissolved in diglyme (6 ml) and an aqueous solution of KOH (334 mg, in 1.5 ml). The solution was heated to 160 ^{o}C overnight, allowed to cool and water (20 ml) was added, followed by a solution of aqueous acetic acid (2 ml glacial in 8 ml water). A precipitate formed which was filtered and washed with water and diethyl ether to remove the digylme. The reaction mixture was then heated under reflux in DCM (20 ml) for 10 min, allowed to cool to room temperature, and filtered; this operation was repeated another two times. Upon filtration a white solid was collected (216 mg), which proved to be insoluble in organic solvents. The combined filtrates were evaporated to dryness and the residue was purified by column chromatography (EtOAc (10%) in DCM) to give a yellow solid. NMR analysis suggested a mixture of 2 compounds, with MS data suggesting formation of the require compound(s), **57a** and **57b**, (combined weight 192 mg, 48%) in a 1:1 ratio by ^{1}H NMR analysis.

Attempt 3: The above reaction was repeated using 2-(2,4-difluoro-3-[(4-methylbenzene)sulfonyl]phenyl)pyridine **16** (400 mg, 1.16 mmol) in diglyme (6 ml), KOH (214 mg, 3.85 mmol) in water (1 ml). The mixture was purified by column chromatography (10% EtOAc in DCM) to yield a mixture of the **57a** and **57b** (342 mg, 86%). A ratio of **57a**:**57b** of 30:70 was revealed by NMR analysis.

2-(2-Fluoro-4-methoxy-3-tosylphenyl)pyridine 58

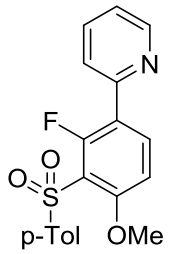

The product mixture **57a**:**57b** (50:50, 50 mg, 0.15 mmol) was dissolved in THF (dry, 2.5 ml) and NaO^{t}Bu (10 mg, 0.10 mmol) was added. The mixture was stirred for 40 min. CH_3I (22 mg, 0.01 ml, 0.16 mmol) was then added rapidly and the mixture was heated to reflux under argon overnight. The mixture was allowed to cool and then DCM (20 ml) and water (20 ml) were added. The mixture was separated and the aqueous layer was extracted with DCM (4 x 20 ml). The fractions were combined and the solvent was removed *in vacuo*. The mixture was then purified by column chromatography (10% MeOH in DCM, increased to 100% MeOH to elute baseline material) to give 2-(2-fluoro-4-methoxy-3-tosylphenyl)pyridine **58** (20 mg, 39%); δ_H (400 MHz; $CDCl_3$; Me_4Si) 8.67 (1H, d, *J* 4.6), 8.14 (1H, t, *J* 8.6), 7.92 (2H, d, *J* 8.40), 7.71-7.80 (2H, m), 7.29 (2H, d, 8.40), 7.23-7.27 (1H, m , 6.84 (1H, dd, *J* 9.0 1.3), 3.84 (3H, s), 2.41 (3H, s); δ_F (376 MHz, $CDCl_3$, Me_4Si) -112.61 (1F, d, *J* 7.9); δ_c (101 MHz, $CDCl_3$, Me_4Si) 158.46 (d, *J* 263.41), 159.08 (d, *J* 3.4), 152.01, 149.82, 144.30,

140.03, 136.74, 136.71, 136.67, 129.36, 127.93, 124.67 (d, *J* 9.7), 122.67, 121.85, 121.70, 118.69 (d, *J* 13.1), 108.72 (d, *J* 3.6), 56.87, 29.82; HRMS (FTMS+ESI): calcd for $[C_{19}H_{16}FNO_3S + H]^+$: 358.0913. Found: 358.0889.

Also obtained was a mixture of N-methylated pyridinium salts (104 mg), isolated when the column was flushed with 100% MeOH.

Demethylation of N-methylpyridiunium salts [9]

The mixture of pyridinium salts obtained from the above reaction (104 mg, 0.214 mmol) was dissolved in DMF (dry, 6 ml) and the solution was stirred. Then PPh_3 was added (73 mg, 0.28 mmol) and the solution was heated to reflux (150 ^oC). The reaction was monitored by TLC. After 6 h TLC showed little change, extra PPh_3 (32 mg, 0.12 mmol) was added. After 20 h the reaction was cooled and DCM (25 ml) and water (25 ml) were added. The layers were separated and the aqueous layer was washed with DCM (2 x 25 ml). The solvent was removed and the residue was purified by column chromatography (10% EtOAc in DCM), changed to DCM:MeOH:NH_3(aq) 15:4:1 to elute the pyridinium ions), resulting in recovered **57a**:**57b** (21 mg, 29%).

Methyl 4-methylbenzenesulfonate

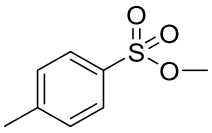

K_2CO_3 (1.45 g, 7.79 mmol) was added to stirred methanol (10 ml). Then tosyl chloride (2.00 g, 10.49 mmol) was added (with caution) to the suspension, which was then stirred overnight at RT. Water (20 ml) was added and the majority of the methanol was removed *in vacuo*. Then DCM (35 ml) was added and the layers were separated. The aqueous layer was then extracted further (2 x 25ml DCM). The solvent was removed *in vacuo* to yield a crystalline semi solid, methyl 4-methylbenzenesulfonate TsOMe (1.60 g, 82%); δ_H (400 MHz; $CDCl_3$; Me_4Si) 7.80 (2H, d, *J* 8.3), 7.36 (2H, d, *J* 7.9), 3.74 (3H, s), 2.46 (3H, s). The NMR data were consistent with the literature data.[10]

2-(2-Fluoro-4-methoxy-3-tosylphenyl)pyridine 58

The product mixture **57a**:**57b** (28:70, 342 mg, 0.99 mmol) was dissolved in THF (15 ml) and NaO^tBu (86 mg, 0.89 mmol) was added. The mixture was stirred at RT for 1.5 h. Then TsOMe (145 mg, 0.78 mmol) was added and the solution was heated to 70 ^oC. The reaction was stirred overnight, then allowed to cool. The volume of THF was reduced to 5 ml then water (50 ml) and DCM (100 ml) were added. An emulsion formed, so dilute HCl (7%, 15 ml) was added. The aqueous layer was then separated and the organic layer was concentrated *in vacuo*. The residue was purified by column chromatography (10% EtOAc in DCM, changed to NH_3(aq):MeOH:DCM (1:4:15, increased to 1:2:14) to elute the pyridinium ions). The product was **58** (65 mg, 18%); NMR data was consistent with that obtained previously.

Also isolated: Starting material mixture **57a**:**57b** (110 mg, 32%), pyridinium ions (110 mg, 30%).

2-(2-Fluoro-4-methoxyphenyl)-pyridine) 60

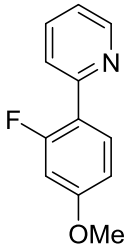

A solution of 2-fluoro-4-methoxyphenylboronic acid **59** (1.00 g, 5.88 mmol) and 2-bromopyridine **11** (0.62 ml, 6.46 mmol) in dioxane (30 ml) was degassed by bubbling argon for 30 min. An aqueous solution of Na_2CO_3 (0.79 g, 7.44 mmol in 4 ml) was added, followed by $Pd(PPh_3)_4$ (70 mg, 0.06 mmol). The mixture was heated to 95 ^oC overnight under argon then allowed to cool and the solvent was removed *in vacuo.* Water and DCM were added and the organic layer was separated, dried over $MgSO_4$ and the solvent was removed *in vacuo*. The crude oil was purified by distillation using a Kuglerohr apparatus. Residual 2-bromopyridine was distilled first (70-80 ^oC, 0.75 mbar), followed at 115 ^oC, 0.75 mbar by 2-(2-fluoro-4-methoxyphenyl)-pyridine) **60** as a pale yellow oil (1.09 g, 91%); δ_H (400 MHz; $CDCl_3$; Me_4Si) 8.68 (1H, ddd, *J* 4.8, 1.8, 1.0), 7.95 (1H, t, *J* 9.0), 7.67-7.77 (2H, m), 7.18 (1H, ddd, *J* 7.0, 4.9, 1.5), 6.81 (1H, ddd, *J* 8.8, 2.5, 0.7), 6.69 (1H, dd, *J* 13.2, 2.5), 3.83 (3H,s); δ_F (376 MHz, $CDCl_3$, Me_4Si) -114.74 (1F, t, *J* 12.3); δ_C (101 MHz; $CDCl_3$; Me_4Si) 161.47 (d, *J* 11.2), 161.32 (d, *J* 249.5), 153.43 (d, *J* 2.8), 149.68, 136.40, 131.63 (d, *J* 4.9), 124.03 (d, 9.8), 121.85, 120.01 (d, *J* 11.9), 110.65 (d, *J* 2.9), 102.00 (d, *J* 27.0), 55.72; HRMS (FTMS+ESI): calcd for $[C_{12}H_{10}NFO+H]^+$: 204.0825. Found: 204.0817.

2-(2-Fluoro-3-iodo-4-methoxyphenyl)-pyridine) 62

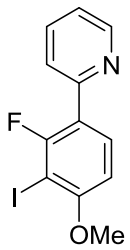

The reaction was conducted using the general procedure B for lithiation followed by iodination. The following reagents were used in the stated quantities: ^{n}BuLi (1.94 ml, 2.5 M), DIPA (0.75 ml, 5.34 mmol), 2-(2-fluoro-4-methoxyphenyl)-pyridine) **60** (790 mg, 3.89 mmol), I_2 (1.38 g, 5.44 mmol) and THF (35 ml, dry). The reaction was worked up as described in the general method, and the product was then purified by column chromatography (hexane:EtOAc 3:2 v/v) to give 2-(2-fluoro-3-iodo-4-methoxyphenyl)-pyridine) **62** (746 mg, 58%) as an off-white solid; m.pt. 107.2-109.7 ^oC; δ_H (400 MHz; $CDCl_3$ Me_4Si) 8.69 (1H, dt, *J* 4.8, 1.5), 7.98 (1H, t, *J* 8.8), 7.71-7.78 (2H, m), 7.19-7.28 (1H, m), 6.76 (1H, dd, *J* 8.8, 1.2), 3.96 (3H, s); δ_F (376 MHz; $CDCl_3$; Me_4Si) -93.14 (d, *J* 10.7); δ_C (101 MHz; $CDCl_3$ Me_4Si) 160.09 (d, *J* 248.0), 160.33 (d, *J* 6.1), 152.82 (d, *J* 3.3), 149.79, 136.62, 131.84 (d, *J* 4.8), 124.23 (d, *J* 9.6), 122.33, 121.25 (d, *J* 14.9), 106.97 (d, *J* 2.9), 75.06 (d, *J* 28.96), 57.02; HRMS (FTMS+ESI): calcd for $[C_{12}H_9NFOI+H]^+$: 329.9791. Found: 329.9787.

2-(2-Fluoro-4-methoxy-3-(methylsulfonyl)phenyl)pyridine 64

The reaction was conducted using the general procedure for sulfone synthesis. The following

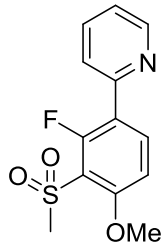

reagents were used in the stated quantities: 2-(2-fluoro-3-iodo-4-methoxyphenyl)-pyridine) **62** (1.02 g, 3.11 mmol), CuI (0.89 g, 4.67 mmol), $MeSO_2Na$ (0.51 g, 4.98 mmol) were added to a stirred solution of in DMF (2.5 ml, dry). The reaction was worked up as described in the general procedure, and the product was purified by column chromatography (DCM:EtOAc 1:1) to give 2-(2-fluoro-4-methoxy-3-(methylsulfonyl)phenyl)pyridine **64** (390 mg, 45%); δ_H (400 MHz; $CDCl_3$; Me_4Si) 8.70 (1H, dt, *J* 4.8, 1.4), 8.23 (1H, dd, *J* 9.0, 8.3), 7.72-7.82 (2H, m), 7.26-7.30 (1H, m), 6.98 (1H, dd, *J* 8.9, 1.3), 4.03 (3H, s), 3.34 (3H, s); δ_F (376 MHz; $CDCl_3$; Me_4Si) -113.56 (d, *J* 9.3); δ_C (176 MHz; $CDCl_3$; Me_4Si) 159.07 (d, *J* 3.4), 158.4 (d, *J* 263.2), 151.87 (d, *J* 1.7), 149.96, 136.87 (d, *J* 6.1), 136.72, 124.60 (d, *J* 9.8), 122.80, 122.20 (d, *J* 14.3), 118.01 (d, *J* 13.6), 108.66 (d, *J* 3.5), 57.28, 45.61; HRMS (FTMS+ESI): calcd for $[C_{13}H_{12}NFO_3S+H]^+$: 282.0600. Found: 282.0615.

Ir complex 68

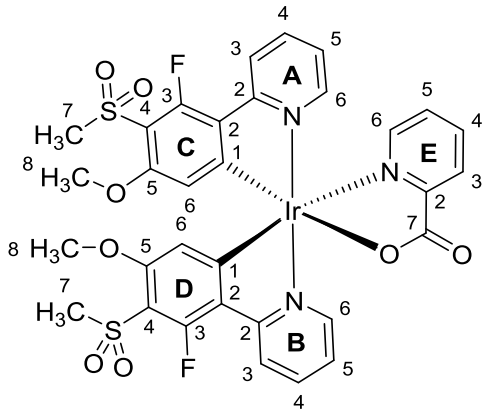

The reaction was conducted as described in the general procedure for synthesis of Iridium pic complexes, Method B. The following reagents were used in the stated quantities: $IrCl_3.3H_2O$ (233 mg, 0.66 mmol), 2-(2-fluoro-4-methoxy-3-(methylsulfonyl)phenyl)pyridine **64** (390 mg, 1.39 mmol), picolinic acid (284 mg, 2.31 mmol), 2-ethoxyethanol (12 ml). The reaction was worked up as described in the general procedure and the residue was purified by column chromatography (5% MeOH in DCM). The yellow solid obtained was then suspended in ethanol and heated to reflux. The solution was filtered to afford complex **68** as a yellow solid (310 mg, 54%); Anal. Calc. for $C_{32}H_{26}N_3F_2O_8S_2Ir$: C, 43.93; H, 3.00; N, 4.80. Found: C, 44.02; H, 3.26; N, 4.97; δ_H (700 MHz; $CDCl_3$; Me_4Si) 8.78 (1H, ddd, *J* 5.8, 1.7, 0.8, H_{A6}), 8.37 (1H, ddd, *J* 7.8, 1.5, 0.8, H_{E3}), 8.34 (1H, d, *J* 8.5, H_{B3}), 8.27 (1H, d, *J* 8.5, H_{A3}), 8.02 (1H, td, *J* 7.8, 1.6, H_{E4}), 7.84 (1H, td, H_{B4}) 7.82 (1H, td, J, H_{A4}), 7.79 (1H, ddd, *J*, H_{E6}), 7.52 (1H, ddd, *J* 7.7, 5.4, 1.5, H_{E5}), 7.46 (1H, ddd, *J* 5.9, 1.6, 0.8, H_{B6}), 7.23 (1H, ddd, *J* 7.3, 5.8, 1.4, H_{A5}), 7.03 (1H, ddd, *J* 7.4, 5.8, 1.4, H_{B5}), 5.73 (1H, s, H_{C6}), 5.57 (1H, s, H_{D6}), 3.56 (3H, s, H_{C8}), 3.51 (3H, s, H_{D8}), 3.25 (3H, s, H_{C7}), 3.20 (3H, s, H_{D7}); δ_F (376 MHz; $CDCl_3$; Me_4Si) -112.10 (1F, s), -112.58 (1F, s); δ_C (176 MHz; $CDCl_3$; Me_4Si) 172.31 (s, C_{E7}), 165.37 (d, *J* 6.2, C_{B2}), 164.21 (d, *J* 6.2, C_{A2}), 161.38 ($C_{C/D2}$), 160.56 ($C_{C/D2}$), 158.69 (d, *J* 3.0, C_{C5}), 158.40 (d, *J* 284.0, C_{C3}), 158.30 (d, *J* 284.0, C_{D3}), 158.18 (d, *J* 2.6, C_{D5}), 151.18 (s, C_{E2}), 148.64 (s, C_{A6}), 148.26 (s, C_{E6}), 148.00 (s, C_{B6}), 138.90(s, C_{E4}), 138.73 (s, $C_{A/B4}$), 138.70 (s, $C_{A/B4}$), 128.81 (s, C_{E3}), 128.78 (s, C_{E5}), 126.12 (d, J,C_{C1}), 125.81 (d, C_{D1}), 123.53 (d, J, C_{B3}), 122.96 (d, J, C_{A3}), 122.41 (s, C_{B5}), 122.35 (s, C_{A5}), 111.28 (d, *J* 11.4, C_{D4}),

111.01 (C_{D6}), 110.93 (d, *J* 11.5, C_{C4}), 110.73 (C_{C6}), 56.09 (s, C_{C8}), 55.97 (s, C_{D8}), 45.29 (s, $C_{C/D7}$), 45.28 (s, $C_{C/D7}$); HRMS (FTMS+ESI): calcd for $[C_{32}H_{26}N_3F_2O_8S_2{}^{191}Ir+H]^+$: 874.0814. Found: 874.0786. Crystals for X-ray analysis were grown by slow vapour diffusion of pentane into a solution of **68** in DCM.

2-(2-Fluoro-4-methoxyphenyl)-4-mesitylpyridine 61

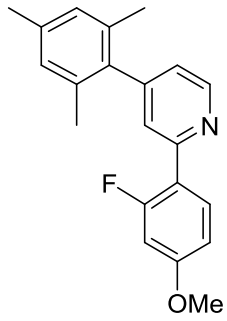

A solution of 2-chloro-4-(2,4,6-trimethylphenyl)pyridine **23** (1.23 g, 5.31 mmol), 2-fluoro-4-methoxyphenylboronic acid **59** (1.00 g, 5.88 mmol), $Pd(OAc)_2$ (73 mg, 0.36 mmol) and PPh_3 (363 mg, 1.52 mmol) in 1,2-dimethoxyethane (60 ml) was degassed with argon for 30 min. Separately a 2 M aqueous solution of sodium carbonate (11 ml, 2.31 g, 24.01 mmol) was degassed for 25 min. The solutions were combined and the mixture was heated to reflux under argon atmosphere for 24 h. The reaction mixture was then cooled to room temperature and the DME was removed *in vacuo*. DCM (50 ml) was then added, followed by brine (50 ml). The organic layer was separated and dried over $MgSO_4$. The solvent was removed *in vacuo* and the residue was purified by column chromatography (EtOAc:hexane 1:5 v/v) to give 2-(2-fluoro-4-methoxyphenyl)-4-mesitylpyridine **61** as a yellow oil (1.35g, 78%); δ_H (400 MHz; $CDCl_3$; Me_4Si) 8.73 (1H, dd, *J* 4.9, 0.9), 8.02 (1H, t, *J* 9.0), 7.55-7.61 (1H, m), 7.03 (1H, dd, *J* 5.0, 1.5), 6.94-6.99 (2H, m), 6.84 (1H, ddd, *J* 8.8, 2.5, 0.7), 6.69 (1H, dd, *J* 13.1, 2.5), 3.85 (3H, s), 2.34 (3H, s), 2.05 (6H, s); δ_F (376 MHz, $CDCl_3$, Me_4Si) -114.38 (1F, t, *J* 13.2); δ_C (101 MHz; $CDCl_3$; Me_4Si) 161.28 (d, *J* 250.1), 161.41 (d, *J* 11.4), 153.50 (d, *J* 2.8), 149.79, 149.69, 137.48, 136.51, 135.28, 131.59 (d, *J* 4.8), 128.33, 125.00 (d, *J* 9.8), 122.86, 119.95 (d, *J* 11.6), 110.58 (d, *J* 3.0), 101.93 (d, *J* 27.2), 55.67, 21.05, 20.62; HRMS (FTMS+ESI): calcd for $[C_{21}H_{20}FNO+H]^+$: 322.1607. Found: 322.1608.

2-(2-Fluoro-3-iodo-4-methoxyphenyl)-4-mesitylpyridine 63

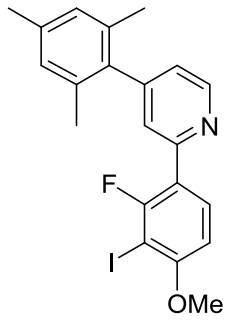

The reaction was conducted using the general procedure B for lithiation followed by iodination. The following reagents were used in the stated quantities: ^{n}BuLi (2.1 ml, 2.5 M), DIPA (0.81 ml, 5.78 mmol), 2-(2-fluoro-4-methoxyphenyl)-4-mesitylpyridine **61** (1.35 g, 4.20 mmol), I_2 (1.49 g, 8.09 mmol) and THF (30 ml, dry). The reaction was worked up as described in the general method, and the product was then purified by column chromatography (hexane:EtOAc 2:1) to give an off-white solid, 2-(2-fluoro-3-iodo-4-methoxyphenyl)-4-mestitylpyridine) **63** (1.03 g, 55%); m.pt. 167.4-168.5 ^oC; δ_H (400 MHz; $CDCl_3$; Me_4Si) 8.73 (1H, dd, *J* 5.0, 0.9), 8.05 (1H, t, *J* 8.8), 7.54-7.61 (1H, m), 7.06 (1H, dd, *J* 5.0, 1.5), 6.96

(2H, s), 6.78 (1H, dd, *J* 8.8, 1.1), 3.97 (3H, s), 2.34 (3H, s), 2.05 (6H, s); δ_F (376 MHz, $CDCl_3$, Me_4Si) -92.81 (d, *J* 12.6); δ_C (101 MHz; $CDCl_3$; Me_4Si) 159.98 (d, *J* 248.3), 160.21 (d, *J* 6.1), 152.81 (d, *J* 3.3), 150.05, 149.76, 137.55, 136.27, 135.17, 131.73 (d, *J* 4.9), 128.34, 125.21 (d, *J* 9.7), 123.27, 121.17 (d, *J* 14.5), 106.83 (d, *J* 2.9), 74.96, 56.88, 21.05, 20.62; HRMS (FTMS+ESI): calcd for $[C_{21}H_{19}NFOI+H]+$: 448.0574. Found: 448.0565.

2-(2-Fluoro-4-methoxy-3-(methylsulfonyl)phenyl)-4-mesitylpyridine 65

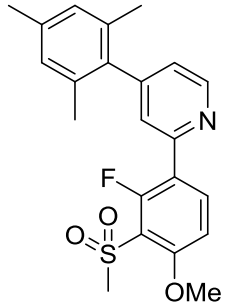

The reaction was conducted using the general procedure for sulfone synthesis. The following reagents were used in the stated quantities: 2-(2-fluoro-3-iodo-4-methoxyphenyl)-4-mestitylpyridine **63** (1.00 g, 2.24 mmol), CuI (0.68 g, 3.58 mmol) and $MeSO_2Na$ (0.34 g, 3.35 mmol) and DMF (3.5 ml, dry). The reaction was worked up as described in the general procedure, and the product was purified by column chromatography (DCM:EtOAc 1:1) to give 2-(2-fluoro-4-methoxy-3-(methylsulfonyl)phenyl)-4-mesitylpyridine **65** (470 mg, 53%); m.pt. 169.2 -170.8 ^oC; (400 MHz; $CDCl_3$; Me_4Si) 8.74 (1H, d, *J* 5.0), 8.30 (1H, t, *J* 8.6), 7.57-7.63 (1H, m), 7.10 (1H, dd, *J* 5.0, 1.5), 7.00 (1H, dd, *J* 9.0, 1.2), 6.92-6.97 (2H, m), 4.05 (3H, s), 3.32 (3H, s), 2.33 (3H, s), 2.03 (6H, s); δ_F (376 MHz; $CDCl_3$; Me_4Si) -113.44 (d, *J* 9.5); δ_C (176 MHz; $CDCl_3$; Me_4Si) 159.09 (d, *J* 3.3), 158.49 (d, *J* 263.0), 152.00, 150.46, 150.07, 137.77, 136.91 (d, *J* 5.9), 136.11, 135.17, 128.49, 125.72 (d, *J* 8.9), 123.89, 122.24 (d, *J* 14.0), 118.06 (d, *J* 13.3), 108.68 (d, *J* 3.4), 57.29, 45.61, 21.18, 20.74; HRMS (FTMS+ESI): calcd for $[C_{22}H_{22}NFO_3S+H]^+$: 400.1383. Found: 400.1379.

Iridium complex 69

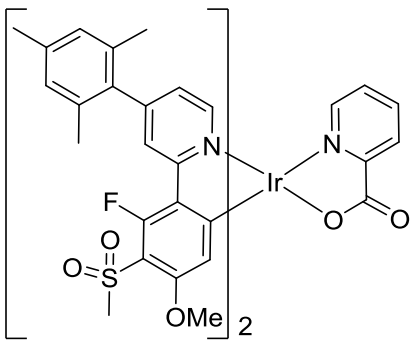

The reaction was conducted as described in the general procedure for synthesis of Iridium pic complexes, Method B. The following reagents were used in the stated quantities: $IrCl_3.3H_2O$ (189 mg, 0.54 mmol), 2-(2-fluoro-4-methoxy-3-(methylsulfonyl)phenyl)-4-mesitylpyridine **65** (450 mg, 1.13 mmol), picolinic acid (231 mg, 1.88 mmol) and 2-ethoxyethanol (20 ml). The reaction was worked up as described in the general procedure and the residue was purified by column chromatography (5% MeOH in DCM). The yellow solid was suspended in ethanol and heated to reflux. The solution was filtered hot to leave pure Ir complex **69** as a yellow solid (420 mg, 70%); Anal. Calc. for $C_{50}H_{46}N_3F_2O_8S_2Ir.CH_2Cl_2$: C, 51.21; H, 4.04; N, 3.51. Found: C, 51.34; H, 3.99; N, 3.55; δ_H (400 MHz; $CDCl_3$; Me_4Si) 8.80-8.87 (m, 1H), 8.44 (1H, dt, *J* 7.8, 0.9), 8.19 (1H, s), 8.12 (1H, s), 8.07 (1H, td, *J*

7.7, 1.5), 7.88 (1H, dt, *J* 5.1, 1.3), 7.57 (1H, ddd, *J* 7.6, 5.3, 1.5), 7.45 (1H, d, *J* 5.9), 7.09 (1H, dd, *J* 5.9, 1.8), 6.93-7.02 (4H, m), 6.87 (1H, dd, *J* 5.9, 1.8), 5.83 (1H, s), 5.77 (1H, s), 3.61 (3H, s), 3.58 (3H, s), 3.23 (3H, s), 3.19 (3H, s), 2.34 (6H, s), 2.09 (3H, s), 2.05 (3H, s), 2.00 (3H, s), 1.95 (3H, s); δ_F (376 MHz; $CDCl_3$; Me_4Si) -111.68 (1F, s), -112.28 (1F, s); HRMS (FTMS+ESI): calcd for $[C_{50}H_{46}N_3F_2O_8S_2{}^{191}Ir+H]^+$: 1110.2379. Found: 1110.2393.

2-(2-Fluoro-4-methoxy-3-tosylphenyl)-4-mesitylpyridine 66

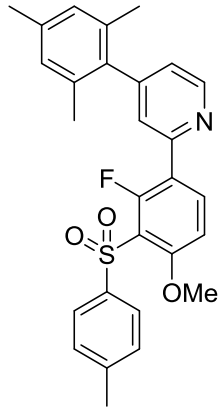

The reaction was conducted using the general procedure for sulfone synthesis. The following reagents were used in the stated quantities: 2-(2-fluoro-3-iodo-4-methoxyphenyl)-4-mesitylpyridine **61** (0.81 g, 1.81 mmol), sodium p-tolylsulfinate (0.52 g, 2.90 mmol), CuI (0.52 g, 2.71 mmol) and DMF (3 ml, dry). The reaction was worked up as described in the general procedure and the product mixture was purified by column chromatography (5% EtOAc in DCM, increased to 20%) to give 2-(2-fluoro-4-methoxy-3-tosylphenyl)-4-mesitylpyridine **66** as an off white solid (0.17 g, 21%); δ_H (400 MHz; $CDCl_3$; Me_4Si) 8.73 (1H, dd, *J* 5.0, 0.9), 8.22 (1H, dd, *J* 8.9, 8.2), 7.88-7.98 (2H, m), 7.56-7.66 (1H, m), 7.26-7.33 (2H, m), 7.08 (1H, dd, *J* 5.0, 1.5), 6.94-6.99 (2H, m), 6.87 (1H, dd, *J* 9.0, 1.2), 3.85 (3H, s), 2.41 (3H,s), 2.34 (3H, s) 2.04 (6H, s); δ_F (376 MHz; $CDCl_3$; Me_4Si) -112.69 (1F, d, *J* 10.9); δ_C (101 MHz; $CDCl_3$; Me_4Si) 158.40 (d, *J* 263.0), 158.98 (d, *J* 3.3), 152.10 (d, *J* 1.8), 150.26, 149.88, 144.17, 139.92, 137.63, 136.68 (d, *J* 6.1), 136.05, 135.10, 129.26, 128.36, 127.82, 125.62 (d, *J* 9.9), 123.64, 121.78 (d, *J* 14.2), 118.64 (d, *J* 13.4), 108.61 (d, *J* 3.6), 56.77, 21.65, 21.07, 20.64; HRMS (FTMS+ESI): calcd for $[C_{28}H_{26}NFO_3S+H]^+$: 476.1696. Found: 476.1718.

p-Tolyl disulfide

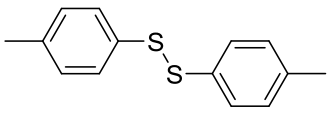

DDQ (0.91 g, 4.01 mmol) was added cautiously to a stirred solution of 4-methylbenzene thiol (1.00 g, 8.05 mmol) in DCM (50 ml) which was cooled by an ice bath. The solution was stirred for 30 min before the solvent was removed. The residue was purified by column chromatography (hexane) to give the product, p-tolyl disulfide (0.90 g, 91%); δ_H (400 MHz; $CDCl_3$; Me_4Si) 7.41 – 7.33 (2H, m), 7.18 – 7.07 (2H, m), 2.32 (3H, s); NMR data are consistent with the literature data.[11]

2-(2-Fluoro-4-methoxy-3-(p-tolylthio)phenyl)pyridine 67

^{n}BuLi (1.35 ml, 2.5 M in hexanes) was added dropwise to a stirred solution of DIPA (0.52 ml, 3.71 mmol) in THF (10 ml, dry) at 0 ^oC under argon. The solution was stirred at 0 ^oC for 30 min before the temperature was lowered to -78 ^oC. A solution of 2-(2-fluoro-4-methoxyphenyl)-4-mesitylpyridine **61** (0.90 g, 2.81 mmol) in THF (20 ml, dry) was added dropwise via cannula and

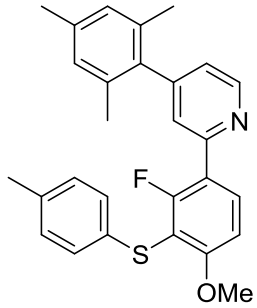

the mixture was stirred at -78 °C for 1 h. A solution of p-Tolyl disulfide (0.90 g, 3.65 mmol) in THF (20 ml, dry) was slowly added, and the reaction mixture was stirred at -78 °C for 1 h before being left to warm to RT overnight. The reaction was quenched with water, DCM was added, and the organic layer separated. The aqueous layer was washed with further DCM (3 x 50 ml), the extracts combined and the solvent removed. The crude oil was purified by column chromatograpy (5% EtOAc in DCM) to give a mixture of unreacted **61** and the desired product, **67**, (22% by NMR) which could not be separated. The residue was used for the next step without further purification.

2-(2-Fluoro-4-methoxy-3-tosylphenyl)-4-mesitylpyridine 66

m-Chloroperoxybenzoic acid (234 mg, 1.36 mmol) was added to a stirred solution of the crude mixture of **67** and **61** from the reaction described above in DCM (50 ml). The solution was stirred at RT overnight. The reaction was quenched with aqueous sodium bisulfite and the organic layer was separated. The aqueous layer was extracted with further DCM. The solvent was removed *in vacuo* and the residue was purified by column chromatography (DCM: EtOAc 4:1) to give a white solid, 2-(2,4-dimethoxy-3-(methylsulfonyl)phenyl)-4-mesitylpyridine **66** (184 mg, 63%). The NMR data was consistent with that obtained previously.

Also isolated was 2-(2-fluoro-4-methoxyphenyl)-4-mesitylpyridine **61** (590 mg), which remained from the previous step.

Iridium complex 70

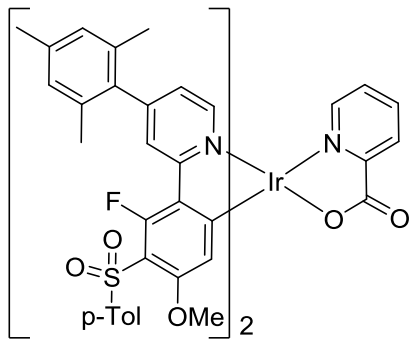

The reaction was conducted as described in the general procedure for synthesis of iridium pic complexes, Method B. The following reagents were used in the stated quantities: $IrCl_3.3H_2O$ (72 mg, 0.20 mmol), 2-(2-fluoro-4-methoxy-3-tosylphenyl)-4-mesitylpyridine **66** (184 mg, 0.42 mmol), picolinic acid (37 mg, 0.30 mmol) and 2-ethoxyethanol (5 ml). The reaction was worked up as described in the general procedure and the residue was purified by column chromatography (EtOAc in DCM 1:4, increased to 1:3) to give a yellow solid. This was purified further by recrystallisation from ethanol to give complex **70** (210 mg, 83%); Anal. Calc. for $C_{62}H_{54}N_3F_2O_8S_2Ir$: C, 58.94; H, 4.31; N, 3.33. Found: C, 58.60; H, 4.26; N, 3.27; δ_H (400 MHz; $CDCl_3$; Me_4Si) 8.74 (1H, d, *J* 5.8), 8.39 (1H, d, *J* 7.8), 8.15 (1H, s), 8.08 (1H, s), 8.04 (1H, td, *J* 7.7, 1.6), 7.85-7.90 (2H, m) 7.77-7.85 (3H, m), 7.56 (1H, ddd, *J* 7.4, 5.3, 1.1), 7.40 (1H, d, *J* 5.9), 7.30 – 7.20 (4H, m), 7.03 – 6.92 (5H, m), 6.81 (1H, dd, *J* 5.9, 1.8), 5.71

(1H, s), 5.63 (1H, s), 3.43 (3H, s), 3.37 (3H, s), 2.38 (6H, s), 2.34 (6H, s), 2.08 (3H, s), 2.00 (3H, s), 1.96 (3H, s), 1.94 (3H, s); δ_F (376 MHz; $CDCl_3$; Me_4Si) -110.60 (1F, s), -111.33 (1F, s); HRMS (FTMS+ESI): calcd for $[C_{62}H_{54}N_3F_2O_8S_2{}^{191}Ir+H]^+$: 1262.3005. Found: 1262.3020.

2-(2,4-Dimethoxyphenyl)-4-mesitylpyridine 72

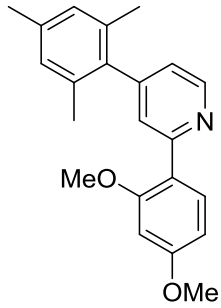

2-Chloro-4-mesitylpyridine **23** (1.16 g, 5.01 mmol), 2,4,6-trimethylphenylboronic acid **71** (1.00 g, 5.50 mmol) and PPh_3 (340 mg, 1.30 mmol) were dissolved in DME (70 ml) and the solution was degased for 20 min by bubbling with argon. Separately, an aqueous solution of Na_2CO_3 (2.16 g, 20.38 mmol) was degassed for 20 min. The solutions were combined and $Pd(OAc)_2$ (68 mg, 0.30 mmol) was added. The mixture was heated to reflux overnight before being cooled. The solvent was removed under reduced pressure and DCM and water were added. The organic layer was separated, and the aqueous layer was extracted with further DCM. The extracts were combined and the solvent removed. The residue was purified by column chromatography (DCM:EtOAc 1:1) to give a white solid, 2-(2,4-dimethoxyphenyl)-4-mesitylpyridine **72** (1.13 g, 68%); m.pt. 143.5-145.3 ^oC; δ_H (400 MHz; $CDCl_3$; Me_4Si) 8.70 (1H, dd, *J* 5.0, 0.9), 7.86 (1H, d, *J* 8.5), 7.65 (1H, dd, *J* 1.6, 0.9), 6.93-7.00 (3H, m), 6.64 (1H, dd, *J* 8.6, 2.4), 6.54 (1H, d, *J* 2.4), 3.86 (3H, s), 3.79 (3H, s), 2.34 (3H, s), 2.07 (6H, s); δ_c (101 MHz; $CDCl_3$; Me_4Si) 161.35, 158.16, 155.89, 149.33, 148.68, 137.30, 136.96, 135.44, 132.01, 128.29, 125.89, 122.14, 105.06, 98.85, 55.60, 55.46, 21.06, 20.64; HRMS (FTMS+ESI): calcd for $[C_{22}H_{23}NO_2+H]^+$: 334.1807. Found: 334.1807.

2,6-Dimethoxythioanisole 75

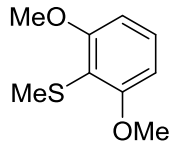

The reaction was conducted as described in the literature method. ^{n}BuLi (18.8 ml, 2.5 M) was added to a stirred solution of TMEDA (6.50 ml, 43.46 mmol) in hexane (30 ml, dry) at 0 ^oC and the solution was stirred for 30 min. A solution of 1,3-dimethoxybenzene **74** (5.00 g, 36.19 mmol) in hexane (20 ml, dry) was added in portions via cannula and the mixture was stirred for a further 1 h. A solution of dimethyl disulfide (4.18 ml, 47.03 mmol) in hexane (20 ml, dry) was added to the flask dropwise. The solution was stirred at 0 ^oC and allowed to warm to RT overnight. The reaction mixture was poured into water (300 ml) and acidified with conc. H_2SO_4 (CAUTION, MeSH produced). The precipitate was filtered off, and the filtrate was extracted with DCM (100 ml). The solvent was removed and the solids combined and recrystallized from hot methanol to give white crystals, 2,6-dimethoxythioanisole **75** (5.14 g, 77%); δ_H (400 MHz; $CDCl_3$; Me_4Si) 7.24 (1H, t, *J* 8.3), 6.58 (2H, d, *J* 8.4), 3.90 (6H, s), 2.37 (3H,s). NMR data are consistent with the literature data.[12]

3-Bromo-2,6-dimethoxythioanisole 76

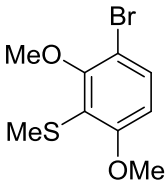

The reaction was conducted as described in the literature method. A solution of Br_2 (0.79 ml, 15.41 mmol) in DCM (20 ml) was added dropwise to a stirred solution of 2,6-dimethoxythioanisole **75** (2.89 g, 15.68 mmol) in DCM (50 ml) cooled by an ice bath. The solution was stirred at 0 ^{o}C for appox. 30 min, by which time the solution was a pale yellow colour. The solvent was removed under reduced pressure (care, may evolve HBr) and the product was distilled using the Kugelrohr apparatus (~150 ^{o}C at 0.6 mbar) to leave a clear oil, 3-bromo-2,6-dimethoxythioanisole **76** (4.07 g, 98%); δ_H (400 MHz; $CDCl_3$; Me_4Si) 7.43 (1H, d, *J* 8.9), 6.59 (1H, *J* 8.9), 3.90 (3H, s), 3.89 (3H, s) 2.42 (3H, s). NMR data are consistent with the literature data.[12]

(2,4-Dimethoxy-3-(methylthio)phenyl)boronic acid 77

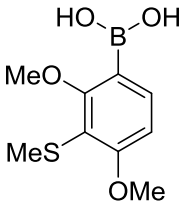

^{n}BuLi (11.25 ml, 2.5 M in hexanes) was added dropwise to a stirred solution of 3-bromo-2,6-dimethoxythioanisole **76** (6.17 g, 23.45 mmol) in THF (15 ml, dry) at -78 ^{o}C. The mixture was stirred at -78 ^{o}C for 1 h. Triisopropyl borate (8.11 ml, 35.15 mmol) was slowly added, and the reaction mixture was stirred at -78 ^{o}C for 1 h before being left to warm to RT overnight. Dilute HCl was added and the solution was extracted with EtOAc. The solvent was removed *in vacuo* to leave a sticky brown solid which was redissolved in EtOAc and was extracted with aqueous KOH (150 ml). The aqueous layer was acidified to pH 5 with dilute HCl and extracted with EtOAc. The solvent was removed *in vacuo* to give a beige solid, (2,4-dimethoxy-3-(methylthio)phenyl)boronic acid **77** (2.80 g, 52%); δ_H (400 MHz; $CDCl_3$; Me_4Si) 7.80 (1H, d, *J* 8.4), 6.79 (1H, d, *J* 8.4), 5.88 (2H, br s), 3.98 (3H, s), 3.97 (3H, s), 2.42 (3H, s); δ_B (128 MHz; $CDCl_3$; Me_4Si) 28.66 (1B, br s); HRMS (FTMS+ESI): calcd for $[C_9H_{13}O_4S^{10}B+H]^+$: 228.0742. Found: 228.0732.

2-(2,4-Dimethoxy-3-(methylthio)phenyl)-4-mesitylpyridine 78

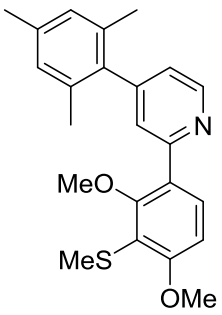

2-Chloro-4-mesitylpyridine **23** (0.72 g, 3.11 mmol), (2,4-dimethoxy-3-(methylthio)phenyl)boronic acid **77** (0.85 g, 3.73 mmol) and PPh_3 (211 mg, 0.80 mmol) were dissolved in DME (50 ml) and the solution was degased for 20 min by bubbling with argon. Separately, an aqueous solution of Na_2CO_3 (1.34 g, 12.64 mmol in 10 ml) was degassed for 20 min. The solutions were combined and $Pd(OAc)_2$ (43 mg, 0.19 mmol) was added. The mixture was heated to reflux for 24 h before being cooled. The solvent was removed under reduced pressure and DCM and water were added. The organic layer was separated, and the aqueous layer was extracted with further DCM. The extracts were combined and the solvent removed. The residue

was purified by column chromatography (DCM:EtOAc 1:1 v/v) to give a white solid, 2-(2,4-dimethoxy-3-(methylthio)phenyl)-4-mesitylpyridine **78** (0.70 g, 60%); m.pt. 133.4-136.2; δ_H (400 MHz; CD_3OD; Me_4Si) 8.65 (1H, dd, *J* 5.1, 0.9), 7.62 (1H, d, *J* 8.6), 7.58 – 7.52 (1H, m), 7.16 (1H, dd, *J* 5.1, 1.6), 6.97 (2H, s), 6.97 (1H, d, *J* 8.7), 3.94 (3 H, s), 3.57 (3 H, s), 2.39 (3H, s), 2.31 (3H, s), 2.05 (6H, s); δ_C ^{13}C NMR (101 MHz, CD_3OD; Me_4Si) 161.38, 159.22, 156.10, 150.69, 148.72, 137.40, 136.03, 134.50, 130.81, 127.99, 126.57, 126.07, 123.18, 119.02, 107.31, 99.99, 19.73 , 19.34, 16.60; HRMS (FTMS+ESI): calcd for $[C_{23}H_{25}NFO_2S+H]^+$: 380.1684. Found: 380.1666.

2-(2,4-Dimethoxy-3-(methylthio)phenyl)-4-mesitylpyridinium chloride 78a

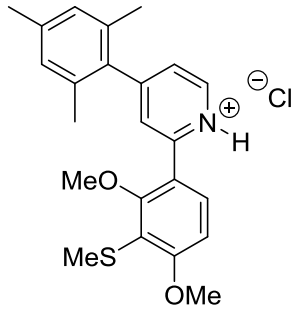

HCl (0.05 ml, 12 M) was added to a stirred solution of 2-(2,4-dimethoxy-3-(methylthio)phenyl)-4-mesitylpyridine **78** (236 mg, 0.62 mmol) in DCM/MeOH (40 ml, 1:1), and the mixture was stirred at RT overnight. The solvent was removed *in vacuo* to leave the product as a white solid, 2-(2,4-dimethoxy-3-(methylthio)phenyl)-4-mesitylpyridinium chloride **78a** (259 mg, 100%); m.pt. 177.3-180.2 ^{o}C; δ_H (400 MHz; CD_3OD; Me_4Si) 8.84 (1H, d, *J* 6.1), 8.18 – 8.12 (m, 1H), 7.87 (1H, dd, *J* 6.1, 1.9), 7.74 (1H, dd, *J* 8.8, 0.9), 7.12 (1H, d, *J* 8.8), 7.09-7.08 (2H, m), 4.03 (s, 3H), 3.75 (s, 3H), 2.47 (s, 3H), 2.37 (s, 3H), 2.14 (s, 6H); δ_C (176 MHz, CD_3OD; Me_4Si) 164.17, 160.76, 159.45, 150.20, 140.89, 139.28, 134.22, 133.75, 130.94, 128.91, 128.51, 126.27, 120.38, 117.78, 109.99, 108.05, 99.79, 60.89, 55.66, 22.77, 19.71, 19.16, 16.28.

2-(2,4-Dimethoxy-3-(methylsulfonyl)phenyl)-4-mesitylpyridine 79

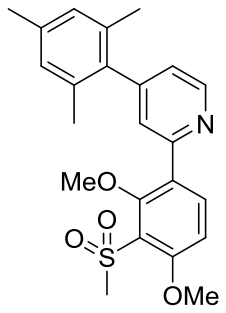

m-Chloroperoxybenzoic acid (436 mg, 2.68 mmol) was added to a stirred solution of 2-(2,4-dimethoxy-3-(methylthio)phenyl)-4-mesitylpyridinium chloride **78a** (510 mg, 1.22 mmol) in DCM (20 ml). The solution was stirred at RT overnight. The reaction was quenched with aqueous $NaHSO_3$ and the organic layer was separated. The aqueous layer was extracted with additional DCM. The organic layers were then washed with aq. NaOH before the solvent was removed *in vacuo* and the residue was purified by reverse phase column chromatography (water/MeOH) to give a white solid, 2-(2,4-dimethoxy-3-(methylsulfonyl)phenyl)-4-mesitylpyridine **79** (420 mg, 83%); m.pt. 155.8-160.8 ^{o}C, started to discolour at 148.7 ^{o}C; δ_H (400 MHz; $CDCl_3$; Me_4Si) 8.75 (1H, dd, *J* 5.0, 0.9), 8.05 (1H, d, *J* 8.9), 7.70 (1H, dd, *J* 1.6, 0.9), 7.09 (1H, dd, *J* 5.0, 1.6), 6.98 (1H, d, *J* 8.9), 6.96 (2 H, s), 4.00 (3 H, s), 3.61 (3 H, s), 3.33 (3 H, s), 2.33 (3 H, s), 2.03 (6 H, s); δ_C (101 MHz, $CDCl_3$, Me_4Si) 158.95, 158.44, 154.71, 150.38, 149.99, 137.74, 137.21,

136.22, 135.07, 128.45, 128.14, 125.69, 123.55, 123.44, 109.10, 63.42, 56.97, 46.25, 21.16, 20.74; HRMS (FTMS+ESI): calcd for $[C_{23}H_{25}NFO_4S+H]^+$: 412.1583. Found: 412.1564.

Iridium complex 80

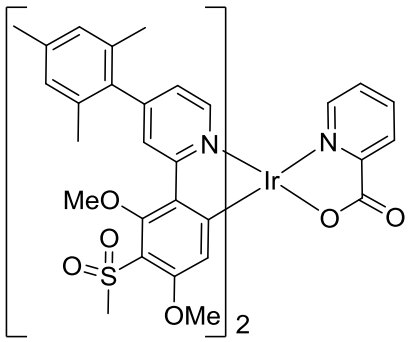

$[Ir(COD)Cl]_2$ (51 mg, 0.19 mmol) was added to a stirred solution of 2-(2,4-dimethoxy-3-(methylsulfonyl)phenyl)-4-mesitylpyridine **30** (130 mg, 0.32 mmol) in 2-ethoxyethanol (5 ml). The solution was heated to 130 ^oC under an argon atmosphere overnight, Picolinic acid (26 mg, 0.21 mmol) was added and the solution was heated at 130 ^oC for 6 h under an argon atmosphere. The solution was cooled and the solvent was removed *in vacuo*. The residue was purified by column chromatography (DCM/CH_3CN 2:1 v/v) to give a yellow solid, iridium complex **80** (70 mg, 40%); Anal. Calc. for $C_{52}H_{52}IrN_3O_{10}S_2.1.5CH_2Cl_2$: C, 50.89; H, 4.39; N, 3.33. Found: C, 50.43; H, 3.97; N, 3.08 δ_H (400 MHz; $CDCl_3$; Me_4Si) 8.84 (1H, d, *J*), 8.50 (1H, dd, *J* 1.8, 0.7 Hz), 8.45 (1H, d, *J* 7.7), 8.37 (1H, dd, *J* 1.8, 0.7), 8.04 (1H, td, *J* 7.8, 1.6), 7.84 (1H, d, *J* 5.3), 7.53 (1H, ddd, *J* 7.4, 5.4, 1.5), 7.45 (1H, d, *J* 5.9), 7.05 (1H, dd, *J* 5.9, 1.9), 7.04 – 6.96 (4H, m), 6.81 (1H, dd, *J* 5.9, 1.9), 5.83 (1H, s), 5.78 (1H, s), 3.92 (3H, s), 3.89 (3H, s), 3.55 (3H, s), 3.54 (3H, s), 3.49 (3H, s), 3.25 (3H, s), 3.20 (3H, s), 2.35 (6H, s), 2.11 (3H, s), 2.05 (3H, s), 2.00 (3H, s), 1.96 (3H, s); HRMS (FTMS+ESI): calcd for $[C_{52}H_{52}N_3O_{10}S_2{}^{191}Ir+H]^+$: 1134.2778. Found: 1134.2792.

Experimental details for chapter 4: Dual emissive phosphorescent materials for white light

(4-Methoxyphenyl)boronic acid 92[13]

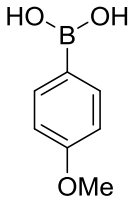

The reaction was conducted according to the literature method. Bromoanisole **91** (10.00 g, 53.5 mmol) was dissolved in dry THF (40 ml) and added dropwise to a stirring mixture of magnesium turnings (1.56 g, 64.2 mmol) in THF (25 ml, dry). A catalytic amount of iodine was added to initiate the reaction. Once addition was completer the mixture was heated to reflux for 3 h. The Grignard reagent was then diluted with THF (20 ml, dry) and added by cannula to a stirred solution of trimethyl borate (9.6 ml, 85.6 mmol in 20 ml of dry THF) at -10^oC, resulting in the formation of a white precipitate. The reaction mixture was stirred at 0 ^oC for 3 h and allowed to warm to room temperature overnight. The mixture was acidified to pH 1 with HCl (10 %) and extracted twice with EtOAc. The organic layers were dried over $MgSO_4$ and the solvent was removed *in vacuo*. The crude boronic acid was

washed with hexane to give a white solid, (4-methoxyphenyl)boronic acid **92** (8.12 g, 90%); δ_H (400s MHz; $CDCl_3$; Me_4Si) 8.13-8.21 (2H, m), 6.96-7.06 (2H, m), 3.90 (3H, s). NMR data are consistent with the literature data.[13]

4,4'-Dimethoxy-2-nitro-1,1'-biphenyl 94

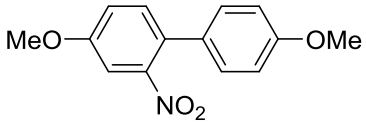

A solution of (4-methoxyphenyl)boronic acid **92** (3.60 g, 23.69 mmol) and 4-bromo-3-nitroanisole **93** (5.00 g, 21.55 mmol) in 1,4-dioxane (100 ml) was degassed with argon for 25 mins. An aqueous solution of Na_2CO_3 (2.97 g, 28.02 mmol in 14 ml) was degassed for 20 mins. The solutions were combined, degassed for a further 5 mins before $Pd(PPh_3)_4$ (498 mg, 0.43 mmol) was added. The mixture was heated to reflux under argon for 72 h before being cooled to RT. The volume of the solution was reduced by 75% before DCM (100 ml) and water (100 ml) were added. The layers were separated and the aqueous layer was futher washed with DCM (2 x 50 ml). The organic layers were combined, dried over $MgSO_4$ and the solvent removed *in vacuo*. The crude product was purified by trituration/recrystallisation from ethanol to give 4,4'-dimethoxy-2-nitro-1,1'-biphenyl **94** as a yellow-green crystalline solid (5.17 g, 92%); δ_H (400 MHz; $CDCl_3$; Me_4Si) 7.29-7.36 (2H, m), 7.18-7.24 (2H, m), 7.13 (1H, dd, *J* 8.6, 2.7), 6.90-6.97 (2H, m), 3.89 (3H, s), 3.84 (3H, s). NMR data are consistent with the literature data.[14]

2,7-Dimethoxycarbazole 95 [15]

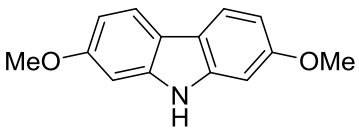

The reaction was conducted as described in the literature. 4,4'-dimethoxy-2-nitro-1,1'-biphenyl **94** (5.17 g, 19.9 mmol) and triethylphosphite (25 ml) were heated to 160 ^oC overnight under an atmosphere of argon (the yellow solution turned cloudy due to the formation of white crystals). The mixture was allowed to cool to RT and methanol was added (10 ml). The solution was left in an ice bath for 2 h before the solution was filtered and washed with cold MeOH to give a white crystalline material, 2,7-dimethoxycarbazole **95** (3.86 g, 85%); δ_H (400 MHz; $CDCl_3$; Me_4Si) 10.96 (1H, s), 7.83 (2H, d, *J* 8.5), 6.93 (2H, d, *J* 2.2), 6.72 (2H, dd, *J* 8.5, 2.2), 3.81 (6H, s). NMR data are consistent with the literature data.[15]

9-(2-Chloropyridin-4-yl)-2,7-dimethoxy-9H-carbazole 96

2,7-Dimethoxycarbazole **95** (3.16 g, 13.90 mmol) and 4-iodo-2-chloropyridine **21** (3.61 g, 13.91 mmol) were dissolved in 10 ml of dry DMF. Then, the reaction mixture was degassed by bubbling argon for 15 mins, following by an addition of CuI (0.77 g, 4.04 mmol), 1,10-phenanthroline (1.43 g, 7.93 mmol) and K_2CO_3 (3.84 g, 27.83 mmol). The reaction mixture was heat at 120 ^oC over the weekend. The solution was cooled and water was added. The precipitate was collected, dried and

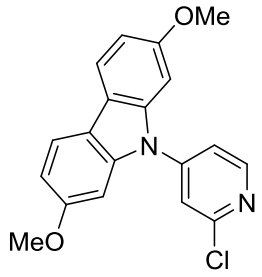

purified by column chromatography (DCM) to give 9-(2-chloropyridin-4-yl)-2,7-dimethoxy-9H-carbazole **96** (4.51 g, 96%) as a white solid; m.pt. 109.3-110.9 °C; δ_H (400 MHz; $CDCl_3$; Me_4Si) 8.62 (1H, dd, *J* 5.4, 0.6), 7.88 (2H, dd, *J* 8.6, 0.5), 7.63 (1H, dd, *J* 1.9, 0.6), 7.52 (1H, dd, *J* 5.4, 1.9), 6.98 (2H, d, *J* 2.2), 6.93 (2H, dd, *J* 8.5, 2.2), 3.87 (6H, s); δ_C (101 MHz; DMSO-d_6; Me_4Si) 158.65, 158.00, 152.43, 152.28, 147.51, 140.59, 121.04, 120.45, 117.89, 110.03, 95.23, 55.97; MS (ASAP+): *m/z* 338.1 (M_+, 100%).

9-(2-Chloropyridin-4-yl)-9H-carbazole-2,7-diol 97

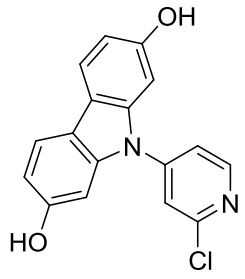

9-(2-Chloropyridin-4-yl)-2,7-dimethoxy-9H-carbazole **96** (4.51 g, 13.31 mmol) was dissolved in DCM (150 ml, dry) and the solution was cooled to 0 °C under an argon atmosphere. BBr_3 (20.01 g, 79.87 mmol) was slowly added over 10 mins. After 1 hour, the reaction was stopped by an addition of water (40 ml). The precipitate was collected, dried and recrystallised from ethanol to give **97** as a white solid (3.00 g, 72%); m.pt. 289.0-290.5 °C; δ_H (400 MHz; DMSO-d_6; Me_4Si) 9.53 (2H, br s), 8.65 (1H, d, *J* 5.4), 7.85 (1H, d, *J* 1.7), 7.83 (2H, d, *J* 8.4), 7.74 (1H, dd, *J* 5.4, 1.9), 6.89 (2H, d, *J* 2.0), 6.73 (2H, dd, *J* 8.4, 2.1); δ_C (151 MHz; DMSO-d_6; Me_4Si) 156.33, 152.23, 152.11, 147.81, 140.42, 120.65, 120.61, 120.06, 117.03, 110.80, 96.48; MS (ASAP+): *m/z* 310.1 (M+, 100%).

9-(2-Chloropyridin-4-yl)-2,7-bis(hexyloxy)-9H-carbazole 98

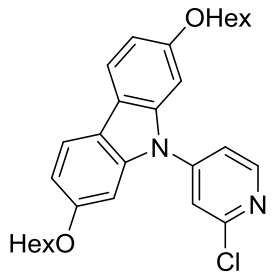

9-(2-Chloropyridin-4-yl)-9H-carbazole-2,7-diol **97** (2.46 g, 7.9 mmol) and K_2CO_3 (3.28 g, 23.7 mmol) was dissolved in DMSO (80 ml) and the solution was stirred at RT for 2 h. 1-bromohexane (3.32 ml, 23.7 mmol) was slowly added over 10 mins. The reaction mixture was stirred at RT overnight. The reaction was stopped by an addition of water (50 ml). The precipitate was collected, dried and purified by column chromatography (DCM) to give a white solid, 9-(2-chloropyridin-4-yl)-2,7-bis(hexyloxy)-9H-carbazole **98** (2.83 g, 75%) as a white solid; m.pt. 176.1-177.5 °C; δ_H (400 MHz; $CDCl_3$; Me_4Si) 8.61 (1H, dd, *J* 5.4, 0.6), 7.86 (2H, d, *J* 8.5), 7.61 (1H, dd, *J* 1.9, 0.6), 7.51 (1H, dd, *J* 5.4, 1.8), 6.87-7.00 (4H, m), 4.00 (4H, t, *J* 6.5), 1.81 (4H, dq, *J* 8.0, 6.6), 1.55 (3H, s), 1.28-1.42 (9H, m), 0.91 (6H, m); δ_C (176 MHz; $CDCl_3$; Me_4Si) 158.08, 153.18, 151.27, 147.86, 140.56, 120.73, 120.32, 119.22, 118.19, 109.64, 95.59, 68.66, 31.59, 29.30, 25.74, 22.57, 14.00; MS (ASAP+): *m/z* 478.2 (M+, 100%).

2,4-Difluoro-3-cyanophenylboronic acid 104

^{n}BuLi (13.8 ml, 2.5 M in hexanes) was added dropwise to a stirred solution of DIPA (5.24 ml, 37.3

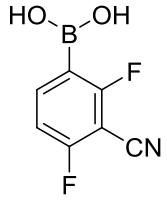

mmol) in THF (40 ml, dry) at 0 °C under argon. The solution was stirred at 0 °C for 30 min before the temperature was lowered to -78 °C. A solution of 2,6-difluorobenzonitrile **103** (4.00 g, 28.8 mmol) in THF (15 ml, dry) was added dropwise via cannula and the mixture was stirred at -78 °C for 1 h. Triisopropyl borate (9.95 ml, 43.1 mmol) was slowly added, and the reaction mixture was stirred at-78 °C for 1 h before being left to warm to RT overnight. Dilute HCl was added and the solution was extracted with EtOAc. The solvent was removed *in vacuo* to leave a sticky brown solid. The solids was redissolved in EtOAc and was extracted with aqueous KOH (150 ml). The aqueous layer was acidified to pH 5 with dilute HCl and extracted with EtOAc. The solvent was removed *in vacuo* to give a beige solid, 2,4-difluoro-3-cyanophenylboronic acid **104** (4.39 g, 84%); δ_H (400 MHz; acetone-d_6; Me_4Si) 8.13 (1H, dt, J 8.6 7.1), 7.71 (2H, s), 7.32 (1H, td, J 8.6 0.9); δ_F (376 MHz; acetone-d_6; Me_4Si) -98.62 (1F, d, J 6.6), -105.73 (1F, t, J 7.6); δ_B (400 MHz; acetone-d_6; Me_4Si) 27.22 (1B, s); NMR data are consistent with the literature data.[16]

2,6-Difluoro-3-(6-methyl-4,8-dioxo-1,3,6,2-dioxazaborocan-2-yl)benzonitrile 100

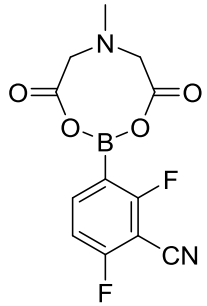

A mixture of **104** (4.39 g, 24.0 mmol), methyliminodiacetic acid (MIDA) (4.24 g, 28.8 mmol), DMSO (40 ml), and toluene (80 ml) was heated under reflux with a Dean Stark trap overnight. The mixture was cooled to room temperature, and water (50 ml) was added. The precipitate was filtered off, washed with water and dried under vacuum to give **100** as an off-white solid (5.10 g, 72%); δ_H (400 MHz; $CDCl_3$; Me_4Si) 7.82 (1H, q, *J* 7.5), 7.39 (1H, t, *J* 8.7), 4.40 (2H, d, *J* 17.3), 4.08 (2H, d, *J* 17.3), 2.62 (3H, s); δ_F (376 MHz; DMSO-d_6; Me_4Si) -97.74 (d, *J* 7.6), -104.91 (ddt, *J* 11.1, 6.6, 3.1); NMR data are consistent with the literature data.[16]

9-(2',6'-Difluoro-[2,3'-bipyridin]-4-yl)-2,7-bis(hexyloxy)-9H-carbazole 101

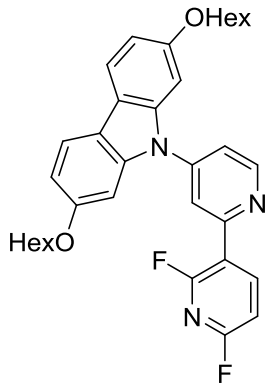

9-(2-Chloropyridin-4-yl)-2,7-bis(hexyloxy)-9H-carbazole **98** (0.80 g, 1.67 mmol), MIDA ester **99** (0.68 g, 2.50 mmol) and SPhos (0.11 g, 0.13 mmol) were dissolved 1,4-dioxane (20 ml) and the reaction mixture was degassed by bubbling argon for 15 mins, before $Pd(OAc)_2$ (30 mg, 0.13 mmol) was added. A degassed aquesous solution of K_3PO_4 (1.28 g, mmol in 4 ml) was added and the reaction mixture was heated to 60 °C for 18h. The solution was cooled and the solvent was removed *in vacuo*. The crude material was dissolved in DCM, which was washed with water before the solvent was removed. The crude material was purified by column chromatography (DCM) to give 9-(2',6'-difluoro-[2,3'-bipyridin]-4-yl)-2,7-bis(hexyloxy)-9H-carbazole **101** (0.81 g,

87%) as a white solid; δ_H (400 MHz; $CDCl_3$; Me_4Si) 8.92 (1H, dd, *J* 5.2, 0.7), 8.78 (1H, dt, *J* 9.7, 8.1), 8.10-8.16 (1H, m), 7.88 (2H, d, *J* 8.6), 7.60 (1H, dd, *J* 5.3, 2.0), 7.08 (2H, d, *J* 2.2), 7.05 (1H, dd, *J* 8.2, 3.0, 0.8), 6.92 (2H, dd, *J* 8.6, 2.2), 4.01 (4H, t, *J* 6.5), 1.81 (4H, dt, *J* 14.3, 6.7), 1.42-1.54 (4H, m), 1.22-1.40 (8H, m), 0.86-0.94 (6H, m); δ_F (376 MHz; $CDCl_3$; Me_4Si) -66.83 (ddd, *J* 10.5, 7.6, 3.0), -69.87 (1F, t, *J* 10.0); δ_C (151 MHz; $CDCl_3$; Me_4Si) 161.45 (dd, *J* 249.6, 14.8), 158.52 (dd, *J* 248.4, 14.2), 158.08, 152.50, 151.67, 146.45, 146.14, 140.65, 120.65 (d, *J* 10.3), 120.30, 119.46, 118.73 (d, *J* 23.8), 118.12, 109.94, 107.20 (d, *J* 34.3), 95.27, 68.56, 31.58, 29.32, 25.75, 22.58, 14.00; MS (ASAP+): *m/z* 557.3 (M+, 100%).

3-(4-(2,7-Bis(hexyloxy)-9H-carbazol-9-yl)pyridin-2-yl)-2,6-difluorobenzonitrile 102

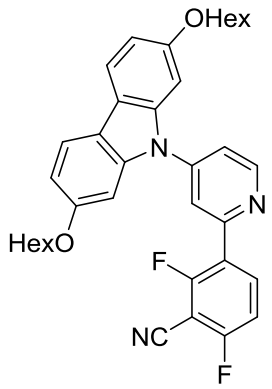

9-(2-Chloropyridin-4-yl)-2,7-bis(hexyloxy)-9H-carbazole **98** (1.00 g, 2.09 mmol), MIDA ester **100** (0.92 g, 3.13 mmol) and SPhos (137 mg, 0.33 mmol) were dissolved 1,4-dioxane (20 ml) and the reaction mixture was degassed by bubbling argon for 15 mins, before $Pd(OAc)_2$ (37 mg, 0.16 mmol) was added.. A degassed aquesous solution of K_3PO_4 (1.77 g, 8.34 mmol in 4 ml) was added and the reaction mixture was heated to 60 ^oC for 72 h. The solution was cooled and the solvent was removed *in vacuo*. The crude material was dissolved in DCM, which was washed with water before the solvent was removed. The crude material was purified by column chromatography (DCM) to give 3-(4-(2,7-bis(hexyloxy)-9H-carbazol-9-yl)pyridin-2-yl)-2,6-difluorobenzonitrile **102** (1.01 g, 83%) as a white solid; m.pt. 126.1-127.9 ^oC; δ_H (400 MHz; $CDCl_3$; Me_4Si) 8.93 (1H, dd, *J* 5.3, 0.7), 8.45 (1H, td, *J* 8.9, 6.4), 8.03-8.07 (1H, m), 7.88 (2H, d, *J* 8.5), 7.63 (1H, dd, *J* 5.3, 2.0), 7.25 (1H, ddd, *J* 9.0, 7.7, 1.2), 7.07 (2H, d, *J* 2.1), 6.93 (2H, dd, *J* 8.5, 2.2), 4.02 (4H, t, *J* 6.6), 1.82 (4H, dq, *J* 8.7, 6.6), 1.42-1.58 (4H, m), 1.27-1.42 (8H, m), 0.84-0.99 (6H, m); δ_F (376 MHz; $CDCl_3$; Me_4Si) -101.89 (1F, ddd, *J* 8.0, 6.4, 1.8), -108.04 (1F, dq, *J* 8.7, 1.9); δ_C (178 MHz; $CDCl_3$; Me_4Si) 163.51 (dd, *J* 265.0, 3.8), 160.7 (dd, *J* 263.8, 4.2), 158.27, 152.39 (d, *J* 1.8), 152.05, 146.65, 140.80, 137.21 (dd, *J* 9.9, 4.8), 124.44 (dd , *J* 10.0, 3.9), 121.16 (d, *J* 9.2), 120.53, 119.94, 118.34, 113.05 (dd, *J* 19.1, 4.0), 110.02, 109.06, 95.51, 93.30 (dd, *J* 20.5, 19.5), 68.78, 31.76, 29.50, 25.91, 22.75, 14.19; HRMS (FTMS+ESI): calcd for $[C_{36}H_{37}N_3F_2O_2+H]^+$: 582.2932. Found: 582.2931.

Ir complex 90

The reaction was conducted as described in the general procedure for synthesis of Iridium pic complexes, Method B. The following reagents were used in the stated quantities: $IrCl_3.3H_2O$ (150 mg, 0.43 mmol), **101** (500 mg, 0.90 mmol), picolinic acid (184 mg, 1.49 mmol) and 2-

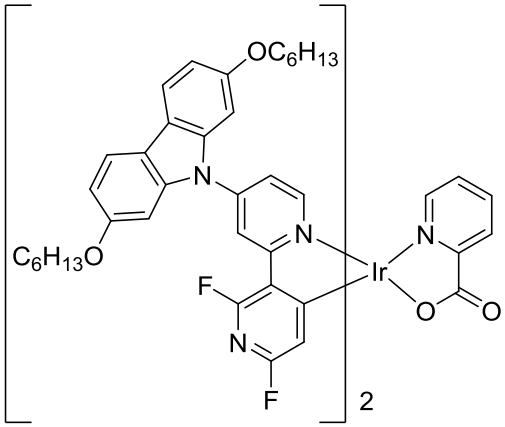

ethoxyethanol (20 ml). The reaction was worked up as described in the general procedure, and the residue was purified by column chromatography (4% EtOAc in DCM) to leave **30** as a yellow solid (55 mg, 9%); δ_H (400 MHz; $CDCl_3$; Me_4Si) 8.95 (1H, d, *J* 6.3), 8.65 (2H, dt, *J* 23.4, 2.4), 8.50 (1H, dt, *J* 7.8, 1.1), 8.14 (1H, td, *J* 7.7, 1.5), 7.99 (1H, dt, *J* 5.3, 1.2), 7.88 (2H, d, *J* 8.5), 7.87 (2H, d, *J* 8.5), 7.67 (2H, ddd, *J* 7.5, 3.9, 2.2), 7.58 (1H, d, *J* 6.4), 7.45 (1H, dd, *J* 6.4, 2.4), 7.18 (2H, d, *J* 2.0), 7.15 (2H, d, *J* 2.0), 6.96 (4H, dd, *J* 8.5, 2.0), 6.11 (1H, t, *J* 1.9), 5.84 (1H, t, *J* 1.9), 4.04 (8H, td, *J* 6.5, 4.7), 1.82 (8H, dtd, *J* 15.8, 6.4, 1.5), 1.41-1.58 (8H, m), 1.28-1.41 (16H, m), 0.82-0.96 (12H, m); δ_F (376 MHz; $CDCl_3$; Me_4Si) -67.83 (1F, dt, *J* 9.1, 2.1), -68.29 (1F, dd, *J* 9.1, 2.4), -68.63 (1H, dt, *J* 9.2, 2.3), -68.96 (1F, dd, *J* 9.1, 2.4); HRMS (FTMS+ESI): calcd for $[C_{74}H_{76}F_4{}^{191}IrN_7O_6+H]$: 1426.5477. Found: 1426.5470.

Ir complex 105

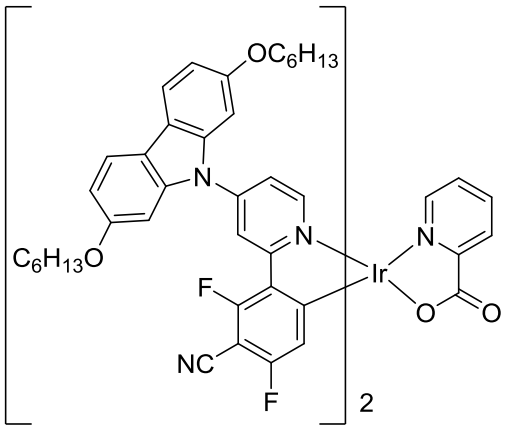

The reaction was conducted as described in the general procedure for synthesis of Iridium pic complexes, Method B. The following reagents were used in the stated quantities: $IrCl_3.3H_2O$ (75 mg, 0.21 mmol), **102** (260 mg, 0.45 mmol), picolinic acid (92 mg, 0.75 mmol) and 2-ethoxyethanol (15 ml). The reaction was worked up as described in the general procedure, and the residue was purified by column chromatography (4% EtOAc in DCM) to leave **105** as a yellow solid (40 mg, 13%); δ_H (400 MHz; $CDCl_3$; Me_4Si) 8.91 (1H, d, *J* 6.4), 8.69 (1H, t, *J* 2.6), 8.64 (1H, t, *J* 2.4), 8.49 (1H, d, *J* 7.8), 8.15 (1H, td, *J* 7.8, 1.6), 7.81-7.95 (5H, m), 7.63-7.74 (2H, m), 7.51-7.58 (1H, m), 7.48 (1H, dd, *J* 6.4, 2.4), 7.17 (2H, d, *J* 2.1), 7.15 (2H, d, *J* 2.1), 6.97 (4H, dd, *J* 8.5, 2.1), 6.26 (1H, d, *J* 8.1), 5.97 (1H, d, *J* 8.2), 4.05 (8H, td, *J* 6.6, 2.4), 1.78-1.90 (8H, m), 1.48-1.56 (8H, m) , 1.28-1.37 (16H, m), 0.80-0.98 (12H, m); δ_F (376 MHz; $CDCl_3$; Me_4Si) -101.18 (1F, dd, *J* 8.2, 4.2), -101.91 (1F, dd, *J* 8.2, 3.9), -105.62 (1F, d, *J* 4.3), -106.62 (1F, t, *J* 4.0); HRMS (FTMS+ESI): calcd for $[C_{78}H_{76}F_4{}^{191}IrN_7O_6]^+$: 1473.5399. Found: 1473.5367.

Bis(4-methoxyphenyl)amine 108

The reaction was conducted according to the literature method. *p*-Anisidine **107** (2.00 g, 16.24 mmol), *p*-bromoanisole **91** (1.76 ml, 14.00 mmol), $Pd_2(dba)_3$ (0.64 g, 0.70 mmol), dppf (0.78 g,

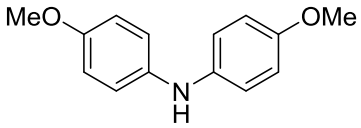

1.41mmol) and NaO^tBu (1.90 g, 19.77 mmol) were combined in toluene (20 ml, dry) and the solution was heated to 90 °C overnight under an argon atmosphere. The solution was cooled and water was added. The organic layer was separated, dried over $MgSO_4$ and the solvent removed. The residue was purified by column chromatography (1:4 EtOAc in hexanes) to give a white solid, bis(4-methoxyphenyl)amine **108** (2.00 g, 62%); δ_H (400 MHz; acetone-d_6; Me_4Si) 6.92-7.01 (4H, m), 6.76-6.88 (4H, m), 3.73 (6H, s). NMR data are consistent with the literature data.[17]

3,7-Dimethoxyphenothiazine 109

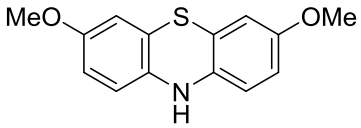

Sulfur (245 mg, 7.64 mmol) and iodine (194 mg, 0.76 mmol) were added to a stirred solution of bis(4-methoxyphenyl)amine (875 mg, 3.82 mmol) in 1,2-dichlorobenzene (10 ml). The solution was heated to reflux for 30 min under an argon atmosphere before being cooled to RT. The solution was applied directly to a silica column (gradient elution 0-20% EtOAc in hexane) to remove the solvent and purify the product. The product was obtained as an off white crystalline solid, 3,7-dimethoxyphenothiazine (300 mg, 30%); δ_H (400 MHz; acetone-d_6; Me_4Si) 7.42 (1H, br s), 6.69-6.62 (2H, m), 6.62-6.55 (4H, m), 3.70 (6H, s). NMR data are consistent with the literature data.[18]

10-(2-Chloropyridin-4-yl)-3,7-dimethoxy-10H-phenothiazine 110

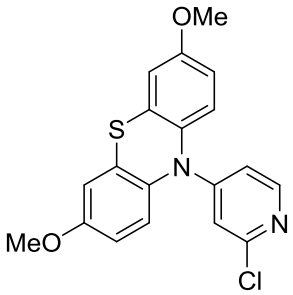

A solution of 3,7-dimethoxyphenothiazine **109** (0.78 g, 3.00 mmol) and 4-iodo-2-chloropyridine **21** (0.72 g, 3.00 mmol) in DMF (10ml, dry) was degassed with bubbling argon for 15 min. CuI (166 mg, 0.87 mmol), 1,10-phenanthroline (309 mg, 1.71 mmol) and K_2CO_3 (0.83 g, 6.02 mmol) were added and the solution was heated to 120 °C for 18 h under an atmosphere of argon. The solution was cooled and water was added, resulting in formation of a dark precipitate. The precipitate was filtered off and purified by column chromatography (1% NEt_3 in DCM) to give a white solid, 10-(2-chloropyridin-4-yl)-3,7-dimethoxy-10H-phenothiazine **110** (0.58 g, 52%); δ_H (400 MHz; CD_3OD; Me_4Si) 7.91 (1H, d, *J* 6.1), 7.48 (2H, d, *J*9.0), 7.16 (2H, d, *J* 2.4), 7.05 (2H, dt, *J* 8.8, 1.9), 6.80 – 6.72 (1H, dd, *J* 6.1, 2.3), 6.70 (1H, d, *J* 2.3), 3.87 (6H, s); δ_C (176 MHz; CD_3OD; Me_4Si) 159.94, 157.50, 152.82, 150.12, 137.70, 133.85, 129.45, 114.79, 114.75, 108.69, 108.25, 56.29; HRMS (FTMS+ESI): calcd for $[C_{19}H_{15}N_2O_2SCl+H]^+$: 371.0621. Found: 371.0611.

10-(2-Chloropyridin-4-yl)-10H-phenothiazine-3,7-diol 111

BBr_3 (0.58 ml, 6.15 mmol) was added cautiously to a stirred solution of 10-(2-chloropyridin-4-yl)-3,7-dimethoxy-10H-phenothiazine **110** (380 mg, 1.02 mmol) in DCM (10 ml, dry) cooled over an

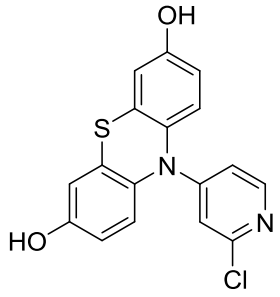

ice bath and under an argon atmosphere. The mixture was stirred at 0 °C for 1 h before water was added to quench the reaction. The precipitate was filtered and washed with water. The bulk of the material was used for the next step without further purification (350 mg, 100%); a small sample was recrystallised from methanol to give analytically pure 10-(2-chloropyridin-4-yl)-10H-phenothiazine-3,7-diol **111**; δ_H (400 MHz; CD_3OD; Me_4Si) 9.70 (1H, d, *J* 7.2), 9.08 (2H, d, *J* 8.6), 8.71 (1H, dd, *J* 7.3, 2.6), 8.67 (1H, d, *J* 2.5), 8.60 (2H, d, *J* 2.6), 8.49 (2H, dd, *J* 8.6, 2.7); δ_C (101 MHz; CD_3OD; Me_4Si) 160.15, 158.72, 144.54, 142.56, 136.79, 130.73, 128.15, 116.51, 116.27, 109.31; HRMS (FTMS+ESI): calcd for $[C_{17}H_{11}N_2O_2SCl+H]^+$: 343.0308. Found: 343.0310.

10-(2-Chloropyridin-4-yl)-3,7-bis(hexyloxy)-10H-phenothiazine 112

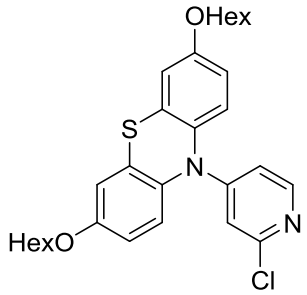

10-(2-Chloropyridin-4-yl)-10H-phenothiazine-3,7-diol **111** (443 mg, 1.29 mmol) was dissolved in DMSO (20 ml) and K_2CO_3 (540 mg, 3.91 mmol) was added. The solution was stirred for 2 h at RT before 1-bromohexane (0.54 ml, 3.88 mmol) was added. The solution was left to stir at RT overnight. Ethyl acetate was added and the organic phase was washed with brine to remove the DMSO. The solvent was removed *in vacuo* and the residue was purified by column chromatography (1% NEt_3 in DCM) to give an oily solid, 10-(2-chloropyridin-4-yl)-3,7-bis(hexyloxy)-10H-phenothiazine **112** (500 mg, 76%); δ_H (400 MHz; acetone-d_6; Me_4Si) 7.95 (1H, d, *J* 5.9), 7.53 (2H, d, *J* 8.7), 7.16 (2H, d, *J* 2.7), 7.05 (2H, dd, *J* 8.7, 2.8), 6.71 (1H, dd, *J* 5.9, 2.3), 6.67 (1H, d, *J* 2.3), 4.07 (4H, t, *J* 6.5), 1.85 – 1.73 (4H, m), 1.55 – 1.42 (4H, m), 1.42 – 1.22 (8H, m), 0.98 – 0.81 (6H, m); δ_C (176 MHz; acetone-d_6; Me_4Si) 158.78, 156.45, 152.83, 150.52, 137.01, 133.47, 129.43, 115.17, 114.94, 108.37, 107.70, 69.26, 32.39, 29.87, 26.40, 23.28, 14.30; HRMS (FTMS+ESI): calcd for $[C_{29}H_{35}N_2O_2SCl+H]^+$: 511.2186. Found: 511.2174.

2-Fluoro-3-pyridylboronic acid 115

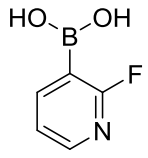

The reaction was conducted according to the literature procedure.[19] ^{n}BuLi (12.36 ml, 2.5 M) was added dropwise to a stirred solution of DIPA (4.69 ml, 33.50 mmol) in THF (40 ml, dry) at 0 °C under an atmosphere of argon. The solution was stirred for 30 min at 0 °C before the temperature was lowered to -78 °C. 2-Fluoropyridine **114** (2.22 ml, 25.75 mmol) was added dropwise and the solution was stirred at -78 °C for 1 h. $B(O^iPr)_3$ (8.90 ml, 38.60 mmol) was then added dropwise and the reaction was left to warm to RT overnight. Dilute NaOH was added and the aqueous layer was separated and acidified to pH 6 with conc HCl. The

aqueous layer was then extracted with EtOAc, and the solvent removed to give a product assumed to be crude 2-fluoro-3-pyridylboronic acid **115**. The material was used for the next step without further purification.

2-Fluoro-3-pyridylboronic MIDA ester 112

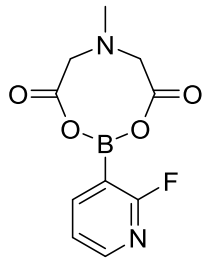

The crude boronic acid **115** (estimated 3.37 g, 23.9 mmol) and MIDA (4.22 g, 28.7 mmol) were dissolved in DMSO (40 ml) and toluene (80 ml) and the solution was heated to reflux (170 ^{o}C) overnight in a Dean-Stark apparatus. The solution was cooled and water (100 ml) was added. The precipitate was filtered and dried to give an off-white solid, 2-fluoro-3-pyridylboronic MIDA ester **112** (3.33 g, 51% for two steps); δ_H (400 MHz; DMSO-d_6; Me_4Si) 8.26 (1H, ddd, *J* 4.9, 2.1, 0.9), 8.00 (1H, ddd, *J* 9.4, 7.1, 2.1), 7.36 (1H, ddd, *J* 7.1, 4.9, 3.0), 4.43 (2H, dd, *J* 17.2, 1.0), 4.14 (2H, d, *J* 17.3), 2.65 (3H, s); δ_F (376 MHz; DMSO-d_6; Me_4Si) -60.50 (1F, dd, *J* 9.7, 2.9); δ_B (128 MHz; DMSO-d_6; Me_4Si) 10.65 (1B, s); δ_C (101 MHz; DMSO-d_6; Me_4Si) 168.87, 165.55 (d, *J* 235.0), 148.81 (d, *J* 15.0), 146.78 (d, *J* 8.4), 121.85 (d, *J* 4.07), 62.45, 47.49; HRMS (FTMS+ASAP): calcd for $[C_{10}H_{10}N_2O_4F^{10}B+H]^+$: 252.0832. Found: 252.0821.

10-(2'-Fluoro-[2,3'-bipyridin]-4-yl)-3,7-bis(hexyloxy)-10H-phenothiazine 113

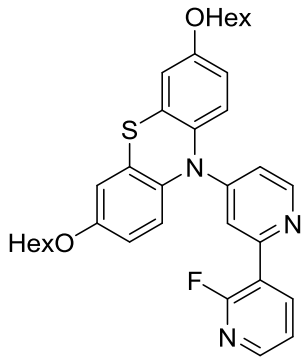

Method 1: A solution of 10-(2-chloropyridin-4-yl)-3,7-bis(hexyloxy)-10H-phenothiazine **111** (500 mg, 0.98 mmol), 2-fluoro-3-pyridylboronic MIDA ester **112** (370 mg, 1.47 mmol) and SPhos (64 mg, 0.16 mmol) in dioxane (20 ml) was degassed with bubbling argon for 15 min. $Pd(OAc)_2$ (18 mg, 0.08 mmol) was added, followed by a degassed solution of K_3PO_4 (1.50 g, 7.07 mmol in 4 ml) and the mixture was heated to 65 ^{o}C under an argon atmosphere overnight. The solution was cooled and the solvent removed *in vacuo*. The crude material was analysed by NMR and showed no sign of product. The 10-(2-chloropyridin-4-yl)-3,7-bis(hexyloxy)-10H-phenothiazine was reclaimed.

Method 2: A solution of 10-(2-chloropyridin-4-yl)-3,7-bis(hexyloxy)-10H-phenothiazine **111** (500 mg, 0.98 mmol), 2-fluoro-3-pyridylboronic MIDA ester **112** (370 mg, 1.47 mmol) and PPh_3 (62 mg, 0.24 mmol) in DME (20 ml) was degassed with bubbling argon for 15 min. $Pd(OAc)_2$ (13 mg, 0.06 mmol) was added, followed by a degassed solution of Na_2CO_3 (423 mg, 4.00 mmol in 4 ml) and the mixture was heated to reflux under an argon atmosphere overnight. The solution was cooled and the solvent removed *in vacuo*. The residue was purified by column chromatography (10-20% EtOAc in DCM) to give 10-(2'-fluoro-[2,3'-bipyridin]-4-yl)-3,7-bis(hexyloxy)-10H-phenothiazine **113**

(450 mg, 81%) as a viscous oil; δ_H (400 MHz; acetone-d_6; Me_4Si) 8.52 (1H, ddd, *J* 9.9, 7.5, 2.0), 8.31 (1H, dd, *J* 5.9, 0.6), 8.21 (1H, ddd, *J* 4.8, 2.0, 1.3), 7.56 (2H, d, *J* 8.7), 7.42 (1H, ddd, *J* 7.6, 4.8, 2.0), 7.39 – 7.36 (1H, m), 7.16 (2H, d, *J* 2.8), 7.07 (2H, dd, *J* 8.7, 2.8), 6.77 (1H, dd, *J* 5.9, 2.5), 4.07 (4H, t, *J*6.6), 1.79 (4H, dq, *J* 7.9, 6.6), 1.55 – 1.43 (4H, m), 1.43 – 1.28 (8H, m), 0.98 – 0.86 (6H, m); δ_F (376 MHz; acetone-d_6; Me_4Si) -70.74 (1F, d, *J* 10.0); δ_C (176 MHz; acetone-d_6; Me_4Si) 161.37 (d, *J* 238.1), 158.64, 154.78, 152.55 (d, *J* 6.8), 151.12, 148.30 (d, *J* 15.8), 142.37 (d, *J* 3.6), 137.04, 133.90, 129.60, 123.45 (d, *J* 26.1), 123.01 (d, *J* 4.25), 115.05, 114.86, 109.00 (d, *J* 10.85), 108.20, 69.24, 32.30, 29.89, 26.41, 23.29, 14.30; HRMS (FTMS+ESI): calcd for $[C_{34}H_{38}N_3O_2SF]^+$: 571.2669. Found: 571.2685.

Iridium complex 116

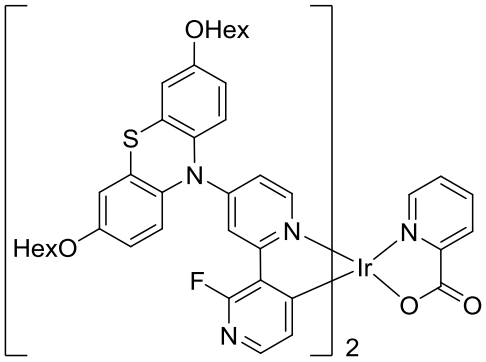

10-(2'-Fluoro-[2,3'-bipyridin]-4-yl)-3,7-bis(hexyloxy)-10H-phenothiazine **113** (450 mg, 0.79 mmol) was dissolved in toluene (10 ml, dry) and $IrCl_3.3H_2O$ (132 mg, mmol) was added. The mixture was heated to reflux overnight under an atmosphere of argon. Picolinic acid (92 mg, 0.75 mmol) was added and the solution was heated for a further 8 h before being cooled to RT. NMR analysis showed mostly the intermediate μ-dimer with little sign of complex or free ligand. The residue was redissolved in 2-ethoxyethanol (5 ml) and Na_2CO_3 (50 mg, 0.47 mmol) and picolinic acid (20 mg, 0.16 mmol) were added. The mixture was heated to 130 ^oC for 6 h before being cooled to RT. The solvent was removed *in vacuo* and the residue was purified by column chromatography (20% EtOAc in DCM) to give a yellow solid, iridium complex **116** (50 mg, 9%); Anal. Calc. for $C_{74}H_{78}F_2IrN_7O_6S_2$: C, 61.05; H, 5.40; N, 6.73. Found: C, 60.57; H, 5.38; N, 6.48; δ_H (400 MHz; acetone-d_6; Me_4Si) 8.20 (1H, d, *J* 6.9), 8.14 (1H, ddd, *J* 7.8, 1.6, 0.8), 8.07 (1H, td, *J* 7.6, 1.5), 7.86 (1H, t, *J* 3.2), 7.84 – 7.74 (2H, m), 7.65 (2H, d, *J* 8.7), 7.63 (2H, d, *J* 8.7), 7.57 (1H, ddd, *J* 7.2, 5.3, 1.6), 7.35 (1H, dd, *J* 5.1, 1.1), 7.32 (1H, dd, *J* 5.1, 1.1), 7.24 (1H, d, *J* 6.9), 7.18 (4H, dd, *J* 2.7, 0.8), 7.08 (2H, dd, *J* 8.7, 2.8), 7.07 (2H, dd, *J* 8.7, 2.8), 6.91 (1H, dd, *J* 6.9, 2.8), 6.66 (1H, dd, *J* 6.9, 2.9), 6.35 (1H, dd, *J* 5.1, 3.1), 6.16 (1H, dd, *J* 5.0, 3.2), 4.07 (8H, td, *J* 6.5, 3.1), 1.85 – 1.72 (8H, m), 1.52-1.42 (8H, m), 1.41 – 1.25 (16H, m), 0.95 – 0.80 (12H, m); MS (MALDI+): m/z = 1455.5 (M+, 100%).

Attempt 2: The above reaction was repeated using 10-(2'-fluoro-[2,3'-bipyridin]-4-yl)-3,7-bis(hexyloxy)-10H-phenothiazine **113** (250 mg, 0.44 mmol), $IrCl_3.3H_2O$ (73 mg, 0.21 mmol),

picolinic acid (51 mg, 0.41 mmol) and Na_2CO_3 (50 mg, 0.47 mmol) in diglyme (6 ml, dry). The reaction was worked up as previously described to give complex **116** (82 mg, 26%).

Iridium complex 117

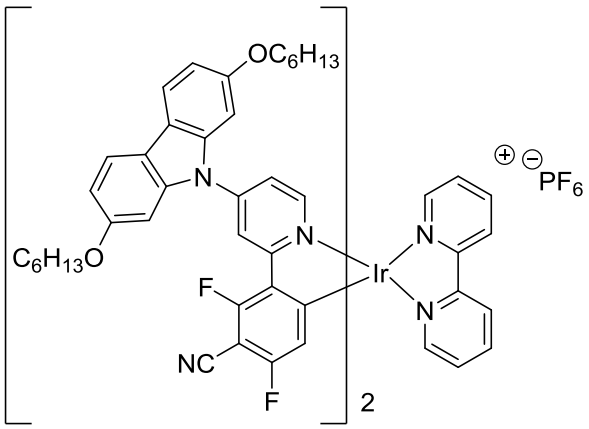

$IrCl_3.3H_2O$ (87 mg, 0.25 mmol) was added to a stirred solution of the **102** (300 mg, 0.52 mmol) in diglyme (6 ml). The mixture was heated to 130 ^oC under an atmosphere of argon overnight. The mixture was then left to cool and the solvent was removed *in vacuo*. The yellow solid, presumed to be the intermediate bis(μ-Cl)dimer complex, was then suspended in a DCM/MeOH mixture (1:1), and 2,2'-bipyridine (42 mg, 0.27 mmol), NH_4PF_6 (400 mg, 2.46 mmol) and $AgPF_6$ (30 mg, 0.12 mmol) and the solution was stirred at RT overnight. The precipitated AgCl was removed by filtration over Celite, and the solvent removed *in vacuo*. The residue was then purified by column chromatography (DCM/MeOH 1:1), and the resultant solid was washed with cold methanol to give **117** (96 mg, 24%); Anal. Calc. for $C_{82}H_{80}F_{10}IrN_8O_4P$: C, 59.52; H, 4.87; N, 6.77. Found: C, 59.41; H, 4.79; N, 6.68; δ_H (400 MHz; $CDCl_3$; Me_4Si) 8.65 (2H, t, *J* 2.5), 8.13-8.10 (2H, m), 7.98 (2H, d, *J* 5.1), 7.95 (2H, d, *J* 8.6), 7.88 (4H, d, *J* 8.5), 7.65 (2H, d, *J* 6.4), 7.60 (2H, t, *J* 6.7), 7.52 (2H, dd, *J* 6.5, 2.5), 7.13 (4H, d, *J* 2.1), 6.97 (4H, dd, *J* 8.6, 2.1), 6.01 (2H, d, *J* 7.9), 4.04 (8H, t, *J* 6.5), 1.81 (8H, p, *J* 6.6), 1.48 (8H, q, *J* 7.2), 1.38–1.32 (16H, m), 0.91 (12H, q, *J* 4.3, 3.8); δ_F (376 MHz; $CDCl_3$; Me_4Si) -72.40 (6F, *J* 713.9), -99.62 (2F), -104.92 (2F); HRMS (FTMS+ESI): calcd for $[C_{82}H_{80}F_4N_8O_4{}^{191}Ir]^+$: 1507.5845. Found: 1507.5798.

Experimental details for chapter 5: New ancillary ligands

Part 1:

4-Chloro-2-cyanopyridine-N-oxide 135 [20]

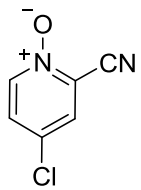

4-Nitro-α-picoline N-oxide **134** (25.00 g, 0.16 mol) was added slowly to stirred acetyl chloride (120 ml) which was cooled by an ice bath. The mixture was stirred at RT for 1.5 h then heated to 60 ^oC for 5 h. The solution was left to cool over the weekend. The acetyl chloride was evapourated *in vacuo* to give an oily residue which was taken up in water (100 ml) and neutralised with solid sodium carbonate. The precipitate was collected, washed with cold toluene and air dried. The aqueous filtrate was extracted with chloroform, and the residue from the extract was dissolved in the minimum amount of boiling

toluene, filtered and cooled (freezer) to give a second crop of the expected product. The solid obtained was recrystallised from toluene to give 4-chloro-2-cyanopyridine-N-oxide **135** (6.00 g, 23%); δ_H (400 MHz; $CDCl_3$; Me_4Si) 8.18 (1H, dd, *J* 7.2, 0.6), 7.63 (1H, dd, *J* 2.9, 0.6), 7.43 (1H, dd, *J* 7.1, 3.0). NMR data are consistent with the literature data.[20]

4-Chloro-2-cyanopyridine 136 [20]

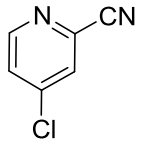

A solution of 4-chloro-2-cyanopyridine-N-oxide **135** (6.00 g, 38.82 mmol) in chloroform (50 ml) was treated with phosphorus trichloride (6.00 ml, 68.75 mmol) at RT for 2 h and then at reflux overnight. The mixture was poured into cold water (100 ml) and neutralised with solid sodium carbonate. The organic layer was separated, and the aqueous layer was further extracted with chloroform. The solvent was removed *in vacuo* and the residue was recrystallised from hexanes to give clear crystals of 4-chloro-2-cyanopyridine **136** (3.96 g, 73%); δ_H (400 MHz; $CDCl_3$; Me_4Si) 8.64 (1H, dd, *J* 5.3, 0.7), 7.73 (1H, dd, *J* 2.0, 0.7), 7.57 (1H, dd, *J* 5.4, 2.0). NMR data are consistent with the literature data.[20]

2-Acetyl-4-chloropyridine 137

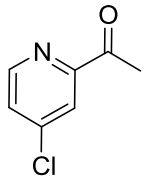

A solution of methylmagnesium chloride (12.6 ml, 3.0 M in THF) was added to a stirred solution of 4-chloro-2-cyanopyridine **136** (3.96 g, 28.6 mmol) in ether (300 ml, dry) dropwise over an ice bath. The resultant mixture was stirred at RT for 2.5 h and poured into aqueous 1 M ammonium chloride solution (300 ml). After acidification to pH 1 with conc. HCl the mixture was stirred for 1 h, neutralised with Na_2CO_3. DCM was added and the organic layer was separated. The aqueous layer was extracted with further DCM. The solvent was removed *in vacuo* and the product was distilled (b.pt. 50^{o}C at 0.6 mbar) giving a colourless oil which crystallised on standing, 2-acetyl-4-chloropyridine **137** (4.10 g, 92%); δ_H (400 MHz; $CDCl_3$; Me_4Si) 8.52 (1H, dd, *J* 5.2, 0.7), 8.04 (1H, dd, *J* 2.1, 0.6), 7.47 (1H, dd, *J* 5.2, 2.1), 2.72 (3H, s); NMR data are consistent with the literature data.[21]

1-(4-Mesitylpyridin-2-yl)ethanone 138

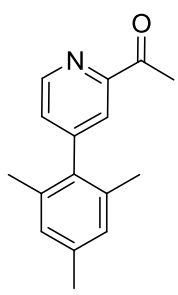

2-Acetyl-4-chloropyridine **137** (1.5 g, 9.68 mmol), 2,4,6-trimethylphenylboronic acid **22** (1.75 g, 10.67 mmol) and PPh_3 (657 mg, 2.50 mmol) were dissolved in DME (70 ml) and the solution was degassed for 20 min by bubbling with argon. Separately, an aqueous solution of Na_2CO_3 (4.18 g, 39.43 mmol in 17 ml) was degassed. The solutions were combined and $Pd(OAc)_2$ (130 mg, 0.58 mmol) was added. The mixture was heated to reflux overnight under an atmosphere of argon. The solution was then cooled to RT, and the majority of the solvent was removed *in vacuo*.

DCM and water were added, and the organic layer separated. The aqueous layer was extracted with further DCM, and the extracts combined and the solvent removed *in vacuo*. The crude residue was purified by column chromatography (DCM), followed by recrystallisation from hexane to give 1-(4-mesitylpyridin-2-yl)ethanone **138** (1.2 g, 52%); m.pt. 118.9-119.9 ^{o}C; δ_H (400 MHz; $CDCl_3$; Me_4Si) 8.74 (1H, dd, *J* 4.9, 0.8), 7.88 (1H, dd, *J* 1.7, 0.8), 7.31 (1H, dd, *J* 4.9, 1.7), 6.95 –6.94 (2H, m), 2.79 (3H, s), 2.33 (3H, s), 1.97 (6H, s); δ_C (101 MHz; $CDCl_3$; Me_4Si) 200.07, 153.73, 151.14, 149.18, 138.05, 135.64, 135.08, 128.61, 128.41, 123.06, 26.19, 21.19, 20.72; HRMS (FTMS+ESI): calcd for $[C_{16}H_{17}NO+H]^+$: 240.1388. Found: 240.1388.

4-Mesityl-2-(3-(trifluoromethyl)-1H-pyrazol-5-yl)pyridine 133

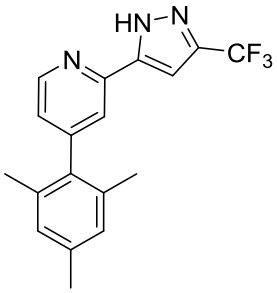

A solution of 4-mesityl-2-acetylpyridine **138** (1.20 g, 5.01 mmol) in THF (15 ml) was added dropwise to a stirred suspension of KO^{t}Bu (0.68 g, 6.06 mmol) in dry THF solution (30 ml), which was cooled in an ice bath. After 5 min ethyl trifluoroacetate (0.65 ml, 5.51 mmol) was added slowly. The solution was allowed to stir at 0 ^{o}C for 15 mins before being removed from the ice bath. The mixture was heated to reflux overnight before being cooled, and the solvent was removed under reduced pressure. Water (30 ml) was added to the resulting solid and the resulting suspension was neutralised with conc. HCl. The solution was then extracted with DCM. The organic phase was dried over $MgSO_4$ and the solvent removed to give the presumed 1,3-dione intermediate **139** (not characterised). This was dissolved in ethanol (30 ml) and hydrazine hydrate (0.34 ml, 95%) was added. The solution was heated to reflux overnight before the solvent was removed *in vacuo*. The residue was dissolved in DCM and washed with water to remove unreacted hydrazine hydrate. The solvent was removed, and the oily residue was redissolved in ethanol and conc. HCl (0.5 ml) was added (to prompt complete dehydration). The solution was heated to reflux for 5 h, before being cooled and the solvent removed. The crude solid was dissolved in DCM and washed with water, before being dried over $MgSO_4$ and concentrated *in vacuo*. The crude solid was purified by column chromatography (1:3 EtOAc:DCM) followed by recrystallisation from hot hexane to give an off-white solid, 4-mesityl-2-(3-(trifluoromethyl)-1H-pyrazol-5-yl)pyridine **133** (277 mg, 20%); m.pt. 171.1-172.9 ^{o}C; δ_H (400 MHz; $CDCl_3$; Me_4Si) 11.95 (1H, br s), 8.70 (1H, dd, *J* 5.0, 0.9), 7.47 (1H, dd, *J* 1.5, 0.9), 7.15 (1H, dd, *J* 5.0, 1.5), 6.96-7.00 (2H, m), 6.91 (1H, s), 2.35 (3H, s), 2.02 (6H, s); δ_F (376 MHz; $CDCl_3$; Me_4Si) -62.34 (3F, s); δ_C (101 MHz; $CDCl_3$; Me_4Si) 151.57, 149.86, 146.91, 144.61, 144.23, 143.10, 138.08, 135.43, 134.97, 128.52, 125.07, 122.48, 121.40, 119.81, 101.34, 21.06, 20.57; HRMS (FTMS+ESI): calcd for $[C_{18}H_{16}N_3F_3+H]^+$: 332.1375. Found: 332.1379.

Iridium complex 140

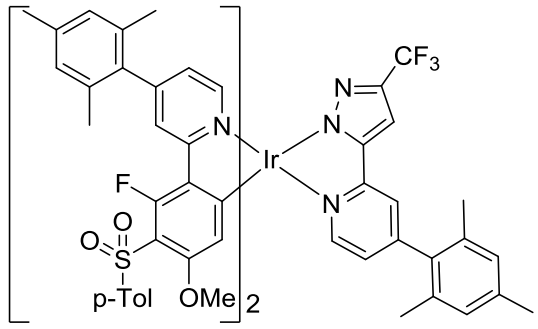

$IrCl_3.3H_2O$ (66 mg, 0.19 mmol) was added to a stirred solution of 2-(2-fluoro-4-methoxy-3-tosylphenyl)-4-mesitylpyridine **66** (169 mg, 0.38 mmol) in 2-ethoxyethanol (5 ml). The solution was heated to 130 °C under an argon atmosphere overnight, during which a bright yellow precipitate formed, presumed to be the dichloro bridged dimer. The solvent was removed *in vacuo*and the precipitate was redissolved in DCM/ethanol (20 ml, 3:1). 4-mesityl-2-(3-(trifluoromethyl)-1H-pyrazol-5-yl)pyridine **133** (77 mg, 0.28 mmol) was added and the solution was heated at 60°C overnight under an argon atmosphere. The solution was cooled and the solvent was removed *in vacuo*. The residue was purified by column chromatography (EtOAc in DCM, 2.5% increased to 4%) to give a yellow solid, iridium complex **140** (190 mg, 70%); Anal. Calc. for $C_{74}H_{65}F_5IrN_5O_6S_2$: C, 60.39; H, 4.45; N, 4.76. Found: C, 59.44; H, 4.42; N, 4.62; δ_H (400 MHz; $CDCl_3$; Me_4Si) 8.12-8.17 (1H, m), 8.03-8.08 (1H, m), 7.89 (2H, d, *J* 8.2), 7.88 (2H, d, *J* 8.2), 7.67 (1H, d, *J* 5.9), 7.64 (1H, d, *J* 5.9), 7.59 (1H, dd, *J* 1.7, 0.8), 7.57 (1H, d, *J* 5.9), 7.27 (4H, t, *J* 8.7 Hz), 7.02 – 6.89 (8H, s), 6.78 (2H, td, *J* 6.1, 1.8), 5.79 (1H, s), 5.74 (1H, s), 3.47 (3H, s), 3.44 (3H,s) 2.39 (3H, s), 2.38 (3H, s), 2.34 (3H, s), 2.33 (6H, s), 2.09 (3H, s), 2.01 (3H, s), 1.98 (3H, s), 1.97 (3H, s), 1.86 (6H, s); %); δ_F (376 MHz; $CDCl_3$; Me_4Si)-59.87 (3F, s), -110.50 (1F, s), -111.36 (1F, s); HRMS (FTMS+ESI): calcd for $[C_{74}H_{65}N_5F_5O_6S_2{}^{191}Ir+H]^+$: 1470.3981. Found: 1470.3995.

Iridium complex 141

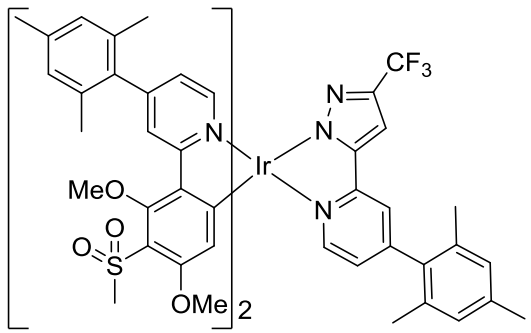

$[Ir(COD)Cl]_2$ (90 mg, 0.13 mmol) was added to a stirred solution of 2-(2,4-dimethoxy-3-(methylsulfonyl)phenyl)-4-mesitylpyridine **79** (226 mg, 0.55 mmol) in 2-ethoxyethanol (5 ml). The solution was heated to 130 °C under an argon atmosphere overnight before being cooled to RT. Water was added and a yellow precipitate formed which was filtered, washed with further water and dried. The precipitate, presumed to be the intermediate dichloro bridged dimer, was dissolved in DCM/ethanol (40 ml, 3:1) and 4-mesityl-2-(3-(trifluoromethyl)-1H-pyrazol-5-yl)pyridine **133** (90 mg, 0.27 mmol) was added and the solution was heated at 55 °C overnight under an argon atmosphere. The solution was cooled and the solvent was removed *in vacuo*. The residue was purified by column chromatography (EtOAc in DCM gradient elution from 0% to 15%) to give a yellow solid, iridium complex **141** (98 mg, 27%);

δ_H (400 MHz; CD_2Cl_2; Me_4Si) 8.47 (1H, d, *J* 1.4), 8.38 (1H, d, *J* 1.4), 7.80 – 7.74 (3H, m), 7.65 (1H, dd, *J* 1.8, 0.8), 6.98 (6H, s), 6.95 (3H, s), 6.91 (1H, dd, *J* 5.7, 1.8), 6.84 (1H, dd, *J* 5.9, 1.9), 6.81 (1H, dd, *J* 5.9, 1.9), 6.03 (1H, s), 6.01 (1H, s), 3.88 (3H, s), 3.85 (3H, s), 3.61 (3H, s), 3.60 (3H, s), 3.22 (3H, s), 3.19 (3H, s), 2.33 (3H, s), 2.32 (3H, s), 2.31 (3H, s), 2.09 (3H, s), 2.06 (3H, s), 2.05 (3H, s), 2.01 (3H, s), 1.88 (3H, s), 1.85 (3H, s); δ_F (376 MHz; $CDCl_3$; Me_4Si) -58.48 (3F, s); HRMS (FTMS+ESI): calcd for $[C_{64}H_{63}F_3N_5O_8S_2{}^{191}Ir+H]^+$: 1342.3754. Found: 1342.3802.

Part 2:

2-Hydroxy-N-(2'-hydroxyethyl)benzamide 155 [22]

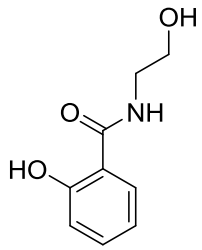

The reaction was conducted as described in the literature.[22] Methyl salicylate **153** (4.26 g, 28.00 mmol) and 2-aminoethanol **154** (1.62 ml, 26.85 mmol) were combined and heated to reflux (~170 °C) for 2 h before the solution was cooled to RT and the methanol produced was removed by vacuum distillation. The crude residue was purified by column chromatography (30:70 EtOAc:DCM to remove impurities, increased to 5:25:70 MeOH:EtOAc:DCM to elute the product) to give a crystalline white solid, 2-hydroxy-N-(2'-hydroxyethyl)benzamide **155** (3.98 g, 82%); δ_H (400 MHz; CD_2Cl_2; Me_4Si) 12.27 (1H, br s), 7.47 – 7.36 (2H, m), 6.98 – 6.91 (1H, dd, *J* 8.4, 1.1), 6.87 (1H, ddd, *J* 7.9, 7.3, 1.2), 6.85 (1H, br s), 3.81 (2H, dd, *J* 5.7, 4.6), 3.60 (2H, td, *J* 5.7, 4.6), 2.13 (1H, br s). NMR data is consistent with

2-(2'-Hydroxyphenyl)-2-oxazoline 152

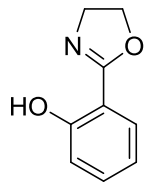

2-Hydroxy-N-(2'-hydroxyethyl)benzamide **155** (3.98 g, 21.98 mmol) was suspended in DCM (100 ml) and $SOCl_2$ (3.19 ml, 43.96 mmol) was added with caution. The solution was stirred under an atmosphere of argon overnight before the HCl salt of the desired product was filtered off and neutralised with a saturated $NaHCO_3$ solution. The aqueous solution was extracted with diethyl ether (3 x 100 ml) and the solvent removed to leave a pale pink oil which solidified on standing. 2-(2'-Hydroxyphenyl)-2-oxazoline **152** (3.39 g, 94%); δ_H (400 MHz; $CDCl_3$; Me_4Si) 12.18 (1H, br s), 7.65 (1H, dd, *J* 7.8, 1.8), 7.37 (1H, ddd, *J* 8.4, 7.3, 1.8), 7.02 (1H, dd, *J* 8.4, 0.9), 6.87 (1H, ddd, *J* 7.8, 7.3, 0.9), 4.49 – 4.40 (2H, m), 4.16 – 4.07 (2H, m). NMR data are consistent with the literature data.[22]

Iridium complex 145

$IrCl_3.3H_2O$ (209 mg, 0.59 mmol) was added to a stirred solution of 2-(2,4-difluorophenyl)pyridine **13** (250 mg, 1.31 mmol) in 2-ethoxyethanol (6 ml) under argon. The solution was heated to 135 °C for 6 h, before 2-(2'-hydroxyphenyl)-2-oxazoline **152** (121 mg, 0.74 mmol) and Na_2CO_3 (315 mg,

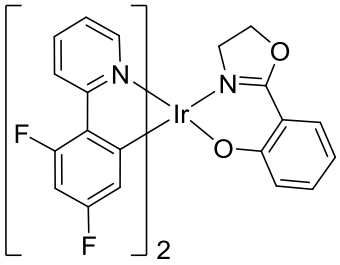

2.97 mmol) were added and the solution was heated to 135 °C overnight. Water was added and the yellow precipitate was collected by filtration. The residue was purified by column chromatography (hexane:EtOAc 4:1) to give complex **145** as a yellow solid (310 mg, 79%); Anal. Calc. for $C_{31}H_{20}F_4IrN_3O_2$: C, 50.68; H, 2.74; N, 5.72. Found: C, 50.43; H, 3.07; N, 5.47; δ_H (400 MHz; CD_2Cl_2; Me_4Si) 8.78 (1H, d, *J* 5.2), 8.39 (1H, d, *J* 5.8), 8.26 (2H, t, *J* 8.9), 7.87 – 7.75 (2H, m), 7.61 (1H, d, *J* 8.1), 7.21 (1H, t, *J* 6.6), 7.14 (2H, t, *J* 7.0), 6.60 (1H, d, *J* 8.7), 6.45 – 6.32 (3H, m), 5.79 (1H, dd, *J* 8.9, 2.3), 5.62 (1H, dd, *J* 8.9, 2.4), 4.36 (1H, q, *J* 9.3), 4.23 (1H, q, *J* 8.5), 3.64 – 3.47 (1H, m), 3.14 – 3.00 (1H, m); δ_F (376 MHz CD_2Cl_2; Me_4Si) -109.30 (1F, q, *J* 9.1), -109.34 (1F, q, *J* 9.3), -110.90 (1F, ddd, *J* 12.4, 10.1, 1.6), -110.95 (1F, ddd, *J* 12.5, 10.1, 2.5); HRMS (FTMS+ESI): calcd for $[C_{31}H_{20}F_4N_3O_2{}^{191}Ir+H]^+$: 734.1176. Found: 734.1186. Crystals for X-ray analysis were grown by slow evaporation of a DCM/Methanol solution of **145**.

3,6-Di-tert-butyl-9H-carbazole

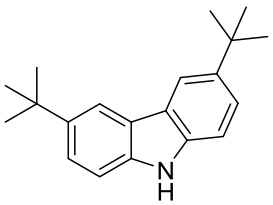

$ZnCl_2$ (4.84 g, 35.50 mmol) was added to a degassed solution of carbazole (2.00 g, 11.96 mmol) in CH_3NO_2 (60 ml) under argon. ^tBuCl (2.6 ml, 23.92 mmol) was added dropwise and the solution was stirred at RT for 2 h. Water (50 ml) was added and the organic layer was separated and washed with further water (2 x 50 ml) before the solvent was removed *in vacuo*. The product was recrystallised from hexane to give a white solid (0.65 g, 19%); δ_H (400 MHz; $CDCl_3$; Me_4Si) 8.07 (2H, d, *J* 1.9), 7.87 (1H, br s), 7.46 (2H, dd, *J* 8.5, 1.9), 7.34 (2H, dd, *J* 8.6, 0.7), 1.45 (18H, s); NMR data are consistent with the literature data.[23]

3,6-Di-tert-butyl-9-(2-chloropyridin-4-yl)-9H-carbazole 149

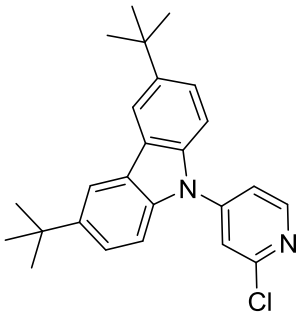

3,6-Di-tert-butyl-9H-carbazole **148** (0.65 g, 2.32 mmol), 2-chloro-4-iodopyridine **21** (0.56 g, 2.32 mmol) and 1,10-phenanthroline (0.24 g, 1.33 mmol) were dissolved in DMF (10 ml, dry) and the solution was degassed for 15 min. CuI (0.13 g, 0.67 mmol) and K_2CO_3 (0.64 g, 4.65 mmol) were added and the solution was heated to 120 °C overnight under an argon atmosphere. The solution was cooled to RT and brine (50 ml) and DCM (50 ml) were added. The phases were separated and the aqueous phase was extracted with further DCM (50 ml). The organic phases were combined and the solvent removed *in vacuo*. The residue was purified by column chromatography (hexane: EtOAc 6:1) to give a white solid, 3,6-di-tert-butyl-9-(2-chloropyridin-4-yl)-9H-carbazole **149** (0.72 g, 79%); m.pt. 175.1-177.2

^{o}C; δ_H (700 MHz; $CDCl_3$; Me_4Si) 8.57 (1H, d, *J* 5.3), 8.11 (2H, dd, *J* 1.9, 0.8), 7.64 (1H, d, *J* 1.8), 7.55 – 7.49 (5H, m), 1.47 (18H, s); δ_C (176 MHz; $CDCl_3$; Me_4Si) 153.18, 151.21, 148.37, 144.94, 137.60, 124.73, 124.39, 120.11, 118.72, 116.79, 109.53, 34.97, 32.04; HRMS (FTMS+ESI): calcd for $[C_{25}H_{27}N_2Cl+H]^+$: 391.1941. Found: 391.1943.

3,6-Di-tert-butyl-9-(2-phenylpyridin-4-yl)-9H-carbazole 151

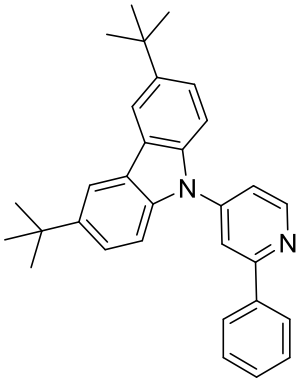

3,6-Di-tert-butyl-9-(2-chloropyridin-4-yl)-9H-carbazole **149** (400 mg, 1.02 mmol) and phenylboronic acid **150** (187 mg, 1.53 mmol) were dissolved in a mixture of toluene (7 ml), EtOH (1.5 ml) and water (7 ml) and the solution was degassed with bubbling argon for 10 min. $Pd(PPh_3)_4$ (71 mg, 1.02 mmol) and Na_2CO_3 (400 mg, 4.17 mmol) were added and the solution was heated to reflux overnight before being cooled to RT. The organic phase was separated and the aqueous layer was extracted with EtOAc (2 x 50 ml). The organic phases were combined, dried over $MgSO_4$ and the solvent was removed *in vacuo*. The residue was purified by column chromatography (hexane:EtOAc 6:1) to give an off-white solid, **151** (460 mg, 58%); m.pt. 176.3-177.0 ^{o}C; δ_H (700 MHz; $CDCl_3$; Me_4Si) 8.89 (1H, d, *J* 5.3), 8.15 (2H, d, *J* 1.9), 8.09 – 8.05 (2H, m), 8.02 (1H, d, *J* 2.0), 7.57 (2H, d, *J* 8.6), 7.55 – 7.50 (5H, m), 7.50 – 7.45 (1H, m), 1.48 (18 H, s); δ_C (176 MHz; $CDCl_3$; Me_4Si) 147.16, 144.45, 137.99, 129.10, 127.25, 124.52, 124.25, 120.88, 118.58, 117.09, 116.74, 115.44, 109.59, 96.05, 34.97, 32.09; HRMS (FTMS+ESI): calcd for $[C_{31}H_{32}N_2+H]^+$: 433.2644. Found: 433.2616.

Iridium complex 146

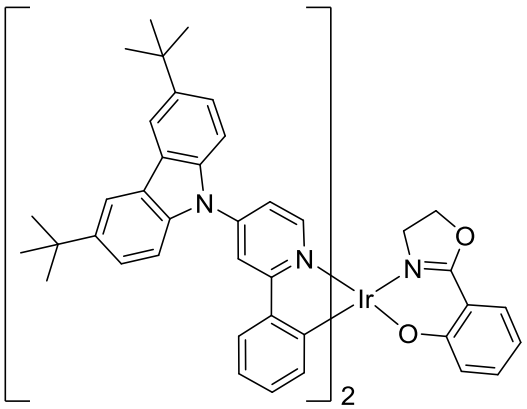

$IrCl_3.3H_2O$ (170 mg, 0.48 mmol) was added to a stirred solution of 3,6-di-tert-butyl-9-(2-phenylpyridin-4-yl)-9H-carbazole **151** (460 mg, 1.06 mmol) and the solution was heated to 135 ^{o}C overnight. 2-(2'-hydroxyphenyl)-2-oxazoline **152** (99 mg, 0.61 mmol) and Na_2CO_3 (256 mg, 2.41 mmol) were added and the solution was heated to 135 ^{o}C for 8 h before being cooled to RT. Water (5 ml) was added and the precipitate was filtered off and dried. The precipitate was purified by column chromatography (hexane:EtOAc 7:1). The product from the column was stirred in hot MeOH, allowed to cool, and filtered. This was repeated to remove soluble impurities. The product

146 was obtained as an orange-yellow solid (109 mg, 19%); δ_H (400 MHz; $CDCl_3$; Me_4Si) 9.09 (1H, d, *J* 6.3), 8.58 (1H, d, *J* 6.3), 8.24 – 8.13 (6H, m), 7.79 – 7.72 (3H, m), 7.72 – 7.65 (2H, m), 7.65 – 7.54 (6H, m), 7.52 (1H, dd, *J* 6.3, 2.3), 7.38 (1H, dd, *J* 6.3, 2.3), 7.23 (1H, ddd, *J* 8.8, 6.7, 2.0), 6.97 – 6.78 (5H, m), 6.60 (1H, dd, *J* 7.5, 1.3), 6.50 (1H, dd, *J* 6.6, 1.9), 6.46 (1H, ddd, *J* 8.1, 6.8, 1.2), 4.42 (1H, q, *J* 9.3), 4.35 (1H, dt, *J* 10.4, 8.2), 3.71 (1H, ddd, *J* 14.0, 10.2, 7.6), 3.21 (1H, dt, *J* 14.0, 10.1), 1.56 (3H, d, *J* 3.3); HRMS (FTMS+ASAP): calcd for $[C_{71}H_{70}N_5O_2{}^{191}Ir]^+$: 1215.5136. Found: 1215.5104.

2-(Oxazol-2-yl)phenol 156

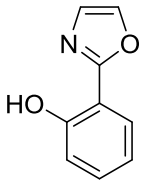

MnO_2 (5.00 g, 57.52 mmol) was added to a stirred solution of 2-(2'-hydroxyphenyl)-2-oxazoline **152** (500 mg, 3.06 mmol) in toluene (20 ml) and the mixture was heated to reflux for 5 h. The mixture was cooled to RT and filtered through a celite plug (DCM) and the solvent was removed *in vacuo*. The residue was purified by column chromatography (DCM) to give a white solid, 2-(oxazol-2-yl)phenol **156** (140 mg, 28%); δ_H (700 MHz; $CDCl_3$; Me_4Si) 11.20 (1H, s), 7.84 (1H, dd, *J* 7.8, 1.7), 7.69 (1H, t, *J* 0.9), 7.39 – 7.34 (1H, m), 7.24 (1H, d, *J* 1.0), 7.08 (1H, dd, *J* 8.3, 1.2), 6.95 (1H, td, *J* 7.5, 1.0); δ_C (176 MHz; $CDCl_3$; Me_4Si) 161.78, 157.35, 137.49, 132.47, 126.51, 126.08, 119.52, 117.31, 111.25; HRMS (FTMS+ESI): calcd for $[C_9H_7NO_2+H]^+$: 162.0555. Found: 162.0542.

N-(2,2-diethoxyethyl)-2-methoxybenzamide 159

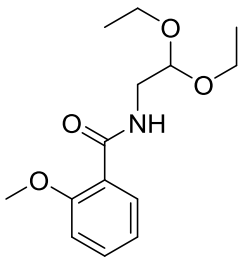

Methyl-2-methoxybenzoate **157** (5.00 g, 28.93 mmol) and aminoacetaldehyde diethylacetal **158** (2.78 g, 17.25 mmol) were combined and the mixture was heated to 160 ^oC for 4 h before being cooled to RT. A crude NMR showed the reaction had not gone to completion, more aminoacetaldehyde diethylacetal **158** (1.00 g, 6.20 mmol) was added and the reaction was heated to 160 ^oC overnight before being cooled to RT. Any methanol produced was removed by rotary evaporation and the oily residue was purified by column chromatography (hexane:EtOAc 1:1) to give an oil, N-(2,2-diethoxyethyl)-2-methoxybenzamide **159** (2.80 g, 36%); δ_H (400 MHz; $CDCl_3$; Me_4Si) 8.21 (1H, dd, *J* 7.8, 1.9), 8.15 (1H, br t, *J* 5.5), 7.45 (1H, ddd, *J* 8.3, 7.3, 1.8), 7.08 (1H, ddd, *J* 7.8, 7.3 1.0), 6.98 (1H, dd, *J* 8.4, 1.0), 4.63 (1H, t, *J* 5.6), 3.97 (3H, s), 3.76 (dq, *J* 9.4, 7.0), 3.67 – 3.54 (4H, m), 1.25 (6H, t, *J* 7.0); HRMS (FTMS+ESI): calcd for $[C_{14}H_{21}NO_4+Na]^+$: 290.1368. Found: 290.1368. The carbon NMR could not be obtained as **159** hydrolysed to the aldehyde in the NMR solvent; δ_H (600 MHz; $CDCl_3$; Me_4Si) 9.76 (1H, d, *J* 0.6), 8.64 (1H, br s), 8.21 (1H, dd, *J* 7.7, 1.9), 7.51 – 7.45 (1H, m), 7.09 (1H, t, *J* 7.6), 7.01 (1H, d, *J* 8.4), 4.41 (2H, dd, *J* 4.8, 0.7), 4.03 (3H, d, *J* 0.6); δ_C (151 MHz; $CDCl_3$; Me_4Si) 196.97, 165.69, 157.96, 133.45, 132.52,

121.48, 120.70, 111.55, 56.20, 51.15.

2-(2-Methoxyphenyl)oxazole 160 and 2-(2-methoxy-5-(methylsulfonyl)phenyl)oxazole 161

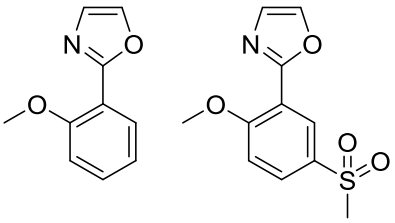

Methanesulfonic acid (35 ml) was added cautiously to N-(2,2-diethoxyethyl)-2-methoxybenzamide **159** (2.80 g, 11.70 mmol) with stirring. P_4O_{10} (4.50 g, 15.85 mmol) was added with caution and the mixture was heated to 180 ^oC overnight. The mixture was cooled to RT and added dropwise to aq. $NaHCO_3$ solution (300 ml) with stirring. The aqueous phase (pH 8) was extracted with DCM (3 x 400 ml) and the solvent was removed *in vacuo* to leave a thick oil. The residue was purified by column chromatography (10-20% EtOAc in DCM) to give the product as a yellow oil **160** (400 mg, 19%); δ_H (400 MHz; $CDCl_3$; Me_4Si) 7.98 (1H, dd, *J* 8.1, 1.8), 7.76 (1H, d, *J* 0.8), 7.46 (1H, ddd, *J* 8.3, 7.4, 1.8), 7.31 (1H, d, *J* 0.8), 7.04- 7.11 (2H, m), 4.00 (3H, s); δ_C (151 MHz; $CDCl_3$; Me_4Si) 160.44, 157.67, 138.31, 138.27, 131.90, 130.41, 128.28, 120.79, 116.61, 112.10, 56.20; HRMS (FTMS+ESI): calcd for $[C_{10}H_9NO_2+H]^+$: 176.0712. Found: 176.0740.

Also isolated as a second fraction was 2-(2-methoxy-5-(methylsulfonyl)phenyl)oxazole **161** (538 mg, 18%); δ_H (400 MHz; $CDCl_3$; Me_4Si) 8.54 (1H, dd, *J* 2.4, 0.8), 8.01 (1H, ddd, *J* 8.8, 2.4, 0.8), 7.78 (1H, d, *J* 0.8), 7.33 (1H, s), 7.18 (1H, d, *J* 8.8), 4.07 (3H, s), 3.09 (3H, s); δ_C (151 MHz; $CDCl_3$; Me_4Si) 161.29 , 139.10 , 131.21 , 130.18 , 128.69 , 112.49 , 56.85 , 44.94 . HRMS (FTMS+ESI): calcd for $[C_{11}H_{11}NO_4S+H]^+$: 254.0487. Found: 254.0471.

2-(Oxazol-2-yl)phenol 156

BBr_3 (0.65 ml, 6.87 mmol) was added dropwise to a stirred solution of 2-(2-methoxyphenyl)oxazole **160** (400 mg, 2.28 mmol) in DCM (10 ml, dry) over an ice bath. The suspension was stirred at RT overnight before the reaction was quenched with water (CAUTION). The solid formed, presumed to be (2-(2-hydroxyphenyl)oxazol-3-ium bromide) was filtered off and suspended in DCM. This was then washed with aq. Na_2CO_3 to neutralise the salt. The organic phase was collected and the aqueous phase was washed with further DCM (3 x 50 ml). The organic phases were combined, dried over $MgSO_4$ and filtered. The solvent was removed *in vacuo* to give an oil, 2-(oxazol-2-yl)phenol **156** (250 mg, 68%). The NMR data was consistent with that obtained previously.

4-(Methylsulfonyl)-2-(oxazol-2-yl)phenol 162

BBr_3 (0.61 ml, 6.37 mmol) was added dropwise to a stirred solution of 2-(2-methoxy-5-

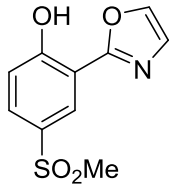

(methylsulfonyl)phenyl)oxazole **161** (538 mg, mmol) in DCM (10 ml, dry) over an ice bath. The suspension was stirred at RT overnight before the reaction was quenched with water (caution!). The solid formed, presumed to be 2-(2-hydroxy-5-(methylsulfonyl)phenyl)oxazol-3-ium bromide, was filtered off and suspended in DCM. This was then washed with aq. Na_2CO_3 to neutralise the salt. The organic phase was collected and the aqueous phase was washed with further DCM (3 x 50 ml). The organic phases were combined, dried over $MgSO_4$ and filtered. TLC revealed a mixture of starting material and product; the crude mixture was redissolved in DCM and extracted with aq. NaOH solution (3 x 50 ml, 1 M). The aqueous phases were combined, acidified to pH 6 with conc. HCl and re-extracted with DCM (4 x 100 ml). The organic phase was dried over $MgSO_4$, the solvent was removed and the residue was purified by silica plug (EtOAc) to give a white solid, 4-(methylsulfonyl)-2-(oxazol-2-yl)phenol **162** (200 mg, 39%). A small sample was recrystallised from methanol to give an analytically pure sample; δ_H (400 MHz; $CDCl_3$; Me_4Si) 11.91 (1H, s), 8.47 (1H, d, *J* 2.4), 7.91 (1H, dd, *J* 8.8, 2.4), 7.79 (1H, d, *J* 0.9), 7.32 (1H, d, *J* 0.9), 7.23 (1H, d, 8.8), 3.10 (3H, s); δ_C (101 MHz; $CDCl_3$; Me_4Si) 161.39, 160.21, 138.54, 131.68, 131.30, 126.78, 126.56, 118.56, 111.65, 45.01; HRMS (FTMS+ESI): calcd for $[C_{10}H_9NO_4S]^+$: 240.0331. Found: 240.0335.

Iridium complex 164

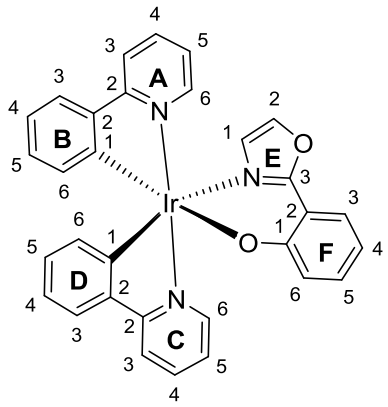

$IrCl_3.3H_2O$ (123 mg, 0.35 mmol) was added to a stirred solution of 2-phenylpyridine **163** (0.11 ml, 0.77 mmol) in 2-ethoxyethanol (10 ml). The solution was heated to reflux (135 ^oC) overnight. Na_2CO_3 (300 mg, 2.83 mmol) and 2-(oxazol-2-yl)phenol **156** (62 mg, 0.38 mmol) and the solution was heated to reflux overnight before being cooled to RT. Water was added and the precipitate was filtered to give a yellow solid. The crude product was filtered and washed with more water to remove water soluble impurities. The product was dried, then washed with hexane and cold diethyl ether to remove traces of ppy **163** ligand. The product was obtained as a yellow solid, **164** (200 mg, 87%); δ_H (700 MHz; $CDCl_3$; Me_4Si) 8.88 (1H, d, *J* 5.7, H_{A6}), 7.99 (1H, d, *J* 5.8, H_{C6}), 7.85 (1H, d, *J* 8.2, H_{C3}), 7.80 (1H, d, *J* 8.2, H_{A3}), 7.72 (1H, dd, *J* 8.2, 1.9, H_{F3}), 7.67 (1H, td, *J* 8.1, 1.5, H_{A4}), 7.65 (1H, td, *J* 8.1, 1.5, H_{C4}), 7.59 (1H, dd, *J* 7.9, 1.1, H_{D3}), 7.56 (1H, dd, *J* 7.6, 1.1, H_{B3}), 7.38 (1H, d, *J* 1.0, H_{E2}), 7.12 (1H, ddd, *J* 8.7, 7.0, 1.9, H_{F5}), 7.07 (1H, ddd, *J* 7.4, 6.0, 1.4, H_{A5}), 6.92 (1H, ddd, *J* 8.1, 5.9, 1.4, H_{C5}), 6.87 (1H, td, *J* 7.5, 1.2, H_{D4}), 6.86 (1H, td, *J* 7.4, 1.2, H_{B4}), 6.80 – 6.75 (2H, m, H_{F6+D5}), 6.73 (1H, dt, *J* 7.3, 1.1, H_{B5}), 6.42 (1H, ddd, *J* 7.9, 6.9, 1.1, H_{F4}), 6.36 (1H, d, *J* 7.6, H_{B6}), 6.28 (1H, d, *J* 7.6,

H_{D6}), 6.20 (1H, d, *J* 1.0, H_{E1}); δ_C (151 MHz; $CDCl_3$; Me_4Si) 169.22 (C_{C2}), 168.10 (C_{A2}), 167.20 (C_{F1}), 158.67 (C_{E3}), 152.67 (C_{D1}), 149.07 (C_{A6}) 148. 72 (C_{B1}), 148.67 (C_{C6}), 144.87 (C_{B2}), 144.83 (C_{D2}), 137.49 (C_{E2}), 136.91 (C_{A4}), 136.74 (C_{C4}), 133.20 (C_{B6}), 132.56 (C_{F5}), 132.48 (C_{D6}), 129.69 (C_{B5}), 129.58 (C_{D5}), 127.39 (C_{F3}), 126.64 (C_{E1}), 125.53 (C_{F6}), 124.18 (C_{B3}), 124.10 (C_{D3}), 122.07 (C_{A5}) 121.80 (C_{C5}), 120.79 (C_{D4}), 119.02 (C_{B4}), 118.73 (C_{C3}), 118.25 (C_{A3}), 113.34 (C_{F4}), 110.94 (C_{F2}); HRMS (FTMS+ESI): calcd for $[C_{31}H_{22}N_3O_4{}^{191}Ir+H]^+$: 660.1396. Found: 660.1406

Iridium complex 165

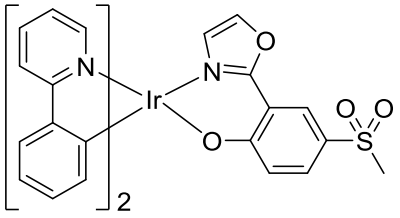

$IrCl_3.3H_2O$ (236 mg, 0.67 mmol) was added to a stirred solution of 2-phenylpyridine **163** (0.21 ml, 1.47 mmol) in 2-ethoxyethanol (10 ml). The solution was heated to reflux (135 ^oC) overnight. Na_2CO_3 (354 mg, 3.34 mmol) and 4-(methylsulfonyl)-2-(oxazol-2-yl)phenol **162** (200 mg, 0.84 mmol) and the solution was heated to reflux overnight before being cooled to RT. Water was added and the precipitate was filtered to give a yellow solid. The crude material was purified by column chromatography (10% EtOAc in DCM) to give the product as a yellow solid. Fractions containing product **165** contaminated with unreacted ppy were combined, the solvent was then removed and the solid was washed with hexane to give further product **165** (combined yield: 281 mg, 57%); δ_H (400 MHz; $CDCl_3$; Me_4Si) 8.75 (1H, ddd, *J* 5.8, 1.5, 0.7), 8.38 (1H, d, *J* 2.6), 7.96 (1H, d, *J* 5.7, 1.5, 0.7), 7.91 (1H, d, *J* 8.1), 7.87 (1H, d, *J* 8.1), 7.75 (1H, td, *J* 7.6, 1.7), 7.73 (1H, td, *J* 7.5, 1.6), 7.60 (1H, td, *J* 8.4, 1.1), 7.57 (1H, dd, *J* 9.2, 2.6), 7.49 (1H, d, *J* 1.0), 7.14 (1H, ddd, *J* 7.3, 5.7, 1.4), 7.01 (1H, ddd, *J* 7.4, 5.8, 1.5), 6.93 (1H, td, *J* 7.5, 1.2), 6.92 (1H, td, *J* 7.5, 1.2), 6.82 (1H, d, *J* 9.2), 6.79 (1H, td, *J* 6.16, 1.2), 6.76 (1H, td, *J* 7.4, 1.4), 6.83 – 6.77 (1H, m), 6.79 – 6.74 (m, 1H), 6.38 (1H, dd, *J* 7.7, 1.0), 6.29 (1H, dd, *J* 7.6, 1.0), 6.27 (1H, d, *J* 1.0), 3.04 (s, 3H); HRMS (FTMS+ESI): calcd for $[C_{32}H_{24}N_3O_4S^{191}Ir]^+$: 737.1094. Found: 737.1118.

Experimental details for chapter 6: 'Cage complexes' for enhanced stability

Tris(2-chloroethyl)amine hydrochloride 176 [24]

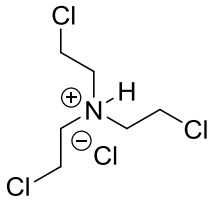

The reaction was conducted as described in the literature. Triethanolamine **175** (2.81 g, 18.84 mmol) was dissolved in chloroform (10 ml) and added dropwise with caution to a stirred solution of thionyl chloride (6.84 ml, 94.14 mmol) in chloroform (10 ml). After the addition was complete, the reaction mixture was stirred for another 2 h at RT before the solvent and excess thionyl chloride were removed *in vacuo*. The remaining product was recrystallised from acetone to give a white solid,

tris(2-chloroethyl)amine hydrochloride **176** (4.33 g, 95%); δ_H (400 MHz; $CDCl_3$; Me_4Si) 4.10 (1H, t, *J* 6.3), 3.66 (1H, t, *J* 6.4). NMR data are consistent with the literature data.[24]

Tris(2-(4-bromophenoxy)ethyl)amine 177

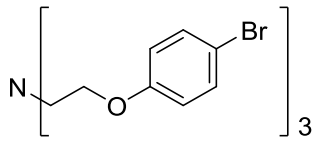

The reaction was conducted as described in the literature. NaOH (0.72 g, 17.98 mmol) was added to a solution of 4-bromophenol (2.28 g, 13.17 mmol) in methanol (50 ml, dry) and stirred at RT for 1 h. Tris(2-chloroethyl)amine hydrochloride **176** (0.96 g, 3.99 mmol) was added and the solution was heated to reflux (100 ^oC) overnight before being cooled to RT. The solvent was removed *in vacuo* and water (50 ml) and chloroform (50 ml) were added. The layers were separated and the aqueous layer was extracted with additional chloroform (50 ml). The organic phases were combined, dried over $MgSO_4$ and the solvent removed. The residue was purified by column chromatography (EtOAc:hexane 1:2) to give a brown oil, tris(2-(4-bromophenoxy)ethyl)amine **177** (1.21 g, 49%); δ_H (400 MHz; $CDCl_3$; Me_4Si) 7.37 – 7.30 (6H, m), 6.76 – 6.69 (6H, m), 4.04 (6H, t, *J* 5.6), 3.12 (6H, t, *J* 5.6). NMR data are consistent with the literature data.[25]
Also isolated was N,N-bis(4-bromophenethyl)-2-chloroethan-1-amine (460 mg, 24%); δ_H (400 MHz; $CDCl_3$; Me_4Si) 7.40 – 7.30 (4H, m), 6.80 – 6.71 (4H, m), 4.03 (4H, t, *J* 5.9), 3.50 (2H, t, *J* 5.7), 3.07 (4H, t, *J* 5.9), 2.89 (2H, t, *J* 5.6).

Tris(2-(4-(1H-imidazol-1-yl)phenoxy)ethyl)amine 178

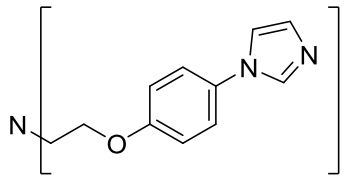

Tris(2-(4-bromophenoxy)ethyl)amine **177** (1.21 g, 1.97 mmol), imidazole (0.53 g, 7.79 mmol) and 1,10-phenanthroline (212 mg, 1.18 mmol) were dissolved in DMSO (6 ml, dry). CuI (112 mg, 0.59 mmol) and Cs_2CO_3 (3.84 g, 11.79 mmol) were added and the solution was heated to 165 ^oC under argon for 40 h before being cooled to RT. DCM (50 ml) and brine (50 ml) were added and the layers were separated. The aqueous layer was extracted with further DCM before the organic layers were combined, dried over $MgSO_4$, filtered and the solvent removed. The residue was purified by crystallisation from a mixture of toluene and acetone to give tris(2-(4-(1H-imidazol-1-yl)phenoxy)ethyl)amine **178** (0.52 g, 46%); δ_H (400 MHz; CD_2Cl_2; Me_4Si) 7.76 (3H, br s), 7.35 – 7.22 (6H, m), 7.25 (3H, br s), 7.15 (3H, br s), 7.02 – 6.95 (6H, m), 4.14 (6H, t, *J* 5.7), 3.18 (6H, t, *J* 5.7); δ_C (176 MHz; CD_2Cl_2; Me_4Si) 158.68, 131.48, 130.49, 123.56, 116.02, 68.09, 55.06; HRMS (FTMS+ESI): calcd for $[C_{33}H_{33}N_7O_3+H]^+$: 576.2723. Found: 576.2722.

Imidazolium ion 179

Tris(2-(4-(1H-imidazol-1-yl)phenoxy)ethyl)amine **178** (520 mg, 0.90 mmol) was suspended in

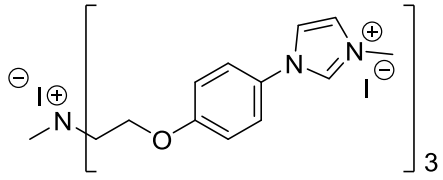

acetonitrile (25 ml) and CH_3I (0.16 ml, 2.61 mmol) was added. The solution was heated to reflux for 4h, during which time a precipitate formed. The solution was cooled and the acetonitrile was decanted. The product was recrystallized by addition of acetone to a solution of the product in methanol. The product was obtained as a brown solid **179** (446 mg, 50%); δ_H (700 MHz; DMSO-d_6; Me_4Si) 9.72 – 9.68 (1H, m), 8.23 (1H, dt, *J* 3.8, 1.8), 7.95 (1H, t, *J* 1.8), 7.79 – 7.74 (2H, m), 7.32 (2H, dd, *J* 9.2, 2.5), 4.71 – 4.67 (2H, m), 4.15 (2H, m), 3.95 (3H, s), 3.42 (1H, d, *J* 5.3); δ_C (176 MHz; DMSO-d_6; Me_4Si) 232.80, 232.79, 158.02, 135.70, 128.54, 124.31, 123.33, 121.17, 121.16, 116.09, 62.01, 61.36, 49.94, 36.14.

4-(2-Pyridyl)phenol 182 [26]

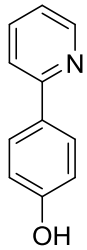

The reaction was conducted according to the literature method. 2-Bromopyridine **11** (1.21 ml, 12.66 mmol), 4-hydroxyphenylboronic acid **181** (2.62 g, 19.00 mmol), $Pd(OAc)_2$ (14 mg, 0.06 mmol) were combined in ethylene glycol (40 ml) and the mixture was heated to 80 ^{o}C for 2 h before being cooled to RT. Water (50 ml), brine (50 ml) and DCM (100 ml) were added and the layers were separated. The aqueous layer was extracted with further DCM (3 x 100 ml) and the extracts were combined and the solvent was removed *in vacuo*. The residue was purified by column chromatography (3:2 to 1:1 hexane: EtOAc) to give a white solid, 4-(2-pyridyl)phenol **182** (1.81 g, 84%); δ_H (400 MHz; $CDCl_3$; Me_4Si) 8.64 (1H, ddd, *J* 4.9, 1.8, 1.0), 7.90 – 7.81 (2H, m), 7.74 (1H, ddd, *J* 8.0, 7.4, 1.8), 7.66 (1H, dt, *J* 8.1, 1.1), 7.20 (1H, ddd, *J* 7.4, 4.9, 1.2), 6.93 – 6.84 (2H, m), 6.15 (1H, br s). NMR data are consistent with the literature data.[26]

Tris(2-(4-(pyridin-2-yl)phenoxy)ethyl)amine 183

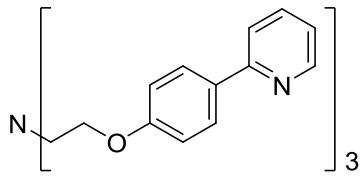

NaOH (0.57 g, 14.34 mmol) was added to a stirred solution of 4-(2-pyridyl)phenol **182** (1.81 g, 10.57 mmol) in MeOH (40 ml, dry) and the solution was stirred at RT for 1 h. Tris(2-chloroethyl)amine hydrochloride (0.77 g, 3.20 mmol) was added and the solution was heated to reflux overnight before being cooled to RT. The solvent was removed *in vacuo* and DCM (50 ml) and water (50 ml) were added. The organic layer was separated and the aqueous phase was extracted with further DCM (2 x 100 ml). The organic phases were combined and the solvent removed *in vacuo*. The residue was purified by using the Biotage® Isolera One ™ purification system (Reverse phase C18 column, H_2O/MeOH gradient

elution) to give a white solid, tris(2-(4-(pyridin-2-yl)phenoxy)ethyl)amine **183** (0.75 g, 40%); δ_H (400 MHz; $CDCl_3$; Me_4Si) 8.64 (3H, ddd, *J* 4.9, 1.8, 1.0), 7.96 – 7.88 (6H, m), 7.69 (3H, ddd, *J* 8.0, 7.2, 1.8), 7.64 (3H, dt, *J* 8.1, 1.3), 7.16 (3H, ddd, *J* 7.2, 4.8, 1.3), 7.03 – 6.94 (2H, m), 4.19 (6H, br t, *J* 4.8), 3.22 (6H, t, *J* 4.8); δ_C (176 MHz; $CDCl_3$; Me_4Si) 159.76, 157.23, 149.66, 136.77, 132.28, 128.32, 121.53, 119.96, 114.91, 67.16, 54.65; HRMS (FTMS+ASAP): calcd for $[C_{39}H_{36}N_4O_3+H]^+$: 609.2866. Found: 609.2861.

2-(2-(4-(Pyridin-2-yl)phenoxy)ethoxy)ethan-1-ol 185

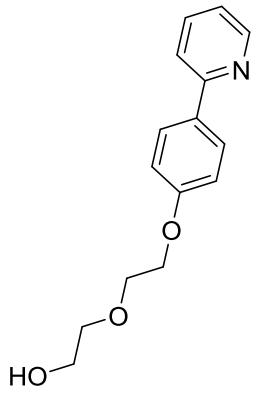

KOH (0.93 g, 16.57 mmol) was added to a stirred solution of 4-(2-pyridyl)phenol **182** (1.42 g, 8.29 mmol) in acetonitrile (30 ml) and the mixture was heated to reflux for 2 h. KI (1.38 g, 8.31 mmol) and 2-(2-chloroethoxy)ethanol (1.75 ml, 16.62 mmol) were added and the mixture was heated to reflux for 40 h before being cooled to RT. The solvent was removed *in vacuo* and DCM (50 ml) and water (50 ml) were added. The organic phase was separated and the aqueous phase was extracted with further DCM (2 x 50 ml). The organic phases were combined, dried over $MgSO_4$, and the solvent removed. The residue was purified by column chromatography (EtOAc) to give an oil which solidified on standing, 2-(2-(4-(pyridin-2-yl)phenoxy)ethoxy)ethan-1-ol **185** (1.88 g, 87%); δ_H (400 MHz; $CDCl_3$; Me_4Si) 8.65 (1H, ddd, *J* 4.7, 1.8, 1.0), 8.02 – 7.85 (2H, m), 7.77 – 7.68 (1H, m), 7.68 – 7.61 (1H, m), 7.23 – 7.10 (1H, m), 7.10 – 6.96 (2H, m), 4.20 (2H, ddd, *J* 4.7, 3.8, 1.4), 3.99 – 3.82 (2H, m), 3.82 – 3.73 (2H, m), 3.69 (2H, ddd, *J* 5.5, 3.3, 1.4); δ_C (101 MHz; $CDCl_3$; Me_4Si) 159.66, 157.17, 149.67, 136.83, 132.49, 128.33, 121.62, 120.01, 114.92, 90.77, 72.76, 69.80, 67.61, 61.94; HRMS (FTMS+ASAP): calcd for $[C_{15}H_{17}NO_3+H]^+$: 260.1287. Found: 260.1290.

Tris(2-iodoethyl)amine [27]

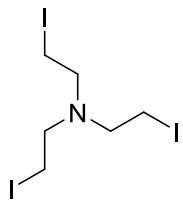

KI (1.38 g, 8.31 mmol) was added to a stirred solution of tris(2-chloroethyl)aminehydrochloride **176** (490 mg, 2.03 mmol) in acetonitrile and the solution was heated to reflux for 3 h before being cooled to RT. The KCl formed was removed by filtration and the filtrate was reduced *in vacuo* to give a yellow solid which was washed with sodium bisulfite solution (1 ml), dried, and used in the next step without further purification.

2-(4-(2-(2-Iodoethoxy)ethoxy)phenyl)pyridine 188

I_2 (896 mg, 3.53 mmol) was added to a stirred solution of PPh_3 (997 mg, 3.80 mmol) and imidazole

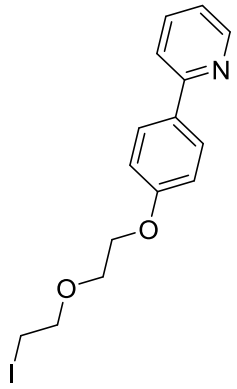

(259 mg, 3.80 mmol) in DCM (10 ml, dry) at 0 °C under argon. The resulting suspension was stirred at 0 °C for 30 mins before a solution of 2-(2-(4-(pyridin-2-yl)phenoxy)ethoxy)ethan-1-ol **185** (657 mg, 2.53 mmol) in DCM (10 ml, dry) was added. The mixture was stirred at RT overnight before the reaction was quenched by aq. NH_4Cl solution. The organic phase was separated and the aqueous layer was extracted with further DCM (2 x 70 ml). The organic phases were combined, concentrated *in vacuo* and the residue obtained was purified by column chromatography (20-50% EtOAc in DCM) to give an oil that solidified to a white solid, 2-(4-(2-(2-iodoethoxy)ethoxy)phenyl)pyridine **188** (764 mg, 82%); δ_H (400 MHz; $CDCl_3$; Me_4Si) 8.66 (1H, ddd, *J* 4.9, 1.8, 1.0), 7.91-7.99 (2H, m), 7.77 – 7.70 (1H, m), 7.70 – 7.65 (1H, m), 7.22 – 7.16 (1H, m), 7.06 – 6.98 (2H, m), 4.24 – 4.18 (2H, m), 3.92 – 3.88 (2H, m), 3.85 (2H, t, *J* 7.2), 3.30 (2H, t, *J* 7.2); δ_C (151 MHz; $CDCl_3$; Me_4Si) 159.79, 156.79, 137.11, 132.28, 128.39, 127.56, 121.65, 114.99, 69.47, 68.85, 67.68, 2.81; HRMS (FTMS+ESI): calcd for $[C_{15}H_{16}{}^{127}INO_2+H]^+$: 370.0304. Found: 370.0295.

2-(2-((Tetrahydro-2H-pyran-2-yl)oxy)ethoxy)ethanol 191[28]

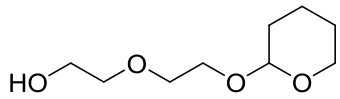

The reaction was conducted as described in the literature. *p*-Toluenesulfonic acid (20 mg, 0.12 mmol) was added to diethylene glycol **190** (9 ml) and the solution was cooled to -10 °C and stirred. 3,4-Dihydro-2H-pyran (1.08 ml, 11.89 mmol) was added dropwise over 15 min. The solution was stirred at -10 °C for 1 h and then at RT for 2 h before aq. NaOH (0.5 M, 60 ml). This was extracted with DCM (4 x 60 ml) and the organic phases were combined and dried over $MgSO_4$, filtered and the solvent was removed *in vacuo*. The crude product was purified by vacuum distillation (Kugelrohr, ~120 °C at 1 mbar) to give a colourless oil, 2-(2-((tetrahydro-2H-pyran-2-yl)oxy)ethoxy)ethanol **191** (2.10 g, 93%); δ_H (400 MHz; $CDCl_3$; Me_4Si) 4.64 (1H, dd, *J* 4.4, 2.9), 3.96 – 3.85 (2H, m), 3.82 – 3.71 (4H, m), 3.68 – 3.64 (3H, m), 3.57 –3.51 (1H, m), 1.91 – 1.68 (2H, m), 1.68 – 1.47 (4H, m). NMR data are consistent with the literature data.[28]

Tris(2-(2-(2-((tetrahydro-2H-pyran-2-yl)oxy)ethoxy)ethoxy)ethyl)amine 192

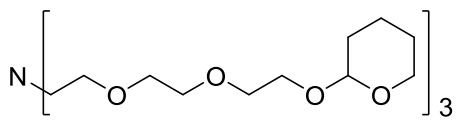

NaOH (210 mg, 5.25 mmol, ground) was added to a stirred solution of THP-protected ethylene glycol **191** (1.00 g, 5.25 mmol) and tetrabutylammonium hydrogensulfate (71 mg, 0.21 mmol) in THF (10 ml, dry) and the solution was heated to reflux for 2 h. The solution was cooled and tris(2-chloroethyl)amine hydrochloride **176** (317 mg, 1.31 mmol)

was added. The solution was heated to reflux over the weekend before being cooled to RT. The solution was filtered to remove any NaCl formed, and the solid was washed with DCM. The solvent was removed *in vacuo* and the residue was purified by column chromatography (EtOAc, stained with $KMnO_4$) to give a yellow oil, tris(2-(2-(2-((tetrahydro-2H-pyran-2-yl)oxy)ethoxy)ethoxy)ethyl)amine **192** (550 mg, 63%); δ_H (400 MHz; $CDCl_3$; Me_4Si) 4.67 (3H, dd, *J* 4.4, 2.9), 3.96 – 3.83 (6H, m), 3.81 – 3.70 (13H, m), 3.70 – 3.60 (9H, m), 3.60 – 3.50 (3H, m), 2.56 (3H, t, *J* 5.0), 1.94 – 1.72 (7H, m), 1.69 – 1.48 (19H, m).

Tris(2-(2-(2-hydroxy)ethoxy)ethyl)amine 193

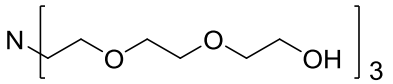

Sodium (1.00 g, 43.48 mmol) was added to a stirred diethylene glycol **190** (25 ml) and the mixture was heated with stirring until the sodium had fully dissolved. Trichloroethylamine (1.78 g, 8.70 mmol, prepared by washing the salt **176** with aq. Na_2CO_3 and extracting) was added and the solution was heated to 130 ^oC overnight before being cooled to RT. The majority of the excess diethylene glycol was removed by vacuum distillation (2 mbar, 108-110 ^oC), with the rest being removed via distillation in the Kugelrohr. The residue was dissolved in DCM and the solution was filtered to remove and NaCl. The solution was then concentrated to give the product **193** (3.55 g, 99%), δ_H (400 MHz; $CDCl_3$; Me_4Si) 3.80 – 3.56 (m, 36H); HRMS (FTMS+ESI): calcd for $[C_{18}H_{39}NO_9+H]^+$: 414.2703. Found: 414.2700.

Tris(2-(2-(2-methanesulfonate-ethoxy)ethoxy)ethyl)amine 195

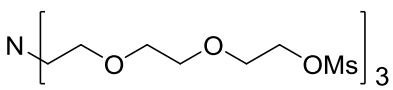

MsCl (2.91 ml, 37.53 mmol) was added dropwise (caution, exothermic) to a stirred solution of tris(2-(2-(2-hydroxy)ethoxy)ethyl)amine **193** (2.22 g, 5.36 mmol) and NEt_3 (20 ml) in DCM (50 ml, dry) over an ice bath under an atmosphere of argon. The solution was left to warm to RT overnight before aq. $NaHCO_3$ (20 ml) was added. The organic layer was separated and the aqueous layer was extracted with further DCM (4 x 100 ml, spiked with iPrOH due to water soluble products). The solvent was removed *in vacuo* and the residue was purified by using the Biotage® Isolera One ™ purification system (Reverse phase C18 column, H_2O/MeOH gradient elution) to give a brown oil containing tris(2-(2-(2-methanesulfonate-ethoxy)ethoxy)ethyl)amine **195**; δ_H (400 MHz;$CDCl_3$;Me_4Si) 4.41 (6H, m), 3.85 – 3.61 (30H, m), 3.09 (9H, s); HRMS (FTMS+ESI): calcd for $[C_{21}H_{45}NO_{15}S_3+H]^+$: 648.2030. Found: 648.2020.

Tris(2-(2-(2-iodoethoxy)ethoxy)ethyl)amine 196

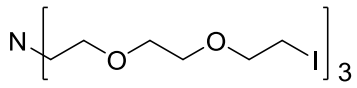

NaI (14.50 g, 96.73 mmol) was added to a solution of tris(2-(2-(2-methanesulfonate-ethoxy)ethoxy)ethyl)amine **195** (1.49 g, 2.30 mmol) in acetonitrile (20 ml) and the solution was heated to reflux overnight before being cooled to RT. The solvent was removed *in vacuo*, and water (20 ml) and chloroform (50 ml) were added. The layers were separated, and the aqueous phase was extracted with further chloroform (3 x 40 ml). The organic phases were combined, dried over $MgSO_4$, and the solvent was removed *in vacuo*. The residue was purified using the Biotage® Isolera One ™ purification system (Reverse phase C18 column, H_2O/MeOH gradient elution) to give a brown oil containing tris(2-(2-(2-iodoethoxy)ethoxy)ethyl)amine **196**; δ_H (400 MHz;$CDCl_3$;Me_4Si) 3.81 –3.75 (m), 3.75 – 3.71 (12H, m), 3.70 – 3.66 12H, m); δ_C (101 MHz; $CDCl_3$; Me_4Si) 95.79, 72.11, 70.26, 67.05, 31.08, 2.86; HRMS (FTMS+ESI): calcd for $[C_{18}H_{36}NO_6{}^{127}I_3+H]^+$: 743.9755. Found: 743.9760.

1,3,5-Benzenetrimethanol 198 [29]

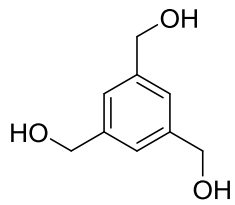

A solution of 1,3,5-trimethylbenzene carboxylate **197** (4.00 g, 15.86 mmol) in THF (40 ml, dry) was added dropwise to a suspension of $LiAlH_4$ (1.80 g, 47.43 mmol, crushed to a powder) in THF (60 ml, dry) over an ice bath, under an argon atmosphere. Once addition was complete the suspension was heated to reflux overnight. The reaction was quenched by slow pouring onto ice (caution, gas evolution). The precipitate formed was filtered through celite and washed with $CHCl_3$ (100 ml). The solvents were then removed *in vacuo* to leave a white solid, 1,3,5-benzenetrimethanol **198** (2.67 g, quant); δ_H (400 MHz; CD_3OH; Me_4Si) 7.26 (3H, p, 0.6), 4.61 (6H, q, 0.6); NMR data is consistent with the literature data.[29]

1,3,5-Tris(bromomethyl)benzene 199 [30]

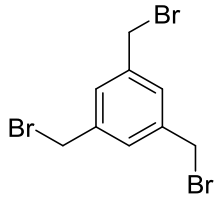

PBr_3 (7.52 ml, 79.17 mmol) was added dropwise to a stirred suspension of 1,3,5-benzenetrimethanol **198** (3.33 g, 19.80 mmol) in diethyl ether (60 ml, dry) over an ice bath under an atmosphere of argon. The solution was stirred at 0 ^oC for 2 h and then at RT for 6 h. The solution was poured over ice and the layers were separated. The aqueous layer was extracted with further diethyl ether (3 x 40 ml) and the organic phases were combined, dried over $MgSO_4$, filtered and the solvent removed *in vacuo*. The residue was purified by column chromatography (3:1 hexane:EtOAc) to give the product as a white crystalline solid, 1,3,5-tris(bromomethyl)benzene (5.15 g, 74%); δ_H (400 MHz; $CDCl_3$; Me_4Si) 7.36 (3H, s), 4.46

(2H, s); NMR data is consistent with the literature data.[30]

1,3,5-Tris((2-(2-((tetrahydro-2H-pyran-2-yl)oxy)ethoxy)ethoxy)methyl)benzene 200

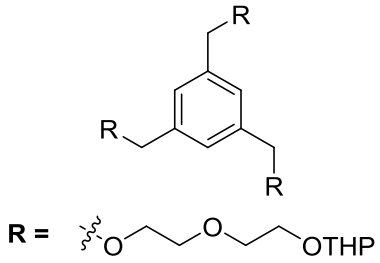

NaOH (1.05 g, 26.25 mmol) was added to a solution of PEG-THP **191** (5.00 g, 26.29 mmol) and $TBAHSO_4$ (357 mg, 1.05 mmol). The mixture was heated to reflux for 2 h before 1,3,5-tris(bromomethyl)benzene **199** (2.32 g, 6.56 mmol) was added. The solution was heated to reflux overnight before being cooled to RT. The mixture was filtered to remove the white precipitate and the solvent was removed *in vacuo*. The residue was purified by column chromatography (50-0% hexane in EtOAc) to give the product as a colourless oil, **200** (1.10 g, 24%); δ_H (400 MHz; $CDCl_3$; Me_4Si) 7.24 (3H, s), 4.64 (6H, q, *J* 4.4), 4.56 (6H, s), 3.90-3.82 (6H, m), 3.78 – 3.59 (7 H, m), 3.59 – 3.46 (1 H, m), 2.05 (1 H, s), 1.83 (1 H, d, *J* 10.1), 1.80 – 1.66 (1 H, m), 1.66 – 1.51 (5 H, m), 1.26 (1 H, t, *J* 7.1); NMR data is consistent with the literature data.[31]

1,3,5-Tris((2-(2-hydroxyethoxy)ethoxy)methyl)benzene 201

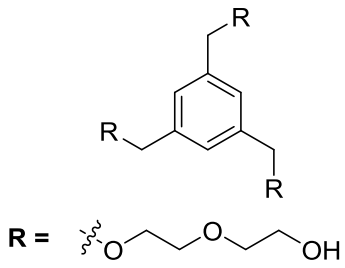

The THP-protected alcohol **200** (1.10 g, 1.61 mmol) was dissolved in DCM/Methanol (1:1, 20 ml) and a drop of conc. HCl (37%) was added. The solution was stirred at RT overnight. Solid $NaHCO_3$ was added and the solvent removed *in vacuo*. The residue was suspended in EtOAc and filtered. The solvent was removed to give the product as a colourless oil, **201** (500 mg, 71%); δ_H (400 MHz; $CDCl_3$; Me_4Si) 7.29 (3H, s), 4.58 (6H, s), 3.79 – 3.56 (32 H, m); NMR data is consistent with the literature data.[31]

1,3,5-Tris((2-(2-hydroxyethoxy)ethoxy)methyl)benzene 201

Sodium (1.67 g, 72.61 mmol) was added to stirred diethylene glycol (30 ml) and the mixture was heated to 80 ^oC for 3 h (until the sodium dissolved). The mixture was cooled and 1,3,5-tris(bromomethyl)benzene **199** (5.15 g , 14.56 mmol) was added and the solution was heated to 100 ^oC overnight before being cooled to RT. The remaining diethylene glycol was removed by vacuum distillation using the Kugelrohr apparatus to leave a mixture of the crude product **201** and diethylene glycol sodium salts.

1,3,5-Tris((2-(2-mesyl-ethoxy)ethoxy)methyl)benzene 202

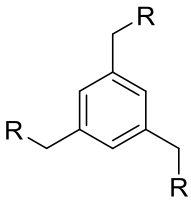

R = 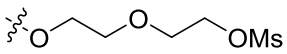

Mesyl chloride (15 ml, 0.19 mol) was added cautiously to a stirred solution of the crude mixture containing **201** (~10 g) and NEt_3 (30 ml) in DCM (50 ml, dry) at 0 °C under argon. The solution was left to stir at 0 °C for 1 h, then allowed to warm to RT overnight. Water (200 ml) was added, and the layers were separated. The aqueous layer was extracted with further DCM (3 x 100 ml) and the organic phases were combined, dried over $MgSO_4$, and the solvent removed to give an oil containing diethylene glycol dimesylate and the product **202**; δ_H (400 MHz; $CDCl_3$; Me_4Si) 7.23 (3H, s), 4.54 (6H, s), 4.39 – 4.37 (6H, m), 3.78 – 3.76 (6H, m), 3.73 – 3.62 (12H, m), 3.03 (9H, s); NMR data is consistent with the literature data.[31]

1,3,5-Tris((2-(2-iodoethoxy)ethoxy)methyl)benzene 203

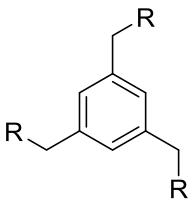

R = 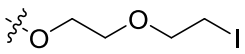

NaI (44.00 g, 0.29 mol) was added to a stirred solution of the crude mixture containing **202** (~26 g) in acetonitrile (120 ml). The mixture was heated to reflux overnight before being cooled to RT. The mixture was cooled and the solvent removed in vacuo. DCM and water were added. The organic phase was separated and the aqueous phase was extracted with further DCM. The organic phases were combined, dried over $MgSO_4$, filtered and the solvent removed. The residue was purified by an alumina column (hexane:EtOAc 1:1) followed by a Kugelrohr distillation to remove bis(2-iodoethyl) ether (b.pt. 110-120 °C at 0.66 mbar[32]). The product **203** was obtained as an orange oil (5.94 g, 54% over three steps); δ_H (400 MHz; $CDCl_3$; Me_4Si) 7.27 (3H, s), 4.58 (6H, s), 3.78 (6H, t, *J* 6.9), 3.71 – 3.68 (6H, m), 3.66 – 3.63 (6H, m), 3.27 (6H, t, *J* 6.9); NMR data is consistent with the literature data.[31]

1,3,5-Tris((2-(2-(4-(pyridin-2-yl)phenoxy)ethoxy)ethoxy)methyl)benzene 223

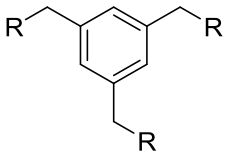

R = 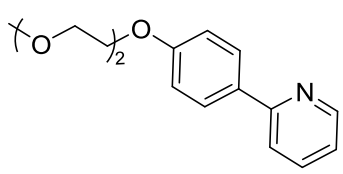

NaOH (93 mg, 2.33 mmol) was added to a stirred solution of 4-(2-pyridyl)phenol **182** (500 mg, 2.92 mmol) in THF (20 ml, dry). The mixture was heated to reflux under argon for 3 h before being cooled to RT. A solution of 1,3,5-tris((2-(2-iodoethoxy)ethoxy)methyl)benzene **203** (445 mg, 0.58 mmol) in THF (5 ml, dry) and the solution was heated to reflux overnight. The solution was then cooled to RT and the solvent was removed *in vacuo*. The residue was purified by column chromatography (EtOAc) to give the

product as a clear oil, 1,3,5-tris((2-(2-(4-(pyridin-2-yl)phenoxy)ethoxy)ethoxy)methyl)benzene **223** (345 mg, 66%); δ_H (400 MHz; $CDCl_3$; Me_4Si) 8.63 (3H, d, *J* 4.3), 7.95 – 7.88 (6H, m), 7.71 – 7.61 (6H, m), 7.26 (3H, s), 7.15 (3H, ddd, *J*7.1, 4.9, 1.5), 7.03 – 6.96 (6H, m), 4.55 (6H, s), 4.17 – 4.15 (6H, m), 3.91 – 3.82 (6H, m), 3.79 – 3.69 (6H, m), 3.69 – 3.59 (6H, m); δ_C (101 MHz; $CDCl_3$; Me_4Si) 159.75, 157.11, 149.58, 138.69, 136.72, 132.22, 128.19, 126.41, 121.49, 119.86, 114.88, 73.19, 70.97, 69.80, 69.67, 67.59; HRMS (FTMS+ESI): calcd for $[C_{54}H_{57}N_3O_9+H]^+$: 892.4173. Found: 892.4181.

Iridium complex 228

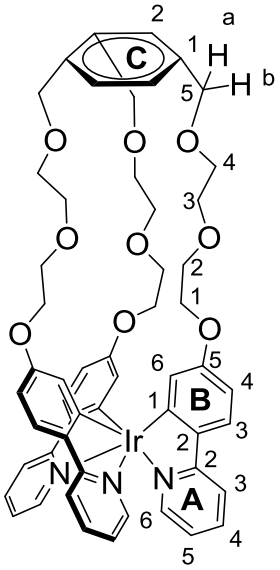

Reaction 1: Ligand **223** (64 mg, 0.07 mmol) was suspended in ethylene glycol (300 ml) and the solution was degassed with bubbling argon. The solution was heated to 140 °C before $Ir(acac)_3$ (21 mg, 0.07 mmol) was added. The solution was heated to 160 °C for 24 h under argon before being cooled. The solvent was removed via trap-to-trap distillation and DCM (20 ml) and water (20 ml) were added. The organic phase was separated and the aqueous phase was extracted with further DCM (2 x 20 ml). The organic phases were combined, dried over $MgSO_4$, and the solvent removed *in vacuo*. TLC analysis showed only unreacted ligand **223**. The ligand and unreacted $Ir(acac)_3$ were reclaimed via column chromatography (DCM to EtOAc).

Reaction 2: Ligand **223** (64 mg, 0.07 mmol) was suspended in ethylene glycol (150 ml) and the solution was degassed with bubbling argon. The solution was heated to 140 °C before $Ir(acac)_3$ (21 mg, 0.07 mmol) was added. The solution was heated to reflux for 24 h under argon before being cooled. The solvent was removed via trap-to-trap distillation and DCM (20 ml) and water (20 ml) were added. The organic phase was separated and the aqueous phase was extracted with further DCM (2 x 20 ml). The organic phases were combined, dried over $MgSO_4$, and the solvent removed *in vacuo*. The residue was purified by column chromatography (DCM:EtOAc 1:1) to give the product **228** as a yellow solid (25 mg, 32%); δ_H (700 MHz; CD_2Cl_2; Me_4Si) 7.77 (3H, dt, *J* 8.4, 1.1, H_{A3}), 7.58 (3H, d, J, H_{B3}), 7.56 (3H, ddd, J, H_{A4}), 7.44 (3H, ddd, *J* 5.4, 1.6, 0.8, H_{A6}), 7.25 (3H, s, H_{C2}), 6.79 (3H, ddd, *J* 7.0, 5.5, 1.3, H_{A5}), 6.43 (3H, dd, *J* 8.6, 2.7, H_{B4}), 6.25 (3H, d, *J* 2.7, H_{B6}), 4.50 (6H, m, H_5), 3.87 – 3.78 (6H, m, H_1), 3.65 (12H, ddt, *J* 7.2, 5.4, 3.9, $H_{2/3}$), 3.60 (6H, t, *J* 5.1, H_4); δ_C (176 MHz; CD_2Cl_2; Me_4Si) 166.64 (C_{A2}), 163.82 (C_{B1}), 160.62 (C_{B5}), 147.50 (C_{A6}), 138.98 (C_{C1}), 137.49 (C_{B2}), 136.44 (C_{A4}), 128.64 (C_{C2}), 125.76 (C_{B3}), 122.36 (C_{B6}), 121.25 (C_{A5}), 118.63 (C_{A3}), 106.22 (C_{B4}), 73.82 (C_5), 71.02 (C_3), 70.45 (C_2), 69.79 (C_4), 67.21 (C_1); HRMS (FTMS+ESI): calcd for $[C_{54}H_{54}IrN_3O_9]^+$: 1079.3466. Found: 1079.3489.

4-Imidazol-1-ylphenol [33]

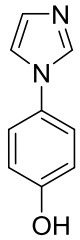

CuI (440 mg, 2.31 mmol) and Cs_2CO_3 (7.53 g, 23.11 mmol) were added to a stirred solution of 4-bromophenol **207** (2.00 g, 11.56 mmol) and imidazole (1.10 g, 16.16 mmol) in DMF (8 ml, dry) under an atmosphere of argon. The mixture was heated to 120 ^{o}C for 48 h before being cooled to RT. EtOAc was added and the suspension was passed through a column of silica to remove any copper salts (eluent: EtOAc/ethanol). The residue obtained was purified by column chromatography (1-5% ethanol in EtOAc) to give the product as a white solid, 4-imidazol-1-ylphenol **204** (250 mg, 14%); δ_H (400 MHz; CD_3OD; Me_4Si) 7.96 (1H, t, *J* 1.2), 7.43 (1H, t, *J* 1.4), 7.39 – 7.30 (2 H, m), 7.12 (1H, t, *J* 1.2), 6.98 – 6.85 (2H, m). NMR data is consistent with the literature.[33]

2-(4-Bromophenoxy)tetrahydro-2H-pyran 208

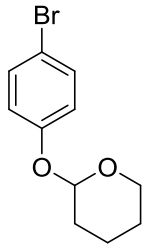

3,4-Dihydro-2H-pyrane (1.05 ml, 11.53 mmol) was added dropwise to a stirred solution of 4-bromophenol **207** (2.00 g, 11.56 mmol) and *p*-toluenesulfonic acid (20 mg, 0.12 mmol) in DCM (20 ml). The solution was stirred at RT for 2 h before dilute aq. NaOH (50 ml) was added. Diethyl ether (50 ml) was added and the layers were separated. The aqueous layer was extracted with further diethyl ether (2 x 50 ml), the organic phases were then combined, dried over $MgSO_4$ and the solvent removed to give an oil. The product was run through a short silica column (eluent: hexane) to give the product as a white crystalline solid, 2-(4-bromophenoxy)tetrahydro-2H-pyran **208** (1.10 g, 37%); δ_H (400 MHz; $CDCl_3$; Me_4Si) 7.41 – 7.32 (2H, m), 6.99 – 6.89 (2H, m), 5.37 (1H, t, *J* 3.2), 3.87 (1H, ddd, *J* 11.5, 9.6, 3.2), 3.60 (1H, dtd, *J* 11.4, 4.1, 1.5), 2.07 – 1.83 (2H, m), 1.81 – 1.64 (2H, m), 1.64 – 1.49 (2H, m). NMR data is consistent with the literature data.[34]

2-(4-Imidazol-1-yl-phenoxy)tetrahydro-2H-pyran 209

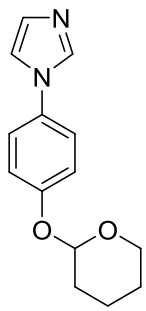

A solution of 2-(4-bromophenoxy)tetrahydro-2H-pyran **208** (962 mg, 3.74 mmol), imidazole (382 mg, 5.61 mmol) and 1,10-phenanthroline (405 mg, 2.25 mmol) in DMSO (5 ml, dry) was degassed with bubbling argon for 10 mins. Cs_2CO_3 (7.33 mg, 22.50 mmol) and CuI (214 mg, 1.12 mmol) were added and the solution was heated to 165 ^{o}C overnight under argon before being cooled to RT. Brine (30 ml) and DCM (30 ml) were added, the organic phase was separated and aqueous phase was extracted with further DCM (2 x 30 ml). The organic phases were combined, dried over $MgSO_4$, and the solvent was removed *in vacuo*. The residue was purified by column chromatography (EtOAc) to give an off-white solid, 2-(4-imidazol-1-yl-phenoxy)tetrahydro-2H-pyran **209** (630 mg,

69%); δ_H (400 MHz; $CDCl_3$; Me_4Si) 7.80 (1H, s), 7.34 – 7.25 (2H, m), 7.22 (1H, s), 7.20 (1H, s), 7.17 – 7.10 (2H, m), 5.45 (1H, t, *J* 3.2), 3.90 (1H, ddd, *J* 11.4, 9.6, 3.1), 3.63 (1H, dtd, *J* 11.3, 4.1, 1.4), 2.12 – 1.91 (2H, m), 1.91 – 1.85 (2H, m), 1.78 – 1.58 (2H, m).

4-Imidazol-1-ylphenol

Conc. HCl (1 ml, 37%) was added to a stirred solution of 2-(4-imidazol-1-yl-phenoxy)tetrahydro-2H-pyran **209** (765 mg, mmol) in MeOH (10 ml). The mixture was stirred at RT overnight before $NaHCO_3$ was added. The solvent was removed *in vacuo* and the mixture was redissolved in EtOAc (20 ml) and filtered. The solvent was removed to give an off-white solid, 4-imidazol-1-ylphenol **204** (500 mg, quant.). The NMR data was consistent with that obtained previously.

6-(2-Thienyl)-3-pyridinol 205

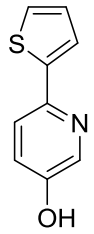

2-Thienylboronic acid **211** (0.88 g, 6.88 mmol) and 2-bromo-5-hydroxypyridine **210** (1.00 g, 5.75 mmol) were combined in DME/water (20/9 ml) and the solution was degassed for 20 min with bubbling argon. $PdCl_2(PPh_3)_2$ (20 mg, 0.03 mmol) and K_2CO_3 (2.22 g, 16.06 mmol) were added and the solution was heated to reflux overnight before being cooled to RT. The solvent was removed *in vacuo* and DCM (50 ml) and water (50 ml) were added. The aqueous layer was acidified to pH 7 with dilute HCl (2.0 M) and the layers were separated. The aqueous layer was extracted with additional DCM (3 x 50 ml) and the organic phases were combined, dried over $MgSO_4$, filtered and the solvent removed to give an off-white solid. NMR revealed a mixture of starting material and product that did not separate on TLC. The starting material removed by sublimation (150 ^oC, 0.1 mbar) using a Kugelrohr apparatus to leave the product as a white solid, 6-(2-thienyl)-3-pyridinol **205** (690 mg, 68%); δ_H (400 MHz; $CDCl_3$; Me_4Si) 8.27 (1H, dd, *J* 2.9, 0.7), 7.58 (1H, dd, *J* 8.6, 0.7), 7.50 (1H, dd, *J* 3.7, 1.1), 7.34 (1H, dd, *J* 5.1, 1.1), 7.25 (1H, dd, *J* 8.6, 2.9), 7.09 (1H, dd, *J* 5.1, 3.7); δ_C (151 MHz; $CDCl_3$; Me_4Si) 151.76, 145.40, 143.71, 136.86, 128.21, 126.75, 124.60, 123.96, 120.39; HRMS (FTMS+ESI): calcd for $[C_9H_7NOS+H]^+$: 178.0327. Found: 178.0324.

1,3,5-Tris((2-(2-((6-(thiophen-2-yl)pyridin-3-yl)oxy)ethoxy)ethoxy)methyl)benzene 226

NaOH (69 mg, 1.73 mmol) was added to a stirred solution of 6-(2-thienyl)- 3-pyridinol **205** (332 mg, 1.87 mmol) in THF (20 ml, dry). The mixture was heated to reflux under argon for 3 h before being cooled to RT. 1,3,5-Tris((2-(2-iodoethoxy)ethoxy)methyl)benzene **103** (210 mg, 0.28 mmol) was added and the solution was heated to reflux overnight. The solution was then cooled to RT and the solvent was removed *in vacuo*. The residue was purified by column chromatography

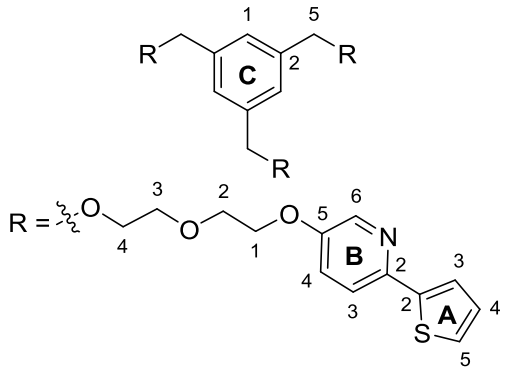

(EtOAc:hexane 3:1) to give intermediate **225** (200 mg, 80%); δ_H (400 MHz; $CDCl_3$; Me_4Si) 8.26 (2H, dd, *J* 2.9, 0.7), 7.55 (2H, dd, *J* 8.7, 0.7), 7.42 (2H, dd, *J* 3.7, 1.2), 7.30 (2H, dd, *J* 5.1, 1.1), 7.24 (3H, s), 7.21 (2H, dd, *J* 8.7, 3.0), 7.05 (2H, dd, *J* 5.1, 3.6), 4.54 (4H, s), 4.53 (2H, s), 4.19 – 4.16 (4H, m), 3.90 – 3.82 (4H, m), 3.79 – 3.72 (6H, m), 3.72 – 3.56 (8H, m), 3.28 – 3.19 (2H, m); HRMS (FTMS+ESI): calcd for $[C_{39}H_{45}N_2O_8S_2I+H]^+$: 861.1760. Found: 861.1735.

NaOH (28 mg, 0.70 mmol) was added to a stirred solution of 6-(2-thienyl)-3-pyridinol **205** (165 mg, 0.93 mmol) in THF (20 ml, dry) and the mixture was heated to reflux for 4 h under an argon atmosphere before being cooled to RT. The intermediate **225** (200 mg, 0.23 mmol) was added and the mixture was heated to reflux overnight before being cooled to RT. The solvent was removed *in vacuo* and the residue was purified by column chromatograpy (hexane:EtOAc 3:1) to give the product as an oil, **226** (105 mg, 50%); δ_H (600 MHz; $CDCl_3$; Me_4Si) 8.26 (3H, d, *J* 2.9, H_{B6}), 7.55 (3H, d, *J* 8.7, H_{B3}), 7.44 (3H, d, *J* 3.6, H_{A5}), 7.31 (3H, dd, *J* 5.1, 1.1, H_{A3}), 7.24 (3H, s, H_{C1}), 7.23 (3H, dd, *J*, 8.7, 2.9, H_{B4}), 7.06 (3H, dd, *J* 5.1, 3.6, H_{A4}), 4.53 (6H, s, H_5), 4.20 – 4.15 (4H, m, H_1), 3.88 – 3.83 (6H, m, H_2), 3.74 – 3.69 (6H, m, H_3), 3.66 – 3.61 (6H, m, H_4). δ_C (151 MHz; $CDCl_3$; Me_4Si) 154.10 (C_{B5}), 145.71 (C_{B2}), 144.34 (C_{A2}), 138.74 (C_{C2}), 137.19 (C_{B6}), 128.12 (C_{A4}), 126.63 (C_{A3}), 126.50 (C_{C1}), 123.57 (C_{A5}), 122.77 (C_{B4}), 119.56 (C_{B3}), 73.29 (C_5), 71.09 (C_3), 69.77 ($C_{2/4}$), 69.76 ($C_{2/4}$), 68.25 (C_1); HRMS (FTMS+ESI): calcd for $[C_{48}H_{51}N_3O_9S_3+H]^+$: 910.2866. Found: 910.2867.

Iridium complex 229

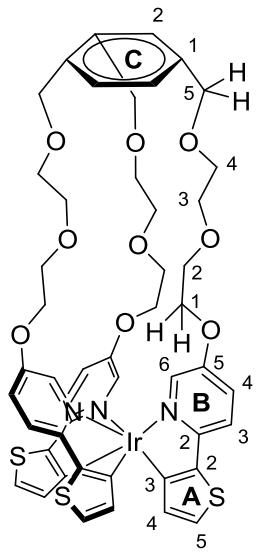

Ligand **226** (105 mg, 0.12 mmol) was suspended in ethylene glycol (150 ml) and the solution was degassed with bubbling argon. The solution was heated to 140 ^oC before $Ir(acac)_3$ (34 mg, 0.12 mmol) was added. The solution was heated to reflux for 24 h under argon before being cooled. The solvent was removed via trap-to-trap distillation and DCM (20 ml) and water (20 ml) were added. The organic phase was separated and the aqueous phase was extracted with further DCM (2 x 20 ml). The organic phases were combined, dried over $MgSO_4$, and the solvent removed *in vacuo*. The residue was purified by column chromatography (DCM:EtOAc 1:1) to give the product as a yellow solid **229** (9 mg, 8%); δ_H (700 MHz; CD_2Cl_2; Me_4Si) 7.38 (3H, dd, *J* 8.9, 0.7, H_{B3}), 7.32 (3H, dd, *J* 2.8, 0.7, H_{B6}), 7.29 (3H, s, H_{C2}), 7.14 (3H, dd, *J* 8.9, 2.7, H_{B4}), 7.07 (3 H, d, *J* 4.6, H_{A5}), 6.20 (3 H, d, *J* 4.6, H_{A4}), 4.50

(3 H, d, *J* 10.9, H_{5a}), 4.46 (3 H, d, *J* 10.9, H_{5b}), 3.97 (3 H, ddd, *J* 9.5, 6.0, 3.1, H_{1a}), 3.83 (3 H, ddd, *J* 10.1, 4.8, 2.8, H_{1a}), 3.69 (6 H, dt, *J* 4.9, 2.7, H_2), 3.67 – 3.61 (12 H, m, $H_{3/4}$); δ_C (176 MHz; CD_2Cl_2; Me_4Si) 156.06 (C_{B2}), 155.41 (C_{A3}), 153.29 (C_{B5}), 139.00 (C_{C1}), 137.26 (C_{B6}), 135.69 (C_{A4}), 134.94 (C_{A2}), 128.77 (C_{C2}), 126.00 (C_{A5}), 122.51 (C_{B4}), 117.78 (C_{B3}), 73.94 (C_5), 71.13 (C_3), 70.32(C_4), 70.13 (C_2), 68.69 (C_1); HRMS (FTMS+ESI): calcd for $[C_{48}H_{48}{}^{191}IrN_3O_9S_3]^+$: 1097.2159. Found: 1097.2152.

5-(4,4,5,5-Tetramethyl-1,3,2-dioxaborolan-2-yl)-3-(trifluoromethyl)-1H-pyrazole [35]

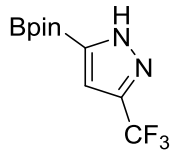

B_2pin_2 (1.87 g, 7.36 mmol), $[Ir(COD)Cl]_2$ (122 mg, 0.18 mmol) and 3,4,7,8-tetramethyl-1,10-phenanthroline (87 mg, 0.37 mmol) were added to degassed THF (20 ml, dry) and the solution was heated to reflux for 1 h. 3-(Trifluoromethyl)pyrazole **213** (1.00 g, 7.35 mmol) was added and the solution was heated to reflux overnight under an atmosphere of argon before being cooled to RT. The reaction was quenched with water and the solvent was removed. DCM and water were added and the organic phase was separated. The aqueous phase was extracted with further DCM; the organic phases were combined, dried over $MgSO_4$, filtered and the solvent removed. The residue was purified by column chromatography (hexane:EtOAc 4:1) to give the product as a white solid, 5-(4,4,5,5-tetramethyl-1,3,2-dioxaborolan-2-yl)-3-(trifluoromethyl)-1H-pyrazole **212** (1.40 g, 73%); δ_H (400 MHz; $CDCl_3$; Me_4Si) 6.99 (1H, d, *J* 0.7), 1.35 (13 H, s); δ_F (376 MHz; $CDCl_3$; Me_4Si) -61.81 (1F, s); δ_B (128 MHz; $CDCl_3$; Me_4Si) 27.28 (br s); NMR data is consistent with the literature data.[35]

1-(Tetrahydro-2H-pyran-2-yl)-3-(trifluoromethyl)- 1H-pyrazole 215 [36]

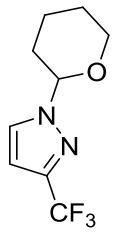

Trifluroroacetic acid (0.16 ml, 2.02 mmol) was added to a stirred solution of 3-(trifluoromethyl)pyrazole **213** (1.85 g, 13.59 mmol) and 3,4-dihydro-2H-pyran (1.30 ml, 14.27 mmol) in toluene (15 ml) and the mixture was heated to 80 ^oC overnight before being cooled to RT. The toluene was removed *in vacuo* and EtOAc (40 ml) and water (40 ml) were added. The organic phase was separated, and the aqueous phase was extracted with further EtOAc (3 x 40 ml). The organic phases were combined, washed with brine then dried over $MgSO_4$ and filtered. The solvent was removed and the residue was purified by column chromatography (hexane:EtOAc 3:1), product visualised with $KMnO_4$ stain) to give the product as a yellow oil, 1-(tetrahydro-2H-pyran-2-yl)-3-(trifluoromethyl)- 1H-pyrazole **215** (2.84 g, 95%); δ_H (400 MHz; $CDCl_3$; Me_4Si) 7.66 (1H, dq, *J* 1.9, 0.9), 6.56 (1H, d, *J* 2.5), 5.44 (1H, dd, *J* 8.6, 3.5), 4.16 – 4.02 (1H, m), 3.78 – 3.63 (1H, m), 2.16 – 1.95 (3H, m), 1.78 – 1.58 (3H, m); δ_F (376 MHz; $CDCl_3$; Me_4Si) -62.01 (3F, s).

1-(Tetrahydro-2H-pyran-2-yl)-5-(4,4,5,5-tetramethyl-1,3,2-dioxaborolan-2-yl)-3-(trifluoromethyl)- 1H-pyrazole 214

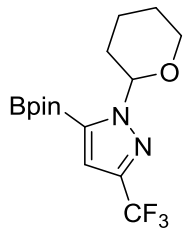

Trifluroroacetic acid (0.017 ml, 0.23 mmol) was added to a stirred solution of 5-(4,4,5,5-tetramethyl-1,3,2-dioxaborolan-2-yl)-3-(trifluoromethyl)- 1H-pyrazole **212** (400 mg, 1.53 mmol) and 3,4-dihydro-2H-pyran (0.146 ml, 1.62 mmol) in toluene (10 ml) and the mixture was heated to 80 ^{o}C overnight before being cooled to RT. The toluene was removed *in vacuo* and EtOAc (40 ml) and water (40 ml) were added. The organic phase was separated, and the aqueous phase was extracted with further EtOAc (3 x 40 ml). The organic phases were combined, washed with brine then dried over $MgSO_4$ and filtered. The solvent was removed and the residue was purified by column chromatography (hexane:EtOAc 3:1, product visualised with $KMnO_4$ stain) to give the product as an orange oil, 1-(tetrahydro-2H-pyran-2-yl)-5-(4,4,5,5-tetramethyl-1,3,2-dioxaborolan-2-yl)-3-(trifluoromethyl)- 1H-pyrazole **214** (126 mg, 24%); δ_H (400 MHz; $CDCl_3$; Me_4Si) 6.96 (1H, s), 5.85 (1H, dd, *J* 10.0, 2.5), 4.04 (1H, dt, *J* 11.6, 2.0), 3.67 (1 H, td, *J* 11.3, 2.7), 2.49 –2.37 (1H, m), 2.16 – 2.03 (1H, m), 1.98 (1H, ddd, *J* 13.0, 3.9, 2.4), 1.82 – 1.63 (2H, m), 1.63 – 1.52 (1 H, m), 1.34 (12H, s); δ_B (128 MHz; $CDCl_3$; Me_4Si) 27.58 (br s); δ_F (376 MHz; $CDCl_3$; Me_4Si) 27.58 (1F, s).

1-(Tetrahydro-2H-pyran-2-yl)-5-(4,4,5,5-tetramethyl-1,3,2-dioxaborolan-2-yl)-3-(trifluoromethyl)-1H-pyrazole 214

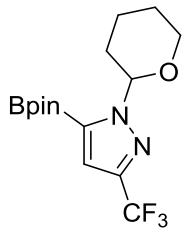

^{n}BuLi (7.76 ml, 2.5 M) was added dropwise to a stirred solution of 1-(tetrahydro-2H-pyran-2-yl)-3-(trifluoromethyl)-1H-pyrazole **212** (3.56 g, 16.17 mmol) in THF (20 ml, dry) under argon at -78 ^{o}C. The mixture was stirred at LT for 1 h before ^{i}PrOBpin (4.29 ml, 21.01 mmol) was added dropwise and the mixture was stirred at LT for 1 h before being allowed to rise to RT overnight. The reaction was quenched with water (20 ml) and DCM (40 ml) was added. The organic phase was separated and the aqueous phase was extracted with further DCM (3 x 40 ml). The organic phases were then combined, dried over $MgSO_4$, filtered and the solvent removed. The residue was purified by column chromatography on alumina (hexane:EtOAc 3:1, product visualised with $KMnO_4$ stain) to give the product as a yellow oil, 1-(tetrahydro-2H-pyran-2-yl)-5-(4,4,5,5-tetramethyl-1,3,2-dioxaborolan-2-yl)-3-(trifluoromethyl)-1H-pyrazole **214** (2.30 g, 41%). The NMR data was consistent with that obtained previously.

2-Cyano-5-hydroxy pyridine 218 [37]

A solution of $NaNO_2$ (1.90 g, 27.54 mmol) in water (17 ml) was added dropwise to a stirred

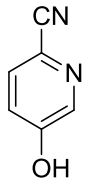

solution of 5-amino-2-cyano pyridine **217** (3.00 g, 25.10 mmol) in conc. H_2SO_4/water (13/45 ml). The temperature was monitored and maintained below 2 ^oC. After addition was complete the solution was stirred at 0 ^oC for 30 min. The mixture was then poured into a boiling mixture of water (33 ml) and conc. H_2SO_4 (3 ml). The mixture was stirred for 30 min at boiling before being cooled to RT and extracted with EtOAc (4 x 100 ml). The organic layers were combined, dried over $MgSO_4$ and filtered. The solvent was removed *in vacuo* to give the product as an orange solid, 2-cyano-5-hydroxy pyridine **218** (3.01 g, 100%), which was used without further purification; δ_H (400 MHz; $CDCl_3$; Me_4Si) 8.34 (6 H, dd, *J* 2.8, 0.6), 7.58 (6 H, dt, *J* 8.6, 0.7), 7.25 (1H, dd, *J* 8.6, 2.8).

2-Cyano-5-methoxypyridine 219

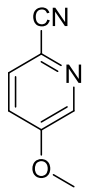

MeI (2.34 ml, 37.62 mmol) was added dropwise to a stirred suspension of K_2CO_3 (3.81 g, 27.57 mmol) and 2-cyano-5-hydroxy pyridine **218** (3.01 g, 25.06 mmol) in acetonitrile (100 ml). The mixture was stirred at RT overnight before the solvent was removed. EtOAc and water were added and the organic phase was separated. The aqueous phase was extracted with further EtOAc. The organic layers were combined, dried over $MgSO_4$, filtered and the solvent was removed *in vacuo*. The residue was purified by column chromatography (hexane:EtOAc 4:1) to give the product as an off-white solid **219** (975 mg, 29%); δ_H (400 MHz, $CDCl_3$; Me_4Si) 8.38 (1 H, dd, *J* 2.9, 0.6), 7.65 (1 H, dd, *J* 8.6, 0.7), 7.24 (1 H, dd, *J* 8.6, 2.9), 3.93 (3 H, s); δ_C (101 MHz; $CDCl_3$; Me_4Si) 157.99, 140.24, 129.66, 125.50, 119.89, 117.60, 56.09; NMR data is consistent with the literature data.[38]

1-(5-Methoxy-2-pyridinyl)-ethanone 220

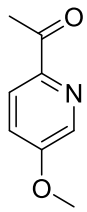

A solution of MeMgBr (3.15 ml, 3.0 M) was added dropwise to a stirred solution of 2-cyano-5-methoxypyridine **219** (0.98 g, 7.27 mmol) in THF (40 ml, dry) at 0 ^oC. The mixture was stirred at LT for 2 h, then allowed to warm overnight. The solution was poured into aq. NH_4Cl (100 ml, 1M) solution and acidified to pH 1 with conc. HCl. The mixture was stirred at RT for 1 h before being neutralised with solid $NaHCO_3$. DCM was added, and the layers were separated. The aqueous layer was extracted with further DCM and the organic phases were combined, dried over $MgSO_4$, filtered and the solvent was removed *in vacuo*. The residue was purified by column chromatography (hexane:EtOAc 1:2) to give the product as a clear oil that solidifies on standing, **220** (0.62 g, 56%); δ_H (400 MHz, $CDCl_3$; Me_4Si) 8.33 (1 H, dd, *J* 2.9, 0.6), 8.05 (1 H, dd, *J* 8.8, 0.6), 7.26 (3 H, dd, *J* 8.7, 2.9), 3.93 (3 H, s), 2.69 (3 H, s); NMR data is consistent with the literature data.[39]

References

1) G. St-Pierre, S. Ladouceur, D. Fortin and E. Zysman-Colman, *Dalton Trans.,* 2011, **40**, 11726-31
2) T. Hofbeck and H. Yersin, *Inorg. Chem.,* 2010, **49**, 9290-9
3) Y. Zhou, W. Li, Y. Liu, L. Zeng, W. Su and M. Zhou, *Dalton Trans.,* 2012, **41**, 9373-81
4) H. Suzuki and H. Abe, *Tetrahedron Lett.,* 1995, **36**, 6239-6242
5) Y. You and S. Y. Park, *J. Am. Chem. Soc.,* 2005, **127**, 12438-9
6) S.-y. Takizawa, H. Echizen, J.-i. Nishida, T. Tsuzuki, S. Tokito and Y. Yamashita, *Chem. Lett.,* 2006, **35**, 748-749
7) C. Fan, Y. Li, C. Yang, H. Wu, J. Qin and Y. Cao, *Chem. Mater.,* 2012, **24**, 4581-4587
8) V. N. Kozhevnikov, Y. Zheng, M. Clough, H. A. Al-Attar, G. C. Griffiths, K. Abdullah, S. Raisys, V. Jankus, M. R. Bryce and A. P. Monkman, *Chem. Mater.,* 2013, **25**, 2352-2358
9) U. Berg, R. Gallo and J. Metzger, *J. Org. Chem.,* 1976, **41**, 2621-2624
10) K. Asano and S. Matsubara, *Org. Lett.,* 2009, **11**, 1757-1759
11) A. Christoforou, G. Nicolaou and Y. Elemes, *Tetrahedron Lett.,* 2006, **47**, 9211-9213
12) P. Jacob and A. T. Shulgin, *J. Med. Chem.,* 1981, **24**, 1348-1353
13) B. M. Rosen, D. A. Wilson, C. J. Wilson, M. Peterca, B. C. Won, C. Huang, L. R. Lipski, X. Zeng, G. Ungar, P. A. Heiney and V. Percec, *J. Am. Chem. Soc.,* 2009, **131**, 17500-17521
14) J. T. Kuethe and K. G. Childers, *Adv. Synth. Catal.,* 2008, **350**, 1577-1586
15) B. A. Kamino, B. Mills, C. Reali, M. J. Gretton, M. A. Brook and T. P. Bender, *J. Org. Chem.,* 2012, **77**, 1663-1674
16) V. N. Kozhevnikov, K. Dahms and M. R. Bryce, *J. Org. Chem.,* 2011, **76**, 5143-8
17) H. Zhao, C. Tanjutco and S. Thayumanavan, *Tetrahedron Lett.,* 2001, **42**, 4421-4424
18) M. Delor, T. Keane, P. A. Scattergood, I. V. Sazanovich, G. M. Greetham, M. Towrie, A. J. H. M. Meijer and J. A. Weinstein, *Nature Chem.,* 2015, **7**, 689-695
19) A. Bouillon, J.-C. Lancelot, V. Collot, P. R. Bovy and S. Rault, *Tetrahedron,* 2002, **58**, 3323-3328
20) E. Bisagni, M. Rautureau and C. Huel, *Heterocycles,* 1989, **29**, 1815
21) E. Busto, V. Gotor-Fernández and V. Gotor, *Tetrahedron: Asymmetry,* 2006, **17**, 1007-1016
22) H. R. Hoveyda, V. Karunaratne, S. J. Rettig and C. Orvig, *Inorg. Chem.,* 1992, **31**, 5408-5416
23) E. Ishow, R. Camacho-Aguilera, J. Guérin, A. Brosseau and K. Nakatani, *Adv. Funct. Mater.,* 2009, **19**, 796-804
24) A. S. Singh and P. K. Bharadwaj, *Dalton Trans.,* 2008, 738-741
25) A. S. Singh, B.-Y. Chen, Y.-S. Wen, C. Tsai and S.-S. Sun, *Org. Lett.,* 2009, **11**, 1867-1870
26) J. S. Ward, J. M. Lynam, J. W. B. Moir, D. E. Sanin, A. P. Mountford and I. J. S. Fairlamb, *Dalton Trans.,* 2012, **41**, 10514-10517
27) W. E. Silva, M. Freire Belian, R. O. Freire, G. F. de Sá and S. Alves Jr, *J. Phys. Chem. A,* 2010, **114**, 10066-10075
28) X. Liu, Z. Tian, C. Chen and H. R. Allcock, *Macromolecules,* 2012, **45**, 1417-1426
29) M. P. Castaldi, S. E. Gibson, M. Rudd and A. J. P. White, *Chem. Eur. J.,* 2006, **12**, 138-148
30) D. W. Brousmiche, J. M. Serin, J. M. J. Fréchet, G. S. He, T.-C. Lin, S.-J. Chung, P. N. Prasad, R. Kannan and L.-S. Tan, *J. Phys. Chem. B,* 2004, **108**, 8592-8600
31) C. Schaffner-Hamann, A. von Zelewsky, A. Barbieri, F. Barigelletti, G. Muller, J. P. Riehl and A. Neels, *J. Am. Chem. Soc.,* 2004, **126**, 9339-48
32) D. F. Taber and J. L. Schuchardt, *Tetrahedron,* 1987, **43**, 5677-5684
33) L. Zhu, P. Guo, G. Li, J. Lan, R. Xie and J. You, *J. Org. Chem.,* 2007, **72**, 8535-8538
34) P.-J. Yang, H.-C. Chu, T.-C. Chen and H.-C. Lin, *J. Mater. Chem.,* 2012, **22**, 12358-12368
35) M. A. Larsen and J. F. Hartwig, *J. Am. Chem. Soc.,* 2014, **136**, 4287-4299
36) K. C. Nicolaou, D. Rhoades, Y. Wang, S. Totokotsopoulos, R. Bai and E. Hamel, *ChemMedChem,* 2015, **10**, 1974-1979
37) WO2006045096 (A2), 2006

38) E. L. P. Chekler, R. Unwalla, T. A. Khan, R. S. Tangirala, M. Johnson, M. St. Andre, J. T. Anderson, T. Kenney, S. Chiparri, C. McNally, E. Kilbourne, C. Thompson, S. Nagpal, G. Weber, S. Schelling, J. Owens, C. A. Morris, D. Powell, P. R. Verhoest and A. M. Gilbert, *J. Med. Chem.,* 2014, **57**, 2462-2471
39) R. M. Garbaccio, E. J. Brnardic, M. E. Fraley, G. D. Hartman, P. H. Hutson, J. A. O'Brien, B. C. Magliaro, J. M. Uslaner, S. L. Huszar, K. L. Fillgrove, J. H. Small, C. Tang, Y. Kuo and M. A. Jacobson, *ACS Medicinal Chemistry Letters,* 2010, **1**, 406-410